

Contributing Editor

ABDULLAH A. AL-BADR

Founding Editor

KLAUS FLOREY

Academic Press is an imprint of Elsevier
225 Wyman Street, Waltham, MA 02451, USA
525 B Street, Suite 1800, San Diego, CA 92101-4495, USA
125 London Wall, London, EC2Y 5AS, UK
The Boulevard, Langford Lane, Kidlington, Oxford OX5 1GB, UK

First edition 2015

© 2015 Elsevier Inc. All rights reserved.

No part of this publication may be reproduced or transmitted in any form or by any means, electronic or mechanical, including photocopying, recording, or any information storage and retrieval system, without permission in writing from the publisher. Details on how to seek permission, further information about the Publisher's permissions policies and our arrangements with organizations such as the Copyright Clearance Center and the Copyright Licensing Agency, can be found at our website: www.elsevier.com/permissions.

This book and the individual contributions contained in it are protected under copyright by the Publisher (other than as may be noted herein).

Notices

Knowledge and best practice in this field are constantly changing. As new research and experience broaden our understanding, changes in research methods, professional practices, or medical treatment may become necessary.

Practitioners and researchers must always rely on their own experience and knowledge in evaluating and using any information, methods, compounds, or experiments described herein. In using such information or methods they should be mindful of their own safety and the safety of others, including parties for whom they have a professional responsibility.

To the fullest extent of the law, neither the Publisher nor the authors, contributors, or editors, assume any liability for any injury and/or damage to persons or property as a matter of products liability, negligence or otherwise, or from any use or operation of any methods, products, instructions, or ideas contained in the material herein.

ISBN: 978-0-12-803300-5

ISSN: 1871-5125 (Series)

For information on all Academic Press publications
visit our website at <http://store.elsevier.com/>



Working together
to grow libraries in
developing countries

www.elsevier.com • www.bookaid.org

PREFACE TO VOLUME 40

The comprehensive profiling of drug substances and pharmaceutical excipients as to their physical and analytical characteristics remains essential to all phases of pharmaceutical development, and such profiles are of immeasurable importance to workers in the field. Consequently, the compilation and publication of comprehensive summaries of physical and chemical data, analytical methods, routes of compound preparation, degradation pathways, uses and applications, etc., have always been and will continue to be a vital function to both academia and industry.

Since this volume of the *Profiles* is the 40th of the series, it seemed appropriate to write a longer preface in the form of a retrospective, and to share thoughts and remembrances regarding where the series came from and where it is going. The early history I will discuss was provided by Klaus Florey (the founding editor of the series), and the latter history is mine.

As part of his internal duties at the Squibb Institute for Medical Research in 1968, Klaus recognized a need for better documentation of new drug substances. His idea was to publish comprehensive profiles of the physical, analytical, and pharmacological properties of the most important drug substances that had been approved by the US Food and Drug Administration. Up until that point in time, information regarding active pharmaceutical ingredients was scattered throughout the literature. Klaus had the vision that monographs collecting in one place everything that was known about a given drug substance would be of great use to the pharmaceutical community.

As his first step in the publication process, Klaus asked Ed Feldman (who was the editor of the *Journal of Pharmaceutical Sciences* at the time) whether he would publish profiles in the journal. But since the interest was not there, Klaus then approached several publishers with the concept of publishing a continuing series of volumes containing these monographs, obtaining significant interest from Marcel Dekker and from Academic Press. Ultimately, the agreement was signed with Academic Press to publish the series as it was initially known, the *Analytical Profiles of Drug Substances*.

Klaus had wanted to obtain cooperation of the Academy of Pharmaceutical Sciences in this endeavor, and so approached Tom Macek (president of the Academy at that time). The arrangement was accepted, and then the question of royalties for individual contributors came up. Klaus thought at the time that the money involved for individual contributors would be

rather puny, since back then all contributors worked in the industry. So the monies derived from sales went to the Analytical Section of APhA, but APhA maintained all copyrights. Upon formation of the American Association for Pharmaceutical Scientists, APhA released the copyright to AAPS and the Analytical and Pharmaceutical Quality section of AAPS received the proceeds from sales.

The first volume in the *Analytical Profiles of Drug Substances* was published in 1972 and contained profiles of Acetohexamide, Chlordiazepoxide and its hydrochloride salt, Cycloserine, Cyclothiazide, Diazepam, Erythromycin Estolate, Halothane, Levarterenol Bitartrate, Meperidine Hydrochloride, Meprobamate, Nortriptyline Hydrochloride, Potassium Phenoxymethyl Penicillin, Propoxyphene Hydrochloride, Cephalothin Sodium, Secobarbital Sodium, Triamcinolone, Triamcinolone Acetonide, Triamcinolone Diacetate, Vinblastine Sulfate, and Vincristine Sulfate. By 1991, Klaus had edited a total of 20 volumes in the series.

My first exposure to the *Analytical Profiles* came in 1988 when Klaus asked me to join the Editorial Advisory Board. At the same time, he and Glenn Brewer (Director of Analytical Research & Development of the Squibb Institute) also asked me to write a profile of Chlorothiazide, which was published in Volume 18. In 1991, while Klaus was developing his last volume in the series, he asked me to take over the editorship of the series. At this time, I had a strong interest in pharmaceutical excipients and envisioned the publication of profiles on excipients. Accordingly, I and my Materials Science team (Susan Bogdanowich, David Bugay, Joseph DeVincentis, Greg Lewen, and Ann Newman) contributed a profile of anhydrous lactose to Klaus' last volume in the *Analytical Profiles* series.

When I took over the editorship in 1991, I determined that the expanded scope of the series necessitated a change in the name of the series. Accordingly, Volume 21 (published in 1992) became the first volume published under the new series name, the *Analytical Profiles of Drug Substances and Excipients*. In addition to the usual drug substance monographs, this volume also contained a profile of Titanium Dioxide. Volumes in the series continued to be published under this name, with Volume 29 (published in 2002) being the last.

Around this time, Academic Press was acquired by Elsevier, and the new contract severed the ongoing relationship with APhA. I viewed this development as an opportunity to further expand the scope of the series beyond profiles of drug substances and excipients, and to now feature review articles summarizing the techniques and methods used by investigators active in

profiling. Hence, beginning with Volume 30 (published in 2003), the title of the series changed again to reflect its new scope and now became the *Profiles of Drug Substances, Excipients, and Related Methodology* (its current title). Not only did Volume 30 contain profiles of various drug substances (Acyclovir, Ceftriaxone Sodium, Ipratropium Bromide, Ornidazole, and Sertraline (L)-Lactate), but it also contained an excipient profile (Propylparaben) and the first methodology chapter (X-Ray Diffraction of Pharmaceutical Materials).

Since 2003, nine volumes in the Profiles series have been published, all of which contain monographs of drug substances, and many of which contain monographs relating to the additional content. In this time period, Volume 33 (published in 2007) stands out in my mind owing to the massive contribution by Richard Pranker in the form of his critical compilation of ionization constant values for numerous pharmaceutical substances. Of course, the success of the series has been greatly aided by the efforts of the Contributing Editors, Abdullah Al-Badr, Gunawan Indrayanto, and Yuri Goldberg.

On the subject of Contributing Editors, Professor Al-Badr has elected to leave the Department of Pharmaceutical Chemistry in King Saud University and to relinquish his position on the *Profiles* editorial team. The enormous contributions made by Professor Al-Badr over the years cannot be adequately summarized, but it shall suffice to say that many fewer volumes in the series would have been published were it not for his tireless efforts in manuscript solicitation and writing. Fortunately, he has indicated a desire to continue as a chapter contributor, and so I look forward to reading his newest works. Professor Abdulrahman A. Al-Majed will become a new Contributing Editor, and I welcome him to the team.

Since the science of pharmaceuticals continues to grow and mature, the need for information continues to expand along new fronts. This continual growth still requires an equivalent growth in the repository sources where investigators find the information they need. The content of the *Profiles* series continues to respond and expand to meet this need, and so chapters are published that fall into one or more of the following main categories:

1. Comprehensive profiles of a drug substance or excipient
2. Physical characterization of a drug substance or excipient
3. Analytical methods for a drug substance or excipient
4. Detailed discussions of the clinical uses, pharmacology, pharmacokinetics, safety, or toxicity of a drug substance or excipient
5. Reviews of methodology useful for the characterization of drug substances or excipients

6. Annual reviews of areas of importance to pharmaceutical scientists

This volume contains comprehensive profiles of cinnarizine, glutathione, losartan, prasugrel hydrochloride, salmeterol, telmisartan, and valsartan, all of which contain state-of-the-art information. As always, I welcome communications from anyone in the pharmaceutical community who might want to provide an opinion or a contribution.

HARRY G. BRITTAIN

Editor, Profiles of Drug Substances,
Excipients, and Related Methodology
hbrittain@centerpharmphysics.com



Cinnarizine: Comprehensive Profile

Nadia G. Haress¹

Department of Pharmaceutical Chemistry, College of Pharmacy, King Saud University, Riyadh, Saudi Arabia

¹Corresponding author: e-mail address: nharess@ksu.edu.sa; nadiaharess@hotmail.com

Contents

1. Description	1
1.1 Nomenclature	1
1.2 Formulae	2
1.3 Elemental Analysis	3
1.4 Appearance	3
1.5 Uses and Applications	3
2. Methods of Preparation	3
3. Physical Characteristics	5
3.1 Ionization Constant	5
3.2 Solubility Characteristics	5
3.3 X-Ray Powder Diffraction Pattern	5
3.4 Thermal Method of Analysis	7
3.5 Spectroscopy	7
4. Methods of Analysis	21
4.1 Compendial Methods	21
4.2 Reported Methods of Analysis	24
5. Biological Analysis	33
6. Stability	35
7. Pharmacokinetics, Metabolism, and Excretion	36
8. Pharmacology	38
Acknowledgment	39
References	39



1. DESCRIPTION

1.1 Nomenclature

1.1.1 Systemic Chemical Names

- 1-(Diphenylmethyl)-4-(3-phenyl-2-propenyl)piperazine
- 1-Cinnamyl-4-diphenylmethylpiperazine

- *N*-Benzhydryl-*N*-*trans*-cinnamylpiperazine
- 1-*trans*-Cinnamyl-4-diphenylmethylpiperazine
- 1-Cinnamyl-4-benzhydrylpiperazine
- 1-Diphenylmethyl-4-*trans*-cinnamylpiperazine [1–4]

1.1.2 Nonproprietary Names

Cinnarizine, cinnarizin [1–4]

1.1.3 Proprietary Names

1.1.3.1 Cinnarizine

Cinniprine[®], 516-MD[®], Aplactan[®], Aplexal[®], Apotomin[®], Artate[®], Car-ecin[®], Cerebolan[®], Cerepar[®], Cinnaperazine[®], Cinazyn[®], Cinnacet[®], Cinnageron[®], Corathiem[®], Denapol[®], Dimitron[®], Eglen[®], Folcodal[®], Giganten[®], Glanil[®], Hilactan[®], Ixertol[®], Katoseran[®], Labyrin[®], Midronal[®], Mitronal[®], Olamin[®], Processine[®], Sedatromin[®], Sepan[®], Siptazin[®], Spaderizine[®], Stugeron[®], Stutgin[®], Toliman[®] [1–4].

1.1.3.2 Cinnarizine Hydrochloride

Linazine[®], Siarizine[®], Silicin[®], Sorebral[®].

1.1.3.3 Mixture with Vitamin B₆

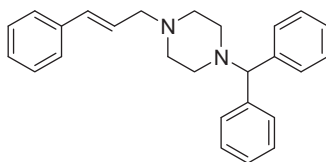
Emasazine[®], C-Sik[®]

1.2 Formulae

1.2.1 Empirical Formula, Molecular Weight, and CAS Number

Cinnarizine	C ₂₆ H ₂₈ N ₂	368.51	298-57-7
Cinnarizine hydrochloride	C ₂₆ H ₂₈ N ₂ ·HCl	404.97	700-58-6

1.2.2 Structural Formulae



1.3 Elemental Analysis

Cinnarizine	C, 84.74%	H, 7.66%	N, 7.60%	
Cinnarizine hydrochloride	C, 77.11%	H, 7.22%	N, 6.92%	Cl, 8.75% [1]

1.4 Appearance

Cinnarizine is a white or almost white powder [1–3].

1.5 Uses and Applications

Cinnarizine is a piperazine derivative with antihistaminic, antiserotonergic, antidopaminergic, and calcium channel-blocking activities. It is currently used for the treatment of nausea, vomiting, and vertigo caused by Meniere's disease and other vestibular disorders. Cinnarizine is also used for prevention and treatment of motion sickness. It is also widely used for the treatment of cerebral thrombosis, cerebral embolism, cerebral arteriosclerosis, and diseases caused by poor peripheral circulation [3]. It is also reported that cinnarizine is effective in the treatment of some allergic diseases, such as chronic urticaria and senile skin pruritus [3].

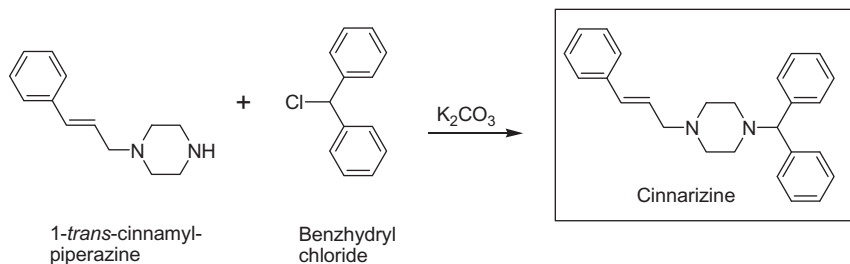
Cinnarizine is given orally as tablets or capsules which may result in a very slow bioavailability and a wide individual variation [3,4].

Intravenous cinnarizine administration is an alternative to oral administration which provides greater bioavailability, faster therapeutic effect, and lower individual difference than oral dosing. However, any injectable dosage forms can cause pain at the injection site, venous irritation, and possible precipitation of the drug after intravenous administration resulting in restriction of their clinical applications and industrial-scale production [3,4].

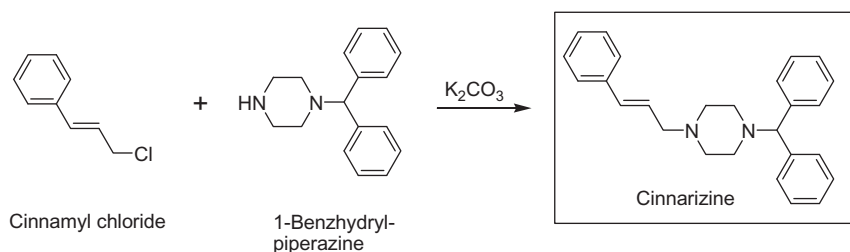


2. METHODS OF PREPARATION

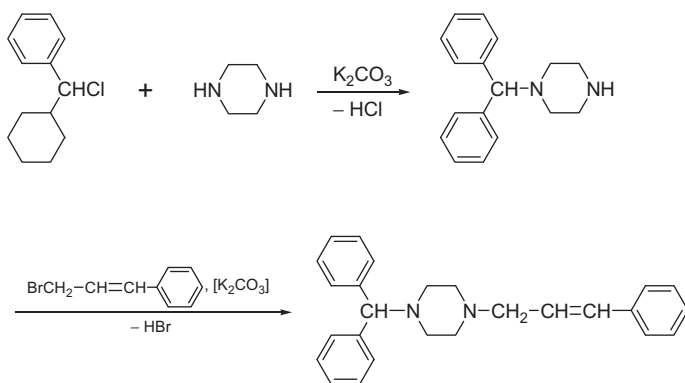
Cinnarizine was prepared by Janssen Pharmaceutical Companies [5] by two methods. The first one was achieved by reacting 1-*trans*-cinnamylpiperazine with benzhydryl chloride in an alkaline medium (Scheme 1), while the other method was performed by the addition of cinnamyl chloride to 1-benzylpiperazine in the presence of sodium carbonate (Scheme 2).



Scheme 1 Synthesis of cinnarizine by Janssen Pharmaceutical Companies (first method).



Scheme 2 Synthesis of cinnarizine by Janssen Pharmaceutical Companies (second method).



Scheme 3 Synthesis of cinnarizine by a reported method.

Cinnarizine was also prepared by the reaction of piperazine with benzhydryl chloride, followed by N-alkylation with cinnamyl bromide or chloride ([Scheme 3](#)) [6].

In addition, Sheng *et al.* [7] reported a convenient synthesis of cinnarizine by Mannich reaction of 1-benzhydrylpiperazine with HCHO and

PhCOMe, followed by the reduction of the resultant propiophenone derivative and subsequent dehydration of the alcohol to afford cinnarizine in quantitative yield.



3. PHYSICAL CHARACTERISTICS

3.1 Ionization Constant

$$\text{p}K_{\text{a}} = 7.8$$

$$\text{Log } P = 6.14 \text{ [8]}$$

3.2 Solubility Characteristics

Cinnarizine: Practically insoluble in water. Slightly soluble in ethanol (96%) and methanol. Soluble in acetone and freely soluble in dichloromethane. Protect from light [1–3].

Cinnarizine hydrochloride: Soluble 2 mg/100 mL in water [1–3].

3.3 X-Ray Powder Diffraction Pattern

The X-ray powder diffraction pattern of cinnarizine was performed using a Bruker-Nonius FR590 diffractometer. Figure 1 shows the X-ray powder diffraction pattern of cinnarizine, which was obtained on a pure sample of the drug substance. Table 1 shows the values for the scattering angles

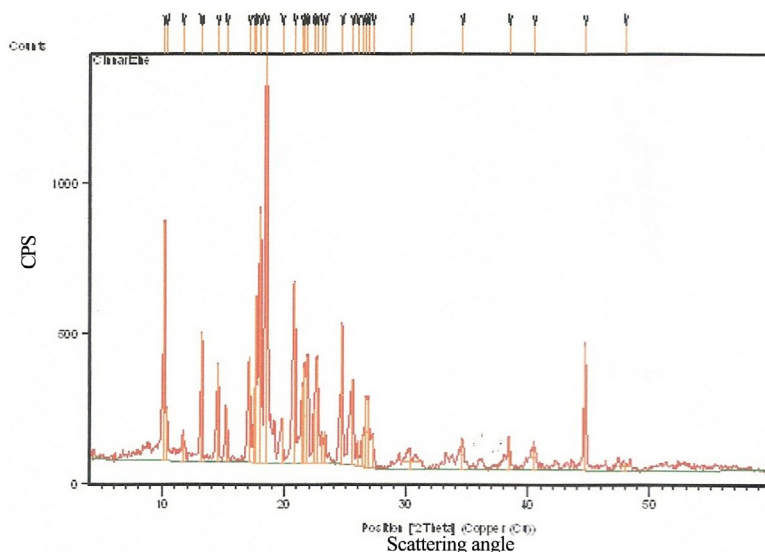


Figure 1 The X-ray diffraction pattern of cinnarizine.

Table 1 The X-Ray Powder Diffraction Pattern of Cinnarizine

Position ($^{\circ} 2\theta$)	Height (cts)	FWHM Left ($^{\circ} 2\theta$)	d-Spacing (\AA)	Relative Intensity (%)
10.1300	789.24	0.0900	8.72502	57.95
10.3243	173.35	0.0900	8.56133	12.73
11.6712	88.89	0.3070	7.58239	6.53
13.1005	232.89	0.0900	6.75258	17.10
13.2245	427.43	0.0768	6.69508	31.39
14.5404	323.93	0.1279	6.09200	23.79
15.2189	181.93	0.2047	5.82191	13.36
17.0963	353.10	0.0900	5.18230	25.93
17.5123	247.33	0.0900	5.06013	18.16
17.6765	554.26	0.0768	5.01763	40.40
18.0114	826.60	0.0900	4.92100	60.70
18.4553	1361.85	0.0900	4.80365	100.00
19.7652	152.87	0.1535	4.49186	11.23
20.7696	603.13	0.0900	4.27330	44.29
21.4551	254.51	0.0900	4.13831	18.69
21.6264	319.60	0.0900	4.10590	23.47
21.8549	352.73	0.0900	4.06349	25.90
22.3690	179.01	0.0900	3.97126	13.14
22.5974	345.14	0.0900	3.93162	25.34
23.0258	101.38	0.0900	3.85943	7.44
23.3257	110.54	0.0900	3.81049	8.12
24.6931	459.60	0.0900	3.60249	33.75
25.5281	285.59	0.0900	3.48652	20.97
25.9534	86.62	0.0900	3.43033	6.36
26.3946	105.73	0.0900	3.37400	7.76
26.6781	233.08	0.0900	3.33877	17.12
27.1980	116.57	0.0900	3.27612	8.56
30.3314	51.89	1.6374	2.94688	3.81

Table 1 The X-Ray Powder Diffraction Pattern of Cinnarizine—cont'd

Position ($^{\circ}2\theta$)	Height (cts)	FWHM Left ($^{\circ}2\theta$)	d-Spacing (\AA)	Relative Intensity (%)
34.5428	96.91	0.3070	2.59664	7.12
40.4625	83.29	0.4093	2.22937	6.12
44.6465	414.33	0.2047	2.02968	30.42
47.9395	27.19	1.2280	1.89767	2.00

(deg, 2θ), the interplanar d-spacing (\AA), and the relative intensities (%) observed for the major diffraction peaks of cinnarizine.

3.4 Thermal Method of Analysis

3.4.1 Melting Behavior

Cinnarizine melts at 118–122 $^{\circ}\text{C}$.

Cinnarizine hydrochloride melts at 192 $^{\circ}\text{C}$ [1].

3.5 Spectroscopy

3.5.1 Ultraviolet Spectroscopy

The UV absorption spectrum of cinnarizine in 0.1 N hydrochloric acid shown in Figure 2 was recorded using an Ultrospec 2100 pro UV/Vis Spectrophotometer. Compound exhibited a maximum at 253 nm (A 1%, 1 cm = 584). Clarke reported the following: aqueous acid—254 nm (A 1%, 1 cm = 584) [2].

3.5.2 Vibrational Spectroscopy

The infrared absorption spectrum of cinnarizine was obtained as KBr disc using a Jasco FT/IR-4100 infrared spectrophotometer. The infrared spectrum is shown in Figure 3, where the principle peaks are observed at 3064, 3021, 2953, 2873, 1134, 997, and 965 cm^{-1} . Assignment for the major infrared absorption bands is shown in Table 2.

Clarke reported principle peaks at 702, 691, 1138, 964, 740, and 1000 cm^{-1} (KBr disc) [2].

3.5.3 Nuclear Magnetic Resonance Spectrometry

3.5.3.1 ^1H NMR Spectrum

The proton NMR spectrum of cinnarizine was obtained using a Bruker instrument operating at 500 MHz. Standard Bruker software was used to execute the recording of DEPT, COSY, and HETCOR spectra. The

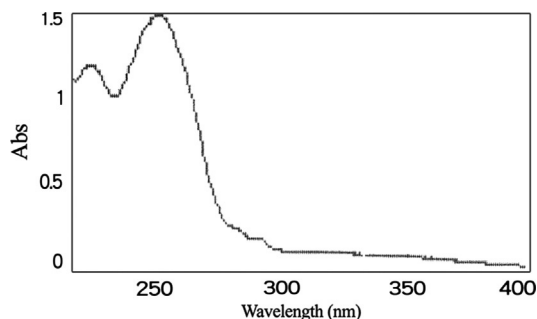


Figure 2 The UV absorption spectrum of cinnarizine.

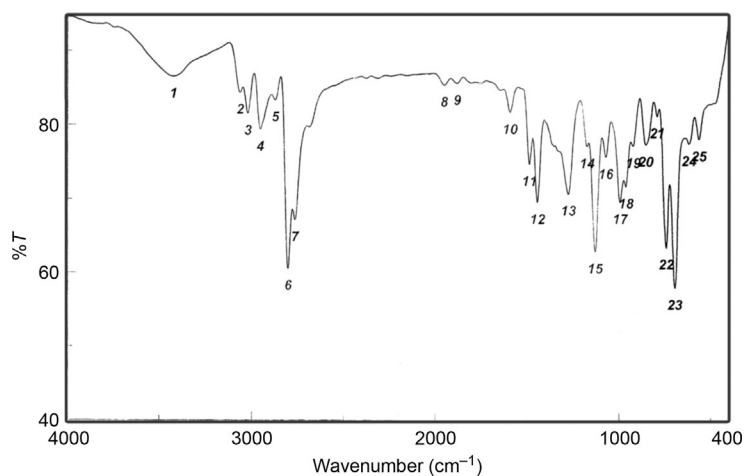


Figure 3 The infrared absorption spectrum of cinnarizine (KBr disc).

Table 2 $\pm R$ (ν , cm^{-1}) Assignments of Cinnarizine

Frequency (cm^{-1})	Assignments
3064, 3021	CH stretching (aromatic and alkene)
2953, 2873	CH stretch (aliphatic)
1134	C—N stretching
997, 965	=C—H out of plane (oop) (alkene and Aromatic)

sample was dissolved in $\text{DMSO}-d_6$ and all resonance bands were referenced to tetramethylsilane (TMS) as internal standard. The ^1H NMR spectra of cinnarizine are shown in [Figures 4–6](#) and the COSY ^1H NMR spectrum is shown in [Figures 7 and 8](#). The ^1H NMR assignments for cinnarizine are provided in [Table 3](#).

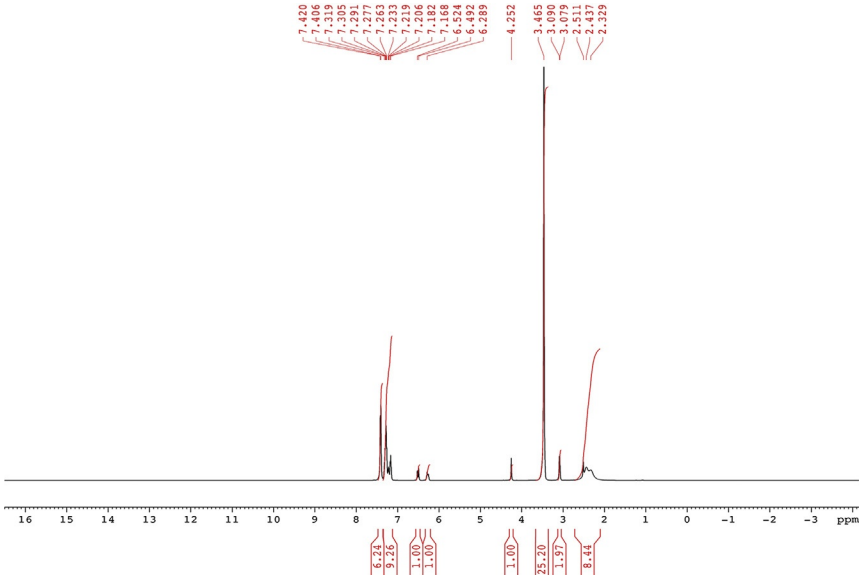


Figure 4 ^1H NMR spectrum of cinnarizine.

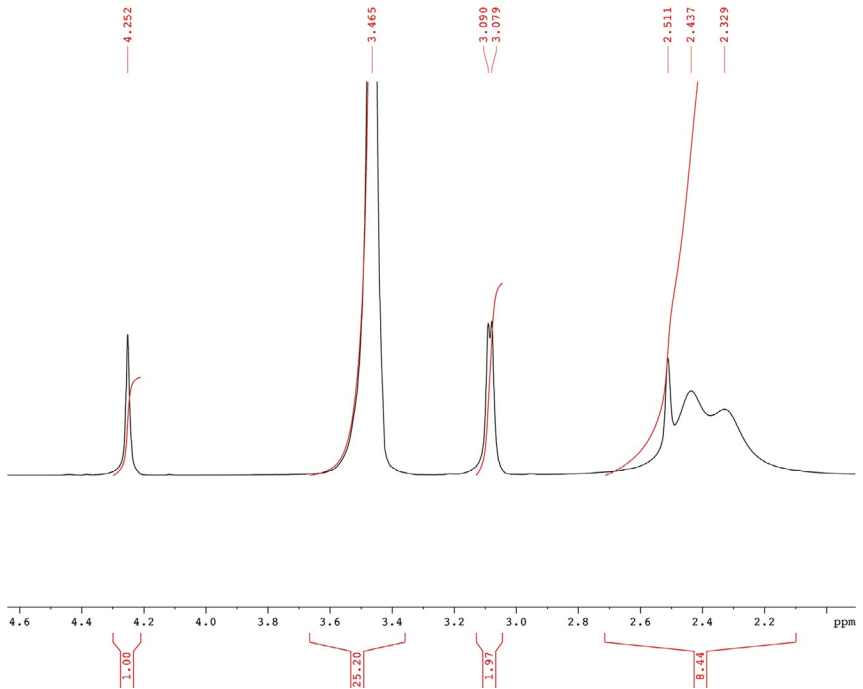


Figure 5 Partial expanded ^1H NMR spectrum (δ 2.1–4.6 ppm) of cinnarizine.

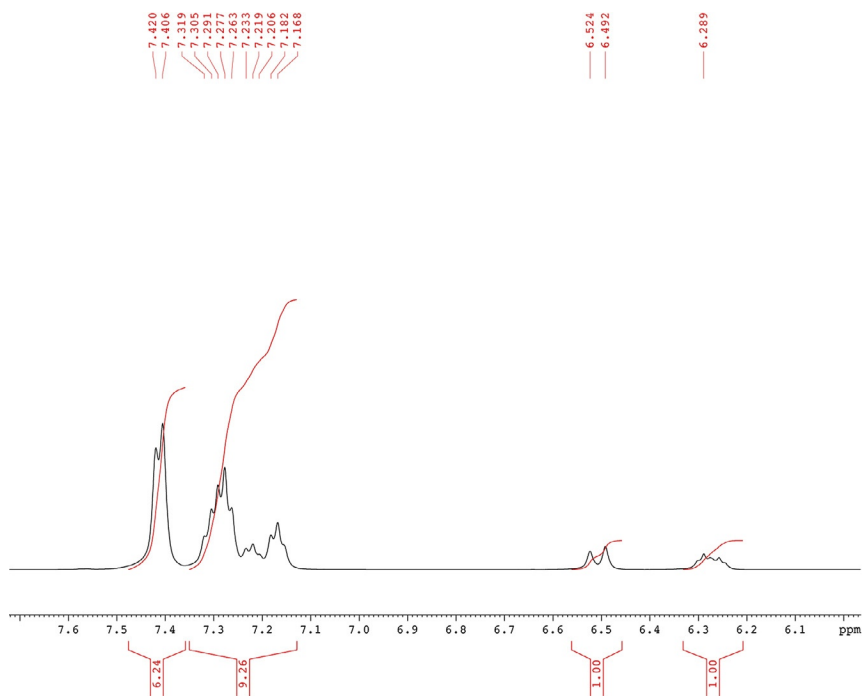


Figure 6 Partial expanded ^1H NMR spectrum (δ 6.2–7.5 ppm) of cinnarizine.

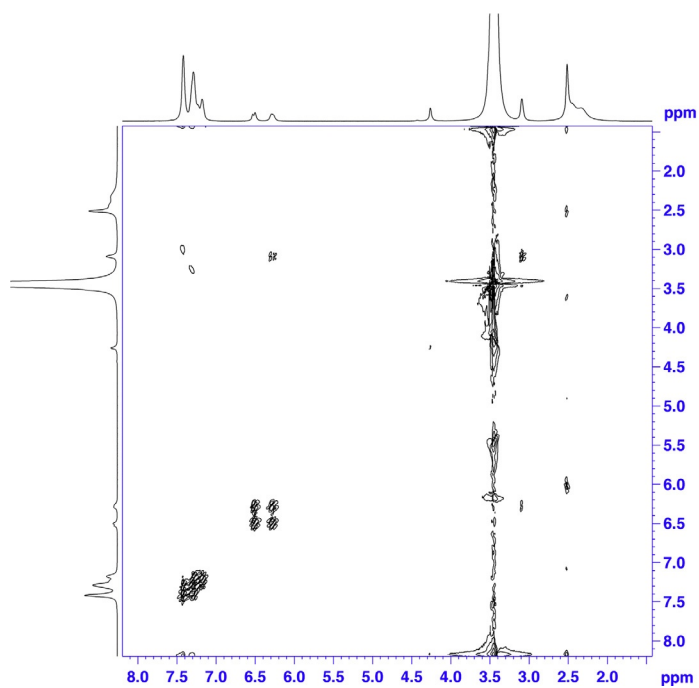


Figure 7 COSY-1 ^1H NMR spectrum of cinnarizine in $\text{DMSO}-d_6$.

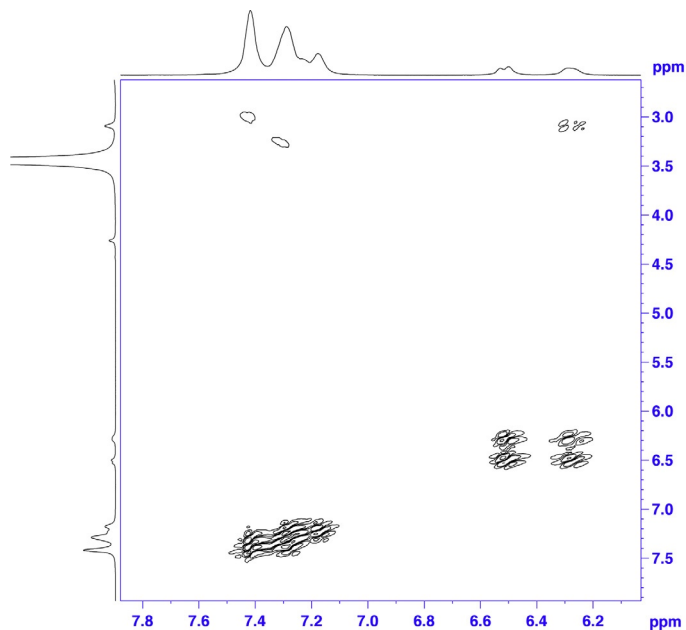


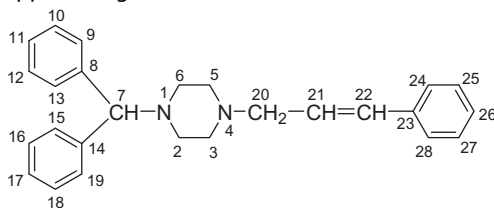
Figure 8 COSY-2 ^1H NMR spectrum of cinnarizine.

3.5.3.2 ^{13}C NMR Spectrum

The carbon-13 NMR spectra of cinnarizine were obtained using a Bruker instrument operating at 125 MHz. The sample was dissolved in $\text{DMSO}-d_6$ and TMS was added to function as the internal standard. The ^{13}C NMR spectra are shown in [Figures 9 and 10](#) and the HSQC and HMBC NMR spectra were shown in [Figures 11–15](#), respectively. The DEPT 90 and DEPT 135 are shown in [Figures 16–19](#), respectively. The assignments for the observed resonance bands associated with the various carbons are listed in [Table 4](#). Summary of assignments for the nuclear magnetic resonance bands of cinnarizine is shown in [Table 5](#).

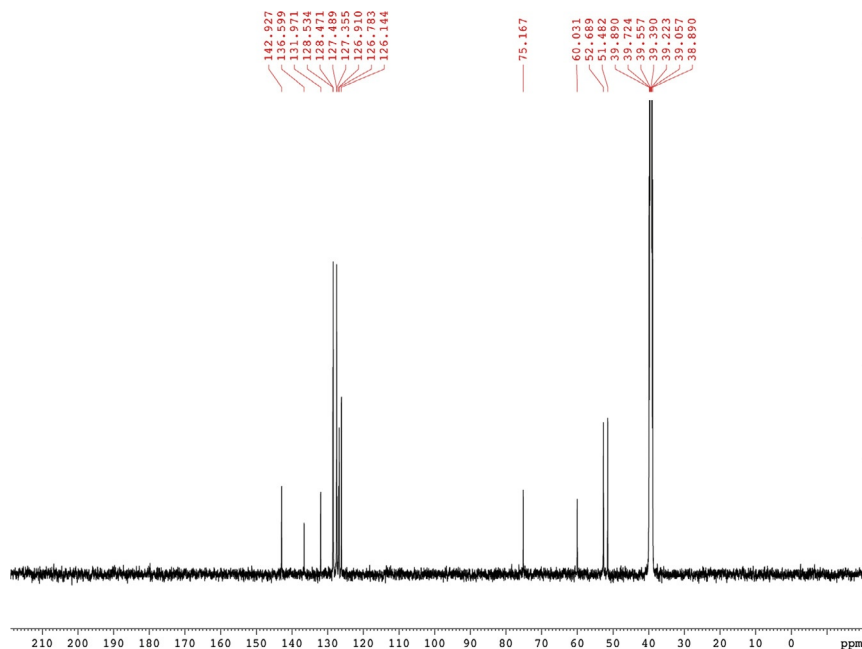
3.5.4 Electron Impact Mass Spectrometry

The electron impact (EI) mass spectrum of cinnarizine was obtained using a Shimadzu QP-2010 plus mass spectrometer. [Figure 20](#) shows the detailed mass fragmentation pattern for cinnarizine. [Table 6](#) shows the proposed mass fragmentation pattern of the drug.

Table 3 ^1H NMR (δ ppm) Assignments of the Resonance Bands in Cinnarizine

Chemical Shift (δ ppm, Relative to TMS)	Number of Protons	Multiplicity ^a	Assignments
2.33	4	m	H-2 and H-6
2.44	4	m	H-3 and H-5
3.08	2	d	H-20
4.25	1	s	H-7
6.29	1	m	H-21
6.51	1	d	H-22
7.17–7.18	2	m	H-11 and H-17
7.21	1	m	H-26
7.22–7.29	6	m	H-9, H-13, H-15, H-19, H-25, and H-27
7.31–7.42	6	m	H-10, H-12, H-16, H-18, H-24, and H-28

^as, singlet; d, doublet; m, multiplet.

**Figure 9** ^{13}C NMR spectrum of cinnarizine in $\text{DMSO}-d_6$.

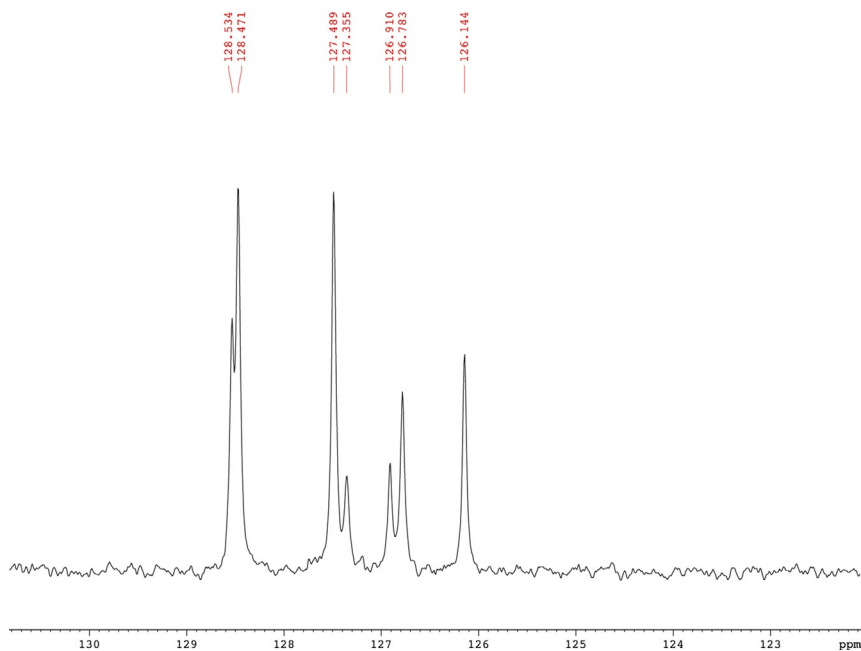


Figure 10 Expanded ^{13}C NMR spectrum of cinnarizine in $\text{DMSO}-d_6$.

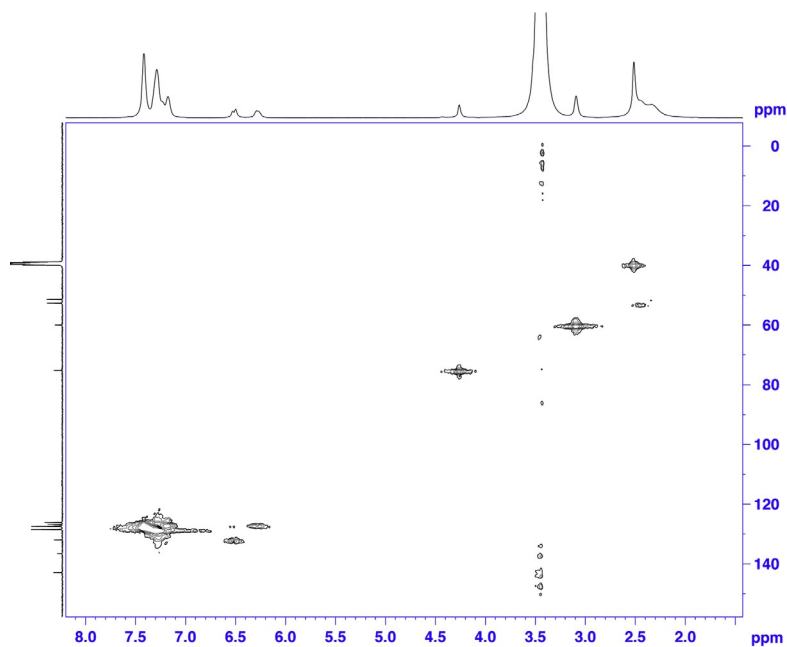


Figure 11 The HMQC-1 spectrum of cinnarizine in $\text{DMSO}-d_6$.

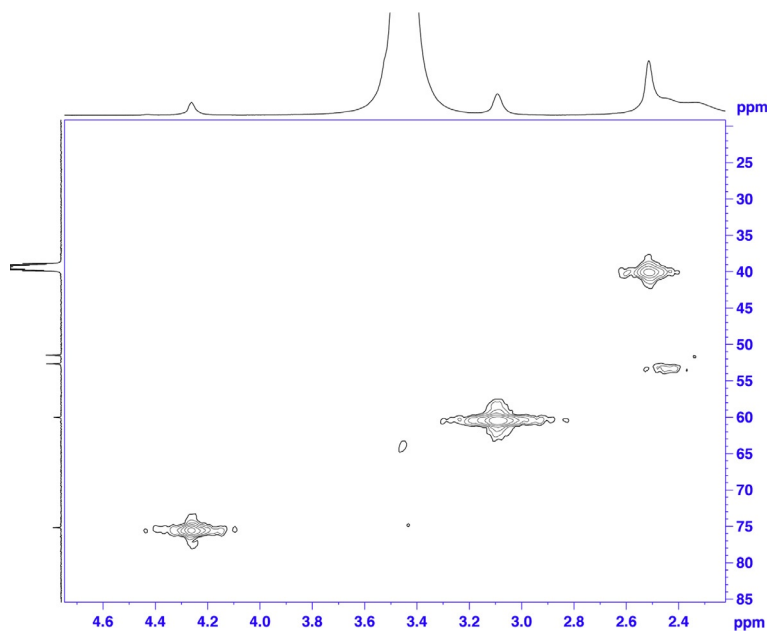


Figure 12 The HMOC-2 spectrum of cinnarizine in DMSO- d_6 .

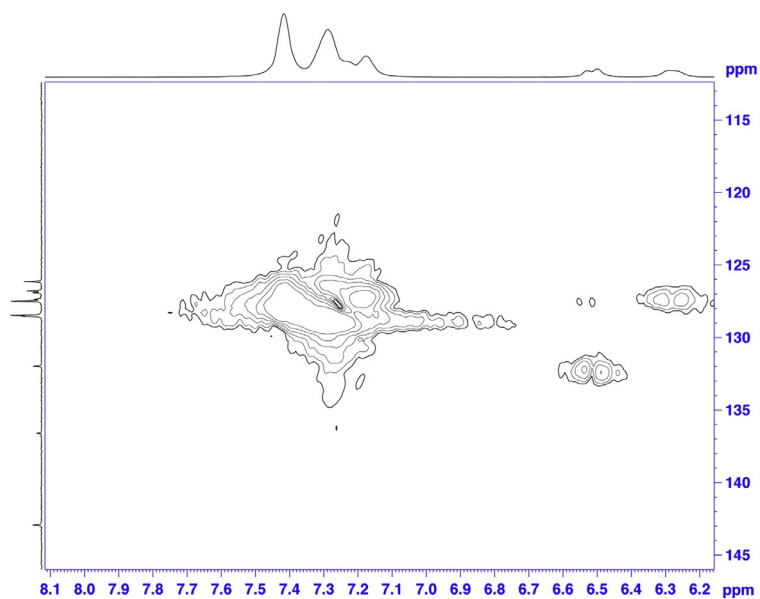


Figure 13 The HMOC-3 spectrum of cinnarizine in DMSO- d_6 .

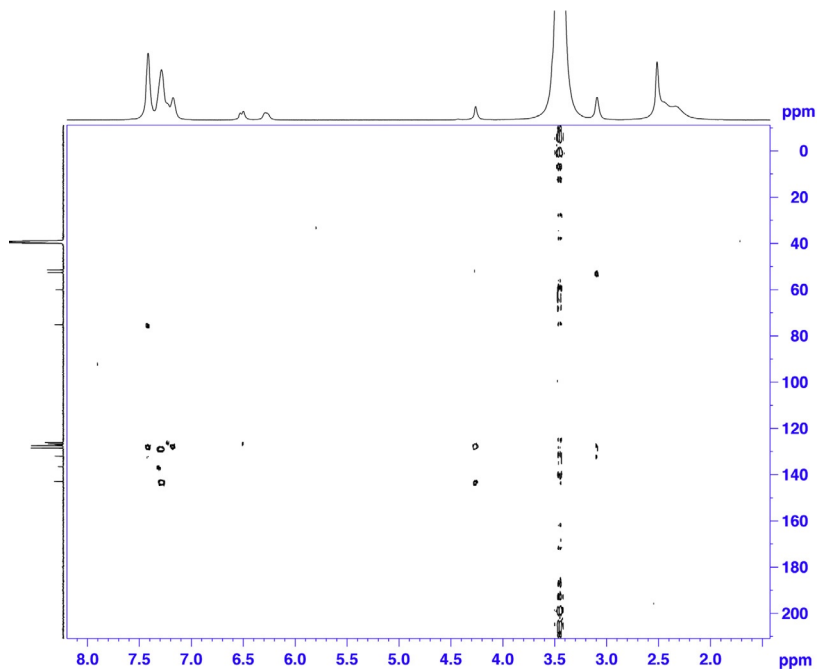


Figure 14 The HMBC-1 spectrum of cinnarizine in DMSO- d_6 .

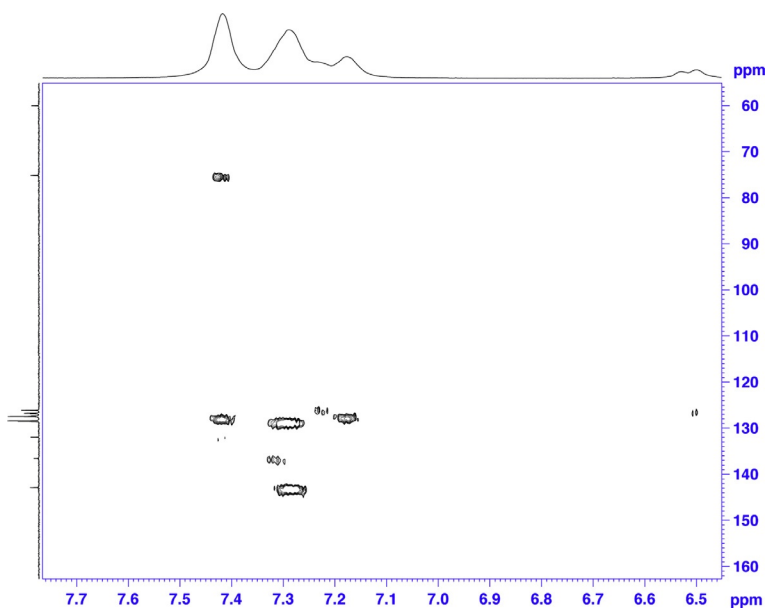


Figure 15 The HMBC-2 spectrum of cinnarizine in DMSO- d_6 .

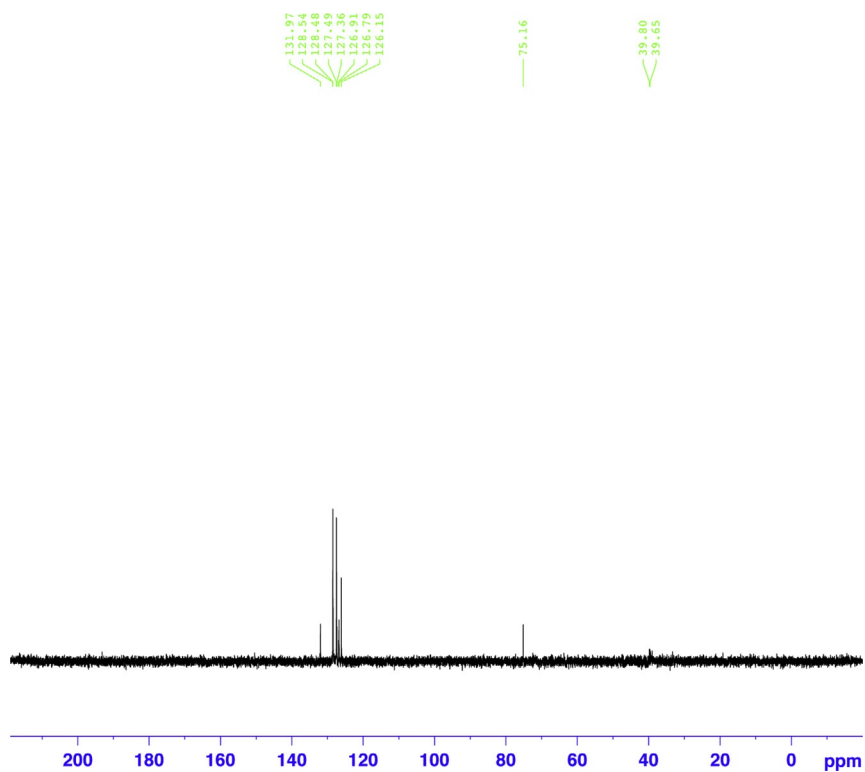


Figure 16 The DEPT 90-1 ^{13}C NMR spectrum of cinnarizine in $\text{DMSO}-d_6$.

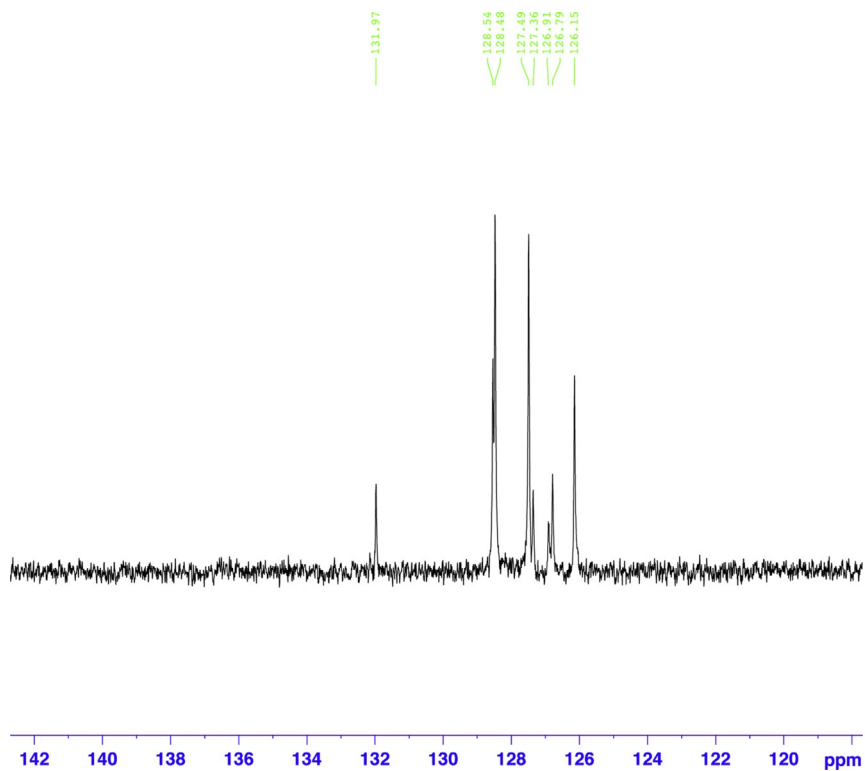


Figure 17 Expanded DEPT 90-2 ^{13}C NMR spectrum of cinnarizine in $\text{DMSO}-d_6$.

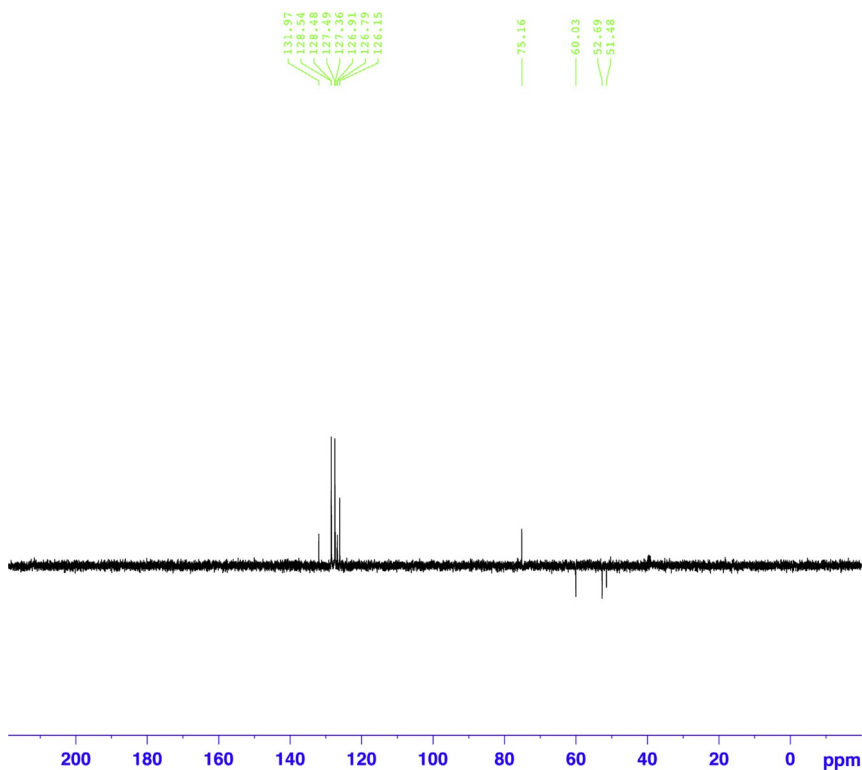


Figure 18 The DEPT 135-1 ^{13}C NMR spectrum of cinnarizine in $\text{DMSO-}d_6$.

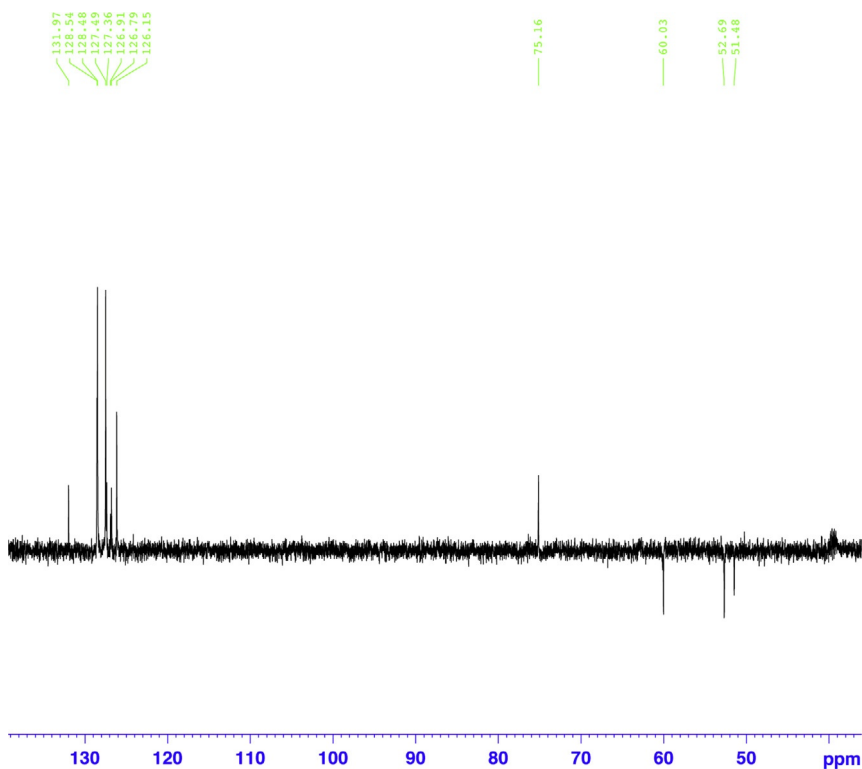
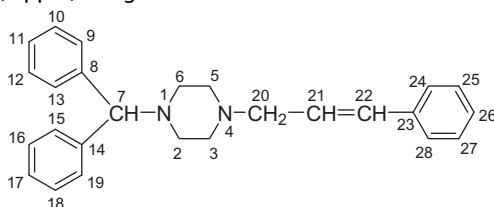
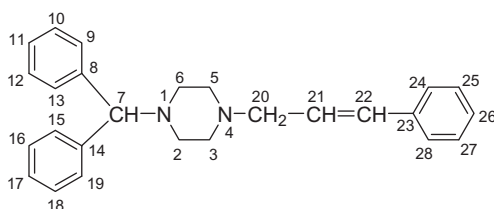


Figure 19 Expanded DEPT 135-2 ^{13}C NMR spectrum of cinnarizine in $\text{DMSO-}d_6$.

Table 4 ^{13}C NMR (δ ppm) Assignments of the Resonance Bands in Cinnarizine

Chemical Shift (δ ppm, Relative to TMS)	Assignments (Carbon Number)
51.50	C-2 and C-6
52.7	C-3 and C-5
60.0	C-20
75.2	C-7
126.1	C-11 and C-17
126.8	C-25 and C-27
126.9	C-26
127.4	C-21
127.5	C-9/C-13, C-15/C-19
128.47	C-10/C-12 and C-16/C-18
128.53	C-24/C-28
132.0	C-22
136.6	C-23
142.9	C-8 and C-14

Table 5 NMR Correlation of Cinnarizine

No.	^{13}C (δ)	^1H (δH) ^a	DEPT 90 ^b	DEPT 135 ^b	COSY	HMBC
1.	—	—	—	—	—	—
2.	51.5	2.33 (2H, m)	—	2	—	—
3.	52.7	2.44 (2H, m)	—	2	—	H-20(³ J)
4.	—	—	—	—	—	—

Table 5 NMR Correlation of Cinnarizine—cont'd

No.	^{13}C (δ)	^1H (δH)	DEPT 90	DEPT 135	COSY	HMBC
5.	52.7	2.44 (2H, m)	—	2	—	H-20(3J)
6.	51.5	2.33 (2H, m)	—	2	—	—
7.	75.2	4.25 (1H, s)	1	1	—	—
8.	142.9	—	0	0	—	H-7(2J), H-9(2J), H-13(2J)
9.	127.5	7.22–7.29 (1H, m)	1	1	—	H-7(3J), H-10
10.	128.47	7.31–7.42 (1H, m)	1	1	—	H-9
11.	126.1	7.17–7.18 (1H, m)	1	1	—	—
12.	128.47	7.31–7.42 (1H, m)	1	1	—	H-13
13.	127.5	7.22–7.29 (1H, m)	1	1	—	H-7(3J), H-12
14.	142.9	—	—	—	—	H-7(2J), H-15(2J), H-19(2J)
15.	127.5	7.22–7.29 (1H, m)	1	1	—	H-7(3J), H-16
16.	128.47	7.31–7.42 (1H, m)	1	1	—	H-15(2J)
17.	126.1	7.17–7.18 (1H, m)	1	1	—	—
18.	128.47	7.31–7.42 (1H, m)	1	1	—	H-19(2J)
19.	127.5	7.22–7.29 (1H, m)	1	1	—	H-7(3J), H-18(2J)
20.	60	3.08 (2H, d, $J=5.5$ Hz)	—	2	H-21	—
21.	127.4	6.29 (1H, m)	1	1	H-20, H-22	H-20(2J), H-22(2J)
22.	132	6.51 (1H, d, $J=16$ Hz)	1	1	H-21	H-20 (3J)
23.	136.6	—	—	—	—	H-25(3J)/H-27(3J)
24.	128.53	7.31–7.42 (1H, m)	1	1	—	—
25.	126.8	7.22–7.29 (1H, m)	1	1	—	H-26 (2J)
26.	126.9	7.21 (1H, m)	1	1	—	—
27.	126.8	7.22–7.29 (1H, m)	1	1	—	H-26 (2J)
28.	128.53	7.31–7.42 (1H, m)	1	1	—	—

^a δ ppm in DMSO- d_6 , J in Hz, 125 MHz for ^{13}C , 500 MHz for ^1H .^bDEPT is the number of attached protons.

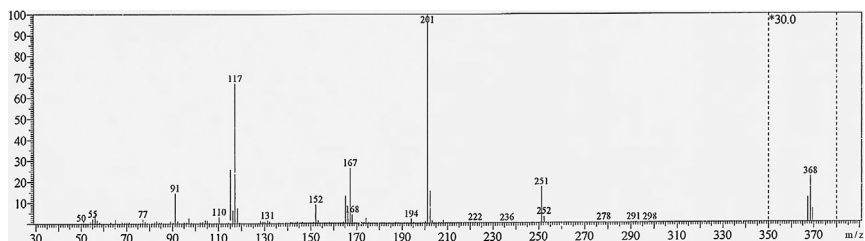


Figure 20 The EI mass spectrum of cinnarizine.

Table 6 Mass Spectral (EI) Assignments in Cinnarizine

		Fragment	
<i>m/z</i>	Relative Intensity (%)	Formula	Structure
368	0.72	$C_{26}H_{28}N_2$	
251	17.11	$C_{17}H_{19}N_2$	
201	100	$C_{13}H_{17}N_2$	
167	26.35	$C_{13}H_{11}$	
117	66.94	C_9H_9	
91	14.50	C_7H_7	
77	2.28	C_6H_5	



4. METHODS OF ANALYSIS

4.1 Compendial Methods

4.1.1 British Pharmacopoeial Methods [9]

Cinnarizine contains not less than 99% and not more than the equivalent of 101% of (*E*)-1-(diphenylmethyl)-4-(3-phenyl-prop-2-enyl)piperazine, calculated with reference to the dried substance.

4.1.1.1 Identification

Test 1. When cinnarizine is tested according to the general method (2.2.14), the melting point of cinnarizine is in the range 118–122 °C.

Test 2. According to the general method (2.2.24), examine cinnarizine by infrared absorption spectrophotometry, comparing with the spectrum obtained with *cinnarizine CRS*. Examine the substance as discs prepared using *potassium bromide R*.

Test 3. According to the general method (2.2.27), examine by thin-layer chromatography using a suitable octadecylsilyl silica gel as the coating substance.

Test solution. Dissolve 10 mg of cinnarizine in *methanol R* and dilute to 20 mL with the same solvent.

Reference solution (a). Dissolve 10 mg of *cinnarizine CRS* in *methanol R* and dilute to 20 mL with the same solvent.

Reference solution (b). Dissolve 10 mg of *flunarizine dihydrochloride CRS* in *methanol R* and dilute to 20 mL with the same solvent.

Apply separately to the plate 5 µL of each solution. Develop over a path of 15 cm using a mixture of 20 volumes of *sodium chloride solution R*, 30 volumes of *methanol R*, and 50 volumes of *acetone R*. Dry the plate in a current of warm air for 15 min and expose to iodine vapor until the spots appear. Examine in daylight. The principal spot in the chromatogram obtained with the test solution is similar in position, color, and size to the principal spot in the chromatogram obtained with reference solution (a). The test is not valid unless the chromatogram obtained with reference solution (b) shows two clearly separated spots.

Test 4. Dissolve 0.2 g of *anhydrous citric acid R* in 10 mL of *acetic anhydride R* in a water bath at 80 °C and maintain the temperature of the water bath at 80 °C for 10 min. Add about 20 mg of cinnarizine. A purple color develops.

4.1.1.2 Tests

Solution S. Dissolve 0.5 g of cinnarizine in *methylene chloride R* and dilute to 20 mL with the same solvent.

Appearance of solution. When the test is carried out as directed in general method (2.2.1), *solution S* is clear and not more intensely colored than reference solution BY₇, as directed in general method (Method II, 2.2.2).

Related substances. Examine by liquid chromatography, as directed in general method (2.2.29).

Test solution. Dissolve 25 mg of cinnarizine in the mobile phase *methanol R* and dilute to 10 mL with the same mobile phase.

Reference solution (a). Dissolve 12 mg of cinnarizine CRS and 15 mg of flunarizine dihydrochloride CRS in *methanol R* and dilute to 100 mL with the mobile phase.

Reference solution (b). Dilute 1 mL of the test solution to 100 mL with *methanol R*. Dilute 5 mL of this solution with the mobile phase.

The chromatographic procedure may be carried out using:

- a stainless steel column 0.1 m long and 4.0 mm in internal diameter packed with octadecylsilyl silica gel for *chromatography R* (3 µm).
- as mobile phase at a flow rate of 1.5 mL/min a solution of 10 g of *ammonium acetate R* in a mixture of 0.2% v/v solution of *glacial acetic acid R* in *acetonitrile R*.
- as detector, a spectrophotometer set at 230 nm.

Equilibrate the column with the mobile phase at a flow rate of 1.5 mL/min for about 25 min.

Adjust the sensitivity of the system so that the height of the principal peak in the chromatogram obtained with 10 µL for reference solution (b) is not less than 50% of the full scale of the recorder.

Inject 10 µL of reference solution (a). When the chromatograms are recorded in the prescribed conditions, the retention times are flunarizine, 11.55 min and cinnarizine, about 11 min. The test is not valid unless the resolution between the peaks corresponding to flunarizine and cinnarizine is not less than 5; if necessary, adjust the condition of the mobile phase.

Inject separately 10 µL of the test solution and 10 µL of reference solution (b). Continue the chromatography for 1.2 times the retention time of the principal peak.

In the chromatogram obtained with the test solution, the area of any peak, apart from the principal peak, is not greater than the area of the principal peak in the chromatogram obtained with reference solution (b) (0.25%); the sum of the areas of all peaks, apart from the principal peak,

is not greater than twice that of the principal peak in the chromatogram obtained with reference solution (b) (0.5%). Disregard any peak due to the solvent and any peak with an area less than 0.2 times the area of the principal peak in the chromatogram obtained with reference solution (b).

4.1.1.3 Acidity or Alkalinity

Suspend 0.5 g of cinnarizine in 15 mL of *water R*. Boil for 2 min. Cool and filter. Dilute the filtrate to 20 mL with carbon dioxide-free *water R*. To 10 mL of this solution, add 0.1 mL of *phenolphthalein solution R* and 0.25 mL of 0.01 M *sodium hydroxide*. The solution is pink. To 10 mL of the solution, add 0.1 mL of *methyl red solution R* and 0.25 mL of 0.01 M *hydrochloric acid*. The solution is red.

4.1.1.4 Loss on Drying

When cinnarizine is tested according to the general method (2.2.32), not more than 0.5%, determined with 1 g by drying in an oven *in vacuo* at 60 °C for 4 h.

4.1.1.5 Heavy Metals

When cinnarizine is tested according to the general method (2.4.8), a maximum 20 ppm is obtained.

4.1.1.6 Sulfated Ash

When cinnarizine is tested according to the general method (2.4.14), not more than 0.1%, determined on 1 g.

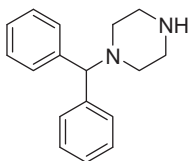
4.1.1.7 Assay

Dissolve 0.15 g of cinnarizine in 50 mL of a mixture of 1 volume of *anhydrous acetic acid R* and 7 volumes of *methyl ethyl ketone R*. Titrate with 0.1 M *perchloric acid*, using 0.2 mL of *naphtholbenzein solution R* as indicator. 1 mL of 0.1 M *perchloric acid* is equivalent to 18.43 mg of $C_{26}H_{28}N_2$.

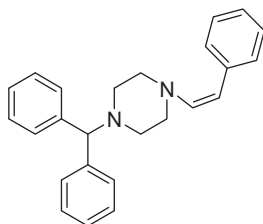
4.1.1.8 Storage

Store in a well-closed container, protected from light.

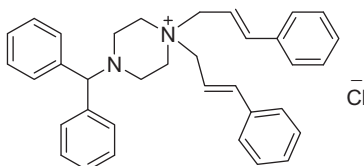
4.1.1.9 Impurities



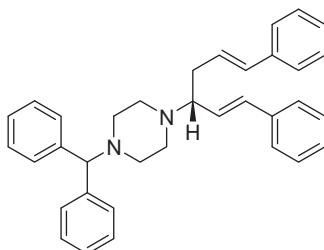
1. 1-(Diphenylmethyl)piperazine



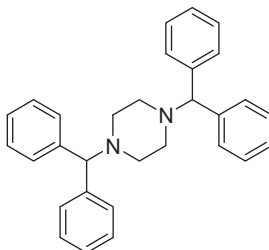
2. (Z)-1-(diphenylmethyl)-4-(3-phenyl-prop-2-enyl)piperazine



3. 4-(Diphenylmethyl)-1,1-bis[(E)-3-phenyl-prop-2-enyl]piperazine chloride



4. 1-(Diphenylmethyl)-4-[(1*RS*,3*E*)-4-phenyl-1-[(*E*)-2-phenylethenyl]but-3-enyl]piperazine



5. 1,4-Bis(diphenylmethyl)piperazine

4.2 Reported Methods of Analysis

4.2.1 Titrimetric Method

Wu *et al.* [10] titrimetrically determined cinnarizine by a simple and reliable method. Cinnarizine tablets were powdered, treated with tartaric acid and

acetic acid, mixed, and titrated with 0.1 N perchloric acid for cinnarizine determination. Tartaric acid was used to eliminate the interference by magnesium stearate and other basic compounds. Recoveries were $\sim 100\%$.

Morait and Nedelcu [11] reported the use of gravimetric, titrimetric, and potentiometric methods for the determination of cinnarizine by using the precipitation reactions of cinnarizine with heteropolyacids (silicowolframic acid, phosphowolframic acids, and phosphomolybdic acid). The obtained results allowed the use of these methods to measure cinnarizine in tablets.

Popa *et al.* [12] established two semimicro-analytical methods for the assay of cinnarizine or dipyridamole by the formation of complexes between sodium lauryl sulfate and these pharmaceutical substances by ionic association, with a lower stability than that of lauryl sulfate–Metanil Yellow Complex. Titration with sodium lauryl sulfate 10^{-2} M solution resulted in that the quantified amounts of substance were about 25 mg; thus, the newly established methods may be used for the analysis of tablets containing cinnarizine and dipyridamole.

4.2.2 Spectrophotometric Methods

4.2.2.1 Ultraviolet Spectrometry

Hanmin and Xiuquan [13] reported the determination of cinnarizine in tablets by ultraviolet spectrophotometry based on the measurement of absorbance at 250 nm. Standard plots of absorbances and the concentrations of cinnarizine were linear for 5–25 $\mu\text{g/mL}$ of cinnarizine. Recoveries were 93.9–98.9%.

Saleh and Askal [14] described a spectrophotometric method for the determination of cinnarizine in capsules and tablets based on the charge-transfer complex formation between cinnarizine as n-donor and either iodine as δ -acceptor or 2,3-dichloro-5,6-dicyano-*p*-benzoquinone (DDQ) as n-acceptor. Ranges for obedience of absorbance at 295 and 460 nm to Beer's law for cinnarizine with iodine and DDQ were 1–6 and 10–8 $\mu\text{g/mL}$, respectively. Recoveries of cinnarizine were $\sim 100\%$ and standard deviations were 0.72–1.15%.

Abdine *et al.* [15] developed a direct, extraction-free spectrophotometric method for the determination of cinnarizine in pharmaceutical preparations. The method was based on ion-pair formation between cinnarizine and three acidic (sulfonephthalein) dyes, namely bromocresol green, bromocresol purple, and bromocresol blue which induced an instantaneous bathochromic shift of the maximum in the drug spectrum. Conformity to Beer's law enabled the assay of dosage forms of cinnarizine. Compared with

a reference method, the results obtained were of equal accuracy and precision.

Elazazy *et al.* [16] used a simple, rapid, sensitive, and accurate spectrophotometric method for the determination of cinnarizine, famotidine, and metoclopramide hydrochloride in pure form and in pharmaceutical formulations. The spectral method is based on the reaction between dichlorophenol indophenol and the cited drugs to give bluish violet radical ions exhibiting maximum absorption at 650, 642, and 654 nm for cinnarizine, famotidine, and metoclopramide, respectively, with molar absorptivities 2.421×10^3 , 4.313×10^3 , and 2.112×10^4 L/mol/cm for cinnarizine, famotidine, and metoclopramide, respectively, and Sandell's sensitivities 6.569×10^{-3} , 1.278×10^{-3} , and 6.646×10^{-3} $\mu\text{g}/\text{cm}^2$.

Devagondanahalli *et al.* [17] described two simple, rapid, and sensitive extractive spectrophotometric methods for the assay of cinnarizine in pure and pharmaceutical formulations. The spectrophotometric methods depend on the formation of chloroform-soluble ion-association complexes of cinnarizine with thymol blue (TB) and with cresol red in sodium acetate-acetic acid buffer of pH 3.6 for TB and in potassium chloride-hydrochloric acid buffer at pH 1.6 for cinnarizine with absorption maxima at 405 and 403 nm for TB and cinnarizine, respectively. Reaction conditions were optimized to obtain the maximum color intensity. The systems obeyed Beer's law in the range of 0.6–15.8 and 0.8–16.6 $\mu\text{g}/\text{mL}$ for TB and cinnarizine, respectively. Various analytical parameters have been evaluated and the results have been validated by statistical data.

Tarkase *et al.* [18] reported the development and validation of spectrophotometric method for simultaneous estimation of cinnarizine and domperidone maleate in pure and tablet dosage form. The spectral method depends on simultaneous equation method at two selected wavelength 254 and 284 nm, respectively, and also on absorbance ratio method at two selected wavelengths 274 nm (isoabsorptive point) and 254 nm (λ_{max} of cinnarizine). The linearity was obtained in the concentration range of 5–20 and 5–20 $\mu\text{g}/\text{mL}$ for cinnarizine and domperidone maleate, respectively. These methods are accurate, precise, reproducible, and economical, and the results have been validated statistically and by recovery studies.

Abdelrahman [19] described a simultaneous determination of cinnarizine and domperidone in a binary mixture by using area under the curve and dual wavelength spectrophotometric methods. In area under the curve method, mixture solutions in the wavelength ranges 241–258 and 280–292 nm were

selected for the determination of cinnarizine and domperidone, and by applying Cramer's rule the concentration of each drug was obtained. In dual wavelength method, two wavelengths were selected for each drug in a way so that the difference in absorbance is zero for another drug. Domperidone shows equal absorbance at 240.2 and 273.2 nm, where the differences in absorbance were measured for the determination of cinnarizine. Similarly, differences in absorbance at 230.8 and 239.2 nm were measured for determination of domperidone. The spectral methods were applied for the determination of cinnarizine and domperidone over the concentration ranges of 2–20 and 2–22 $\mu\text{g/mL}$, respectively. Both methods were found to be simple, accurate, sensitive, precise, and inexpensive which could be used in routine and quality control analysis of the cited drugs in pharmaceutical formulations containing them.

Issa *et al.* [20] reported the determination of cinnarizine in pure and in its pharmaceutical dosage forms by spectrophotometric methods carried out to investigate the charge-transfer complex formation between cinnarizine and dipicrylamine (DPA) or 2,6-dinitrophenol (DNP). The colored products were quantified spectrophotometrically at 430 and 440 nm for cinnarizine complexes with DPA in a mixture of 15% dioxane in dichloroethane and 15% ethyl acetate in chloroform, respectively. On the other hand, cinnarizine complexes formed with DNP in acetonitrile and in a mixture of 30% dichloroethane in ethyl alcohol were quantified at 460 and 430 nm, respectively. Beer's law was obeyed in the concentration range of 1–36.8 $\mu\text{g/mL}$. These methods utilize a single-step reaction and have the advantages of being simple, accurate, sensitive, rapid, and suitable for routine analysis in control laboratories.

4.2.2.2 Spectrofluorimetric Method

Walash *et al.* [21] suggested the use of second-derivative synchronous fluorimetric method for the determination of cinnarizine and domperidone in different pharmaceutical formulations. The fluorimetric method is based upon measurement of the native fluorescence of these drugs at λ_{max} 315 and 324 nm for cinnarizine and domperidone, respectively, after excitation at 280 nm. The synchronous fluorescence spectra of cinnarizine with domperidone were recorded using the optimum $\Delta\lambda$ 80 nm in aqueous methanol (50% v/v). The produced fluorescence-concentration plots were rectilinear obeying Beer's law in the concentration range of 0.1–1.3 and 0.1–3 $\mu\text{g/mL}$ for cinnarizine and domperidone, respectively, with lower detection limits of 0.017 and 5.77×10^{-3} $\mu\text{g/mL}$ and quantification limits of 0.058 and

0.02 $\mu\text{g/mL}$ for cinnarizine and domperidone, respectively. This simple, rapid, and highly sensitive method was successfully applied for the determination of cinnarizine in biological fluids.

4.2.2.3 Chemiluminescence Method

Townsend *et al.* [22] reported a flow-injection chemiluminescence method for the determination of cinnarizine by using the chemiluminescence of permanganate system in the presence of polyphosphoric acid, ethanol, and Tween 60. Five hundred-microliter samples were injected and the sample throughput was 130 h^{-1} . Preliminary experiments identified Tween 60 as the surfactant of choice, improving the detection limit of cinnarizine system 20-fold. Optimum chemiluminescence signals were obtained using $7.5 \times 10^{-4}\text{ mol/L}$ potassium permanganate in 0.02 mol/L polyphosphoric acid as the oxidant stream and a carrier stream of 10% (v/v) of ethanol in aqueous $1.5 \times 10^{-3}\text{ mol/L}$ Tween 60 with a total flow rate of 7.6 mL/min. The calibration curve was linear from 0.5 to 6 $\mu\text{g/mL}$ with recoveries of 98.4–100.2%.

4.2.3 Voltammetric Methods

El-Sayed *et al.* [23] studied the voltammetric behavior and determination of cinnarizine in pharmaceutical formulations and serum. Cinnarizine was reduced by cyclic linear sweep adsorptive voltammetric method at glassy carbon electrode in Britton–Robinson buffers over the pH range 2.5–11.5. A well-defined adsorption-controlled cathodic peak was obtained at pH 2.5. By cathodic adsorptive linear sweep voltammetry, a linear calibration plot was obtained in the concentration range of 2×10^{-7} to $5 \times 10^{-6}\text{ mol/L}$ with detection limit of $9 \times 10^{-9}\text{ mol/L}$. The method is fast, simple, and accurate and has been successfully applied for the determination of cinnarizine in commercial formulations, showing mean recovery and relative standard deviation of 100.24% and 1.46, respectively.

Hegde *et al.* [24] investigated the voltammetric oxidation of cinnarizine in pH 2.5 Britton–Robinson buffer. An irreversible oxidation peak at about 1.2 V at a multi-walled carbon nanotube-modified glassy carbon electrode was obtained. The electrocatalytic behavior was further exploited as a sensitive detection scheme for the determination of cinnarizine by differential pulse voltammetry. Under optimized conditions, the concentration range and detection limit were 9×10^{-8} to 6×10^{-6} and $2.58 \times 10^{-9}\text{ M}$, respectively, for cinnarizine. This method offered the advantage of accuracy, simplicity, and was successfully applied for the determination of cinnarizine in pharmaceutical samples.

4.2.4 Polarographic Method

Nin'o [25] described a polarographic method for the determination of cinnarizine by using a dropping mercury electrode. Cinnarizine tablets were treated with ethanol and then filtered. Ammonium chloride (0.1 M) in 50% ethanol was added to the filtrate and the solution was measured. The method was sensitive to 0.37 mg/mL.

4.2.5 Chromatographic Methods

4.2.5.1 Thin-Layer Chromatography

Clarke [2] recommended the following three thin-layer chromatographic systems:

System 1

Plates: Silica gel G, 250 μm thick, dipped in, or sprayed with, 0.1 M potassium hydroxide in methanol, and dried.

Mobile phase: Methanol:strong ammonia solution (100:1.5).

Reference compounds: Diazepam $R_F=75$, chlorprothixene $R_F=56$, and codeine $R_F=33$, $R_F=76$ [26].

System 2

Plates: Use the same plates as system 1 with which it may be used because of the low correlation of R_F values.

Mobile phase: Cyclohexane:toluene:diethylamine (75:15:10).

Reference compounds: Dipipanone $R_F=66$, pethidine $R_F=37$, desipramine $R_F=20$, and codeine $R_F=06$, $R_F=51$ [26].

System 3

Plates: This system uses the same plates as systems 1 and 2 with which it may be used because of the low correlation of R_F values.

Mobile phase: Chloroform:methanol (90:10).

Reference compounds: Meclozine $R_F=79$, caffeine $R_F=58$, dipipanone $R_F=33$, and desipramine $R_F=11$, $R_F=78$ (acidified iodoplatinate solution, positive) [26].

Hassan *et al.* [27] reported the use of an accurate method of thin-layer densitometry for quantification of cinnarizine in dosage forms in the presence of its photodegradation products and metabolites in serum. The thin-layer chromatography mobile phases consisted of benzene:methanol:formic acid (80:17:3) for the resolution of cinnarizine from the associated substances. The samples were applied to precoated silica gel F₂₅₄ plates (20 \times 20 cm) and slid into the tank which contained the mobile phase. Visualization of the spots was possible under ultraviolet light and scanning densitometry at 250 nm allowed quantitation. The drug was well separated from the other

related substances and was determined by comparison with standards. Calibration graphs were linear from 10^{-3} to 10^{-6} M of the drug. The lower detection limits were $16 \mu\text{L}^{-1}$ of cinnarizine with standard deviation of 1.3% and an average recovery of 98.6%.

Bagade *et al.* [28] described a simple high-performance thin-layer chromatographic method for simultaneous estimation of cinnarizine and domperidone in tablet dosage form. It was performed on silica gel 60 GF₂₅₄ thin-layer chromatographic plates using mobile phase comprising of methanol:toluene:ethyl acetate:glacial acetic acid in the ratio of 2:9:0.5:0.5, and the detection was carried out at 216 nm showing R_F value 0.61 for cinnarizine and 0.16 for domperidone. The calibration curve response was observed between 5–14 g for cinnarizine and 4–11 g for domperidone by height and by area. The percentage of drug estimated from cinnarizine and domperidone for marketed formulation was found to be 99.95, 99.82 by height and 100.85, 100.08 by area, respectively. The recovery of drugs was carried out by standard addition method and was found to be 100.13 and 100.18 for cinnarizine and 100.06 and 100.72 for domperidone.

4.2.5.2 Gas Chromatography

Clarke recommended the following gas chromatographic system for the separation of cinnarizine [2].

Column: 2.5% SE-30 on 80–100 mesh Chromosorb G (acid washed and dimethyldichlorosilane-treated), $2 \text{ m} \times 4 \text{ mm}$ internal diameter glass column. It is essential that the support is fully activated.

Carrier gas: Nitrogen at 45 mL/min.

Reference compounds: *n*-Alkanes with an even number of carbon atoms.

Retention indices: RI 3065 [29].

Akada *et al.* [30] applied gas chromatography for the determination of cinnarizine in plasma by using an alkali flame ionization detector. The detection limit and determination were, respectively, 0.1 and 0.2 ng/mL. The recovery of cinnarizine in plasma was 104.1%.

Woestenborghs *et al.* [31] developed a sensitive gas chromatographic method for the determination of cinnarizine and flunarizine in plasma, urine, and milk samples from man and animals. The drugs and their internal standard were extracted from the biological samples at alkaline pH, back-extracted into sulfuric acid, and re-extracted into the organic phase (heptane-isoamyl alcohol). The analyses were carried out by gas chromatography using a nitrogen-selective thermionic specific detector. The detection limit was 0.5 ng/mL of biological fluid and extraction recoveries were 87–94%.

Xitian *et al.* [32] used a highly sensitive gas chromatographic method for direct quantitative determination of cinnarizine in tablets. The conditions of determination were FID detector at 280 °C, OV-101 (12 m × 0.25 mm), and fused-silica capillary column, and carbamazepine was used as an internal standard. The temperature was programmed from 200 to 275 °C at 40 °C/min. The response was linear between concentrations 1 and 1.2 mg/mL. The average recovery was 99.98% and the coefficient of variation was 0.92.

4.2.5.3 Gas Chromatography-Mass Spectrometric Method

Maurer and Pfleger [33] described an automated screening procedure using gas chromatography-mass spectrometry (GC-MS) for identification of cinnarizine and other drugs after their extraction from biological sample. This novel analytical procedure has been developed, using computerized GC-MS to detect ethylenediamine and piperazine antihistamines and their metabolites in urine which was used because the drug concentrations are higher in urine than in plasma. After acid hydrolysis and acetylation of the sample, the acetylated extract was analyzed by computerized GC-MS. By using ion chromatography with the selective ions m/z 58, 72, 85, 125, 165, 183, 198, and 201, the possible presence of cinnarizine or piperazine antihistamines or their metabolites was indicated. The identity of positive signals in the reconstructed ion chromatogram was then confirmed by a visual for computerized comparison of the stored full mass spectra with the reference spectra. The ion chromatograms, reference mass spectra, and gas chromatographic retention indices (OV-101) were documented.

4.2.5.4 High-Performance Liquid Chromatographic Methods

Nowacka-Krukowska *et al.* [34] used a high-performance liquid chromatographic method for the determination of cinnarizine in plasma. Cinnarizine was extracted from plasma with a mixture of chloroform and *n*-hexane (2:3, v/v) and separated by high-performance liquid chromatography column MicroSpher C₁₈ with a fluorescence detector at $\lambda_{\text{ex}}=245$ nm and $\lambda_{\text{em}}=310$ nm. The mobile phase was 0.01 M ammonium dihydrogen phosphate buffer (pH 4.2) containing 0.038% triethylamine and acetonitrile (25:75, v/v). The flow rate was 1 mL/min. The calibration curves were linear over the range 1–100 ng/mL. Recovery was 97%. The intra- and inter-day relative standard deviations were less than 10% and the accuracy of the assay expressed by bias was in the range 0.14–2.37%. The minimum detectable concentration of cinnarizine was determined at 1.25 ng/mL and the lowest limit of quantitation was found to be 1 ng/mL of plasma.

Heda *et al.* [35] established a simple and precise reverse-phase high-pressure liquid chromatographic method for the determination of cinnarizine in pharmaceutical formulation. A sample containing 75 mg of cinnarizine was dissolved in 40 mL of a mixture of ethanol and acetate buffer (pH 5.5) in 1:1 proportion, ultrasonicated for 10 min, and then the volume was made up to 50 mL with the same mixture. The solution was filtered and 20 µg/mL of the filtrate was analyzed by reverse-phase high-pressure liquid chromatography on a column (length \times OD \times ID = 33 \times 8 \times 6 mm, 1.5 µm) of MICRA-NPS C₁₈ with a mobile phase prepared by mixing acetonitrile, triethylamine buffer (adjusted to pH 4.5 with 10% potassium hydroxide), and tetrahydrofuran in the ratio of 30:66:4, respectively, at a flow rate of 0.5 mL/min. Detection was at 253 nm. The calibration graph was rectilinear for 20–100 µg/mL of cinnarizine. Recovery was within the range of 100 \pm 2%. The limit of detection and limit of quantification were found to be 0.0592 and 0.1794 µg/mL, respectively.

4.2.5.5 High-Performance Liquid Chromatography-Mass Spectrometry

Liu *et al.* [36] used a high-performance liquid chromatography coupled with tandem mass spectrometry (LC-MS/MS) with electrospray ionization (ESI) to separate and simultaneously quantify cinnarizine, sodium ferulate, salicylic acid, and vitamin B₁ in human plasma. The internal standards used were lomerizine for cinnarizine and vitamin B₁, whereas gemfibrozil was used for sodium ferulate and salicylic acid. The plasma samples were prepared by one-step protein precipitation followed by an isocratic elution with 10 mM ammonium acetate buffer:acetonitrile (35:65, v/v) at pH 5 on an Agilent Zorbax SB-CN column (150 mm \times 2 mm ID, 5 µm). The precursor and product ions of cinnarizine and the other drugs were monitored on a triple quadrupole mass spectrometer, operating in the selected reaction monitoring mode with polarity switch, in the negative-ion mode for sodium ferulate, salicylic acid, and gemfibrozil, and in the positive-ion mode for cinnarizine, vitamin B₁, and lomerizine. The results showed that the calibration curves were linear in the range from 2 to 500 ng/mL for cinnarizine, $r=0.9992$ with recoveries ranging from 98.4 to 100.33%, whereas for sodium ferulate in the range of 1.5–1000 µg/mL, $r=0.9991$ with recoveries 99.24–88.83%, while salicylic acid in the range of 20–5000 µg/mL, $r=0.9988$ showed recoveries in the range of 93.2–82.45% and vitamin B₁ in the range of 1–30 ng/mL, $r=0.9928$ with recoveries 94.61–86.59%.

Van De Steene and Lambert [37] developed a quantitative liquid chromatography-electrospray tandem mass spectrometric (ESI)-MS/MS method for the simultaneous analysis of cinnarizine and other pharmaceuticals in environmental waters. Sample preparation consisted of solid-phase extraction on a Speedisk phenyl and an NH_2 solid-phase extraction tube for sample clean-up. Chromatography was performed on a pentafluorophenyl column in a total run time of 24 min. Standard addition was the only method to perform accurate quantification due to different matrix effects measured in different surface water samples. Limits of detection and determination were in the range of <0.05 –1 and 0.05–10 ng/L, respectively. Recoveries were in the range of 60–100%. The method was successfully applied to influent, effluent, and surface water samples. Also, removal percentage of these drugs could be estimated.

4.2.5.6 Capillary Electrophoresis

Abdelal *et al.* [38] described a validated simultaneous determination of cinnarizine and domperidone and cinnarizine and nicergoline in their coformulated tablets by capillary electrophoresis which was performed using a CAPI-3100 CE system equipped with a multiwavelength ultraviolet-visible detector and an automated sampler. An uncoated fused-silica capillary ($40 \times 50 \mu\text{m}$) was used for the separation. Optimization of capillary electrophoretic method was established by using a running buffer, methanol-acetate buffer (pH 3, 10 mM) (80:20 v/v) for cinnarizine and nicergoline at wavelength 227 nm. The voltage applied was 20 kV and the hydrodynamic injection was performed at a height of 25 mm for 30 s. Under these conditions, the calibration graphs were linear over the ranges 0.25–20 and 0.375–15 $\mu\text{g/mL}$ for cinnarizine and domperidone, whereas they were linear over the ranges 0.25–25 and 0.4–10 $\mu\text{g/mL}$ with detection limits at 0.072 and 0.116 $\mu\text{g/mL}$ for cinnarizine and nicergoline. The relative standard deviation was $\leq 2.34\%$ ($n = 3$).



5. BIOLOGICAL ANALYSIS

Siegler *et al.* [39] described a human bioassay for cinnarizine. The assays were carried out by a double-blind method with placebo in groups of 30–60 patients. The doses were determined at which the antihistamines produced a beneficial effect in 50% and toxic effects in 25% of the patients which were 12 and 25 mg for cinnarizine.

A comparative bioassay of vasoactive drug, cinnarizine, by using isolated perfused arteries was developed by Van Nueten [40]. A simple and reliable assay for cinnarizine is described by using potassium chloride–depolarized central artery preparations from the rabbit ear and saphenous artery preparation from the hind leg. Cinnarizine was assayed for potency, rate of onset, and duration of action (inhibiting potassium chloride–induced vasoconstriction).

Dhall *et al.* [41] assessed the vasopressor activity of human amniotic fluid of 46 primigravidas during the third trimester of pregnancy. The samples of amniotic fluid showing vasopressor activity were lyophilized and subjected to gel filtration using Sephadex G-100. The various fractions thus obtained were monitored at 280 nm and the pressor activity was re-estimated. It was observed that most of the amniotic fluid of the toxemic patients was capable of causing contraction of the rat colon as well as a significant rise in the systolic blood pressure of the intact rat. Furthermore, this activity was found to be heat-labile and was completely blocked by cinnarizine.

Ogata *et al.* [42] evaluated beagle dogs as an animal model for bioavailability testing of cinnarizine capsules. The bioavailability of cinnarizine 25 mg from two commercial capsules were determined in beagle dogs and compared with that previously found in humans given the same preparations. The gastric acidity did not affect the bioavailability of cinnarizine in beagle dogs, although the human study had shown a distinct effect of gastric acidity on the bioavailability. Consequently, beagle dogs cannot be used as an animal model for predicting the human bioavailability of cinnarizine, since they do not affect the gastric acidity dependency that is observed in humans.

Also, Hassan *et al.* [27] developed a new high-performance (HPLC) and thin-layer densitometric (TLC) methods for quantification of cinnarizine in dosage forms in the presence of its photodegradation products, related substances, and in the presence of its metabolites in serum. The methods applied provided assessment of cinnarizine purity, bioavailability, stability, and tablet dissolution rate.

Konieczna *et al.* [43] studied the relationships between experimental and computational descriptors of antihistamine drugs, including cinnarizine by using principal component analysis (PCA). A matrix of 18×49 data, including high-performance chromatography and ultraviolet and infrared spectroscopic data, together with molecular modeling studies, was evaluated by the PCA method. The obtained clusters of drugs were consistent with the drugs' chemical structure classification, and hence, it may potentially help limit the number of biological assays in the search of new drugs.



6. STABILITY

Tokumura *et al.* [44] investigated the stability of cinnarizine in aqueous solution at various pH values and temperatures. The degradation of cinnarizine was observed as a pseudo-first-order reaction. By determining the degradation rate of cinnarizine at various pH values, it was found that the degradation rate of cinnarizine increased with decreasing pH within the range of 3–1. The rate of degradation remained unchanged below pH 1.2 and cinnarizine was stable above pH 3. The rate constant (k) at 60 °C was found to be $1.85 \times 10^{-5}/\text{min}^{-1}$ which is 100 times less than that at 90 °C. Consequently, the results indicate that the degradation rate of cinnarizine increases with increasing temperature.

Shi *et al.* [45] studied the stability, formulation, and degradation kinetics of intravenous cinnarizine lipid emulsion. Cinnarizine was loaded in the lipid emulsion to develop an intravenous formulation with good physical and chemical stability. The lipid emulsion was prepared by using high-pressure homogenization. The factors influencing the stability of cinnarizine lipid emulsion, such as different loading methods, pH, temperature, sterilization methods, and time, were monitored by high-performance liquid chromatography. The degradation of cinnarizine in aqueous solution and lipid emulsion both followed apparent first-order kinetics. Also, a possible degradation mechanism was postulated by the bell-shaped pH-rate profile of cinnarizine. It was found that localization of the drug in the interfacial lecithin layer significantly improved the chemical stability of cinnarizine. The activation energy of cinnarizine in lipid emulsion was calculated to be 51.27 kJ/mol which was similar to that in aqueous solution. Furthermore, the shelf-life of cinnarizine in lipid emulsion was estimated to be 1471.6 days at 4 °C, which is much longer compared with 19.8 days in aqueous solution.

Shahba *et al.* [46] assessed the stability of cinnarizine in self-emulsifying drug delivery systems. The chemical and physical stability of cinnarizine was evaluated within self-emulsifying drug delivery systems. The selected formulations were enrolled into both accelerated and long-term stability studies up to 6 and 12 months. The chemical stability of the formulations was assessed periodically based on the intact cinnarizine level, while the physical stability was evaluated based on the physical appearance and color change patterns of the formulations. The accelerated stability study revealed significant cinnarizine degradation within 6 months of storage. On the other hand, the long-term stability study showed no significant degradation or

change of color of cinnarizine within the formulations containing 100% saturated medium chain glycerides (as oil component). However, the formulations containing 50% unsaturated long chain fatty acids showed considerable drug degradation as well as significant discoloration. Thus, the formulations containing 100% saturated medium chain glycerides provide excellent chemical and physical stability pattern and have the potential to provide a stable dosage form of cinnarizine.



7. PHARMACOKINETICS, METABOLISM, AND EXCRETION

Castañeda-Hernández *et al.* [47] studied the pharmacokinetics of cinnarizine after single and repetitive dosing in healthy volunteers. Blood samples were drawn from six young healthy male subjects after receiving a 75-mg cinnarizine tablet for 72 h. Cinnarizine plasma levels were determined by gas chromatography. Then, after a 2-week washout period, five of these subjects received 75-mg tablets for 15 days. Blood samples were drawn for 12 h and cinnarizine plasma levels were measured. The results indicated that cinnarizine accumulates with repetitive dosing due to its pharmacokinetic properties.

Kariya *et al.* [48] investigated the potentialities of cinnarizine and its fluorine derivative flunarizine to induce Parkinsonism as an adverse effect. The study was evaluated pharmacokinetically and pharmacodynamically in rats after giving them a daily dose of 20 $\mu\text{mol/kg}$ of cinnarizine or flunarizine for 1, 5, 10, 15, and 30 days. The active metabolites of their cinnamyl moiety in the plasma and striatum were determined 24 h after the final dose. The results indicate that on the basis of the equimolar dosing performed, flunarizine is a more potent inducer of Parkinsonism than cinnarizine and that their active metabolites contribute to the development of Parkinsonism during chronic medication with cinnarizine and flunarizine.

Tokumura *et al.* [49] studied the improvement of oral bioavailability of flurbiprofen from flurbiprofen/ β -cyclodextrin inclusion complex by the action of cinnarizine. Flurbiprofen and flurbiprofen/ β -cyclodextrin were administered to fasted rats at a dose of 20 mg/kg as flurbiprofen. After 30 min of drug administration, 0.17 mg/kg of cinnarizine dissolved in pH 4 buffer solution was administered to the rats. Blood samples were taken from the rats and the concentrations of flurbiprofen in plasma samples were determined by high-performance liquid chromatography. It was found that cinnarizine had no effect on plasma concentrations of flurbiprofen after oral administration of the drug. On the other hand, the mean plasma levels after

oral administration of flurbiprofen/ β -cyclodextrin with cinnarizine were larger than those of flurbiprofen and those of flurbiprofen/ β -cyclodextrin. Consequently, this result is considered to be caused by the action of cinnarizine as a competing agent *in vivo* which was supported by the decrease in solubility of flurbiprofen in β -cyclodextrin upon the addition of cinnarizine.

Shi *et al.* [50] assessed the potential of cinnarizine loaded in lipid emulsion to modify the pharmacokinetics, tissue distribution, and safety of the drug. The cinnarizine-loaded emulsion was prepared by high-pressure homogenization. The pharmacokinetics and tissue distributions of cinnarizine lipid emulsion were evaluated by comparing with the solution form after intravenous administration to rats at a dose of 2 mg/kg. The cinnarizine lipid emulsion showed significantly higher area under the concentration/time curve and lower clearance and distribution volume than those of a solution form. This helped cinnarizine to reach higher level in vessel and circulate in the blood stream for a longer time, resulting in better therapeutic effect. While the tissue distribution showed a significantly lower uptake of cinnarizine lipid emulsion in lung and brain, indicating the advantage of the emulsion over the solution form in reducing drug precipitation *in vivo* and toxicity in the central nervous system. In addition, the intravenous safety investigation proved that cinnarizine lipid emulsion was safe as an intravenous injection.

Soudijn and van Wijngaarden [51] studied the metabolism and excretion of ^{14}C cinnarizine in male rats after a single intraperitoneal administration at a dose of 20 mg/kg. Urine and feces were collected separately once a day for 3 weeks. After administration of ^{14}C cinnarizine, the excretion of radioactive material was maximal during the first 5 days. After 10 days, less than 1% was excreted and after 3 weeks residual radioactivity was less than 0.1% of the administered dose and amounted to 5 μg per rat, mainly concentrated in the liver, gastrointestinal tract, and carcass. It was found that the major metabolite in urine was benzhydrol, mainly in the conjugated form, while the main metabolites in the feces were benzhydrylpiperazine and benzophenone, with small amounts of unaltered cinnarizine. Thus, N-dealkylation was the major pathway of metabolism of cinnarizine in rats. About one-third of the radioactive metabolites were excreted in the urine and two-thirds in the feces, predominantly during the first 5 days after administration of the drug.

Kariya *et al.* [52] investigated the oxidative metabolism of cinnarizine in rat liver by the microsomal monooxygenase system, including P450 to

1-(diphenylmethyl)piperazine, 1-(diphenylmethyl)-4[3-(4'-hydroxyphenyl)-2-propenyl]piperazine, benzophenone, and 1-[(4'-hydroxyphenyl)-phenylmethyl]-4-(3-phenyl-2-propenyl)piperazine. The reactions required NADPH and were inhibited by carbon monoxide and SKF 525-A. The results indicate that cinnarizine is oxidized by cytochrome P450 and that the formation of 1-(diphenylmethyl)-4-[3-(4-hydroxyphenyl)-2-propenyl]piperazine is related to debrisoquine/spartein-type polymorphic drug oxidation.



8. PHARMACOLOGY

Cinnarizine is a piperazine derivative with antihistaminic and calcium channel-blocking activities. It inhibits calcium translocation across the vestibular sensory cells in the ampullae and maintains endolymph flow by preventing constriction of the stria vascularis. Cinnarizine is a potent dilator of the peripheral vessels, with no corresponding calcium-blocking actions in the heart [53].

Elimadi *et al.* [54] investigated the effects of cinnarizine on mitochondrial permeability transition, ATP synthesis, membrane potential, and NAD(P)H oxidation. Cinnarizine was effective in inhibiting the mitochondrial permeability transition induced either by calcium (Ca^{2+}) alone or in the presence of *tert*-butylhydroperoxide. At low concentration of cinnarizine ($<50 \mu\text{M}$), the protective effect occurred which was accompanied by the inhibition of NAD(P)H oxidation and the restoration of the mitochondrial membrane potential decreased by a high concentration of Ca^{2+} ($25 \mu\text{M}$). However, at higher concentrations ($>50 \mu\text{M}$) of cinnarizine and in the absence of both *tert*-butylhydroperoxide and Ca^{2+} , the effects of cinnarizine on the mitochondria were reversed as the mitochondrial permeability transition was generated, mitochondrial NAD(P)H was oxidized, and the membrane potential collapsed. It was found that both effects might be linked to the binding of cinnarizine to mitochondrial hydrophobic sites and the shift from the inhibition to induction of the mitochondrial permeability transition being dependent on the concentration of cinnarizine.

Terland and Flatmark [55] reported that cinnarizine inhibited the MgATP-dependent generation of transmembrane proton electrochemical gradient in chromaffin granule ghosts and thus inhibiting proton pumping and catecholamine uptake in storage vesicles *in vivo*. This mechanism of action may contribute to the drug-induced Parkinsonism observed as a side effect of cinnarizine.

ACKNOWLEDGMENT

The author wishes to thank Mr. Tanvir Ahmed Butt, Department of Pharmaceutical Chemistry, College of Pharmacy at King Saud University, for his secretarial assistance in drafting this chapter.

REFERENCES

- [1] S. Budavari (Ed.), *The Merck Index*, 14th ed., Merck and Co, NJ, 2006, p. 385.
- [2] A.C. Moffat (Ed.), *Clarke's Isolation and Identification of Drugs*, second ed., The Pharmaceutical Press, London, 1989, p. 471.
- [3] S.C. Sweetman (Ed.), *Martindale: The Complete Drug Reference*, 33rd ed., Pharmaceutical Press, London, 2002, p. 413.
- [4] Swiss Pharmaceutical Society (Ed.), *Index Nominum 2000: International Drug Directory*, 17th ed., MedPharm GmbH Scientific Publishers, Stuttgart, 2000, p. 238.
- [5] P.A. Janssen, U.S. Patent 2882271 (1959).
- [6] H.J. Roth, A. Kleeman, T. Beisswenger, In: *Pharmaceutical Chemistry: Drug Synthesis*, vol. 1, Halstead Press/E. Horwood Ltd., Horwood, Chichester, 1988, p. 298.
- [7] J. Sheng, L. Sheng-He, C. Yu-Ping, W. Jin-Y, W. Chang-Ying, *Huaxue* 6 (1980) 341.
- [8] M.A. Martinez, M.M. Carril-Aviles, S. Sagrado, R.M. Villanueva-Camanas, M.J. Medina-Hernandez, Characterization of antihistamine-human serum protein interactions by capillary electrophoresis, *J. Chromatogr. A* 1147 (2007) 266.
- [9] *The British Pharmacopoeia*, vol. 1, Her Majesty's Stationary Office, London, 2013, p. 534.
- [10] Q. Wu, R. Yu, H. Xu, Improved method for determination of filcilin and cinnarizine in tablets, *Nanjing Yaoxueyuan Xuebao* 16 (2) (1985) 64.
- [11] G.H. Morait, A. Nedelcu, Analytical study of cinnarizine. New methods for quantitative determination using cinnarizine reactions with heteropolyacids. Note I, *Farmacia* 46 (5) (1998) 37.
- [12] C.M. Popa, A. Nedelcu, C. Arama, A. Neagu, Quantitative determination of dipyridamole and cinnarizine. Note I. New titrimetric methods, *Farmacia* 46 (2) (1998) 29.
- [13] C. Hanmin, Y. Xiuquan, UV spectrophotometric analysis of cinnarizine tablets, *Yaowu Fenxi Zazhi* 6 (1) (1986) 31.
- [14] G.A. Saleh, H.F. Askal, Spectrophotometric analysis of cinnarizine via charge-transfer complexation reaction, *Pharmazia* 45 (3) (1990) 220.
- [15] H. Abdine, F. Belal, N. Zoman, Simple spectrophotometric determination of cinnarizine in its dosage forms, *Farmaco* 57 (2002) 267.
- [16] M.S. Elazazy, A. Shalaby, M.N. Elbolikiny, H.M. Khalil, M. Hawa, Spectrophotometric determination of cinnarizine, famotidine, and metoclopramide hydrochloride using 2,6-dichlorophenol indophenol, *Drug Res.* 25 (2004) 107.
- [17] M.H. Devagondanahalli, S.M.T. Shaikh, S. Jaldappagari, S.K. Ramanaboyina, H. Kasalanti, Determination of cinnarizine in pure and pharmaceutical formulations, *J. Chin. Chem. Soc.* 54 (1) (2007) 63.
- [18] K.N. Tarkase, M.K. Tarkase, M.D. Dokhe, V.S. Wagh, Development and validation of spectrophotometric method for simultaneous estimation of cinnarizine and domperidone maleate in pure and tablet dosage form, *Int. J. Pharm. Sci. Res.* 3 (8) (2012) 2700.
- [19] M.M. Abdelrahman, Simultaneous determination of cinnarizine and domperidone by area under curve and dual wavelength spectrophotometric methods, *Spectrochim. Acta A Mol. Biomol. Spectrosc.* 113 (2013) 291.

- [20] Y.M. Issa, A.F.A. Youssef, W.F. El-Hawary, E.A. Abdel-Ghaffar, Spectrophotometric determination of cinnarizine through charge-transfer complex formation with polynitro compounds, *Eur. Chem. Bull.* 2 (7) (2013) 507.
- [21] M.I. Walash, F. Belal, N. El-Enany, A.A. Abdelal, Second-derivative synchronous fluorometric method for the simultaneous determination of cinnarizine and domperidone in pharmaceutical preparations. Application to biological fluids, *J. Fluoresc.* 18 (2008) 61.
- [22] A. Townsend, N. Youngvise, R.A. Wheatley, S. Liawuangrath, Flow-injection determination of cinnarizine using surfactant-enhanced permanganate chemiluminescence, *Anal. Chim. Acta* 499 (2003) 223.
- [23] G.O. El-Sayed, S.A. Yasin, A.A. El Badawy, Voltammetric behavior and determination of cinnarizine in pharmaceutical formulations and serum, *Anal. Lett.* 41 (2008) 3021.
- [24] R.N. Hegde, R.R. Hosamani, S.T. Nandibewoor, Voltammetric oxidation and determination of cinnarizine at glassy carbon electrode modified with multi-walled carbon nanotubes, *Colloids Surf. B Biointerfaces* 72 (2009) 259.
- [25] N. Nin'o, Polarographic method for the analysis of cinnarizine (1-benzhydryl-4-cinnamylpiperazine) tablets, *Trudove na Nauchnoizsledovatel'skiya Khimikofarmatsevtichen Institut* 9 (1974) 445.
- [26] A.H. Stead, R. Gill, T. Wright, J.R. Gibbs, A.C. Moffat, Standardized thin-layer chromatographic systems for identification of drugs and poisons, *Analyst* 707 (1982) 1106.
- [27] S.S.M. Hassan, M.A.F. Elmosallamy, A.B. Abbas, LC and TLC determination of cinnarizine in pharmaceutical preparations and serum, *J. Pharm. Biomed. Anal.* 28 (2002) 711.
- [28] S.B. Bagade, S.G. Walode, M.S. Charde, M.R. Tajne, A.V. Kasture, Simultaneous HPTLC estimation of cinnarizine and domperidone in their combined dose tablet, *Asian J. Chem.* 17 (2) (2005) 1116.
- [29] R.E. Ardrey, A.C. Moffat, Gas-liquid chromatographic retention indices of 1318 substances of toxicological interest on SE-30 or OV-1 stationary phase, *J. Chromatogr.* 220 (1981) 195.
- [30] S. Akada, M. Shimoda, Y. Takahashi, Y. Saito, Determination of cinnarizine in biological samples by gas chromatography and its bioavailability, *Eisel Kagaku* 22 (5) (1976) 291.
- [31] R. Woestenborghs, L. Michielsen, W. Lorreyne, J. Heykants, Sensitive gas chromatographic method for the determination of cinnarizine and flunarizine in biological samples, *J. Chromatogr.* 232 (1) (1982) 85.
- [32] X. Xitian, G. Wu, C. Liu, Determination of cinnarizine in tablets by gas chromatography, *Sepu* 11 (5) (1993) 315.
- [33] H. Maurer, K. Pflieger, Toxicological detection of ethylenediamine and piperazine antihistamines and their metabolites in urine by computerized gas chromatography-mass spectrometry, *Fresenius Z. Anal. Chem.* 331 (1998) 744.
- [34] H. Nowacka-Krukowska, M. Rakowska, K. Neubart, M. Kobylinska, High-performance liquid chromatographic assay for cinnarizine in human plasma, *Acta Pol. Pharm.* 63 (2007) 407.
- [35] A.A. Heda, A.R. Sonawane, G.H. Naranje, P.K. Puranik, A rapid determination of cinnarizine in bulk and pharmaceutical dosage form by LC, *E-J. Chem.* 7 (3) (2010) 1080.
- [36] N. Liu, C. Yang, Z. Zhang, Y. Tian, F. Xu, Y. Chen, Simultaneous quantification of sodium ferulate, salicylic acid, cinnarizine and vitamin B1 in human plasma by LC tandem MS detection, *Chromatographia* 67 (2008) 583.
- [37] J.C. Van De Steene, W. Lambert, Validation of solid-phase extraction and liquid chromatography-electrospray tandem mass spectrometric method for the determination of nine basic pharmaceuticals in wastewater and surface water samples, *J. Chromatogr. A* 1182 (2008) 153.

- [38] A.A. Abdelal, S. Kitagawa, H. Ohtani, N. El-Enany, F. Belal, M.I. Walash, Method development and validation for the simultaneous determination of cinnarizine and co-formulated drugs in pharmaceutical preparations by capillary electrophoresis, *J. Pharm. Biomed. Anal.* 46 (2008) 491.
- [39] P.E. Siegler, T. Bodi, M. Gershenfeld, E.B. Brown, A.D. Ducanes, J.H. Nodine, Human bioassay of antihistaminic agents, *Ann. Allergy* 20 (1962) 37.
- [40] J.M. Van Nueten, Comparative bioassay of vasoactive drugs using isolated perfused rabbit arteries, *Eur. J. Pharmacol.* 6 (3) (1969) 286.
- [41] K. Dhall, M. Kumar, G.I. Dhall, P. Jain, K.T. Singh, R.N. Chakravorti, Identification of vasopressor constituents of amniotic fluid in pregnancy toxemia, *Ric. Clin. Lab.* 9 (1) (1979) 25.
- [42] H. Ogata, N. Aoyagi, N. Kaniwa, A. Ejima, T. Kitaura, T. Ohki, K. Kitamura, Evaluation of beagle dogs as animal model for bioavailability testing of cinnarizine capsules, *Int. J. Pharm.* 29 (1986) 121.
- [43] L. Konieczna, L. Bober, M. Belka, T. Ciesielski, T. Baczek, Chemometric exploration of the dependencies between molecular modeling descriptors and analytical chemistry data of antihistaminic drugs, *J. AOAC Int.* 95 (2012) 713.
- [44] T. Tokumura, T. Ichikawa, N. Sugawara, K. Tatsuishi, M. Kayano, Y. Machida, H. Hoshida, T. Nagai, Kinetics of degradation of cinnarizine in aqueous solution, *Chem. Pharm. Bull.* 33 (5) (1985) 2069.
- [45] S. Shi, H. Chen, Y. Cui, X. Tang, Formulation, stability and degradation kinetics of intravenous cinnarizine lipid emulsion, *Int. J. Pharm.* 373 (2009) 147.
- [46] A.A. Shahba, F.K. Alanazi, K. Mohsin, M. Abdel-Hamid, Stability assessment of cinnarizine in self-emulsifying drug delivery systems, *Lat. Am. J. Pharm.* 31 (4) (2012) 549.
- [47] G. Castañeda-Hernández, Y. Vargas-Alvarado, F. Aguirre, F.J. Flores-Murrieta, Pharmacokinetics of cinnarizine after single and multiple dosing in healthy volunteers, *Arzneimittelforschung* 43 (5) (1993) 539.
- [48] S. Kariya, S. Isozaki, Y. Masubuchi, T. Suzuki, S. Narimatsu, Possible pharmacokinetic and pharmacodynamic factors affecting parkinsonism inducement by cinnarizine and flunarizine, *Biochem. Pharmacol.* 50 (10) (1995) 1645.
- [49] T. Tokumura, A. Muraoka, Y. Machida, Improvement of oral bioavailability of flurbiprofen from flurbiprofen/ β -cyclodextrin inclusion complex by action of cinnarizine, *Eur. J. Pharm. Biopharm.* 73 (2009) 202.
- [50] S. Shi, H. Chen, X. Lin, X. Tang, Pharmacokinetics, tissue distribution and safety of cinnarizine delivered in lipid emulsion, *Int. J. Pharm.* 383 (2010) 264.
- [51] W. Soudijn, I. van Wijngaarden, The metabolism and excretion of cinnarizine by rats, *Life Sci.* 7 (1968) 231.
- [52] S. Kariya, S. Isozaki, S. Narimatsu, T. Suzuki, Oxidative metabolism of cinnarizine in rat liver microsomes, *Biochem. Pharmacol.* 44 (1992) 1471.
- [53] B.N. Singh, The mechanism of action of calcium antagonists relative to their clinical applications, *Br. J. Clin. Pharmacol.* 21 (1986) 1095.
- [54] A. Elimadi, L. Bouillot, R. Sapena, J.-P. Tillement, D. Morin, Dose-related inversion of cinnarizine and flunarizine effects on mitochondrial permeability transition, *Eur. J. Pharmacol.* 348 (1998) 115.
- [55] O. Terland, T. Flatmark, Drug-induced parkinsonism: cinnarizine and flunarizine are potent uncouplers of the vacuolar H^+ -ATPase in catecholamine storage vesicles, *Neuropharmacology* 38 (1999) 879.



Glutathione

Amer M. Alanazi, Gamal A.E. Mostafa, Abdullah A. Al-Badr¹

Department of Pharmaceutical Chemistry, College of Pharmacy, King Saud University, Riyadh, Saudi Arabia

¹Corresponding author: e-mail address: abadr@ksu.edu.sa

Contents

1. Description	44
1.1 Nomenclature	44
1.2 Formulae	44
1.3 Elemental Composition	45
1.4 Appearance	45
2. Uses and Applications	45
3. Methods of Preparation	46
3.1 History of Glutathione Structure	46
3.2 Biosynthesis of Glutathione	47
3.3 Synthesis of Glutathione	47
4. Physical Characteristics	49
4.1 Solubility	49
4.2 X-ray Powder Diffraction Pattern	49
4.3 Crystal Structure	49
4.4 Thermal Methods of Analysis	82
4.5 Spectroscopy	83
4.6 Mass Spectrometry	86
5. Methods of Analysis	90
5.1 Compendial Methods	90
5.2 Electrochemical Methods	95
5.3 Spectrophotometric Methods	106
5.4 Spectrofluorimetric Methods	108
5.5 Chemiluminescence Methods	110
5.6 Chromatographic Methods	113
5.7 Immunoassay Methods	143
6. Stability	146
7. Reviews	147
Acknowledgments	148
References	148



1. DESCRIPTION

1.1 Nomenclature

1.1.1 Systematical Chemical Names

- Glycine, *N*-(*N*- γ -glutamyl-L-cysteinyl).
- γ -L-Glutamyl-L-cysteinylglycine.
- *N*-(*N*-L- γ -Glutamyl-L-cysteinyl) glycine.
- (2*S*)-2-Amino-5-[[*(2R)*-1-(carboxymethylamino)-1-oxo-3-sulfanylpropan-2-yl]amino]-5-oxo-pentanoic acid.
- (2*S*)-2-amino-4-{[[*(1R)*-1-[(carboxymethyl)carbamoyl]-2-sulfanylethyl]carbamoyl}butanoic acid.
- 2-Amino-5-[[1-(carboxymethylamino)-1-oxo-3-sufanylpropan-2-yl]amino]5-oxobutanoic acid.
- 2-Amino-5-[[2-(carboxymethy-amino)-2-keto-1-(mercaptomethyl)ethyl]amino]-5-ketovaleric acid.
- 2-Amino-5-[[2-(carboxymethylamino)-2-oxo-1-(sulfanylmethyl)ethyl]amino]-5-oxo-pentanoic acid.
- 2-Azanyl-5-[[1-(carboxymethylamino)-1-oxo-3-sulfanylpropan-2-yl]amino]-5-oxopentanoic acid [1–4].

1.1.2 Nonproprietary Name

Glutathione, Glutathion, L-Glutathion, Glutathione SH, GSH.

1.1.3 Proprietary Names

Agifutol[®]; Atomolan[®]; Beamthion[®]; Copren[®]; Deltathione[®]; Glutamed[®]; Glutasan[®]; Glutathin[®]; Glutathiol[®]; Glutathion[®]; Gluthion[®]; Glutanil[®]; Glutoxil[®]; Ipatox[®]; sethion[®]; Maglut[®]; Neuthion[®]; Novatox[®]; Ridutox[®]; Rition[®]; Scavenger[®]; Tad[®]; Tathiclon[®]; Tathion[®]; Tationil[®]; Thioxene[®]; Titon[®]; Triptide[®] [3,4].

1.2 Formulae

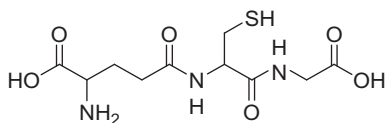
1.2.1 Empirical Formula, Molecular Weight, and CAS Number

C₁₀H₁₇N₃O₆S

307.32

70-18-8

1.2.2 Structural Formula



1.3 Elemental Composition

C 39.08%, H 5.58%, N 13.67%, O 31.24%, S 10.43%.

1.4 Appearance

A white or almost white, crystalline powder or colorless crystals [3,4]

2. USES AND APPLICATIONS

Glutathione is an endogenous peptide with antioxidant and other metabolic functions. Glutathione and glutathione sodium are used to prevent neurotoxicity associated with cisplatin or oxaliplatin. They have also been used to prevent other adverse effects of antineoplastic and radiation therapy, as well as in a wide range of other disorders including poisoning with heavy metals and other compounds, liver disorders, corneal disorders, and eczema. Glutathione has also been tried in idiopathic pulmonary fibrosis and peripheral vascular disorders [3]. Glutathione reduces the incidence of neurotoxicity induced by cisplatin therapy. In a double-blind, randomized trial [5] in 50 patients receiving cisplatin for advanced gastric cancer, administration of glutathione significantly reduces the incidence of neuropathy assessed within 1 week of completing cisplatin therapy. There did not appear to be any reduction in cytotoxic activity. Similar benefit was observed in a randomized, double-blind, placebo-controlled trials involving 52 patients receiving oxaliplatin [6]. Glutathione is an important extracellular antioxidant in the lung and high concentrations are found in lung epithelial lining fluid. A deficiency of glutathione may contribute to the epithelial damage that occurs in various lung disorders, and treatment with nebulized glutathione has therefore been investigated. Small studies have found beneficial biochemical results in patients with cryptogenic fibrosing alveolitis (idiopathic pulmonary fibrosis) [7] and in cystic fibrosis [8], but the clinical effects of these changes are not clear. Another study in cystic fibrosis [9] found no

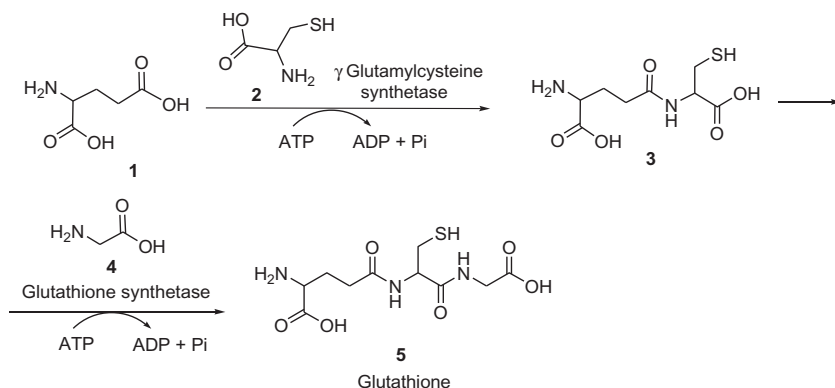
effect on oxidative markers after treatment for 2 weeks, but there was a small improvement in lung function. Benefit has also been reported [10] in a patient with emphysema. However, in a study [11] of patients with mild asthma, inhalation of glutathione solution was associated with bronchoconstriction, leading to cough or breathlessness in some patients, possibly due to sulfite formation [3].



3. METHODS OF PREPARATION

3.1 History of Glutathione Structure [12]

Glutathione was discovered by J. de Rey-Paiade in 1888 from extracts of yeast and many animal tissues (beef skeletal muscle and liver, fish skeletal muscle, lamb small intestine, and sheep brain) and in fresh egg white. de Rey-Paiade named this substance *philothion* meaning love and sulfur in Greek. In 1921, Hopkins suggested that the *philothion* isolated from liver, skeletal muscle, and yeast is a dipeptide consisting of cysteine and glutamate but these authors overlooked the presence of glycine in *philothion* possibly due to misinterpretation of the Van Slyke amino N data. Honoring the history of the discovery of *philothion*, Hopkins named the substance “glutathione.” Based on the content of nitrogen and sulfur in Glutathione isolated from yeast, blood, and liver, Hunter and Eagles indicated in 1927 that Glutathione is not a dipeptide containing Glutamate–Cysteine but is a tripeptide consisting of Glutamate–Cysteine and an additional low-molecular-weight amino acid (possibly serine). Using an acid hydrolysate of Glutathione, Hopkins proposed in 1929 that Glutathione is a tripeptide formed from cysteine, glutamate, and glycine. This proposal was supported by the independent work of Kendall and coworkers in 1929 and 1930. Based on titration of Glutathione in water and formaldehyde as well as the observed pK values, Pirie and Pinhey reported in 1929 that the structure of Glutathione is γ -Glutamate–Cysteine–Glycine. The structure of Glutathione was confirmed by Harington and Mead in 1935 through chemical synthesis from *N*-carbobenzoxy cystine and glycine ethyl ester. One year later, another chemical synthesis of Glutathione was performed by du Vigneaud and Miller using *S*-benzylcysteinylglycine methyl ester and the acid chloride of *N*-carbobenzoxyglutamate- α -methyl ester. During the past half century, glutathione has been found in all cells. Related substances reported to date include γ -Glu-Cys-Gly-spermidine in *E. coli* and $(\gamma$ -Glu-Cys) $_n$ -Gly in plants [12–20].



Scheme 1 Biosynthesis of glutathione [21,22].

3.2 Biosynthesis of Glutathione

Noctor *et al.* [21,22] reviewed the biosynthesis, metabolism, and relationship to stress tolerance explored in transformed plants. The pathway of glutathione biosynthesis involves two sequential ATP-dependent reactions allow the synthesis of γ -glutamylcysteine from L-glutamate **1** and L-cysteine **2**, followed by the formation of glutathione **5** by addition of glycine **4** to the C-terminal end of the γ -glutamylcysteine **3** [23]. These reactions are catalyzed by γ -glutamylcysteine synthetase and glutathione synthetase (Scheme 1).

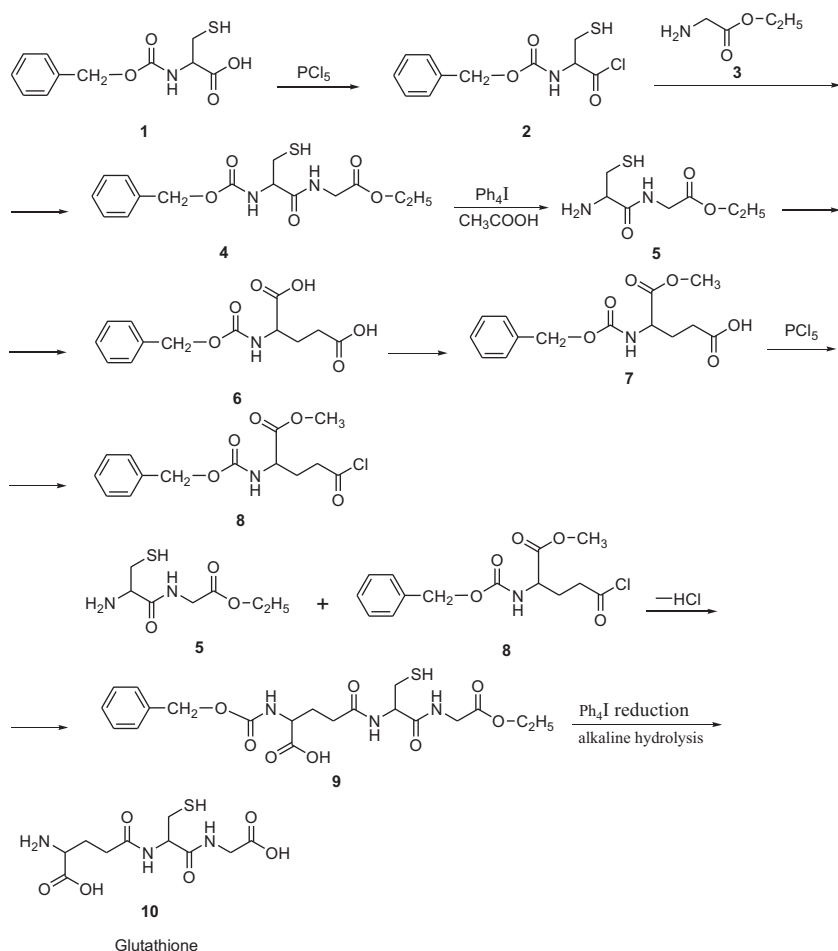
Johnston and Bloch [24] enzymatically synthesized glutathione. Extracts of the acetone-dried pigeon liver catalyze reactions leading to the synthesis of glutathione from glutamic acid, cysteine, and glycine. Magnesium ion, phosphate, and adenine nucleotide are necessary for the synthesis of the tripeptide glutathione. The preparation and some properties of the enzyme system are described. Adenosine diphosphate and adenosine triphosphate are equally effective in supporting glutathione synthesis. Adenylic acid can replace adenine triphosphate in crude extracts, presumably because the adenosine monophosphate is converted to adenosine diphosphate or adenosine triphosphate. Crude liver extracts catalyze both the splitting and the synthesis of glutathione. From these preparations, the hydrolytic activity can be separated by centrifugation at high speed.

3.3 Synthesis of Glutathione

3.3.1 First Method

The synthesis of glutathione was described by Harrington and Mead [13] as follows: *N*-benzyloxycarbonyl cysteine **1** [25] was converted into the acid

chloride **2** and the latter coupled with glycine ethyl ester **3**, the product **4** on treatment with phosphonium iodide in acetic acid was converted into cysteylglycyl ethyl ester **5** which was conveniently isolated as the hydroiodide. *N*-benzyloxycarbonylglutamic acid **6** was then converted into the anhydride which with sodium methoxide in methyl alcohol yielded the α -monomethyl ester of *N*-benzyloxycarbonyl glutamic acid **7** [26]; Treatment with phosphorous pentachloride converted the latter compound **7** into the corresponding acid chloride **8** which was coupled with the cysteylglycyl ester **5** to give the ester **9**. The ester groups were removed from **9** by very careful hydrolysis in an alkaline aqueous dioxian solution and the



Scheme 2 Synthesis of glutathione [13].

resulting acid was treated with phosphonium iodide under the usual conditions. From the reaction mixture, there was obtained in small yield the tripeptide glutathione **10** which proved to be identical in every respect with an authentic sample of glutathione obtained from natural sources (Scheme 2).

3.3.2 Second Method

Berse *et al.* [27] described a method for the preparation of glutathione. Di(*N*-*p*-nitrocarboboxy) L-cystine **1** was condensed with glycine ethyl ester **2** in the presence of *N,N'*-dicyclohexylcarbodiimide; the intermediate ester **3** was partially reduced to uncover the amino groups of the L-cysteine residue without cleaving its disulfide linkage. The resulting diethyl L-cysteinyl diglycinate **4** was condensed with 2 equivalents of *p*-nitrocarboboxy-L-glutamic acid **5** to provide an ester **6** in which the glutathione structure has been assembled. Saponification (a) and partial reduction (b) of **6** lead to the oxidized glutathione **5**. Complete hydrogenation on palladium catalyst leads to glutathione **7** (Scheme 3).



4. PHYSICAL CHARACTERISTICS

4.1 Solubility

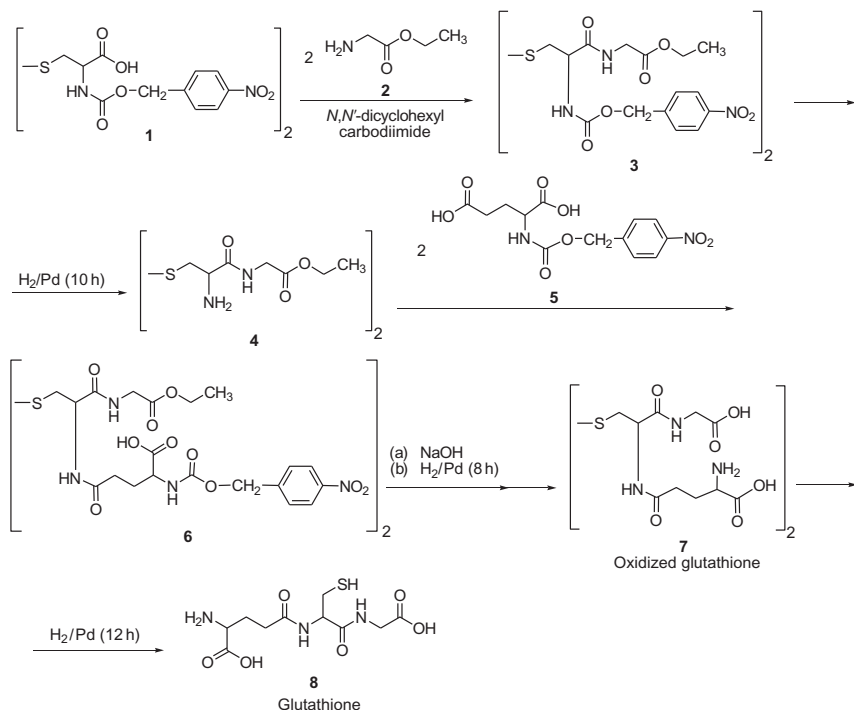
Freely soluble in water, diluted alcohol, liquid ammonia, and dimethyl formamide. A white or almost white, crystalline powder, or colorless crystals. Very slightly soluble in alcohol and in dichloromethane [2–4].

4.2 X-ray Powder Diffraction Pattern

X-ray powder diffraction pattern has been obtained on D8-Advanced, Bruker AXE Germany (Figure 1) diffractometer equipped with scintillation detector using copper Ka ($\lambda 1.5406 \text{ \AA}$) radiation with scanning range between 2γ and 50γ (theta) at scanning speed of 2/min. Detail process for preparing the glutathione amorphous and its polymorph form was described. A full data summary is compiled in Table 1.

4.3 Crystal Structure

Wright [28] described the crystal structure of glutathione and provided a comparison of the methods used in the attempt to determine its crystal structure [29].



Scheme 3 Synthesis of glutathione [27].

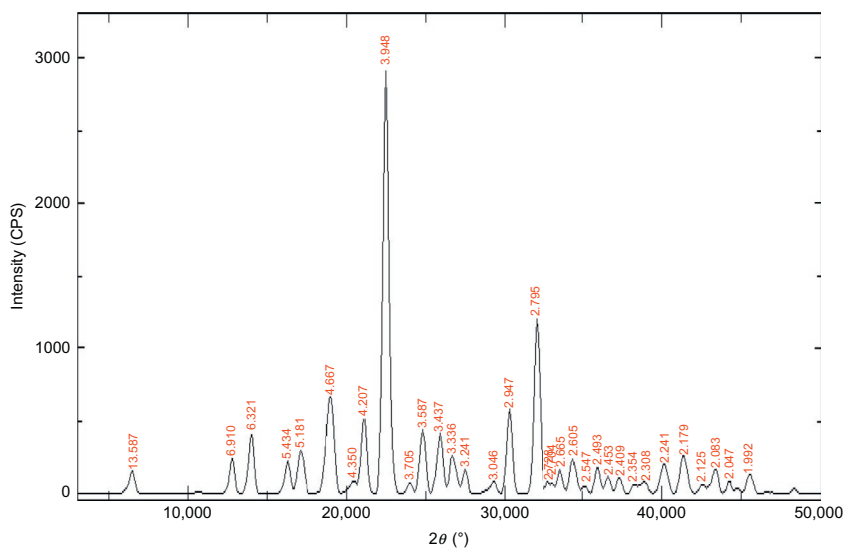


Figure 1 The X-ray powder diffraction pattern of glutathione.

Table 1 Data Deduced from the X-ray Powder Diffraction Patterns of Glutathione

S. No.	Diffraction Angel (2θ)	Intensity, I/I_0 (%)	S. No.	Diffraction Angel (2θ)	Intensity, I/I_0 (%)
1	6.500	6	16	30.300	21
2	12.800	9	17	32.000	42
3	14.000	15	18	32.800	3
4	16.300	8	19	33.100	3
5	17.100	11	20	33.600	6
6	19.000	23	21	34.400	9
7	20.400	3	22	35.200	2
8	21.100	18	23	36.000	7
9	22.500	100	24	36.600	4
10	24.000	3	25	37.300	4
11	24.800	15	26	38.200	3
12	25.900	15	27	39.000	3
13	26.700	9	28	40.200	7
14	27.500	6	29	41.400	10
15	29.300	3	30	42.500	3

The tripeptide glutathione crystallizes in the orthorhombic system with space group $P2_12_12_1$ and unit-cell dimensions $a=28.05\pm0.02$, $b=8.802\pm0.002$, $c=5.630\pm0.002$ Å. The position of the sulfur atoms in the unit cell was determined from the Harker sections of the three-dimensional Patterson function. The structure was finally determined from a c -axis Fourier projection pattern, based on terms with signs derived by the method of Cochran and Douglas, used in conjunction with a three-dimensional electron-density distribution based on terms with phase angles given by the sulfur atoms only. The structure was refined by two- and three-dimensional Fourier syntheses. The molecule contains no unusual bond lengths or angles and adopts a curled configuration with the planes of the glycine carboxyl group and the amino-carboxyl group both parallel to the c -axis and the planar peptide linkages inclined at 94.4° to one another. The sulfur atoms from zig-zag chains about alternate screw diad axes parallel to c , the S–S distances being 4.41 Å. The structure is held together by a

three-dimensional network of hydrogen bonds, but there are no internal hydrogen bonds in the molecule [28].

The investigation of the crystal structure of the naturally occurring tripeptide glutathione γ -L-glutamyl-L-cysteinylglycine was undertaken with a view to providing additional information about the molecular configuration of the amino acids present in proteins. But it was also considered to be of especial interest in that the two peptide linkages present in the molecule might bear the same spatial relationship to one another as do neighboring peptide linkages in protein chains, for which certain structure such as the α -helix have been postulated [30]. Various structures have been postulated for the glutathione molecule in solution [31], such as those involving internal hydrogen-bond formation to the sulfur atom, which would account for the increased reactivity of the mercaptan group in the presence of urea and guanidinium salts, a phenomenon also observed with protein. The possibility of this type of hydrogen-bond formation and of the presence of other internal hydrogen bonds in the molecule was considered during the trial structure work [28].

Most of the well-known methods of crystal-structure analysis were tried during the preliminary attempts to determine the structure. The trials were made on the c -axis projection, which was considered to contain the least overlap and has the additional advantage of a center of symmetry. It was found that most of the methods tried gave essentially the same c -axis projection Fourier pattern, on which it was possible to place the molecule in a variety of different ways; but only one of the patterns, derived by the method of Cochran and Douglas [32,33] suggested a configuration of the molecule in which the maximum number of hydrogen bonds could be formed without strain. This pattern, used in conjunction with a three-dimensional electron-density distribution calculated using phase angles based on the coordinates of the sulfur atoms only, served to locate the positions of all the atoms in the unit cell, and the atomic parameters were then refined by two- and three-dimensional Fourier methods [28].

It is proposed in this account to outline the methods which actually led from the experimental data to the determination of the crystal structure, and in a subsequent account [29] to give an outline of all the other methods which were tried, together with some comparison and discussion of the results obtained in each case.

The crystals of glutathione used for the X-ray investigation were grown, in a reducing atmosphere, from solutions in water saturated with hydrogen sulfide, in order to keep the substance in the reduced form. They grew as

thin flat plates, normal to the a -axis and slightly elongated parallel to the c -axis, the predominant form being $\{100\}$. The crystals showed straight extinction, and refractive indices parallel to the b - and c -axes of 1.589 ± 0.002 and 1.591 ± 0.002 , respectively. Oscillation and Weissenberg photographs established the crystals as belonging to the orthorhombic system, with space group $P2_12_12_1$. The unit-cell dimensions, determined from high-order equatorial reflexions on oscillation photographs, were found to be

$$a = 28.05 \pm 0.02, \quad b = 8.802 \pm 0.002, \quad c = 5.630 \pm 0.002 \text{ \AA}$$

substantially in agreement with the values found by Bernal [34]. There are four molecules in the unit cell, which gives a calculated value for the density of 1.467 g/cm^3 . The density of the crystals, determined by flotation in mixtures of benzene and carbon tetrachloride, is 1.47 g/cm^3 .

Three-dimensional intensity data were obtained from equi-inclination Weissenberg photographs, using the multiple-film technique and taken with the crystals oscillating about the b -axis ($k=0-6$), and about the c -axis ($l=0-4$). Of the 1830 reflexions which could have been recorded using Cu $K\alpha$ radiation ($\lambda=1.5418 \text{ \AA}$), only 1186 were actually observed. Although, therefore, only 65% of the (hkl) reflexions, 77% of the $(hk0)$, and 66% of the $(h0l)$, were actually observed, these values represent 90%, 97%, and 94%, respectively, of the total structure amplitude in each case, estimated on the assumption that $|F_o|$ for the unobserved reflexions is equal to half the minimum observable value in each zone. The intensities of the reflexions were estimated visually by comparison with a set of spots of standard intensity, and a correction for variation in spot shape was made by the method given by Broomhead [35] to allow for the nonuniform cross section of the crystals. As the crystals were very thin, no correction was made for absorption. An empirical correction to allow for the variation in background on the films was applied, and Lorentz and polarization corrections were made by the method of Goldschmidt and Pitt [36]. For the 393 reflexions which were measured about both axes, the probable error was calculated and was found to be of the order of 13.3% for $|F_o(hk0)|^2$ and 9.7% for $|F_o(hk0)|^2$ where $l=1, 2$, or 3 [28].

The values of $|F_o(hkl)|^2$ were placed on an absolute scale, using Wilson's method [37], and the value of B in the temperature factor $\exp [-B(\sin^2 \theta)/\lambda^2]$ was found to be 3.396 \AA^2 . Atomic scattering-factor curves for carbon, nitrogen, and oxygen [38], and for sulfur [39] were modified by this

temperature factor and used for the two-dimensional work. For the three-dimensional work, the values of atomic scattering factors for the different kinds of atoms in the structure, uncorrected for temperature effects, versus values of $2 \sin \theta$ at intervals of 0.0185 in the latter, were held in the computer during all structure-factor calculations. For each reflection, the appropriate values of the atomic scattering factors were selected by the machine and multiplied by a calculated temperature factor for which the value of B had been derived, by a least-squares method, in a previous round of the structure-factor calculations [28].

4.3.1 Determination of the Positions of the Sulfur Atoms in the Unit Cell

The three-dimensional intensity data were used to calculate the three Harker sections and the three zero sections of the three-dimensional Patterson function. From the Harker sections, it was possible to recognize the S-S vector peaks at $(2x - \frac{1}{2}, 2y, \text{peak height } 350)$ in $P(x, y, \frac{1}{2})$, at $(2x, 2z - \frac{1}{2}, \text{peak height } 250)$ in $P(x, \frac{1}{2}, z)$, and at $(2y, -\frac{1}{2}, 2z, \text{peak height } 503)$ in $P(\frac{1}{2}, y, z)$, where x , y , and z are the fractional coordinates of a sulfur atom in the unit cell and the peak heights are in arbitrary units. The sulfur coordinates were found to be (0.291, 0.641, 0.335), so that the sulfur atoms in the structure form zig-zag chains along alternate screw diad axes parallel to c , the distance between neighboring sulfur atoms in the chains being 4.40 Å [28].

4.3.2 The Cochran and Douglas Method [33] Applied to the c-Axis Projection

By this method the sets of terms for which

$$\chi = \Sigma Y(h, h') P(h, h')$$

is large and positive are determined, as it can be shown that the extent to which χ is positive is a measure of the plausibility of a particulate set of signs. $Y(h, h')$ is defined as $S(h)S(h')S(h + h')$, and $P(h, h')$ is defined as $|U(h)U(h')U(h + h')|$, where $S(h)$ is the sign of the unitary structure factor $U(h)$. It has also been noted by Cochran and Douglas [32] that if the signs of about 20 of the largest structure factors are known correctly, it is often possible from the resulting Fourier map to recognize the correct configuration of the molecule [28].

The $|U|$ values were calculated for 28 of the strongest ($hk0$) reflexions for glutathione, the signs of two of them were chosen in order to fix the origin

of the projection, and the signs of the remaining 26 were represented by letters. Of the largest product terms, 47 were calculated and set in order of magnitude, and the χ values corresponding to the various sign combinations were calculated on the electronic computer EDSAC, and set in order of magnitude. Of the nine sets of sign combinations which gave the largest χ values, only four differed from one another by more than one or two signs. These four sets of signs were used to derive the signs of the next largest structure factors, using the sign relationship

$$S(h)S(h') \approx S(h+h'),$$

and from the results four c -axis Fourier projections were calculated. All four patterns have at least one heavy peak which could correspond to a sulfur atom, but only one pattern (Figure 2) has a heavy peak in the position already chosen for a sulfur atom from the Harker sections. It was possible to place the molecule on the system of peaks as shown in Figure 2, in a curled configuration in which the maximum number of hydrogen bonds could be formed without straining the molecule [28].

Calculation of $F(hk0)$ for this molecular arrangement gave a reliability (R) index of 47.5% for 101 terms. By rearrangement of the amino-carboxyl group of the glutamic acid end of the molecule, so that an external instead of an internal hydrogen bond is formed from N_2 to O_5 , R decreased to 38%

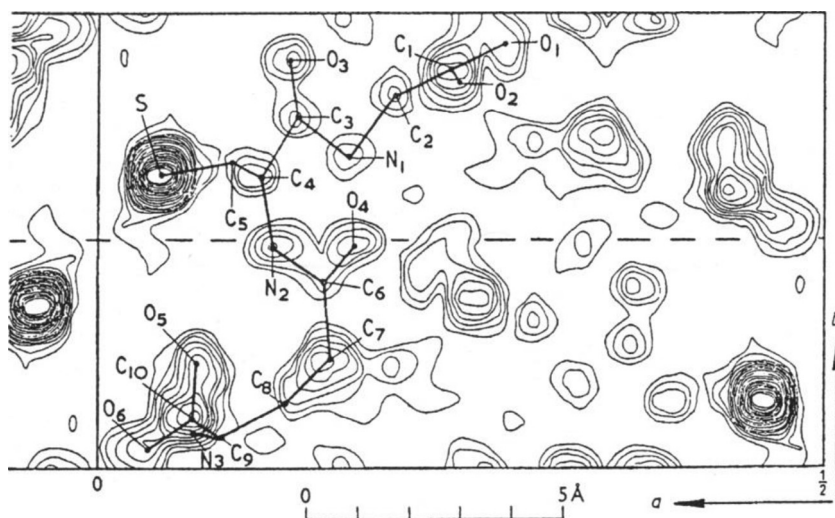


Figure 2 The c -axis Fourier projection based on 90 terms whose signs were derived by the method of Cochran and Douglas. Contours are at arbitrary intervals [28].

over 127 terms. Although two atoms, C₄ and C₅, had been placed on one Fourier peak (Figure 2), the peak height corresponded to only one and a half carbon atoms, and it was therefore concluded that C₅ must lie on the sulfur peak in this projection [28].

4.3.3 The Use of the Heavy-Atom Technique

The z coordinates of the atoms were determined from a three-dimensional electron-density distribution, calculated using the sulfur atom in the asymmetric unit as a heavy atom. The phase angles and structure amplitudes of the 1186 (hkl) reflexions for which values of $|F_o(hkl)|$ were actually observed were calculated from the sulfur coordinates, and the 598 reflexions to which the sulfur was making more than 50% of its maximum contribution were used to calculate a three-dimensional electron-density distribution. The electron density was evaluated over one quarter of the unit cell, at intervals of $a/64$, $b/32$, and $c/16$, on the electronic computer LEO [28].

This distribution showed the sulfur peak, maximum density $20 \text{ e.}\text{\AA}^{-3}$, at (0.294, 0.642, 0.337), and immediately beneath it in the c direction at (0.292, 0.644, 0.031) a peak, maximum density $3 \text{ e.}\text{\AA}^{-3}$, corresponding to carbon atom C₅. None of the other regions of positive electron density was greater than $2 \text{ e.}\text{\AA}^{-3}$. The x and y coordinates of the atoms determined from the c -axis projection, used in conjunction with this three-dimensional distribution, and with generally accepted values of bond lengths and bond angles, enabled the positions of all the atoms in the asymmetric unit to be located in the unit cell. Neither of the two alternative arrangements of the amino-carboxyl group, allowing for the formation of either an external or an internal hydrogen bond from N₂ to O₅, could be eliminated, as there were small peaks in the three-dimensional distribution which would allow for either possibility [28].

The b -axis Fourier projection containing 65 terms, whose signs were determined from the sulfur coordinates, was calculated (Figure 3). The positions of the atoms, which have x coordinates obtained from the c -axis projection and z coordinates obtained from the three-dimensional distribution, are shown, with the two alternative positions for atoms N₃, C₁₀, O₅, and O₆. The arrangement for the formation of an internal hydrogen bond to O₅ being indicated by the broken line bonding between the atoms, and the arrangement for this end of the molecule allowing for external hydrogen bonding between N₂ and O₅ being shown by the full-line bonding between the atoms. The z parameters of the atoms were adjusted slightly as indicated by this Fourier map, and the ($h0l$) structure factors were calculated for the two alternative

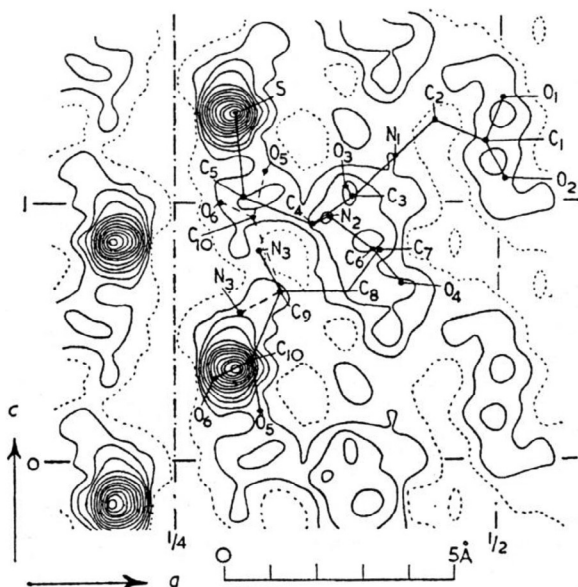


Figure 3 The b -axis Fourier projection based on 65 terms whose signs were determined from the sulfur atoms only. Contours are at arbitrary intervals [28].

arrangements. For the internal hydrogen-bond arrangement R was 52% over 65 terms, and for the external hydrogen-bond arrangement R was 35%. It was therefore concluded that the latter arrangement was the correct one, confirming the findings on the c -axis projection [28].

The atomic parameters were partially refined by three c -axis and three b -axis Fourier projections. The third c -axis projections, for which R is 25.5% over 246 terms, are shown in Figure 4, and the third b -axis projection, for which R is 27.5% over 132 terms, is shown in Figure 5. The atomic parameters obtained from these two Fourier maps are given in Table 2, column (i) [28].

4.3.4 The Refinement of the Structure

Throughout the partial refinement of the structure in projections, oxygen atom O_1 , which is resolved in the c -axis projection, gave an electron-density peak (Figure 4) which was much more diffuse than the peaks corresponding to any of the other oxygen atoms. This diffuseness was not considered to be entirely due to thermal motion and for this reason the normal method of Fourier refinement was used in three dimensions, so that the shapes of the peaks in the electron-density function could be ascertained at each stage

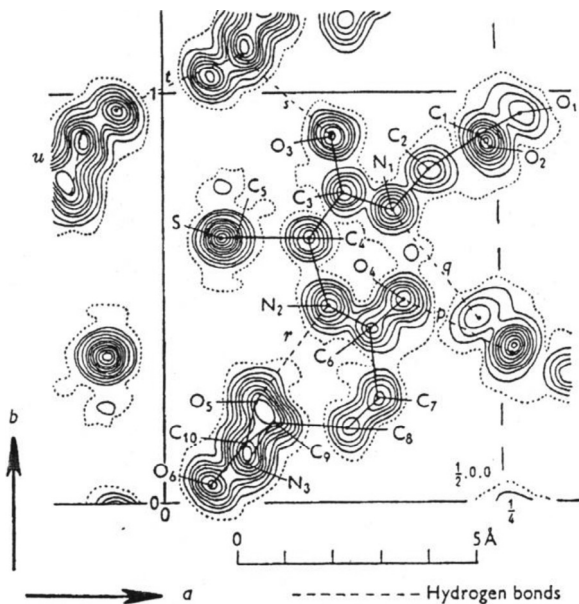


Figure 4 The c -axis Fourier projection for which $R=25.5\%$ for 246 terms. Contours at intervals of $1 \text{ e.}\text{\AA}^{-3}$, beginning at $1 \text{ e.}\text{\AA}^{-3}$ (broken line), except in the case of the sulfur atom, which has contours at $2 \text{ e.}\text{\AA}^{-3}$ intervals [28].

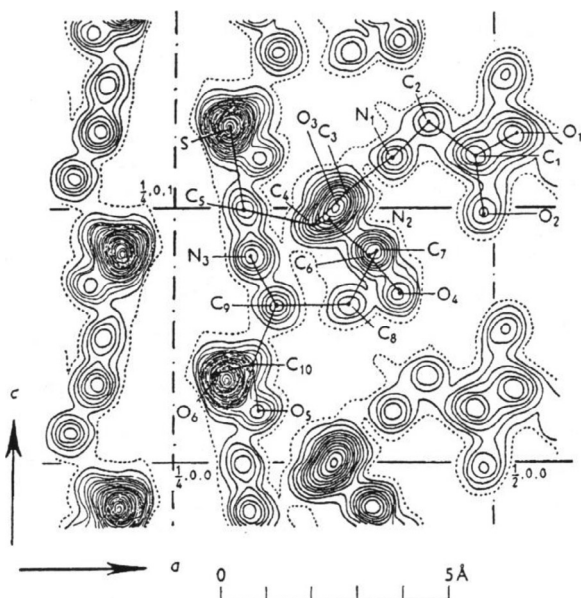


Figure 5 The b -axis Fourier projection for which $R=27.5\%$ for 132 terms. Contours at intervals of $1 \text{ e.}\text{\AA}^{-3}$, beginning at $3 \text{ e.}\text{\AA}^{-3}$ (broken line) [28].

Table 2 Atomic Parameters [28]

	(i)	(ii)	(iii)	(iv)	(v)	(vi)
The x parameters						
C ₁	0.487	0.4868	0.4867	0.4868	–	0.4897
C ₂	0.450	0.4486	0.4476	0.4478	0.4479	0.4474
C ₃	0.384	0.3849	0.3855	0.3862	0.3849	0.3852
C ₄	0.358	0.3570	0.3563	0.3563	0.3570	0.3566
C ₅	0.304	0.3036	0.3033	0.3031	0.3036	0.3036
C ₆	0.402	0.4032	0.4040	0.4039	0.4032	0.4039
C ₇	0.410	0.4090	0.4083	0.4084	0.4085	0.4087
C ₈	0.385	0.3844	0.3840	0.3841	0.3848	0.3848
C ₉	0.331	0.3296	0.3286	0.3293	0.3310	0.3309
C ₁₀	0.310	0.3090	0.3083	0.3084	0.3084	0.3088
N ₁	0.421	0.4196	0.4184	0.4189	0.4195	0.4196
N ₂	0.370	0.3711	0.3719	0.3715	0.3715	0.3724
N ₃	0.310	0.3102	0.3103	0.3104	0.3108	0.3109
O ₁	0.516	0.5157	0.5155	0.5159	–	0.5186
O ₂	0.496	0.4942	0.4929	0.4934	–	0.4920
O ₃	0.377	0.3773	0.3775	0.3775	0.3766	0.3761
O ₄	0.427	0.4269	0.4268	0.4264	0.4266	0.4270
O ₅	0.317	0.3164	0.3160	0.3161	0.3161	0.3161
O ₆	0.284	0.2829	0.2821	0.2829	0.2829	0.2829
S	0.293	0.2915	0.2905	0.2908	0.2915	0.2910
The y parameters						
C ₁	0.890	0.8937	0.8963	0.8943	–	0.8833
C ₂	0.810	0.8156	0.8195	0.8126	0.8107	0.8126
C ₃	0.759	0.7554	0.7529	0.7567	0.7587	0.7577
C ₄	0.643	0.6410	0.6396	0.6397	0.6407	0.6399
C ₅	0.648	0.6511	0.6533	0.6531	0.6511	0.6526
C ₆	0.425	0.4218	0.4196	0.4207	0.4218	0.4207
C ₇	0.259	0.2562	0.2542	0.2545	0.2534	0.2520

Continued

Table 2 Atomic Parameters [28]—cont'd

	(i)	(ii)	(iii)	(iv)	(v)	(vi)
C ₈	0.171	0.1747	0.1773	0.1762	0.1775	0.1775
C ₉	0.198	0.1910	0.1861	0.1882	0.1921	0.1909
C ₁₀	0.151	0.1528	0.1541	0.1534	0.1534	0.1541
N ₁	0.710	0.7105	0.7109	0.7115	0.7119	0.7117
N ₂	0.480	0.4822	0.4837	0.4837	0.4822	0.4837
N ₃	0.097	0.0936	0.0912	0.0924	0.0922	0.0912
O ₁	0.980	0.9586	0.9576	0.9578	—	0.9506
O ₂	0.860	0.8626	0.8644	0.8653	—	0.8699
O ₃	0.895	0.8945	0.8941	0.8941	0.8951	0.8938
O ₄	0.491	0.4928	0.4941	0.4932	0.4937	0.4937
O ₅	0.247	0.2484	0.2494	0.2487	0.2487	0.2487
O ₆	0.037	0.0380	0.0387	0.0404	0.0404	0.0404
S	0.644	0.6419	0.6404	0.6411	0.6417	0.6415
The z parameters						
C ₁	0.214	0.2211	0.2261	0.2276	—	0.2066
C ₂	0.351	0.3406	0.3333	0.3380	0.3521	0.3531
C ₃	0.054	0.0589	0.0623	0.0599	0.0589	0.0574
C ₄	0.938	0.9284	0.9217	0.9248	0.9240	0.9240
C ₅	0.985	0.9989	0.0016	0.0055	0.9989	0.9977
C ₆	0.817	0.8157	0.8148	0.8166	0.8156	0.8166
C ₇	0.826	0.8219	0.9190	0.8208	0.8219	0.8231
C ₈	0.629	0.6239	0.6203	0.6215	0.6160	0.6100
C ₉	0.621	0.6185	0.6167	0.6169	0.6167	0.8178
C ₁₀	0.379	0.3819	0.3839	0.3822	0.3832	0.3832
N ₁	0.188	0.1929	0.1963	0.1951	0.1965	0.2000
N ₂	0.978	0.9635	0.9533	0.9571	0.9590	0.9574
N ₃	0.805	0.8042	0.8036	0.8045	0.8070	0.8086
O ₁	0.339	0.3390	0.3390	0.3378	—	0.3190
O ₂	0	0.9906	0.9840	0.9843	—	0.9777

Table 2 Atomic Parameters [28]—cont'd

	(i)	(ii)	(iii)	(iv)	(v)	(vi)
O ₃	0.031	0.0266	0.0235	0.0245	0.0266	0.0245
O ₄	0.679	0.6731	0.6690	0.6684	0.6731	0.6712
O ₅	0.201	0.2075	0.2121	0.2111	0.2111	0.2140
O ₆	0.348	0.3507	0.3526	0.3536	0.3536	0.3560
S	0.321	0.3117	0.3052	0.3072	0.3070	0.3072

of the refinement. As the crystals of glutathione were of an unsuitable shape and size for accurate intensity measurements, the method of least squares, which minimizes $\Sigma(|F_o| - |F_c|)^2$, was not used for the later stages of the refinement. The positional parameters were therefore refined by two complete rounds of structure-factor calculations followed by full three-dimensional electron-density calculations, several pairs of *b*- and *c*-axis difference syntheses in projection, and a final three-dimensional difference synthesis containing 17 atoms, i.e., omitting three atoms which might have been wrongly placed [28].

1. First Round of the Refinement

The atomic parameters given in Table 2, column (i) were used for the first round of the refinement together with a temperature factor $B = 3.396 \text{ \AA}^2$ and a scaling factor $K = 1.30$, both determined by Wilson's statistical method. 1557 $|F_c|$ values and phase angles were calculated and for this number of terms, which includes 371 for which the value of $|F_o|$ was taken as one-half the minimum observed value, *R* was 29.4%. The value calculated for *K* in this round was 1.435, the high values for both *R* and *K* being attributed to the inclusion of the 371 terms with uncertain $|F_o|$ values [28].

A three-dimensional electron-density function containing 1186 terms was calculated and the peak positions were calculated from the equation representing a Gaussian ellipsoid [40], solving for the 10 unknowns in this equation from the 10 ϱ values suitably disposed about the maximum ϱ value for each peak. The atomic parameters calculated in this way are shown in Table 2, column (ii). Column (iii) shows the values obtained if allowance is made for the phase angles of 70% of the structure factors, by taking $1.7 \times$ atomic shifts [28].

In connection with this electron-density distribution the following points were noted:

1. Oxygen atom O₁, which in the *c*-axis projection produced a peak elliptical in shape, diffuse, and lower in height than the peaks corresponding to the other oxygen atoms, gave a diffuse avoid-shaped electron-density distribution in three dimensions, the maximum ρ value being only 6 e.Å⁻³, whereas all other oxygen atoms, with the exception of O₂, gave peaks with maximum ρ values of 9–11 e.Å⁻³ [28].
2. The change in parameters of carbon atom C₁ had resulted in an unusual set of values for the bond lengths at the glycine end of the molecule, the peculiarities being enhanced by taking 1.7 × atomic shifts. Therefore, although this allowance for the phase angles would probably have speeded up the refinement process, on the assumption that some of the atomic positions might have been overshoot in the first round, the actual shifts were used in calculating the parameters for the second round of the refinement [28].

2. Second Round of the Refinement

The structure amplitudes and phase angles for the second round of the refinement were calculated from the atomic parameters shown in Table 2, column (ii), *R* was 25.7% over 1557 terms and 22.2% for the 1186 terms for which $|F_o|$ values were actually obtained. *K* and *B* were 1.450 and 2.983 Å², respectively [28].

Atomic parameters calculated from the second three-dimensional electron-density distribution are given in Table 2, column (iv). Figure 6A and B is composite diagram of this second distribution, representing views down the *c*- and *b*-axes, respectively. Peak heights for the atoms are given in Table 3. In general, the apparent atomic shifts calculated from this second round were in the same direction as those calculated from the first round, so that taking 1.7 × the shifts would have been justified. The peak for atom O₁ was again diffuse (Figure 6), and lower in height than the peaks for other oxygen atoms in the structure, while the values for the bond lengths at the glycine end of the molecule were not in agreement with generally accepted values for such bonds [28].

Three pairs of *c*-axis and *b*-axis difference syntheses in projection were calculated in an unsuccessful attempt to determine the true positions of atoms C₁, O₁, and O₂, and to improve the shape of the peak for O₁. The parameters obtained from the final pair, for the 17 other atoms in the asymmetric unit, are shown in Table 2, column (v) [28].

3. A Three-Dimensional Difference Synthesis

During the investigation of the structure of vitamin B₁₂ (Hodgkin, private communication), it has been found that there is a tendency, in electron-density functions involving phase angles, for a peak one-third

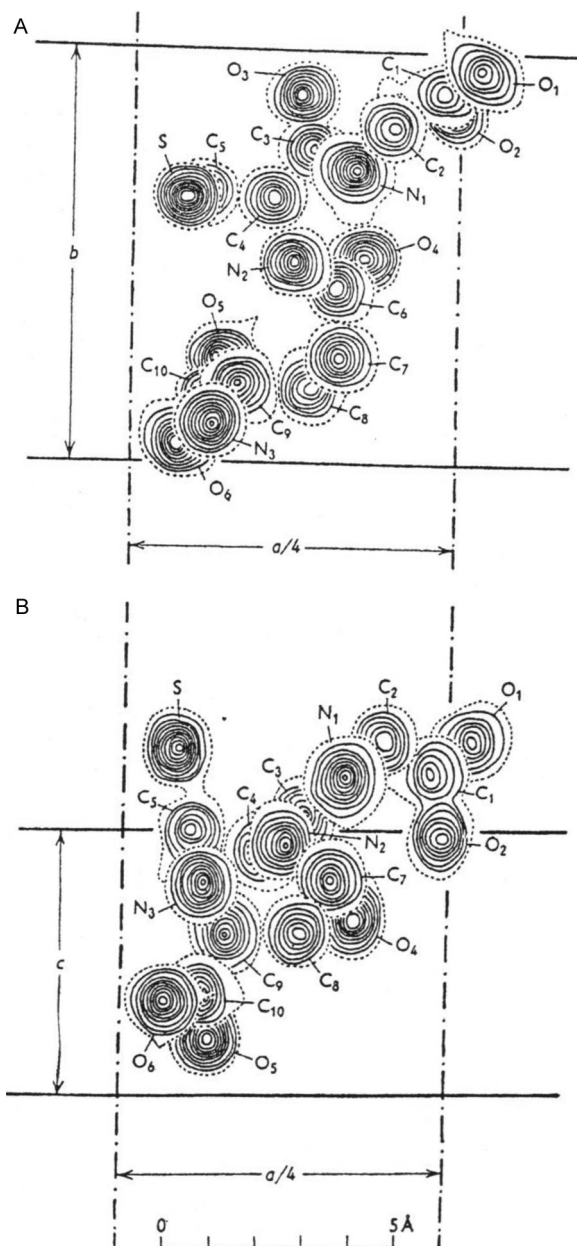


Figure 6 Composite diagrams of the second three-dimensional electron-density distribution: (A) viewed down the c -axis and (B) viewed down the b -axis. Contours are at intervals of $1 \text{ e.}\text{\AA}^{-3}$, beginning at $1 \text{ e.}\text{\AA}^{-3}$ (broken line), except in the case of the sulfur atom, which has contours at $2 \text{ e.}\text{\AA}^{-3}$ intervals [28].

Table 3 Peak Electron-Density Values Obtained in the Second Round of the Three-Dimensional Refinement [28]

C₁	6.1 e.Å⁻³	N₁	10.3 e.Å⁻³
C ₂	6.8	N ₂	9.1
C ₃	7.6	N ₃	10.4
C ₄	8.0		
C ₅	7.0	O ₁	7.3
C ₆	7.9	O ₂	8.0
C ₇	8.6	O ₃	10.0
C ₈	7.0	O ₄	9.8
C ₉	9.0	O ₅	10.9
C ₁₀	8.2	O ₆	10.3
		S	21.2

of the normal height to be produced for atoms not included in the calculation, or included in incorrect positions, provided that the positions of most of the other atoms in the structure are known with reasonable accuracy. Therefore, a three-dimensional difference synthesis, omitting atoms C₁, O₁, and O₂, and based on the 17 atoms with parameters as in Table 2, column (v), was calculated. The distribution obtained is represented by the composite diagrams showing a view down the *c*-axis (Figure 7A) and down the *b*-axis (Figure 7B). The results may be summarized as follows:

1. There are peaks with maximum ρ values 3 e.Å⁻³ in the difference distribution corresponding to the atoms C₁, O₁, and O₂ omitted from the calculation, as predicted from the work on vitamin B₁₂. The atomic parameters calculated from these three peaks are given in Table 2, column (vi).
2. Other peaks in the difference distribution did not have ρ values exceeding 1 e.Å⁻³ except for the negative peak at the position of the sulfur atom, indicating that the sulfur atom requires a larger temperature factor than the overall one which was used in the calculation. O₆ appears to have an anisotropic thermal motion, and several other atoms require small adjustments to their temperature factors.
3. Corrections to the atomic parameters for C₂, C₇, C₉, and N₃ were indicated and were calculated from the difference distribution by the usual methods.

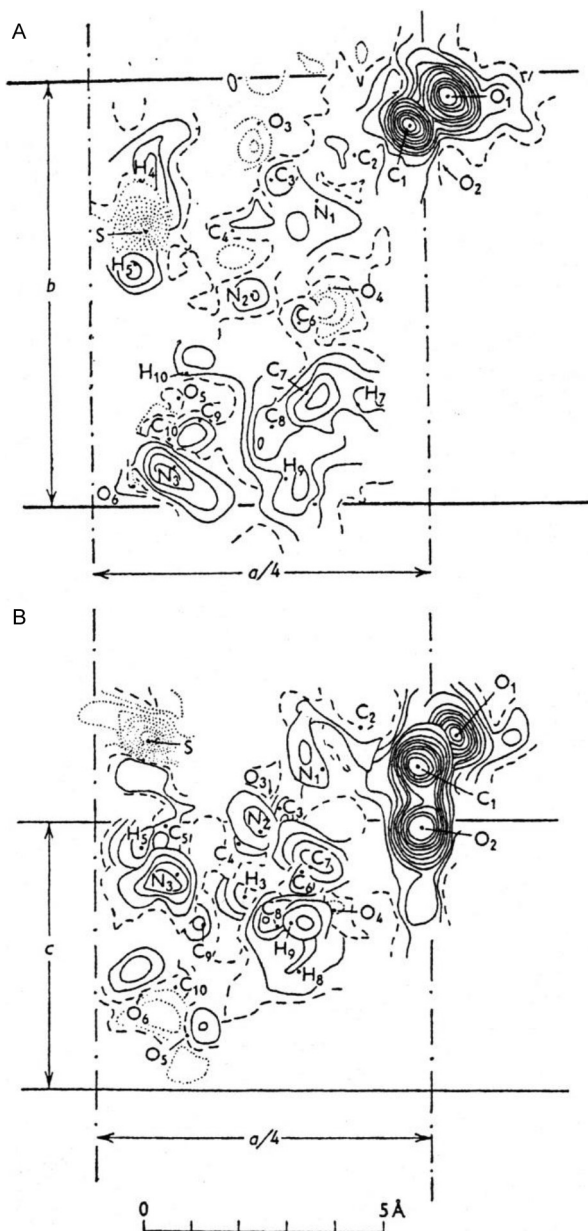


Figure 7 Composite diagrams representing the three-dimensional difference synthesis: (A) viewed down the *c*-axis and (B) viewed down the *b*-axis. Contours are at intervals of $0.25 \text{ e.}\text{\AA}^{-3}$, with the zero contour line broken and the negative contour lines dotted [28].

4. There are small peaks, maximum ρ values 0.7–1.0 e.Å⁻³ (Figure 7A and B), in positions corresponding to eight of the covalently bonded hydrogen atoms, and parameters calculated for these atoms are given in Table 4.

The final atomic parameters calculated from the three-dimensional differences synthesis are given in Table 2, column (vi). The final $|F_c|$ values, which include a contribution from the eight covalently bonded hydrogen atoms, are shown together with the $|F_a|$ values in Table 5. R for 1557 terms was 25.3% and for 1186 terms 21.0% [28].

Accuracy

An approximate value of the standard deviation $\sigma(x)$, etc., in the atomic parameters was calculated by the method of Cruickshank [41]. $\sigma(x)$ was found to be about 0.020 Å, which gives a value for the standard deviation in bond length of about 0.028 Å. Therefore, differences less than 0.08 Å between the values calculated for the bond lengths in this structure and generally accepted values for such bond lengths cannot be considered as significant [28].

Discussion of the structure

The values of bond lengths and bond angles determined in the final round of the refinement are shown in Figure 8. The two peptide linkages in the molecule are planar, with the –NH and –CO groups in the *trans* configuration. The best representative planes, determined by the method of least squares on the assumption that the z parameters are the least accurate, are

$$2.5959x + 0.0436y - 0.5705z = 1 \text{ for atoms } C_2, N_1, C_3, O_3 \text{ and } C_4, \text{ and} \\ 1.6389x + 0.1242y + 0.3552z = 1 \text{ for atoms } C_4, O_6, N_2, O_4 \text{ and } C_7.$$

Table 4 Atomic Parameters of the Eight Covalently Bonded Hydrogen Atoms Included in the Final Structure-Factor Calculations [28]

	<i>x</i>	<i>y</i>	<i>z</i>
H ₃	0.3601	0.6589	0.7332
H ₄	0.2888	0.7595	0.9325
H ₅	0.2840	0.5612	0.9112
H ₆	0.3939	0.2088	0.9892
H ₇	0.4465	0.2230	0.8231
H ₈	0.4002	0.2230	0.4472
H ₉	0.3939	0.0568	0.6189
H ₁₀	0.3217	0.3091	0.8587

Table 5 Final Values of Observed and Calculated Structure Amplitudes
For each entry the upper is the observed value

$\frac{c-o}{h^2}$	0	1	2	3	4	5	6	7	8	9	10	11
0			39.4 39.6		18.2 20.8		9.1 11.2		23.7 24.8		3.4 12.0	
1		10.7 13.6	26.2 34.6	9.3 6.2	45.0 54.8	5.4 5.2	9.6 3.4	28.8 32.6	7.2 3.2	<4.2 1.4	<3.5 5.0	6.6 9.4
2	24.6 19.2	2.3 0.6	18.9 24.2	9.5 7.4	26.2 24.0	43.9 50.6	10.6 9.8	16.3 14.8	<4.4 5.2	7.6 6.0	13.5 13.2	<2.1 2.2
3		47.2 48.6	122.6 169.8	73.4 95.8	28.8 22.2	17.7 25.6	16.5 16.0	11.3 14.4	15.5 21.4	5.4 4.4	5.2 2.6	2.4 2.8
4	50.6 48.0	44.7 36.6	35.8 45.8	30.3 38.4	33.4 43.6	28.2 30.4	10.9 9.8	<3.5 0.4	4.4 1.0	14.8 15.8	7.8 10.2	4.8 6.0
5		18.0 22.4	76.8 69.0	15.8 5.6	27.0 15.6	<3.5 0.2	14.9 14.0	6.4 6.6	12.6 12.0	7.1 5.2	<3.3 0.6	3.2 1.8
6	39.0 35.2	16.8 14.4	10.1 5.4	15.5 10.5	43.5 59.0	35.7 55.8	9.3 0.6	19.1 13.2	<4.4 4.6	<4.0 3.8	<3.3 6.0	<1.8 0.4
7		26.1 16.6	92.0 110.8	9.6 5.8	14.5 18.6	15.9 5.2	13.5 17.0	7.1 6.0	9.1 11.8	<4.0 5.4	11.0 14.2	5.5 6.2
8	42.0 25.2	16.5 12.2	46.4 49.2	18.1 19.0	15.2 22.2	19.1 16.2	10.6 11.6	<4.5 2.4	6.2 3.8	<4.0 5.0	<3.2 2.8	
9		10.7 12.6	10.7 19.6	36.2 43.4	10.9 20.2	3.7 1.0	7.4 7.6	<4.5 11.4	18.3 18.6	7.2 8.8	<3.0 3.2	
10	140.8 154.8	69.6 71.2	21.8 16.8	7.1 1.6	20.4 31.0	17.0 26.6	10.6 11.2	26.0 55.2	14.5 16.2	7.3 8.4	10.1 14.2	
11		22.5 16.0	4.3 9.2	15.5 8.2	19.3 22.0	<4.4 1.0	14.8 13.6	9.5 8.2	10.2 9.4	12.2 12.4	<2.4 5.2	
12	46.8 59.2	56.4 55.8	20.8 17.0	3.8 3.6	35.1 31.4	<4.5 11.0	14.8 18.0	<4.4 0.8	7.7 5.0	6.1 5.8	7.2 9.6	
13		25.9 13.0	21.6 29.2	54.1 42.8	7.1 4.6	6.1 1.6	18.4 19.8	28.5 54.8	12.5 9.2	<3.5 5.8	8.0 5.2	
14	44.0 41.2	29.4 20.8	28.1 40.8	6.6 10.0	18.9 24.6	4.0 5.8	32.3 25.0	<4.4 2.8	15.6 15.0	<5.5 1.4	5.5 4.2	
15		46.3 42.8	24.6 16.2	51.3 41.0	<3.8 5.2	3.3 5.0	16.7 10.8	<4.4 0.8	5.2 6.0	<3.4 1.4	3.7 2.6	
16	36.8 56.0	53.5 50.0	<3.5 6.6	8.5 4.6	<3.9 4.6	28.0 59.8	11.5 1.8	<4.3 4.8	9.1 9.2	<3.2 5.6	5.7 7.2	
17		15.6 15.4	38.9 45.8	23.1 52.6	15.6 12.2	43.0 45.2	20.4 21.2	<4.2 4.0	11.0 8.6	<3.0 4.0		

Continued

[illegible]

Table 5 Final Values of Observed and Calculated Structure Amplitudes—cont'd

$\frac{c-1}{h^k}$	0	1	2	3	4	5	6	7	8	9	10
0		104.6 90.2	<3.2 3.0	14.5 19.2	<5.2 10.0	30.0 28.4	<7.4 7.4	<8.0 1.8	12.9 13.6	<6.7 2.0	6.8 8.8
1	21.3 25.6	62.3 56.2	41.5 45.1	24.9 22.6	18.2 11.6	54.4 41.5	7.4 7.5	<8.0 8.8	<7.1 5.1	10.0 11.4	<5.4 5.4
2	55.3 67.8	16.8 22.6	44.5 57.8	40.4 40.3	11.0 2.5	10.3 16.8	28.8 25.4	15.9 18.6	21.6 25.6	<6.7 4.6	<5.4 6.0
3	23.0 19.6	96.0 75.6	34.4 34.5	38.0 41.5	22.9 17.2	44.5 42.2	5.2 7.4	13.9 17.3	14.6 18.8	10.0 6.7	9.7 12.0
4	16.7 17.8	70.0 56.3	20.1 14.2	15.9 21.4	17.4 25.9	21.7 12.7	11.7 14.0	17.9 16.4	11.4 10.7	<6.5 6.2	<5.2 4.3
5	102.0 138.0	43.2 37.2	18.3 22.7	29.0 51.9	12.0 12.2	14.2 15.7	19.7 14.8	7.0 10.2	16.4 16.5	5.2 6.5	10.2 16.6
6	68.0 76.0	42.6 45.4	51.0 53.5	25.3 25.9	16.5 20.7	41.8 37.8	6.5 12.4	4.1 10.1	16.4 13.2	5.2 3.1	<5.1 2.6
7	41.2 39.2	35.1 34.0	49.7 52.3	38.8 35.8	32.4 26.0	28.8 34.5	22.4 23.0	14.6 9.3	<7.1 4.0	5.2 7.3	<4.9 8.9
8	18.1 25.4	30.2 48.5	48.8 50.1	61.7 64.4	26.7 17.7	9.3 12.3	18.4 14.0	26.1 28.2	12.0 11.5	<6.2 4.0	<4.8 8.4
9	37.2 44.2	45.0 36.0	56.4 40.8	59.9 61.9	18.1 21.6	16.7 17.0	16.9 11.7	4.1 5.6	12.0 9.1	<6.2 5.9	<4.6 4.6
10	43.4 52.8	25.2 27.3	42.5 41.3	10.1 6.0	19.9 23.9	<6.2 8.5	8.8 6.7	23.9 17.3	14.9 13.3	<6.1 6.1	<4.6 4.8
11	27.5 18.2	29.4 24.8	50.3 55.3	28.5 22.0	16.4 11.9	22.5 54.2	6.6 3.1	17.4 16.9	9.7 7.5	<5.9 7.4	<4.5 6.2
12	28.7 39.4	35.0 37.2	16.4 23.6	13.2 18.9	10.3 8.4	12.5 17.0	22.6 19.6	12.9 7.2	18.3 15.5	<5.8 5.5	<4.1 5.5
13	8.8 12.6	13.0 17.1	14.8 13.2	<5.7 5.3	18.7 16.4	27.2 20.2	27.0 7.0	14.1 14.6	13.2 11.3	10.8 11.3	<3.8 7.3
14	16.4 6.2	14.9 4.8	36.0 33.4	15.4 16.3	11.2 11.5	25.6 21.1	<7.1 4.8	<7.1 7.7	<6.5 8.8	<5.4 3.4	<3.5 5.3
15	31.4 25.4	24.8 24.8	22.8 26.9	22.4 24.3	15.9 21.4	19.3 17.1	<7.1 0.7	17.1 16.3	<6.4 3.7	8.4 10.9	
16	23.6 24.6	30.8 25.3	33.2 31.2	19.0 19.3	10.0 12.9	18.7 17.8	10.0 8.5	12.6 10.5	8.7 6.6	<4.9 4.5	

Continued

Table 5 Final Values of Observed and Calculated Structure Amplitudes—cont'd

$\frac{c-1}{h^k}$	0	1	2	3	4	5	6	7	8	9	10
17	18.4 16.6	20.2 21.3	9.0 10.1	13.6 9.6	14.5 18.2	14.8 14.9	18.3 19.3	<6.8 2.6	<5.9 2.4	<4.6 5.4	
18	25.2 33.4	16.9 9.6	12.3 8.5	10.7 14.1	24.6 25.2	17.9 15.0	10.7 6.0	16.8 22.7	<5.8 7.6	<4.5 5.5	
19	22.0 17.8	<5.1 5.0	30.4 35.1	10.9 11.0	12.7 18.9	19.7 16.1	16.1 14.6	7.4 3.5	<5.5 7.5	<4.1 0.9	
20	17.4 15.0	10.0 10.7	21.1 8.4	22.7 19.1	<7.1 3.1	7.1 4.7	11.9 9.7	14.5 11.8	<5.2 3.8	<3.5 9.4	
21	20.2 22.2	9.9 12.5	21.3 9.3	15.1 15.1	14.8 15.5	11.4 12.8	15.5 11.4	4.9 8.7	<4.9 3.7		
22	13.3 14.2	9.7 6.4	9.0 9.0	30.3 32.7	10.9 11.7	12.7 9.1	9.3 12.8	<5.7 3.6	<4.5 3.7		
23	11.3 7.4	14.8 20.0	11.2 9.9	17.7 17.1	10.9 7.8	14.2 12.6	<6.3 3.7	<5.4 6.8	<4.1 1.4		
24	<7.1 4.6	7.7 5.9	17.7 21.1	<7.1 7.0	<7.0 3.7	8.6 8.5	4.9 4.4	6.5 6.6	<3.5 5.1		
25	<7.1 4.4	22.3 24.8	14.5 18.6	<7.1 2.7	<5.8 9.9	12.9 13.5	<5.7 6.4	<4.6 3.0			
26	6.5 12.4	16.5 16.9	14.6 14.2	<7.0 1.7	<6.7 2.8	<6.1 6.7	7.3 9.6	<4.1 3.4			
27	<7.1 6.0	<4.1 5.7	9.0 11.5	<6.7 6.3	10.5 12.7	10.6 11.3	5.7 10.6	<3.5 2.9			
28	5.7 8.2	<4.1 5.6	10.3 12.4	<6.7 6.8	<6.1 4.9	<5.4 8.1	<4.3 3.5				
29	<6.7 3.0	<5.4 4.6	<6.7 3.8	<6.2 2.4	7.4 10.9	7.7 9.7	<3.8 2.4				
30	6.4 7.2	<5.2 3.2	<6.1 2.6	10.1 12.2	<5.2 4.0	<4.5 3.6					
31	13.0 19.8	<4.8 3.2	<5.8 1.7	<5.4 1.7	<4.8 4.1	<3.8 1.6					
32	<6.1 3.0	7.1 9.8	<5.4 2.5	<5.7 6.5	<4.1 7.6						
33	<5.5 3.2	<4.1 8.1	<4.8 5.1	8.1 10.1	<3.3 2.6						
34	<4.9 4.0	<3.6 2.9	<4.1 4.6	<4.1 4.4							

Table 5 Final Values of Observed and Calculated Structure Amplitudes—cont'd

$\frac{c-2}{h^k}$	0	1	2	3	4	5	6	7	8	9	10
0	40.7	18.4	11.4	40.4	11.4	14.0	12.5	8.3	<4.2	<3.6	<2.8
	46.4	18.2	7.4	46.2	20.4	17.2	11.4	5.9	1.2	1.8	3.4
1	42.4	5.4	34.6	26.6	29.9	21.1	6.3	13.8	7.7	6.4	10.4
	49.0	9.8	33.4	26.4	32.1	15.6	11.4	17.9	7.3	2.7	11.4
2	15.9	30.4	16.8	19.1	24.3	21.6	21.6	21.6	8.8	6.2	8.0
	10.4	38.0	22.6	21.8	29.0	22.3	19.6	21.3	13.2	1.4	8.9
3	38.7	30.0	32.6	24.6	21.1	22.3	14.7	16.2	5.8	7.7	4.5
	60.4	30.5	33.7	27.4	23.4	25.8	14.0	17.0	4.5	4.7	4.5
4	40.3	44.2	55.3	17.9	11.9	17.7	11.0	6.6	11.2	7.7	<2.8
	52.2	52.3	60.8	21.6	9.9	15.2	9.1	8.1	8.6	8.6	1.2
5	19.6	40.4	34.8	31.1	9.5	18.0	12.8	16.8	10.4	6.1	5.1
	14.6	48.2	41.7	20.6	3.8	12.5	17.0	14.3	9.0	7.2	0.7
6	22.1	16.7	43.5	12.8	16.7	33.7	13.3	11.9	13.5	6.7	<2.7
	22.2	16.3	44.7	9.1	17.4	33.5	14.8	13.0	14.8	7.0	1.8
7	17.4	26.2	13.3	23.1	21.6	18.3	15.5	10.3	<4.0	5.9	2.5
	8.0	16.8	18.5	21.4	24.1	22.4	10.8	11.2	2.9	5.8	2.5
8	69.4	38.0	15.2	11.0	13.9	24.4	11.6	4.2	15.5	6.0	2.5
	91.5	41.4	16.8	8.4	9.5	21.4	6.2	3.6	18.4	7.5	3.6
9	28.0	23.8	31.7	8.0	28.6	27.2	14.9	7.9	9.4	3.4	7.0
	29.2	15.8	29.1	10.3	27.0	28.6	16.0	8.8	7.9	5.0	9.6
10	28.4	10.9	20.8	16.5	8.3	<3.9	11.7	3.0	8.8	7.7	<2.1
	52.8	2.4	20.9	16.0	5.8	3.9	10.6	2.7	4.6	6.1	4.5
11	41.1	27.2	17.7	26.3	10.1	22.8	13.5	7.9	6.1	<3.3	<2.1
	30.4	25.6	16.5	25.6	10.9	22.8	13.6	8.7	8.1	3.5	0.7
12	27.2	38.0	2.2	<3.6	26.9	13.4	11.7	15.5	7.1	6.5	4.9
	29.0	37.9	5.1	8.9	27.6	13.4	12.4	16.4	2.9	4.8	6.4
13	38.0	13.7	4.8	20.2	13.5	12.2	19.8	10.9	5.2	<3.0	
	52.4	7.2	5.5	22.7	17.2	12.7	16.1	10.8	4.5	4.1	
14	12.9	16.9	19.3	18.8	9.2	17.7	16.4	13.3	8.9	3.6	
	11.4	12.3	13.3	24.3	7.7	18.7	16.8	16.0	5.1	5.0	
15	18.2	17.6	23.7	10.1	10.9	7.1	7.9	9.8	4.9	7.6	
	17.0	22.4	27.9	6.7	7.3	6.7	4.9	6.7	7.3	6.3	
16	28.7	13.8	29.8	23.8	14.0	7.9	8.9	9.2	10.1	3.6	
	31.6	12.2	35.0	21.0	13.5	6.0	6.5	9.1	10.8	2.4	

Continued

Table 5 Final Values of Observed and Calculated Structure Amplitudes—cont'd

$\frac{c-3}{h^k}$	0	1	2	3	4	5	6	7	8	9
0		45.2	15.7	15.5	29.4	<5.4	<5.8	24.4	<5.3	3.0
		59.4	17.2	24.4	26.0	12.8	1.2	21.2	2.0	9.0
1	28.0	9.1	27.2	41.8	14.3	19.4	12.7	14.2	15.8	5.0
	27.0	14.2	29.1	33.1	13.2	17.4	11.6	16.3	18.2	7.0
2	34.0	23.3	20.6	5.4	14.3	15.7	29.4	14.2	5.9	5.0
	41.0	23.6	22.3	7.3	14.6	22.1	32.2	14.0	6.3	6.3
3	15.6	24.2	31.5	14.8	17.5	6.3	13.0	9.2	7.3	5.0
	9.0	28.1	36.3	19.0	17.7	7.2	11.0	11.8	9.6	5.0
4	28.4	29.2	28.7	7.9	20.3	21.4	9.2	17.2	7.3	<5.0
	34.8	24.2	30.0	7.4	21.6	20.4	7.6	19.4	3.3	4.9
5	10.2	26.4	24.1	41.4	25.2	24.2	14.7	7.3	10.6	<4.1
	24.4	19.4	19.4	48.9	25.5	21.4	12.1	1.1	11.4	3.3
6	15.0	16.3	9.6	19.3	13.8	<5.4	17.8	<6.4	6.4	6.9
	17.2	12.5	17.3	18.3	17.6	4.7	22.7	4.0	3.2	9.1
7	20.1	14.5	20.1	22.3	9.1	16.7	8.1	17.0	6.4	5.1
	17.4	28.3	19.0	24.6	3.0	16.8	5.7	19.7	7.0	5.4
8	18.0	19.8	24.6	12.4	10.2	9.1	13.2	<5.4	6.9	<4.0
	27.4	11.3	25.0	12.9	9.4	6.6	14.1	2.0	6.1	2.4
9	5.3	22.1	22.9	22.3	14.8	7.9	15.5	8.9	11.9	<5.8
	5.6	25.7	24.2	25.7	6.6	6.6	21.2	9.8	9.7	1.3
10	38.3	30.2	12.7	15.5	7.1	7.3	14.7	15.6	6.6	4.1
	38.6	33.0	18.3	17.2	9.5	5.6	10.6	11.5	8.0	9.4
11	<2.8	<2.8	26.2	14.7	18.8	13.8	10.4	6.1	9.9	<3.5
	3.5	2.0	31.1	14.0	10.2	13.4	7.5	3.1	13.5	1.4
12	24.4	21.6	20.0	8.7	12.5	19.0	19.0	6.1	<5.1	<3.3
	32.8	24.7	26.1	7.8	15.5	23.5	19.0	3.5	2.2	0.6
13	10.1	18.6	7.4	7.6	15.3	9.4	10.7	3.9	6.1	<3.0
	13.0	11.5	9.1	8.8	15.9	5.0	15.1	3.7	9.3	5.2
14	36.2	15.7	15.4	5.4	<5.6	23.2	15.3	5.9	5.4	<2.8
	45.0	17.3	6.5	10.4	6.6	30.2	9.2	6.1	3.5	4.9
15	<3.1	34.8	18.5	6.4	17.0	<5.8	<4.5	5.8	5.3	
	5.0	40.5	25.7	4.7	15.5	3.9	1.5	7.5	7.4	
16	8.9	12.5	19.3	14.5	11.9	9.7	13.0	6.1	9.1	
	8.4	12.2	13.0	12.3	13.6	6.8	12.9	4.2	12.4	

Continued

Table 5 Final Values of Observed and Calculated Structure Amplitudes—cont'd

$\frac{c-3}{h^2}$	0	1	2	3	4	5	6	7	8	9
17	<3.1 5.6	10.6 11.3	12.5 13.3	21.3 27.8	16.1 11.0	7.3 10.7	6.1 0.6	9.9 12.7	6.4 5.6	
18	<4.6 7.0	9.1 3.4	9.7 8.4	15.8 15.5	13.0 12.1	<6.3 6.5	5.9 4.2	5.8 6.9	<3.3 1.5	
19	<4.6 1.2	17.0 16.8	13.8 8.2	18.1 17.0	18.7 20.0	12.0 7.5	10.2 11.5	5.4 5.1	3.3 1.8	
20	33.3 33.6	19.3 16.1	13.5 11.0	11.9 7.3	11.5 5.1	<6.1 5.3	9.1 2.3	5.4 5.9		
21	14.3 8.0	7.4 5.4	14.3 14.6	7.3 7.3	11.7 5.4	<5.9 5.6	5.9 8.0	7.6 10.8		
22	15.6 20.6	11.9 5.9	17.2 18.2	13.5 9.1	<5.3 4.2	9.4 8.5	<4.9 4.6	<3.3 3.6		
23	16.6 7.0	9.7 3.4	10.7 9.5	10.4 6.5	9.4 10.5	<5.4 2.5	5.6 6.5	3.3 2.7		
24	11.9 7.2	<6.3 3.0	10.9 9.3	<6.4 5.1	5.8 5.6	12.2 15.6	<4.1 3.5			
25	<5.4 0.4	11.2 10.2	9.1 7.4	5.8 7.4	6.1 4.0	5.3 1.5	3.8 4.3			
26	9.9 9.0	5.4 9.7	11.1 7.0	8.7 3.7	9.2 9.3	5.4 4.4	<3.1 5.9			
27	<4.9 3.2	<4.0 3.3	10.4 12.7	5.9 6.1	5.3 1.3	4.0 0.9				
28	5.4 4.2	<3.8 3.7	8.7 6.0	<4.3 3.1	<3.8 3.8	<2.8 6.9				
29	8.1 8.0	6.1 9.3	5.4 2.5	9.4 8.7	4.1 6.6					
30	8.7 10.0	<3.3 3.3	<3.8 0.8	<3.5 2.4						
31	9.7 9.4	<3.6 3.7	<3.3 4.0	<2.8 4.9						
32	<3.1 1.6	<3.0 4.8								

Table 5 Final Values of Observed and Calculated Structure Amplitudes—cont'd

$\frac{c-4}{h^k}$	0	1	2	3	4	5	6	7	8	9
0	12.0 0.8	15.3 19.6	7.7 4.0	16.8 26.8	7.3 12.2	19.7 20.4	16.3 10.8	8.5 12.4	11.2 13.8	<3.0 2.6
1	16.4 22.6	19.3 15.0	16.7 15.4	16.7 10.4	18.3 24.3	17.6 13.8	14.5 8.1	8.5 8.1	<4.3 1.6	5.0 7.9
2	13.7 6.8	20.2 20.3	11.5 7.0	12.8 10.6	14.0 8.1	18.0 13.7	9.2 2.1	12.2 8.0	7.3 9.1	<2.8 3.4
3	12.8 21.8	16.7 22.2	22.0 19.7	16.0 7.3	11.5 7.0	8.2 14.5	21.5 21.5	8.8 11.3	6.0 4.7	5.7 9.8
4	4.2 2.2	12.7 18.5	25.0 27.2	14.8 23.1	14.8 12.3	16.0 11.3	9.2 6.7	16.3 18.8	6.0 2.2	5.3 7.4
5	6.8 0.6	19.5 20.2	12.2 7.7	14.5 7.4	<5.8 4.6	12.3 7.4	<5.5 6.0	<5.0 4.1	<4.2 2.4	
6	10.2 14.6	3.3 1.0	25.5 36.9	14.5 10.5	13.7 5.7	12.8 10.7	16.3 14.0	10.0 4.7	6.7 6.7	
7	11.2 16.2	5.3 11.6	18.0 21.1	13.8 13.8	14.5 13.0	27.2 32.5	17.2 14.9	<5.0 1.9	6.5 3.6	
8	14.3 15.8	11.2 8.6	11.5 12.6	<5.7 3.3	9.5 11.8	<5.7 2.4	14.0 13.4	8.0 7.1	7.8 10.8	
9	20.5 24.8	7.2 12.2	16.5 18.8	15.2 17.1	18.0 21.2	9.3 9.0	<5.3 0.4	<4.7 4.6	5.3 3.1	
10	<4.5 13.6	14.7 17.2	13.8 17.0	17.2 22.8	7.5 8.1	10.8 6.4	8.7 4.1	12.0 14.1	<3.7 7.4	
11	24.5 27.4	13.8 16.2	<5.7 7.9	13.3 10.5	16.3 13.4	9.8 6.3	<5.3 5.5	7.5 8.9	<3.5 7.8	
12	5.7 0.6	10.4 12.2	12.3 12.6	9.5 12.1	<5.8 0.8	14.3 14.5	<5.2 2.8	7.7 8.0	<3.3 2.4	
13	10.9 21.2	22.2 24.2	11.0 5.3	12.5 7.2	13.2 15.2	<5.5 0.9	<3.0 3.4	<4.2 6.1	<3.0 2.5	
14	<5.8 5.6	<4.7 2.6	13.7 8.4	10.0 19.3	11.8 11.3	13.8 13.3	8.5 5.3	<4.0 5.7	<2.8 2.0	
15	5.8 9.2	7.5 8.3	<5.8 4.2	10.0 10.9	<5.5 6.2	<5.3 5.0	<4.7 6.1	<4.0 4.8		
16	12.0 14.8	15.3 15.3	11.5 16.9	<5.7 4.8	9.3 5.7	<3.2 3.3	7.5 8.3	<3.7 2.7		

Continued

Table 5 Final Values of Observed and Calculated Structure Amplitudes—cont'd

$\frac{c-4}{h^k}$	0	1	2	3	4	5	6	7	8	9
17	24.5 33.0	12.0 9.6	12.3 11.5	13.8 13.7	10.8 7.5	14.2 16.7	<4.5 5.8	<3.5 4.8		
18	7.3 9.2	8.8 9.8	<5.7 4.5	7.8 5.2	10.7 11.9	7.8 7.6	<4.2 8.2	7.3 2.3		
19	11.8 6.6	10.9 10.1	9.7 9.1	<5.3 4.6	<5.2 2.6	10.4 14.3	<4.0 3.7	<2.8 5.3		
20	<5.5 1.0	13.7 19.5	13.3 19.2	<5.3 4.0	<5.0 4.5	<4.5 2.2	8.5 6.7			
21	12.7 8.6	10.3 14.1	<5.3 8.1	12.2 13.8	<4.7 4.1	<4.2 2.5	<3.3 7.5			
22	<5.3 2.0	7.5 3.1	<5.2 2.4	8.5 10.3	<4.5 4.6	<4.0 5.7	<2.8 0.5			
23	8.0 11.6	5.8 3.0	8.0 8.5	7.7 6.3	9.5 13.4	6.0 8.3				
24	5.0 4.4	6.2 8.4	<4.7 4.0	8.8 9.3	6.7 5.5	6.8 7.2				
25	9.0 10.0	<3.8 0.7	<4.3 4.6	6.7 7.1	5.0 3.3					
26	<4.3 3.2	8.3 9.7	5.8 5.2	6.3 8.1	<3.0 2.2					
27	4.7 7.0	3.2 3.5	<3.7 3.4	7.0 10.0						
28	4.2 2.8	3.0 3.9	4.7 5.7	4.5 4.6						
29	4.3 4.6	5.0 3.8	<2.3 2.7							
$\frac{c-5}{h^k}$	0	1	2	3						
0					30.8 22.6		12.4 5.2		<13.6 1.7	
1		<8.4 0.4			9.8 11.7		10.3 7.8		13.6 13.5	
2		27.9 22.0			18.9 22.9		10.3 14.7		<13.6 8.0	
3		<8.4 3.2			15.3 13.3		<12.4 9.4		13.6 10.3	

Table 5 Final Values of Observed and Calculated Structure Amplitudes—cont'd

$\frac{c-5}{h^k}$	0	1	2	3
4	15.3 5.2	4.8 7.2	<12.4 6.8	
5	20.3 22.2	18.2 14.2	<12.4 7.1	
6	<8.4 4.8	16.2 13.1	<10.3 4.3	
7	<8.4 1.2	4.8 10.4	12.4 7.1	
8	<8.4 8.6	6.0 15.2	12.2 3.7	
9	<8.4 5.4	<4.8 8.6	12.2 15.6	
10	12.4 8.2	<4.8 14.6		
11	16.8 15.2	<4.8 5.9		
12	29.0 30.0	4.8 12.		
13	<6.5 4.0	<4.8 1.6		
14	<6.5 6.4	7.9 8.2		
15	16.5 9.0	6.4 13.3		
16	5.5 5.0	<4.5 6.2		
17	<6.2 6.6	<4.3 3.0		
18	13.2 21.8	<4.2 4.3		
19	<5.7 6.4	<4.1 7.2		
20	10.0 9.8	<4.0 3.3		
21	<5.2 2.4	<3.6 4.5		

Continued

Table 5 Final Values of Observed and Calculated Structure Amplitudes—cont'd

$\frac{c-5}{h^k}$	0	1	2	3
22	<4.8 10.2	<3.4 2.8		
23	<4.5 3.0	<3.1 6.1		
24	<4.1 2.8	<2.9 1.5		
$\frac{c-6}{h^k}$	0	1		
0		21.5 24.0		<5.4 5.5
1		<9.5 5.0		<5.4 7.5
2		<9.5 2.6		<5.4 8.2
3		<9.5 7.2		<5.4 4.7
4		9.5 9.8		<5.4 6.0
5		10.8 5.2		14.3 20.2
6		9.3 5.4		
7		<9.1 2.2		
8		11.0 8.4		
9		<8.9 2.6		
10		15.1 14.0		
$\frac{c-7}{h^k}$	0	1		
0				3.3 4.0
1		<6.2 1.0		<3.3 7.9
2		14.1 7.8		3.3 10.2

Table 5 Final Values of Observed and Calculated Structure Amplitudes—cont'd

$\frac{c-z}{h^k}$	0	1
3	<4.3 3.2	<3.3 3.0
4	11.5 3.0	<3.3 7.7
5	<4.8 5.0	6.7 9.1
6	5.5 1.0	

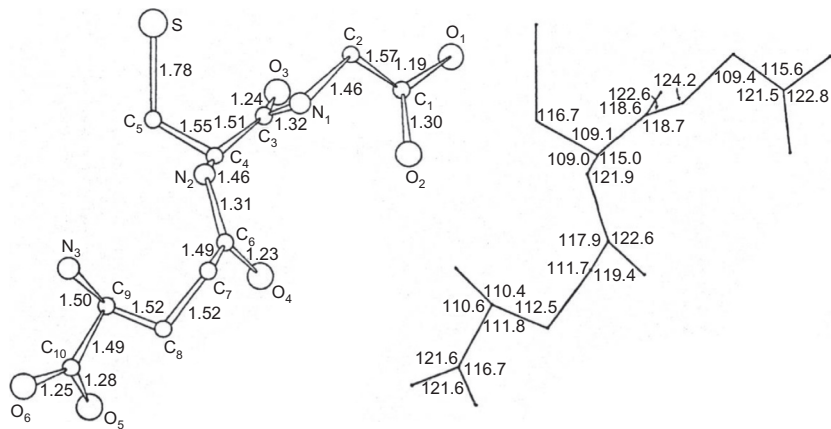


Figure 8 The glutathione molecule showing values of bond lengths and bond angles [28].

Table 6 Displacements of the Atoms from the Planes of the Peptide Links [28]

Displacement (Å)		Displacement (Å)	
C ₂	+0.034	C ₄	−0.090
N ₁	−0.045	N ₂	+0.121
C ₃	−0.002	C ₆	+0.049
C ₃	−0.009	C ₄	−0.005
C ₄	+0.022	C ₇	−0.075

The displacements of the atoms from these planes are shown in Table 6. The planes make angles of 42.4° and 2.0°, and 47.6°, and 42.1°, 9.3°, and 46.4° with the *a*-, *b*-, and *c*-axes, respectively, and the angle between the planes is 94.4° [28].

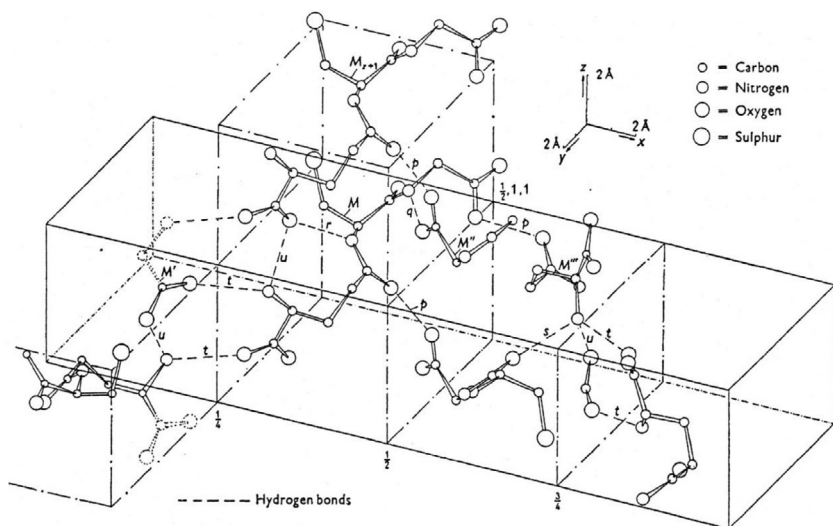


Figure 9 Clinographic projection of the structure, showing the hydrogen-bonding arrangement [28].

The structure is represented by the clinographic projection (Figure 9), which shows two complete molecules and certain portions of others which illustrate the hydrogen-bonding arrangement. Molecule M is related to molecules M' , M'' , M''' by the screw diad axes at $(\frac{1}{4}, 0, z)$, $(\frac{1}{2}, \gamma, \frac{1}{4})$, and $(\frac{1}{2}, \gamma, \frac{3}{4})$, respectively, and to molecules M_{z+1} , M_{y-1} by unit translations in the z and $-y$ directions, respectively. The molecule has adopted an S-shaped configuration, running diagonally downward in the c direction from the glycine carboxyl group at $x = \frac{1}{2}$, $\gamma = 1$, $z = 1 + \frac{1}{3}$, to the glutamic acid carboxyl group at $x = \frac{1}{2}$, $\gamma = 0$, $z = \frac{1}{2}$ approximately. Certain interatomic distances and angles present in the structure are given in Table 7 [28].

There are no internal hydrogen bonds in the molecule, the shortest distance N_1-O_4 being 3.5 Å, and the nearest oxygen atom, O_3 , to the sulfur atom being at a distance of 3.6 Å from it [28].

The molecules are held together in the structure by a three-dimensional network of hydrogen bonds. Oxygen atom O_2 of the glycine carboxyl group, which lies in a plane almost parallel to the c -axis, forms a hydrogen bond with carbonyl oxygen atom O_4 of molecule M''' . This bond is 2.66 Å long, and is represented by bonds of the type p in Figures 4 and 9. Peptide nitrogen atom N_1 forms a hydrogen bond, q , 2.88 Å long, to glycine carboxyl oxygen atom O_1 of molecule M^2 . Peptide nitrogen atom N_2 forms

Table 7 Interatomic Distances and Angles [28]

Distance (Å)		Angle (°)	
S–O ₃	3.63		
S–O _{6z+1} y+1	3.53		
S–O _{5z+1}	3.57		
S–S'	4.41		
S–O _{5z+1} y+1	3.90		
N ₁ –O ₄	3.55	C ₃ –N ₁ –O ₁ ²	131.5
N ₁ –O _{4z+1}	3.28	C ₂ –N ₁ –O ₁ ²	100.7
N ₁ –O ₁ ²	2.88	C ₁ ² –O ₁ ² –N ₁	142.1
O ₁ –C ₆	3.00	C ₁ –O ₂ –O ₄ ^{'''}	108.6
O ₂ –O ₄ ^{'''}	2.66	C ₆ ^{'''} –O ₄ ^{'''} –O ₂	116.6
O ₁ –O ₄ ^{'''}	3.18	N ₂ –O _{5z+1} –N ₃	88.6
O ₁ –O _{4z+1} ^{'''}	3.27	C _{10z+1} –O _{5z+1} –N ₃	153.7
N ₂ –O _{5z+1}	2.98	C ₆ –N ₂ –O _{5z+}	110.9
N ₃ –O _{6z+1}	3.21	C ₄ –N ₂ –O _{5z+1}	123.8
N ₃ –O ₆ '	2.89	C ₉ –N ₃ –O ₆	130.0
N ₃ –O _{5z+1}	2.68	C ₁₀ –O ₆ –N ₃	149.9
		C ₉ –N ₃ –O _{5z+1}	106.7
		C _{10z+1} –O _{5z+1} –N ₃	106.8
N ₃ –O _{3y+1}	2.81	C ₉ –N ₃ –O _{3y+1}	115.3
		N ₃ –O _{3y-1} –C _{3y-1}	124.7

a hydrogen bond of type *r*, 2.98 Å long, to oxygen atom O₅ of molecule *M*_{z+1}. As the plane of the amino-carboxyl group lies almost parallel to the *c*-axis, nitrogen atom N₃ is in a position to form three hydrogen bonds: type *s*, 2.81 Å long, with oxygen atom O₃ of molecule *M*_{y-1}; type *t*, 2.89 Å long, with oxygen atom O₆ of molecule *M'*; and type *u*, 2.68 Å long, with oxygen atom O₅ of molecule *M*_{z+1} [28].

All other nonbonded atoms in the structure are at the usual van der Waals distances from one another, with the exception of C₆ and O₁ of molecule

M^2 , which are 3.00 Å apart. The sulfur atom has four oxygen atoms as nearest neighbors (Table 7), and the distance between neighboring sulfur atoms is 4.41 Å [28].

4.4 Thermal Methods of Analysis

4.4.1 Melting Behavior

Melting point: 195 °C

4.4.2 Differential Scanning Calorimetry

The glutathione has been characterized by differential scanning calorimetry which exhibits a significant endo peak around 200 °C. The differential scanning calorimetry thermogram of glutathione is substantially depicted as in Figure 10. Differential scanning calorimetry studies were carried out using differential scanning calorimeter equipped with an intercooler (Shimadzu DSC-60, Shimadzu Corporation, Koyoto, Japan). Indium/zinc standard were used to calibrate the temperature and enthalpy scale. The samples were hermetically sealed in an aluminum pans and heated at a constant rate of 10 °C/min over a temperature range of 25–300 °C. Inert atmosphere was maintained by purging nitrogen gas at a flow rate of 50 ml/min.

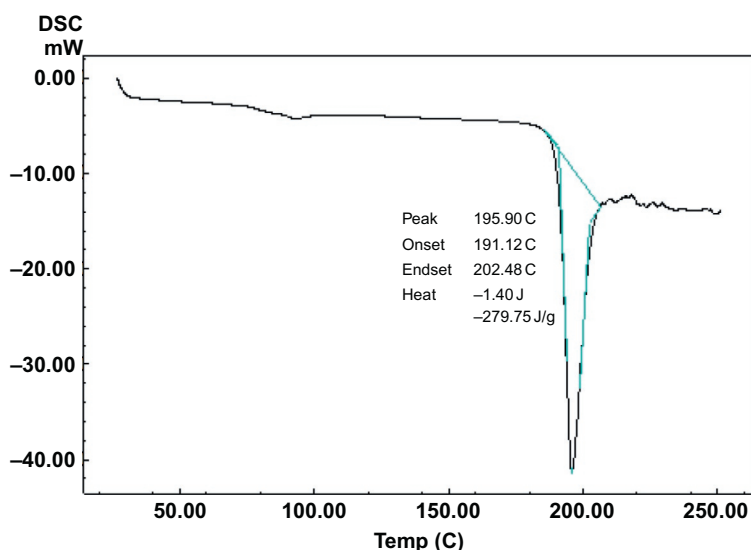


Figure 10 Differential scanning calorimetry thermogram of glutathione.

4.5 Spectroscopy

4.5.1 UV-Vis Spectroscopy

The ultraviolet (UV) absorption spectrum of glutathione in aqueous methanol was scanned from 200 to 400 nm, using UV/VIS spectrometer (Shimadzu ultraviolet–visible spectrophotometer 1601 PC). The compound exhibited a maximum at 206 nm (Figure 11).

4.5.2 Vibrational Spectroscopy

The infrared absorption spectrum of glutathione was obtained in KBr pellet using a Perkin-Elmer infrared spectrophotometer. The IR spectrum is shown in Figure 12. The principal peaks were observed at (3250–3628), 3020, 2523, 1712, 1598 cm^{-1} . Assignments for the major infrared absorption band are listed in Table 8. Principal peaks are at 3348.2, 3252.4, 3029.6, 2525.49, 1712.6, and 1601.9 cm^{-1} .

4.5.3 Nuclear Magnetic Resonance Spectrometry

The Proton and Carbon-13 nuclear magnetic resonance (NMR) spectra of glutathione were registered with a Varian Gemini 200 spectrometer (200 MHz). Chemical shifts were expressed in parts per million (ppm) with respect to the tetramethylsilane (TMS) signal for ^1H and ^{13}C NMR spectra (Figures 13 and 14, respectively).

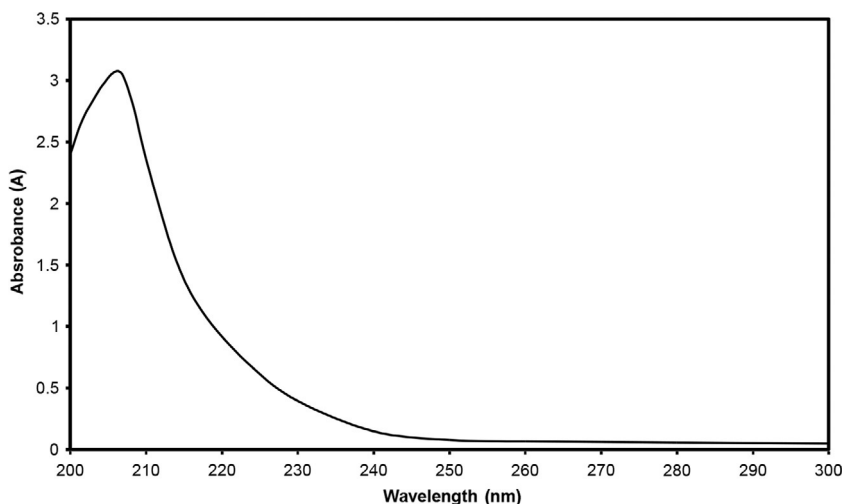


Figure 11 Ultraviolet absorption spectrum of glutathione in aqueous methanol.

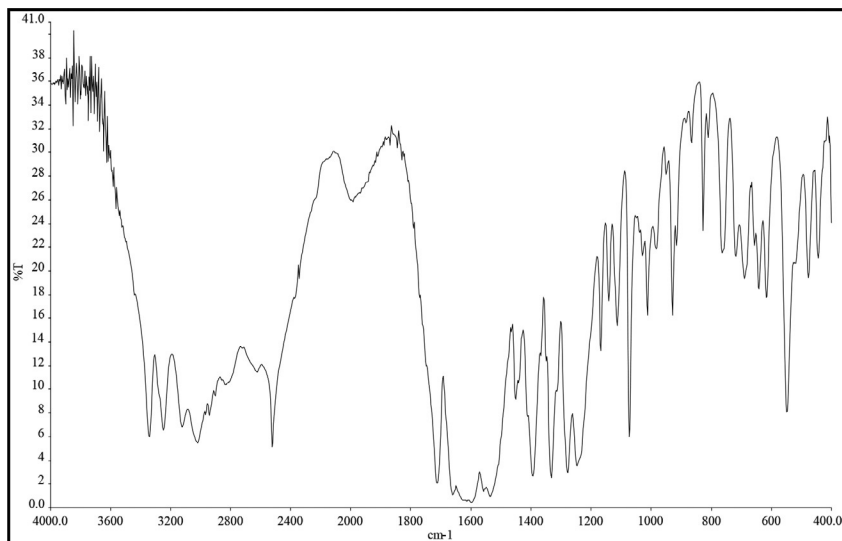


Figure 12 The infrared absorption spectrum of glutathione (KBr disc).

Table 8 Vibrational Assignments for the Glutathione Infrared Absorption Bands
Frequency (cm^{-1})

Frequency (cm^{-1})	Assignment
3250–3628	–OH, NH, NH_2
3020	C–H
2523	–SH
1712	–C=O acid
1598	–C=O amide

4.5.3.1 ^1H NMR Spectra

The one-dimensional proton ^1H NMR spectrum of glutathione dissolved in DMSO is shown in [Figure 13](#). The corresponding spectral assignments of ^1H NMR for glutathione are listed in [Table 9](#).

4.5.3.2 ^{13}C NMR Spectra

The one-dimensional ^{13}C NMR spectrum of glutathione dissolved in DMSO, which was recorded at 24 °C, is shown in [Figure 14](#). The assignments for the observed resonance bands associated with the various carbons are listed in [Table 10](#). [Figures 15–19](#) show the HMBC, DEPT 90, and DEPT 135, COSY and HSQC NMR spectra, respectively.

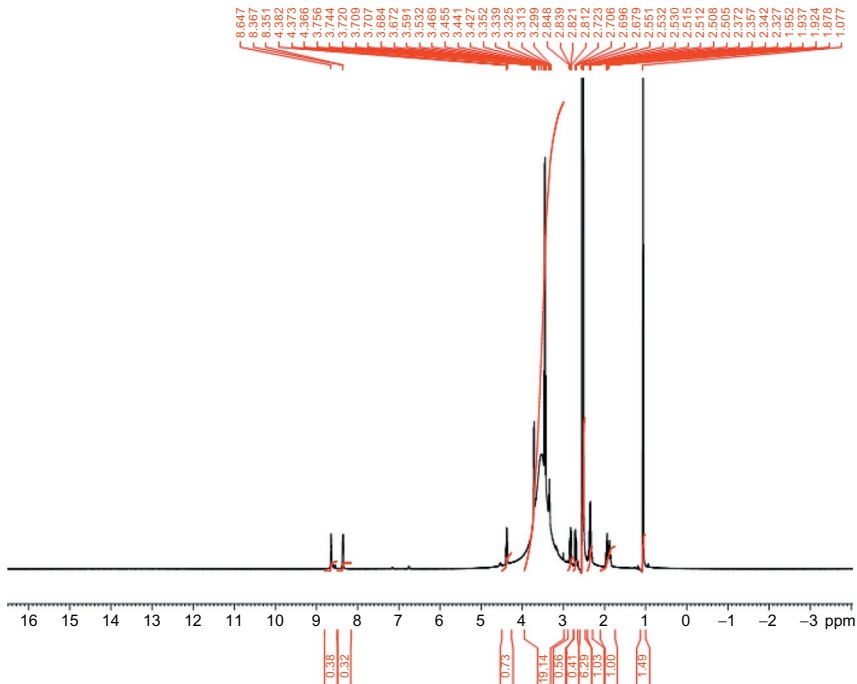


Figure 13 The ¹H NMR spectrum of glutathione in DMSO-d₆.

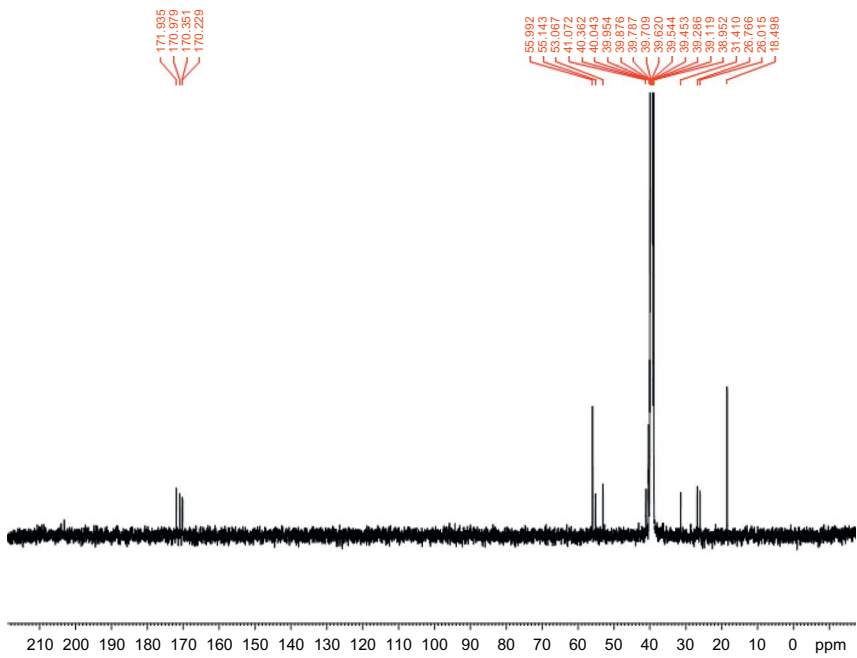
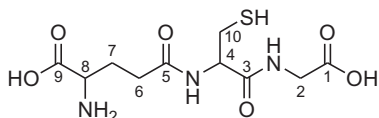


Figure 14 The ¹³C NMR spectrum of glutathione in DMSO-d₆.

Table 9 Assignment of the Resonance Bands in the ^1H NMR Spectrum of Glutathione

Chemical Shift Relative to TMS	Number of Protons	Multiplicity	Assignment (Proton at Carbon Atom)
3.72	2	m	2
4.37	1	m	4
2.35	2	m	6
1.94	2	m	7
3.33	1	m	8
2.83	1	dd (13.5, 4.5)	10a
2.70	1	dd (13.5, 8.5)	10b

Table 10 Assignment of the Resonance Bands in the ^{13}C NMR Spectrum of Glutathione

Chemical Shift (ppm)	Carbon Number
171.94	1
41.07	2
170.23	3
55.14	4
170.98	5
31.41	6
26.77	7
53.07	8
170.35	9
26.02	10

4.6 Mass Spectrometry

Mass spectra of glutathione, carried out with electron impact method, were registered using Agilent 1200 series HPLC/MS spectrometer. [Figure 20](#) shows the detailed mass fragmentation pattern and [Table 11](#) shows the proposed mass fragmentation pattern of the drug substance.

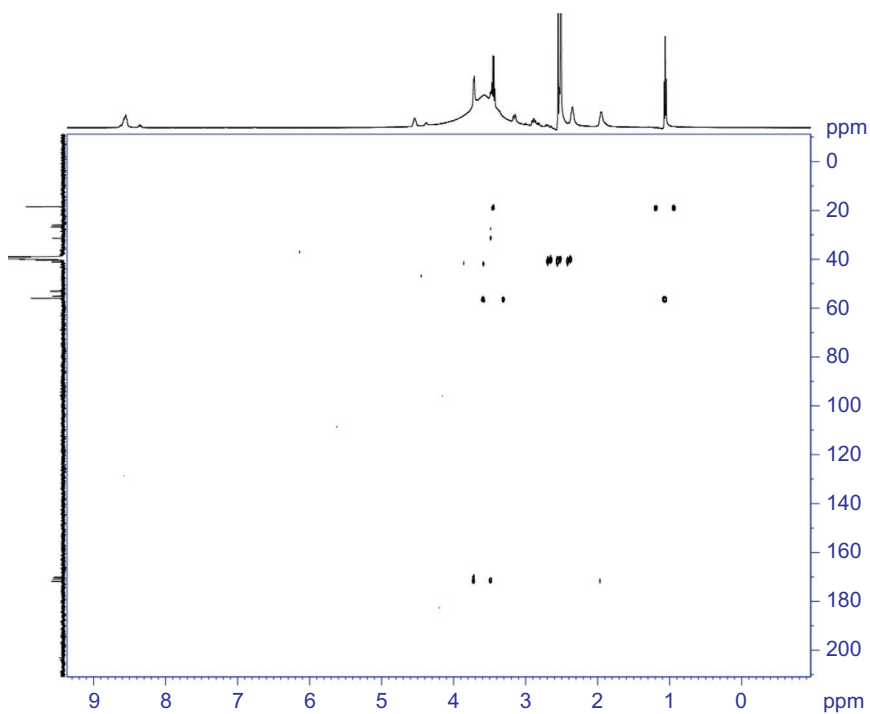


Figure 15 The HMBC NMR spectrum of glutathione in DMSO-d₆.

55.14
53.02
52.20
40.02
39.16
39.70
39.53
39.36

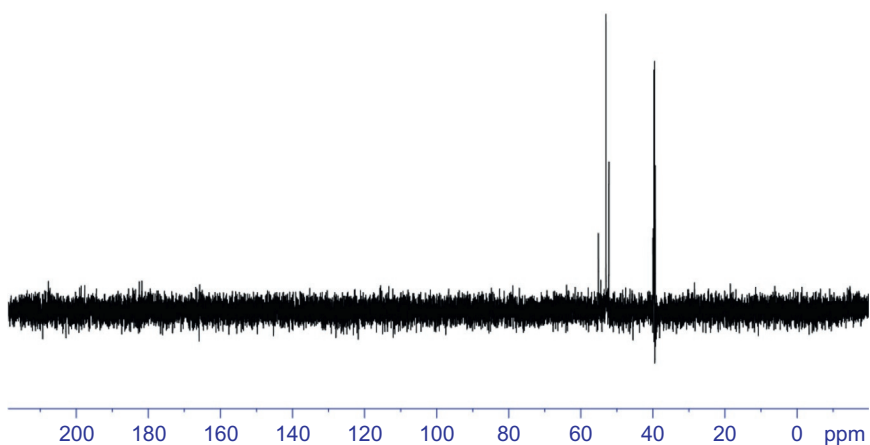


Figure 16 The DEPT-90 ¹³C NMR of glutathione in DMSO-d₆.

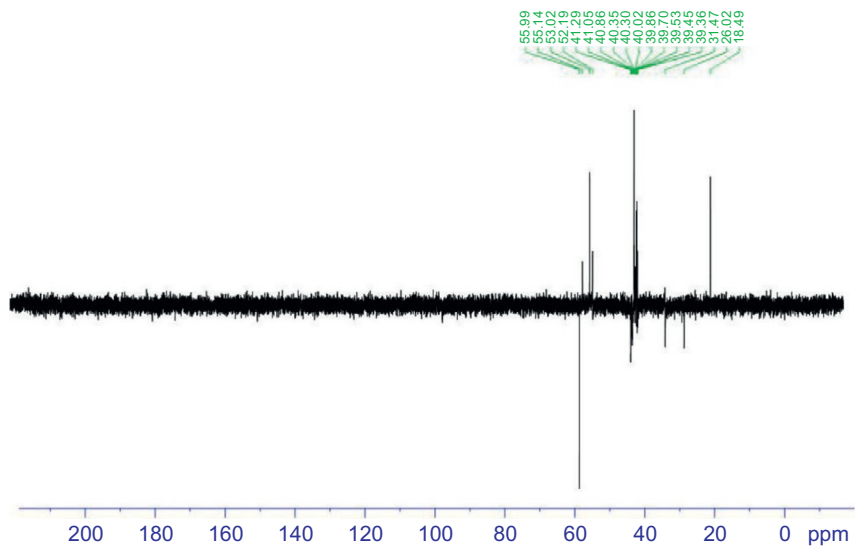


Figure 17 The DEPT 135 ¹³C NMR of glutathione in DMSO-d₆.

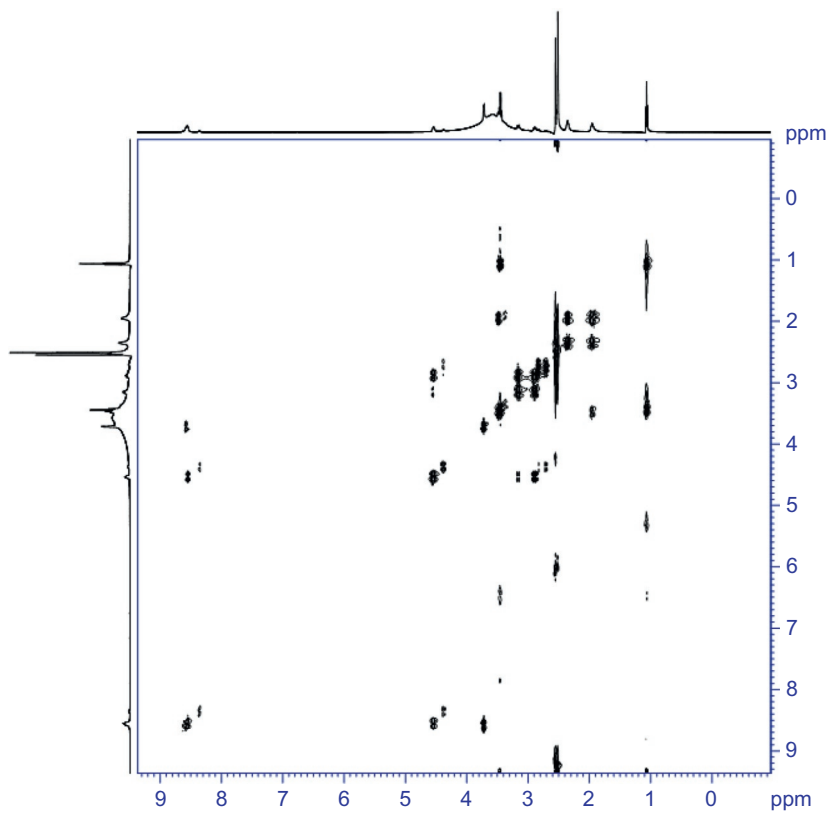


Figure 18 The COSY NMR spectrum of glutathione in DMSO-d₆.

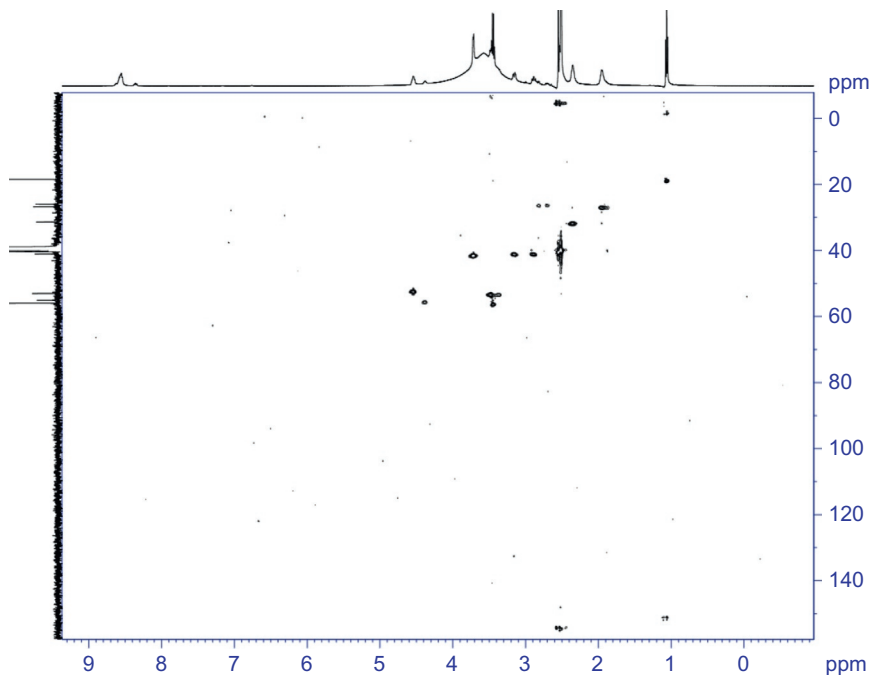


Figure 19 The HSQC NMR spectrum of glutathione in DMSO-d₆.

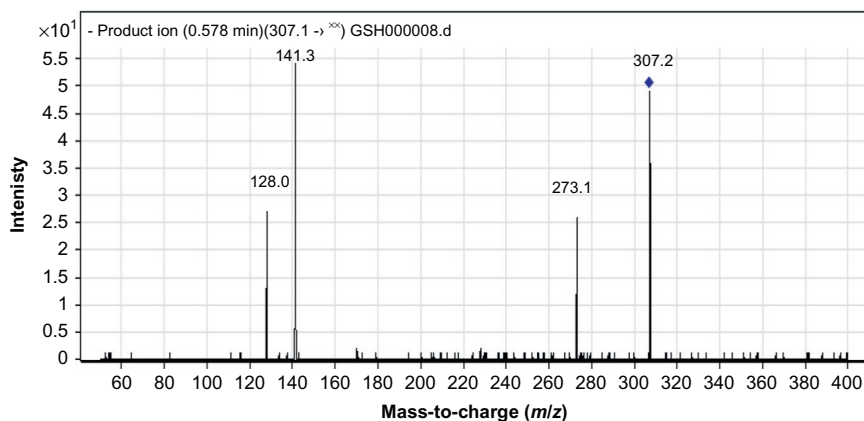
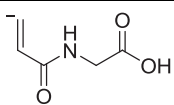
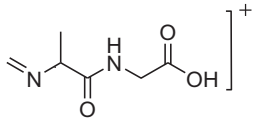
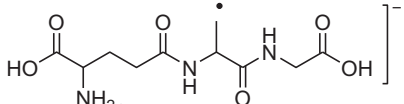
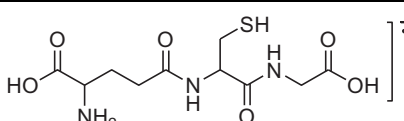


Figure 20 Mass spectrum of glutathione.

Thakur and Balaram [42] studied the fragmentation of the positive and negative ions of oxidized glutathione and contryphan, the peptide disulfides under mass spectrometric conditions which yields distinctly different product ion distributions. A negative ion upon collision induced dissociation yields intense product ion, which correspond to cleavage at the disulfide linkage.

Table 11 Mass Spectral Fragmentation Pattern of Glutathione

<i>m/z</i>	Relative Intensity (%)	Formula	Structure
128.0	50.0	C ₅ H ₆ NO ₃	
141.3	100.0	C ₆ H ₉ N ₂ O ₂	
273.1	48.15	C ₁₀ H ₁₅ N ₃ O ₆	
307.2	90.74	C ₁₀ H ₁₇ N ₃ O ₆ S	

The complete assignment of the product ions obtained upon fragmentation of oxidized glutathione in an ion trap is presented. The cleavage at the disulfide site is mediated by abstraction of C^αH and C^βH protons resulting in product ions derived by neutral loss of H₂S₂ and H₂S. The formation of peptide thioaldehydes and persulfides at the cysteine sites is established. Dehydroalanine formation at the cysteine residue is predominant.



METHODS OF ANALYSIS

5.1 Compendial Methods

5.1.1 British Pharmacopeia Methods [4]

Identification

- A.** It complies with the test for specific optical rotation (see Tests).
- B.** Infrared absorption spectrophotometry The infrared absorption spectrum should be carried out as described in the general procedure (2.2.24) using KBr Pellet and be compared with an infrared absorption spectrum obtained from *glutathione CRS*.

Tests:

Solution S

Dissolve 5.0 g in *distilled water R* and dilute to 50 ml with the same solvent.

Appearance of solution

When the test is carried out according the general procedure (2.2.1), Solution S is clear and when the test is carried out as described in the general procedure (2.2.2, *Method II*), solution S is colorless.

Specific optical rotation

When the test is carried out as described in the general procedure (2.2.7), and using a dried substance, the specific optical rotation is -15.5 to -17.5 . Dissolve 1.0 g of dried glutathione in *water R* and dilute to 25.0 ml with the same solvent.

Related substances

Capillary electrophoresis: Carry out this experiment according to the general procedure (2.2.47), *Prepare the solutions immediately before use*.

Internal standard solution (a) Dissolve 0.100 g of *phenylalanine R* in the electrolyte solution and dilute to 50.0 ml with the same solution.

Internal standard solution (b) Dilute 10.0 ml of internal standard solution (a) to 100.0 ml with the electrolyte solution.

Test solution (a) Dissolve 0.200 g of glutathione in the electrolyte solution and dilute to 10.0 ml with the same solution.

Test solution (b) Dissolve 0.200 g of glutathione in internal standard solution (b) and dilute to 10.0 ml with the same solution.

Reference solution (a) Dissolve 20 mg glutathione in internal standard solution (a) and dilute to 10.0 ml with the same solution.

Reference solution (b) Dilute 5.0 ml of reference solution (a) to 50.0 ml with the electrolyte solution.

Reference solution (c) Dissolve 0.200 g of the substance to be examined in 5 ml of the electrolyte solution. Add 1.0 ml of internal standard solution (a), 0.5 ml of a 2 mg/ml solution of *L-cysteine R* (impurity B) in the electrolyte solution, 0.5 ml of a 2 mg/ml solution of *L-glutathione, oxidized R* (impurity C) in the electrolyte solution and 0.5 ml of a 2 mg/ml solution of *L- γ -glutamyl-L-cysteine R* (impurity D) in the electrolyte solution. Dilute to 10.0 ml with the electrolyte solution.

Capillary:

- *Material*: uncoated fused silica,
- *Size*: length to the detector cell = 0.5 m;
total length = 0.6 m; $\varnothing = 75\ \mu\text{m}$.

Temperature: 25 °C.

Electrolyte solution: Dissolve 1.50 g of *anhydrous sodium dihydrogen phosphate R* in 230.0 ml of *water R* and adjust to pH 1.80 with *phosphoric acid*

R. Dilute to 250.0 ml with *water R*. Check the pH and, if necessary, adjust with *phosphoric acid R* or *dilute sodium hydroxide solution R*.

Detection: Spectrophotometer at 200 nm.

Preconditioning of a new capillary: Rinse the new capillary before the first injection with 0.1 M *hydrochloric acid* for 20 min at 138 kPa and with *water R* at 138 kPa for 10 min; for complete equilibration, condition the capillary with the electrolyte solution for 40 min at 350 kPa, and subsequently for 60 min at a voltage of 20 kV;

Preconditioning of the capillary: Rinse the capillary at 138 kPa with the electrolyte solution for 40 min;

Between-run rinsing: Rinse the capillary with *water R* at 138 kPa for 1 min, with 0.1 M *sodium hydroxide* for 2 min, with *water R* at 138 kPa for 1 min, with 0.1 M *hydrochloric acid* for 3 min, and with the electrolyte solution at 138 kPa for 10 min.

Injection: Under pressure (3.45 kPa) for 5 s; inject the electrolyte solution (blank solution), reference solutions (b) and (c) and test solutions (a) and (b).

Migration: Apply a voltage of 20 kV.

Run time: 45 min.

Relative migration: With reference to the internal standard (about 14 min): impurity A = about 0.77; impurity B = about 1.04; impurity E = about 1.2; impurity C = about 1.26; impurity D = about 1.3.

System suitability:

- *resolution*: minimum 1.5 between the peaks due to the internal standard and impurity B in the chromatogram obtained with reference solution (c); if necessary increase the pH with *dilute sodium hydroxide solution R*;
- *peak-to-valley ratio*: minimum 2.5, where H_p = height above the baseline of the peak due to impurity D and H_v = height above the baseline of the lowest point of the curve separating this peak from the peak due to glutathione in the chromatogram obtained with reference solution (c); if necessary lower the pH with *phosphoric acid R*;
- check that in the electropherogram obtained with test solution (a) there is no peak with the same migration time as the internal standard (in such case, correct the area of the phenylalanine peak).

Limits

Test solution (b):

- *Corrected areas*: divide all the peak areas by the corresponding migration times;

- *Correction factors*: for the calculation of contents, multiply the ratio of time corrected peak areas of impurity and the internal standard by the corresponding correction factor: impurity B = 3.0; impurity D = 1.4;
- *Impurities A, B, E*: for each impurity, not more than 0.5 times the ratio of the area of the peak due to glutathione to the area of the peak due to the internal standard in the electropherogram obtained with reference solution (b) (0.5%);
- *Impurities C, D*: for each impurity, not more than 0.7 times the ratio of the area of the peak due to glutathione to the area of the peak due to the internal standard in the electropherogram obtained with reference solution (b) (0.7%);
- *Any other impurity*: for each impurity, not more than 0.1 times the ratio of the area of the peak due to glutathione to the area of the peak due to the internal standard in the electropherogram obtained with reference solution (b) (0.1%);
- *Total*: not more than twice the ratio of the area of the peak due to glutathione to the area of the peak due to the internal standard in the electropherogram obtained with reference solution (b) (2.0%);
- *Disregard limit*: 0.05 times the ratio of the area of the peak due to glutathione to the area of the peak due to the internal standard in the electropherogram obtained with reference solution (b) (0.05%); disregard any peak due to the blank.

Chlorides. When this test is carried out according to general procedure (2.4.4), maximum 200 ppm.

Dilute 2.5 ml of solution S to 15 ml with *water R*.

Sulfates. When this test is carried out according to general method (2.4.13), maximum 300 ppm.

Dilute 5 ml of solution S to 15 ml with *distilled water R*.

Ammonium. When this test is carried out as directed in the general method (2.4.1), maximum 200 ppm.

50 mg complies with limit test B. Prepare the reference solution using 0.1 ml of *ammonium standard solution (100 ppm NH₄) R*.

Iron. When this test is carried out according to general procedure (2.4.9), maximum 10 ppm.

In a separating funnel, dissolve 1.0 g in 10 ml of *dilute hydrochloric acid R*. Shake with three quantities, each of 10 ml, of *methyl isobutyl ketone R1*, shaking for 3 min each time. To the combined organic layers, add 10 ml of *water R* and shake for 3 min. The aqueous layer complies with the test.

Heavy metals. When this test is carried out according to general procedure (2.4.8), maximum 10 ppm. 12 ml of solution S complies with limit test A. Prepare the reference solution using *lead standard solution (1 ppm Pb) R*.
Loss on drying. When this test is carried out according to general procedure (2.2.32), maximum 0.5%, determined on 1.000 g by drying in an oven at 100–105 °C for 3 h.

Sulfated ash. When this test is carried out according to general procedure (2.4.14), maximum 0.1%, determined on 1.0 g.

Assay

In a ground-glass-stoppered flask, dissolve 0.500 g of glutathione and 2 g of *potassium iodide R* in 50 ml of *water R*. Cool the solution in iced water, add 10 ml of *hydrochloric acid R1* and 20.0 ml of 0.05 M *iodine*. Stopper the flask and allow to stand in the dark for 15 min. Titrate with 0.1 M *sodium thiosulfate* using 1 ml of *starch solution R*, added toward the end of the titration, as indicator. Carry out a blank titration.

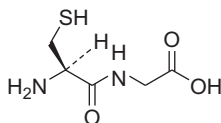
1 ml of 0.05 M *iodine* is equivalent to 30.73 mg of $C_{10}H_{17}N_3O_6S$.

Storage

Protected from light.

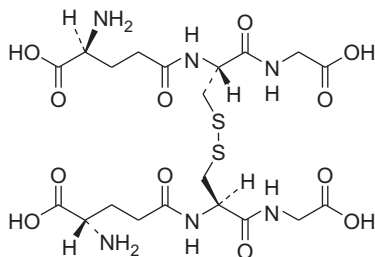
Impurities

Specified impurities A, B, C, D, E.



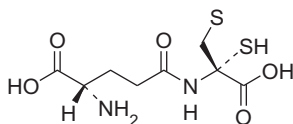
A. L-cysteinylglycine,

B. cysteine,



C. bis(L-γ-glutamyl-L-cysteinylglycine) disulfide (L-glutathione oxidized),

- D. L- γ -glutamyl-L-cysteine,
- E. unknown structure (product of degradation).



5.2 Electrochemical Methods

5.2.1 Potentiometric Methods

The potentiometric flow-injection determination of vitamin C and glutathione with a chemically prepared tubular silver electrode was studied by Kolar *et al.* [43]. The electrode was used as a potentiometric sensor for the indirect determination of vitamin C and glutathione in a carrier iodine. A simple flow-injection analysis system that consists of a peristaltic pump, an injection T valve, a tubular silver electrode, and a saturated calomel reference electrode was used. Some typical flow-injection analysis parameters such as flow rate, tube length, sample volume, and composition of the carrier stream were varied. After optimization of these parameters, the electrode was further characterized by a constant linear response within the concentration range for the vitamin C between 5×10^{-5} and 5×10^{-3} M at the slope of 60.5 ± 1.0 mV/p (vitamin C). Glutathione has a linear concentration range between 5×10^{-5} and 10^{-2} M at a slope of 55.2 ± 1.0 mV/p glutathione. The experimental slope was in good agreement with the theoretical values. Some pharmaceutical products containing vitamin C were also tested.

Potentiometric membrane sensors were described by El-Kosasy *et al.* [44] for determination of glutathione. Four glutathione-selective electrodes were developed with different techniques and in different polymeric matrices. Precipitation-based technique with bathophenanthroline-ferrous as cationic exchanger in polyvinyl chloride matrix was used for sensor 1 fabrication. β -Cyclodextrin (β -CD)-based technique with either tetrakis(4-chlorophenyl)borate or bathophenanthroline-ferrous as fixed anionic and cationic sites in polyvinyl chloride matrix was used for fabrication of sensors 2 and 3, respectively. β -Cyclodextrin-based technique with tetrakis(4-chlorophenyl)borate as fixed anionic site in polyurethane (Tecoflex) matrix was used for sensor 4 fabrications. Linear responses of 1×10^{-5} to 1×10^{-4} and 1×10^{-6} to 1×10^{-3} M with slopes of 37.5 and 32.0 mV/decade within pH 7–8 were obtained by using electrodes 1 and

3, respectively. On the other hand, linear responses of 1×10^{-5} to 1×10^{-2} and 1×10^{-5} to 1×10^{-3} M with slopes of 47.9 and 54.3 mV/decade within pH 5–6 were obtained by using electrodes 2 and 4, respectively. The percentage recoveries for determination of glutathione by the four glutathione-selective electrodes were $100 \pm 1\%$, $100.5 \pm 0.7\%$, $100 \pm 1\%$, and $99.0 \pm 0.8\%$ for sensors 1, 2, 3, and 4, respectively. Determination of glutathione in capsules by the proposed electrodes revealed their applicability for determination of glutathione in its pharmaceutical formulations. Also, they were used to determine glutathione selectively in the presence of its oxidized form (GSSG). Sensor 4 was successfully applied for determination of glutathione in plasma with average recovery of $100.4 \pm 1.11\%$. The method was compared with a reported one. No significant difference for both accuracy and precision was observed.

5.2.2 Voltammetric Methods

Voltammetric sensor for glutathione determination based on ferrocene-modified carbon-paste electrode was reported by Bakhsh *et al.* [45]. The electrocatalytic oxidation of glutathione has been studied at the surface of ferrocene-modified carbon-paste electrode. Cyclic voltammetry, double potential-step chronoamperometry, and differential-pulse voltammetry techniques were used to investigate the suitability of incorporation of ferrocene into ferrocene-modified carbon-paste electrode as a mediator for the electrocatalytic oxidation of glutathione in buffered aqueous solution. Results showed that pH 7 is the most suitable for this purpose. In the optimum condition (pH 7), the electrocatalytic ability of about 480 mV can be found and the heterogeneous rate constant of catalytic reaction was calculated as $k'h = 1.83 \times 10^{-1}$ cm/s. Also, the diffusion coefficient of glutathione, D , was found to be 3.61×10^{-5} cm²/s. The electrocatalytic oxidation peak current of glutathione at the surface of this modified electrode was linearly dependent on the glutathione concentration and the linear analytical curves were obtained in the ranges of 3.2×10^{-5} – 1.6×10^{-3} M and 2.2×10^{-6} – 3.5×10^{-3} M with cyclic voltammetry and differential-pulse voltammetry methods, respectively. The detection limits (3σ) were determined as 1.8×10^{-5} and 2.1×10^{-6} M using cyclic voltammetry and differential-pulse voltammetry, respectively. Finally, the electrocatalytic oxidation of glutathione at the surface of this modified electrode can be employed as a new method for the voltammetric determination of glutathione in real samples such as human plasma.

Cyclic voltammetry, double potential-step chronoamperometry, and differential-pulse voltammetry were used by Raoof *et al.* [46] to investigate

the suitability of this ferrocene derivative as a mediator for the electrocatalytic oxidation of glutathione in aqueous solutions with various pH. Electrooxidation of glutathione was studied at the surface of 2,7-bis (ferrocenyl ethyl) fluoren-9-one modified carbon-paste electrode. Results showed that pH 7 is the most suitable pH for this purpose. At the optimum pH, the oxidation of glutathione at the surface of this modified electrode occurs at a potential of about 0.410 V versus $\text{Ag}|\text{AgCl}|\text{KCl}_{\text{sat}}$. The kinetic parameters such as electron transfer coefficient, $\alpha=0.61$, and rate constant for the chemical reaction between glutathione and redox site in 2,7-bis (ferrocenyl ethyl) fluoren-9-one modified carbon-paste electrode, $k_h=1.73 \times 10^3 \text{ cm}^3/\text{mol/s}$, were also determined using electrochemical approaches. Also, the apparent diffusion coefficient, D_{app} , for glutathione was found to be $5.0 \times 10^{-5} \text{ cm}^2/\text{s}$ in aqueous buffered solution. The electrocatalytic oxidation peak current of glutathione showed a linear dependence on the glutathione concentration, and linear calibration curves were obtained in the ranges of 5.2×10^{-5} – 4.1×10^{-3} and 9.2×10^{-7} – $1.1 \times 10^{-5} \text{ M}$ with cyclic voltammetry and differential-pulse voltammetry methods, respectively. The detection limits (3σ) were determined as 1.4×10^{-5} and $5.1 \times 10^{-7} \text{ M}$ for the cyclic voltammetry and differential-pulse voltammetry methods, respectively. This method was also examined as a selective, simple, and precise new method for voltammetric determination of glutathione in real sample such as hemolyzed erythrocyte.

Karimi-Maleh *et al.* [47] proposed isoprenaline as a new mediator for the rapid, sensitive, and highly selective voltammetric determination of glutathione using multiwall carbon nanotubes paste electrode. It has been shown by direct current cyclic voltammetry, double-step chronoamperometry, and electrochemical impedance spectroscopy that this modified electrode can catalyze the oxidation of glutathione in an aqueous solution. The kinetic parameter of the system including electron transfer coefficient, and catalytic rate constant were also determined using the electrochemical approaches. In addition, linear sweep voltammetry was used for quantitative analysis. Linear sweep voltammetry showed wide linear dynamic range (0.5–300 μM glutathione) with a detection limit 0.9 μM glutathione. The method was examined as a selective, simple, and precise electrochemical sensor for the determination of glutathione in real samples such as hemolyzed erythrocyte, tablets, and urine.

Sezginturk and Dinckaya [48] investigated the applicability of the glassy carbon electrode coated with thin mercury film layer to the determination of reduced glutathione. Mercury coating process parameters were studied such

as concentration of mercury coating solution, coating current, and coating temperature. Then, working conditions were investigated. At the end of these studies, it is concluded that the sensor would be applicable to the determination of reduced glutathione. For the determination of glutathione, the glassy carbon electrode, coated with mercury thin film, was placed into the electrochemical cell contained 20 ml of phosphate buffer purged with nitrogen (pH 7.5, 0.05 M). A potential scanning from 0 to -750 mV at 20 mV/s was done to determine the reduction potential of glutathione at mercury thin film. After determination of the reduction potential of glutathione at the sensor surface, the potential scanning was carried out without glutathione. Then, glutathione standard solution was injected into the reaction cell and the second potential scanning was started. After injection of glutathione standard solution, a reduction peak was observed because the reduction of the $-SH$ group of glutathione at mercury film. The difference between the first and the second current values was used to quantify the change of glutathione reduction current. Measurements were carried out by the change of $-SH$ reduction current related to glutathione concentration added to the electrochemical reaction cell.

5.2.3 Amperometric Methods

A flow-injection determination of glutathione with amperometric monitoring of the enzymic reaction was reported Satoh *et al.* [49]. Glutathione sulfhydryl oxidase was immobilized on to Eupergit-C (oxiran-acrylic beads; 100–200 μm diam.) and the preparation was packed into a plastic column (2.2 cm \times 7.1 mm), which was incorporated into a flow-injection system for indirect determination of glutathione. The flow-through amperometric detector comprised a cellulose acetate membrane-covered platinum anode and Ag–AgCl reference electrode. Glutathione sample solution (0.2 ml) was introduced into the enzyme column at 30° via a rotary injection valve, the carrier solution was 0.1 M potassium phosphate buffer (pH 7) containing 0.1 M potassium chloride, and the peak current arising from oxidation of hydrogen peroxide was measured. The calibration graph was rectilinear for 0.5–1.0 mM glutathione and the coefficient of variation ($n=10$) was 2%.

A voltammetry and amperometry were used by Wring *et al.* [50] to study the behavior of reduced glutathione (I) at a carbon-paste electrode either unmodified or modified with cobalt phthalocyanine (II). Cobalt phthalocyanine reduced the potential necessary for the oxidation of glutathione to an extent that depended on the glutathione and pH of the supporting electrolyte; the oxidation of glutathione in the presence of cobalt phthalocyanine

occurred at 0.27 and 0.75 V versus the saturated calomel electrode. By using differential-pulse voltammetry, the first wave gave optimum sensitivity for 2.5–62.5 μM glutathione, and the second wave for 0.125–2.5 mM glutathione. An electrode based on a C-epoxy-resin composite-containing cobalt phthalocyanine was superior to the paste electrode in flowing solution and could be used for ≥ 10 h. The calibration graph was rectilinear from 0.1 μM to 5.5 mM glutathione, and the detection limit was 10 ng/ml by amperometry or 450 pg injected by high-performance liquid chromatography with electrochemical detection; the latter technique is suitable for determining glutathione in human plasma.

A flow-injection amperometry method for determination of cysteine and glutathione at an electrode modified with a ruthenium-containing inorganic film was reported by Cox and Gray [51]. A vitreous-carbon electrode modified with a thin film of Ru oxides (prep. described) promotes the diffusion-controlled oxidation of cysteine and glutathione at +0.92 V (vs. Ag/AgCl). In flow-injection amperometry, a calibration graphs were rectilinear over three orders of magnitude and detection limits (injection vol. 7.5 μl) were 1 μM . Up to 60 samples/h could be analyzed, and there was no evidence of electrode fouling during use. The electrode exhibited no change in sensitivity after regular use during 2 weeks.

A chemically modified with selected mediators and their application as sensors for the determination of reduced glutathione using voltammetric behavior of screen-printed carbon electrodes was reported by Wring *et al.* [52]. Screen-printed C electrodes were chemically modified with selected mediators. Cyclic voltammetry was used to study the effect of pH on the electrochemical behavior of the mediators, and amperometry in stirred solution was used to record hydrodynamic voltammograms, which were used to show the steady-state behavior of the electrodes. Amperometry in stirred solution was also used for quantitative measurements and to determine calibration response factors and the limits of detection for reduced glutathione for each of the mediators. The most promising mediators for detection of reduced glutathione were Co or Fe phthalocyanine and ferrocene carboxaldehyde. By careful selection of the potential, the selectivity and sensitivity of the electrodes can be altered to suit the requirements of the applications. By using such electrodes in conjunction with enzymes, it should be possible to prepare selective biosensors for reduced glutathione in biological materials.

A development of an amperometric assay for the determination of reduced glutathione, using glutathione peroxidase and screen-printed

carbon electrodes chemically modified with cobalt phthalocyanine was reported by Wring *et al.* [53]. Reduced glutathione was determined in 0.05 M phosphate buffer solution (pH 7) at 25°. Glutathione peroxidase solution (10 μ l) was injected into the electrochemical cell containing glutathione in the cited buffer solution and the current at 250 mV was measured with a Co phthalocyanine modified screen-printed carbon electrode. The calibration graph was rectilinear from 10 to 50 μ M glutathione. The coefficient of variation ($n=5$) was 7.3% (for solution containing 40 μ M glutathione).

A cathodic-stripping voltammetry of glutathione in natural waters was reported by Le-Gall and Van-den-Berg [54]. Sample was adjusted to pH 5 or 8.5 by the addition of acetate or borate buffer. The stirred solution was purged with nitrogen for 8 min and a deposition potential of -0.225 V (pH 5) or -0.25 V (pH 8.5) was applied for 1 min at a new mercury drop. Stirring was stopped and 15 s later a negative differential-pulse potential scan was made at 20 mV/s and pulse amplitude 25 mV. The procedure was repeated after the addition of copper and again after the standard addition of glutathione. The calibration graph was linear up to 5 nM glutathione without added copper; in the presence of 150 nM copper, the calibration graph was linear up to 200 nM glutathione. The detection limit was 1.2 nM glutathione, which was decreased to 0.4 nM by extending the adsorption time to 5 min and with the addition of 200 nM copper. The relative standard deviation for the determination of 5 nM glutathione in seawater was 8.3% in the presence of 200 nM copper and using 1 min adsorption at pH 8.5. Interference by surface-active organic compounds was minimized by passing the samples through a Sep-pak C18 cartridge; interference from copper complexing compounds was prevented by omitting the addition of copper to the sample.

A catalytic cathodic-stripping voltammetric method for glutathione determination was described by Banica *et al.* [55]. A 20-ml portion of phosphate/acetate buffer of pH 7 was purged with nitrogen for 10 min. Glutathione solution and 1 mM Ni(II) were added and the resulting solution was analyzed by differential-pulse stripping voltammetry at a hanging mercury drop electrode, by applying a deposition potential of -0.2 to -0.3 V versus Ag/AgCl for 2 min, with a vitreous C rod as auxiliary electrode. After a 30-s quiescence period, stripping was effected by scanning cathodically at 10 mV/s (pulse height 50 mV, pulse interval 0.5 s); the current was measured at -0.6 V versus Ag/AgCl. The calibration graph was linear from the detection limit (10 nM) to 120 nM glutathione. Slight interferences

from *N*-acylcysteine derivatives, Zn(II), sodium chloride, and low concentrations of strong complexants were observed. Copper (II), cysteine, and human serum albumin interfered more strongly.

An amperometric method for determination of glutathione using an amperometric enzyme microsensor was reported by Huang *et al.* [56]. A sensor (30 μm diameter) for glutathione was formed by bonding reduced glutathione sulphydryl oxidase via glutaraldehyde to a cellulose acetate membrane coated on to the tip of a platinum wire (25 μm diameter) sealed into glass. For use, the sensor was operated at +0.65 V versus Ag/AgCl in a stirred 10-ml vessel containing phosphate buffer saline of pH 7.4 and enclosed in a Faraday cage. The calibration graph was linear from 0.01 (detection limit) to 0.19 mM glutathione. The sensor could be used in media of pH ranging from 3.8 to 11.

A cathodic-stripping voltammetry determination of oxidized glutathione at a hanging-mercury-drop electrode in the presence of nickel ion was reported by Banica *et al.* [57]. Oxidized glutathione (glutathione disulfide) was determined after accumulation on a hanging-mercury-drop electrode at $E > -0.3$ V versus a Ag/AgCl reference electrode producing reduced glutathione. Using catalytic cathodic-stripping voltammetry with a hanging-mercury-drop electrode, a Ag/AgCl reference electrode and a vitreous-carbon auxiliary electrode and supporting electrolyte of 0.05 M 3-(*N*-morpholino)propanesulfonic acid of pH 7 adjusted with 10% sodium hydroxide or 25 mM sodium phosphate/25 mM sodium acetate buffer of pH 7 adjusted with 10% sulfuric acid containing 0.5–1 mM Ni(II) the reduced glutathione catalyzed the reduction of the Ni(II) giving a peak at -0.6 V. The working parameters were 50 mV pulse height, 0.5 s pulse interval, and 10 mV/s scan rate. The calibration graph was linear with a detection limit of 10 nM glutathione disulfide. The effects of interferences including human serum albumin are discussed.

An amperometric determination of glutathione in yeast extract using a membrane-covered phthalocyanine embedded carbon-paste electrode was reported Kinoshita *et al.* [58]. Twelve yeast extracts were analyzed for glutathione using a membrane-covered cobalt phthalocyanine embedded C-paste electrode and a photometric method. The results from both methods were comparable, with a correlation coefficient of 0.96. The detection limit achieved with the membrane-covered electrode was 2 μM glutathione at 200 mV versus saturated calomel electrode. The addition of 5,5'-dithiobis(2-nitrobenzoic acid) resulted in a 3.5-fold increase in the current due to glutathione and in a 13% decrease in current due to cysteine. Little interference from coexisting substances was detected.

A new amperometric biosensor based on glutathione sulfhydryl oxidase and osmium-polyvinylpyridine gel polymer (Os-gel-HRP) bilayer film modified glassy carbon electrode was demonstrated by Mao and Yamamoto [59], for glutathione and glutathione disulfide. Osmium-polyvinylpyridine gel polymer was applied at glassy carbon electrode with a surface coverage of $7.1 \mu\text{l}/\text{cm}$ to sense hydrogen peroxide based on horseradish peroxide catalytic reaction mediated by osmium. Glutathione sulfhydryl oxidase was immobilized at osmium-polyvinylpyridine gel polymer cast coated glassy carbon electrode with an approximate surface coverage of $7 \text{ U}/\text{cm}^2$ by cross-linking with BAS-glutathione sulfhydryl oxidase in glutaraldehyde vapor for 5 min. The resultant bioenzyme-based sensor was tested toward glutathione and glutathione disulfide with techniques of cyclic voltammetry, flow cell amperometry, and flow-injection analysis. The sensor was polarized at 0.0 V (vs. Ag/AgCl, 3 M potassium chloride) electrode for the detection of glutathione and glutathione disulfide in a flow system at a flow rate of $6 \mu\text{l}/\text{min}$. Linear response to glutathione and glutathione disulfide in a concentration range from 1 to $200 \mu\text{M}$ and 2 to $120 \mu\text{M}$ was obtained at the sensor with a sensitivity of 1.195 and $0.60 \text{ nA}/\mu\text{M}$ for glutathione and glutathione disulfide, respectively. The dependence of current response on pH value of the buffer glutathione disulfide and operating potential was also tested and optimized.

A modified gold electrode for electrochemical studies of the reaction of phospholipid-hydroperoxide glutathione peroxidase with glutathione and glutathione disulfide was developed Lehmann *et al.* [60]. Glutathione peroxidases catalyze the reduction of hydroperoxides to the corresponding alcohols under consumption of glutathione. Glutathione is oxidized to glutathione disulfide while the enzyme is regenerated. Here, the reaction of phospholipid-hydroperoxide glutathione peroxidase with glutathione and glutathione disulfide at modified electrodes, prepared by self-assembly of glutathione, mercaptoundecanoic acid, or dodecanethiol on to silver electrodes, was investigated electrochemically. The modified electrodes were characterized by cyclic voltammetry using the redox compounds $[\text{Ru}(\text{NH}_3)_6]^{2+}$ and $[\text{Fe}(\text{CN})_6]^{4-}$. Apart from the reaction with hydroperoxides and glutathione, monomeric phospholipid-hydroperoxide glutathione peroxidase reacted with glutathione disulfide leading to a mixed selenadisulfide. The tetrameric cytosolic glutathione peroxidases did not react. From the results, the transhydrogenase activity of phospholipid-hydroperoxide glutathione peroxidase is discussed.

An amperometric determination of glutathione and cysteine on a palladium-iridium dioxide modified electrode with high-performance

liquid chromatography was developed by Xu *et al.* [61]. A Pd/IrO₂ coelectrodeposited glassy carbon electrode was prepared and the electrochemical behavior of glutathione at this chemically modified electrode has been studied by cyclic voltammetry. The results indicated that the modified electrode efficiently exhibited electrocatalytic oxidation for glutathione with relatively high sensitivity, stability, and long life. Coupled with high-performance liquid chromatography, the Pd/IrO₂-modified electrode was utilized for the electrochemical detection of the thio-compounds, glutathione, and cysteine. The peak currents were linear with the substance concentrations in the range of 1.0×10^{-5} to 8.0×10^{-4} M for glutathione and 4.0×10^{-6} to 2.0×10^{-4} M for cysteine. The detection limits were 2.0×10^{-6} M for glutathione and 5.0×10^{-7} M for cysteine with signal-to-noise ratio of 3. The method has been successfully applied to assess the contents of glutathione and cysteine in rat brain microdialysates.

A renewable three-dimensional chemically modified carbon ceramic electrode containing Ru[(tpy)(bpy)Cl]PF₆ was constructed by Salimi and Pourbeyram [62] using sol-gel technique for detection of L-cysteine and glutathione. It exhibits an excellent electrocatalytic activity for oxidation of L-cysteine and glutathione at pH range 2–8. Cyclic voltammetry was employed to characterize the electrochemical behavior of the chemically modified electrode. The electrocatalytic behavior is further exploited as a sensitive detection scheme for L-cysteine and glutathione by hydrodynamic amperometry. Optimum pH value for detection is 2 for both L-cysteine and glutathione. Under the optimized condition, the calibration curves are linear in the concentration ranges of 5–685 and 5–700 μ M for L-cysteine and glutathione determination, respectively. The detection limit (S/N=3) and sensitivity is 1 μ M, 5 nA/ μ M for L-cysteine, and 1 μ M, 7.8 nA/ μ M for glutathione. The relative standard deviation for the amperogram's currents with five injections of L-cysteine or glutathione at concentration range of linear calibration is <1.5%. The advantages of this amperometric detector are: high sensitivity, good catalytic effect, short response time ($t < 3$ s), remarkable long-term stability, simplicity of preparation, and reproducibility of surface fouling (relative standard deviation for six successive polishing is 3.31%). This sensor can be used as a chromatographic detector for analysis of L-cysteine and glutathione.

The development of an amperometric sensor for the determination of reduced glutathione was described by Calvo-Marzal *et al.* [63]. The sensor was based on tetrathiafulvalene-tetracyanoquinodimethane incorporated into the graphite powder/Nujol oil matrix. The electrooxidation of glutathione was monitored amperometrically at 200 mV versus saturated calomel

electrode. The amperometric response of the sensor was linearly proportional to the glutathione concentration between 20 and 300 μM , in 0.1 M phosphate buffer (pH 8.0), containing 0.1 M potassium chloride and 0.5 M disodium dihydrogen EDTA, as supporting electrolyte. The detection limit, considering signal-to-noise ratio equal three, was 4.2 μM for glutathione and the repeatability obtained as relative standard deviation was of 5.1% for a series of 10 successive measurements.

An amperometric biosensor based on cucumber tissue homogenate was developed by Sezgenturk and Dinckaya [64] for the determination of glutathione. Cucumber (*Cucumis sativus* L.) tissue homogenate was used as the biological material. The cucumber tissue homogenate was cross-linked with gelatine using glutaraldehyde and fixed on a pretreated teflon membrane. The principle of the measurements was based on the determination of the decrease in the differentiation of oxygen level which had been caused by the inhibition of ascorbate oxidase in the biological material by glutathione. Determinations were carried out by standard curves which were obtained by the measurement of the decrease in the consumed oxygen level related to glutathione concentration. Optimization and characterization studies of the biosensor were carried out and linearity in the glutathione concentration range of 0.1–2 μM was obtained, when 600 μM ascorbic acid was used as a substrate. The biosensor useful lifetime was at least 2 months. The results of some plant samples analyzed with the presented biosensor agreed well with the spectrophotometric method (Ellman's reagent) used as a reference.

A direct simultaneous electrochemical determination of glutathione and glutathione disulfide was presented by Afsaneh *et al.* [65] using a nanoscale copper hydroxide carbon ionic liquid composite electrode. To the best of our knowledge, this is the first report on the simultaneous determination of these two biologically important compounds based on their direct electrochemical oxidation. Incorporation of copper(II) hydroxide nanostructures in the composite electrode results in complexation of Cu(II) with the thiol group of glutathione and leads to a significant decrease in glutathione oxidation overpotential, while an anodic peak corresponding to the direct oxidation of glutathione disulfide as the product of glutathione oxidation is observed at higher overvoltages. Low detection limits of 30 nM for glutathione and 15 nM for glutathione disulfide were achieved based on a signal-to-noise ratio of 3. The method is free from interference of cysteine, homocystein, ascorbic acid, and uric acid. No electrode surface fouling was observed during successive scans. Stability, high sensitivity, and low detection limits made the electrode applicable for the analysis of biological fluids.

Electrocatalytic activity of cobalt phthalocyanine adsorbed on a graphite electrode for the oxidation of reduced L-glutathione and the reduction of glutathione disulfide at physiological pH was reported by Pereira-Rodrigues *et al.* [66]. Modified electrodes coated by adsorbed cobalt phthalocyanines were known to show substantial electrocatalytic activity for the electrooxidation of several thiols in alkaline aqueous solution. In this context, we explore in this study the electrocatalytic activity of adsorbed cobalt phthalocyanine on ordinary pyrolytic graphite electrode for the oxidation of reduced L-glutathione and the reduction of its glutathione disulfide at physiological pH. Cyclic and rotating disk voltammetries were performed and the amperometric results show that a stable electrochemical sensing material, with good reproducibility and sensitivity (in accordance with the concentrations of glutathione expected in biological media), can be easily achieved. This opens the way for the design of an electrochemical sensor able to detect these two analytes in biologically relevant experimental conditions (in terms of pH).

A modified carbon-paste electrode was prepared by incorporating titanium oxide nanoparticles and ferrocene carboxylic acid in carbon-paste matrix by Raoof *et al.* [67]. Electrochemical impedance spectroscopy indicates that the titanium oxide nanoparticles efficiently decreased the charge transfer resistance value of electrode and increased the porous microcrystalline structure of it to improve the electron transfer kinetic between ferrocene carboxylic acid and electrode. Ferrocene carboxylic acid acted as a mediator between the analyte and electrode surface. The electrocatalytic oxidation of glutathione and tryptophan is individually and simultaneously investigated at the surface of ferrocene carboxylic acid–titanium oxide modified electrode using cyclic voltammetry and differential-pulse voltammetry. The electrode is able to completely resolve the voltammetric response of glutathione and tryptophan from potentially interfering species, e.g., ascorbic acid and tyrosine, respectively. The linear range of the analytical plot remains constant in binary mixture solutions of glutathione and tryptophan. High sensitivity and selectivity together with very low detection limit of the electrode response make it very suitable for simultaneous and individual determination of trace amounts of glutathione and tryptophan in pharmaceutical and clinical preparations.

Chlorpromazine was used as a new mediator for a rapid, sensitive, and highly selective voltammetric method for the determination of glutathione using multiwall carbon nanotubes paste electrode was reported by Ensafi *et al.* [68]. The experimental results showed that the carbon nanotubes paste

electrode has a highly electrocatalytic activity for the oxidation of glutathione in the presence of chlorpromazine as a mediator. Cyclic voltammetry, double potential-step chronoamperometry, and differential-pulse voltammetry are used to investigate the suitability of chlorpromazine at the surface of multiwall carbon nanotubes paste electrode as a mediator for the electrocatalytic oxidation of glutathione in aqueous solutions. It is shown that chlorpromazine can catalyze the oxidation of glutathione in an aqueous buffer solution to produce a sharp oxidation peak current at about +0.70 versus Ag/AgCl as a reference electrode. Kinetic parameters such as electron transfer coefficient and catalytic reaction rate constant, k/h , are also determined. Using differential-pulse voltammetry and under the optimum conditions at pH 4.0, the electrocatalytic oxidation peak current of glutathione shows a linear dependence on glutathione concentration in the glutathione concentration range of 0.3–18.3 μM . The detection limit (3σ) is determined to be 0.16 μM . The relative standard deviation for 1.5 and 5.0 μM glutathione are found to be 3.7% and 2.5%, respectively. The method may, thus, also be used as a novel, selective, simple, and precise method for the voltammetric determination of glutathione in such real samples as hemolyzed erythrocyte.

5.3 Spectrophotometric Methods

A spectrophotometric determination of cysteine, penicillamine, glutathione, and 6-mercaptopurine was reported by Besada *et al.* [69], based on reaction with Cu^{2+} –neocuproine. Sample solution (≤ 5 ml) was adjusted to pH 7.8 for 6-mercaptopurine or pH 6 for other thiols with acetate buffer solution, and Cu^{2+} –neocuproine reagent solution was added, with shaking for ~ 2 min. The mixture was diluted to 25 ml with water, and after ~ 15 min, Cu I–neocuproine was detected at 458 nm versus a reagent blank. Calibration graphs were rectilinear for 40–200 $\mu\text{g/ml}$.

A spectrophotometric determination of glutathione and of its oxidation product in pharmaceutical dosage forms was reported by Raggi *et al.* [70]. Lyophilized sample was dissolved in water and treated with 6 mM diammonium palladium tetrachloride. After 5 min, the absorbance of the mixture was measured at 380 nm versus a reagent blank. The calibration graph was rectilinear for 50–600 μM glutathione. Recoveries and coefficient of variation obtained in the analysis of three pharmaceuticals are tabulated. The method could also be used to determine the oxidation product of glutathione.

A derivative spectrophotometric method was developed by Boutolleau *et al.* [71] for determination of glutathione. The analytical performances of the assay were improved by using derivative spectrophotometry. The second-order derivative spectrophotometry gave identical signals with either a glutathione standard solution or erythrocyte lysate containing the same amount of glutathione, whereas the corresponding absorbances were different. The linearity range of the method was 20–2000 $\mu\text{M/l}$.

Avi-Dor and Lipkin [72] described a spectrophotometric method for the determination of reduced glutathione. The method which is based on the interaction between fluoropyruvic acid and glutathione in borate solution compares favorably in its sensitivity with other methods. The method allows the quantitative estimation of glutathione and cysteine. The procedure which is rapid, simple and allows in one determination the estimation of both concentration of cysteine and glutathione. Addition of borate to the product of interaction between fluoropyruvic acid and thiol compounds which have no free amino group in the α or β position produced a shift in the absorption peak from 275 to 290 nm with a concomitant increase in absorbency. The high extinction of the resulting borate complex was utilized for the spectrophotometric determination of reduced glutathione. The spectral differences existing between the glutathione fluoropyruvic acid and the corresponding cysteine derivative, made possible the determination of both mercaptides in a mixture of the two. Some aspects of the mechanism of the reaction are discussed.

Redegeld *et al.* [73] presented a sensitive and specific assay method for glutathione using recycling reaction followed by spectrophotometric detection in a flow-injection analysis system. The method provides specific amplification of the response to glutathione by combined use of the enzyme glutathione disulfide reductase and the chromogenic reagent 5,5'-dithiobis(2-nitrobenzoic acid). Both oxidized glutathione and reduced glutathione are detected, so that oxidized glutathione must be determined separately after alkylation of the glutathione with *N*-ethylmaleimide. The sensitivity is controlled by the number of times the cycle occurs and therefore by the residence time of the sample in the reactor. This time depends on the reactor length and the flow rate. The influence of the residence time, temperature, and enzyme concentration on the response has been studied and the optimum reaction conditions have been selected. The sample throughput is as high as 30/h and the detection is 1 pmol glutathione at a signal-to-noise ratio of 3. The method has been evaluated by the quantitation of glutathione and oxidized glutathione in isolated hepatocytes. A high

correlation between the new flow-injection analysis method and the original spectrophotometric batch assay has been found (slope = 1.039, intercept = 0.6, $n = 216$, and $r = 0.977$). The main advantages of the method are high sample throughput, high sensitivity, and good reproducibility.

Teare *et al.* [74] used an automated spectrophotometric method for determining oxidized and reduced glutathione in liver. An enzymatic recycling method has been applied to the measurement of total and oxidized glutathione in the liver, with a centrifugal analyzer. When the reduced form of glutathione was masked with 2-vinylpyridine to measure the oxidized glutathione, the time to insure full derivatization was three times longer than has been reported. The method is quick, simple, accurate, and precise (1.27% for glutathione, 3.3% for oxidized glutathione intra-assay coefficient of variation; 2.15% for glutathione, 5% for oxidized glutathione intra-assay coefficient of variation), and the automation allows large numbers of samples to be conveniently assayed.

5.4 Spectrofluorimetric Methods

Revised protocols for the determination of glutathione and glutathione disulfide using *o*-phthalaldehyde derivatization are presented by Senft *et al.* [75]. The assays were performed in phosphate buffer, at a lower pH using more *o*-phthalaldehyde, and using dithionite as reductant for glutathione disulfide. Fluorescence was measured at 430 nm (excitation at 365 nm). Calibration graphs were linear for up to 10 nmol of glutathione and glutathione disulfide and the detection limit was 20 pM. Using these protocols, interference from nonspecific reactants in tissue was minimized. Similar results were obtained for glutathione and glutathione disulfide in mouse liver extracts determined using this method and by high-performance liquid chromatography.

A spectrofluorimetric method for cysteine and glutathione using the fluorescence system of Zn(II)-8-hydroxyquinoline-5-sulfonic acid complex was developed by Wang *et al.* [76]. The method is based on the principle that the presence of thiol compounds such as cysteine and glutathione reduce the fluorescence intensity of the Zn(II)-8-hydroxyquinoline-5-sulfonic acid complex in boric acid-sodium tetraborate buffer medium of pH 8.5 owing to the formation of nonfluorescent Zn(II)-cysteine or Zn(II)-glutathione complexes. The relative decrease in fluorescence intensity at 512 nm (excitation at 365 nm) was linear in the ranges of 0.8–2.2 $\mu\text{g/ml}$ of cysteine and 0–8 $\mu\text{g/ml}$ of glutathione and the detection limits were 0.017 and 0.6 $\mu\text{g/ml}$

for cysteine and glutathione, respectively. For 17 amino acids investigated, the most serious interferences were produced by tyrosine and tryptophan, which exhibit strong native fluorescence. Tolerable amounts of Ca(II) and Mg(II) were increased to 43 and 6 $\mu\text{g}/\text{ml}$, respectively in the presence of 3.33 mM tartaric acid. The method has been applied in the determination of cysteine in protein hydrolysate and cystine electrolyte and of glutathione in blood serum with recoveries in the range of 95.6–104.5%. Within-day relative standard deviation were 0.9% and 1.1% ($n=7$) for cysteine and glutathione, respectively, and the corresponding between-day relative standard deviation were 1.8% and 2.5% ($n=7$).

Spectrofluorimetric determination of reduced glutathione was developed by Shen *et al.* [77] with *N*-[*p*-(2-benzothiazolyl) phenyl] maleimide. The maximum fluorescence for the reagent and the adduct were both at excitation and emission wavelengths of 323.2 and 388.8 nm, respectively. *N*-[*p*-(2-benzothiazolyl) phenyl] maleimide reacted with glutathione at 50 °C for 35 min in boric acid (potassium chloride)/sodium carbonate buffer (pH 7.50) to give a highly fluorescent derivative. The relative fluorescence intensity was linear with the glutathione concentration in the range of 4–240 nM. The detection limit was 0.32 nM (signal-to-noise ratio = 3). The method was applied to human blood and satisfactory results were obtained.

A new thiol fluorescence probe, 5-maleimidyl-2-(*m*-methylphenyl) benzoxazole has been developed by Liang *et al.* [78], for the direct determination of reduced glutathione in real samples. Compared to the reported *N*-substituted maleimide type of thiol reagents, the main advantage of 5-maleimidyl-2-(*m*-methylphenyl)benzoxazole is its rather high selectivity for glutathione to cysteine, which often coexists with glutathione in biological samples. Under mild conditions similar to the physiological environment, 5-maleimidyl-2-(*m*-methylphenyl)benzoxazole reacted with glutathione to give a highly fluorescent derivative with the excitation and emission wavelengths of 299.2 and 355.8 nm, respectively. In the presence of 0.40-fold (molar ratio) of cysteine, a linear relationship was found in the range of $0\text{--}1.62 \times 10^{-7}$ M with the detection limit (3σ) of 3.23×10^{-10} M for glutathione determination. Many other amino acids (100-fold) did not interfere with the determination. Since the molar ratio of cysteine to glutathione in mammalian tissues and blood does not exceed the value of 0.40:1, the method has been used in the direct determination of glutathione in these kinds of biological samples, such as human blood, pig's liver, and heart, with the recoveries of 94.3–104.5%.

Hashmat Ullah *et al.* [79] studied the concentration- and time-dependent effect of cadmium nitrate tetrahydrate on glutathione in aqueous medium by using ultraviolet–visible spectrophotometer. Different concentrations of cadmium nitrate tetrahydrate were introduced to constant concentration of glutathione to determine the effect of cadmium on the concentration of glutathione. It was found that higher concentration of cadmium causes greater decrease in glutathione concentration than lower concentration of cadmium nitrate tetrahydrate with the passage of time, at different time of intervals, there was a gradual depletion in the concentration of glutathione that was indicating either binding of cadmium with glutathione or conversion of glutathione into oxidized glutathione.

Yakubu *et al.* [80] developed a spectrofluorimetric assay method for glutathione and glutathione transferase using monobromobimane, the non-fluorescent compound with an electrophilic site. Monobromobimane slowly reacted with glutathione to form fluorescent glutathione conjugate and that the reaction was catalyzed by glutathione transferase. Both non-enzymatic and enzymatic reaction products of monobromobimane, in the presence of glutathione in phosphate buffer (pH 6.5), were measured by following increase of fluorescence at wavelength 475 nm. For validation of the assay method, the kinetic parameters such as the apparent Michaelis–Mente constant and maximum rates of conjugate formation as well as the specific activity of rat hepatic glutathione transferase were determined. The method was found to be sensitive and thus applied to measure glutathione contents of crude preparation of rat hepatic cytosol fraction.

5.5 Chemiluminescence Methods

A chemiluminescence method for simultaneous determination of cysteine and glutathione via use of time-resolved luminol was reported by Kamidate *et al.* [81]. Hydrogen peroxide produced from the Cu(II)-catalyzed oxidation of cysteine and glutathione was detected using *Arthromyces ramosus* peroxidase-catalyzed chemiluminescence. The use of *Arthromyces ramosus* peroxidase gave a chemiluminescence response curve time-resolved into two peaks for the simultaneous determination of cysteine and glutathione. Calibration graphs were linear in the range of 1–50 and 3–50 μM for cysteine and glutathione, respectively. The relative standard deviation ($n = 5$) was 2.5% and 2.8% at 5 μM cysteine and 10 μM glutathione, respectively.

Peroxidase-catalyzed luminol chemiluminescence method for the determination of glutathione was reported by Kamidate and Watanabe [82].

Solution containing 10 μM luminol and 0.5 μM *Arthromyces ramosus* peroxidase was saturated with oxygen, 10 μM Cu(II) solution and glutathione solution were added simultaneously and the chemiluminescence produced was monitored. The calibration graph was linear for 0.75–30 μM glutathione with a detection limit of 0.75 μM . The relative standard deviation ($n=5$) was 1.6% at 3 μM glutathione.

A rapid flow-injection method with chemiluminescence detection was described by Wang *et al.* [83] for the determination of glutathione. The method is based on the chemiluminescence reaction of luminol and hydrogen peroxide. Glutathione can greatly enhance the chemiluminescence intensity in 0.1 M borax-sodium hydroxide buffer solution (pH 9.7). The maximum chemiluminescence intensity was directly proportional to the concentration of glutathione in the range of 3.0×10^{-7} – 2.0×10^{-5} M, and the detection limit was 6.8×10^{-8} M. The relative standard deviation was 3.4% for 5.0×10^{-6} M of glutathione ($n=11$).

The chemiluminescence method for determination of glutathione was reported by Ensafi *et al.* [84], based on the effect of glutathione on the chemiluminescence signal of the oxidation of luminol by sodium periodate in basic solution. In this work, a new sensitive method is introduced for analysis of glutathione at trace levels in blood samples. The influence of chemical and manifold variables on the sensitivity was studied. At the optimized conditions, the linear range for the determination of glutathione was 1.0×10^{-8} – 1.0×10^{-5} mol/l with the detection limit (3σ) of 8×10^{-9} mol/l. The relative standard deviation for 10 repeated measurements of 1.0×10^{-6} mol/l of glutathione was 4%. The results of the method were compared with the Ellman reference method and no significant difference was found. The influence of potential interference substances on the determination of glutathione was studied. The method was applied for the determination of glutathione in real samples such as erythrocyte hemolyzed in normal subjects and diabetes.

A sensitive chemiluminescence method for the determination of glutathione, L-cysteine and 6-mercaptopurine was reported by Ping *et al.* [85]. Glutathione, L-cysteine and 6-mercaptopurine inhibit the chemiluminescence reaction of luminol–hydrogen peroxide catalyzed by gold colloids. In order to explore this, Glutathione, L-cysteine, and 6-mercaptopurine were injected into the chemiluminescence system of luminol and hydrogen peroxide catalyzed by gold colloids. The results showed that gold colloids interact with Glutathione, L-cysteine and 6-mercaptopurine and decrease the chemiluminescence emission. Based on this phenomenon, a simple,

sensitive, and convenient flow-injection chemiluminescence method was developed for the determination of Glutathione, L-cysteine, and 6-mercaptopurine. This method provides a novel, and effective chemiluminescence assay for Glutathione, L-cysteine, and 6-mercaptopurine that has been applied to the determination of Glutathione in human serum.

Thompson and Watson [86] studied the nitroprusside method for the determination of blood glutathione. The earlier methods have been modified in order to increase the sensitivity and decrease rate of fading of the final color. In the following method, all solutions must be prepared with glass-distilled water, and all glassware must be scrupulously clean. A quantity, 0.5 ml of freshly drawn blood (oxalated or heparinized), is added to 1.5 ml of glass-distilled water in a 15-ml centrifuge tube and allowed to stand for 5 min to take. Then, 2 ml of 10% trichloroacetic acid is added, and the mixture well stirred with a glass rod and allowed to stand for 5 min, after which it is centrifuged for 5 min at 3000 rpm. Then, 2 ml of clear, protein-free supernatant are pipetted into a stopper 10 ml graduated cylinder. Solid ammonium sulfate is added to saturate the solution (by tipping in 1.4 g contained in a marked tube); after shaking the volume is made up to 3 ml with saturated ammonium sulfate. For the production of the color 0.5 ml of 0.05 M nitroprusside reagent is added, followed by 0.7 ml of 8 N ammonium hydroxide. After transferring into cells of 1 cm optical depth, the color intensity is read in a photoelectric colorimeter 30 s after the addition of ammonium hydroxide, using an Ilford spectrum green (604) filter. A reagent blank determination is carried out using 1 ml water and 1 ml 10% trichloroacetic acid, with all subsequent additions as for the blood filtrate. All tubes are compared against water. The standard glutathione solution is diluted 10-fold with water to give a solution containing 100 μg glutathione/ml. To prepare a standard curve, 0.2, 0.4 . . . 1.0 ml samples (i.e., 20, 40 . . . 100 μg glutathione) are each diluted with water to 1 ml. Then, 1 ml of 10% trichloroacetic acid is added to each, and the estimation carried out as for the blood filtrate. One standard tube (containing 60 or 80 μg glutathione) is included in each series of blood estimations.

Owens and Belcher [87] described a rapid colorimetric and apparently specific micro-method for the determination of total glutathione in small amounts of tissue. Generally, less than 30 mg of tissue is sufficient and this is homogenized in ice-cold 3% metaphosphoric acid. The product is filtered through sintered glass and neutralized or diluted before being added to a cuvette containing phosphate buffer, pH 7.1, 5,5'-dithiobis(2-nitrobenzoic acid), EDTA, and glutathione reductase. Addition of NADPH_2 to the

system initiate a progressive reduction of 5,5'-dithiobis(2-nitrobenzoic acid) by catalytic amount of glutathione, and this causes a color increase at 412 nm. The rate of this change, calculated over 5 min, is proportional to the total amount of glutathione present, and consequently unknown concentrations are determined by reference to standards.

Tipple and Rogers [88] presented a method for determination of glutathione levels in complex biological samples and plasma. The 5,5'-dithiobis(2-nitrobenzoic acid)/glutathione reductase enzyme recycling method is sensitive and requires no specialized equipment. Glutathione is oxidized by 5,5'-dithiobis(2-nitrobenzoic acid) resulting in the formation of oxidized glutathione and 5-thio-2-nitrobenzoic acid. Oxidized glutathione is then reduced to glutathione by glutathione reductase using reducing equivalent provided by NADPH. The rate of 5-thio-2-nitrobenzoic acid formation is proportional to the sum of glutathione and glutathione disulfide present in the sample and is determined by measuring the formation of 5-thio-2-nitrobenzoic acid at 412 nm. Specific changes have been described to increase assay sensitivity enabling measurements in plasma from populations with inherently low glutathione and glutathione disulfide levels.

Cappiello *et al.* [89] described a simple and rapid colorimetric coupled enzymatic assay for the determination of glutathione. The method is based on the specific reaction catalyzed by γ -glutamyltransferase, which transfers the γ -glutamyl moiety from glutathione to an acceptor, with the formation of the γ -glutamyl derivative of the acceptor and cysteinylglycine. The latter dipeptide is a substrate of leucyl aminopeptidase, which hydrolyzes cysteinylglycine to glycine and cysteine that can be easily measured spectrophotometrically. The method was used to measure the content of glutathione in acid extracts of bovine lens, to follow the NADPH-dependent reduction of glutathione disulfide to reduced glutathione catalyzed by the enzyme glutathione reductase, and to determine the glutathione content in human astrocytoma ADF cells subjected to oxidative stress. The results showed that the method can be suitably used for the determination of glutathione and oxidized glutathione in different biological samples and to monitor tissue or cell redox status under different conditions. It is also applicable for following reactions involving glutathione and/or glutathione disulfide.

5.6 Chromatographic Methods

5.6.1 High-Performance Liquid Chromatography–Ultra Violet

Glutathione and oxidized glutathione were determined by standard addition using high-performance liquid chromatography by Yoshida [90]. Standard

solutions were prepared by mixing 2 mg/ml glutathione and 0.8 mg/ml oxidized glutathione in 20 mM 1,10-phenanthroline solution. Erythrocytes were hemolyzed by adding 0.4 ml of the standard solutions. Metaphosphoric acid (10%, 0.3 ml) was added, the solutions were vortex-mixed and centrifuged. The supernatant was mixed with 0.1 ml of 400 mM iodoacetic acid, neutralized with sodium bicarbonate powder (~ 20 mg) and allowed to react for 1 h in the dark using a wave rotor to form the S-carboxymethyl derivative of glutathione. A 0.5-ml portion of 5% 2,4-dinitrofluorobenzene in ethanol was added and the mixture was allowed to react for 20 h in the dark, then centrifuged. Derivatives were determined on a 5 μ m LiChrospher 100 NH_2 column (25 cm \times 4 mm i.d.) with a guard column of the same material (4 cm \times 4 mm i.d.) with gradient elution (1.2 ml/min) with solvent A/solvent B [3:1–1:19 (held for 15 min) in 30 min] where solvent A was water/methanol (1:4) and solvent B was 2 M sodium acetate of pH 4.6/methanol (9:16); detection was at 365 nm. Relative standard deviation for Glutathione and oxidized glutathione were 6% and 8%, respectively ($n=10$). Calibration graphs are shown.

Determination of glutathione and other thiols in human mononuclear blood cells using high-performance liquid chromatography method was reported by Raggi *et al.* [91]. Portions (2 ml) of a standard glutathione solution, or 800 μ l filtrate of human mononuclear blood cell lysate, were treated with 200 and 80 μ l, respectively, 0.1 mM Ellman reagent. After 5 min, a 20- μ l portion of the reaction mixture was analyzed by HPLC on a 4.5 μ m RP-18 column (25 cm \times 4.6 mm i.d.) with 0.023 M ammonium formate of pH 5/methanol (9:1) as mobile phase (1 ml/min) and detection at 280 nm. The retention peak for glutathione was at 5.8 min. The calibration graph was linear from 3 to 60 μ M I with a detection limit of 1.5 μ M. The average recovery of I from cell lysate was 96% and the intraday RSD ($n=5$) was 2% for 20 μ M I. Cysteine and N-acetylcysteine were also investigated. Results are tabulated.

A sensitive high-performance liquid chromatographic method for quantification of glutathione and other sulfhydryl and disulfide amino acids in human plasma using ultra violet spectrophotometric detection was developed by Katrusiak *et al.* [92]. Precolumn derivatization with 5,5'-dithiobis-nitrobenzoic acid and an optional prederivatization reaction with dithiothreitol allowed both quantitative reduction of disulfides for measurement of total amino acid levels and the measurement of the reduced forms. A dynamic range of 500 nM to 750 μ M allowed the major analytes of interest to be quantified in plasma without sample dilution. The assay is a sensitive

and precise method for the determination of sulfhydryl and disulfide amino acids in plasma and cell extracts.

A rapid procedure for high-performance liquid chromatography analysis of ascorbic acid and glutathione in plant tissues was described by Davey *et al.* [93]. After sample preparation, samples were analyzed on a "Rocket" high-performance liquid chromatography column (53 × 7 mm i.d.) custom packed with LiChrosorb RP C18-endcapped stationary phase (3 μm spherical particle size), equipped with a guard cartridge packed with the same material. The column was eluted at 3 ml/min with a 3-min linear gradient of 1–30% acetonitrile in mobile phase (400 μl *o*-phosphoric acid, 0.1 mM EDTA, and 0.25% methanol, pH similar to 2.5). Photodiode array detection was used, with UV spectra collected over the range of 195–300 nm and quantification of ascorbic acid and glutathione at 243 and 197 nm, respectively. Analyses were complete within 6 min. Optimization of parameters such as choice of extraction buffer, tissue disruption technique, sample stability, and separation conditions were carried out. Inclusion of dithiothreitol as a stabilizer in extracts with high phenolic content was found to promote oxidation of these antioxidants. The method is suitable for high resolution screening of large numbers of samples.

Methods for quantification of glutathione and oxidized glutathione and cysteine and oxidized cysteine and the disulfide glutathione–cysteine resulting from the oxidation of the mixture of cysteine and glutathione were performed by Vignaud *et al.* [94]. The fractionation of the disulfides, oxidized glutathione, oxidized glutathione–cysteine, and oxidized cysteine, was achieved by size exclusion using a Superdex peptide column coupled with ultraviolet detection at 254 nm. The conditions of separation of these compounds by reversed-phase high-performance liquid chromatography were optimized using the response surface methodology. Optimal peak resolution and retention times were obtained on a C18 YMC ODS AQ column with 20 mM of ammonium phosphate at pH 2.5 and 2% of acetonitrile in the elution phase. In these experimental conditions, cysteine, cysteine disulfide, glutathione, and glutathione disulfide were eluted within 20 min. Coulometric detection enabled a sensitivity 100 times higher for the disulfides than the ultraviolet detection at 220 nm. These methods were applied to follow the consumption of thiols and the disulfide formation by three oxidizing systems, sulfhydryl oxidase, and glutathione dehydroascorbate oxidoreductase and potassium bromate. This study revealed that the relative proportions of the disulfides formed were similar for the three oxidizing systems when the reactions are in their state of equilibrium.

Glutathione quantification was optimized and validated by Garcia *et al.* [95] using high-performance liquid chromatography-ultraviolet for determination of reduced glutathione. Important aspects such as acid deproteinization and glutathione stability were established. The erythrocytes were hemolyzed, deproteinized, derivatized with 5,5-dithiobis(2-nitrobenzoic) acid, and analyzed using high-performance liquid chromatography, on an RP₁₈ gradient elution, $\lambda = 330$ nm. The method was applied to hemodialysis patients ($n = 75$) compared with healthy subjects ($n = 40$). The assay was linear from 0.5 to 3.0 mM ($r^2 > 0.99$). The intra- and interrater reproducibilities were obtained with coefficient of variation percentage of $< 10\%$. The accuracy (bias %) ranged from 1.32% to 6.38%, and the recovery was $> 94\%$. The derivatized sample was stable for 60 days at -20°C . This method used ultraviolet detection, reduction of the phosphate concentration in the mobile phase, and effective protein removal with trichloroacetic acid. The method proved to be reproducible, precise, accurate, and stable. Thus, it can be utilized for routine laboratory tests for the verification of physiopathological conditions.

A validation of a novel reversed-phase high-pressure liquid chromatography method for the quantification of reduced glutathione in pharmaceutical formulations utilizing simple ultraviolet detection was reported by Sutariya *et al.* [96]. The separation utilized a C18 column at room temperature and ultraviolet absorption was measured at 215 nm. The mobile phase was an isocratic flow of a 50/50 (v/v) mixture of water (pH 7.0) and acetonitrile flowing at 1.0 ml/min. Validation of the method assessed the method's ability in seven categories: linearity, range, limit of detection, limit of quantification, accuracy, precision, and selectivity. Analysis of the system suitability showed acceptable levels of suitability in all categories. Likewise, the method displayed an acceptable degree of linearity ($r^2 = 0.9994$) over a concentration range of 2.5–60 $\mu\text{g/ml}$. The detection limit and quantification limit were 0.6 and 1.8 $\mu\text{g/ml}$, respectively. The percent recovery of the method was 98.80–100.79%. Following validation, the method was employed in the determination of glutathione in pharmaceutical formulations in the form of a conjugate and a nanoparticle. The method offers a simple, accurate, and inexpensive way to quantify reduced glutathione.

5.6.2 High-Performance Liquid Chromatographic-Fluorescence

Winters *et al.* [97] described a reversed-phase high-performance liquid chromatographic method to separate and quantify derivative of glutathione and other biological thiols. *N*-(1-pyrenyl)maleimide reacts with free sulfhydryl

groups to form fluorescent derivatives. Separation and quantitation of glutathione, cysteine homocysteine, cysteinylglycine, and γ -glutamylcysteine derivatives are achieved. The method allows for the measurement of glutathione disulfide by masking free glutathione with 2-vinylpyridine, reducing glutathione disulfide with glutathione reductase and measuring the resulting glutathione. Coefficient of variation for various thiols measured by the *N*-(1-pyrenyl)maleimide method range from 1.5% to 8.8%. The lower detection limit is around 50 pmol of glutathione. *N*-(1-pyrenyl)maleimide derivatives are shown to be stable for 2 months at 4 °C. Between 94.2% and 97.2% of glutathione and/or glutathione disulfide added to a sample is recovered using *N*-(1-pyrenyl)maleimide method. The *N*-(1-pyrenyl)maleimide method is compared to the monobromobimane high-performance liquid chromatography method and the Tietze assay by measuring glutathione in homogenates from five different cell lines. The method offers some advantages over the currently accepted techniques, including specificity, speed, sensitivity, and ease to use.

Tipple and Rogers [88] presented a high-performance liquid chromatography for the separation and fluorometric detection of glutathione and other thiols. This technique is using iodoacetic acid as the thiol alkylating agent followed by dansyl chloride derivatization for fluorometric detection. The method is advantageous because it is amenable to small samples quantities and detects thiols and disulfides of several small molecules, glutathione, oxidized glutathione, cysteine, cystine, and mixed disulfides in a single run using ion-pairing chromatography.

Determination of glutathione, cysteine, and *N*-acetylcysteine in rabbit eye tissues using high-performance liquid chromatography and postcolumn derivatization with 5,5'-dithiobis(2-nitrobenzoic acid) was reported by Nozal *et al.* [98]. Samples of rabbit eye tissues, 0.2 g lens, 0.04 g retina, or 0.7 g vitreous, were homogenized, diluted with 2 ml 2 mM EDTA at pH 6, sonicated and centrifuged at 2500 $\times g$ and 4 °C. The supernatants were frozen at -80 °C until required for high-performance liquid chromatography analysis. The analysis was carried out on a Spherisorb 5 ODS 2 column (25 cm \times 4.6 mm i.d., 5 μ m) with an injection volume of 100 μ l, 0.05 M phosphate buffer at pH 3 as the mobile phase (1 ml/min), post-column addition (0.25 ml/min) of the chromogenic reagent containing 40 mg/l 5,5'-dithiobis(2-nitrobenzoic acid) and 80 mg/l hexadecyltrimethylammonium bromide at pH 9 and ultraviolet detection at 412 nm. The detection limits for glutathione, cysteine, and *N*-acetylcysteine in eye tissue were 0.21, 0.92, and 0.61 μ mol/g wet tissue, respectively.

An ion-pairing high-performance liquid chromatography method was used by Yoo *et al.* [99], for the determination of glutathione in biological samples. Plasma (300 μ l) was deproteinized with 0.6 M perchloric acid (300 μ l) and centrifuged. The supernatant was treated with 1.55 M sodium hydroxide (10 μ l), then 0.125 M sodium tetraborate (125 μ l, pH 9.6) and with derivatizing agents monobromobimane or 4-fluoro-7-sulfobenzofurazan. The mixture was incubated at 60 °C for 20 min or 40 °C for 30 min and then cooled on crushed ice. Acetic acid (10 μ l) was then added. Analysis was performed on a 5- μ m LiChrospher 100 C18 column (25 cm \times 4 mm i.d.), ammonium phosphate buffer/methanol (30%), plus 11.8 μ g/ml *N*-acetylcysteine (internal standard) as mobile phase (1 ml/min), fluorescence detection. Monobromobimane gave 200-fold greater sensitivity than 4-fluoro-7-sulfobenzofurazan. The detection limit was 0.03 μ g/ml. Linear range was 0.08–8.33 μ g/ml, with a correlation coefficient of 0.998.

Analysis of glutathione and glutathione disulfide in whole cells and mitochondria by postcolumn derivatization high-performance liquid chromatography with *o*-phthalaldehyde was reported by Lenton *et al.* [100]. Glutathione and glutathione disulfide were determined by high-performance liquid chromatography on a 5 μ m ODS column (15 cm \times 4.6 mm i.d.) with 50 mM phosphate buffer of pH 3 as mobile phase (1 ml/min). Postcolumn reaction with 373 μ M *o*-phthalaldehyde in 200 mM phosphate buffer of pH 12 was performed (with solutions combined in a ratio 1:1) in a 2-m reaction loop at 60 °C. Fluorescence was monitored at 425 nm (excitation at 340 nm). The method was applied to the determination of glutathione and glutathione disulfide in whole cell and mitochondrial extracts of primary human lymphocytes and granulocytes (preparation details given). Calibration graphs were linear from 0.4 to 200 pmol glutathione disulfide and the detection limit was approaching 100 fmol. Intra- and interassay relative standard deviations of glutathione disulfide in a mitochondrial fraction were 2.9% and 4.3%, respectively. Recovery of glutathione disulfide from *N*-ethylmaleimide-treated Jurkat whole-cell lysates was 98.2%. The method was sensitive enough to detect whole-cell glutathione disulfide in 10,000 cells or mitochondrial glutathione disulfide in 20 million cells.

An improved simultaneous measurement of oxidized and reduced glutathione in biological samples by high-performance liquid chromatography following derivatization with dansyl chloride was published by Nishijima *et al.* [101]. Tissue was homogenized in 5% ice-cold trichloroacetic acid containing lithium hydroxide at pH 7 to yield a 10% homogenate with

deproteinization; the homogenate was immediately centrifuged for 10 min at 4 °C. A 200- μ l portion of the supernatant solution was treated with 200 μ l 0.5 M boric acid/lithium hydroxide buffer of pH 8.5 and 4 μ l 1 mM iodoacetic acid in the dark for 30 min at 25 °C; 400 μ l of 1 mg/ml dansyl chloride in acetonitrile was added for derivatization over 1 h. The reaction mixture was washed with 400 μ l chloroform, and then the upper phase was centrifuged for 5 min. The derivatized reduced and oxidized glutathiones, respectively, were separated and determined by high-performance liquid chromatography on a 5 μ m LiChrospher-NH₂ column (12.5 cm \times 4 mm i.d.) equipped with a precolumn, operated at 35 °C, with linear gradient elution at 1 ml/min with aqueous 80% methanol (solvent A) and 50 ml sodium acetate/acetic acid/water (272 g:378 ml:122 ml) added to 450 ml A (solvent B) from 0% to 100% B over 26 min, and fluorimetric detection at 541 nm (excitation at 328 nm). Recoveries were 94.9–106%, with relative standard deviation of 2.88–4.65%. The method was applied to rat kidney and liver tissues. Results were compared with those obtained by the enzymic assay. There was no interference.

An automated high-performance liquid chromatography analysis of glutathione and thiol-containing compounds in grape juice and wine using precolumn derivatization with fluorescence detection was reported by Park *et al.* [102]. Grape juice samples (0.5 ml) were diluted with 5 mM sodium acetate buffer (0.5 ml) then derivatized using an automated procedure in an auto sampler. *o*-Phthalaldehyde (2 μ l) was taken up in autosampler syringe, 5 μ l of grape juice was taken, and finally 2 μ l, 2-aminoethanol was taken and mixed for 1 min inside the capillary. The derivatized sample was injected and analyzed by high-performance liquid chromatography on a Ultramex 3 C18 column (100 cm \times 4.6 mm i.d.), 0.05 M sodium acetate buffer and methanol as mobile phase with gradient elution and fluorescence detection at 450 nm (excitation at 340 nm). Glutathione, cysteine, methanethiol, and ethanethiol were separated with detection limits of 1 μ g/l, 2.7 mg/l, 12.8 and 11 μ g/l, respectively. Linear responses were achieved for Glutathione up to 40 mg/l and for cysteine up to 21 mg/l. Results for these compounds in grape juice and wine are presented graphically and discussed.

A very sensitive high-performance liquid chromatography method for the determination of total glutathione and γ -glutamyl-cysteine content in cell lysates was presented by Sack *et al.* [103]. It is based on a precolumn derivatization with *o*-phthalaldehyde using tris(2-carboxyethyl)phosphine as a reducing agent. Separation of the peptide derivatives is carried out by

reversed-phase chromatography on a C18 column, followed by fluorimetric detection. The fluorescence response of glutathione and γ -glutamyl-cysteine derivatives is linear from 0.05 to 100 and 1 to 25 μM , respectively, with good precision. The detection limits approach 26 and 60 fmol on column, respectively. In contrast the detection limit for glutathione in the presence of dithiothreitol, which is often used as the reducing agent, is 250 fmol glutathione on-columns. The results for the glutathione concentration of cell lysates are in agreement with a radiotracer method based on metabolic labeling of glutathione with [^{35}S]-cysteine.

A new rapid and highly sensitive high-performance liquid chromatography method with *o*-phthalaldehyde precolumn derivatization was developed by Cereser *et al.* [104] for determination of reduced glutathione and total glutathione in human red blood cells and cultured fibroblasts. *o*-Phthalaldehyde derivatives were separated on a reversed-phase high-performance liquid chromatography column with an acetonitrile/sodium acetate gradient system and detected fluorimetrically. An internal standard (glutathione ethyl ester) was added to facilitate quantitation. The total glutathione was determined after reduction of disulfide groups with dithiothreitol; the oxidized glutathione was determined by difference. The assay showed high sensitivity (50 fmol per injection, the lowest reported), good precision (relative standard deviation <5%), an analytical recovery of glutathione, and oxidized glutathione close to 100% and linearity ($r > 0.999$). This high-performance liquid chromatography technique is very simple and rapid. Its wide applicability and high sensitivity make it a convenient and reliable method for glutathione determination in various biological samples.

Three methods for the determination of rat hepatocellular thiols by high-performance liquid chromatography with fluorescence detection were developed by Toyo'oka *et al.* [105]. The thiols in the cells were tagged with three fluorogenic reagents, ammonium 7-fluoro-2,1,3-benzoxadiazole-4-sulfonate (SBD-F), 4-(aminosulfonyl)-7-fluoro-2,1,3-benzoxadiazole (ABD-F), and 4-(*N,N*-dimethylaminosulfonyl)-7-fluoro-2,1,3-benzoxadiazole (DBD-F). These reagents could permeate into cells and effectively reacted with thiols to produce highly fluorescent derivatives. These derivatives fluoresced in the long wavelength region at around 530 nm (excitation at around 380 nm). The five biological thiols tagged were perfectly separated by reversed-phase liquid chromatography and were sensitively and selectively detected without any interference from endogenous substances. The main thiols in the cells were reduced glutathione and the concentration was at the mM level. The procedures were applied to the

determination of hepatocellular glutathione after treatment of environmental pollutants such as volatile organic compounds and endocrine disrupting chemicals. From the comparison of intracellular glutathione concentration, the test compounds were classified into four groups: compounds of strong depletion (e.g., triphenyltin chloride, hexachlorocyclohexane, nonylphenol, bromoacetic acid, 4-chlorobenzyl chloride, and 1,3-dichloropropene), slight decrease (e.g., bisphenol A, benzo[*a*]pyrene, carbon tetrachloride, and benzene), slight increase (e.g., bromoform and toluene), and no effect (e.g., 1,1,1-trichloroethane, 1,1,2-trichloroethane, and 1,2-dichloroethane). Although the decrease of glutathione concentration does not reflect the cytotoxicity of chemicals, the procedure utilizing isolated rat hepatocytes seems to be useful for investigating the bioactivation of volatile organic compounds, endocrine disrupting chemicals, etc. Principal component analysis and classification methods are used to extract maps of the pure components from a degradation image data set. The maps are compared with elemental X-ray photoelectron spectroscopy images and maps of the pure components extracted from an images-to-spectra data set. Analysis of the image data provides insight into the difficulties in basing quantification on the C 1s photopeak curve fits.

A simple and widely used homocysteine high-performance liquid chromatography procedure was applied by Abukhalaf *et al.* [106] for the high-performance liquid chromatography identification and quantitation of glutathione in plasma. The method which utilizes SBD-F as a derivatizing agent utilizes only 50 μl of sample volume. Linear quantitative response curve was generated for glutathione over a concentration range of 0.3125–62.50 $\mu\text{M/l}$. linear regression analysis of the standard curve exhibited correlation coefficient of 0.999. Limit of detection and limit of quantitation values were 5.0 and 15 pmol, respectively. Glutathione recovery using this method was nearly complete (above 96%). Intra-assay and interassay precision studies reflected a high level of reliability and reproducibility of the method. The applicability of the method for the quantitation of glutathione was demonstrated using human and rat plasma samples.

A high-performance liquid chromatography-based method for quantifying glutathione, cysteine and cysteine-containing peptides was described by Ohmori *et al.* [107]. *N*-(2,4-dinitrophenylaminoethyl)maleimide was synthesized from ethylenediamine, 2,4-dinitrochlorobenzene, and maleic anhydride. The maleimide was allowed to react at 40 °C and pH 5.8 for 10 min with thiol compounds such as glutathione or cysteine. An aliquot of the reaction mixtures was applied to a reversed-phase column (15 cm \times 4.6 mm i.d.)

for high-performance liquid chromatography. When glutathione and cysteine were simultaneously assayed, the column was eluted with a gradient of acetonitrile in potassium phosphate (pH 7). The derivatives were monitored at 350 nm. Good linear relationships existed between peak area and concentration of glutathione or cysteine from 10 pmol to 2 nmol. The recovery results from rat liver homogenate were $99.7 \pm 2.2\%$ for glutathione and $104.9 \pm 3.8\%$ for cysteine. By this method, γ -glutamylcysteine, cysteinylglycine, and homocysteine could also be quantified. The determination limits of glutathione, cysteine, and other thiol compounds were 5 pmol. The method is simple: a sample solution is mixed with the labeling reagent and an aliquot of the reaction mixture is applied to a standard high-performance liquid chromatography. The hepatic levels of cysteine and glutathione in precancerous rats were determined by this method. The cysteine level in precancerous livers was extremely elevated in comparison to that of the control groups, while no difference was observed in the glutathione contents between the precancerous and control groups.

A method for the simultaneous quantification of reduced and oxidized glutathione in human plasma employing a two-dimensional chromatographic system with parallel porous graphitized carbon columns coupled with fluorescence and coulometric electrochemical detection was developed by Sakhi *et al.* [108]. Postsampling oxidation of reduced glutathione was prevented by derivatizing the thiol group with monobromobimane and the glutathione-bimane adduct was detected by fluorescence. Oxidized glutathione was detected by electrochemical detection optimized to give lowest possible limits of detection. The method is fully validated and is currently used for the determination of glutathione and oxidized glutathione and its redox potential in different clinical studies.

A robust method for the simultaneous quantification of endogenous reduced glutathione and oxidized glutathione in as little as 5 μ l human plasma employing two-dimensional chromatographic system with parallel Hypercarb columns coupled with dual fluorescence detectors was developed by Sakhi *et al.* [109]. After sample preparation, 10 μ l of supernatant was injected into the chromatographic system. The limits of detection of glutathione and oxidized glutathione were 0.5 and 0.040 pmol on column, respectively. Derivatization of glutathione and oxidized glutathione with monobromobimane and *o*-phthalaldehyde provides a sensitivity and specificity that allows analysis after fingertip sampling, blood sampling from infants, or multiple blood sampling from mice or other small experimental animals without sacrificing the animal.

A sensitive, reproducible, and robust high-performance liquid chromatography method was validated by Nolin *et al.* [110] for simultaneously determining total concentrations of the aminothiols homocysteine, cysteine, cysteinylglycine, and glutathione in human plasma. Plasma aminothiols are reduced via incubation with tris-(2-carboxyethyl)-phosphine hydrochloride, followed by protein precipitation with trichloroacetic acid and derivatization with ammonium-7-fluorobenzo-2-oxa-1,3-diazole-4-sulfonic acid. Separation of aminothiols and the internal standard mercaptopropionylglycine is achieved using reversed-phase high-performance liquid chromatography conditions and fluorescence detection. Excellent linearity is observed for all analytes over their respective concentration ranges with correlation coefficients (r) > 0.99. The intra- and interday precision and accuracy were within $\pm 10\%$. This method utilizes an internal standard, employs phosphate buffered saline-based standards and quality controls, and demonstrates excellent plasma recovery and improved sensitivity. This assay is well suited for high-throughput quantitative determination of aminothiols in clinical studies and is currently being used to support investigations of oxidative stress in patients with chronic kidney disease.

A high-performance liquid chromatography method for determination of both reduced and oxidized glutathione in plasma, whole blood, and rat hepatocytes was developed and evaluated by Kand'ár *et al.* [111]. Reduced glutathione reacts with *o*-phthalaldehyde to form a stable, highly fluorescent tricyclic derivate at pH 8, while oxidized glutathione reacts with *o*-phthalaldehyde at pH 12. At measurement of oxidized glutathione, glutathione was complexed to *N*-ethylmaleimide. For the separation, reverse phase column Discovery C18, 150 mm \times 4 mm, 5 μ m, was used. The mixture of methanol and 25 mM sodium hydrogen phosphate (15:85, v/v), pH 6.0, was used as mobile phase. The analytical performance of this method is satisfactory for both glutathione and oxidized glutathione. The intra-assay coefficients of variation were 1.8% and 2.1% for whole blood, 2.0% and 1.9% for rat hepatocytes, and 4.3% and 5.2% for plasma. The interassay coefficients of variation were 5.8% and 6.2% for whole blood, 6.6% and 7.1% for rat hepatocytes, and 6.9% and 7.8% for plasma. The recoveries were 98.2% (coefficients of variation 3.5%) and 101.5% (coefficients of variation 4.2%) for whole blood, 99.1% (2.5%) and 102.3 (4.4%) for rat hepatocytes, 94.1% (coefficients of variation 7.5%), and 103.5% (coefficients of variation 8.5%) for plasma. The calibration curve was linear in the whole range tested. The limit of detection was 14.0 and 5.6 fmol, respectively. The preliminary reference ranges of reduced and oxidized glutathione in a group of blood

donors are (4.69 ± 0.93) and $(0.28 \pm 0.12) \mu\text{M/gHb}$ for whole blood (1.82 ± 0.55) and $(0.154 \pm 0.044) \mu\text{M}$ for plasma.

A modified preparation of sample was developed by Lucija *et al.* [112] for the determination of glutathione content in grape juice and wine by high-performance liquid chromatography with fluorescence detection, using on-line precolumn derivatization. Ice-cold deoxygenated methanol was used to deactivate the oxidation enzymes in juices or wines and keep the glutathione stable. The optimum recovery of glutathione content in grape juice and wine was obtained when either the sample of grape juice or wine was mixed in ice-cold deoxygenated methanol in the ratio 10:90 (v/v) and further diluted in sodium acetate buffer in the ratio 1:1 (v/v). The optimized method was validated for linearity, limit of detection, limit of quantification, precision, and uncertainty. According to the validation data, the method is appropriate for the determination of glutathione content in grape juice and wine. Glutathione contents in grape juices made from White Muscat grapes and Sauvignon Blanc wines were analyzed. The average glutathione content in 28 young Sauvignon Blanc wines was 12.5 mg/l.

A method for the determination of the content of total glutathione was introduced by Ma *et al.* [113] based on high-performance liquid chromatography with dansylation. The minimum detection concentration of total glutathione was 0.5 $\mu\text{g/ml}$ and the measurable range of 1.0–300 $\mu\text{g/ml}$. Total glutathione in yeasts was obtained by hot-water extraction, glutathione complete autooxidation to oxidized glutathione in alkaline solution and purification by thin-layer chromatography. The quantitative determination of oxidized glutathione was derived by dansyl chloride at pH 9.5, 60 °C for 60 min, and assayed by high-performance liquid chromatography.

A simple and automated high-performance liquid chromatography method for the separation and quantitative determination of γ -glutamylcysteine and reduced glutathione in wines was reported by St phanie and de Revel [114]. This technique involves the use of a precolumn derivatization with 2,3-naphthalenedialdehyde, an isocratic separation in presence of β -cyclodextrin and a fluorimetric detection. The quantification of oxidized glutathione has also been studied, for the first time in wines, using an additive pre-derivatization step for reduction using glutathione reductase. The method has been designed for use in laboratories with limited equipment. The assay has been optimized and presents very good performances in terms of sensitivity and selectivity. Then, it has been validated for linearity, limit of detection, limit of quantitation, precision, and accuracy.

A high-performance liquid chromatography fluorescence method was established by Ju *et al.* [115] for simultaneous determination of cysteine, glutathione, and phytochelatins (2–6) after treatment with disulfide reductant of tris (2-carboxyethyl) phosphine hydrochloride and thiolite reagent of monobromobimane. The separation of thiol derivatives was performed on an Agilent Zorbax Eclipse XDB-C18 column (4.6 mm × 30 mm, 1.8 μ m) with a linear gradient elution of 0.1% (v/v) trifluoroacetic acid–acetonitrile at 0.8 ml/min. The temperature of the column was maintained at 25 °C. The excitation and emission wavelengths were set at 380 and 470 nm, respectively. The thiol derivatives were well separated in 19 min, and the total analysis time was 30 min. The established method was proved selective, specific and reproducible, and could be applicable to determine cysteine, glutathione, and phytochelatins (2–6).

A developed, valid, and application of a new green liquid chromatographic method for the determination of glutathione in vegetable samples was published by Zacharis *et al.* [116]. Ethyl propiolate was introduced as an advantageous post-column derivatization reagent for thiolic compounds. glutathione (t_r = 6.60 min) and *N*-acetylcysteine (internal standard) (t_r = 11.80 min) were separated efficiently from matrix endogenous compounds by using a 100% aqueous mobile phase (0.1%, v/v, acetic acid in 1 mmol/l EDTA, $Q(V)$ = 0.5 ml/min) and a Prevail[®] reversed-phase column that offers the advantage of stable packing material in aqueous mobile phases. The parameters of the postcolumn reaction (pH, amount concentration of the reagent, flow rates, length of the reaction coil and temperature) were studied. The linear determination range for glutathione was 1–200 μ mol/l and the limit of detection was 0.1 μ mol/l (signal-to-noise ratio = 3). Total endogenous glutathione was determined in broccoli, potato, asparagus, and Brussels sprouts using the standards addition approach. The accuracy was evaluated by both recovery experiments (R = 91–110%) and comparison to an *o*-phthalaldehyde/glycine corroborative post-column derivatization fluorimetric method.

An optimized rapid, sensitive, and accurate reversed-phase high-performance liquid chromatography methodology with fluorescence detection, for the simultaneous determination of the total concentrations of cysteine, homocysteine, cysteinylglycine, and glutathione in blood plasma, as well as its application to the evaluation of those thiols levels in plasma of a group of Azorean subjects was reported by Rita *et al.* [117]. Amino thiols were reduced with tri-*n*-butylphosphine and derivatized with a thiol-specific fluorogenic reagent ammonium 7-fluorobenzo-2-oxa-1,3-diazole-4-sulfonate.

The thiols adducts were separated by an isocratic elution on a Platinum EPS C18 analytical column (53 mm \times 7 mm, 3 μ m) using a phosphate buffer containing 4% of acetonitrile as a mobile phase. Results indicated an excellent linearity for all the analytes over their respective concentration ranges with correlation coefficients ($r^2 \geq 0.99$). The limit of detection for the four plasma thiols was lower than 0.10 μ mol/l, while limit of quantitation varied from 0.5 to 15 μ mol/l. For both intra- and interday precision, the relative standard deviation (%) values were lower than 1.9%, and the coefficient of variation (%) values were found under 0.5%. The recovery ranged from 92% to 100% indicating a high degree of the method's accuracy. This method allows a simultaneous, complete analysis of the four plasma aminothiols and the internal standard in 6 min. By reducing the total run time, a larger number of analyses can be performed daily.

A high-performance liquid chromatography method that uses the thiol-specific, fluorogenic reagent, 4-fluoro-7-aminosulfonylbenzofurazan for the simultaneous determination of total glutathione, cysteine, cysteinylglycine, and homocysteine in cell culture medium was described by Steele *et al.* [118]. 4-Fluoro-7-aminosulfonylbenzofurazan-labeled thiols were separated using an isocratic mobile phase consisting of 14% methanol and 86% 0.1 M acetate buffer at pH 4.0. The method was validated for linearity, accuracy, and intra- and interday precision, and the lower and upper limits of quantitation, were determined using a Dionex RF-2000 detector set to medium sensitivity. In addition, the suitability of *N*-acetylcysteine as an internal standard was evaluated by external and internal standard calibration methods. Although both calibration methods showed acceptable linearity (correlation coefficients >0.99) and intra- and interday precision (relative standard deviations = 10.2% and 6.6%, respectively), the external standard calibration method performed better in terms of accuracy (recovery = 93.7–125%) and also had lower limits of quantitation values for all analytes (cysteine = 6.3 μ M, cysteinylglycine = 0.8 μ M, homocysteine = 0.8 μ M, and glutathione = 1.6 μ M).

A rapid and highly sensitive high-performance liquid chromatography method with fluorescence detection has been developed by Wang *et al.* [119] for determination of glutathione in human plasma. A simple precolumn derivatization procedure with 7-fluoro-4-nitrobenzo-2-oxa-1,3-diazole (NBD-F) reagent was employed. The separation of the derivatized glutathione was performed using a mobile phase consisting of phosphate buffer (0.02 mol/l, pH 6.0)–acetonitrile (77:23, v/v) at a flow rate of 1.0 ml/min with the column temperature 2 $^{\circ}$ C. The eluted derivatives were fluorometrically detected at an excitation wavelength 470 nm and an emission

wavelength 530 nm. Under the optimum chromatographic conditions, the calibration curve was linear over the range of 0.1–10.0 $\mu\text{mol/l}$ with the correlation coefficient of 0.9988. The precision of the method was satisfactory with the intra- and interday coefficient of variation being 6.3% and 6.9%, respectively. This method has been used to determine glutathione concentrations in plasma samples from healthy individuals.

5.6.3 High-Performance Liquid Chromatography–Chemiluminescence

High-performance liquid chromatographic separation of glutathione and some mercapto-compounds with chemiluminescence detection was described by Li *et al.* [120]. The method was based on the chemiluminescence reaction between Ce(IV) and the mercapto group with detection based on Rhodamine B as a sensitizer in a flow system. High-performance liquid chromatography was performed with acetonitrile/water/0.1 M sodium acetate–acetic acid buffer (2:18:3) as mobile phase (0.9 ml/min; column details not given). Postcolumn chemiluminescence detection was performed after mixing with 0.4 mM Rhodamine B and 8 mM Ce(IV). Chemiluminescence detection was at 580 nm (excitation at 406 nm).

A direct determines intracellular glutathione based on a rapid chromatographic separation coupled with acidic potassium permanganate chemiluminescence detection was reported by McDermott *et al.* [121]. The procedure avoids derivatization of glutathione (thus minimizing autooxidation) and overcomes problems encountered when deriving the concentration of oxidized glutathione from total glutathione. The linear range and limit of detection for both analytes were 7.5×10^{-7} to 1×10^{-5} M, and 5×10^{-7} M, respectively. Glutathione and oxidized glutathione were determined in cultured muscle cells treated for 24 h with glucose oxidase (0, 15, 30, 100, 250, and 500 mU/ml), which exposed them to a continuous source of reactive oxygen species. Both analyte concentrations were greater in myotubes treated with 100 or 250 mU/ml glucose oxidase (compared to untreated controls), but were significantly lower in myotubes treated with 500 mU/ml ($p < 0.05$), which was rationalized by considering measurements of hydrogen peroxide and cell viability. However, the glutathione/oxidized glutathione ratio in myotubes treated with 100, 250, and 500 mU/ml glucose oxidase exhibited a dose-dependent decrease that reflected the increase in intracellular reactive oxygen species.

5.6.4 High-Performance Liquid Chromatography/Mass Spectrometry

A sensitivity and specificity afforded by coupling high-performance liquid chromatography to a tandem mass spectrometer to produce an assay for

glutathione concentrations in liver tissue was reported by Norris *et al.* [122]. The sensitivity suggests it may also be suitable for extrahepatic tissues. The method has been validated for glutathione using mouse liver samples and also allows the assay of glutathione disulfide. The stability of glutathione under conditions relevant to the assay has been determined. A 20- μ l amount of a diluted methanol extract of tissue was injected with detection limits of 0.2 pmol for glutathione and 2 pmol for oxidized glutathione. High-performance liquid chromatography was affected on a 5 μ m Altima C18 column (15 cm \times 4.6 mm i.d.) operated at 35 $^{\circ}$ C. Chromatography utilized a linear gradient from 0% to 10% methanol in 0.1% formic acid over 5 min, with a final isocratic stage holding at 10% methanol for 5 min. Total flow rate was 0.8 ml/min. The transitions from the $[M+H]^+$ ion (308.1 m/z for glutathione and 613.3 m/z for oxidized glutathione) to the 162.0 m/z glutathione and 355.3 m/z oxidized glutathione fragments, respectively, were monitored.

A rugged liquid chromatography-mass spectrometry-mass spectrometric method was developed by Loughlin *et al.* [123] to quantify reduced glutathione and oxidized glutathione in rat hepatocytes. In addition, conjugates of glutathione can be detected, characterized, and measured in the same analysis. Samples were treated with acetonitrile and iodoacetic acid to precipitate proteins and trap-free glutathione, respectively. These highly polar analytes were separated by ion exchange chromatography using conditions that were developed to be amenable to electrospray ionization and provide baseline chromatographic resolution. A solvent gradient with a total run time of 13 min was used to elute the analytes, as well as any highly retained components in the samples that would otherwise accumulate on the high-performance liquid chromatography column and degrade the chromatography. The analytes were detected using either selected-ion monitoring using an ion-trap mass spectrometry or selected reaction monitoring using a triple quadrupole mass spectrometry. The ranges for quantification of glutathione and oxidized glutathione using an ion trap were 0.651–488 and 0.817–327 μ M, respectively. Using selected reaction monitoring with the triple quadrupole instrument, the ranges of quantification for glutathione and oxidized glutathione were 0.163–163 and 0.0816–81.6 μ M, respectively. The accuracy and precision for both methods were within 15%. The utility of the method was demonstrated by treating rat hepatocytes with model compounds menadione(III) and precocene glutathione(IV). Menadione, which contains a quinone moiety that undergoes redox cycling and induces concentration- and time-dependent oxidative stress in hepatocytes,

resulted in decrease concentrations of glutathione with concomitant increase in concentrations of oxidized glutathione, as well as a glutathione–menadione conjugate. When hepatocytes were incubated with precocene glutathione, a time-dependent decrease in the concentration of glutathione was observed with concomitant increase in a glutathione–precocene glutathione conjugate. Concentrations of oxidized glutathione did not increase in the presence of precocene glutathione, consistent with its lack of redox activity. This analytical method has general utility for simultaneously investigating the potential of test compounds to induce both oxidative stress from redox cycling *in vitro* and the formation of conjugates of glutathione.

A sensitive and specific liquid chromatography–electrospray ionization mass spectrometric assay method for the simultaneous determination of reduced and oxidized glutathione in peripheral blood mononuclear cells was developed by Camera *et al.* [124]. Following derivatization with *N*-ethylmaleimide to prevent glutathione autooxidation, addition of thiosalicylic acid as internal standard and protein precipitation with cold acetonitrile, the samples were injected into a diol column, eluted with acetonitrile/1% acetic acid (1:3), and detected by the electrospray ionization mass spectrometric system. The optimized method exhibited a good detection limit for both analytes (10 and 50 nM for glutathione and oxidized glutathione, respectively). Good linearity was reached in the 0.01–20 μ M range for glutathione and 0.05–20 μ M for oxidized glutathione. The mean recoveries of glutathione and oxidized glutathione were 98.5–100.6% and 105.8–111.5%, respectively. The run-to-run repeatability for retention time and peak area was 0.06% and 1.75% relative standard deviation for glutathione and 0.18% and 2.5% relative standard deviation for oxidized glutathione. The optimized method was applied to glutathione and oxidized glutathione assay in peripheral blood mononuclear cells analyzing 20 healthy individuals.

A validated high-performance liquid chromatography–mass spectrometry method for determination of glutathione in spruce needles was reported by Gucek *et al.* [125]. Freeze-dried sample (50 mg) was homogenized with 2 ml 0.1 M HCl, the mixture was centrifuged, and the supernatant liquid was analyzed by LC on a 5- μ m Nova-Pak C18 column (15 cm \times 3.9 mm) operated with gradient elution (0.3 ml/min) with methanol in aqueous 0.1% trifluoroacetic acid (program details given) and electrospray ion-trap or triple-quadrupole mass spectrometric detection with both selected-ion monitoring of the $[M+H]^+$ ion of glutathione at m/z 308 (precursor) and multiple reaction monitoring of the characteristic fragments at m/z 179

and 162. Whereas the former technique offered the selectivity of MSn scans, the latter permitted the detection also of the dimer and trimer of glutathione and its sulfonate and sulfinic acid analogues. Although results obtained by the external-standard and standard-additions methods showed acceptable agreement, neither method was entirely satisfactory, and the use of [^{15}N] glutathione as internal standard is envisaged.

A new, fast, and reliable method to measure reduced or oxidized glutathione in whole blood was described by Steghens *et al.* [126]. The method is based on a liquid chromatography-mass spectrometry measurement in positive electrospray ionization mode after a chromatographic separation on a specific column which does not need any counter-ion in the mobile phase, improving the sensitivity of detection. A 50- μl sample of whole blood is sufficient for analysis. The lack of an alkylating agent during the sample preparation brings out an underestimation of glutathione and an artefactual production of oxidized glutathione corresponding to 2–3% of glutathione. The simultaneous use of *N*-ethylmaleimide and a strong deproteinizing acid prevents these two drawbacks. This efficient and new method of preparation and analysis lets us show that, unexpectedly, glutathione is stable in whole blood for some hours and that deproteinized samples can be stored without glutathione loss for at least 3 weeks at -20 or -80 °C. The reference interval, measured on 22 volunteers, on blood samples collected either with heparin or with EDTA, is 1310 ± 118 μM for glutathione and 0.62 μM for oxidized glutathione. The within-run precision of this method, with γ -glutamyl-glutamic acid as an internal standard, evaluated in three successive series ($n = 30$), lies between 2.1% and 4.8% for a glutathione level at 580 or 1150 μM . The one step sample preparation we propose seems well suited for glutathione routine measurements in hospital laboratories and avoids any underestimation of glutathione, a now well accepted biomarker of oxidative stress.

A liquid chromatography-mass spectrometry method was developed by Guan *et al.* [127] for simultaneous detection and quantitation of glutathione, glutathione disulfide, cysteine, homocysteine, and homocystine in biological samples (rat brain, lung, liver, heart, kidneys, erythrocytes, and plasma). Thiols were derivatized with a large excess of Ellman's reagent, a thiol-specific reagent, to ensure an instantaneous and complete derivatization. The derivatization blocked the oxidation of the thiols to disulfides, preventing errors caused by thiol oxidation. The samples were then analyzed by liquid chromatography-mass spectrometry. The method provides a highly selective and sensitive assay for these endogenous thiols and their

corresponding disulfides. The detection limits for glutathione, glutathione disulfide, cysteine, homocysteine, and homocystine were 3.3, 3.3, 16.5, 29.6, and 14.9 pmol, respectively. An attempt for cystine analysis was unsuccessful due to earlier elution of the compound and strong interferences caused by other endogenous compounds. This method will be a useful tool in the investigation of the roles of these important thiol-containing compounds and their corresponding disulfides in physiological and pathological processes.

A simple and robust isotope dilution mass spectrometry-based assay was developed by Shuford *et al.* [128], for the determination of free cysteine and glutathione in aquatic insects. Several experimental parameters were evaluated and optimized to provide specific and sensitive detection of both compounds by *in situ* derivatization with *N*-ethylmaleimide followed by acid alkylation quenching and reversed-phase liquid chromatography coupled with selected reaction monitoring. For both targets, the assay was evaluated over a concentration range of 0.313–320 μM and was demonstrated to have a quantitative dynamic range spanning nearly three orders of magnitude, with lower limits of quantification being 0.330 μM for glutathione and 0.370 μM for cysteine. Additionally, measurements were observed to be highly reproducible over the course of several days. When applied to the analysis of four different species of insects, large biological variation between and within species was observed. Different feeding regimens were also tested within two species of insects but statistical comparisons revealed no significant difference in the levels of either compounds.

A simple, highly selective, sensitive, and reproducible liquid chromatography-electrospray ionization/mass spectrometry (time of flight) method has been developed by Rellán-Álvarez *et al.* [129] for the direct and simultaneous determination of glutathione and related compounds such as homoglutathione in different plant tissues. These compounds are low-molecular mass antioxidants involved in cellular redox homeostasis in plants, and efforts are being made to develop methods to determine the concentrations of oxidized and reduced forms of these compounds and their ratio. Many of the methodologies developed so far, however, are time-consuming and complex; therefore, analytes can decompose and their redox status can change during the analysis process. The method allows the simultaneous determination of reduced forms (glutathione and homoglutathione) and oxidized forms (glutathione disulfide) of these compounds and is also suitable for the determination of ascorbic acid and *S*-nitrosglutathione. Quantification was done using isotopically labeled glutathione and ascorbic

acid as internal standards. All compounds were base peak resolved in less than 6 min, and limits of detection were 60 pmol for glutathione, 30 pmol for homogluthathione, 20 pmol for oxidized glutathione, 100 pmol for ascorbic acid, and 30 pmol for S-nitrosogluthathione. The intraday repeatability values were approximately 0.4% and 7% for retention time and peak area, respectively, whereas the interday repeatability values were approximately 0.6% and 9% for retention time and peak area, respectively. Analyte recoveries found were between 92% and 105%. The method was used to determine the concentrations of glutathione, oxidized glutathione, homogluthathione, and ascorbic acid in extracts from several plant tissues.

5.6.5 High-Performance Liquid Chromatography/Electrochemical

The determination of reduced glutathione in human whole blood by high-performance liquid chromatography with electrochemical detection by graphite–epoxy resin electrode chemically modified with cobalt phthalocyanine was developed by Wring *et al.* [130]. Blood was treated with sulfosalicylic acid, set aside in the dark for 5 min and centrifuged at 3000 rpm for 10 min. A 10- μ l portion of the filtered supernatant solution was analyzed by high-performance liquid chromatography on a column (30 cm \times 3.9 mm) of μ Bondapac (10 μ m), equipped with a guard column containing 30–40 μ m ODS pellicular packing, with 0.05 M phosphate buffer (pH 2.3) containing 1 mM EDTA as mobile phase (1 ml/min) and electrochemical detection by means of a graphite–epoxy resin composite electrode, modified with cobalt phthalocyanine at +0.5 V versus Ag–AgCl. The calibration graph was rectilinear and the detection limit was 450 pg of glutathione; recoveries were 95%.

A simultaneous quantitation of oxidized and reduced glutathione in equine biological fluids by reversed-phase high-performance liquid chromatography using electrochemical detection was published by Smith *et al.* [131]. For plasma, a 0.5-ml portion was vortex-mixed with 500 μ l 5% perchloric acid, the mixture was centrifuged at $13,000 \times g$ for 5 min and the supernatant was diluted (1:1) with mobile phase. For haemolysates, a 200 μ l portion was treated with perchloric acid and centrifuged as for plasma and the supernatant was treated with 40 μ l 10 M potassium hydroxide. The mixture was centrifuged at $1300 \times g$ for 2 min and the supernatant was diluted 1:10 with mobile phase. Portions (10 μ l) of each diluted supernatant/mobile phase solution were analyzed by high-performance liquid chromatography on a 3- μ m Hypersil ODS column (15 cm \times 4.6 mm i.d.) with 10 mM sodium dihydrogen phosphate buffer of pH 2.7 containing 5%

methanol as mobile phase (1 ml/min) and electrochemical detection at +0.35 and +0.85 V, for reduced glutathione and oxidized glutathione, respectively. The calibration graph was linear from 1 to 100 and 5 to 500 ng/ml, respectively, for glutathione and oxidized glutathione and the corresponding detection limits were 5 and 10 ng/ml. Recoveries were 99.05% and 99.1%, respectively, of glutathione and oxidized glutathione, in plasma and haemolysate. Inter- and intra-assay relative standard deviation ($n=6$) were 8.8% and 2%, and 10.8% and 5.1%, respectively, for glutathione and oxidized glutathione. The method was also applied to bronchoalveolar lavage fluid and to the analysis of glutathione and oxidized glutathione in biological fluids during stressful physiological conditions.

The determination of cysteine and reduced glutathione in human plasma by liquid chromatography with pulsed amperometric electrochemical detection using a platinum-particle modified glassy carbon electrode was developed by Liu *et al.* [132]. Blood (100 μ l) was vortex-mixed with 700 μ l EDTA (1 g/l) and 200 μ l 20% perchloric acid and the mixture was kept in the dark for 5 min. The mixture was centrifuged at 3000 rpm for 5 min and the supernatant was decanted and filtered (2 μ m). Portions (20 μ l) of filtrate were injected onto a high-performance liquid chromatography column with 0.1 M potassium phosphate buffer of pH 4.5 containing 50 μ M EDTA as mobile phase (1 ml/min) and pulsed amperometric detection at -1.0 V versus Ag/AgCl at a Pt particles dispersed chemically modified electrode. The calibration graph was linear from 0.1 to 5000 μ M cysteine and reduced glutathione and the detection limit was 1 pmol. The relative standard deviation ($n=10$) was 9.5%. The mean recovery ($n=3$) of cysteine was 97.2% in the concentration range of 5–3000 μ M. The method was applied to the analysis of cysteine and reduced glutathione in human plasma.

A validated high-performance liquid chromatography electrochemical method for determination of glutathione and glutathione disulfide in small tissue samples was published by Lakritz *et al.* [133]. Mouse trachea or lung was homogenized in methanesulfonic acid containing 5 mM diethylenetriamine pentaacetic acid (at pH < 2) and precipitated proteins were removed by centrifugation. Glutathione and glutathione disulfide were determined by high-performance liquid chromatography on a 5- μ m ODS-2 column (20 cm \times 4 mm i.d.) with 50 mM sodium dihydrogen phosphate/0.05 mM octanesulfonic acid/2% acetonitrile, adjusted to pH 2.7 with phosphoric acid as mobile phase (1 ml/min) and coulometric detection at 850–880 mV. The intraday relative standard deviation were

4.7–5.9% for glutathione and 4.4–5.7% for the disulfide; corresponding interday relative standard deviation ($n=5$) were 6.0–7.6% and 5.5–23%. Recovery was 86.2–98.3%. The calibration graph was linear from 0.8 pmol (detection limit) to 1.63 nmol of glutathione and the detection limit was 1.63 pmol of glutathione disulfide.

A simultaneous measurement of ascorbic acid and glutathione was reported using an online high-performance liquid chromatography with Au/Hg electrode was reported by Yang *et al.* [134]. A microdialysis perfusion system was coupled online with the liquid chromatography with electrochemical system to allow continuous analysis of extracellular fluids from anesthetized rat liver. Microdialysis probes (24 mm length) were perfused with Ringer's solution (2 μ l/min) before taking measurements. The microdialysates (19.6 μ l) were collected at 10 min intervals. Separation was achieved on a 5- μ m Econosphere C18 column (15 cm \times 4.6 mm i.d.) with 0.1 M monochloroacetic acid, 2 mM heptane sulfonic acid (sodium salt), and 0.046 M sodium hydroxide in 2% acetonitrile of pH 3 as mobile phase (0.8 ml/min) and electrochemical detection at +0.15 V versus Ag/AgCl. Good reproducibility was achieved. Results are discussed.

A novel assay for glutathione reductase activity by high-performance liquid chromatography with electrochemical detection was described by Ohkuwa *et al.* [135]. The enzyme sample (1–5 μ g of protein) was incubated in 0.1 M phosphate buffer of pH 7, containing 1 mM glutathione disulfide and 0.1 mM NADPH (total volume 0.1 ml) for 20 min at 37 °C. The reaction was stopped by addition of 0.1 ml 0.1 M perchloric acid containing 0.1 mM EDTA and 0.1 mM sodium meta-bisulfite. The mixture was cooled and centrifuged at 4 °C and the supernatant liquid was filtered (0.45 μ m). Portions were analyzed on a 5- μ m Biophase ODS-IV column (11 cm \times 4 mm i.d.) with 0.1 M monochloroacetic acid, adjusted to a pH of 3 with sodium hydroxide as mobile phase (0.8 ml/min). The thiol and disulfide forms of glutathione, separated by high-performance liquid chromatography, were detected at a dual electrode; the disulfide was reduced at the first, gold electrode and the thiol was detected at the second mercury electrode by oxidation at 0.1 V. Calibration graphs were linear up to at least 400 pmol of the thiol injected. Recovery of 250 pmol added to the incubation mixture was 96–97%, with intraday and interday relative standard deviation ($n=6$) of 3% and 2.8%, respectively. The method was applied to aqueous extracts of rat liver, heart, and brain.

A reversed-phase high-performance liquid chromatography with dual-electrochemical detection was used by Manna *et al.* [136] for determination

of oxidized and reduced glutathione in pharmaceuticals. Powder from one injection phial of a commercial pharmaceutical preparation was diluted to 100 ml with mobile phase and further diluted to give about 6 $\mu\text{g}/\text{ml}$ of the thiol drug. After filtration, 20 μl portions of the diluted solution were analyzed by high-performance liquid chromatography on a 5- μm Supelcosil LC-18 DB column (10 cm \times 4.6 mm i.d.), with aqueous 2% acetonitrile containing 0.1% trifluoroacetic acid as mobile phase (1.2 ml/min) and dual-electrochemical detection at 0.45 V for reduced glutathione and 0.75 V for oxidized glutathione. Calibration graphs were linear from 3 to 122 and 0.65 to 13 ng, respectively, for glutathione and glutathione disulfide, with corresponding detection limits of 0.6 and 0.15 ng, respectively. Intra- and interassay relative standard deviation for 0.771, 1.52, and 3.04 $\mu\text{g}/\text{ml}$ of glutathione were 0.5–2.7% ($n=5$ on 3 days); for 0.0604, 0.121, and 0.604 $\mu\text{g}/\text{ml}$ of glutathione disulfide relative standard deviation were 0.6–3.4% ($n=5$ on 3 days). In five commercial preparations, the results were 96.7–103.8% of the claimed 600 mg of glutathione; the amounts of the glutathione disulfide impurity were 1.3–2%. 5-(Pentafluorobenzoylamino) fluorescein: a selective substrate for the determination of glutathione concentration and glutathione S-transferase activity.

A glassy carbon electrode modified by the electrodeposition of a cobalt hexacyanoferrate (CoHCF) thin film as a detector with high-performance liquid chromatography was developed by Shi *et al.* [137], for determination of glutathione. The process was carried out using a solution containing 0.5 mM potassium ferricyanide and 1 mM cobaltous chloride in 0.1 M potassium dihydrogen phosphate at pH 3 by cycling the potential between 1.2 and -0.2 V versus Ag/AgCl at 0.1 V/s. The film was deposited over 30 cycles. The modified electrode was used as an amperometric detector in liquid chromatography for determining glutathione, cysteine, and N-acetylcysteine. The chromatography was performed on a Hypersil ODS column (20 cm \times 4.6 mm i.d.) with 0.1 M potassium dihydrogen phosphate at pH 3 as the mobile phase (0.8 ml/min). The detector was maintained at $+0.8$ V versus Ag/AgCl (stainless steel counter electrode). Calibration graphs were linear for 5–100 μM glutathione, 1.5–200 μM cysteine, and 3–100 μM N-acetylcysteine and detection limits were 1–2.5 μM . The method was applied to determine glutathione in the microdialysate of rat brain.

The simultaneous determination of glutathione, homocysteine, cysteinylglycine, and methionine in plasma by high-performance liquid chromatography with electrochemical detection was described by Houze

et al. [138]. Separation was carried out on an Inertsil 5 ODS 3 column with 1 ml/min of a mobile phase containing 8% methanol and 92% buffer (15 mM disodium hydrogen phosphate/15 mM monopotassium dihydrogen phosphate/1 μ M 1-octanesulfonate sodium salt adjusted to pH 2.6 with phosphoric acid) and electrochemical detection. Detection limits were 1 μ M for methionine and 0.5 μ M/ml for other analytes. Experimental details are given and the results are discussed.

A simultaneous determination of reduced and oxidized glutathione in freshly isolated rat hepatocytes and cardiomyocytes by high-performance liquid chromatography with electrochemical detection was reported by Remiao *et al.* [139]. A rapid and sensitive isocratic reversed-phase high-performance liquid chromatography method using coulometric detection was implemented for the simultaneous detection of glutathione and glutathione disulfide, in freshly isolated hepatocytes and cardiomyocytes of the rat. The method implemented proved to be effective for the measurement of glutathione and glutathione disulfide in control conditions and for the detection of variations in this redox system, induced by *tert*-butylhydroperoxide. *t*-Butylhydroperoxide is an organic peroxide, which has been used as a model molecule for inducing oxidative stress in isolated cells. A comparative study with a previously published high-performance liquid chromatography electrochemical detection method was performed.

5.6.6 Capillary Electrophoresis

A capillary zone electrophoresis with electrochemical detection for the determination of glutathione in human red blood cells without pre-separation of haemoglobin was reported by Jin *et al.* [140]. Interference is studied for the determination of glutathione in human red blood cells using capillary zone electrophoresis with end-column amperometric detection at a gold-mercury amalgam microelectrode. It is found that when interference substances such as haemoglobin in the haemolysate flow off from the end of the separation capillary, they can be adsorbed on the surface of the electrode and interfere with the signal of glutathione. If the concentration of haemolysate is lower 0.5% (v/v), this phenomenon can be overcome because they are adsorbed on the surface of the capillary wall and do not flow off from the capillary. A method is developed for the determination of glutathione in human erythrocytes without the pre-separation of haemoglobin.

Glutathione was determined by Jin *et al.* [141] in individual macrophages without the need for derivatization, by capillary zone electrophoresis on a fused-silica capillary (40 cm \times 20 μ m i.d.). Separation was performed at an

applied voltage of 20 kV in buffer consisting of 1.22 mM disodium hydrogen phosphate/7.8 mM sodium dihydrogen phosphate (pH 7) and 2 mM disodium dihydrogen EDTA with electrochemical end-column amperometric detection at a gold/mercury amalgam microelectrode. Macrophages could be lysed in 0.01 M sodium hydroxide. Glutathione levels of 5.8 fmol were determined in individual mouse peritoneal macrophage by this method.

A method for the simultaneous determination of nucleosides, bases, intracellular free ribonucleotides, and oxidized and reduced glutathione, in myocardial tissues by capillary electrophoresis was described by Carlucci *et al.* [142]. Biopsy specimens (<2 mg) were homogenized with >20 μ l 0.4 M perchloric acid and centrifuged. The pellet was resuspended in a similar volume of 0.1 M sodium hydroxide for analysis of protein content [143], whilst the supernatant was neutralized with 5 M potassium carbonate and centrifuged. A portion of the supernatant was hydrodynamically injected (12 s; 17.4 nl) into a bare CElect-Fs capillary (60 cm \times 75 μ m; 52.5 cm to detector) and separated at 26–27 $^{\circ}$ C with 20 mM borate buffer (pH 10), an applied potential of 20 kV, and detection at 185 nm. Under these conditions, 13 compounds were separated within 20 min. Calibration graphs were linear from 2 to 550 μ M for nucleotides, nucleosides and bases, and from 5 to 500 μ M for glutathione forms; detection limits were typically sub-nmol/mg protein. Intra- and interassay relative standard deviation ($n=8$) for peak area were 3.79% and 4.78%, respectively. Sampling relative standard deviation ($n=6$) for multiple analyses in the same heart are tabulated. The method offers comparable resolution to high-performance liquid chromatography, with the advantage of fast simultaneous measurement of cell nucleotide metabolism and redox state.

Determination of the reduced glutathione/oxidized glutathione ratio in blood by capillary zone electrophoresis was reported by Serru *et al.* [144]. Both forms of glutathione were determined on a fused-silica capillary using a boric acid/Tris buffer (3:1, pH 8.4) with detection at 200 nm. Methodology (assays linear over the range of 0.5–40 μ M) is presented and application to real samples discussed. Precolumn derivatization high-performance liquid chromatographic method for determination of cysteine, cysteinylglycine, homocysteine and glutathione in plasma, and cell extracts.

A method for the determination of rat hepatocellular glutathione by capillary electrophoresis with laser-induced fluorescence detection utilizing He–Cd laser line at 325 nm was developed by Toyo'oka *et al.* [145]. The glutathione in hepatocyte cells was tagged with three fluorogenic

reagents, ammonium 7-fluoro-2,1,3-benzoxadiazole-4-sulfonate (SBD-F), 4-(aminosulfonyl)-7-fluoro-2,1,3-benzoxadiazole (ABD-F), and 4-(*N,N*-dimethylaminosulfonyl)-7-fluoro-2,1,3-benzoxadiazole (DBD-F). These reagents were permeable into cells and reacted with glutathione to produce highly fluorescent derivatives, but the efficiency was different among the reagents. Judging from fluorescence microscope analysis, 4-(aminosulfonyl)-7-fluoro-2,1,3-benzoxadiazole seems to be suitable for the tagging of hepatocellular glutathione, in terms of the permeability to the cells and the reaction selectivity to glutathione. The resulting ABD-glutathione was effectively resolved by capillary zone electrophoresis with a running buffer of 20 mM phosphate (pH 7.5) at 30 kV applied potential. The determination of intracellular glutathione in isolated rat hepatocytes before and after treatments with environmental pollutants was carried out with the capillary electrophoresis conditions. The glutathione concentrations in untreated cells obtained from 8- to 11-year-old rats were calculated as 14–103 fmol per cell. On the other hand, the hepatocellular glutathione levels after treatment of bisphenol A and 1,3-dichloropropene were obviously decreased as compared with control glutathione concentrations. The degrees of the depletion were essentially similar to results obtained from high-performance liquid chromatography fluorescence method.

A simultaneous analysis of oxidized and reduced glutathione in cell extracts by capillary zone electrophoresis was reported by Yang *et al.* [146]. In this study, a capillary zone electrophoresis method is described that enables the quantitation of glutathione and oxidized glutathione from cellular extracts. The capillary zone electrophoresis buffer used was 20 mM ammonium acetate containing 5% (v/v) acetic acid at pH 3.1 in conjunction with a polybrene-coated capillary operated in reverse polarity mode. Effects of different acids used to prepare cell samples on capillary zone electrophoresis performance were investigated. The acids included metaphosphoric acid, trichloro acetic acid, phosphoric acid, and sulfosalicylic acid and were used to stabilize glutathione and oxidized glutathione before performing capillary zone electrophoresis analysis. The method features a limit of detection of 4 μM and a limit of quantification of 12 μM for both glutathione and oxidized glutathione and recoveries of 94% for glutathione and 100% for oxidized glutathione. Quantitative analysis of oxidized glutathione and glutathione in HaCaT cell extracts (5% sulfosalicylic acid, w/v) was performed with this method and changes in the ratio of glutathione to oxidized glutathione in a *N*-ethylmaleimide-treated cell sample were observed by comparing with control cell samples.

An optimization of the principal parameters for the ultrarapid electrophoretic separation of reduced and oxidized glutathione by capillary electrophoresis was studied by Carru *et al.* [147]. The optimized time, efficiency and resolution of the electrophoretic separation of reduced glutathione, and oxidized glutathione by studying the influence of the most important factors affecting the separation, i.e., the pH and ionic strength of the electrolyte solution, the capillary length, and temperature. Best results in the shortest time are obtained at 25 °C, using an uncoated 37 cm × 75 µm i. d. capillary and a 300 mM/l borate buffer pH 7.8. These conditions give a good reproducibility of the corrected peak areas (relative standard deviation 1.41% and 1.31%) and of the migration time (relative standard deviation 0.22% and 0.26%) for glutathione and oxidized glutathione, respectively. The high concentration buffer, besides permitting a good resolution of standard glutathione and oxidized glutathione mix, allows also *N*-nitrosoglutathione detection. By shortening the capillary length to 27 cm, the separation time of glutathione and oxidized glutathione can be further decreased to less than 60 s. This shortened method, the most rapid described in literature, can detect and quantify glutathione in red blood cells despite a loss of sensitivity. To compare the new method here described with the Beutler colorimetric method, the data relative to the glutathione content of red blood cells from young normal subjects were analyzed by the Passing and Bablok regression and the Bland–Altman test.

A simultaneous determination of tryptophan and glutathione in individual rat hepatocytes by capillary zone electrophoresis with electrochemical detection at a carbon fiber bundle–Au/Hg dual electrode was reported by Jin *et al.* [148]. The parallel mode was used. Different potentials were applied to both electrodes of the dual electrode. Tryptophan and glutathione, which could not be simultaneously detected by normal capillary zone electrophoresis with electrochemical detection, could be simultaneously and selectively detected by capillary zone electrophoresis with electrochemical detection at the dual electrode in one run, respectively. The capillary zone electrophoresis with electrochemical detection system with the dual electrode was applied to determine them in individual rat hepatocytes.

A sensitive capillary electrophoretic method using low pH with direct ultraviolet detection was developed by Novatchev and Holzgrabe [149], to evaluate the impurity profile of reduced glutathione obtained from its production and purification. The method is characterized by high detection sensitivity and selectivity. Validation has been performed with model mixtures consisting of the main known related substances, oxidized glutathione,

glutamylcysteine, cysteinylglycine, and cysteine. The results from this study show that with respect to quantification criteria the method is acceptable for routine control of reduced glutathione for pharmaceutical application.

A method for determination of glutathione in single human hepatocarcinoma cells was described by Wang [150] using capillary zone electrophoresis with electrochemical detection at a gold/mercury amalgam microdisk electrode. When human hepatocarcinoma cells were washed with the running buffer instead of physiological buffer saline, only one electrophoretic peak for glutathione is depicted on the electropherograms of single human hepatocarcinoma cells. When electroosmotic injection of 0.01 mol/l sodium hydroxide for lysing the cell introduced into the capillary, the lysis time can be shortened to 5 s. The whole-cell injection and no need to derivatization reaction leads to more accurate and precise results. The average amount of glutathione in an individual human hepatocarcinoma cells is 22.3 ± 5.8 fmol (mean \pm standard deviation), which is consistent with that of its homogenate.

Govindaraju *et al.* [151] developed a suitable technique for analysis of glutathione and oxidized glutathione in microliter samples using capillary sampling followed by capillary zone electrophoresis analysis with conductivity detection. Capillary zone electrophoresis was carried out in 100 mM 2-(cyclohexylamino)-ethansulfonic acid and 40 mM lithium hydroxide with 5 mM spermine at pH 9.1 under an applied electric field of -416 V/cm. To prevent any autooxidation of glutathione during sample manipulations, the samples were treated with *N*-ethylmaleimide (50 mM) to alkylate free thiol group. Under these conditions, glutathione and oxidized glutathione were cleanly separated without interference from common anions (e.g., Cl^- , PO_4^{3-} , HCO_3^- , etc.) and the limit of detection for airway surface liquid analysis was $11 \mu\text{M}$ for glutathione and $8 \mu\text{M}$ for oxidized glutathione (signal-to-noise ratio = 3). Glutathione and oxidized glutathione were also measured in rat plasma. Baseline values of $897 \pm 210 \mu\text{M}$ glutathione and $215 \pm 61 \mu\text{M}$ oxidized glutathione were obtained for rat airway surface liquid ($n=8$), whereas $12.4 \pm 2.7 \mu\text{M}$ glutathione and $14.8 \pm 6.7 \mu\text{M}$ oxidized glutathione were obtained for rat plasma ($n=5$).

A micellar electrokinetic capillary electrophoresis was reported by Havel *et al.* [152] for quantitation of oxidized and reduced glutathione in plasma. Samples (0.1 ml) were mixed with 0.1 ml saline and 0.3 ml 20 mM phosphoric acid in acetonitrile and the mixture was centrifuged. The supernatant liquid (0.2 ml) was diluted with 0.8 ml 0.1 M hydrochloric acid and filtered ($0.2 \mu\text{m}$). A known amount of

N-acetyl-L-cysteine (10 µg/ml; internal standard) was added and portions were injected at 50 mbar for 10 s into the capillary (80.5 cm × 75 µm i.d., 72 cm to high-sensitivity flow cell detector). Electrophoresis was carried out at an applied voltage of 14.5 V, with 25 mM monosodium phosphate and 15 mM tetraborate buffer of pH 8, containing 50 mM sodium dodecyl sulfate as running buffer and detection at 195 nm. Calibration graphs were linear for 5–25 µg/ml of both the reduced glutathione and oxidized glutathione, with detection limits of 0.8 and 0.4 µM, respectively. With use of the internal standard, the relative standard deviation of peak areas for 5, 10, and 25 µg/ml were 0.72–1.29 and 1.45–2.22%, respectively, for glutathione and glutathione disulfide.

A quantitative determination of glutathione in single human erythrocytes by capillary zone electrophoresis with electrochemical detection was reported Jin *et al.* [153]. Human blood was centrifuged; the erythrocytes removed, washed repeatedly using fourfold phosphate-buffered saline and centrifugation, and then diluted 1:500 with phosphate-buffered saline. A 50-µl portion of suspension was placed on a glass slide, and a single-erythrocyte was electrokinetically injected (2 kV) into a fused-silica capillary (30 cm × 10 µm i.d.). Separations were performed on a capillary zone electrophoresis system, with 6.1 mM disodium hydrogen phosphate/3.9 mM sodium dihydrogen phosphate of pH 7 as running buffer, an applied potential of 25 kV, and end-column amperometric detection: Au/Hg-amalgam microelectrode at 0.06 V versus saturated calomel electrode (platinum auxiliary electrode). Peaks due to phosphate-buffered saline and glutathione were separated within 4 min. The calibration graph was linear from 0.2 to 20 µM glutathione, and the detection limit was 0.1 µM. For quantification of glutathione in single erythrocytes, the calibration was generated on a capillary with haemoglobin adsorbed on its surface: 4.97 fmol was injected into the capillary prior to sample injection. The method was rapid, selective, sensitive, and did not require derivatization procedures.

The determination of oxidized and reduced forms of glutathione in biological samples by capillary electrophoresis based on sample stacking was reported Shihabi *et al.* [154]. Prepared samples were deproteinized with acetonitrile and injected for 50 s onto the capillary column. Electrophoresis was effected on a fused-silica capillary (33 cm × 50 µm i.d.) operated at an applied voltage of 10 kV, with 250 mM borate and 50 mM Tris buffer of pH 8 and detection at 214 nm. The calibration graph was linear in the range of 5–100 mg/l for both forms of the peptide and the detection limit was improved 10–20-fold by sample stacking.

A very rapid high-performance capillary electrophoresis method for the separation and quantification of reduced glutathione and oxidized glutathione in red blood cells was described by Carru *et al.* [155]. Two procedures for sample preparation have been compared, Microcon-10 membrane filtration and acid precipitation. The separation is obtained in an uncoated capillary using a high ionic strength borate buffer at pH 7.8. The intra-assay coefficients of variation are 1.53 and 1.66 for glutathione and oxidized glutathione, respectively. The run is shorter than 90 s and the migration time is highly reproducible both for glutathione; coefficient of variation, 0.22, and oxidized glutathione; coefficient of variation 0.17. When the filtration step is used only glutathione is found, whereas both glutathione and oxidized glutathione are detectable after acid precipitation, suggesting that oxidized glutathione revealed after acid treatment may be an artifact due to glutathione oxidation. Because of its good analytical performance, this method could be used for routine red blood cell glutathione measurement in healthy or pathological conditions.

5.6.7 Gas Chromatography/Mass Spectrometry

Gas chromatographic-mass spectrometric method for the analysis of stable isotopes of cysteine and glutathione in biological samples was reported by Capitan *et al.* [156]. The method was applied to a study of synthesis rate and the isotopic enrichment in glutathione after infusion of radiolabeled into humans and rats. Blood samples (2 ml) were diluted with 1 ml 0.2 M phosphate buffer of pH 8.5, containing 5 mM ethylene diamine tetraacetic acid and 80 mM dithiothreitol (buffer A) and the proteins were precipitated with 0.2 ml 50% sulfosalicylic acid. The mixture was diluted to 4 ml with buffer A and centrifuged. Tissues (0.2–0.4 g) were homogenized in 2 ml buffer A and centrifuged. Glutathione in 1 ml aliquots of the supernatant liquids was converted into a derivative with use of ethyl chloroformate, the derivative was extracted from acid solution into ethyl ether, the extract was evaporated and the residue was dissolved in 50–100 μ l ethyl acetate. Portions (1–2 μ l) were analyzed by gas chromatography on a fused-silica column (10 m \times 0.25 mm i.d.) coated with HP5 MS (0.25 μ m), operated with temperature programming from 200 to 295 $^{\circ}$ C, with helium (1.15 ml/min) as carrier gas and 70 eV electron impact mass spectrometry detection operated in selected-ion monitoring mode at m/z 363 and 365, respectively, for glutathione. Calibration graphs were linear for the enrichment ratios investigated and the relative standard deviation for repeated infusions were 0.3–1.2% ($n=3-8$). A similar method was used to determine cysteine.

Bouligand *et al.* [157] developed a liquid chromatography/tandem mass spectrometry assay method for the analysis of glutathione, glutathione disulfide, and precursors (γ -glutamylcysteine, cysteinylglycine, cysteine, cystine, homocysteine, and homocystine) to study glutathione synthesis in mice liver. After iodoacetic acid derivatization, the analytes were analyzed using reversed-phase gradient high-performance liquid chromatography and detected using multiple reaction monitoring. Linear calibration were performed over the concentrations range of 100–10,000 ng/ml for thiol-containing precursors and extended up to 100,000 ng/ml for glutathione and glutathione disulfide. The method was validated for each compound with interday accuracy below 11.9% and with precision below 15%. The method showed low limits of quantitation of 100 ng/ml for each thiol-containing compound and oxidized glutathione and of 200 ng/ml for other disulfides.

5.7 Immunoassay Methods

Semiquantitative bioluminescent assay of glutathione was developed by Romero and Mueller-Klieser [158]. The enzyme cocktail comprised a basic aqueous solution or 60 g/l gelatine/0.3 M glycerol/30 g/l polyvinylpyrrolidone/0.2 M sodium phosphate buffer and 0.1 M disodium hydrogen arsenate and the following components: 100 mM NADP, 0.4 mM FMN, 8 mM MgCl_2 , 0.5 mM 1,4-dithiothreitol, 8 mM decanal, 20 V/ml glutathione reductase, 0.017–0.100 V/ml luciferase, and 6.7 V/ml NAD(F)H-FMN-oxidoreductase. The enzyme solution was mixed with solutions containing different amounts of glutathione. The bioluminescent intensity of the luciferase reaction was measured. A Hamamtsu Photronics ARGUS 100 imaging photon-counting system was used. A calibration curve was obtained for the range 0–2.5 μM , although the assay can probably be used for a greater range of glutathione concentrations by adjusting cocktail concentrations.

Glutathione was determined by Kamencic *et al.* [159] in tissue homogenates by incubation with monochlorobimane (100 μM) and glutathione S-transferase (1 iu/ml) for 30 min. The glutathione-monochlorobimane adduct was measured fluorimetrically at 470 nm (excitation at 380 nm). Calibration graphs were linear for 0.5–50 μM glutathione. Results were compared with those obtained by high-performance liquid chromatography, with precolumn derivatization using 5,5'-dithiobis(2-nitrobenzoic acid), and identical results were obtained. The method was applied to the determination of glutathione in rat liver and spinal cord.

A microtiter plate assay for quantitation of reduced glutathione and oxidized glutathione in the rat liver tissue and bile was described by Shaik and Reza [160]. The assay is based on the established enzymatic recycling method and a new thiol-masking reagent, 1-methyl-4-vinyl-pyridinium trifluoromethane sulfonate. Samples were first processed by homogenization with (liver) or addition of (bile) sulfosalicylic acid. The total glutathione and oxidized glutathione were then determined before and after rapid (≤ 2 min) and efficient (100%) masking of the glutathione content of the samples with 1-methyl-4-vinyl-pyridinium trifluoromethane sulfonate followed by the enzymatic recycling assay. The percentages of error and coefficient of variation of the assay were within the accepted guidelines, indicating the accuracy and precision of the assay in the range of 6.25–100 pmol glutathione per microplate well and 2.17–140 pmol oxidized glutathione per well, with lower limit of quantitation of 6.25 and 2.17 pmol per well for glutathione and oxidized glutathione, respectively. Furthermore, the recoveries of added glutathione or oxidized glutathione from the liver and bile samples were accurate and precise. The assay was applied to measurement of glutathione, oxidized glutathione, and glutathione: oxidized glutathione ratio in the liver and serially collected bile samples in sham-operated and ischemic rat livers, demonstrating a depletion of glutathione and a decrease in the glutathione: oxidized glutathione ratio as a result of ischemia. The developed assay is rapid, sensitive, accurate, and precise and is suitable for studies of the redox status of liver under physiologic and pathophysiologic condition.

The plate reader method was reported by Guillaume and Noctor [161], for determination of glutathione. Glutathione, NAD, and NADP are key nonprotein redox couples in the aqueous phase of virtually all cells, whereas in plant cells ascorbate also plays an important role in redox homeostasis. The development and validation of plate reader assays that allow rapid analysis of these four redox couples in extracts of *Arabidopsis* leaves is presented. Analytical methods were adapted and validated for specific measurement of oxidized and reduced forms. Oxidized and reduced forms of glutathione and ascorbate, as well as NAD^+ and NADP^+ , were measured in hydrochloric acid extracts, NADH, and NADPH in parallel alkaline extracts. Both standards and extracts gave linear assay responses, and recovery quotients of added metabolites through the extraction procedure were generally high. The plate reader method was validated against more conventional spectrophotometric assays and also, for glutathione, by high-performance liquid chromatography analysis. The method was shown to yield quantitative data for six independent extracts with a total sample preparation and analysis time

of 4 h. Analysis of the four redox couples throughout *Arabidopsis* rosette development showed that redox states were relatively constant but that total pools of NAD, glutathione, and ascorbate were significantly modified by day length and developmental stage.

The spectrophotometric/microplate reader assay method for glutathione involves oxidation of glutathione by the sulfhydryl reagent 5,5'-dithiobis(2-nitrobenzoic acid) to form the yellow derivative 5'-thio-2-nitrobenzoic acid, measurable at 412 nm was reported by Rahman *et al.* [162]. The glutathione disulfide formed can be recycled to glutathione by glutathione reductase in the presence of NADPH. The assay is composed of two parts: the preparation of cell cytosolic/tissue extracts and the detection of total glutathione. The method is simple, convenient, sensitive, and accurate. The lowest detection for glutathione and glutathione disulfide is 0.103 nM in a 96-well plate. This method is rapid and the whole procedure takes no longer than 15 min including reagent preparation. The method can assay glutathione in whole blood, plasma, serum, lung lavage fluid, cerebrospinal fluid, urine, tissues, and cell extracts and can be extended for drug discovery/pharmacology and toxicology protocols to study the effects of drugs and toxic compounds on glutathione metabolism.

A sequential injection analysis system for determination of total and oxidized glutathione in human whole blood was reported by Araujo *et al.* [163]. A simple, robust, automated sequential injection analysis system for the enzymatic determination of total and oxidized glutathione in human whole blood was developed. The reduced glutathione concentration is then obtained as the difference between the total glutathione and oxidized glutathione concentrations. The determination was based on the dithiobis-2-nitro-5-thiobenzoic acid-oxidized glutathione reductase recycling assay, which couples the specificity of the oxidized glutathione reductase with an amplification of the response to glutathione, followed by spectrophotometric detection of the 2-nitro-5-thiobenzoic acid formed ($\lambda = 412$ nm). The implementation of this reaction in a sequential injection analysis flow system with an in-line dilution strategy permitted the necessary distinct application ranges for total glutathione and for oxidized glutathione. It also guaranteed the exact timing of fluidic manipulations and precise control of the reaction conditions. The influence of parameters such as reagents concentration, temperature, pH, flow rate of the carrier buffer solution, as well as reaction coil length, etc., on the sensitivity and performance of the sequential injection analysis system were studied and the optimum reaction conditions subsequently selected. Linear calibration plots were obtained for

glutathione and oxidized glutathione concentrations up to 3.00 and 1.50 μM , with detection limits of 0.031 and 0.014 μM , respectively. The developed methodology showed good precision, with a relative standard deviation, $<5.0\%$ ($n=10$) for determination of both glutathione forms. Statistical evaluation showed good compliance, for a 95% confidence level, between the results obtained with the sequential injection analysis system and those furnished by the comparison batch procedure.



6. STABILITY

Stability studies have indicated that L-glutathione is stable when stored in an airtight container at room temperature and normal relative humidity levels for 39 months. When glutathione is dissolved in water and stored under conditions of variable pH for 7 days at room temperature, L-glutathione is more stable at pH values of 3–6 (approximately 80% of the original amount of L-glutathione remaining in the solution) than at lower or higher values (approximately 65% remaining in the solution at pH 2 and 7). The major degradation products formed at lower pH values are cysteinylglycine (up to 20% of the original amount of L-glutathione is degraded to cysteinylglycine) and pyroglutamic acid (up to 10%), while at higher pH values, L-glutathione is primarily oxidized (up to 30%, with 5% cysteinylglycine formed as well). When stored at various temperatures for 7 days at a constant pH of 3, L-glutathione dissolved in water is stable at lower temperatures (more than 85% L-glutathione remaining at 4–25 °C, with up to 10% cysteinylglycine formed), but is degraded primarily to cysteinylglycine and pyroglutamic acid at higher temperatures. At 60 °C, approximately 20% L-glutathione remains, with 40%, 35%, and 5% of cysteinylglycine, pyroglutamic acid, and oxidized glutathione formed, respectively. Minor degradation products include oxidized cysteinylglycine (occurring at 0.5–2%) and glutathione-cysteinylglycine mixed disulfide (occurring at 0.5–5%). Both cysteinylglycine and pyroglutamic acid are intermediates formed in the metabolism of reduced glutathione. Glutathione is metabolized to cysteinylglycine and γ -glutamylamino acid, the latter of which is converted to pyroglutamic acid (also known as 5-oxoproline). Pyroglutamic acid is subsequently converted to the amino acid glutamate, which is one of the components of glutathione. Oxidized glutathione occurs naturally in various foods at levels two- to threefold higher than glutathione [164], and there is evidence of a mechanism in the small intestine of rats that reduces oxidized glutathione [165]. Oxidized cysteinylglycine, also known

as cysteinylglycine disulfide, occurs in the human plasma at higher levels than the reduced form [166]. Although glutathione-cysteinylglycine mixed disulfide has not been measured in humans, it is likely present as mixed disulfides are commonly occurring compounds. Furthermore, if ingested glutathione cysteinylglycine mixed disulfide were to be reduced, the resulting products would be glutathione and cysteinylglycine, which occur endogenously. Therefore, the formation of these products during storage of L-Glutathione in solution at various pH levels and temperature is of no safety concern [167].



7. REVIEWS

An in-depth review of the method used for the determination of glutathione and glutathione disulfide in biological samples was presented by Monostori *et al.* [168]. The review provides a state-of-the-art overview of issues relating to sample pretreatment and choice for the separation and detection of glutathione and glutathione disulfide. High-performance liquid chromatography, capillary electrophoresis, and gas chromatography (as techniques with separation step) with photometric, fluorimetric, electrochemical, and mass spectrometric detection are discussed, stress being laid on novel approaches.

Iwasaki *et al.* [169] reviewed the chromatographic and mass spectrometric analysis of glutathione in biological samples. Measurement of glutathione and glutathione disulfide is a useful indicator for oxidative stress and disease risk. Many publications have reported successful determination of glutathione and glutathione disulfide in biological samples. This review covers the newly developed techniques, such as liquid chromatography coupled with mass spectrometry and tandem mass spectrometry, for identifying glutathione bound to proteins, or for localizing glutathione in bound or free forms at specific sites in organs and in cell locations.

Methods of sample preparation for chromatography and capillary electrophoresis were reported by Bolonska-Sikora *et al.* [170]. Authors have concluded that sample preparation appears as the most important and the most complicated step at once in procedures of determination of glutathione and other thiols. This is connected with difficulties with removing sometimes complicated matrixes used for glutathione determination. Glutathione content in mammals has been analyzed generally in plasma, whole blood, and erythrocytes. However, those analytical methods are also helpful for determination of amino thiols almost in every tissue and organ, what makes

them more useful than enzymatic methods based on blood analysis commonly used in laboratories, Araujo *et al.* [163].

Sample preparation stages are similar for all chromatographic and electrophoretic methods. Every tissues and organs must be chilled after collecting and storage at low temperature from -20 to -80 °C what depends on time from preparation to samples processing. Blood or plasma samples must be protected from coagulation by adding to fresh collected blood chelating reagents or placing blood in special tubes with chelator. Deproteinization, reduction, and derivatization procedures are not demand in very chromatographic or electrophoretic method. It also depends on kind of analyzed tissue or cell. Those with high concentration of glutathionylated proteins or γ -glutamyl transpeptidase must be deproteinized necessarily. Determination of total glutathione or quantification of disulfide bonds concentration requires reduction of disulfides. Derivatization step is necessary almost for all analytical methods described above, except for CE or tandem mass spectrometry what makes them less laborious and time-consuming than the other methods. Elimination of this step protect from undesirable derivatives; derivatizing reagent—other amino thiols, which are not determined.

Hartfield *et al.* [171] reviewed the electrochemical determination of glutathione. Analysis of context in which physiological glutathione measurement can be undertaken electrochemically and compares it to current assay approaches, while also covering the current literature for glutathione disulfide detection. The various characteristics and limitation of the methodologies are compared and contrasted, with the analytical parameters (matrix, pH, limit of detection, etc.) are tabulated to aid comparison.

ACKNOWLEDGMENTS

The authors wish to thank Mr. Tanvir A. Butt, Department of Pharmaceutical Chemistry, College of Pharmacy, King Saud University for his secretarial assistance in preparing this profile.

REFERENCES

- [1] Index Nominum, International Drug Directory, in: Swiss Pharmaceutical Society (Ed.), seventieth ed., Medpharm Scientific GmbH Publishers, Stuttgart, 2000, p. 495.
- [2] The Merck index, An Encyclopedia of Chemicals, Drugs and Biologicals, fourteenth ed., Merck & Co., Inc., Whitehouse Station, NJ, USA, 2006, p. 4475.
- [3] S. Sweetman (Ed.), Martindale: The Complete Drug Reference, Pharmaceutical Press, London, 2007, Electronic version.
- [4] British Pharmacopoeia, vol. 1, Her Majesty's Stationary Office, London, United Kingdom, 2005, pp. 924–926.

- [5] S. Cascinu, L. Cordella, E. Del Ferro, M. Fronzoni, G. Catalano, Neuroprotective effect of reduced glutathione on cisplatin-based chemotherapy in advanced gastric cancer: a randomized double-blind placebo controlled trial, *J. Clin. Oncol.* 13 (1995) 26–32.
- [6] S. Cascinu, V. Catalano, L. Cordella, R. Labianca, P. Giordani, A.M. Baldelli, G.D. Beretta, E. Ubiali, G. Catalano, Neuroprotective effect of reduced glutathione on oxaliplatin-based chemotherapy in advanced colorectal cancer: a randomized double-blind placebo-controlled trial, *J. Clin. Oncol.* 20 (2002) 3478–3483.
- [7] Z. Borok, R. Ruhl, G.J. Grims, A.D. Bokser, R.C. Hubbard, K.J. Holroyd, J.H. Roum, D.B. Czerski, A.M. Cantin, R.G. Crystal, Effect of glutathione aerosol on oxidant-antioxidant imbalance in idiopathic pulmonary fibrosis, *Lancet* 338 (1991) 215–216.
- [8] J.H. Roum, Z. Borok, N.G. McElvaney, G.J. Grims, A.D. Bokser, R. Bohi, R.C. Crystal, Glutathione aerosol suppresses lung epithelial surface inflammatory cell-derived oxidants in cystic fibrosis, *J. Appl. Physiol.* 87 (1999) 438–443.
- [9] M. Griese, J. Ramakers, A. Krasselt, V. Starosta, S. van Koningsbruggen, R. Fischer, F. Ratjen, B. Mullinger, R.M. Huber, K. Maier, E. Reittschel, G. Scheuch, Improvement of alveolar glutathione and lung function but not oxidative state cystic fibrosis, *Am. J. Respir. Crit. Care Med.* 169 (2004) 822–828.
- [10] D.W. Lamson, M.S. Brignall, The use of nebulized glutathione in the treatment of emphysema: a case report, *Altern. Med. Rev.* 5 (2000) 429–431.
- [11] R.M. Marrades, J. Roca, J.A. Barbera, L. de Jover, W. MacNee, R. Rodriguez-Roisin, Nebulized glutathione induces bronchoconstriction in patients with mild asthma, *Am. J. Respir. Crit. Care Med.* 156 (1997) 25–430.
- [12] G. Wu, *Amino Acids: Biochemistry and Nutrition*, CRC Press, New York, 2013, pp. 140–150.
- [13] C.R. Harington, T.H. Mead, Synthesis of glutathione, *Biochem. J.* 29 (1935) 1602–1611.
- [14] F.G. Hopkins, On an autooxidisable constituent of the cell, *Biochem. J.* 15 (1921) 286–305.
- [15] F.G. Hopkins, M. Dixon, On glutathione, II. A thermostable oxidation-reduction system, *J. Biol. Chem.* 54 (1922) 527–563.
- [16] J.H. Quastel, C.P. Stewart, H.E. Tunncliffe, On glutathione, constitution, *Biochem. J.* 17 (1923) 586–592.
- [17] C.P. Stewart, H.E. Tanniciffe, Glutathione synthesis, *Biochem. J.* 19 (1925) 207–217.
- [18] G. Hunter, B.A. Eagles, Glutathione, a critical study, *J. Biol. Chem.* 72 (1927) 147–166.
- [19] F.G. Hopkins, On glutathione, a reinvestigation, *J. Biol. Chem.* 84 (1929) 269–320.
- [20] E.C. Kendall, B.F. McKenzie, H.L. Mason, A study of glutathione, its preparation in crystalline form and its identification, *J. Biol. Chem.* 84 (1929) 657–674.
- [21] G. Noctor, M. Strohm, L. Jouanin, K.J. Kunert, C.H. Foyer, H. Rennenberg, Synthesis of glutathione in leaves of transgenic poplar overexpressing γ -glutamylcysteine synthetase, *Plant Physiol.* 112 (1996) 1070–1078.
- [22] G. Noctor, A.-C.M. Arisi, L. Jouanin, Karl J. Kunert, H. Rennenberg, C.H. Foyer, Glutathione: biosynthesis, metabolism and relationship to stress tolerance explored in transformed plants, *J. Exp. Bot.* 49 (1998) 623–647.
- [23] A. Meister, Glutathione metabolism and its selective modification, *J. Biol. Chem.* 263 (1988) 17205–17208.
- [24] R.B. Johnston, K. Bloch, Enzymatic synthesis of glutathione, *J. Biol. Chem.* 188 (1951) 221–240.
- [25] M. Bergmann, L. Zervas, Ube ein all-gemeines verfahren der peptid-synthetase, *Ber.* 65 (1932) 1192.

- [26] J. Melville, Labile glutamine peptides, and their bearing on the origin of the ammonia set free during the enzymic digestion of proteins, *Biochem. J.* 49 (1935) 179–186.
- [27] C. Berse, R. Boucher, L. Piche, A shorter synthesis of glutathione, *Can. J. Chem.* 37 (1959) 1733–1736.
- [28] W.H. Wright, The crystal structure of glutathione, *Acta Cryst.* 11 (1958) 632–642.
- [29] W.H. Wright, A comparison of the methods used in the attempt to determine the crystal structure of glutathione, *Acta Cryst.* 11 (1958) 642–653.
- [30] L. Pauling, R.B. Corey, Atomic coordinates and structure factors for two helical configurations of polypeptide chains, *Proc. Natl. Acad. Sci. U.S.A.* 37 (1951) 235–240.
- [31] M. Calvin, Glutathione, in: S.P. Colowick, A. Lazarow, E. Racker, D.R. Schwarz, E. Stadtman, H. Walesch (Eds.), *Proceeding of the Symposium Held at Ridgefield, Connecticut, 1953*, Academic Press, Inc., New York, 1954, p. 21.
- [32] W. Cochran, A.S. Douglas, A new application of EDSAC to crystal structure analysis, *Nature (London)* 171 (1953) 1112–1113.
- [33] W. Cochran, A.S. Douglas, The use of high speed digital computer for the direct determination of crystal structures. I, *Proc. R. Soc. Lond. A* 227 (1955) 486–500.
- [34] J.D. Bernal, Cuprous glutathione, with a note on the crystallography of glutathione by N.W. Pirie, *Biochem. J.* 26 (1932) 75–79.
- [35] J.M. Broomhead, The structure of pyrimidines and purines, II. A determination of the structure of adenine hydrochloride by X-ray methods, *Acta Cryst.* 1 (1948) 324–329.
- [36] G.H. Goldschmidt, G.J. Pitt, The correction of X-ray intensities for Lorentz-polarization and rotation factors, *J. Sci. Instrum.* 25 (1948) 397–398.
- [37] A.J.C. Wilson, The probability distribution of X-ray intensities, *Acta Cryst.* 2 (1949) 318–321.
- [38] R. McWeeny, X-ray scattering by aggregates of bonded atoms I. Analytical approximations in single-atom scattering, *Acta Cryst.* 4 (1951) 513–519.
- [39] R.W. James, G.W. Brindley, Some numerical values of the atomic scattering factors, *Z. Kristallogr.* 7 (1931) 470–476.
- [40] P.D. Shoemaker, J. Donohue, V. Schomaker, R.B. Corey, The crystal structure of LS-threonine, *J. Am. Chem. Soc.* 72 (1950) 2328–2349.
- [41] D.W.J. Cruickshank, The accuracy of electron density maps in X-ray analysis with special reference to dibenzyl, *Acta Cryst.* 2 (1949) 65–82.
- [42] S.S. Thakur, P. Balaram, Fragmentation of peptide disulfides under conditions of negative ion mass spectrometry: studies of oxidized glutathione and contryphan, *J. Am. Soc. Mass Spectrom.* 19 (2008) 358–366.
- [43] M. Kolar, D. Dobcnik, N. Radic, Potentiometric flow-injection determination of vitamin C and glutathione with a chemically prepared tubular silver electrode, *Pharmazie* 55 (2000) 913–916.
- [44] A.M. El-Kosasy, A.S. Mostafa, Y.H. Nagib, S.F. Ahmad, A.E. Badr, Membrane electrodes for the determination of glutathione, *Talanta* 66 (2005) 746–754.
- [45] R.J. Bakhsh, R. Ojani, M. Kolbadinezhad, Voltammetric sensor for glutathione determination based on ferrocene-modified carbon paste electrode, *J. Solid State Electrochem.* 13 (2009) 1411–1416.
- [46] J.B. Raoof, R. Ojani, H. Karimi-Maleh, Electrocatalytic oxidation of glutathione at carbon paste electrode modified with 2,7-bis (ferrocenyl ethyl)fluoren-9-one: application as a voltammetric sensor, *J. Appl. Electrochem.* 39 (2009) 1169–1175.
- [47] H. Karimi-Maleh, M. Keyvanfar, K. Alizad, V. Khosravi, M. Asnaashariisfahani, Electrocatalytic determination of glutathione using multiwall carbon nanotubes paste electrode as a sensor and isoprenaline as a mediator, *Int. J. Electrochem. Sci.* 7 (2012) 6816–6830.

- [48] M.K. Sezgenturk, E. Dinckaya, Glutathione (GSH) determination by a very simple electrochemical method, *Int. J. Pept. Res. Ther.* 17 (2011) 87–92.
- [49] I. Satoh, S. Arakawa, A. Okamoto, Flow-injection determination of glutathione with amperometric monitoring of the enzymic reaction, *Anal. Chim. Acta* 214 (1988) 415–419.
- [50] S.A. Wring, J.P. Hart, B.J. Birch, Development of an improved carbon electrode chemically modified with cobalt phthalocyanine as a re-usable sensor for glutathione, *Analyst* 114 (1989) 1563–1570.
- [51] J.A. Cox, T.J. Gray, Flow-injection amperometry of cysteine and glutathione at an electrode modified with a ruthenium-containing inorganic film, *Electroanalysis* 2 (1990) 107–111.
- [52] S.A. Wring, J.P. Hart, B.J. Birch, Voltammetric behaviour of screen-printed carbon electrodes, chemically modified with selected mediators, and their application as sensors for the determination of reduced glutathione, *Analyst* 116 (1991) 123–129.
- [53] S.A. Wring, J.P. Hart, B.J. Birch, Development of an amperometric assay for the determination of reduced glutathione, using glutathione peroxidase and screen-printed carbon electrodes chemically modified with cobalt phthalocyanine, *Electroanalysis* 4 (1992) 299–309.
- [54] A.C. Le-Gall, C.M.G. Van-den-Berg, Cathodic-stripping voltammetry of glutathione in natural waters, *Analyst* 118 (1993) 1411–1415.
- [55] F.G. Banica, A.G. Fogg, J.C. Moreira, Catalytic cathodic-stripping voltammetry at a hanging mercury drop electrode of glutathione in the presence of nickel ion, *Analyst* 119 (1994) 2343–2349.
- [56] Z.X. Huang, R.L. Villarta-Snow, G.J. Lubrano, G.G. Guilbault, Glutathione amperometric enzyme microsensor, *Anal. Lett.* 27 (1994) 263–271.
- [57] F.G. Banica, A.G. Fogg, J.C. Moreira, Catalytic cathodic-stripping voltammetry of oxidized glutathione at a hanging-mercury-drop electrode in the presence of nickel ion, *Talanta* 41 (1995) 227–234.
- [58] H. Kinoshita, T. Miya, S. Kamihira, Amperometric determination of glutathione in yeast extract using a membrane-covered phthalocyanine embedded carbon-paste electrode, *Bunseki Kagaku* 48 (1999) 117–120.
- [59] L. Mao, K. Yamamoto, An amperometric biosensor for glutathione based on osmium-polyvinylpyridine gel polymer and glutathione sulphhydryl oxidase, *Electroanalysis* 12 (2000) 577–582.
- [60] C. Lehmann, U. Wollenberger, R. Brigelius-Flohe, F.W. Scheller, Modified gold electrodes for electrochemical studies of the reaction of phospholipid-hydroperoxide glutathione peroxidase with glutathione and glutathione disulfide, *Electroanalysis* 13 (2001) 364–369.
- [61] F. Xu, L. Wang, M.N. Gao, L.T. Jin, J.Y. Jin, Amperometric determination of glutathione and cysteine on a palladium-iridium dioxide modified electrode with high performance liquid chromatography in rat brain microdialysate, *Anal. Bioanal. Chem.* 372 (2002) 791–794.
- [62] A. Salimi, S. Pourbeyram, Renewable sol-gel carbon ceramic electrodes modified with a ruthenium-complex for the amperometric detection of L-cysteine and glutathione, *Talanta* 60 (2003) 205–214.
- [63] P. Calvo-Marzal, K.Y. Chumbimuni-Torres, N.F. Hoehr, G. de-Oliveira-Neto, L.T. Kubota, Determination of reduced glutathione using an amperometric carbon paste electrode chemically modified with TTF-TCNQ, *Sensors Actuators B* 100 (2004) 333–340.
- [64] M.K. Sezgenturk, E. Dinckaya, An amperometric inhibitor biosensor for the determination of reduced glutathione (GSH) without any derivatization in some plants, *Biosens. Bioelectron.* 19 (2004) 835–841.

- [65] S. Afsaneh, N. Maleki, E. Farjami, F.A. Mahyari, Simultaneous electrochemical determination of glutathione and glutathione disulfide at a nanoscale copper hydroxide composite carbon ionic liquid electrode, *Anal. Chem.* 81 (2009) 7538–7543.
- [66] N. Pereira-Rodrigues, R. Cofré, J.H. Zagal, F. Bedioui, Electrocatalytic activity of cobalt phthalocyanine CoPc adsorbed on a graphite electrode for the oxidation of reduced l-glutathione (GSH) and the reduction of its disulfide (GSSG) at physiological pH, *Bioelectrochemistry* 70 (2007) 147–154.
- [67] J.B. Raoof, O. Reza, B. Mehdi, Simultaneous electrochemical determination of glutathione and tryptophan on a nano- TiO₂/ferrocene carboxylic acid modified carbon paste electrode, *Sensors Actuators B* 143 (2009) 261–269.
- [68] A.A. Ensafi, M. Taei, T. Khayamian, H. Karimi-Maleh, F. Hasanpour, Voltammetric measurement of trace amount of glutathione using multiwall carbon nanotubes as a sensor and chlorpromazine as a mediator, *J. Solid State Electrochem.* 14 (2010) 1415–1423.
- [69] A. Besada, N.B. Tadros, Y.A. Gawargious, Copper (II)—neocuproine as colour reagent for some biologically active thiols: spectrophotometric determination of cysteine, penicillamine, glutathione and 6-mercaptopurine, *Mikrochim. Acta* III (1989) 143–146.
- [70] M.A. Raggi, L. Nobile, A.G. Giovannini, Spectrophotometric determination of glutathione and of its oxidation product in pharmaceutical dosage forms, *J. Pharm. Biomed. Anal.* 9 (1991) 1037–1040.
- [71] D. Boutolleau, G. Lefevre, J. Etienne, Determination of glutathione with the GSH-400 method: value of derivative spectrophotometry, *Ann. Biol. Clin. (Paris)* 5 (1997) 592–596.
- [72] Y. Avi-Dor, R. Lipkin, A spectrophotometric method for the determination of reduced glutathione, *J. Biol. Chem.* 233 (1958) 69–72.
- [73] F.A.M. Redegeld, M.A.J. Van Opstal, F. Houdkamp, W.P. Van Bennekom, Determination of glutathione in biological material by flow-injection analysis using an enzymatic recycling reaction, *Anal. Biochem.* 174 (1988) 489–495.
- [74] J.P. Teare, N.A. Punchard, J.J. Powell, P.J. Lumb, D.W. Mitchell, R.P.H. Thompson, Automated spectrophotometric method for determining oxidized and reduced glutathione in liver, *Clin. Chem.* 39 (1993) 688–689.
- [75] A.P. Senft, T.P. Dalton, H.G. Shertzer, Determining glutathione and glutathione disulfide using the fluorescence probe o-phthalaldehyde, *Anal. Biochem.* 280 (2000) 80–86.
- [76] H. Wang, W.S. Wang, H.S. Zhang, A Spectrofluorimetric method for cysteine and glutathione using the fluorescence system of Zn(II)–8-hydroxyquinoline–5-sulfonic acid complex, *Spectrochim. Acta A* 57A (2001) 2403–2407.
- [77] Z. Shen, H. Wang, S.C. Liang, Z.M. Zhang, H.S. Zhang, Spectrofluorimetric determination of reduced glutathione in human blood using N-[p-(2-benzothiazolyl) phenyl] maleimide, *Anal. Lett.* 35 (2002) 2269–2278.
- [78] S.C. Liang, H. Wang, Z.M. Zhang, X. Zhang, H.S. Zhang, Direct spectrofluorimetric determination of glutathione in biological samples using 5-maleimidyl-2-(m-methylphenyl) benzoxazole, *Anal. Chim. Acta* 451 (2002) 211–219.
- [79] H. Ullah, M.F. Khan, F. Hashmat, Determination of glutathione concentration after its interacting with cadmium nitrate tetrahydrate by using Elman's modified method, *Gomal Univ. J. Res.* 27 (2011) 18–25.
- [80] S.I. Yakubu, I.A. Yakasai, A. Musa, Spectrofluorimetric assay method for glutathione and glutathione transferase using monobromobimane, *J. Basic Clin. Pharmacol.* 2 (2011) 151–158.
- [81] T. Kamidate, I. Kuniya, H. Watanabe, Simultaneous determination of cysteine and glutathione via use of time-resolved luminol chemiluminescence method, *Chem. Lett.* 12 (1993) 2049–2052.

- [82] T. Kamidate, H. Watanabe, Peroxidase-catalysed luminol chemiluminescence method for the determination of glutathione, *Talanta* 43 (1996) 1733–1738.
- [83] L. Wang, Y.X. Li, D.H. Zhao, C.Q. Zhu, A novel enhancing flow-injection chemiluminescence method for the determination of glutathione using the reaction of luminol with hydrogen peroxide, *Microchim. Acta* 141 (2003) 41–45.
- [84] A.A. Ensafi, T. Khayamian, F. Hasanpour, Determination of glutathione in hemolysed erythrocyte by flow injection analysis with chemiluminescence detection, *J. Pharm. Biomed. Anal.* 48 (2008) 140–144.
- [85] Y. Ping, Y. Chen, Q. Zhu, F. Wang, L. Wang, Y. Li, Sensitive chemiluminescence method for the determination of glutathione, L-cysteine and 6-mercaptopurine, *Microchim. Acta* 163 (2008) 263–269.
- [86] R.H.S. Thompson, D. Watson, The nitroprusside method for the determination of blood glutathione, *J. Clin. Pathol.* 5 (1952) 25–29.
- [87] C.W.I. Owens, R.V. Belcher, A colorimetric micro-method for the determination and glutathione, *Biochem. J.* 94 (1965) 705–711.
- [88] T.E. Tipple, L.K. Rogers, Methods for the determination of plasma or tissue glutathione levels, in: C. Harris, J.M. Hansen (Eds.), *Developmental Toxicology: Methods and Protocols, Methods in Molecular Biology*, 889 2012, pp. 315–324.
- [89] M. Cappiello, E. Peroni, A. Lepore, R. Moschini, A. Del Corso, F. Balestri, U. Mura, Rapid colorimetric determination of reduced and oxidized glutathione using an end point coupled enzymatic assay, *Anal. Bioanal. Chem.* 405 (2013) 1779–1785.
- [90] T. Yoshida, Determination of reduced and oxidised glutathione in erythrocytes by high-performance liquid chromatography with ultra-violet absorbance detection, *J. Chromatogr. B* 678 (1996) 157–164.
- [91] M.A. Raggi, R. Mandrioli, G. Casamenti, D. Musiani, M. Marini, HPLC determination of glutathione and other thiols in human mononuclear blood cells, *Biomed. Chromatogr.* 12 (1998) 262–266.
- [92] A.E. Katrusiak, P.G. Paterson, H. Kamencic, A. Shoker, A.W. Lyon, A sensitive high-performance liquid chromatographic method for quantification of sulfhydryl and disulfide amino-acids in human plasma using ultra violet spectrophotometric detection, *J. Chromatogr. B* 758 (2001) 207–212.
- [93] M.W. Davey, E. Dekempeneer, J. Keulemans, Rocket-powered high-performance liquid chromatographic analysis of plant ascorbate and glutathione, *Anal. Biochem.* 216 (2003) 74–81.
- [94] C. Vignaud, L. Rakotozafy, A. Falguières, J. Potus, J. Nicolas, Separation and identification by gel filtration and high-performance liquid chromatography with UV or electrochemical detection of the disulfides produced from cysteine and glutathione oxidation, *J. Chromatogr. A* 1031 (2004) 125–133.
- [95] S.C. Garcia, K. Schott, M. Charão, A. Moro, R. Bulcão, D. Grotto, J. Valentini, D. Bohrer, S. Cardoso, V. Pomblum, Quantification of reduced glutathione by HPLC-UV in erythrocytes of hemodialysis patients, *Biomed. Chromatogr.* 22 (2008) 460–468.
- [96] V. Sutariya, D. Wehrung, W.J. Geldenhuys, Development and validation of a novel RP-HPLC method for the analysis of reduced glutathione, *J. Chromatogr. Sci.* 50 (2012) 271–276.
- [97] R.A. Winters, J. Zukowski, N. Ercal, R.H. Matthews, D.R. Spitz, Analysis of glutathione, glutathione disulfide, cysteine, homocysteine and other biological thiols by high-performance liquid chromatography following derivatization by N-(1-pyrenyl) maleimide, *Anal. Biochem.* 227 (1995) 14–21.
- [98] M.J. Nozal, J.L. Bernal, L. Toribio, P. Marinero, O. Moral, L. Manzanar, Determination of glutathione, cysteine and N-acetylcysteine in rabbit eye tissues using

- high-performance liquid chromatography and post-column derivatization with 5,5'-dithiobis-(2-nitrobenzoic acid), *J. Chromatogr. A* 778 (1997) 347–353.
- [99] J.Y. Yoo, K.O. Lee, H.S. Shin, Determination of glutathione in biological samples by ion-pairing HPLC-FLD, *Anal. Sci. Technol.* 12 (1999) 28–33.
- [100] J. Lenton, H. Therriault, J.R. Wagner, Analysis of glutathione and glutathione disulfide in whole cells and mitochondria by postcolumn derivatization high-performance liquid chromatography with ortho-phthalaldehyde, *Anal. Biochem.* 274 (1999) 125–130.
- [101] H. Nishijima, M. Yoshida, A. Takeya, M. Hara, M. Sagi, N. Sakata, T. Mukai, K. Yamazaki, An improved simultaneous measurement of oxidized and reduced glutathione in biological samples by high-performance liquid chromatography following derivatization with dansyl chloride, *J. Health Sci.* 45 (1999) 324–328.
- [102] S.K. Park, R.B. Boulton, A.C. Noble, Automated HPLC analysis of glutathione and thiol-containing compounds in grape juice and wine using pre-column derivatization with fluorescence detection, *Food Chem.* 68 (2000) 475–480.
- [103] R. Sack, A. Willi, P.E. Hunziker, Determination of total glutathione in cell lysates by high-performance liquid chromatography with o-phthalaldehyde precolumn derivatization in the presence of tris(2-carboxyethyl)phosphine, *J. Liq. Chromatogr. Relat. Technol.* 23 (2000) 2947–2962.
- [104] C. Cereser, J. Guichard, J. Drai, E. Bannier, I. Garcia, S. Boget, P. Parvaz, A. Revol, Quantitation of reduced and total glutathione at the femtomole level by high-performance liquid chromatography with fluorescence detection: application to red blood cells and cultured fibroblasts, *J. Chromatogr. B* 752 (2001) 123–132.
- [105] T. Toyo'oka, J. Tanabe, H. Jinno, Determination of rat hepatocellular glutathione by reversed-phase liquid chromatography with fluorescence detection and cytotoxicity evaluation of environmental pollutants based on the concentration change, *Biomed. Chromatogr.* 15 (2001) 240–247.
- [106] I.K. Abukhalaf, N.A. Silvestrov, J.M. Menter, D.A. von-Deutsch, M.A. Bayorh, R.R. Socci, A.A. Ganafa, High performance liquid chromatographic assay for the quantitation of total glutathione in plasma, *J. Pharm. Biomed. Anal.* 28 (2002) 637–643.
- [107] S. Ohmori, T. Kawase, M. Higashiura, Y. Chisaka, K. Nakata, Y. Yamasaki, High-performance liquid chromatographic method to analyse picomole levels of glutathione, cysteine and cysteinylglycine and its application to pre-cancerous rat livers, *J. Chromatogr. B* 762 (2001) 25–32.
- [108] A.K. Sakhi, K.M. Russnes, S. Smeland, R. Blomhoff, T.E. Gundersen, Simultaneous quantification of reduced and oxidized glutathione in plasma using a two-dimensional chromatographic system with parallel porous graphitized carbon columns coupled with fluorescence and coulometric electrochemical detection, *J. Chromatogr. A* 1104 (2006) 179–189.
- [109] A.K. Sakhi, B. Rune, E.G. Thomas, Simultaneous and trace determination of reduced and oxidized glutathione in minute plasma samples using dual mode fluorescence detection and column switching high performance liquid chromatography, *J. Chromatogr. A* 1142 (2007) 178–184.
- [110] T.D. Nolin, M.E. McMenamin, J. Himmelfarb, Simultaneous determination of total homocysteine, cysteine, cysteinylglycine, and glutathione in human plasma by high-performance liquid chromatography: application to studies of oxidative stress, *J. Chromatogr. B* 852 (2007) 554–561.
- [111] R. Kand'ár, P. Záková, H. Lotková, O. Kucera, Z. Cervinková, Determination of reduced and oxidized glutathione in biological samples using liquid chromatography with fluorimetric detection, *J. Pharm. Biomed. Anal.* 43 (2007) 1382–1387.

- [112] J. Lucija, K. Lisjak, A. Vanzo, Determination of glutathione content in grape juice and wine by high-performance liquid chromatography with fluorescence detection, *Anal. Chim. Acta* 674 (2010) 239–242.
- [113] Y. Ma, F. Xiang, W. Jin, L. Yu, Determination of total glutathione in yeasts by high-performance liquid chromatography with dansylation, *Z. Naturforsch. C* 65 (2010) 391–394.
- [114] M. Stéphanie, G. de Revel, A HPLC fluorescence-based method for glutathione derivatives quantification in must and wine, *Anal. Chim. Acta* 660 (2010) 158–163.
- [115] X.H. Ju, S. Tang, Y. Jia, J. Guo, Y. Ding, Z. Song, Y. Zhao, Determination and characterization of cysteine, glutathione and phytochelatin (PC_{2-6}) in *Lolium perenne* L. exposed to Cd stress under ambient and elevated carbon dioxide using HPLC with fluorescence detection, *J. Chromatogr. B* 879 (2011) 1717–1724.
- [116] C.K. Zacharis, D.T. Paraskevas, Z. Anastasia, Ethyl propiolate as a post-column derivatization reagent for thiols: development of a green liquid chromatographic method for the determination of glutathione in vegetables, *Anal. Chim. Acta* 690 (2011) 122–128.
- [117] F. Rita, M.L. Pavão, J. Baptista, Methodology for a rapid and simultaneous determination of total cysteine, homocysteine, cysteinylglycine and glutathione in plasma by isocratic RP-HPLC, *J. Chromatogr. B* 911 (2012) 15–20.
- [118] M.L. Steele, L. Ooi, G. Münch, Development of a high-performance liquid chromatography method for the simultaneous quantitation of glutathione and related thiols, *Anal. Biochem.* 429 (2012) 45–52.
- [119] X. Wang, D. Chi, D. Song, G. Su, L. Li, L. Shao, Quantification of glutathione in plasma samples by HPLC using 4-fluoro-7-nitrobenzofurazan as a fluorescent labeling reagent, *J. Chromatogr. Sci.* 50 (2012) 119–122.
- [120] H.N. Li, Y.X. Ci, L. Huang, High-performance liquid-chromatographic separation of glutathione and some mercapto-compounds with chemiluminescence detection, *Anal. Sci.* 13 (1997) 821–824.
- [121] G.P. McDermott, P.S. Francis, K.J. Holt, K.L. Scott, S.D. Martin, N. Stupka, N.W. Barnett, X.A. Conlan, Determination of intracellular glutathione and glutathione disulfide using high performance liquid chromatography with acidic potassium permanganate chemiluminescence detection, *Analyst* 136 (2011) 2578–2585.
- [122] R.L. Norris, G.K. Eaglesham, G.R. Shaw, M.J. Smith, R.K. Chiswell, A.A. Seawright, M.R. Moore, A sensitive and specific assay for glutathione with potential application to glutathione disulfide, using high-performance liquid chromatography-tandem mass spectrometry, *J. Chromatogr. B* 762 (2001) 17–23.
- [123] A.F. Loughlin, G.L. Skiles, D.W. Alberts, W.H. Schaefer, An ion exchange liquid chromatography-mass spectrometry method for the determination of reduced and oxidized glutathione and glutathione conjugates in hepatocytes, *J. Pharm. Biomed. Anal.* 26 (2001) 131–142.
- [124] E. Camera, M. Rinaldi, S. Briganti, M. Picardo, S. Fanali, Simultaneous determination of reduced and oxidized glutathione in peripheral blood mononuclear cells by liquid chromatography-electrospray mass spectrometry, *J. Chromatogr. B* 757 (2001) 69–78.
- [125] M. Gucek, S. Makuc, A. Mlakar, J. Bericnik-Vrbovsek, J. Marsel, Determination of glutathione in spruce needles by liquid chromatography-tandem mass spectrometry, *Rapid Commun. Mass Spectrom.* 16 (2002) 1186–1191.
- [126] J.P. Steghens, F. Flourie, K. Arab, C. Collombel, Fast liquid chromatography-mass spectrometry glutathione measurement in whole blood: micromolar GSSG is a sample preparation artifact, *J. Chromatogr. B* 798 (2003) 343–349.
- [127] X.M. Guan, B. Hoffman, C. Dwivedi, D.P. Matthees, A simultaneous liquid chromatography/mass spectrometric assay of glutathione, cysteine, homocysteine and their disulfides in biological samples, *J. Pharm. Biomed. Anal.* 31 (2003) 251–261.

- [128] C.M. Shuford, M.D. Poteat, D.B. Buchwalter, D.C. Muddiman, Absolute quantification of free glutathione and cysteine in aquatic insects using isotope dilution and selected reaction monitoring, *Anal. Bioanal. Chem.* 402 (2012) 357–366.
- [129] R. Rellán-Álvarez, L.E. Hernández, J. Abadía, A. Alvarez-Fernández, Direct and simultaneous determination of reduced and oxidized glutathione and homogluthathione by liquid chromatography–electrospray/mass spectrometry in plant tissue extracts, *Anal. Biochem.* 356 (2006) 254–264.
- [130] S.A. Wring, J.P. Hart, B.J. Birch, Determination of reduced glutathione in human whole blood by high-performance liquid chromatography with electrochemical detection by a graphite–epoxy resin electrode chemically modified with cobalt phthalocyanine, *Talanta* 38 (1991) 1257–1260.
- [131] N.C. Smith, M. Dunnett, P.C. Mills, Simultaneous quantitation of oxidised and reduced glutathione in equine biological fluids by reversed-phase high-performance liquid chromatography using electrochemical detection, *J. Chromatogr. B* 673 (1995) 35–41.
- [132] A.H. Liu, T. Li, E.K. Wang, Determination of cysteine and reduced glutathione in human plasma by liquid chromatography with pulsed amperometric electrochemical detection using a platinum-particles modified glassy carbon electrode, *Anal. Sci.* 11 (1995) 597–603.
- [133] J. Lakritz, C.G. Plopper, A.R. Buckpitt, Validated high-performance liquid chromatography–electrochemical method for determination of glutathione and glutathione disulfide in small tissue samples, *Anal. Biochem.* 247 (1997) 63–68.
- [134] C.S. Yang, S.C. Chang, P.J. Tsai, W.Y. Chen, J.S. Kuo, Simultaneous measurement of ascorbic acid and glutathione: application of microdialysis and online HPLC with Au/Hg electrode in anaesthetized rat liver, *J. Liq. Chromatogr. Relat. Technol.* 21 (1998) 3139–3148.
- [135] T. Ohkuwa, Y. Sato, M. Naoi, Novel assay for glutathione reductase activity by high-performance liquid chromatography with electrochemical detection, *J. Chromatogr. B* 705 (1998) 23–28.
- [136] L. Manna, L. Valvo, P. Betto, Determination of oxidized and reduced glutathione in pharmaceuticals by reversed-phase high-performance liquid chromatography with dual electrochemical detection, *J. Chromatogr. A* 846 (1999) 59–64.
- [137] G.Y. Shi, J.X. Lu, F. Xu, W.L. Sun, L.T. Jin, K. Yamamoto, S. Tao, J. Jin, Determination of glutathione in vivo by microdialysis using liquid chromatography with a cobalt hexacyanoferrate chemically modified electrode, *Anal. Chim. Acta* 391 (1999) 307–313.
- [138] P. Houze, S. Gamra, I. Madelaine, B. Bousquet, B. Gourmel, Simultaneous determination of total plasma glutathione, homocysteine, cysteinylglycine and methionine by HPLC with electrochemical detection, *J. Clin. Lab. Anal.* 15 (2001) 144–153.
- [139] F. Remiao, H. Carmo, F. Carvalho, M.L. Bastos, Simultaneous determination of reduced and oxidized glutathione in freshly isolated rat hepatocytes and cardiomyocytes by HPLC with electrochemical detection, *Biomed. Chromatogr.* 14 (2000) 468–473.
- [140] W.R. Jin, W. Li, Q. Xu, Capillary zone electrophoresis with electrochemical detection for the determination of glutathione in human red blood cells without pre-separation of haemoglobin, *J. Chromatogr. Sci.* 38 (2000) 545–550.
- [141] W.R. Jin, Q. Dong, X.Y. Ye, D.Q. Yu, Assay of glutathione in individual mouse peritoneal macrophages by capillary zone electrophoresis with electrochemical detection, *Anal. Biochem.* 285 (2000) 255–259.
- [142] F. Carlucci, A. Tabucchi, B. Biagioli, G. Sani, G. Lisi, M. Maccherini, F. Rosi, E. Marinello, Capillary electrophoresis in the evaluation of ischemic injury: simultaneous determination of purine compounds and glutathione, *Electrophoresis* 21 (2000) 1552–1557.

- [143] M.M. Bradford, A rapid and sensitive method for the quantitation of microgram quantities of protein utilizing the principle of protein-dye, *Anal. Biochem.* 72 (1976) 248–254.
- [144] V. Serru, B. Baudin, F. Ziegler, J.P. David, M.J. Cals, M. Vaubourdolle, N. Mario, Quantification of reduced and oxidized glutathione in whole blood samples by capillary electrophoresis, *Clin. Chem.* 47 (2001) 1321–1324.
- [145] T. Toyo'oka, J. Tanabe, Y. Kashiara, Determination of intracellular glutathione in rat hepatocytes after treatment of environmental pollutants by capillary electrophoresis with laser-induced fluorescence detection, *Anal. Chim. Acta* 433 (2001) 1–12.
- [146] Q. Yang, C. Krautmacher, D. Schilling, M.R. Pittelkow, S. Naylor, Simultaneous analysis of oxidized and reduced glutathione in cell extracts by capillary zone electrophoresis, *Biomed. Chromatogr.* 16 (2002) 224–228.
- [147] C. Carru, A. Zinellu, S. Sotgia, G. Marongiu, M.G. Farina, M.F. Usai, G.M. Pes, B. Tadolini, L. Deiana, Optimization of the principal parameters for the ultrarapid electrophoretic separation of reduced and oxidized glutathione by capillary electrophoresis, *J. Chromatogr. A* 1017 (2003) 233–238.
- [148] W.R. Jin, X.J. Li, N. Gao, Simultaneous determination of tryptophan and glutathione in individual rat hepatocytes by capillary zone electrophoresis with electrochemical detection at a carbon fiber bundle-Au/Hg dual electrode, *Anal. Chem.* 75 (2003) 3859–3864.
- [149] N. Novatchev, U. Holzgrabe, Capillary electrophoresis method for determination of related substances in glutathione reduced drug substance, *Chromatographia* 57 (2003) 345–349.
- [150] W. Wang, H. Xin, H.L. Shao, W.R. Jin, Determination of glutathione in single human hepatocarcinoma cells by capillary electrophoresis with electrochemical detection, *J. Chromatogr. B* 789 (2003) 425–429.
- [151] K. Govindaraju, V. Govindarajub, D.H. Eidelman, Analysis of glutathione in rat airway surface liquid by capillary zone electrophoresis with conductivity detection, *J. Chromatogr. B* 788 (2003) 369–376.
- [152] K. Havel, K. Pritts, T. Wielgos, Quantitation of oxidized and reduced glutathione in plasma by micellar electrokinetic capillary electrophoresis, *J. Chromatogr. A* 853 (1999) 215–223.
- [153] W.R. Jin, W. Li, Q.A. Xu, Quantitative determination of glutathione in single human erythrocytes by capillary zone electrophoresis with electrochemical detection, *Electrophoresis* 21 (2000) 774–779.
- [154] Z.K. Shihabi, M.E. Hinsdale, C.P. Cheng, Analysis of glutathione by capillary electrophoresis based on sample stacking, *Electrophoresis* 22 (2001) 2351–2354.
- [155] C. Carru, A. Zinellu, G.M. Pes, G. Marongiu, B. Tadolino, L. Deiana, Ultrarapid capillary electrophoresis method for the determination of reduced and oxidized glutathione in red blood cells, *Electrophoresis* 23 (2002) 1716–1721.
- [156] P. Capitan, T. Malmezat, D. Breuille, C. Obled, Gas chromatographic-mass spectrometric analysis of stable isotopes of cysteine and glutathione in biological samples, *J. Chromatogr. B* 732 (1999) 127–135.
- [157] J. Bouligand, A. Deroussent, A. Paci, J. Morizet, G. Vassal, Liquid chromatography-tandem mass spectrometry assay of reduced and oxidized glutathione and main precursors in mice liver, *J. Chromatogr. B* 832 (2006) 67–74.
- [158] F.J. Romero, W. Mueller-Klieser, Semiquantitative bioluminescent assay of glutathione, *J. Biolumin. Chemilumin.* 13 (1998) 263–266.
- [159] H. Kamencic, A. Lyon, P.G. Paterson, B.H.J. Juurlink, Monochlorobimane fluorimetric method to measure tissue glutathione, *Anal. Biochem.* 286 (2000) 35–37.
- [160] I.H. Shaik, M. Reza, Rapid determination of reduced and oxidized glutathione levels using a new thiol-masking reagent and the enzymatic recycling method: application to the rat liver and bile samples, *Anal. Bioanal. Chem.* 385 (2006) 105–113.

- [161] Q. Guillaume, G. Noctor, A plate reader method for the measurement of NAD, NADP, glutathione, and ascorbate in tissue extracts: application to redox profiling during *Arabidopsis* rosette development, *Anal. Biochem.* 363 (2007) 58–69.
- [162] I. Rahman, A. Kode, S.K. Biswas, Assay for quantitative determination of glutathione and glutathione disulfide levels using enzymatic recycling method, *Nat. Protoc.* 1 (2007) 3159–3165.
- [163] R.T.S.A. Araujo, M. Lucia, M.F.S. Saraiva, J.L.F.C. Lima, Determination of total and oxidized glutathione in human whole blood with a sequential injection analysis system, *Talanta* 74 (2008) 1511–1519.
- [164] G.T. Wierzbicka, T.M. Hagen, D.P. Jones, Glutathione in food, *J. Food Compos. Anal.* 2 (1989) 327–337.
- [165] T.M. Hagen, G.T. Wierzbicka, B.B. Bowman, T.Y. Aw, D.P. Jones, Fate of dietary glutathione: disposition in the gastrointestinal tract, *Am. J. Physiol.* 259 (4, Pt 1) (1990) G530–G535.
- [166] M.A. Mansoor, A.M. Svoldal, P.M. Ueland, Determination of the in vivo redox status of cysteine, cysteinylglycine, homocysteine, and glutathione in human plasma, *Anal. Biochem.* 200 (2) (1992) 218–229.
- [167] L-Glutathione GRAS Notification (2008) Pages 8–9. http://www.accessdata.fda.gov/scripts/fcn/gras_notices/804895A.PDF.
- [168] P. Monostori, G. Wittmann, E. Karg, S. Turi, Determination of glutathione and glutathione disulfide in biological samples: an in-depth review, *J. Chromatogr. B* 877 (2009) 3331–3346.
- [169] Y. Iwasaki, Y. Saito, Y. Nakano, K. Mochizuki, O. Sakata, R. Ito, K. Saito, H. Nakazawa, Chromatographic and mass spectrometric analysis of glutathione in biological samples, *J. Chromatogr. B* 877 (2009) 3309–3317.
- [170] E. Bolonska-Sikora, J. Ozczuldlowski, Z. Witkiewicz, D. Widel, Glutathione: method of sample preparation for chromatography and capillary electrophoresis, *Chemik* 66 (2012) 929–942.
- [171] A.J.C. Hartfield, C. Bachelor-McAuley, R.C. Compton, Electrochemical determination of glutathione: a review, *Analyst* 137 (2012) 2285–2296.



Losartan: Comprehensive Profile

**Abdul-Rahman A. Al-Majed¹, Ebrahim Assiri, Nasr Y. Khalil,
Hatem A. Abdel-Aziz**

Department of Pharmaceutical Chemistry, College of Pharmacy, King Saud University, Riyadh,
Saudi Arabia

¹Corresponding author: e-mail address: almajed99@yahoo.com

Contents

1. Description	160
1.1 Nomenclature	160
1.2 Formulae	160
1.3 Elemental Analysis	160
1.4 Appearance	160
1.5 Uses and Applications	161
2. Methods of Preparation	161
3. Physical Characteristics	163
3.1 Ionization Constant	163
3.2 Solubility	163
3.3 X-Ray Powder Diffraction Pattern	163
3.4 Thermal Methods of Analysis	164
3.5 Spectroscopy	164
3.6 Mass Spectrometry	165
3.7 NMR Spectrometry	165
4. Methods of Analysis	165
4.1 Compendial Methods	165
4.2 Reported Methods of Analysis	174
4.3 Chromatography	180
5. Stability	188
6. Pharmacokinetics, Metabolism, and Excretion	188
6.1 Pharmacokinetics	188
6.2 Metabolism	189
6.3 Excretion	189
7. Pharmacology	190
References	191



1. DESCRIPTION

1.1 Nomenclature

1.1.1 Systemic Chemical Names

2-Butyl-4-chloro-1-[[2'-(2*H*-tetrazol-5-yl)[1,1'-biphenyl]-4-yl]methyl]-1*H*-imidazole-5-methanol; 2-*n*-butyl-4-chloro-5-hydroxymethyl-1-[[2'-(1*H*-tetrazol-5-yl)biphenyl-4-yl]methyl]imidazole; 2-butyl-4-chloro-1-[*p*-(*o*-1*H*-tetrazol-5-ylphenyl)benzyl]imidazole-5-methanol [1]

1.1.2 Nonproprietary Names

Losartan potassium [1–4]

1.1.3 Proprietary Names

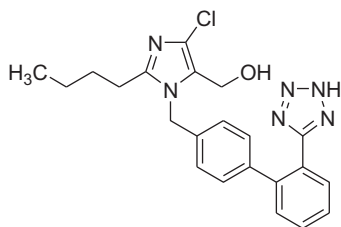
Proprietary Names for losartan include: Cozaar™ (Merck & Co), Losaprex™ (Paramount Pharmaceuticals), Lortaan™ (Merck Pharmaceuticals), Neo-Lotan™, Oscaar™. It is also an ingredient of Hyzaar™ (Merck & Co) and Losazid™ (Sigma-Tau) [2].

1.2 Formulae

1.2.1 Empirical Formula, Molecular Weight, and CAS Number

$C_{22}H_{23}ClN_6O$	422.91	[114798-26-4] [2]
----------------------	--------	-------------------

1.2.2 Structural Formula



1.3 Elemental Analysis

C 62.48%, H 5.48%, Cl 8.38%, N 19.87%, O 3.78% [1]

1.4 Appearance

White to off-white free-flowing crystalline powder [1]

1.5 Uses and Applications

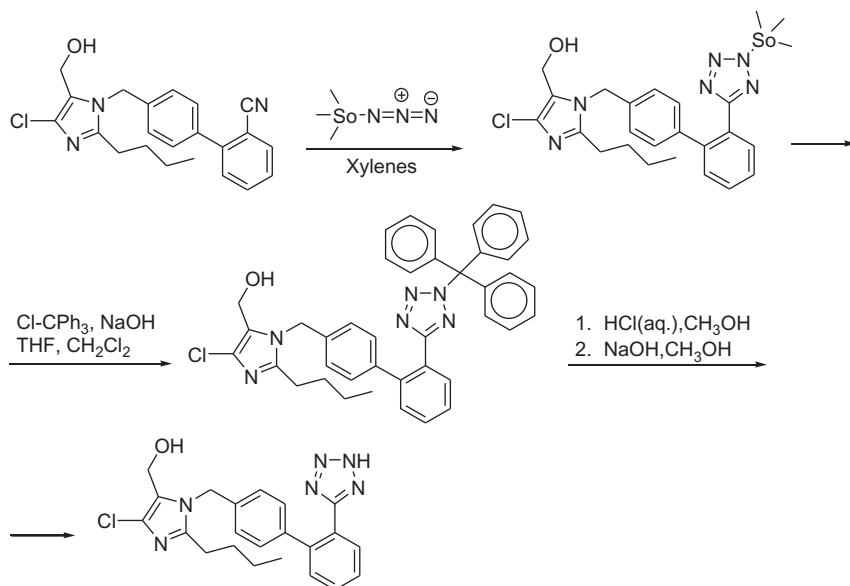
Losartan is an angiotensin II receptor antagonist (AIIRA) with antihypertensive activity due mainly to selective blockade of AT₁ receptors and the consequent reduced pressor effect of angiotensin II. It is used in the management of hypertension and heart failure, particularly in patients who develop cough with ACE inhibitors. It is also used to reduce the risk of stroke in patients with left ventricular hypertrophy, and in the treatment of diabetic nephropathy, and has been tried in myocardial infarction. Losartan is given orally as the potassium salt. The maximum hypotensive effect is achieved in about 3–6 weeks after starting treatment. In hypertension, the usual dose of losartan potassium is 50 mg once daily. The dose may be increased, if necessary, to 100 mg daily as a single dose or in two divided doses. An initial dose of 25 mg once daily should be given to patients with intravascular fluid depletion and to those with hepatic impairment. Losartan potassium is used for heart failure in those aged 60 years and above. An initial dose of 12.5 mg is given once daily and may be doubled at weekly intervals to a usual maintenance dose of 50 mg once daily. In diabetic nephropathy, losartan potassium is given in an initial dose of 50 mg once daily, increased to 100 mg once daily depending on the blood pressure [3]. Because of its mechanism of action, the product avoids the side effects of calcium antagonists and thus has been the origin of a whole family of analogs, “the sartans” [5].



2. METHODS OF PREPARATION

Losartan has been prepared by a variety of synthetic pathways. In several of these synthetic pathways, the penultimate product is 2-butyl-4-chloro-1-[[2'-(2-triphenylmethyl-2*H*-tetrazol-5-yl)[1,1'-biphenyl]-4-yl]methyl]-1*H*-imidazole-5-methanol (trityl losartan). Trityl losartan is an intermediate in processes described in U.S. Patents Nos. 5,138,069; 5,962,500; and 5,206,374.

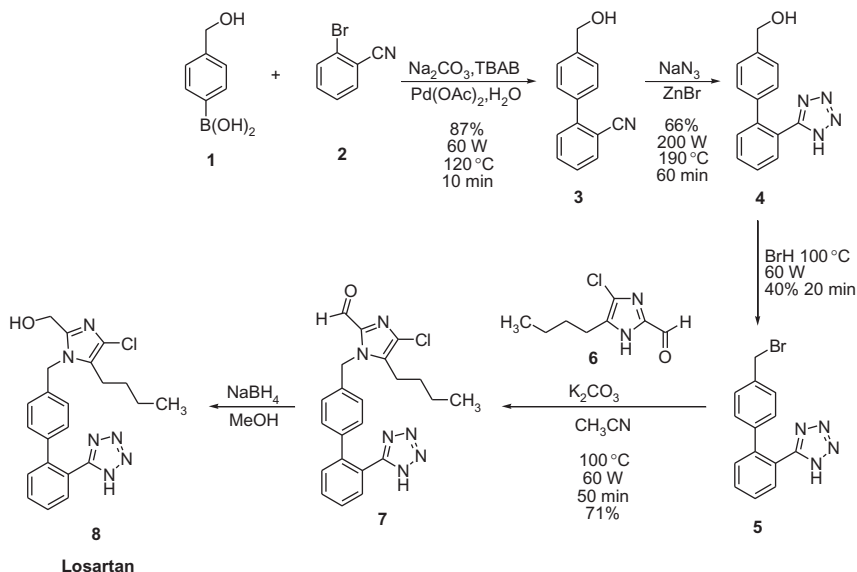
In a process described in Example 316 of U.S. Patent No. 5,138,069, the tetrazole ring of losartan is formed by reacting 1-[(2'-cyanobiphenyl-4-yl)methyl]-2-butyl-4-chloro-5-hydroxymethylimidazole with trimethyltin azide. The reaction gives a trimethylstannyl-substituted tetrazole compound directly. The trimethylstannyl group is cleaved from the product by reacting with trityl chloride. This reaction results in attachment of the trityl group to the tetrazole ring. In the last step, the trityl group is cleaved with acid to give losartan (Scheme 1).



Scheme 1 Preparation of Losartan according to Example 316 of U.S. Patent No. 5,138,069.

In the last step, trityl losartan was suspended in methanol and cooled to $\sim 10^{\circ}\text{C}$. 3.4 N Hydrochloric acid was added to the slurry. After a period of time, the pH of the reaction mixture was raised to 13 with 10 N NaOH. Methanol was then distilled off while makeup water was added. After distillation, additional water and toluene were added. The toluene phase was separated and the aqueous phase was extracted once more with toluene. Ethyl acetate and acetic acid were then added to the aqueous phase. Losartan was recovered from the aqueous phase as a solid and further purified by slurrying in ethyl acetate. Losartan was obtained in 88.5% yield and 98.8% purity as determined by high-performance liquid chromatographic (HPLC). This process is also described in U.S. Patents Nos. 5,128,355 and 5,155,188.

Another approach for the preparation of losartan was a microwave-mediated synthesis where water is heated well above its boiling point in sealed vessels, helping organic substrates become partially soluble [6]. Losartan has been prepared using this technique in most of the steps [7–9]. The synthetic strategy has been redesigned in relation with the conventional preparation methods to prevent the use of protecting groups, thus simplifying the whole procedure (Scheme 2).



Scheme 2 Preparation of Losartan via a microwave-mediated procedure using sealed vessels.



3. PHYSICAL CHARACTERISTICS

3.1 Ionization Constant

$\text{p}K_a$ 5–6 [1].

3.2 Solubility

Freely soluble in water; soluble in alcohols; slightly soluble in common organic solvents, such as acetonitrile and methyl ethyl ketone [1].

3.3 X-Ray Powder Diffraction Pattern

Raghavan *et al.* [10] reported the X-ray powder diffraction (XRPD) patterns for losartan using an automated X-ray diffractometer APD 3720 with copper tube K alpha radiation. They first performed a differential scanning calorimetry (DSC), which showed a minor endotherm at an extrapolated onset temperature of 229.5 °C and a major melting endotherm at an extrapolated onset temperature of 273.2 °C. The minor endotherm disappeared from samples which were heated to 255 °C. The XRPD pattern of the samples heated past the minor endotherm indicated a change in the crystal structure.

From these facts, it was concluded that the minor endotherm corresponds to an enantiotropic polymorphic transition. The major endotherm is the melting of the high temperature form.

3.4 Thermal Methods of Analysis

3.4.1 Melting Behavior

Losartan melts at 183.5–184.5 °C [2]

3.4.2 Differential Scanning Calorimetry

The DSC provides information about the physical properties of the sample as crystalline or amorphous nature and demonstrates a possible interaction between drug and polymers in formulations. The output of a DSC is a plot of heat flux (rate) versus temperature at a specified temperature rate. In addition to the data found by Raghavan *et al.* [10], Aswartha *et al.* [11] also reported a DSC for losartan over the temperature range of 50–300 °C. The pure drug losartan potassium showed an endothermic peak at 260.91 °C. The DSC of physical mixture of the losartan potassium and chitosan also showed an endothermic peak at 260.91 °C.

3.5 Spectroscopy

3.5.1 Ultraviolet Spectroscopy

The ultraviolet absorption spectrum of losartan in methanol is shown in Figure 1. The spectrum was recorded using a Shimadzu ultraviolet–visible spectrophotometer 1601 PC. The drug exhibits three maxima at 205, 225, and 255 nm.

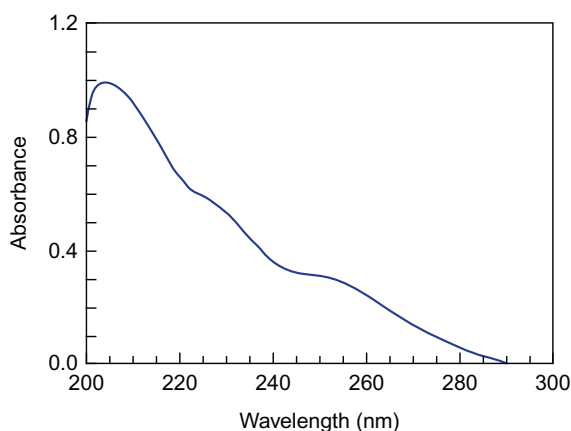


Figure 1 Ultraviolet absorption spectrum of losartan-K (10 µg/mL).

3.5.2 Infrared Spectroscopy

The infrared absorption spectrum of losartan is shown in Figure 2. The spectrum was obtained in a KBr pellet using Shimadzu FT-IR infrared spectrophotometer (model 8400S) equipped with IR Solution software, version 1.0, over the range of 500–4250 cm^{-1} at a resolution of 4 cm^{-1} . The OH absorption band appeared at 3192 cm^{-1} while C=N absorption band appeared at 1578 cm^{-1} .

3.6 Mass Spectrometry

The mass spectrum of losartan was obtained using an Agilent Triple Quadrupole 6410 QQQ LC/MS equipped with an ESI (electrospray ionization) source. Figure 3 shows the detailed mass fragmentation pattern $m/z = 445.2$ [losartan + Na]⁺ and 423.2 [losartan]⁺. Clarke reported the presence of the following principal peaks at m/z 192, 201, 249, 165, and 450 (losartan-2ME) [2].

3.7 NMR Spectrometry

3.7.1 ¹H NMR Spectrometry

¹H NMR spectrum of losartan was scanned in DMSO-*d*₆ on a Bruker NMR spectrometer operating at 500 MHz. Chemical shifts are expressed in δ values (ppm) relative to TMS as an internal standard (IS). Coupling constants (*J*) are expressed in Hz (Table 1 and Figure 4).

3.7.2 ¹³C NMR Spectrometry

¹³C NMR spectrum of losartan was scanned in DMSO-*d*₆ on a Bruker NMR spectrometer operating at 125 MHz. Chemical shifts are expressed in δ values (ppm) relative to TMS as an IS (Table 2 and Figure 5).



4. METHODS OF ANALYSIS

4.1 Compendial Methods

4.1.1 British Pharmacopoeia Methods [4]

Losartan contains not less than 98.5% and not more than 101.5% dried substance.

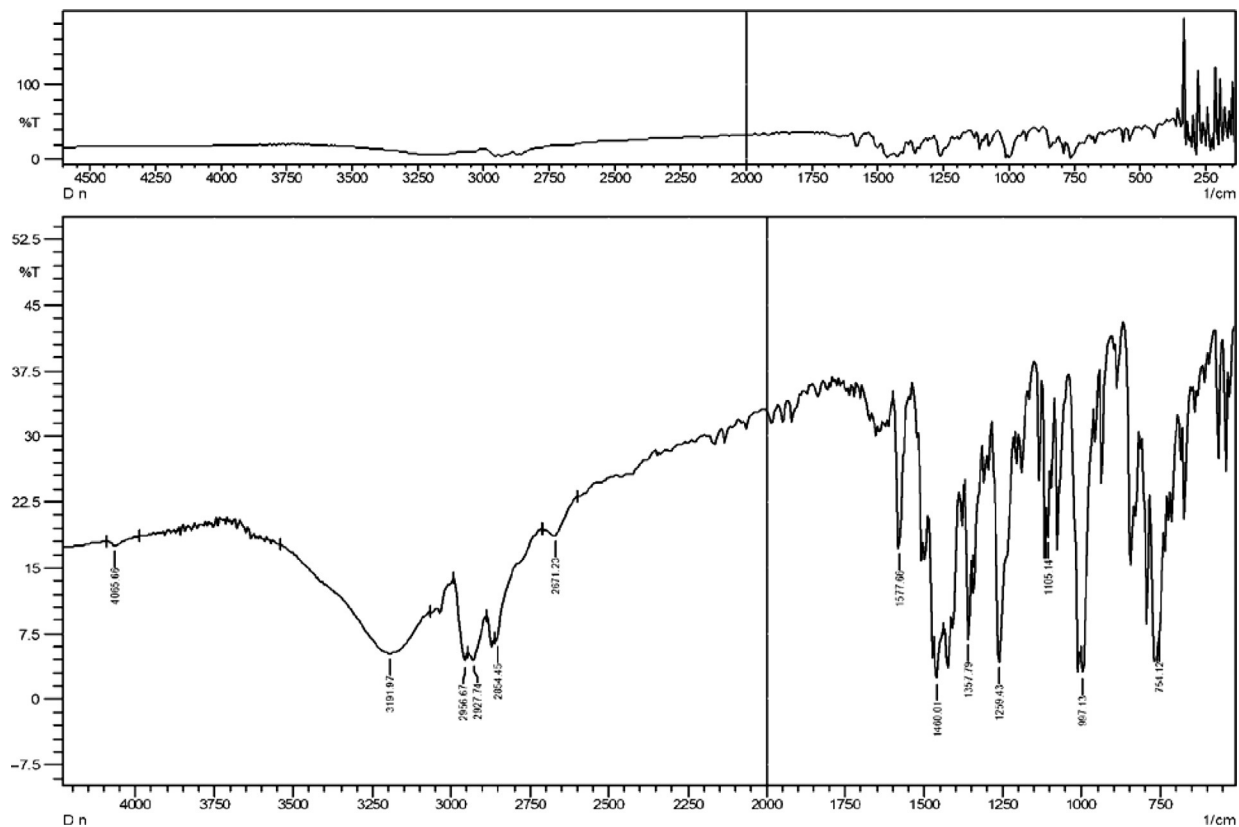


Figure 2 Infrared absorption spectrum of losartan (KBr pellet).

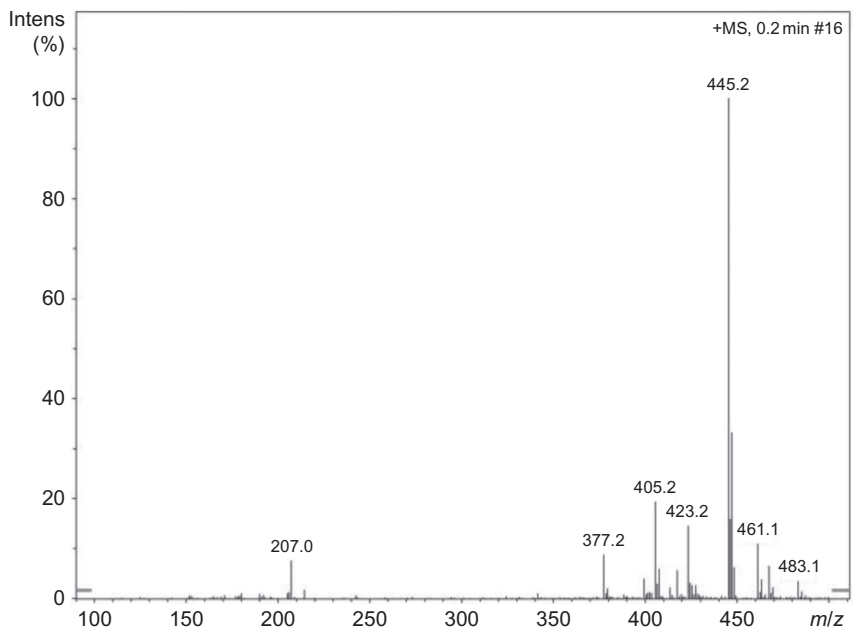


Figure 3 Mass spectrum of losartan.

Table 1 ¹H NMR of Losartan (DMSO-*d*₆)

Signal	Location (δ)	Shape	Integration	Correspondences
1	0.82	t, <i>J</i> = 7.5 Hz	3H	—CH ₃
2	1.26	Sext	2H	—CH ₂ —CH ₂ —CH ₂ —CH ₃
3	1.49	Quint	2H	—CH ₂ —CH ₂ —CH ₂ —CH ₃
4	2.52	t, <i>J</i> = 2.0 Hz	2H	—CH ₂ —CH ₂ —CH ₂ —CH ₃
5	4.43	d, <i>J</i> = 5.0 Hz	2H	—CH ₂ —OH
6	5.22	s	2H	—CH ₂ —Ar
7	5.32	t, <i>J</i> = 5.0 Hz	1H	—OH
8	6.91	d, <i>J</i> = 8.0 Hz	2H	ArHs
9	7.10	d, <i>J</i> = 8.0 Hz	2H	ArHs
10	7.27–7.29	m	1H	ArH
11	7.35–7.37	m	2H	ArHs
12	7.54–7.56	m	1H	ArH

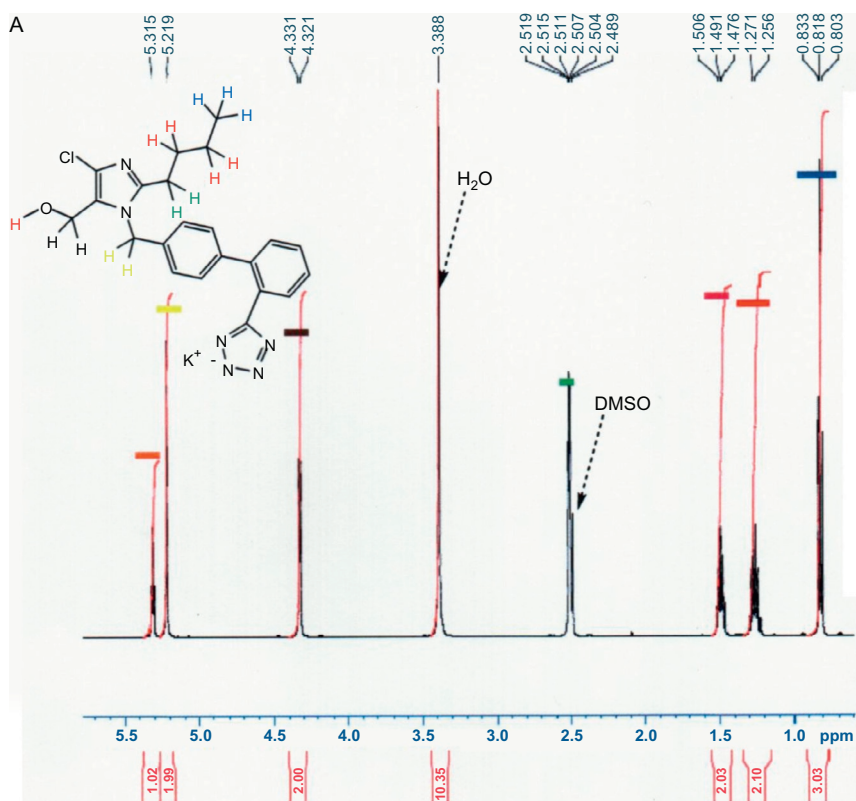
Identification

- A.** Shake a quantity of the powdered tablets containing 0.1 g of losartan potassium with 25 mL of *acetone* for 15 min, filter (Whatman GF/C is suitable), and evaporate to dryness under a stream of nitrogen. The *infrared absorption spectrum* of the residue, Appendix II A [4], is concordant with the *reference spectrum* of losartan (*RS 453*).
- B.** Shake a quantity of the powdered tablets containing 0.2 g of losartan potassium with 5 mL of *water*, filter (Whatman GF/C is suitable), and pass the filtrate through a 0.45- μm membrane filter. 1 mL of the filtrate yields reaction B characteristic of *potassium salts*, Appendix VI [4].

Tests

Dissolution

Comply with the requirements in the *dissolution test for tablets and capsules*, Appendix XII B1 [4].



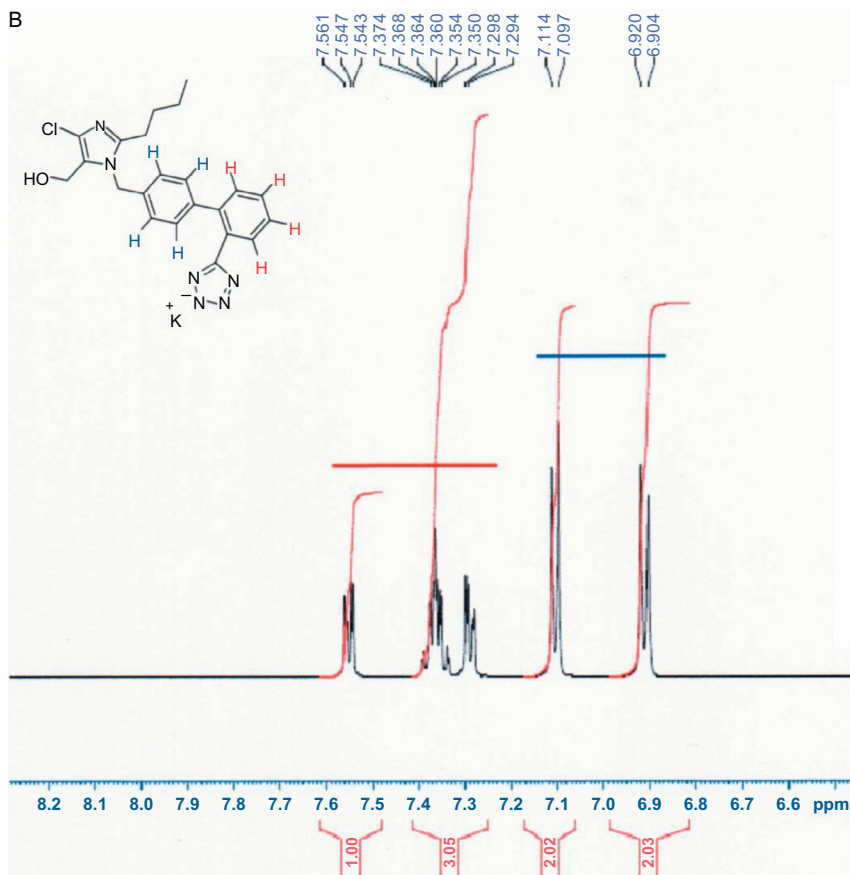


Figure 4 (A) ^1H NMR spectrum of losartan (aliphatic region). (B) ^1H NMR spectrum of losartan (aromatic region).

Test conditions

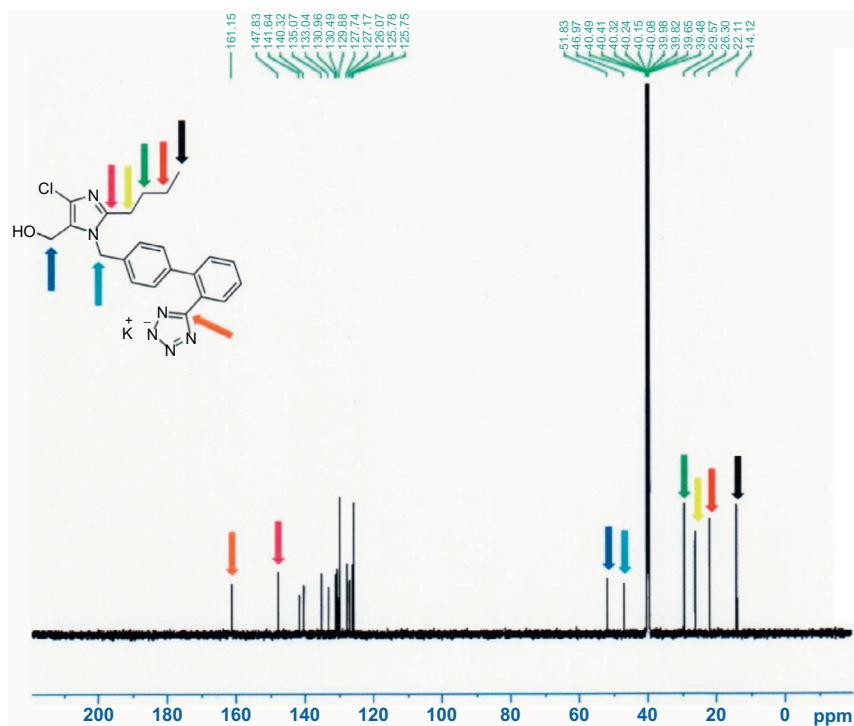
- (a) Use Apparatus 2, rotating the paddle at 75 revolutions/min.
- (b) Use 900 mL of *water*, at a temperature of 37° , as the medium.

Procedure

- (1) After 30 min, withdraw a sample of the medium and measure the *absorbance* of the filtered sample, suitably diluted with the dissolution medium if necessary, at the maximum at 250 nm, Appendix II B [4], using *water* in the reference cell.
- (2) Measure the *absorbance* of a suitable solution of *losartan potassium BPCRS* using *water* in the reference cell.

Table 2 ^{13}C NMR of Losartan ($\text{DMSO}-d_6$)

Signal	Location (δ)	Correspondences
1	14.12	$-\underline{\text{C}}\text{H}_3$
2	22.11	$-\text{CH}_2-\text{CH}_2-\underline{\text{C}}\text{H}_2-\text{CH}_3$
3	26.30	$-\underline{\text{C}}\text{H}_2-\text{CH}_2-\text{CH}_2-\text{CH}_3$
4	29.57	$-\text{CH}_2-\underline{\text{C}}\text{H}_2-\text{CH}_2-\text{CH}_3$
5	46.97	$-\underline{\text{C}}\text{H}_2-\text{Ar}$
6	51.83	$-\underline{\text{C}}\text{H}_2-\text{OH}$
7	125.75 (2C), 125.78, 126.07, 127.17, 127.74, 129.88 (2C), 130.49, 130.96, 133.04, 135.07, 140.32, 141.64,	Aromatic C_s , C4 and C5 of imidazole
8	147.83	C2 imidazole
9	161.51	C tetrazole

**Figure 5** ^{13}C NMR spectrum of losartan.

Determination of content

Calculate the total content of losartan potassium, $C_{22}H_{22}ClKN_6O$, in the medium from the absorbances obtained and using the declared content of $C_{22}H_{22}ClKN_6O$ in losartan potassium BPCRS.

Limits

The amount of losartan potassium released after 30 min is not less than 70% (Q) of the stated amount.

Related substances

Carry out the method for *liquid chromatography*, Appendix III D [4], using the following solutions.

- (1) To a quantity of the powdered tablets containing 62.5 mg of losartan potassium, add 125 mL of mobile phase A and mix with the aid of ultrasound for 15 min, shaking the samples intermittently. Mix for a further 10 min with the aid of ultrasound. Add sufficient mobile phase A to produce a solution containing 0.025% w/v of losartan potassium.
- (2) Dilute 1 volume of solution (1) to 100 volumes and further dilute 1 volume to 10 volumes with mobile phase A.
- (3) Dissolve 12 mg of *losartan potassium BPCRS* in 5 mL of *water*, add 5 mL of 0.1 M *hydrochloric acid*, and heat at 105 °C for 4 h. Cool to ambient temperature. Add 5 mL of 0.1 M *sodium hydroxide* and dilute to 50 mL with *water*. Adjust the pH of the solution to 6.0 with 0.1 M *hydrochloric acid*.

Chromatographic conditions

- (a) Use a stainless steel column (15 cm × 3.9 mm) packed with *octylsilyl silica gel for chromatography* (5 µm) (Waters Symmetry C8 is suitable).
- (b) Use gradient elution and the mobile phase described below.
- (c) Use a flow rate of 1 mL/min.
- (d) Use an ambient column temperature.
- (e) Use a detection wavelength of 250 nm.
- (f) Inject 10 µL of each solution.

Mobile phase

Mobile phase A: 3 volumes of *acetonitrile* and 17 volumes of *mixed phosphate buffer, pH 7.0*

Use the chromatogram obtained with solution (3) to identify the peaks due to impurities L and M. When the chromatograms are recorded under the prescribed conditions, the relative

retentions with reference to losartan (retention time = about 2.6 min) are: impurity L = about 2.4; impurity M = about 2.9.

Mobile phase B: Acetonitrile

Time (min)	Mobile Phase A (% v/v)	Mobile Phase B (% v/v)	Comment
0–10	80 → 40	20 → 60	Linear gradient
10–11	40 → 80	60 → 20	Linear gradient
11–15	80	20	Reequilibration

System suitability

The test is not valid unless, in the chromatogram obtained with solution (3), the *resolution factor* between the peaks due to impurity L and impurity M is at least 2.0.

Limits

In the chromatogram obtained with solution (1):

The area of any peak corresponding to impurity M is not greater than five times the area of the principal peak in the chromatogram obtained with solution (2) (0.5%); the area of any peak corresponding to impurity L is not greater than five times the area of the principal peak in the chromatogram obtained with solution (2) (0.5%); the area of any other *secondary peak* is not greater than twice the area of the principal peak in the chromatogram obtained with solution (2) (0.2%); the sum of the areas of all the *secondary peaks* is not greater than 10 times the area of the principal peak in the chromatogram obtained with solution (2) (1%). Disregard any peak with an area less than the area of the principal peak in the chromatogram obtained with solution (2) (0.1%).

Assay

Weigh and powder 20 tablets. Carry out the method for *liquid chromatography*, Appendix III D [4], using the following solutions in the mobile phase.

- (1) Mix with the aid of ultrasound for 15 min a quantity of the powdered tablets containing 25 mg of losartan potassium with 30 mL of mobile phase and allow to cool. Add sufficient mobile phase to produce 50 mL and filter through a 0.45- μ m PTFE filter.
- (2) 0.05% w/v of *losartan potassium BPCRS*.

Chromatographic conditions

- (a) Use a stainless steel column (25 cm × 4.6 mm) packed with *octadecylsilyl silica gel for chromatography* (5 μm) (Prodigy C18 is suitable).
- (b) Use isocratic elution and the mobile phase described below.
- (c) Use a flow rate of 1.5 mL/min.
- (d) Use an ambient column temperature.
- (e) Use a detection wavelength of 250 nm.
- (f) Inject 10 μL of each solution.

Mobile phase

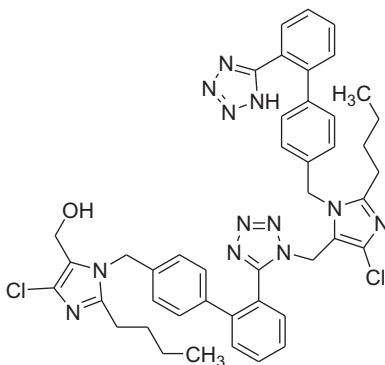
3 Volumes of *acetonitrile* and 7 volumes of a solution containing 0.39% w/v of *sodium dihydrogen orthophosphate* and 0.35% v/v of *triethylamine* adjusted to pH 7.0 with *orthophosphoric acid*. When the chromatograms are recorded under the prescribed conditions, the retention time of losartan is about 7 min.

Determination of content

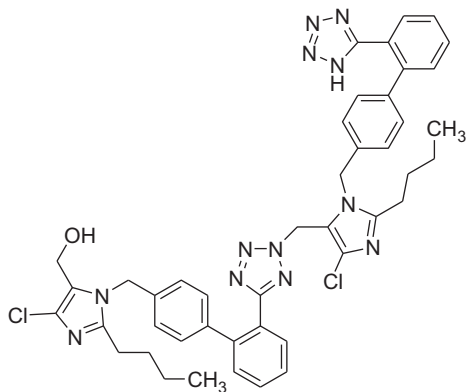
Calculate the content of $C_{22}H_{22}ClKN_6O$ in the tablets using the declared content of $C_{22}H_{22}ClKN_6O$ in *losartan potassium BPCRS*.

Impurities

The impurities limited by the requirements of this monograph include impurities L and M listed under losartan potassium.



L. [2-Butyl-1-[[[2'-[1-[[2-butyl-4-chloro-1-[[2'-(1*H*-tetrazol-5-yl)biphenyl-4-yl]methyl]-1*H*-imidazol-5-yl]methyl]-1*H*-tetrazol-5-yl]biphenyl-4-yl]methyl]-4-chloro-1*H*-imidazol-5-yl]methanol (European Pharmacopoeia Impurity L)



M. [2-Butyl-1-[[2'-[2-[[2-butyl-4-chloro-1-[[2'-(1H-tetrazol-5-yl)biphenyl-4-yl]methyl]-1H-imidazol-5-yl]methyl]-2H-tetrazol-5-yl]biphenyl-4-yl]methyl]-4-chloro-1H-imidazol-5-yl]methanol (European Pharmacopoeia Impurity M).

4.2 Reported Methods of Analysis

4.2.1 Titrimetric Method

de Oliveira Rossini *et al.* [12] reported a simple conductometric titration in aqueous medium for the losartan analysis in pharmaceutical formulations. The first step of the titration occurs with the protonation of losartan producing a white precipitate and resulting in a slow increase in conductivity. When the protonation stage is complete, a sharp increase in conductivity occurs which was determined to be due to the presence of excess of acid. The titrimetric method was applied to the determination of losartan in pharmaceutical products and the results are comparable with values obtained using a chromatographic method recommended by the United States Pharmacopoeia. The relative standard deviation for successive measurements of a 125 mg/L (2.71×10^{-4} mol/L) losartan solution was approximately 2%. Recovery study in tablet samples ranged between 99% and 102.4%. The procedure is fast, simple, and represents an attractive alternative for losartan quantification in routine analysis. In addition, it avoids organic solvents, minimizes the risk of exposure to the operator, and the waste treatment is easier compared to classical chromatographic methods.

4.2.2 Spectrophotometric Methods

4.2.2.1 Ultraviolet Spectrometry

Stolarczyk *et al.* [13] described two methods, spectrophotometric and chromatographic–densitometric methods, for determination of losartan potassium, quinapril hydrochloride, and hydrochlorothiazide in pharmaceutical preparations. The spectrophotometric method involved derivative spectrophotometry and zero-order spectrophotometry. In the derivative spectrophotometric method, the measurements were carried out at $\lambda = 224.0$ nm for quinapril, $\lambda = 261.0$ nm for hydrochlorothiazide, and $\lambda = 270.0$ nm for losartan. When zero-order spectrophotometry was applied for the determination of hydrochlorothiazide, $\lambda = 317.0$ nm was used. In chromatographic–densitometric studies, high-performance thin-layer chromatographic (HPTLC) plates were used as stationary phase and a mixture of solvents, *n*-butanol:acetic acid:water (15:5:1, v/v/v), as mobile phase. Under the established conditions, good resolution of examined constituents was obtained. Retardation factor (R_f) for quinapril hydrochloride was ~ 0.70 , for losartan potassium ~ 0.85 , and for hydrochlorothiazide ~ 0.78 . The developed methods are characterized by high sensitivity and accuracy. For quantitative analysis, densitometric measurements were carried out at $\lambda = 218.0$ nm for quinapril, $\lambda = 275.0$ nm for hydrochlorothiazide, and $\lambda = 232.0$ nm for losartan.

Tarkase *et al.* [14] reported a simple UV–spectrophotometric method for determination of losartan potassium. The spectrum shows an absorbance maximum close to 200 nm and other two maxima but with lower intensities around 220 and 260 nm. The first-derivative spectrum shows an intense maximum at 234 nm with evidently useful characteristics from the analytical viewpoint. The linearity of spectrophotometric measurement for losartan potassium solutions within the concentration range 4.00–88.00 $\mu\text{g/mL}$, equivalent to 80–120% of the nominal value of a tablet, was satisfactory. The accuracy studied by means of assays of recovery in losartan potassium solutions and losartan potassium with excipients gave mean values of 99.66% and 102.25%, respectively.

Thomas *et al.* [15] developed two simple, accurate, and reproducible spectrophotometric methods for the simultaneous estimation of hydrochlorothiazide (HCTZ), atenolol (Atn), and losartan potassium (LOS) in combined tablet dosage forms. The first method involves determination using the simultaneous equation method, and the sampling wavelengths selected

are 272.5, 224, and 250 nm over the concentration ranges of 0.5–30, 1–50, and 1–60 $\mu\text{g/mL}$ for HCTZ, Atn, and LOS, respectively. The second method is the first-order derivative method, and the sampling wavelengths selected for estimation of HCTZ, Atn, and LOS are 280.5, 233, and 244 nm with linearity in the concentration ranges of 0.5–30, 1–50, and 1–60 $\mu\text{g/mL}$, respectively.

Ulu *et al.* [16] developed UV- and second-derivative spectrophotometric and HPLC methods for the determination of losartan in tablets. For UV-spectrophotometric method, absorbances of the standard solutions were measured at 206.6 nm. For second-derivative spectrophotometric method, the distance between two extremum values (peak-to-peak amplitudes), 219.6 nm and 228.8 nm, was measured in the second-order derivative spectra of standard solutions. Calibration curves were constructed by plotting $d^2A/d\lambda^2$ values against concentrations. These wavelengths were selected depending on the obtained maximum values. The two methods were applied to determine losartan in tablets.

Bonfilio *et al.* [17] reported a direct and first-derivative UV-spectrophotometric method for determination of losartan in capsules. Based on losartan potassium spectrophotometric characteristics, a signal at 205 nm of the zero-order spectrum and a signal at 234 nm of the first-derivative spectrum were found adequate for quantification. The results were used to compare these instrumental techniques. The linearity between the signals and concentrations of losartan potassium in the ranges of 3.0–7.0 and 6.0–14.0 mg/L for direct and first-derivative spectrophotometry in aqueous solutions, respectively, presented a correlation coefficient (r) of 0.9999 in both cases. The methods were applied for losartan potassium in capsule dosage obtained from local pharmacies, and were shown to be efficient, easy to apply, and low cost. These methods do not use polluting reagents and require relatively inexpensive equipment.

Ansari *et al.* [18] developed a first-derivative UV-spectroscopic method for determination of losartan in the tablet dosage form. The first-derivative spectrum recorded between 220 and 320 nm, and a zero-crossing technique for first-derivative measurement at 232.5 nm was selected. It is found that the selectivity and sensitivity of method to be in desirable range. In comparison with the direct UV method, the first-derivative UV spectroscopy has a definite through without any interference from UV-absorbing excipients. This method is also fast and economical in comparison to the more time-consuming HPLC method regularly used for formulation screening and quality control, and can be used routinely by any laboratory possessing a

spectrophotometer with a derivative accessory. The linear concentration ranges were 2–50 $\mu\text{g/mL}$ ($\text{DI} = -0.0159\text{C} - 0.0056$, $r = 0.9994$, $n = 6$) where DI is the value of the first derivative of losartan absorbency at 232.5 nm and C is the concentration of losartan (mg/L). Between-days $\text{CV\%} \leq 2.9$, within-day $\text{CV\%} \leq 2.1$, analytical recovery close to 98.1% shows the suitability of the method for determination in quality control.

Rao *et al.* [19] reported a second-derivative UV-spectrophotometric method for the estimation for losartan potassium in solid pharmaceutical dosage form. The λ -max of losartan potassium was found to be 234 nm for both crude and marketed samples. Beer's law was obeyed at the concentration range of 8–22 $\mu\text{g/mL}$. The method was validated statistically and by recovery studies. The LOD (limit of detection) and LOQ (limit of quantification) were found to be 9.7 and 29.74 $\mu\text{g/mL}$, respectively. The correlation coefficient value (r) was found to be 0.9989. The purity was found to be 98%.

4.2.2.2 Colorimetry

Prabhakar and Giridhar [20] described two new rapid reproducible and economical spectrophotometric methods for the determination of losartan potassium in bulk and in synthetic mixture for solid dosage forms. Both methods are based on the formation of an orange-red and orange ion-pair complex due to the action of calmagite (CGT) and orange-II (O-II) on losartan potassium in acidic medium (pH 1.2). Under optimized conditions, they show an absorption maxima at 491 nm (CGT) and 486 nm (O-II), with molar absorptivities of 1.74×10^3 and 1.75×10^3 L/mol/cm and Sandell's sensitivities of 0.2649 and 0.2637 per 0.001 absorbance unit for CGT and O-II, respectively. The color is stable for 5 min after extraction. In both cases, Beer's law is obeyed between 10 and 100 $\mu\text{g/mL}$. The proposed method was successfully extended to synthetic mixture for solid dosage forms.

Darwish [21] published a method involving charge-transfer (CT) complexes between losartan and various acceptors. The studies were carried out to investigate the charge-transfer reactions of losartan potassium (LOS) as n -electron donor with iodine as electron acceptor. Other acceptors were also studied including 7,7,8,8-tetracyanoquinodimethane, 1,3,5-trinitrobenzene, 2,3-dichloro-5,6-dicyano-1,4-benzoquinone, *p*-chloranilic acid, tetracyanoethylene, 2,3,5,6-tetrabromo-1,4-benzoquinone, 2,3,5,6-tetrachloro-1,4-benzoquinone, and 2,4,7-trinitro-9-fluorenone. Different colored charge-transfer complexes and radical anions were obtained. Different variables affecting the reactions were studied and optimized. The formed complexes and the site of interaction were examined by UV-vis,

IR, and ^1H NMR techniques, and computational molecular modeling. The formation of the colored complexes was utilized in the development of simple, rapid, and accurate spectrophotometric methods for the analysis of LOS in pure form as well as in its pharmaceutical tablets. Under the optimum reaction conditions, linear relationships with good correlation coefficients (0.9985–0.9998) were found between the absorbance values and the concentration of LOS-K in the range of 2–200 $\mu\text{g/mL}$. The limits of assay detection ranged from 0.61 to 19.65 $\mu\text{g/mL}$. No interference could be observed from the coformulated hydrochlorothiazide (HCTZ), as well as from the additives commonly present in the tablets. The methods were successfully applied to the analysis of tablets from different manufacturers that contain LOS, alone or combined with HCTZ, with good accuracy and precision; the recovery percentages ranged from $98.96 \pm 1.62\%$ to $101.58 \pm 1.29\%$. The results were compared favorably with a reported method.

4.2.2.3 Spectrofluorimetric Method

El-Shaboury *et al.* [22] developed a highly sensitive spectrofluorimetric method for determination of some AIIRAs, namely losartan potassium (LOS), irbesartan (Irb), valsartan (VAL), and candesartan cilexetil (Cand) in pure forms as well as in their pharmaceutical dosage forms. All the variables affecting the relative fluorescence intensity were studied and optimized. Under the optimum conditions, linear relationships with good correlation coefficients (0.9982–0.9991) were obtained over the concentration range from 0.006 to 1.7 $\mu\text{g/mL}$. Good accuracy and precision were successfully obtained for the analysis of tablets containing each drug alone or combined with hydrochlorothiazide (HCTZ) without interferences from the coformulated HCTZ or the additives commonly present in tablets.

4.2.3 Electrochemical Method

4.2.3.1 Calorimetry

De Paula *et al.* [23] reported a low soluble supramolecular complex between the losartan potassium (LOS) and hydroxypropyl- β -cyclodextrin (HP β CD). The methods were characterized throughout phase solubility, NMR techniques (^1H and 2D-ROESY), and isothermal titration calorimetry (ITC) in order to attain physical–chemical knowledge of the system. In addition, the hypertensive effect of composition losartan/HP β CD was evaluated aiming to obtain a more efficient oral pharmaceutical composition. Mass spectrometry and ITC blank experiment showed the presence of losartan clusters at 30 mM pure solution. Phase-solubility experiments showed a “Bs” type system, due to the formation of a less soluble complex than pure losartan.

NMR demonstrated the short distance interactions between the losartan and the cyclodextrin, where several possibilities of interactions were observed. ITC data suggested an average 1:1 stoichiometry of losartan and the cyclodextrin. The complex demonstrated efficiency in hypertension control, presenting antagonist action on the pressure effect of angiotensin II within 30 h, as compared to losartan alone (6 h), indicating that inclusion of losartan in HP β CD enhanced the extent and duration of its antagonistic action. In this work, a model of interaction between losartan and HP β CD was proposed based on dissociation of self-assembled losartan followed by complexation with HP β CD.

4.2.3.2 Voltammetric Methods

Ensaifi and Hajarri [24] developed a square-wave voltammetric procedure for the electroanalytical determination of losartan and triamterene in Britton–Robinson buffer (pH 3.0, 0.1 mol/L) as a supporting electrolyte containing 30 ng/mL of copper ions. Opposite to the case of triamterene, losartan cannot be reduced at a mercury electrode alone, but a new peak appears at -0.25 V in the presence of copper due to the formation of a complex between copper(II) and losartan. An accumulation potential of -0.30 V during 80 s for the prior adsorption of losartan–copper(II) and triamterene on the electrode surface was used. The response of the system was found to be linear in the range of 30.0–270.0 nmol/L for losartan and two linear dynamic ranges containing 0.5–200.0 and 200.0–400.0 nmol/L of triamterene. The limits of detection were 9.7 and 0.3 nmol/L for losartan and triamterene, respectively. The relative standard deviations for five replicate analyses of 100.0 and 10.0 nmol/L losartan and triamterene were 5.5%. Applicability to assay the drugs in urine and pharmaceutical formulations was illustrated with satisfactory results. The direct current polarography of triamterene indicates that the reduction of a related drug is strongly dependent on the pH of the solution. A linear segment was found with slope value of -63.6 mV pH (-1) in the pH range of 2.0–6.0. The stoichiometry and complex formation constant (β) for losartan–Cu(II), number of transfer electrons (n), transfer coefficients (α), and number of proton transfers were also estimated.

Habib *et al.* [25] described a cathodic stripping voltammetric determination of losartan using hanging mercury drop electrode (HMDE). The method was based on adsorptive accumulation of the species at HMDE and at pH 7, followed by alternating current (AC) sweep. The behavior of adsorptive stripping response was studied under various experimental conditions, e.g., type of supporting electrolyte, pH, accumulation time, scan

rate, and mode of sweep (direct current DC, differential pulse DP, square wave SW, and AC). In Britton–Robinson buffer solution, pH 7, a quasi-reversible reaction took place. The reduction response was more sensitive than the oxidation one and it was linear over the concentration range of 0.16–1.2 $\mu\text{g/mL}$. The determination of the cited compound in oral dosages was achieved using the standard addition method. The average of determinations obtained by SW adsorptive voltammetric method with its standard deviation was $100.1 \pm 3\%$.

4.3 Chromatography

4.3.1 Thin-Layer Chromatography

Tsvetkova and Obreshkova [26] developed a thin-layer chromatographic (TLC)-densitometric method for simultaneous identification and determination of losartan potassium, telmisartan, and valsartan in tablets, by the following chromatographic system: stationary phase: TLC plates with silica gel G60 F254, mobile phase composed of chloroform–methanol–acetone–toluene–acetic acid (7.5 : 1.5 : 5.5 : 0.01 : 0.03, v/v). The UV detection was at $\lambda = 254 \text{ nm}$.

Santhana and Lakshmi [27] established a simple HPTLC method for separation and quantitative analysis of losartan potassium in bulk and in pharmaceutical formulations. After extraction with methanol, sample and standard solutions were applied to silica gel plates and developed with chloroform:methanol:acetone:formic acid (7.5:1.3:0.5:0.03, v/v/v/v) as mobile phase. Zones were scanned densitometrically at 254 nm. The R_f values of amlodipine besylate, hydrochlorothiazide, and losartan potassium were 0.35, 0.57, and 0.74, respectively. Calibration plots were linear in the ranges 500–3000 ng/spot for losartan potassium, amlodipine, and hydrochlorothiazide; the correlation coefficients, r , were 0.998, 0.998, and 0.999, respectively.

Shah *et al.* [28] reported, in the HPTLC method, a mobile phase of chloroform–methanol–acetone–formic acid (7.5 + 1.5 + 0.5 + 0.03, v/v) and a prewashed silica gel G60 F254 TLC plate as the stationary phase were used to resolve LST and HCTZ in a mixture. Two well-separated and sharp peaks for LST and HCTZ were obtained at R_f values of 0.61 ± 0.02 and 0.41 ± 0.02 , respectively. LST and HCTZ were quantitated at 254.0 nm. The linearity ranges obtained for the HPTLC method are 400–1200 and 100–300 ng/spot with corresponding correlation coefficients of 0.9944 and 0.9979, for LST and HCTZ, respectively. Both methods were validated, and the results were compared statistically.

Sathe and Bari [29] established a simple HPTLC method for separation and quantitative analysis of losartan potassium in bulk and in pharmaceutical formulations. After extraction with methanol, sample and standard solutions were applied to prewashed silica gel plates and developed with toluene–methanol–triethylamine 6.5:4:0.5 (v/v) as mobile phase. Zones were scanned densitometrically at 274 nm. The R_f values of losartan potassium, atenolol, and hydrochlorothiazide were 0.60, 0.43, and 0.29, respectively. Calibration plots were linear in the ranges 1000–5000 ng/band for losartan potassium and atenolol and 250–1250 ng/band for hydrochlorothiazide; the correlation coefficients, r , were 0.9994, 0.9993, and 0.9994, respectively.

4.3.2 HPLC Methods

A stability-indicating reversed-phase liquid chromatographic method was developed and validated by Kollipara *et al.* [30] for simultaneous determination of losartan potassium and ramipril. Separations were achieved using a C18 column with mobile phase consisting of acetonitrile (0.2% v/v, pH 2.5) and aqueous trifluoroacetic acid (45:55, v/v) in isocratic mode at 1 mL/min flow rate. Column effluent was monitored at 210 nm using an UV detector.

Soltani *et al.* [31] developed a HPLC method for simultaneous determination of carvedilol and losartan in human plasma and urine samples. The analytes were extracted by a dispersive liquid–liquid microextraction method. A mobile phase of 15 mM sodium dihydrogen phosphate buffer (pH 4.0)/acetonitrile/2-propanol (70/27.5/2.5, v/v/v) was used to separate the drugs using a Waters[®] ODS column (250 × 4.6 mm) and detected by an UV detector at 222 nm.

Czerwińska and Mazurek [32] developed an isocratic system for determination of losartan potassium in bulk substances and tablets: Lorista tablets 50 mg, Diovan tablets 160 mg, Micardis tablets 20 mg, Aprovel tablets 300 mg, Teveten tablets 600 mg, and Blopress tablets 16 mg. The determination was carried out using Zorbax SB-Phenyl column with UV–vis detector set at 230 nm and the following mobile phases: 0.1 mol/L sodium acetate (pH 5.5)–acetonitrile–methanol in 35:9:6 v/v/v ratio for eprosartan mesylate and valsartan, in 15:6:4 v/v/v ratio for losartan potassium and irbesartan, and in 10:9:6 v/v/v ratio for telmisartan and candesartan cilexetil. The recovery from simulated tablets was determined and amounted to for eprosartan mesylate—99.04%, valsartan—100.0%, losartan potassium—100.03%, irbesartan—100.35%, telmisartan—100.06%, and candesartan cilexetil—100.40%.

Dubey *et al.* [33] described a HPLC method for simultaneous determination of losartan potassium and metolazone in formulation. This method is based on a HPLC separation of the two drugs on the Thermo Hypersil BDS-C₁₈ (250 × 4.6 mm, 5.0 μm) with isocratic conditions and a simple mobile phase containing acetonitrile:water (60:40) at a flow rate of 0.8 mL/min using UV detection at 237 nm. This method has been applied to a marketed formulation without interference of excipients. The linear regression analysis data for the calibration plots showed a good linear relationship over the concentration range of 2–12 μg/mL for losartan potassium and 0.2–1.2 μg/mL for metolazone. The method was validated for precision, robustness, and recovery. Statistical analysis showed that the method is repeatable and selective for the estimation of losartan potassium and metolazone.

Wankhede *et al.* [34] reported a reverse-phase high-performance liquid chromatographic (RP-HPLC) method using 0.025 M phosphate buffer (pH 3.7):acetonitrile (57:43, v/v) as the mobile phase and Kromasil C18 (4.6 mm i.d. × 250 mm) column as stationary phase with detection wavelength of 232 nm. Linearity was obtained in the concentration range of 2–14, 20–140, and 5–40 μg/mL for amlodipine besilate, losartan potassium, and hydrochlorothiazide, respectively. Both UV-spectrophotometric and RP-HPLC methods were statistically validated and can be used for analysis of combined dose tablet formulation containing amlodipine besilate, losartan potassium, and hydrochlorothiazide.

Bonfilio *et al.* [35] described a HPLC using 2⁵⁻¹ fractional factorial and Doehlert designs for the determination of losartan potassium in capsules. This multivariate approach allows a considerable improvement in chromatographic performance using fewer experiments, without additional cost for columns or other equipment. The HPLC method utilized potassium phosphate buffer (pH 6.2; 58 mmol/L)–acetonitrile (65:35, v/v) as the mobile phase, pumped at a flow rate of 1.0 mL/min. An octylsilane column (100 mm × 4.6 mm i.d., 5 μm) maintained at 35 °C was used as the stationary phase. UV detection was performed at 254 nm. The method was validated according to the ICH guidelines, showing accuracy, precision (intraday relative standard deviation (RSD) and interday RSD values <2.0%), selectivity, robustness, and linearity ($r=0.9998$) over a concentration range from 30 to 70 mg/L of losartan potassium. The limits of detection and quantification were 0.114 and 0.420 mg/L, respectively. The validated method may be used to quantify losartan potassium in capsules and to determine the stability of this drug.

Jalalizadeh *et al.* [36] developed a sensitive HPLC method for determination of losartan in plasma. Losartan was extracted from plasma by a two-step extraction procedure using chloroform as extracting solvent in acidic medium. HPLC analysis was performed on a cyano reversed-phase column using phosphate buffer (pH 4.3):acetonitrile (750:250, v/v) as the mobile phase with a flow rate of 0.9 mL/min. Sodium diclofenac was selected as IS. Excellent linearity between the peak area ratios and losartan concentrations over the range of 2–200 ng/mL of plasma was observed. The limit of determination with UV detection at 225 nm with a CV <5% was 2 ng/mL in 500 μ L of plasma sample. The assay was rapid, safe, and reliable for use in pharmacokinetic studies of losartan in human being.

Patel *et al.* [37] developed a simple, fast, and precise RP-HPLC method for the simultaneous estimation of losartan potassium and perindopril erbumine in its tablet form. The HPLC method involved by using HiQSil-C-18W ODS (250 mm \times 4.5 mm i.d., 5 μ m) column and mobile phase was ACN:water in proportion of 50:50 v/v, pH adjusted to 3.2 ± 0.1 with 1% *o*-phosphoric acid. The flow rate was 1.0 mL/min and effluent was monitored at 210 nm. The retention time of losartan potassium and perindopril erbumine was eluted at 6.7 and 4.5 min, respectively. The method was validated in terms of linearity, precision, accuracy, and LOD. The method was found to be linear in the range of 2–18 g/mL for both the drug. The coefficient of variance for both the drug was more than 0.999. The mean percentage recovery was found to be 98.40% for losartan potassium and 97.50% for perindopril erbumine. The limits of quantification of losartan potassium and perindopril erbumine were found to be 0.109 and 0.041 g/mL. The method has been successfully applied for determination of losartan potassium and perindopril erbumine in combined dosage form.

Kirtawade *et al.* [38] reported a RP-HPLC method for simultaneous estimation of losartan potassium (LOS) and atenolol (AT) on RP C-18 Column (Microsorb-MV 100-5, 250 \times 4.6 mm) using acetonitrile:methanol:25 mM phosphate buffer (35:35:30), pH adjusted to 3 with *o*-phosphoric acid as mobile phase at a flow rate of 1.0 mL/min and the detection wavelength was 225 nm. The retention time for LOS and AT was found to be 5.40 and 2.44 min, respectively. Proposed method was validated for precision, accuracy, linearity range, robustness, and ruggedness.

del Rosario Brunetto *et al.* [39] developed a validated HPLC method for quantification of losartan, telmisartan, and valsartan in human urine. Urine samples were diluted on the extraction mobile phase (1:4, v/v) and a volume of 20 μ L of this mixture was directly injected onto the HPLC system, and

detected by fluorescence at 259 and 399 nm as excitation and emission wavelength, respectively. The separation of losartan, telmisartan, and valsartan was achieved on a Chromolith RP-18e monolithic column. The method provides extraction recoveries from spiked urine samples greater than 93%. Intra- and interday precision were generally acceptable; the intraday-assay CV was <3.5 for all compounds and the interday-assay CV was <3.7%. The estimated calibration range was 0.001–2.5 µg/mL with excellent coefficient of determination (>0.9981). The detection limits for losartan, telmisartan, and valsartan at a signal-to-noise ratio of 5:1 were 0.002, 0.0002, and 0.001 µg/mL when a sample volume of 20 µL was injected. The proposed method permitted the simultaneous determination of losartan, telmisartan, and valsartan in 8 min, with an adequate precision and sensitivity. However, the overlap of the sample cleanup step with the analysis increases the sampling frequency to 12 samples/h.

González *et al.* [40] developed a HPLC assay coupled to fluorescence detection for the detection of some AIIRAs: losartan, irbesartan, valsartan, candesartan cilexetil and its metabolite candesartan MI. The analytes and the IS (bumetanide, a high-ceiling diuretic) were extracted from plasma under acidic conditions by means of solid-phase extraction using C8 cartridges. This procedure allowed recoveries close to 80% for all these drugs excluding candesartan cilexetil (70%) which presented adsorption processes on glass and plastic walls. The analytes and potential interferences were separated on a reversed-phase column, muBondapak C18, at room temperature. A gradient elution mode was used to carry out the separation, the optimal mobile phase being composed of acetonitrile–5 mM acetate buffer, pH 4, at variable flow rates (from 1.0 to 1.2 mL/min). Fluorescence detector was set at an excitation wavelength of 250 nm and an emission wavelength of 375 nm. Intra- and interday RDs for all the compounds were lower than 8% except for losartan (12%) and the method assesses a quite good accuracy (percentage of relative error approximately 6% in most of the cases). The limit of quantitation for these compounds was 3 ng/mL for candesartan cilexetil and M1, 16 ng/mL for losartan, and 50 ng/mL for irbesartan and valsartan, which allows their determination at expected plasma concentration levels.

4.3.3 HPLC-Mass Spectrometry

Kumar *et al.* [41] developed randomized, open-label, crossover, bioavailability study methods which were conducted separately in healthy Asian Indian and Japanese volunteers. One tablet either of test or of reference product was

administered after 10 h of overnight fasting. After dosing, serial blood samples were collected for a period of 48 h for both the studies. Plasma samples were analyzed for losartan, losartan carboxylic acid, and hydrochlorothiazide by a validated liquid chromatographic and mass spectrometric method (LC-MS/MS). The pharmacokinetic parameters AUC_{0-t} (Area under the curve from time 0 to the last measurable concentration), $AUC_{0-\infty}$ (Area under the curve from time 0 extrapolated to infinite time), C_{max} (Peak concentration), t_{max} (Time for peak concentration), and other pharmacokinetics parameters were determined from plasma concentration–time profiles for both test and reference formulations of losartan/hydrochlorothiazide 50 + 12.5 mg tablets. Statistical evaluations were done to evaluate bioequivalence between generic test formulation (EPR0001) and Japanese reference product (Preminent). Results: losartan, losartan carboxylic acid, and hydrochlorothiazide were well tolerated by subjects in all periods of each study under fasted conditions. No serious adverse events were observed. The ratios of least square means for AUC_{0-t} and C_{max} and the affiliated 90% confidence intervals were within acceptance range.

Yuan *et al.* [42] described a LC-MS/MS method to evaluate bioavailability and bioequivalence of losartan and its metabolite after oral administration of test preparation and reference preparation of losartan potassium in healthy volunteers. This was an open, randomized, single-dose, and 2×2 crossover trial. A total of 24 Chinese healthy male subjects were orally given with 50 mg losartan test or reference preparation. Blood samples were collected 24 h after administration. Plasma concentrations of losartan and losartan acid (LA) were determined by LC-MS/MS.

Salvadori *et al.* [43] developed a method based on a simple liquid–liquid extraction (LLE) followed by HPLC with negative ion ESI tandem mass spectrometry (HPLC-ESI-MS/MS) detection for the simultaneous determination of losartan (LOS) and hydrochlorothiazide (HCTZ) in human plasma, using valsartan (VAL) and chlorthalidone (CHTD) as an IS, respectively. The acquisition was performed in multiple reaction monitoring (MRM) and the limit of quantification was 4 ng/mL for both LOS and HCTZ. The method was linear in the studied range (4–800 ng/mL for LOS and 4–500 ng/mL for HCTZ). The intra-assay precisions ranged from 2.6% to 11.9% for LOS and 1.4% to 8.2% for HCTZ, while the interassay precisions ranged from 1.0% to 8.0% for LOS and 2.5% to 7.7% for HCTZ. The intra-assay accuracies ranged from 91.3% to 107.6% for LOS and 91.5% to 105.8% for HCTZ, while the interassay accuracies ranged from 99.9% to 106.4% for LOS and 97.4% to 101.4% for HCTZ.

Prasaja *et al.* [44] developed a liquid chromatography-tandem mass spectrometry (LC-MS/MS) method employing electrospray ionization for quantification of losartan and its carboxylic acid metabolite in human plasma using irbesartan as IS. Following a simple pretreatment procedure, the analytes were separated using a gradient mobile phase on reverse-phase C18 column. Selected reaction monitoring was specific for losartan, LA, and irbesartan. The method validation demonstrated the specificity, lower limit of quantification, accuracy, and precision of measurements. The assay exhibited a linear dynamic range of 2.0–400 ng/mL for losartan and 1.85–370 ng/mL for LA. A run time of 3.5 min for each sample made it possible to analyze more than 200 samples per day.

Polinko *et al.* [45] developed analytical methods for the simultaneous determination of losartan and its active metabolite EXP3174 in human plasma and urine with limited plasma sample size to support a pediatric clinical program. In both methods, analytes are extracted from the matrixes by LLE and separated using RP-HPLC. A tandem mass spectrometer (MS/MS) with a TurboIonSpray (TIS) interface in MRM mode is used for detection of the analytes in both methods. The plasma method has a lower LOQ of 1 ng/mL with a linearity range of 1–500 ng/mL for losartan and EXP3174 using 100 μ L of plasma. For the urine method, the LOQ for both losartan and EXP3174 is 2 ng/mL using 0.5 mL of urine, and the linearity range for both analytes is 2–1000 ng/mL. Validation procedures have proven that both methods are robust, accurate, and reproducible. Both methods have been used to assay clinical samples and provided satisfactory results.

Shah *et al.* [46] developed a rapid LC-MS/MS method for the determination of losartan (LOS) and its metabolite LA (EXP3174) in human plasma using multiplexing technique (two HPLC units connected to one MS/MS). LOS and LA were extracted from human plasma by SPE technique using Oasis HLB cartridge without evaporation and reconstitution steps. Hydroflumethiazide (HFTZ) was used as an IS. The analytes were separated on Zorbax SB C-18 column. The mass transition $[M - H]$ ions used for detection were m/z 421.0 \rightarrow 127.0 for LOS, m/z 435.0 \rightarrow 157.0 for LA, and m/z 330.0 \rightarrow 239.0 for HFTZ. The proposed method was validated over the concentration range of 2.5–2000 ng/mL for LOS and 5.0–3000 ng/mL for LA with correlation coefficient ≥ 0.9993 . The overall recoveries for LOS, LA, and IS were 96.53%, 99.86%, and 94.16%, respectively. Total MS run time was 2.0 min/sample. The validated method has been successfully used to analyze human plasma samples for applications in 100 mg fasted and fed pharmacokinetic studies.

4.3.4 Capillary Electrophoresis

Quaglia *et al.* [47] reported a capillary electrophoresis (CE) and a capillary electrochromatography (CEC) to determine losartan and hydrochlorothiazide. The CE separation was carried out in an uncoated capillary filled with a 100 mM sodium borate pH 9 solution containing trimethyl-beta-cyclodextrins. CEC was performed using a capillary packed with a RP-18 stationary phase. The mobile phase was a mixture of 50 mM ammonium acetate pH 7, water, and acetonitrile (1/1.5/7.5). By CE and CEC, suitable methods to determine simultaneously losartan and hydrochlorothiazide in working standard mixture or pharmaceutical form were obtained. The proposed methods are very simple and both gave accurate and precise results.

González *et al.* [48] reported a capillary zone electrophoretic (CZE) method for the separation of five AIIRAs (losartan, irbesartan, valsartan, telmisartan, and eprosartan) and two of their metabolites (EXP3174 and Candesartan M1) by means of experimental design methodologies. The aim of this study was to define rapidly experimental conditions under which the analytes can be resolved for quantitation. The effects of the buffer (pH, concentration, and composition), the organic modifier, and voltage were studied. Critical factors were identified in a screening design (fractional factorial design), and sequentially an optimization design (central composite design) was used to choose optimal conditions for separation. The most favorable electrophoretic conditions were found by setting the resolution at a threshold value ($R_s \leq 1.5$) and minimizing, if possible, analysis time. Successful results were obtained with a 50 mM potassium dihydrogen phosphate:boric acid (25:75, v/v) buffer at pH 5.5 in the presence of 5% methanol and application of a 25 kV voltage. Analysis time was 8 min in a conventional fused-silica capillary (50 cm effective length) in a normal cationic mode (anode at the inlet and cathode at the outlet) after hydrostatic sample injection for 30 s.

Balesteros *et al.* [49] reported an alternative methodology by CZE for the determination of losartan potassium (LOS) associated with chlorthalidone (CHTD) or hydrochlorothiazide (HCTZ) in capsules, using 50 mmol/L of sodium carbonate buffer with detection at 226 nm. The electrolyte system was optimized, taking into account peak profiles, resolution, run times, baseline stability, and repeatability (adsorption absence). The method was successfully applied to the analysis of pharmaceutical formulations purchased in manipulation drugstores. The analytes were baseline separated in less than 5 min. The results did not present significant difference in the 95% confidence interval in relation to the label claim values.



5. STABILITY

Lusina *et al.* [50] reported a stability study of losartan/hydrochlorothiazide tablets. Stability study of losartan/hydrochlorothiazide tablets consisted of three steps: stress test (forced degradation study), preliminary testing (selection of packaging), and formal stability testing. The results of stress test suggested that losartan/hydrochlorothiazide tablets are sensitive to moisture. It was demonstrated that the developed analytical methods are stability indicating. Additional preliminary testing was performed in order to select appropriate packaging for losartan/hydrochlorothiazide tablets. OPA/Al/PVC//Al blisters were found to provide adequate protection for the product. Based on the first 12 months of the formal stability study, a shelf life of 24 months was proposed. Losartan/hydrochlorothiazide tablets in OPA/Al/PVC//Al blisters are demonstrated to be chemically, physically, and microbiologically stable.



6. PHARMACOKINETICS, METABOLISM, AND EXCRETION

6.1 Pharmacokinetics

Sica *et al.* [51] reported the pharmacokinetics of losartan. It is rapidly absorbed, reaching maximum concentrations 1–2 h postadministration. After oral administration, approximately 14% of a losartan dose is converted to the pharmacologically active E3174 metabolite. E3174 is 10- to 40-fold more potent than its parent compound and its estimated terminal half-life ranges from 6 to 9 h. The pharmacokinetics of losartan and E3174 are linear, dose-proportional, and do not substantially change with repetitive administration. The recommended dosage of losartan 50 mg/day can be administered without regard to food. There are no clinically significant effects of age, sex, or race on the pharmacokinetics of losartan, and no dosage adjustment is necessary in patients with mild hepatic impairment or various degrees of renal insufficiency. Losartan, or its E3174 metabolite, is not removed during hemodialysis. The major metabolic pathway for losartan is by the cytochrome P450 (CYP) 3A4, 2C9, and 2C10 isoenzymes. Overall, losartan has a favorable drug–drug interaction profile, as evidenced by the lack of clinically relevant interactions between this drug and a range of inhibitors and stimulators of the CYP450 system. Losartan does not have a drug–drug interaction with hydrochlorothiazide, warfarin, or digoxin. Losartan should be avoided in pregnancy, as is the case with all other angiotensin

receptor antagonists. When given in the second and third trimester of pregnancy, losartan is often associated with serious fetal toxicity. Losartan is a competitive antagonist that causes a parallel rightward shift of the concentration–contractile response curve to angiotensin II, while E3174 is a noncompetitive “insurmountable” antagonist of angiotensin II. The maximum recommended daily dose of losartan is 100 mg, which can be given as a once-daily dose or by splitting the same total daily dose into two doses.

6.2 Metabolism

Stearns *et al.* [52] reported the losartan is metabolized *in vivo* in humans to a carboxylic acid derivative E3174 that is pharmacologically more active than the parent compound. We have investigated the mechanism of this biotransformation in human liver preparations. The oxidation of both losartan and the putative aldehyde intermediate E3179 was catalyzed by the microsomal fraction, required both NADPH and molecular oxygen, and was inhibited by SKF 525-A, implicating CYP. When incubations with each substrate were performed under an atmosphere of $^{18}\text{O}_2$, the extent of ^{18}O incorporation into the carboxylic acid product was consistent with a mechanism for losartan oxidation involving an aldehyde intermediate. To substantiate the involvement of CYP in these reactions, incubations with losartan and the aldehyde E3179 were performed in the presence of isoform-selective inhibitors. Inhibitors of CYP3A4/5 (gestodene and ketoconazole) and CYP2C9/10 (sulfaphenazole) attenuated the oxidation of both substrates. It was then demonstrated that microsomes containing either recombinant human liver CYP2C9 or CYP3A4 were capable of oxidizing both losartan and the aldehyde E3179 to the carboxylic acid E3174. Subsequently, it was shown that rabbit anti-CYP2C9 and anti-CYP3A3/4 inhibited the oxidation of losartan to E3174 in incubations with human liver microsomes.

6.3 Excretion

Losartan is readily absorbed from the gastrointestinal tract after oral doses, but undergoes substantial first-pass metabolism resulting in a systemic bioavailability of about 33%. It is metabolized to an active carboxylic acid metabolite E3174 (EXP3174), which has greater pharmacological activity than losartan; some inactive metabolites are also formed. Metabolism is mainly by CYP isoenzymes CYP2C9 and CYP3A4. Peak plasma concentrations of losartan and E3174 occur about 1 and 3–4 h, respectively, after an oral dose. Both losartan and E3174 are more than 98% bound to plasma

proteins. Losartan is excreted in the urine, and in the feces via bile, as unchanged drug and metabolites. About 4% of an oral dose is excreted unchanged in urine and about 6% is excreted in urine as the active metabolite. The terminal elimination half-lives of losartan and E3174 are about 1.5–2.5 and 3–9 h, respectively [3].



7. PHARMACOLOGY

Goa and Wagstaff [53] reported that losartan potassium is an orally active, nonpeptide AII₁RA. It is the first of a new class of drugs to be introduced for clinical use in hypertension. This novel agent binds competitively and selectively to the AII subtype 1 (AT₁) receptor, thereby blocking AII-induced physiological effects. An active metabolite, E3174, contributes substantially to its antihypertensive effect, which persists throughout 24 h after once-daily administration. In patients with mild to moderate hypertension, losartan potassium 50–100 mg once daily as monotherapy lowers blood pressure to a similar degree to enalapril, atenolol, and felodipine extended release. Losartan potassium combined with hydrochlorothiazide reduces blood pressure further than either drug given separately. About one-third of patients with severe hypertension have responded to the combination product. Losartan potassium appears to be effective in elderly patients. Losartan potassium is very well tolerated. In clinical trials, dizziness was the only drug-related event reported more frequently with losartan potassium monotherapy than with placebo. First-dose hypotension is uncommon. An aspect of the drug's tolerability profile which may prove to be particularly advantageous is that it is associated with a similar incidence of cough to placebo in patients with a history of ACE inhibitor-related cough. Additionally, clinically relevant adverse metabolic effects or laboratory abnormalities have not been documented during losartan potassium therapy, and renal function is preserved in patients with or without renal insufficiency. The adverse effect profile of the losartan potassium–hydrochlorothiazide combination resembles those for losartan potassium monotherapy and placebo. Long-term tolerability data are limited (<2 years) but support the very good tolerability profile in shorter studies. Elements of the drug's profile yet to be assessed or reported fully in the literature include long-term efficacy, potential to favorably influence cardiovascular and renovascular systems (and ultimately mortality) in patients with hypertension, and lastly, cost effectiveness and influence on quality of life. In summary, losartan potassium is the first AT₁ receptor antagonist to

become available for the management of hypertension, and as such, it is an important new antihypertensive agent. Pending long-term data as outlined above, it is likely to find initial use in patients with mild to severe hypertension who are unresponsive to, or intolerant of, their current therapy. However, with its novel mechanism of action, good efficacy, and favorable tolerability profile, losartan potassium is well placed to claim a prominent position in the management of patients with essential hypertension in the future.

REFERENCES

- [1] M.J. O'Neil (Ed.), *The Merck Index*, in: 13th ed., Merck & Co, NJ, 2001, p. 5262.
- [2] A.C. Moffat, M.D. Ossltton, B. Widdop, J. Watts (Eds.), *Clarke's Analysis of Drugs and Poisons*, fourth ed., The Pharmaceutical Press, London, 2011.
- [3] S.C. Sweetman (Ed.), *Martindale, The Complete Drug Reference*, 36th ed., Pharmaceutical Press, London, 2009, p. 1326.
- [4] *British Pharmacopoeia*, *British Pharmacopoeia*, vol. III, Her majesty's Stationary Office, London, 2012.
- [5] D.J. Carini, J.V. Duncia, S.M. Wang, U.S. Patent No. 5,138,069, 1986.
- [6] N.E. Leadbeater, M. Marco, Rapid and amenable Suzuki coupling reaction in water using microwave and conventional heating, *J. Org. Chem.* 68 (2003) 888–892.
- [7] N.E. Leadbeater, S.J. Pillsbury, E. Shanahan, V.A. Williams, An assessment of the technique of simultaneous cooling in conjunction with microwave heating for organic synthesis, *Tetrahedron* 61 (2005) 3565–3585.
- [8] Z.P. Demka, K.B. Sharpless, An expedient route to the tetrazole analogues of α -amino acids, *Org. Lett.* 4 (2002) 2525–2527.
- [9] M.C. Reid, J.H. Clark, D.J. Macquarrie, Solventless microwave-assisted chlorodehydroxylation for the conversion of alcohols to alkyl chlorides, *Green Chem.* 8 (2006) 437–438.
- [10] K. Raghavan, A. Dwivedi, G.C. Campbell Jr., E. Johnston, D. Levorse, J. McCauley, M. Hussain, Spectroscopic investigation of losartan polymorphs, *Pharm. Res.* 10 (6) (1993) 900–904.
- [11] U. Aswartha, J. Sreeramulu, P. Satyanarayana, Formulation development of losartan potassium microspheres using natural polysaccharides and their in-vitro evaluation, *Res. J. Pharm. Biol. Chem. Sci.* 3 (2012) 725–734.
- [12] P. de Oliveira Rossini, F.S. Felix, L. Angnes, et al., A simple and precise conductometric method for the determination of losartan in pharmaceutical products, *Cent. Eur. J. Chem.* 10 (2012) 1842–1849.
- [13] M. Stolarczyk, A. Maslanka, A. Apola, J. Krzek, Determination of losartan potassium, quinapril hydrochloride and hydrochlorothiazide in pharmaceutical preparations using derivative spectrophotometry and chromatographic–densitometric method, *Acta Pol. Pharm.* 70 (6) (2013) 967–976.
- [14] K.N. Tarkase, S.S. Suryawanshi, R.S. Joshi, Simultaneous derivative spectrophotometric determination and validation of losartan potassium in pharmaceutical dosage forms, *Int. J. Pharm. Sci. Rev. Res.* 13 (2012) 31–34.
- [15] A.B. Thomas, U.B. Chavan, R.K. Nanda, L.P. Kothapalli, A.D. Deshpande, S.N. Jagdale, S.B. Dighe, Simultaneous spectrophotometric estimation of hydrochlorothiazide, atenolol and losartan potassium in tablet dosage form, *Hindustan Antibiot. Bull.* 51 (2009) 33–38.

- [16] S.T. Ulu, S. Sağlık, Comparison of UV- and second derivative spectrophotometric and high-performance liquid chromatographic methods for the determination of losartan in tablets, *Turkish J. Pharm. Sci.* 3 (2004) 165–175.
- [17] R. Bonfilio, L.B. Favoretto, G.R. Pereira, R. de Cássia Pimentel Azevedo, M.B. de Araújo, Comparative study of analytical methods by direct and first-derivative UV spectrophotometry for evaluation of losartan potassium in capsules, *Braz. J. Pharm. Sci.* 46 (2010) 147–155.
- [18] M. Ansari, M. Kazemipour, M. Baradaran, H. Jalalizadeh, Derivative spectrophotometric method for determination of losartan in pharmaceutical formulations, *Iran. J. Pharmacol. Ther.* 3 (2004) 21–25.
- [19] P.L.K.M. Rao, V. Venugopal, A. Kumar, B. Rajesh, G. Prasad, D. Ravindergoud, Quantitative estimation of losartan potassium in pharmaceutical dosage forms by UV spectrophotometry, *IJRPC* 1 (2011) 295–302.
- [20] A.H. Prabhakar, R. Giridhar, A rapid colorimetric method for the determination of losartan potassium in bulk and in synthetic mixture for solid dosage form, *J. Pharm. Biomed. Anal.* 6 (2002) 861–866.
- [21] I.A. Darwish, Analytical study for the charge-transfer complexes of losartan potassium, *Anal. Chim. Acta* 549 (2005) 212–220.
- [22] S.R. El-Shaboury, S.A. Hussein, N.A. Mohamed, M.M. El-Sutohy, Spectrofluorimetric method for determination of some angiotensin II receptor antagonists, *J. Pharm. Anal.* 2 (2012) 12–18.
- [23] W.X. De Paula, A.M. Denadai, M.M. Santoro, A.N. Braga, R.A. Santos, R.D. Sinisterra, Supramolecular interactions between losartan and hydroxypropyl- β -CD: ESI mass-spectrometry, NMR techniques, phase solubility, isothermal titration calorimetry and anti-hypertensive studies, *Int. J. Pharm.* 404 (2011) 116–123.
- [24] A.A. Ensafi, R. Hajiarn, Determination of losartan and triamterene in pharmaceutical compounds and urine using cathodic adsorptive stripping voltammetry, *Anal. Sci.* 24 (2008) 1449–1454.
- [25] I.H.I. Habib, S.A. Weshahy, S. Toubar, M.M.A. El-Alamin, Cathodic stripping voltammetric determination of losartan in bulk and pharmaceutical products, *Port. Electrochim. Acta* 26 (2008) 315–324.
- [26] D.D. Tsvetkova, D.P. Obreshkova, Application of validated TLC-densitometric method for simultaneous identification and determination of losartan potassium, telmisartan, and valsartan in tablets, *J. Planar Chromatogr. Mod. TLC* 25 (2012) 326–330.
- [27] L. Santhana, S. Lakshmi, Simultaneous analysis of losartan potassium, amlodipine besylate, and hydrochlorothiazide in bulk and in tablets by high-performance thin layer chromatography with UV-absorption densitometry, *J. Anal. Methods Chem.* 2012 (2012) 108281.
- [28] S. Shah, I. Rathod, B. Suhagia, S. Savale, J. Patel, Simultaneous determination of losartan and hydrochlorothiazide in combined dosage forms by first-derivative spectroscopy and high-performance thin-layer chromatography, *J. AOAC Int.* 6 (2001) 1715–1723.
- [29] S.R. Sathe, S.B. Bari, Simultaneous analysis of losartan potassium, atenolol, and hydrochlorothiazide in bulk and in tablets by high-performance thin-layer chromatography with UV absorption densitometry, *Acta Chromatogr.* 19 (2007) 270–278.
- [30] S. Kollipara, G. Bende, Y. Bansal, R. Saha, Stability-indicating reversed-phase liquid chromatographic method for simultaneous determination of losartan potassium and ramipril in tablets, *Indian J. Pharm. Sci.* 74 (2012) 201–210.
- [31] S. Soltani, A.M. Ramezani, N. Soltani, A. Jouyban, Analysis of losartan and carvedilol in urine and plasma samples using a dispersive liquid-liquid microextraction isocratic HPLC-UV method, *Bioanalysis* 4 (2012) 2805–2821.

- [32] K. Czerwińska, A.P. Mazurek, Identification and determination of selected angiotensin II receptor antagonist group drugs by HPLC method, *Acta Pol. Pharm.* 68 (2011) 831–837.
- [33] R. Dubey, V.K. Bhusari, S.R. Dhaneshwar, Validated RP-HPLC method for simultaneous quantitation of losartan potassium and metolazone in bulk drug and formulation, *Sci. Pharm.* 79 (2011) 545–554.
- [34] S. Wankhede, K. Raka, S. Wadkar, S. Chitlange, Spectrophotometric and HPLC methods for simultaneous estimation of amlodipine besilate, losartan potassium and hydrochlorothiazide in tablets, *Indian J. Pharm. Sci.* 72 (2010) 136–140.
- [35] R. Bonfilio, C. Tarley, G. Pereira, H. Salgado, M. De Araújo, Multivariate optimization and validation of an analytical methodology by RP-HPLC for the determination of losartan potassium in capsules, *Talanta* 80 (2009) 236–241.
- [36] H. Jalalizadeh, E. Souri, H. Farsam, M. Ansari, A high-performance liquid chromatographic assay for the determination of losartan in plasma, *Iran. J. Pharmacol. Ther. (IJPT)* 2 (2003) 18–21.
- [37] A.I. Patel, C.K. Oza, J.P. Prajapati, A.J. Vyasand, P. Mehta, RP-HPLC method for the determination of losartan potassium and perindopril erbumine in combined tablet dosage form, *Int. J. Pharm. Bio Sci.* 2 (2011) 709–715.
- [38] R.R. Kirtawade, P.L. Salve, A.S. Kulkarni, P.N. Dhabale, RP-HPLC method for simultaneous estimation of losartan potassium and atenolol in tablet formulation, *Pharm. Sci. Monitor* 1 (2010) 50–57.
- [39] M. del Rosario Brunetto, Y. Contreras, S. Clavijo, D. Torres, Y. Delgado, F. Ovalles, C. Ayala, M. Gallignani, J.M. Estela, V.C. Martin, Determination of losartan, telmisartan, and valsartan by direct injection of human urine into a column-switching liquid chromatographic system with fluorescence detection, *J. Pharm. Biomed. Anal.* 50 (2009) 194–199.
- [40] L. González, J.A. López, R.M. Alonso, R.M. Jiménez, Fast screening method for the determination of angiotensin II receptor antagonists in human plasma by high-performance liquid chromatography with fluorimetric detection, *J. Chromatogr. A* 949 (2002) 49–60.
- [41] S. Kumar, T. Monif, A. Khuroo, S. Reyar, R. Jain, A.K. Singla, K. Kurachi, Pharmacokinetic comparison and bioequivalence evaluation of losartan/hydrochlorothiazide tablet between Asian Indian and Japanese volunteers, *Int. J. Clin. Pharmacol. Ther.* 52 (2014) 39–54.
- [42] F. Yuan, J. Xu, H. Wang, N. Chu, H. Xu, X. Li, W. Chen, Determination of losartan and its metabolite in human plasma by LC-MS/MS, and bioequivalence study of losartan potassium tablets, *Chin. J. Clin. Pharm.* 22 (2013) 13–18.
- [43] M. Salvadori, R. Moreira, B. Borges, M. Andraus, C. Azevedo, R. Moreno, N. Borges, Simultaneous determination of losartan and hydrochlorothiazide in human plasma by LC/MS/MS with electrospray ionization and its application to pharmacokinetics, *Clin. Exp. Hypertens.* 31 (2009) 415–427.
- [44] B. Prasaja, L. Sasongko, Y. Harahap, L.W. Hardiyanti, M. Grigg, Simultaneous quantification of losartan and active metabolite in human plasma by liquid chromatography-tandem mass spectrometry using irbesartan as internal standard, *J. Pharm. Biomed. Anal.* 49 (2009) 862–867.
- [45] M. Polinko, K. Riffel, H. Song, M.W. Lo, Simultaneous determination of losartan and EXP3174 in human plasma and urine utilizing liquid chromatography/tandem mass spectrometry, *J. Pharm. Biomed. Anal.* 33 (2003) 73–84.
- [46] H. Shah, M. Kundlik, N. Patel, G. Subbaiah, D. Patel, B. Suhagia, C. Patel, Rapid determination of losartan and losartan acid in human plasma by multiplexed LC-MS/MS, *J. Sep. Sci.* 32 (2009) 3388–3394.

- [47] M. Quaglia, E. Donati, G. Carlucci, P. Mazzeo, S. Fanali, Determination of losartan and hydrochlorothiazide in tablets by CE and CEC, *J. Pharm. Biomed. Anal.* 29 (2002) 981–987.
- [48] L. González, U. Akesolo, R. Jiménez, R. Alonso, Application of capillary zone electrophoresis to the screening of some angiotensin II receptor antagonists, *Electrophoresis* 23 (2002) 223–229.
- [49] M.R. Balesteros, A.F. Faria, M.A.L. de Oliveira, Determination of losartan associated with chlorthalidone or hydrochlorothiazide in capsules by capillary zone electrophoresis, *J. Braz. Chem. Soc.* 18 (2007) 554–558.
- [50] M. Lusina, T. Cindric, J. Tomaic, M. Peko, L. Pozaic, N. Musulin, Stability study of losartan/hydrochlorothiazide tablets, *Int. J. Pharm.* 291 (2005) 127–137.
- [51] D. Sica, T. Gehr, S. Ghosh, Clinical pharmacokinetics of losartan, *Clin. Pharmacokinet.* 44 (2005) 797–814.
- [52] R.A. Stearns, P.K. Chakravarty, R. Chen, S.H. Chiu, Biotransformation of losartan to its active carboxylic acid metabolite in human liver microsomes. Role of cytochrome P450C and 3A subfamily members, *Drug Metab. Dispos.* 23 (1995) 207–215.
- [53] K. Goa, A. Wagstaff, Losartan potassium: a review of its pharmacology, clinical efficacy and tolerability in the management of hypertension, *Drugs* 51 (1996) 820–845.



Prasugrel Hydrochloride

**Mahmoud M.H. Al Omari^{*,†}, Nidal A. Qinna[†], Iyad S. Rashid^{*},
Khalidoun A. Al-Sou'od[‡], Adnan A. Badwan^{*}**

^{*}The Jordanian Pharmaceutical Manufacturing Co., Naor, Jordan

[†]Faculty of Pharmacy and Medical Sciences, Petra University, Amman, Jordan

[‡]Department of Chemistry, Al al-Bayt University, Mafraq, Jordan

¹Corresponding author: e-mail address: momari@jpm.com.jo

Contents

1. Description	196
1.1 Nomenclature	196
1.2 Formulae	196
1.3 Elemental Analysis	197
1.4 Appearance	197
2. Methods of Preparation	197
2.1 Drug-Free Base and Its Hydrochloride Salt	197
2.2 Drug Intermediates and Its Acid Salts	239
2.3 Drug Analogues	246
3. Physical Characteristics	250
3.1 Ionization Constants	250
3.2 Solubility Characteristics	253
3.3 Partition Coefficients	253
3.4 Optical Activity	254
3.5 Polymorphism	254
3.6 Particle Morphology	254
3.7 Hygroscopicity	255
3.8 Molecular Modeling	255
3.9 Crystallographic Properties	255
3.10 Thermal Analysis	267
3.11 Spectroscopy	270
3.12 Mass Spectrometry	276
4. Methods of Analysis	277
4.1 Compendial Methods	277
4.2 Titrimetric Methods	278
4.3 Spectroscopic Methods	280
4.4 Chromatographic Methods	284
5. Stability	287
5.1 Solid-State Stability	287
5.2 Solution-Phase Stability	295
5.3 Stability in Biological Fluids	295

6. Pharmacology	303
6.1 Uses, Applications, and Pertinent History	303
6.2 Absorption	303
6.3 Distribution	304
6.4 Metabolism	305
6.5 Elimination	309
6.6 Pharmacological Effects	309
References	311



1. DESCRIPTION

1.1 Nomenclature

1.1.1 Systematic Chemical Names

5-[(1*RS*)-2-cyclopropyl-1-(2-fluorophenyl)-2-oxoethyl]-4,5,6,7-tetrahydrothieno[3,2-*c*]pyridin-2-yl acetate hydrochloride [1,2].

(±)-2-[2-Acetyloxy-6,7-dihydrothieno[3,2-*c*]pyridin-5(4*H*)-yl]-1-cyclopropyl-2-(2-fluorophenyl)ethanone hydrochloride [3].

2-Acetoxy-5-(α-cyclopropylcarbonyl-2-fluorobenzyl)-4,5,6,7-tetrahydrothieno[3,2-*c*]pyridine (Prasugrel) [4]

1.1.2 Nonproprietary Names

Recommended international nonproprietary name: Prasugrel [1].

Synonyms: CS-747, LY-640315 [5].

1.1.3 Proprietary Names

Effient, Efient, Prasita (Daiichi Sankyo Co.) [5].

1.2 Formulae

1.2.1 Empirical Formula, Molecular Weight, CAS Number [1,3,5]

Prasugrel	C ₂₀ H ₂₀ FNO ₃ S	373.44	[150322-43-3]
Prasugrel HCl	C ₂₀ H ₂₁ ClFNO ₃ S	409.90	[389574-19-0]

1.2.2 Structural Formula

Prasugrel is a member of the thienopyridine class of an adenosine diphosphate (ADP) receptor inhibitors, like ticlopidine (trade name Ticlid[®]) and clopidogrel (trade name Plavix[®]) (Figure 1) [6].

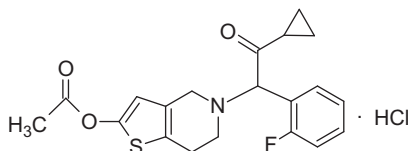


Figure 1 Chemical structure of prasugrel HCl.

Table 1 The Theoretical and Experimental Elemental Compositions of Prasugrel and Its HCl Salt

Compound	Molecular Formula	%						
		C	H	Cl	F	N	O	S
Prasugrel	C ₂₀ H ₂₀ FNO ₃ S	64.33 (64.46)	5.40 (5.39)	—	5.09	3.75 (3.73)	12.85	8.59
Prasugrel HCl	C ₂₀ H ₂₁ ClFNO ₃ S	58.60	5.16	8.65	4.63	3.42	11.71	7.82

Values between brackets represent the experimental data.

1.3 Elemental Analysis

The theoretical values of elemental analysis of prasugrel and its HCl salt are listed in Table 1. The experimental values of elemental analysis (C, H, and N) for prasugrel [4] agree well with the theoretical values.

1.4 Appearance

Prasugrel HCl is white to light brown crystalline solid, slightly hygroscopic [1].

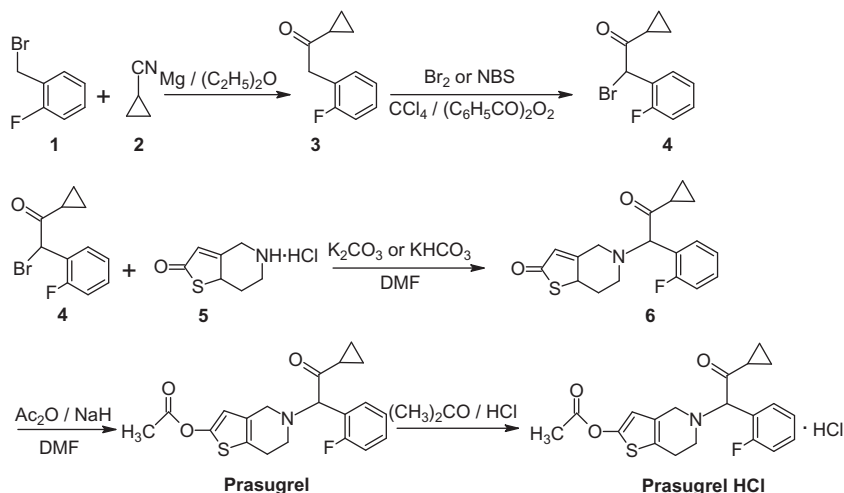


2. METHODS OF PREPARATION

2.1 Drug-Free Base and Its Hydrochloride Salt

2.1.1 Method 1 [4,7,8]

2-Fluorobenzyl bromide (1) is reacted with cyclopropyl cyanide (2) in a mixture of metallic magnesium and anhydrous diethyl ether to give α -cyclopropyl-2-fluorobenzyl ketone (3), which is then reacted with bromine or *N*-bromosuccinimide (NBS)/benzoyl peroxide in carbon tetrachloride to give α -cyclopropylcarbonyl-2-fluorobenzyl bromide (4). Condensation of compound (4) with 5,6,7,8-tetrahydrothieno[3,2-*c*]pyridin-2(4*H*)-one HCl (5) in the presence of potassium carbonate or



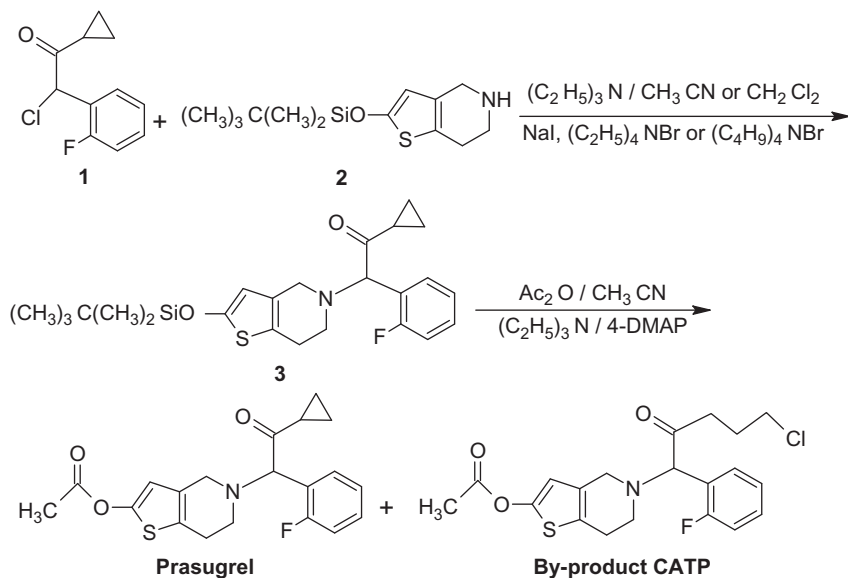
Scheme 1 Preparation of prasugrel and its HCl salt.

potassium bicarbonate in dimethylformamide gives 5-(2-cyclopropyl-1-(2-fluorophenyl)-2-oxoethyl)-5,6,7,7a-tetrahydrothieno[3,2-c]pyridine-2(4*H*)-one (OXTp) (**6**), which is finally reacted with acetic anhydride and sodium hydride in dimethylformamide to yield prasugrel [4,8]. The HCl salt of prasugrel is prepared by reacting prasugrel-free base with HCl in acetone (Scheme 1) [7].

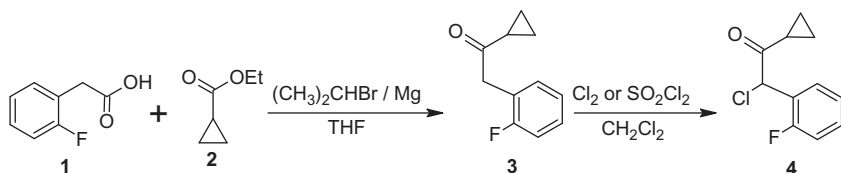
2.1.2 Method 2 [9,10]

α -Cyclopropylcarbonyl-2-fluorobenzyl chloride (**1**) is reacted with 2-(*tert*-butyldimethylsiloxy)-4,5,6,7-tetrahydrothieno[3,2-c]pyridine *p*-toluenesulfonate (**2**) in the presence of triethylamine with or without sodium iodide, tetraethyl or tetrabutylammonium bromide in dichloromethane or acetonitrile to give 2-(*tert*-butyldimethylsiloxy)-5-(2-cyclopropyl-1-(2-fluorophenyl)-2-oxoethyl)-5,6,7,7a-tetrahydrothieno[3,2-c]pyridine (**3**), which is finally reacted with acetic anhydride in the presence of triethylamine and 4-dimethylaminopyridine (4-DMAP) in acetonitrile to yield prasugrel (Scheme 2).

α -Cyclopropylcarbonyl-2-fluorobenzyl chloride (**1**) (Scheme 2) is prepared by the reaction of 2-fluorophenyl acetic acid (**1**) with ethyl cyclopropane carboxylate (**2**) in the presence of isopropyl magnesium bromide in tetrahydrofuran to give α -cyclopropyl-2-fluorobenzyl ketone (**3**), which is reacted with a chlorinating agent such as chlorine gas or sulfonyl chloride in dichloromethane to yield the desired compound (Scheme 3) [9].

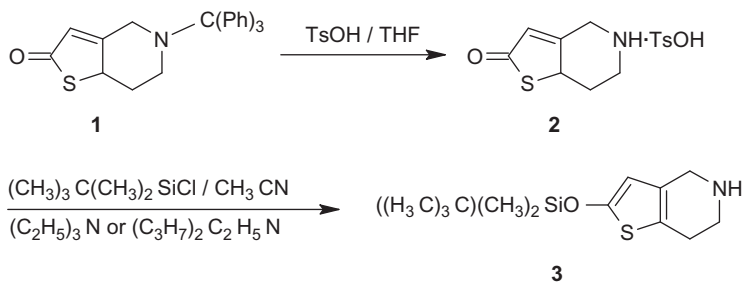


Scheme 2 Preparation of prasugrel.

Scheme 3 Preparation of α -cyclopropylcarbonyl-2-fluorobenzyl chloride (1) (Scheme 2).

On the other hand, 2-(*tert*-butyldimethylsilyloxy)-4,5,6,7-tetrahydrothieno[3,2-*c*]pyridine (2) (Scheme 2) is prepared by the reaction of 5-trityl-5,6,7,7*a*-tetrahydro-4*H*-thieno[3,2-*c*]pyridin-2-one (1) with *p*-toluenesulfonic acid (TsOH) in tetrahydrofuran to give 5,6,7,7*a*-tetrahydro-4*H*-thieno[3,2-*c*]pyridin-2-one *p*-toluenesulfonate (2), which is reacted with *tert*-butyldimethylsilyl chloride in presence of triethylamine or diisopropylethylamine in acetonitrile to yield the desired compound (Scheme 4) [9].

Miyata *et al.* have found that the large-scale production of prasugrel HCl by using the above procedures shows a contamination with the by-product 5-(5-chloro-1-(2-fluorophenyl)-2-oxopentyl)-4,5,6,7-tetrahydrothieno[3,2-*c*]pyridin-2-yl-acetate (CATP, Scheme 2) [10]. However, they improved the procedures to give highly pure prasugrel HCl with a reduced content of



Scheme 4 Preparation of 2-*(tert-butyl)dimethylsilyloxy*-4,5,6,7-tetrahydrothieno[3,2-*c*]pyridine (**2**) (Scheme 2).

CATP by controlling the reaction temperature at low values in the chlorination step.

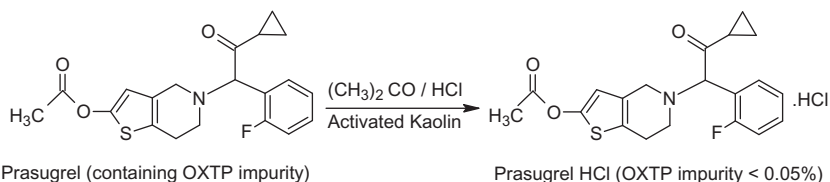
2.1.3 Method 3 [11]

The method describes a process to prepare highly pure prasugrel and its HCl salt. The same process in Section 4.1.2 is followed to prepare prasugrel as a free base, which contains OXTP as by-product. To produce highly pure prasugrel HCl, acetone is added to a mixture of prasugrel containing OXTP impurity and activated kaolin, stirred at 32 °C, and filtered. HCl is added dropwise at 52 °C to the filtrate over a period of 1 min and then prasugrel HCl crystals are added as a seed crystal, and the resultant mixture is then stirred at the same temperature for 1 h. In addition, HCl is added dropwise over a period of 1 h, and the resultant mixture is then stirred at 40 °C for 2 h and further at 30 °C for 1 h. The precipitated crystal is collected by filtration, washed with acetone, and dried under reduced pressure at 50 °C for 5 h to yield highly pure prasugrel HCl (OXTP impurity <0.05%) (Scheme 5).

Furthermore, high-pure prasugrel-free base is produced by dissolving prasugrel-free base in acetonitrile at 40 °C, followed by cooling the reaction solution to −15 °C. Then water is added dropwise and the resultant mixture is then stirred at the same temperature for 30 min. The precipitated crystals are collected by filtration, washed with a pre-cooled acetonitrile–water mixture, and dried under reduced pressure at 45 °C for 5 h to yield highly pure prasugrel-free base.

2.1.4 Method 4 [12,13]

The method describes preparation of 2-alkoxy-5-(α -cyclopropylcarbonyl-2-fluorobenzyl)-4,5,6,7-tetrahydrothieno[3,2-*c*]pyridine and OXTP, which is an intermediate for preparing prasugrel and its HCl salt.



Scheme 5 Preparation of prasugrel HCl containing <0.05% OXTP impurity.

For example, 2-methoxy-5-benzyl-4,5,6,7-tetrahydrothieno[3,2-*c*]pyridine (**1**) is reacted with sodium hydroxide in water and then with phenyl chloroformate in the presence of diisopropylethylamine in toluene and then with HCl in diethyl ether to give 2-methoxy-4,5,6,7-tetrahydrothieno[3,2-*c*]pyridine HCl (**2**). The later compound is reacted with sodium hydroxide, followed by reaction with α -cyclopropylcarbonyl-2-fluorobenzyl chloride (**3**) in the presence of potassium carbonate and sodium iodide in acetonitrile and then converted to hydrochloride salt by HCl in diethyl ether to give 2-methoxy-5-(α -cyclopropylcarbonyl-2-fluorobenzyl)-4,5,6,7-tetrahydrothieno[3,2-*c*]pyridine HCl (**4**). The later compound is demethylated by HCl to give OXTP HCl (**5**), which is finally reacted with sodium carbonate and then with acetic anhydride and sodium hydride in dimethylformamide to yield prasugrel. Prasugrel HCl is prepared by addition of HCl in diethyl ether ([Scheme 6](#)).

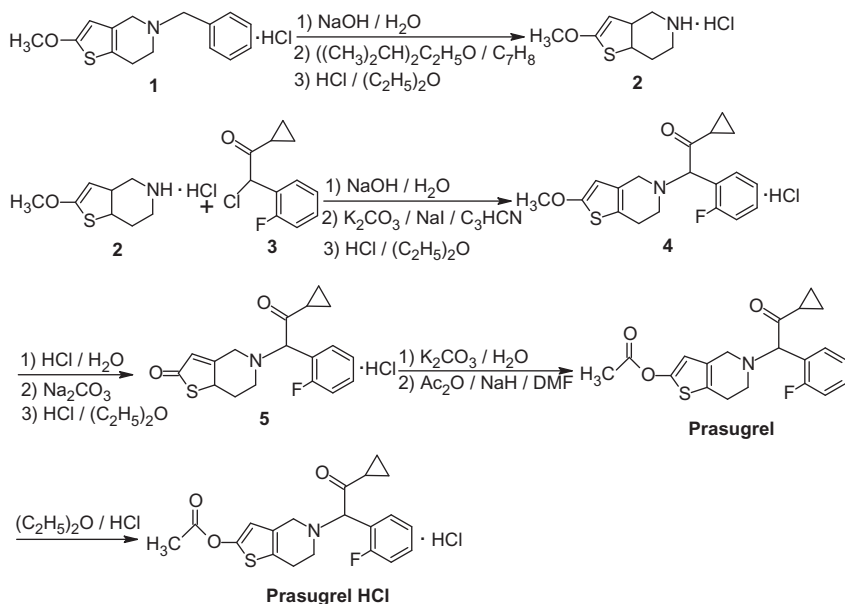
2.1.5 Method 5 [14]

The method describes a process for preparation of 1-cyclopropylcarbonyl-2-(2-fluorophenyl)-2-*R*-sulfonyl-ethanone derivatives as intermediates for preparing prasugrel, where *R* is methyl, ethyl, phenyl, *p*-tolyl, or *p*-nitrophenyl.

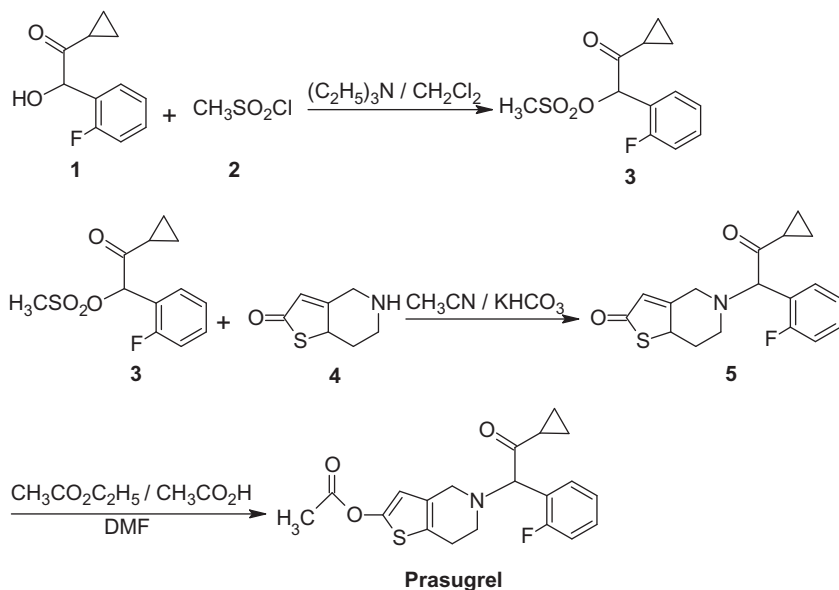
For example, 1-cyclopropyl-2-(2-fluorophenyl)-2-hydroxyethanone (**1**) is sulfonylated with methanesulfonyl chloride (**2**) (*R* is methyl) in the presence of triethylamine in dichloromethane to give 1-cyclopropyl-2-(2-fluorophenyl)-2-methanesulfonyl-ethanone (**3**). Condensation of compound (**3**) with 5,6,7,8-tetrahydrothieno[3,2-*c*]pyridin-2(1*H*)-one HCl (**4**) in the presence of potassium bicarbonate in acetonitrile produces OXTP (**5**), which is finally reacted with ethyl acetate in the presence of acetic acid in dimethylformamide to yield prasugrel ([Scheme 7](#)).

2.1.6 Method 6 [15]

The method describes an improved process for preparing prasugrel and its intermediates and pharmaceutically acceptable salts.



Scheme 6 Preparation of prasugrel intermediate 2-methoxy-5-(α -cyclopropylcarbonyl-2-fluorobenzyl)-4,5,6,7-tetrahydrothieno[3,2-*c*]pyridine (**4**), 5-(2-(cyclopropyl)-1-(2-fluorophenyl)-2-oxoethyl)-5,6,7,7a-tetrahydrothieno[3,2-*c*]pyridine-2(4*H*)-one (**5**) and prasugrel HCl.



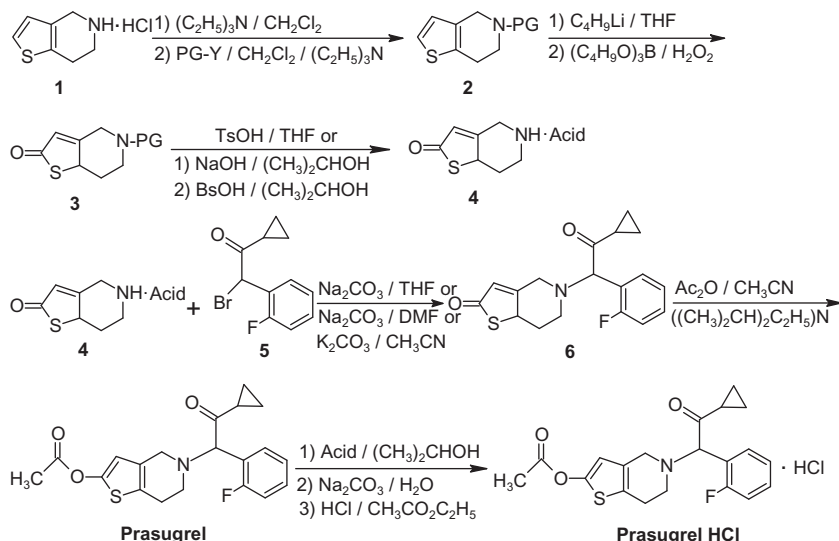
Scheme 7 Preparation of 1-cyclopropyl-2-(2-fluorophenyl)-2-methanesulfonylethanone (**3**) and prasugrel.

For example, 4,5,6,7-tetrahydrothieno[3,2-*c*]pyridine (**1**) is reacted with a protecting agent (PG-Y) such as triphenyl methyl chloride, benzoyl chloride, and di-*tert*-butyl dicarbonate ((Boc)₂O) in the presence of triethylamine in dichloromethane to give 5-PG-4,5,6,7-tetrahydrothieno[3,2-*c*]pyridine (**2**), followed by converting compound (**2**) by introducing a boronic group -B(OR')₂ using tri-*n*-butyl borate in second position of thieno[3,2-*c*]pyridine skeleton through a lithium derivative using *n*-butyl lithium in tetrahydrofuran, and then treating with H₂O₂ to give 5-PG-5,6,7,7*a*-tetrahydrothieno[3,2-*c*]pyridin-2(4*H*)-one (**3**). Compound (**3**) is reacted with a suitable acid such as TsOH in tetrahydrofuran or benzene sulfonic acid in isopropanol to give 5,6,7,7*a*-tetrahydro-4*H*-thieno[3,2-*c*]pyridine-2(4*H*)-one acid addition salt (**4**). The later compound is reacted α-cyclopropylcarbonyl-2-fluorobenzyl bromide (**5**) in presence of sodium carbonate in tetrahydrofuran or dimethylformamide or potassium carbonate in acetonitrile to give OXTP (**6**). Compound (**6**) is reacted with acetic anhydride in the presence of diisopropylethylamine in acetonitrile to yield prasugrel.

Optionally, converting the prasugrel into its acid addition salts by treating it with fumaric, malic, benzene sulfonic, or *p*-toluenesulfonic acid in isopropanol gives prasugrel acid salt. Prasugrel HCl can be prepared by treating prasugrel acid salt such as fumarate with sodium carbonate in water, followed by treating with HCl in ethyl acetate (Scheme 8).

In this work, a process for the purification of prasugrel is carried out by recrystallization. For example, prasugrel is dissolved in ethyl acetate at 60–65 °C to give a clear solution. The reaction mixture is stirred for an hour at 60–65 °C; cyclohexane is added to the reaction mixture and stirred for 1 h. The reaction mixture is cooled to 0–5 °C and stirred for 1 h. The solid obtained is filtered, washed with cyclohexane, and then dried to give high-pure prasugrel (Purity: 99.90%). Another example, a mixture of prasugrel fumarate and ethyl acetate and aqueous sodium carbonate is stirred for 30 min. The aqueous and organic layers are separated. The combined organic layer is washed with water and distilled the organic layer completely under reduced pressure and isolated pure prasugrel (Purity: 99.89%).

Also an improved process for the preparation of α-cyclopropyl-2-fluorobenzyl ketone is also described by treating 2-fluorobenzyl bromide with magnesium metal in higher volumes of diethyl ether to provide 2-fluorobenzyl magnesium bromide, which is condensed with 5-cyclopropyl cyanide in higher volumes of diethyl ether to provide highly pure α-cyclopropyl-2-fluorobenzyl ketone with low content of 2-fluorobenzyl dimer impurity.



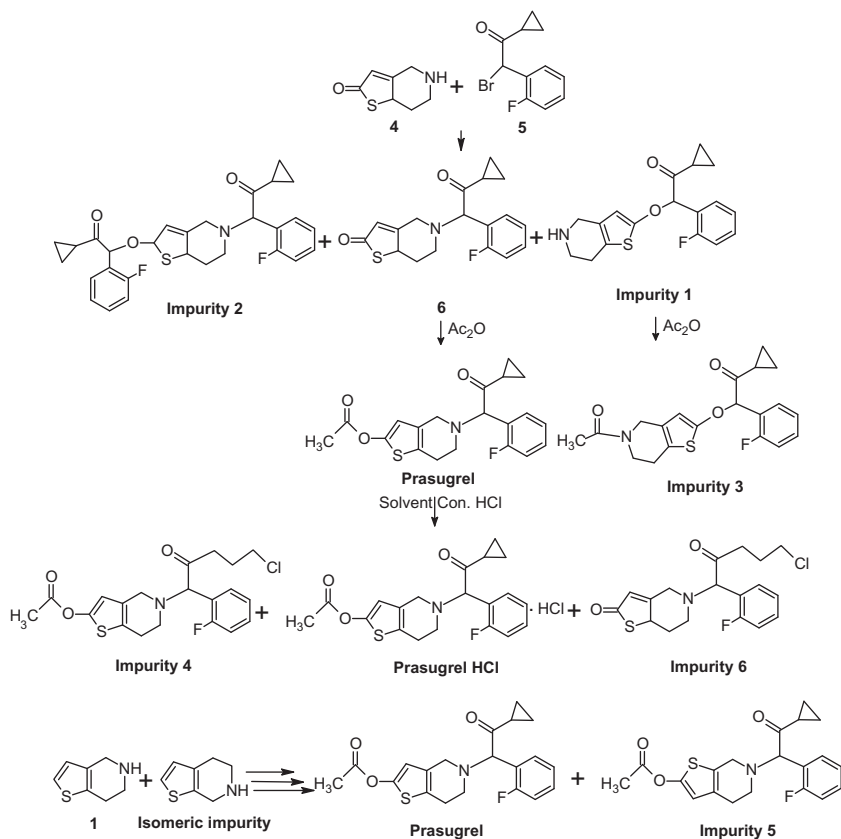
Scheme 8 Preparation of prasugrel HCl. PG is trityl, benzoyl, or *tert*-butyl carbonate (Boc) group. Acid is fumaric, malic, *p*-toluenesulfonic, or benzenesulfonic acid.

The formation of several impurities ([Scheme 9](#)) during the preparation of prasugrel and its acid addition salts by the above procedures have been controlled and minimized by using specific reagents and specific reaction conditions. These impurities are 2-(α -cyclopropylcarbonyl-2-fluorobenzoyloxy)-5-*H*-4,5,6,7-tetrahydrothieno[3,2-*d*]pyridine (**Impurity 1**), 2-(α -cyclopropylcarbonyl-2-fluorobenzoyloxy)-5-(α -cyclopropylcarbonyl-2-fluorobenzyl)-4,5,6,7-tetrahydrothieno[3,2-*d*]pyridine (**Impurity 2**), 2-(α -cyclopropylcarbonyl-2-fluorobenzoyloxy)-5-acetoxy-4,5,6,7-tetrahydrothieno[3,2-*d*]pyridine (**Impurity 3**), CATP (**Impurity 4**), 6-(2-cyclopropyl-1-(2-fluorophenyl)-2-oxoethyl)-4,5,6,7-tetrahydrothieno[2,3-*c*]pyridin-2-yl-acetate (**Impurity 5**), 5-(5-chloro-1-(2-fluorophenyl)-2-oxopentyl)-5,6,7,7*a*-tetrahydrothieno[3,2-*d*]pyridin-2(4*H*)-one (**Impurity 6**).

2.1.7 Method 7 [16]

The method describes a process for preparing prasugrel intermediate OXTP and prasugrel.

For example, α -cyclopropylcarbonyl-2-fluorobenzyl bromide (**1**) is condensed with 2-thiophenylethylamine (**2**) in the presence of potassium carbonate in dichloromethane to give 1-cyclopropyl-2-(2-fluorophenyl)-

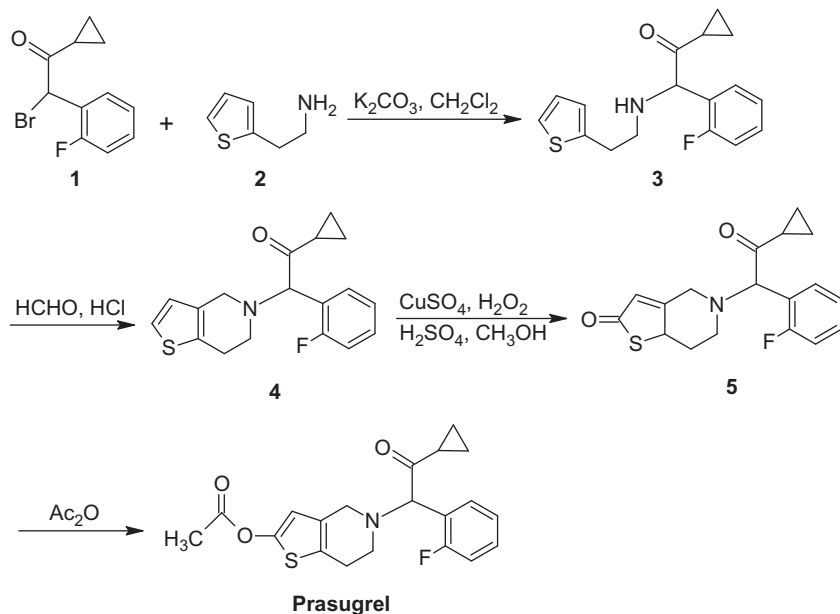


Scheme 9 The pathways of formation of impurities 1–6.

2-*N*-(2-thiophenylethylamine)ethanone (3), then compound (3) is reacted with formaldehyde in the presence of HCl in methanol to give 5-(2-cyclopropyl-1-(2-fluorophenyl)-2-oxoethyl)-5,6,7,7a-tetrahydrothieno[3,2-*c*]pyridine (4), further oxidation with H₂O₂ in the presence of copper sulfate and sulfuric acid in methanol is carried out to give OXTP (5), followed by acetic anhydride esterification of intermediate (5) to obtain prasugrel (Scheme 10).

2.1.8 Method 8 [17]

The method describes a process for preparing prasugrel intermediates 2-acetoxy-5-trityl-4,5,6,7-tetrahydrothieno[3,2-*c*]pyridine and 2-acetoxy-4,5,6,7-tetrahydrothieno[3,2-*c*]pyridine and prasugrel.



Scheme 10 Preparation of prasugrel.

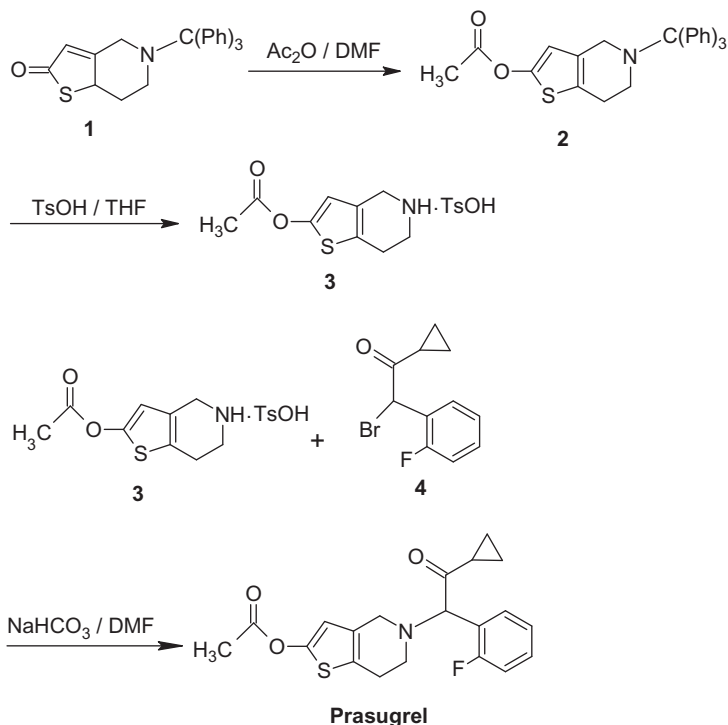
For example, 5-trityl-5,6,7,7*a*-tetrahydro-4*H*-thieno[3,2-*c*]pyridine-2-one (1) is reacted with acetic anhydride in dimethylformamide to give 2-acetoxy-5-trityl-4,5,6,7-tetrahydrothieno[3,2-*c*]pyridine (2), followed by hydrolysis with TsOH in tetrahydrofuran to give 2-acetoxy-4,5,6,7-tetrahydrothieno[3,2-*c*]pyridine-*p*-toluenesulfonate (3). The later compound is condensed with α -cyclopropylcarbonyl-2-fluorobenzyl bromide (4) in the presence of sodium bicarbonate in dimethylformamide to obtain prasugrel (Scheme 11).

α -cyclopropylcarbonyl-2-fluorobenzyl bromide (4) is prepared following a procedure similar to that mentioned in Section 4.1.1 (Scheme 1).

2.1.9 Method 9 [18]

The method describes a process for preparing prasugrel HCl.

For example, 5,6,7,7*a*-tetrahydrothieno[3,2-*c*]pyridine-2(4*H*)-one *p*-toluenesulfonate (1) is reacted with trityl chloride in acetonitrile and diisopropylethylamine to give 5-trityl-4,5,6,7-tetrahydrothieno[3,2-*c*]pyridine-2(3*H*)-one (2), followed by reaction with 2-fluorobenzyl bromide (3) in the presence of potassium carbonate in acetonitrile to give 2-trityl-2-fluorobenzyl-4,5,6,7-tetrahydrothieno[3,2-*c*]pyridine-2(3*H*)-one

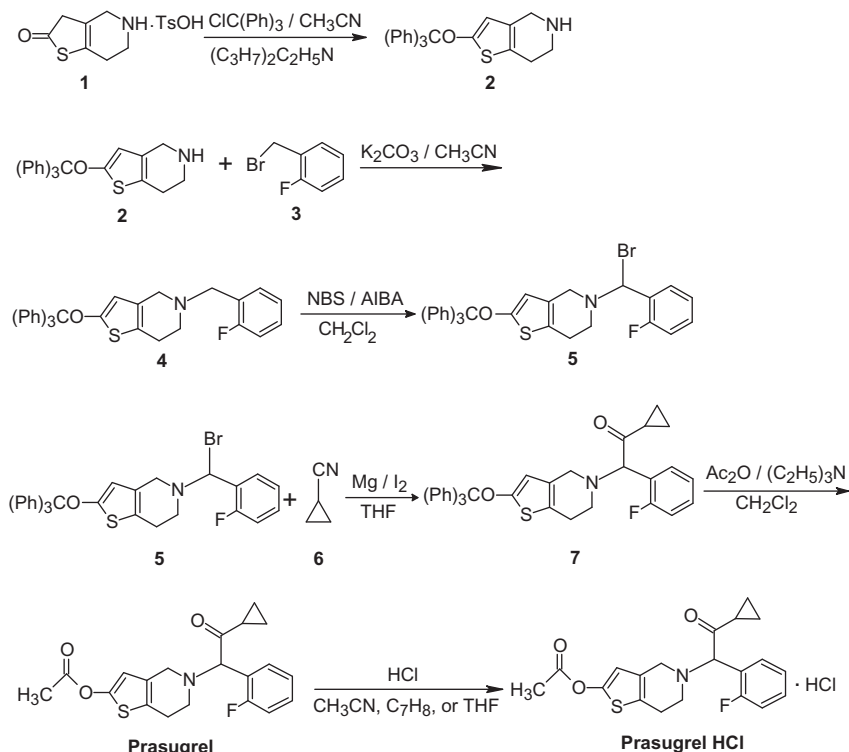


Scheme 11 Preparation of 2-acetoxy-5-trityl-4,5,6,7-tetrahydrothieno[3,2-*c*]pyridine (**2**), 2-acetoxy-4,5,6,7-tetrahydrothieno[3,2-*c*]pyridine (**3**), and prasugrel.

(4). The later compound is reacted with NBS in the presence of azobisisobutyronitrile (AIBN) in dichloromethane to give 2-trityl-5-(α -bromo-2-fluorobenzyl)-4,5,6,7-tetrahydrothieno[3,2-*c*]pyridine-2(3*H*)-one (**5**), followed by reaction with cyclopropyl cyanide (**6**) in the presence of magnesium powder and iodine in tetrahydrofuran to give 2-trityl-5-(α -cyclopropylcarbonyl-2-fluorobenzyl)-4,5,6,7-tetrahydrothieno[3,2-*c*]pyridine-2(3*H*)-one (**7**). Acetylation of compound (**7**) with acetic anhydride in dichloromethane and acetonitrile yields prasugrel. Prasugrel HCl is prepared by reacting prasugrel with concentrated HCl in organic solvent such as acetonitrile, toluene, or tetrahydrofuran ([Scheme 12](#)).

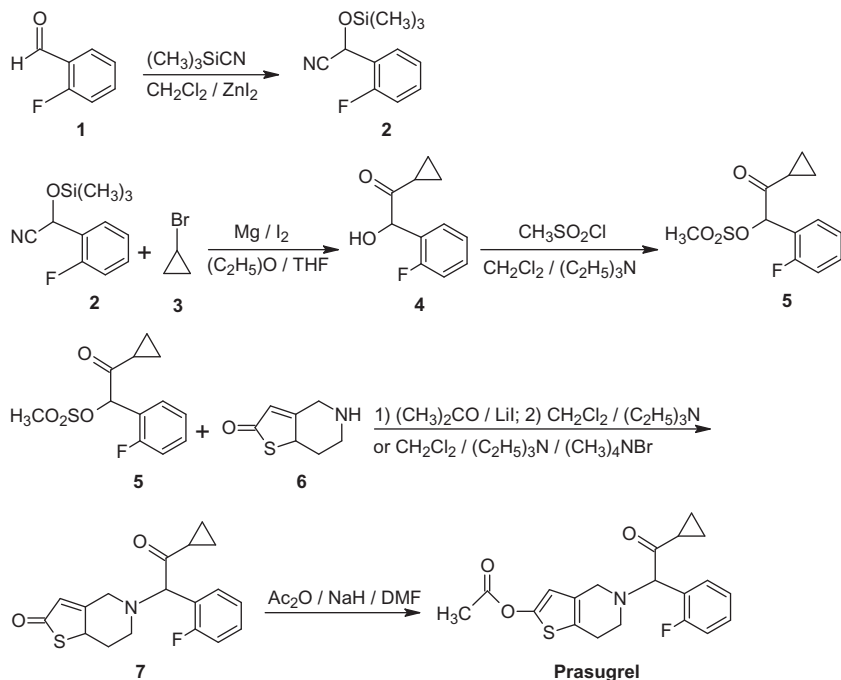
2.1.10 Method 10 [19]

2-Fluorobenzaldehyde (**1**) is reacted with trimethylsilyl cyanide in dichloromethane in the presence of anhydrous zinc iodide as a catalyst to give the silylated nitrile of 2-fluoromandelic acid (**2**), which is then reacted with



Scheme 12 Preparation of prasugrel HCl.

cyclopropyl bromide (**3**) in the presence of magnesium and iodine in a mixture of diethyl ether and tetrahydrofuran to give 1-cyclopropyl-2-(2-fluorophenyl)-2-hydroxyethanone (**4**). The later compound is further reacted with methanesulfonyl chloride in the presence of triethylamine in dichloromethane to give 1-cyclopropyl-2-(2-fluorophenyl)-2-methanesulfonyl ethanone (**5**), which is further treated with lithium iodide in acetone, followed by reaction with 5,6,7,7a-tetrahydrothieno[3,2-c]pyridin-2(4H)-one (**6**) in the presence of triethylamine with or without tetramethylammonium bromide in dichloromethane to give 5-(2-(cyclopropyl-1-(2-fluorophenyl)-2-oxoethyl)-5,6,7,7a-tetrahydrothieno[3,2-c] pyridine-2(4H)-one (**7**). Compound (**7**) can be also prepared by condensation of compound (**5**) with compound (**6**) in the presence of tetramethylammonium bromide and triethylamine in dichloromethane. Finally, compound (**7**) is reacted with acetic anhydride and sodium hydride in dimethylformamide to obtain prasugrel (Scheme 13).

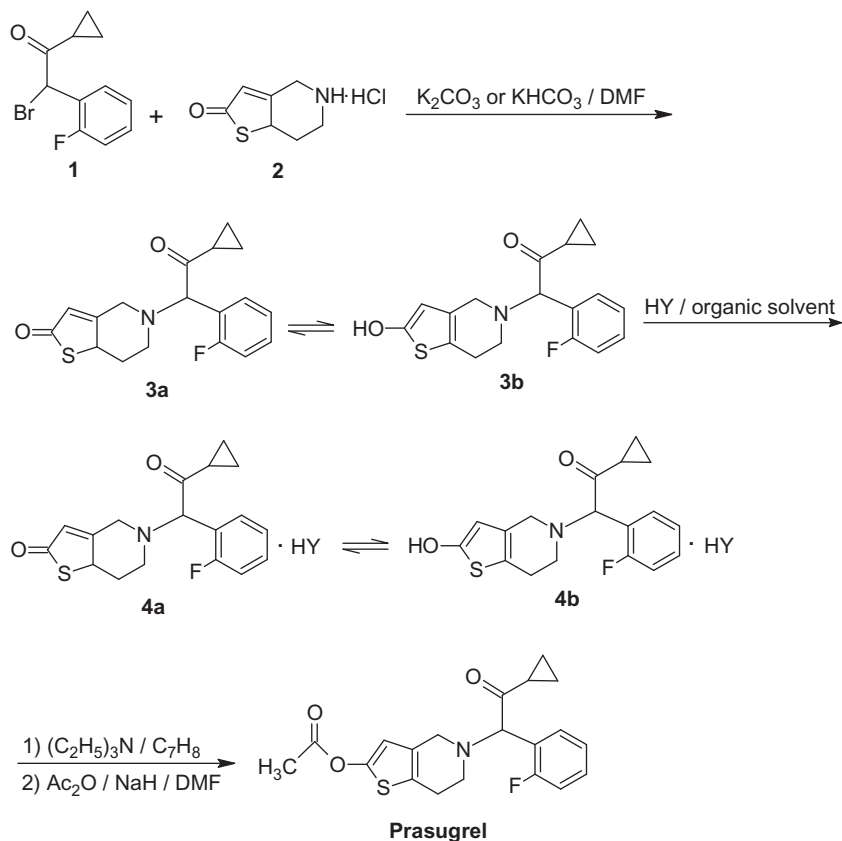


Scheme 13 Preparation of prasugrel.

2.1.11 Method 11 [20]

The method describes a process for preparing prasugrel using an intermediate additive salt having a ketone–enol tautomer structure.

For example, α -cyclopropylcarbonyl-2-fluorobenzyl bromide (**1**) is condensed with 5,6,7,8-tetrahydrothieno[3,2-*c*]pyridin-2(4*H*)-one HCl (**2**) in the presence of potassium carbonate or potassium bicarbonate in dimethylformamide to give a crude intermediate OXTP (**3a** keto and **3b** enol tautomers). Organic solvent such as diethyl ether, acetone, toluene, or isopropanol is added to the crude prasugrel intermediate (**3**), stirred, filtered, and then the filtrate is washed with the organic solvent. The solution of HY such as HCl, H₂SO₄, HNO₃, methanesulfonic, or maleic acid in organic solvent such as methanol, ethanol, acetone, or diethyl ether is slowly added dropwise, then filtered, washed with the organic solvent, and dried by vacuum drying to give pure prasugrel intermediate OXTP HY salt (**4a** keto and **4b** enol tautomers). The prasugrel intermediate (**4**) is reacted with triethylamine in toluene. The obtained organic phase is washed with aqueous sodium chloride solution, dried, and then evaporated to give the free



Scheme 14 Preparation of prasugrel. HY is HCl, H₂SO₄, HNO₃, maleic or methanesulfonic acid.

base of the intermediate (4) as a viscous residue, which is finally reacted with acetic anhydride and sodium hydride in dimethylformamide to obtain prasugrel (Scheme 14).

Also prasugrel can be prepared from the intermediate (4) by one-step method without the separation of the free base of the intermediate (4) by treating with triethylamine in dimethylformamide and followed by reacting with acetic anhydride and sodium hydride in dimethylformamide to obtain prasugrel.

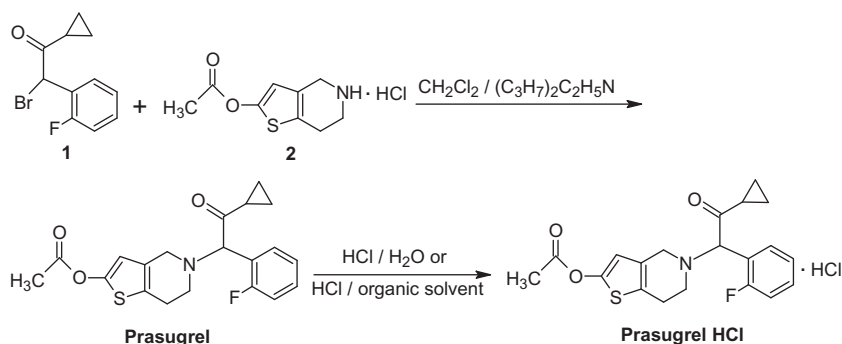
2.1.12 Method 12 [21]

The method describes a process for preparing prasugrel intermediates α -cyclopropylcarbonyl-2-fluorobenzyl bromide, 2-acetoxy-4,5,6,7-tetrahydrothieno[3,2-*c*]pyridine HCl (2), and prasugrel HCl.

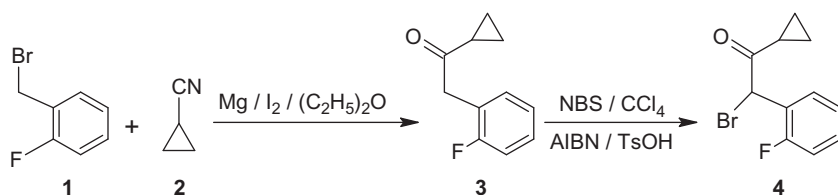
For example, α -cyclopropylcarbonyl-2-fluorobenzyl bromide (**1**) is reacted with 2-acetoxy-4,5,6,7-tetrahydrothieno[3,2-*c*]pyridine HCl (**2**) in a mixture of dichloromethane and diisopropylethylamine to yield prasugrel, which is then reacted with HCl in aqueous or in an organic solvent such as methanol, ethanol, ethyl acetate, isopropanol, acetone to obtain prasugrel HCl (Scheme 15).

α -Cyclopropylcarbonyl-2-fluorobenzyl bromide (**1**) (Scheme 15) is prepared by reacting 2-fluorobenzyl bromide (**1**) with cyclopropyl cyanide (**2**) in a mixture of metallic magnesium, iodine, and anhydrous diethyl ether to give cyclopropyl 2-fluorobenzyl ketone (**3**), which is then reacted with NBS in carbon tetrachloride in the presence of AIBN and TsOH to obtain the desired compound (Scheme 16).

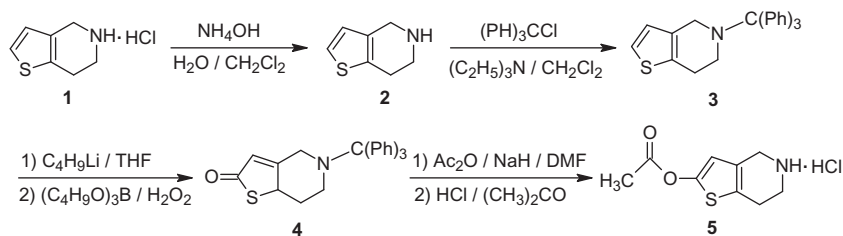
2-Acetoxy-4,5,6,7-tetrahydrothieno[3,2-*c*]pyridine HCl (**2**) (Scheme 15) is prepared by reacting 4,5,6,7-tetrahydrothieno[3,2-*c*]pyridine HCl (**1**) with ammonium hydroxide in a mixture of water and dichloromethane to give 4,5,6,7-tetrahydrothieno[3,2-*c*]pyridine (**2**), which is then reacted with trityl chloride in a mixture of triethylamine and dichloromethane to give 5-trityl-4,5,6,7-tetrahydrothieno[3,2-*c*]pyridine (**3**). The later compound is then reacted with *n*-butyl lithium, tri-*n*-butyl borate, and hydrogen peroxide in tetrahydrofuran to give 5-trityl-5,6,7,7a-tetrahydrothieno[3,2-*c*]pyridin-2



Scheme 15 Preparation of prasugrel HCl.



Scheme 16 Preparation of α -cyclopropylcarbonyl-2-fluorobenzyl bromide (**1**) (Scheme 15).



Scheme 17 Preparation of 2-acetoxy-4,5,6,7-tetrahydrothieno[3,2-*c*]pyridine HCl (**2**) (Scheme 15).

(4*H*)-one (**4**). The later compound is reacted with acetic anhydride and sodium hydride in dimethylformamide, followed by reaction with HCl in acetone to obtain the desired compound (Scheme 17).

2.1.13 Method 13 [22]

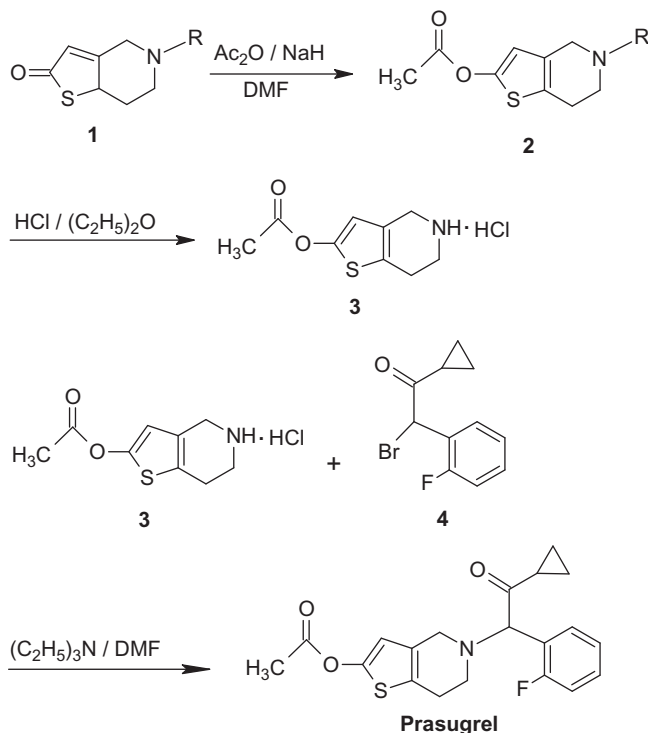
The same procedure in Section 4.1.1 is followed to prepare α -cyclopropylcarbonyl-2-fluorobenzyl bromide or chloride (**4**) but using different halogenating agents.

For example, α -cyclopropyl-2-fluorobenzyl ketone (**3**) is halogenated in a mixture of aqueous hydrogen halide and aqueous hydrogen peroxide in the presence of a water miscible solvent or in the presence of a phase transfer catalyst; or halogenation is carried out in a mixture of H_2SO_4 and alkali metal salt of aqueous hydrogen halide. This method produces prasugrel intermediate (**4**) with a purity of $\geq 90\%$ with a low content of the monohalo and dihalo derivative obtained by the ring opening of the cyclopropane ring.

2.1.14 Method 14 [23]

This method describes a process for the preparation of 2-acetoxy-4,5,6,7-tetrahydrothieno[3,2-*c*]pyridine HCl as intermediate for producing prasugrel.

For example, 5-*R*-5,6,7,7*a*-tetrahydro-4*H*-thieno[3,2-*c*]pyridine-2-one (**1**) is reacted with acetic anhydride in dimethylformamide in the presence of sodium hydride to give 2-acetoxy-5-*R*-5,6,7,7*a*-tetrahydro-4*H*-thieno[3,2-*c*]pyridine (**2**), followed by reaction with gaseous HCl in diethyl ether to give 2-acetoxy-4,5,6,7-tetrahydrothieno[3,2-*c*]pyridine HCl (**3**). The intermediate (**3**) is then reacted with α -cyclopropylcarbonyl-2-fluorobenzyl bromide (**4**) in dichloromethane or acetonitrile in the presence of triethylamine to obtain prasugrel (Scheme 18).

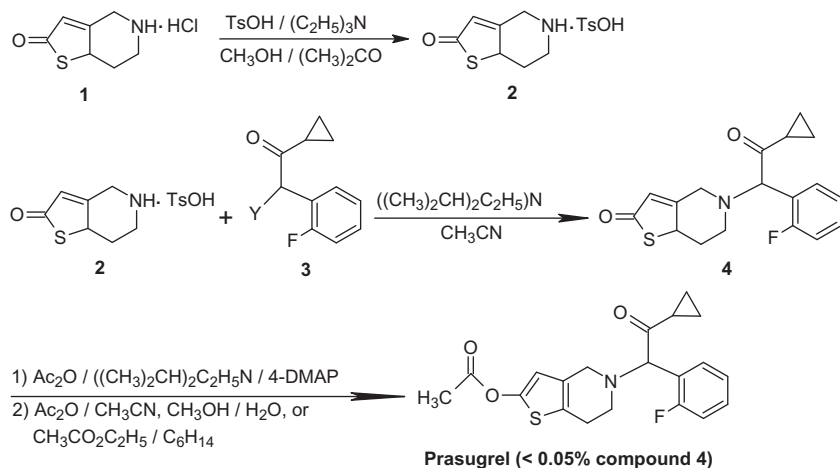


Scheme 18 Preparation of prasugrel. R is hydrogen, trityl, or *tert*-butyloxy carbonyl group.

2.1.15 Method 15 [24]

The method describes a process for preparing highly pure prasugrel.

For example, 5,6,7,7*a*-tetrahydrothieno[3,2-*c*]pyridin-2(4*H*)-one HCl (**1**) is reacted with TsOH in a mixture of triethylamine, methanol, and acetone to give 5,6,7,7*a*-tetrahydrothieno[3,2-*c*]pyridin-2(4*H*)-one TsOH (**2**). The later compound is reacted with α -cyclopropylcarbonyl-2-fluorobenzyl bromide, methanesulfonate, or *p*-toluene sulfonate (**3**) in the presence of diisopropylethylamine in acetonitrile to give OXTP (**4**), followed by reaction with acetic anhydride in the presence of diisopropylethylamine and dimethylaminopyridine as a catalyst to give prasugrel with a low content of the compound (**4**) as undesired impurity (<0.1%). Crude prasugrel is further treated with acetic anhydride in acetonitrile to give pure prasugrel (compound **4** <0.05%). Optionally, purification of crude prasugrel by recrystallization from a mixture of acetone and water, methanol and water, or ethyl acetate and hexane yields prasugrel with <0.05% of compound (**4**) (Scheme 19).



Scheme 19 Preparation of prasugrel containing <0.05% of compound (4).

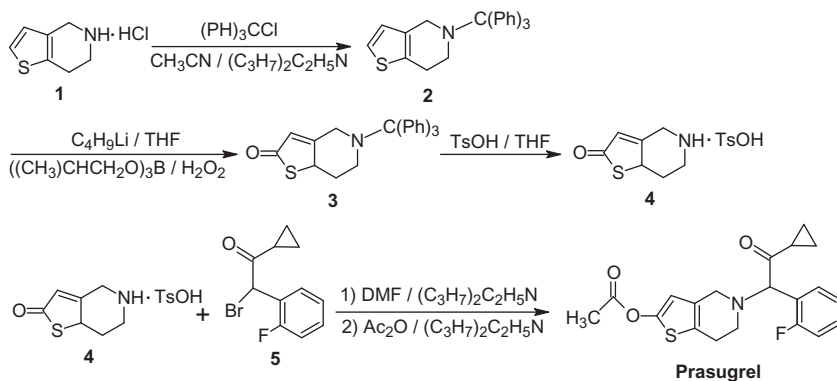
2.1.16 Method 16 [25]

The method describes a one-pot process for preparing prasugrel.

4,5,6,7-Tetrahydrothieno[3,2-*c*]pyridine HCl (**1**) is reacted with trityl chloride in acetonitrile in the presence of diisopropylethylamine to give 5-trityl-4,5,6,7-tetrahydrothieno[3,2-*c*]pyridine (**2**). The later compound is then reacted with *n*-butyl lithium, tri-isobutyl borate, and hydrogen peroxide in tetrahydrofuran to give 5-trityl-5,6,7,7*a*-tetrahydrothieno[3,2-*c*]pyridin-2(4*H*)-one (**3**). The later compound is reacted with TsOH in tetrahydrofuran to give 5,6,7,7*a*-tetrahydro-4*H*-thieno[3,2-*c*]pyridine-2-one *p*-toluenesulfonate (**4**). Compound (**4**) is reacted with α -cyclopropylcarbonyl-2-fluorobenzyl bromide (**5**) and then with acetic anhydride in dimethylformamide in the presence of diisopropylethylamine to obtain prasugrel (Scheme 20).

2.1.17 Method 17 [26]

The method describes a process for preparing prasugrel intermediate 5-*R*-2-(amino-*R*₁*R*₂)-4,5,6,7-tetrahydrothieno[3,2-*c*]pyridine and/or acid addition salts, where *R* is a hydrogen atom or a nitrogen-protecting group or an α -cyclopropylcarbonyl-2-fluorobenzyl group. *R*₁, *R*₂ are independently a C₁-C₁₀ alkyl group, with an option of having one or more carbons substituted by a hydroxyl group, or *R*₁, *R*₂ together with the bridging nitrogen forming a ring comprising 3 to 10 carbon atoms, optionally also comprising another nitrogen, oxygen, or sulfur atom in the ring and/or a nitrogen-, oxygen-, or sulfur-comprising substituent on the ring.



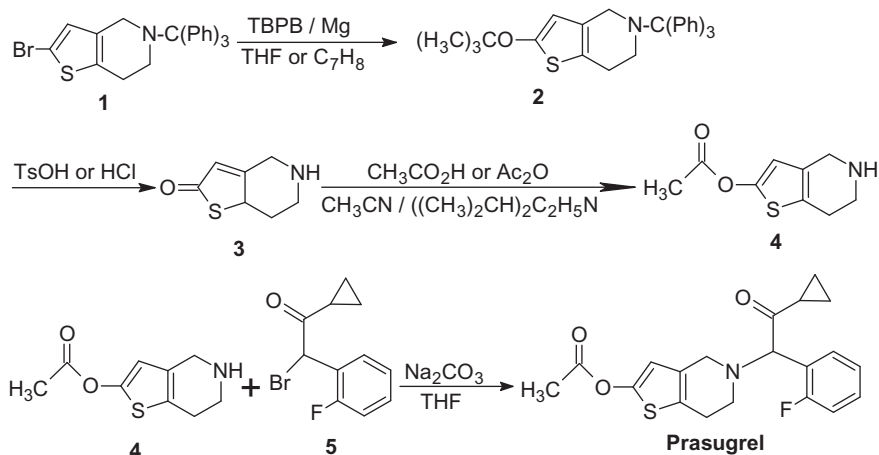
Scheme 20 Preparation of prasugrel.

For example, 4,5,6,7-tetrahydrothieno[3,2-*c*]pyridine HCl (**1**) is reacted with bromine in a mixture of dichloromethane and water, followed by pH adjustment to 8.5 to give 2-bromo-4,5,6,7-tetrahydrothieno[3,2-*c*]pyridine (**2**). The later compound is reacted with (Boc)₂O in dichloromethane in the presence of triethylamine to give 2-bromo-5-*tert*-butyloxycarbonyl-4,5,6,7-tetrahydrothieno[3,2-*c*]pyridine (**3**), followed by reaction with morpholine in dimethylethanolamine in the presence of copper powder, copper iodide, and potassium phosphate tribasic to give 2-(1-morpholinyl)-5-*tert*-butyloxycarbonyl-4,5,6,7-tetrahydrothieno[3,2-*c*]pyridine (**4**). Hydrolysis of compound (**4**) with gaseous HCl in diethyl ether, followed by neutralization with aqueous NaOH gives 2-(1-morpholinyl)-4,5,6,7-tetrahydrothieno[3,2-*c*]pyridine (**5**). Condensation of compound (**5**) with α -cyclopropylcarbonyl-2-fluorobenzyl bromide (**6**) in acetonitrile in the presence of triethylamine produces 2-(*N*-morpholinyl)-5-(α -cyclopropylcarbonyl-2-fluorobenzyl)-4,5,6,7-tetrahydrothieno-[3,2-*c*]pyridine (**7**). Compound (**7**) is hydrolyzed with aqueous HCl, followed by adjusting pH to 10 to give OXTP (**8**). Prasugrel is prepared by reaction of compound (**8**) with acetic anhydride in dimethylformamide in the presence of sodium hydride (Scheme 21).

2.1.18 Method 18 [27]

The method describes a one-pot process for preparing prasugrel.

For example, 5,6,7,7*a*-tetrahydrothieno[3,2-*c*]pyridin-2(4*H*)-one HCl (**1**) is reacted with trimethylsilyl chloride in the presence of triethylamine in dichloromethane to give 2-(trimethylsilyloxy)-4,5,6,7-tetrahydrothieno[3,2-*c*]pyridine (**2**), followed by condensation with α -cyclopropylcarbonyl-2-fluorobenzyl bromide (**3**), and finally acetylation with acetic anhydride (**4**) to obtain prasugrel (Scheme 22).



Scheme 23 Preparation of prasugrel.

For example, 2-bromo-5-trityl-4,5,6,7-tetrahydrothieno[3,2-*c*]pyridine (**1**) is reacted with *tert*-butyl peroxybenzoate (TBPB) in the presence of Mg powder in tetrahydrofuran or toluene to give 2-*tert*-butoxy-5-trityl-4,5,6,7-tetrahydrothieno[3,2-*c*]pyridine (**2**), followed by hydrolysis with acid such as *p*-toluenesulfonic or HCl acid to give 5,6,7,7*a*-tetrahydrothieno[3,2-*c*]pyridin-2(4*H*)-one (**3**). The later compound undergoes acetylation with acetic acid or acetic anhydride in the presence of diisopropylethylamine in acetonitrile to give 2-acetoxy-4,5,6,7-tetrahydrothieno[3,2-*c*]pyridine HCl (**4**), followed by amidation with α-cyclopropylcarbonyl-2-fluorobenzyl bromide (**5**) in the presence of Na₂CO₃ in tetrahydrofuran to yield prasugrel (Scheme 23).

2.1.20 Method 20 [29]

The method describes a process for preparing prasugrel intermediate 5,6,7,7*a*-tetrahydrothieno[3,2-*c*]pyridin-2(4*H*)-one using protecting agent (PG) such as formyl, acetyl, chloroacetyl, 9-fluorenyl-carbonyl, or *p*-toluenesulfonyl group at position 5.

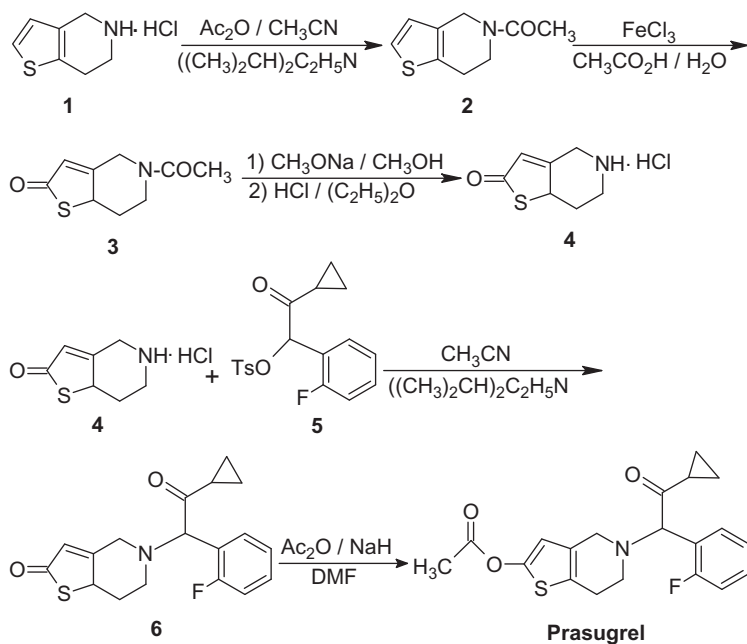
For example, 4,5,6,7-tetrahydrothieno[3,2-*c*]pyridine (**1**) is reacted with acetyl anhydride in the presence of diisopropylethylamine in acetonitrile to give 5-acetyl-4,5,6,7-tetrahydrothieno[3,2-*c*]pyridine (**2**, PG is acetyl), followed by oxidation in an autoclave with ferric chloride in a mixture of acetic acid and water to give 5-acetyl-5,6,7,7*a*-tetrahydrothieno[3,2-*c*]pyridin-2(4*H*)-one (**3**). Compound (**3**) is reacted with sodium methoxide in methanol to give 5,6,7,7*a*-tetrahydro-4*H*-thieno[3,2-*c*]pyridine-2-one

(4), which is fully milled in HCl/diethyl ether system to give the HCl salt of compound (4). Compound (4) is condensed with 1-cyclopropyl-2-tosyloxy-2-(2-fluorophenyl)ethanone (5) in the presence of diisopropylethylamine in acetonitrile to give OXTP (6), followed by acetylation with acetic anhydride in dimethylformamide in the presence of sodium hydride to yield prasugrel (Scheme 24).

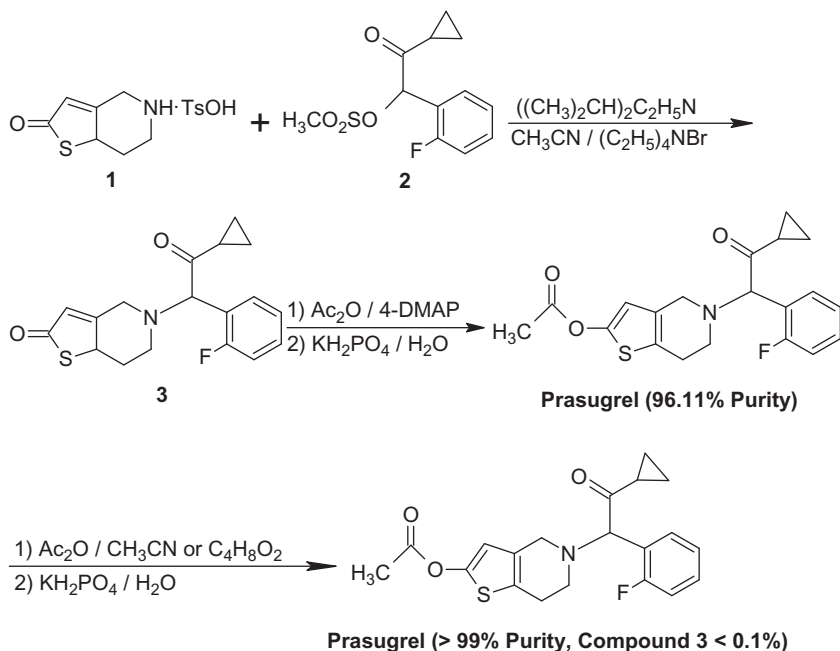
2.1.21 Method 21 [30]

The method describes a process for preparing a highly pure prasugrel containing not more than 0.1% of OXTP.

For example, 5,6,7,7a-tetrahydro-4*H*-thieno[3,2-*c*]pyridine-2-one *p*-toluenesulfonate (1) is reacted with 1-cyclopropyl-2-methanesulfonyloxy-2-(2-fluorophenyl)ethanone (2) in the presence of diisopropylethylamine and tetraethylammonium bromide in acetonitrile to give OXTP (3), followed by acetylation with acetic anhydride in the presence of 4-DMAP and aqueous solution of KH_2PO_4 is added to give crystallized prasugrel with a purity of ~96%.



Scheme 24 Preparation of prasugrel and its intermediate 5,6,7,7a-tetrahydrothieno [3,2-*c*]pyridin-2(4*H*)-one (4).



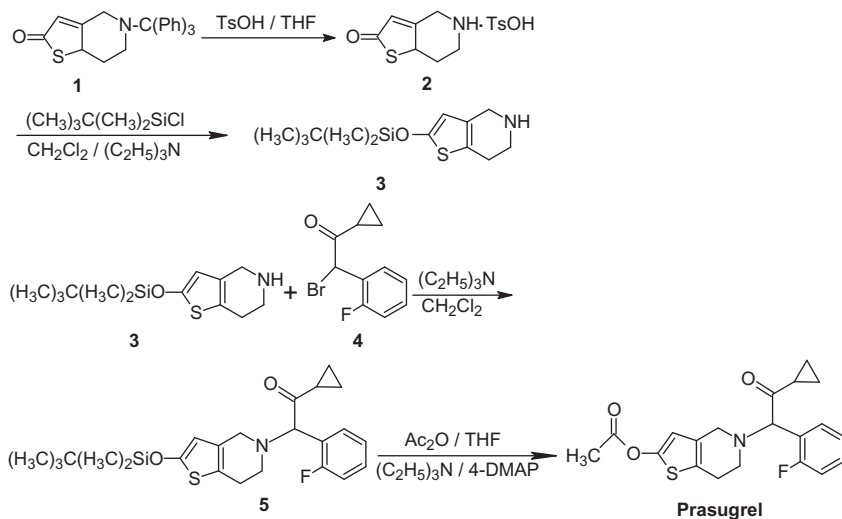
Scheme 25 Preparation of prasugrel containing <0.1% of compound (3).

A highly pure prasugrel is obtained by recrystallization in organic solvent such as acetonitrile or 1,4-dioxane and addition of aqueous solution of KH_2PO_4 to give prasugrel with >99% purity and containing <0.1% of OXTP (3) (Scheme 25).

2.1.22 Method 22 [31]

The method describes a process for preparing prasugrel by using organosilicon protective agent.

For example, 5-trityl-5,6,7,7a-tetrahydrothieno[3,2-c]pyridin-2(4H)-one (1) is reacted with TsOH in tetrahydrofuran to give 5,6,7,7a-tetrahydrothieno[3,2-c]pyridin-2(4H)-one *p*-toluenesulfonate (2), followed by reacting with *tert*-butyldimethylsilyl chloride in the presence of triethylamine in dichloromethane to give 2-(*tert*-butyldimethylsiloxy)-4,5,6,7-tetrahydrothieno[3,2-c]pyridine (3). Alkylation of compound (3) by α -cyclopropylcarbonyl-2-fluorobenzyl bromide (4) in the presence of triethylamine in dichloromethane is carried out to give 2-(*tert*-butyldimethylsiloxy)-5-(α -cyclopropylcarbonyl-2-fluorobenzyl)-4,5,6,7,7a-hexahydrothieno[3,2-c]pyridine (5), followed by acetylation with acetic



Scheme 26 Preparation of prasugrel.

anhydride in the presence of triethylamine as acid acceptor and 4-DMAP as catalyst in tetrahydrofuran to give prasugrel (Scheme 26).

2.1.23 Method 23 [32]

The method describes a process for preparing prasugrel and its high pure intermediates 5,6,7,7a-tetrahydrothieno[3,2-c]pyridin-2(4H)-one *p*-toluenesulfonate or its HCl salt, 1-cyclopropyl-2-fluorobenzyl ketone, α -cyclopropylcarbonyl-2-fluorobenzyl bromide, and OXTP.

For example, 5,6,7,7a-tetrahydrothieno[3,2-c]pyridin-2(4H)-one *p*-toluenesulfonate or its HCl salt in addition to its organosilicon derivative are prepared by reacting 2-triphenylethylamine (1) with *p*-formaldehyde in dichloromethane, followed by salt formation with HCl in dimethylformamide to give 4,5,6,7-tetrahydrothieno[3,2-c]pyridine HCl (2). The later compound is reacted with trityl chloride in the presence of triethylamine in dichloromethane to give 5-trityl-4,5,6,7-tetrahydrothieno[3,2-c]pyridine (3), followed by reaction with *n*-butyl lithium, trimethyl borate, and then treatment with hydrogen peroxide in a mixture of tetrahydrofuran and toluene to give 5-trityl-5,6,7,7a-tetrahydrothieno[3,2-c]pyridin-2(4H)-one (4). The later compound is reacted with TsOH in tetrahydrofuran or HCl in acetone to give 5,6,7,7a-tetrahydrothieno[3,2-c]pyridin-2(4H)-one *p*-toluenesulfonate or

HCl salts (**5**), respectively, followed by reaction with *tert*-butyldimethylsilyl chloride in the presence of triethylamine in dichloromethane to give 2-(*tert*-butyldimethylsiloxy)-4,5,6,7-tetrahydrothieno[3,2-*c*]pyridine (**6**). Alkylation of the later compound with α -cyclopropylcarbonyl-2-fluorobenzyl bromide (**7**) in the presence of triethylamine in dichloromethane gives 2-(*tert*-butyldimethylsiloxy)-5-(α -cyclopropylcarbonyl-2-fluorobenzyl)-4,5,6,7,7*a*-hexahydrothieno[3,2-*c*]pyridine (**8**), followed by reaction with HCl in ethyl acetate to give OXTP (**9**). Acetylation of the later compound (**9**) by acetyl chloride in a mixture of toluene and acetic acid or by acetic anhydride in acetic acid, followed by reaction with HCl in diisopropyl ether to give prasugrel HCl (Scheme 27).

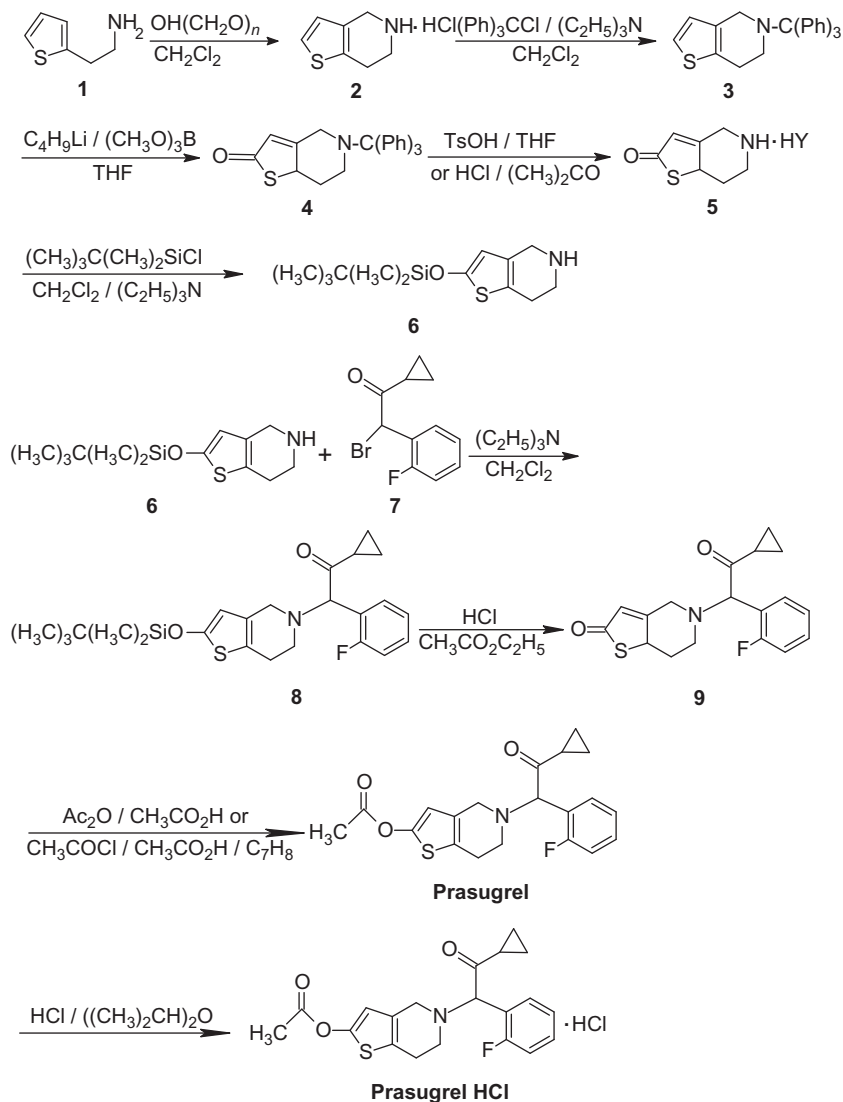
An alternative method to prepare compound (**9**) (Scheme 27) and prasugrel can be achieved by reacting 5,6,7,7*a*-tetrahydrothieno[3,2-*c*]pyridin-2(4*H*)-one HCl (**5**) (Scheme 27) with α -cyclopropylcarbonyl-2-fluorobenzyl bromide (**7**) (Scheme 27) in the presence of ammonium bicarbonate in dichloromethane to give OXTP (**9**) (Scheme 27), followed by acetylation with acetyl chloride in a mixture of toluene and acetic acid to give prasugrel.

Furthermore, 1-cyclopropyl-2-fluorobenzyl ketone and α -cyclopropylcarbonyl-2-fluorobenzyl bromide (**7**) (Scheme 27) are prepared by reacting 2-fluorobenzyl chloride (**1**) with sodium cyanide in the presence of tetrabutyl ammonium bromide in a mixture of dichloromethane and water to give 2-fluorobenzyl cyanide (**2**), followed by hydrolysis in water in the presence of NaOH to give 2-fluorophenyl acetic acid (**3**). The later compound is reacted with methyl cyclopropyl carboxylate (**4**) in the presence of Grignard reagent (prepared from isopropyl bromide and suspension of magnesium in tetrahydrofuran) in toluene to give 1-cyclopropyl-2-fluorobenzyl ketone (**5**), followed by bromination with NBS in the presence of benzoyl peroxide in dichloromethane, ethyl acetate, or a mixture of dichloromethane and ethyl acetate to give the desired compound (Scheme 28).

2.1.24 Method 24 [33]

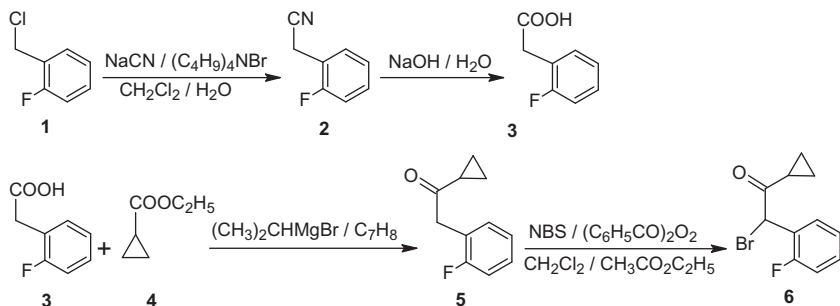
The method describes a process for preparing prasugrel by hydrolysis a crude prasugrel, adding activated carbon for adsorption and purification, and then carrying out esterification under the catalysis of strong acid salt to obtain a highly pure prasugrel.

For example, a crude prasugrel dispersed in water and NaOH solution as a catalyst is added, followed by heating at 70 °C with stirring to

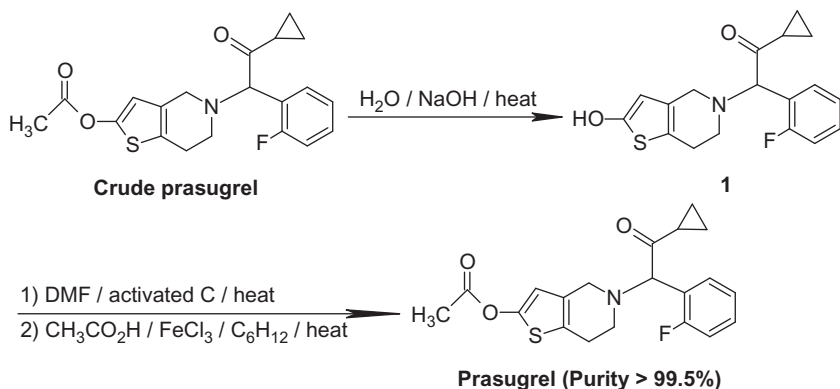


Scheme 27 Preparation of 5,6,7,7a-tetrahydrothieno[3,2-c]pyridin-2(4H)-one *p*-toluenesulfonate or its HCl salt (**5**) and 5-(2-(cyclopropyl-1-(2-fluorophenyl)-2-oxoethyl)-5,6,7,7a-tetrahydrothieno[3,2-c]pyridine-2(4H)-one (**9**) and prasugrel HCl. HY is *p*-toluenesulfonic or HCl acid.

give 2-hydroxy-5-(α -cyclopropylcarbonyl-2-fluorobenzyl)-2,4,5,6,7,7a-hexahydrothieno[3,2-c]pyridine (**1**) as a solid precipitate. The later compound is dissolved in dimethylformamide, followed by addition of carbon, heating at 80 °C with stirring and then filtration. Acetic acid is added to the filtrate and then ferric chloride as a catalyst and cyclohexane as a water



Scheme 28 Preparation of 1-cyclopropyl-2-fluorobenzyl ketone (5) and α -cyclopropylcarbonyl-2-fluorobenzyl bromide (7) (Scheme 27).



Scheme 29 Preparation of highly pure prasugrel (>99.5%).

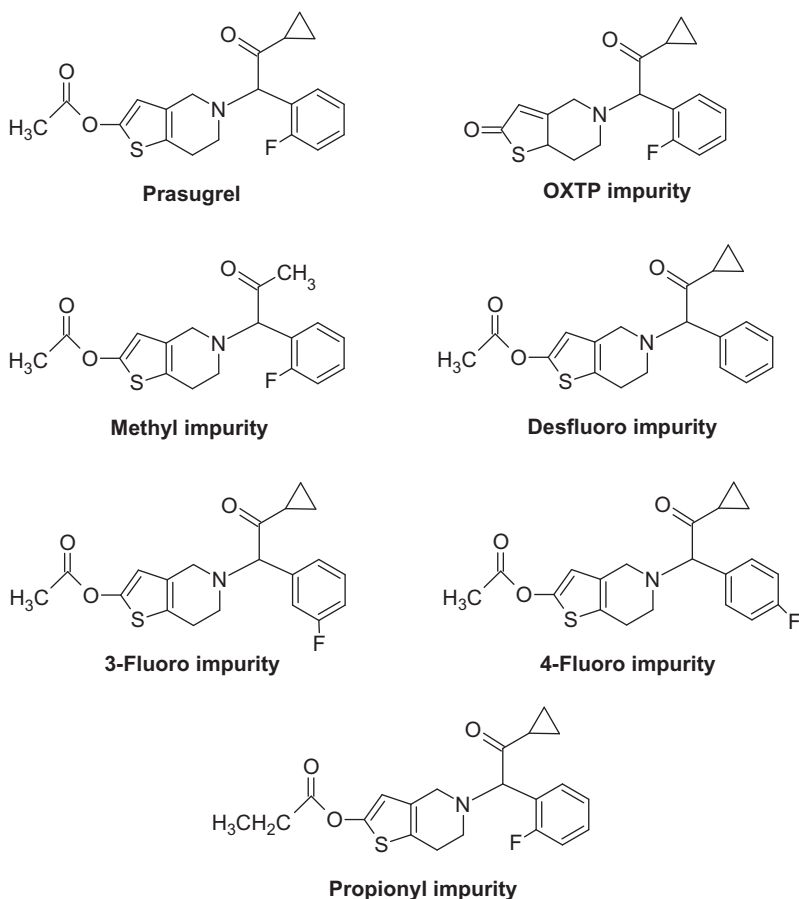
carrier. The solution is heated at 40 °C with stirring and then the filtrate is dried under vacuum to remove dimethylformamide at 60 °C to give a highly pure prasugrel (Yield >90%, purity >99.5%) (Scheme 29).

2.1.25 Method 25 [34]

The method describes a process for preparing prasugrel having a low content of impurities by purification of the starting material 2-fluorophenyl acetic acid, which is a precursor to prepare the prasugrel intermediate α -cyclopropylcarbonyl-2-fluorobenzyl bromide.

Different types of impurities may exist in prasugrel including unreacted starting materials, by-products and intermediates. Some of these impurities are 5-(2-cyclopropyl-1-(2-fluorophenyl)-2-oxoethyl)-5,6,7,7a-tetrahydrothieno[3,2-c]pyridin-2(4H)-one (OXT[®]), 5-[(1*RS*)-2-methyl-1-(2-fluorophenyl)-2-oxoethyl]-4,5,6,7-tetrahydrothieno[3,2-c]pyridin-2-yl

acetate (**Methyl impurity**), 5-[(1*RS*)-2-cyclopropyl-2-oxo-1-phenylethyl]-4,5,6,7-tetrahydrothieno[3,2-*c*]pyridin-2-yl acetate (**Desfluoro impurity**), 5-[(1*RS*)-2-cyclopropyl-1-(3-fluorophenyl)-2-oxoethyl]-4,5,6,7-tetrahydrothieno[3,2-*c*]pyridin-2-yl acetate (**3-Fluoro impurity**), 5-[(1*RS*)-2-cyclopropyl-1-(4-fluorophenyl)-2-oxoethyl]-4,5,6,7-tetrahydrothieno[3,2-*c*]pyridin-2-yl acetate (**4-Fluoro impurity**), 5-[(1*RS*)-2-cyclopropyl-1-(2-fluorophenyl)-2-oxoethyl]-4,5,6,7-tetrahydrothieno[3,2-*c*]pyridin-2-yl propionate (**Propionyl impurity**) (Scheme 30). These impurities are monitored in this preparation to be less than 0.1%.

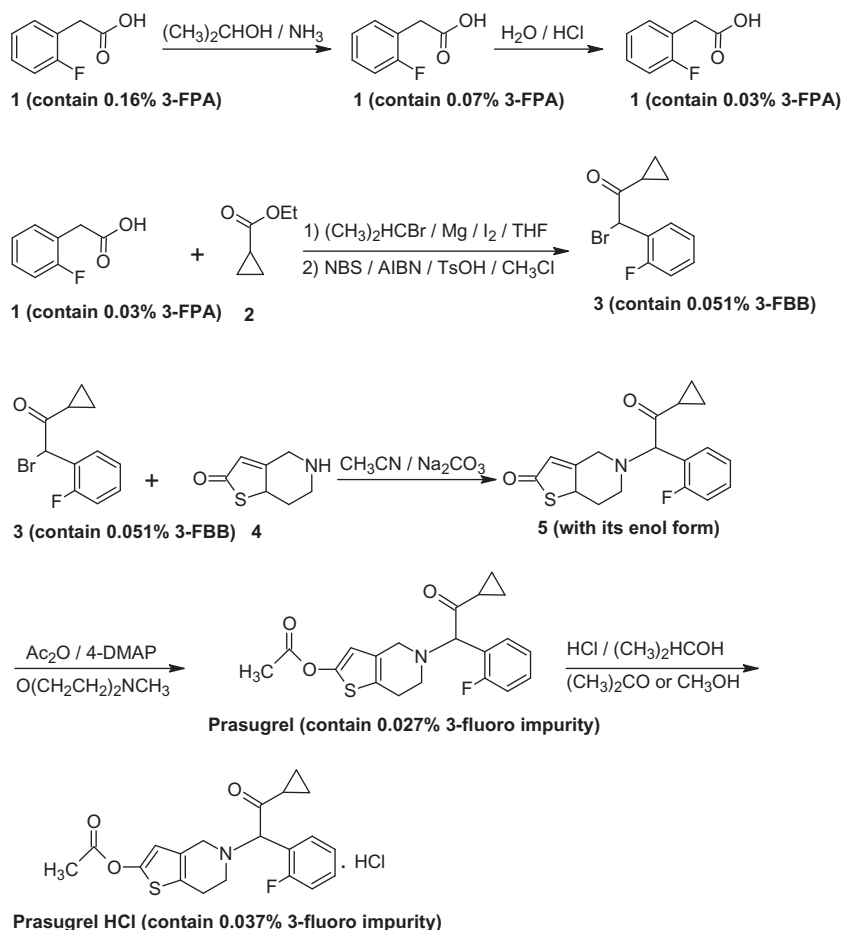


Scheme 30 Prasugrel potential impurities.

For example, a highly pure prasugrel can be prepared as follows. 2-Fluorophenyl acetic acid (**1**) containing 0.16% 3-fluorophenyl acetic acid (3-FPA) impurity is purified by isopropanol and ammonia gas to adjust the pH in the range of 8 to 9. The reaction mass is cooled, filtered, washed with chilled isopropanol, and then dried under vacuum to give 2-fluorophenyl acetic acid with a purity of 99.93% and containing 0.07% 3-FPA as ammonium salt impurity. Further purification by dispersion in water is carried out, followed by addition of concentrated HCl. The solid is collected by filtration, washed with water, and then dried under vacuum to obtain a highly pure 2-fluorophenyl acetic acid (**1**) with a purity of 99.97% and containing 0.03% 3-FPA impurity. Compound (**1**) is then reacted with ethyl cyclopropane carboxylate (**2**) in the presence of magnesium turnings, iodine, and isopropyl bromide in tetrahydrofuran, followed by bromination with NBS in the presence of AIBN and TsOH in chloroform to give α -cyclopropylcarbonyl-2-fluorobenzyl bromide (**3**) containing 0.051% α -cyclopropylcarbonyl-3-fluorobenzyl bromide (3-FBB) impurity. Compound (**3**) is reacted with 5,6,7,7a-tetrahydrothieno[3,2-c]pyridin-2(4H)-one (**4**) in the presence of sodium carbonate, *N*-methylmorpholine and 4-DMAP in acetonitrile to give OXTP (**5**), followed by acetylation with acetic anhydride to give prasugrel with 99.57% purity and containing 0.027% 3-fluoro impurity. Prasugrel HCl is prepared by dissolving prasugrel in organic solvent such as acetone, methylethyl ketone, or methanol, followed by reaction with HCl in isopropanol (Scheme 31).

Alternatively, prasugrel HCl can be prepared by reacting 5,6,7,7a-tetrahydrothieno[3,2-c]pyridin-2(4H)-one HCl (**1**) with *tert*-butyldimethylsilyl chloride in the presence of triethylamine in dichloromethane to give 2-(*tert*-butyldimethylsiloxy)-4,5,6,7-tetrahydrothieno[3,2-c]pyridine (**2**), followed by alkylation of the later compound with α -cyclopropylcarbonyl-2-fluorobenzyl bromide (**3**) in the presence of sodium iodide and triethylamine in dichloromethane to give 2-(*tert*-butyldimethylsiloxy)-5-(α -cyclopropylcarbonyl-2-fluorobenzyl)-4,5,6,7,7a-hexahydrothieno[3,2-c]pyridine (**4**). The later compound is treated with triethylamine in the presence of 4-DMAP in acetonitrile to give OXTP (**5**). Acetylation of compound (**5**) by acetyl anhydride in acetonitrile gives prasugrel. Prasugrel HCl is prepared by dissolving prasugrel in organic solvent such as acetone, methylethyl ketone, or methanol, followed by reacting with HCl in isopropyl alcohol to give prasugrel HCl (Scheme 32).

Pure prasugrel can be prepared by dissolving it at 50 °C in acetonitrile and cooling to 1 °C, followed by addition of water. The solid is then filtered,



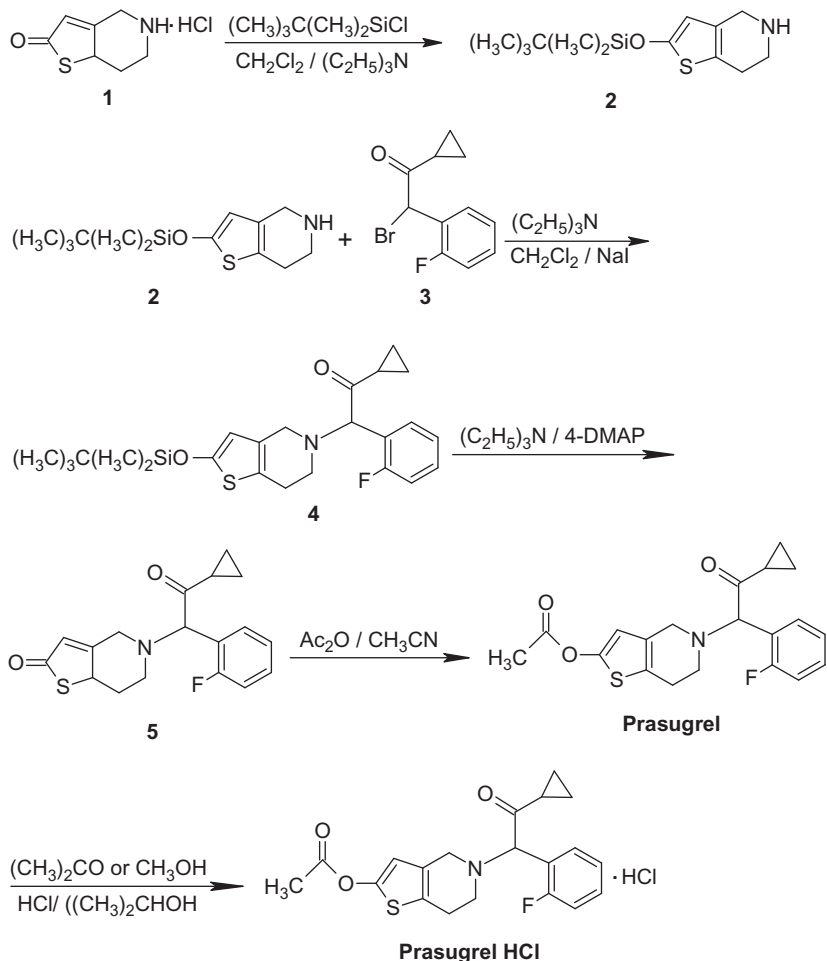
Scheme 31 Preparation of prasugrel HCl containing 0.037% of 3-fluoro impurity.

washed with mixture of acetonitrile and water, and dried under vacuum at 60 °C to yield prasugrel with 99.88% purity containing 0.03% 3-fluoro impurity.

2.1.26 Method 26 [35]

The method describes a process for preparing prasugrel.

For example, 2-fluorobenzaldehyde (**1**) is reacted with cyclopropylmethyl triphenylphosphonium bromide (**2**) in the presence of sodium *tert*-butoxide in tetrahydrofuran to give 1-cyclopropyl-2-fluorobenzyl ethane (**3**). The resulting compound (**3**) is reacted with H_2O_2 in the presence of NaOH in methanol to give 1-cyclopropyl-2-fluorobenzyl epoxyethane (**4**), followed by reaction with 5,6,7,8-tetrahydrothieno[3,2-*c*]pyridin-2(4*H*)-one (**5**) in

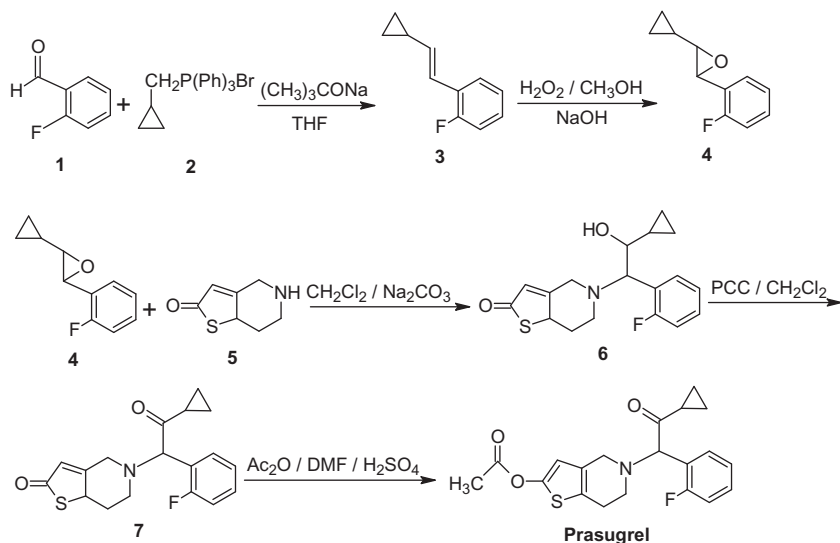


Scheme 32 Preparation of prasugrel HCl.

the presence of K_2CO_3 in dichloromethane to give 5-(2-cyclopropyl-1-(2-fluorophenyl)-2-hydroxyethyl)-5,6,7,7a-tetrahydrothieno[3,2-c]pyridine-2(4H)-one (**6**). Oxidation of compound (**6**) by pyridinium chlorochromate in dichloromethane to give OXTP (**7**), followed by acetylation with acetic anhydride in the presence of H_2SO_4 in dimethylformamide to give prasugrel (**Scheme 33**).

2.1.27 Method 27 [36]

The method describes a process to prepare 5,6,7,7a-tetrahydrothieno[3,2-c]pyridin-2(4H)-one *p*-toluenesulfonate. Furthermore, it offers a process for preparing prasugrel whereby the content of impurities is reduced. It also

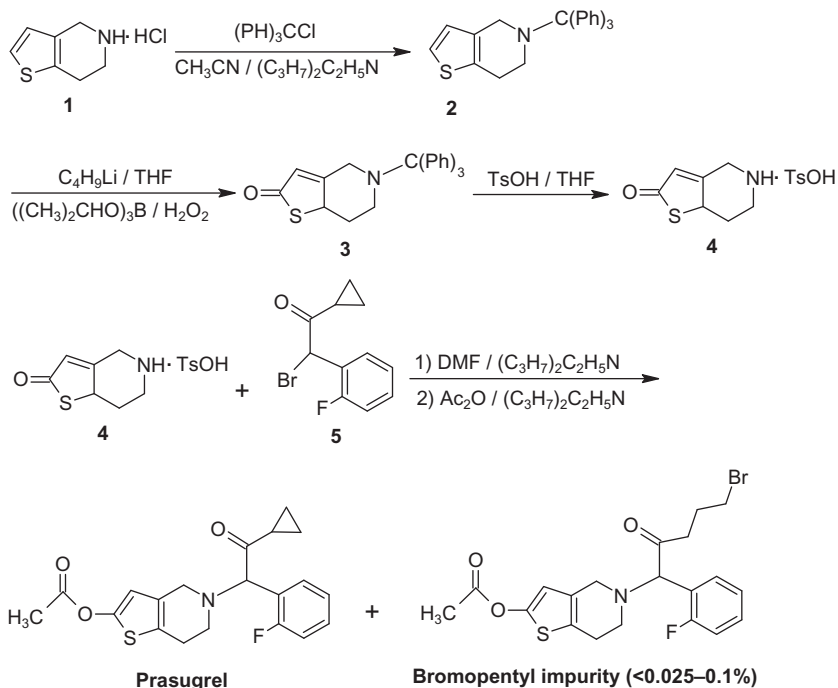


Scheme 33 Preparation of prasugrel.

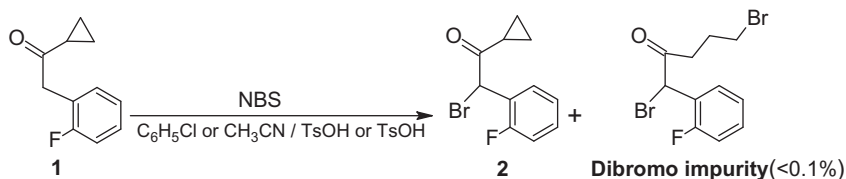
offers a process to prepare the intermediates α -cyclopropylcarbonyl-2-fluorobenzyl halide (halide is Br or Cl) without a radical initiator such as an elemental halogen, an organic peroxide, or AIBN.

For example, reaction of 4,5,6,7-tetrahydrothieno[3,2-*c*]pyridine HCl (1) with trityl chloride in the presence of diisopropylethylamine in acetonitrile gives 5-trityl-4,5,6,7-tetrahydrothieno[3,2-*c*]pyridine (2). The later compound is then reacted with *n*-butyl lithium, tri-isopropyl borate, and hydrogen peroxide in tetrahydrofuran to give 5-trityl-5,6,7,7a-tetrahydrothieno[3,2-*c*]pyridin-2(4*H*)-one (3). The later compound is reacted with TsOH in tetrahydrofuran to give 5,6,7,7a-tetrahydro-4*H*-thieno[3,2-*c*]pyridine-2-one *p*-toluenesulfonate (4). Prasugrel is prepared by reacting compound (4) with α -cyclopropylcarbonyl-2-fluorobenzyl bromide (5) and then with acetic anhydride in the presence of diisopropylethylamine in dimethylformamide to give prasugrel containing <0.025–0.1% 5-(5-bromo-1-(2-fluorophenyl)-2-oxopentyl)-4,5,6,7-tetrahydrothieno[3,2-*c*]pyridin-2-yl-acetate (bromopentyl impurity) (Scheme 34).

α -Cyclopropylcarbonyl-2-fluorobenzyl bromide (5) (Scheme 34) is prepared by bromination of 1-cyclopropyl-2-fluorobenzyl ketone (1) by NBS in different solvents such as chlorobenzene, acetonitrile containing TsOH or only in the presence TsOH to produce α -cyclopropylcarbonyl-2-fluorobenzyl



Scheme 34 Preparation of prasugrel containing <0.025–0.1% bromopentyl impurity.

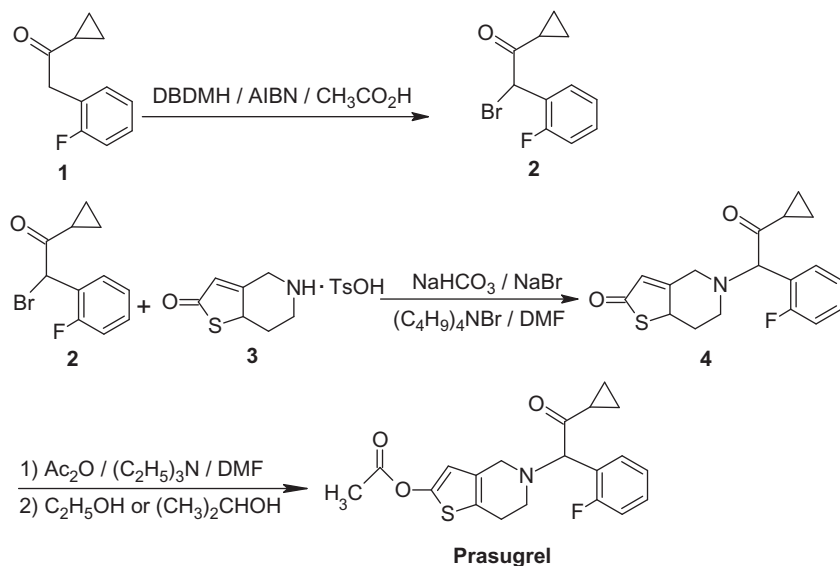


Scheme 35 Preparation of α -cyclopropylcarbonyl-2-fluorobenzyl bromide (**5**) (Scheme 34) containing <0.1 of dibromo impurity.

bromide (**2**) containing <0.1% 1,5-dibromo-1-(2-fluorophenyl)-2-pentanone (dibromo impurity) (Scheme 35).

2.1.28 Method 28 [37]

The method describes a process for preparing prasugrel by converting 1-cyclopropyl-2-fluorobenzyl ketone into α -cyclopropylcarbonyl-2-fluorobenzyl halide (halide is Br or Cl) using 1,3-dihalo-5,5-dimethylhydantoin as the halogenating reagent and acetic acid as the solvent.



Scheme 36 Preparation of prasugrel.

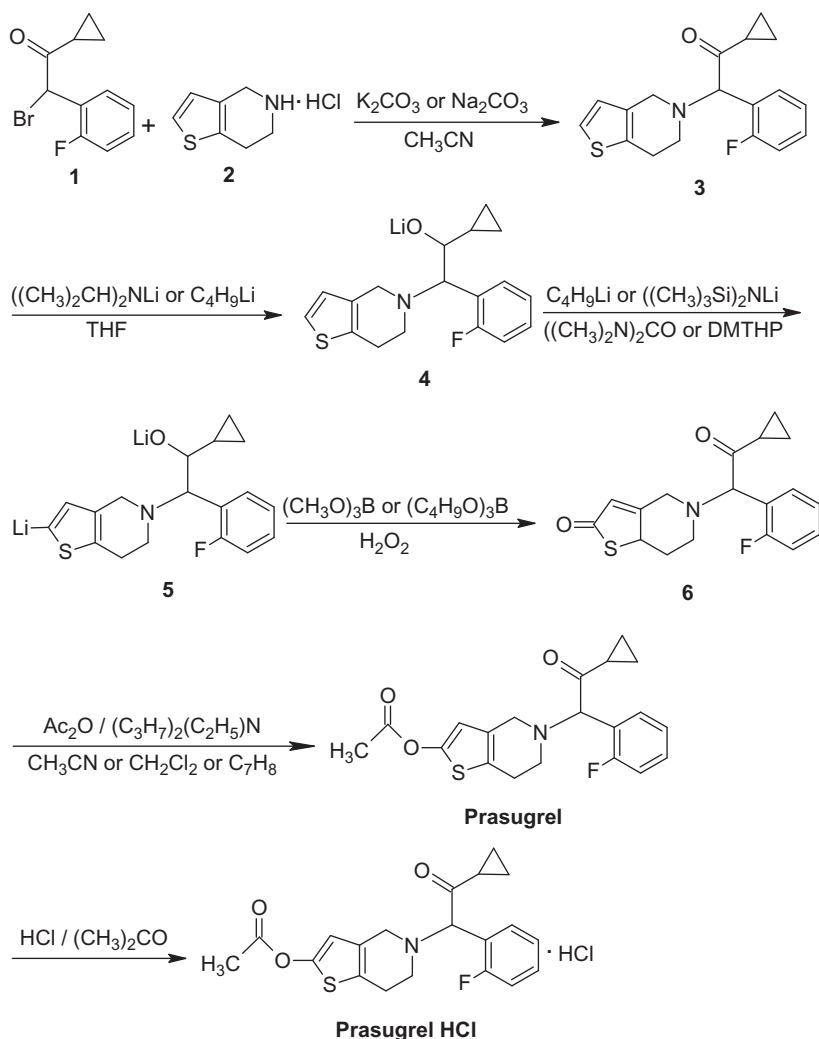
For example, 1-cyclopropyl-2-fluorobenzyl ketone (**1**) is halogenated by 1,3-dibromo-5,5-dimethylhydantoin (DBDMH) in the presence of AIBN in acetic acid to give α -cyclopropylcarbonyl-2-fluorobenzyl bromide (**2**), followed by reaction with 5,6,7,7a-tetrahydro-4H-thieno[3,2-c]pyridine-2-one *p*-toluenesulfonate (**3**) in the presence of sodium bicarbonate, sodium bromide, tetrabutylammonium bromide in dimethylformamide to give OXTP (**4**). Acetylation of compound (**4**) is carried out by acetyl anhydride in the presence of triethylamine in dimethylformamide to give prasugrel. The later is purified by alcohol such as ethanol or isopropanol to give pure prasugrel (Scheme 36).

2.1.29 Method 29 [38]

The method describes a process for preparing prasugrel and its intermediates.

For example, α -cyclopropylcarbonyl-2-fluorobenzyl bromide (**1**) is reacted with 4,5,6,7-tetrahydrothieno[3,2-c]pyridine HCl (**2**) in the presence of a base such as potassium carbonate or sodium carbonate in acetonitrile to give 5-(2-cyclopropyl-1-(2-fluorophenyl)-2-oxoethyl)-5,6,7,7a-tetrahydrothieno[3,2-c]pyridine (**3**). The later compound is reacted with lithium diisopropylamide or *n*-butyllithium in tetrahydrofuran to give mono-lithium salt derivative (**4**) and then with *n*-butyllithium or lithium hexamethyldisilazide in the absence or presence of tetramethylurea or

1,3-dimethyl-3,4,5,6-tetrahydro-2(1*H*)-pyrimidinone to give di-lithium salt derivative (**5**), followed by oxidation with H_2O_2 in the presence of trimethyl borate or tri-*n*-butyl borate to give OXTP (**6**). Acetylation of compound (**6**) or its HBr salt with acetic anhydride is carried out in the absence or presence of diisopropylethylamine in acetonitrile, dichloromethane, or toluene to give prasugrel, followed by reaction with HCl in acetone to give prasugrel HCl (Scheme 37).



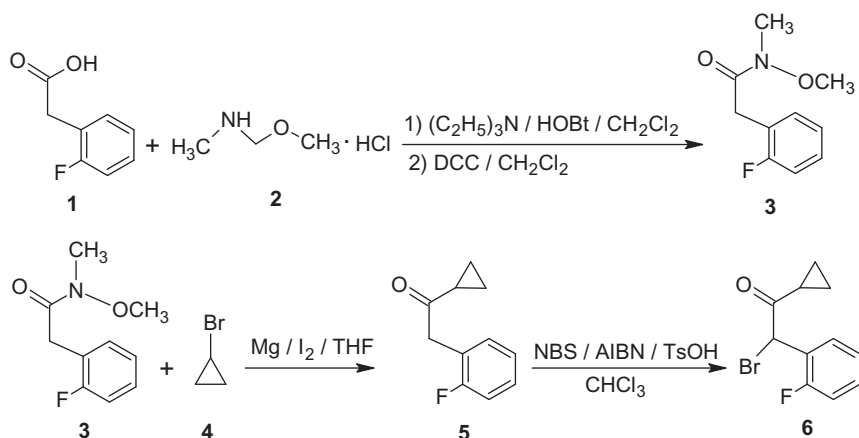
Scheme 37 Preparation of prasugrel HCl.

Another method is offered to prepare prasugrel, which is similar to what is described in [Section 4.1.27 \(Scheme 34\)](#), but using different chemicals and solvents.

Purification of 4,5,6,7-tetrahydrothieno[3,2-*c*]pyridine HCl (**2**) ([Scheme 37](#)) is carried out by recrystallization from a mixture of methanol and dichloromethane and 5,6,7,7*a*-tetrahydro-4*H*-thieno[3,2-*c*]pyridine-2-one HCl (**3**) in [Section 4.1.27 \(Scheme 34\)](#) from a mixture of methanol, dichloromethane, and dimethylformamide to give pure compounds.

α -Cyclopropylcarbonyl-2-fluorobenzyl bromide (**1**) ([Scheme 37](#)) is prepared by reacting 2-fluorophenyl acetic acid (**1**) with *N,O*-dimethyl hydroxylamine HCl (**2**) in the presence of triethylamine and 1-hydroxybenzotriazole in dichloromethane, followed by treatment with dicyclohexylcarbodiimide in dichloromethane to give 2-(2-fluorophenyl)-*N*-methoxy-*N*-methylacetamide (**3**). The later compound is reacted with cyclopropyl bromide (**4**) in the presence of magnesium powder and iodine in tetrahydrofuran to give 1-cyclopropyl-2-fluorobenzyl ketone (**5**), followed by bromination with NBS in the presence of AIBN and TsOH in chloroform to give the desired compound ([Scheme 38](#)).

Purification of 1-cyclopropyl-2-fluorobenzyl ketone (**5**) ([Scheme 38](#)) is carried out by fraction distillation of crude 1-cyclopropyl-2-fluorobenzyl ketone (having purity of 93.41% and containing 3.73% of 1-methyl-2-fluorobenzyl ketone) prepared as per the reported process to give a purity of 98.53% and 1-methyl-2-fluorobenzyl ketone of 0.02%. Such purification gives pure prasugrel HCl with low content of methyl impurity (<0.1%) mentioned in [Section 4.1.25 \(Scheme 30\)](#).



Scheme 38 Preparation of α -cyclopropylcarbonyl-2-fluorobenzyl bromide (**1**) ([Scheme 37](#)).

2.1.30 Method 30 [39]

The method describes a process for preparing prasugrel intermediate 2-(2-fluorophenyl)-2-(2-RO-6,7-dihydrothieno[3,2-*c*]pyridin-5(4*H*)-yl)acetonitrile, where R is alkyl or silyl group.

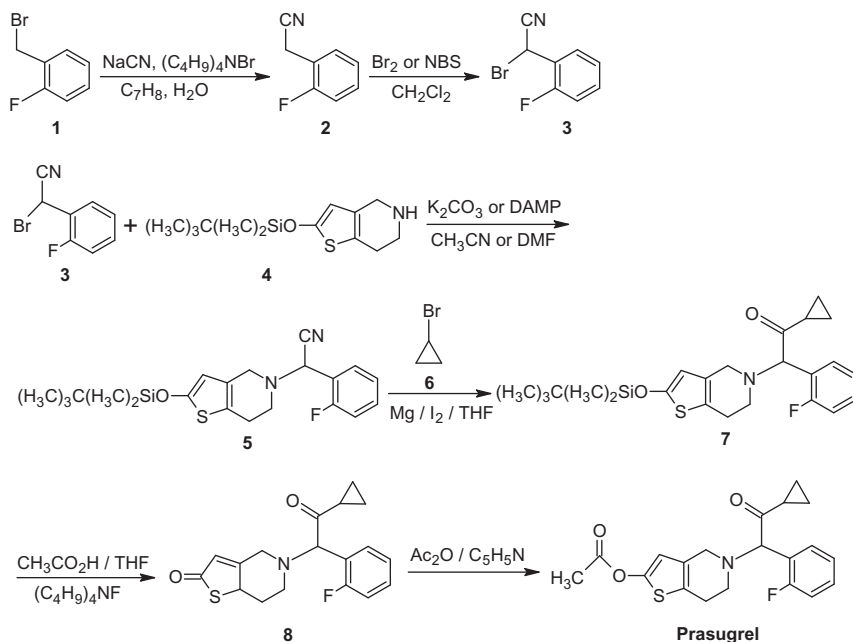
For example, 2-fluorobenzyl bromide (**1**) is reacted with sodium cyanide in the presence of *tert*-butylammonium bromide in a mixture of toluene and water to give 2-fluorobenzyl cyanide (**2**), followed by bromination with bromine or NBS in dichloromethane to give 2-bromo-2(2-fluorophenyl)acetonitrile (**3**). The later compound is reacted with 2-(*tert*-butyldimethylsiloxy)-4,5,6,7-tetrahydrothieno[3,2-*c*]pyridine (**4**) in the presence of anhydrous potassium carbonate or 1,3-pentanediamine in acetonitrile or dimethylformamide to give 2-(2-fluorophenyl)-2-(*tert*-butyldimethylsiloxy)-6,7-dihydrothieno[3,2-*c*]pyridin-5(4*H*)-yl)acetonitrile (**5**), followed by reaction with cyclopropyl bromide (**6**) in the presence of magnesium powder and iodine in tetrahydrofuran to give 2-(*tert*-butyldimethylsiloxy)-5-(α -cyclopropylcarbonyl-2-fluorobenzyl)-4,5,6,7,7*a*-hexahydrothieno[3,2-*c*]pyridine (**7**). The later compound is treated with acetic acid, followed by tetrabutylammonium fluoride in tetrahydrofuran to give OXTP (**8**). Acetylation of compound (**8**) is carried out with acetic anhydride in the presence of pyridine to give prasugrel (Scheme 39).

2-(*Tert*-butyldimethylsiloxy)-4,5,6,7-tetrahydrothieno[3,2-*c*]pyridine (**4**) (Scheme 39) is prepared by reacting 5,6,7,7*a*-tetrahydrothieno[3,2-*c*]pyridin-2(4*H*)-one HCl (**1**) with *tert*-butyldimethylsilyl chloride in the presence of triethylamine, pyridine, or 4-DMAP in dichloromethane to give the desired compound (Scheme 40).

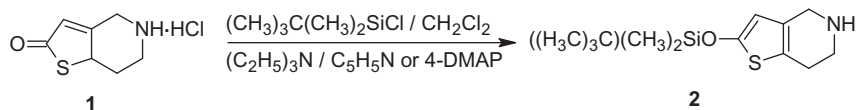
2.1.31 Method 31 [40]

The method describes a process for preparing prasugrel.

2-Bromo-2-(2-fluorophenyl)acetonitrile (**1**) is reacted with 2-methoxy-4,5,6,7-tetrahydrothieno[3,2-*c*]pyridine (**2**) in the presence of potassium carbonate in ethanol to give 2-(2-fluorophenyl)-2-methoxy-6,7-dihydrothieno[3,2-*c*]pyridin-5(4*H*)-yl)acetonitrile (**3**), followed by reaction with cyclopropyl-magnesium bromide (**4**) in tetrahydrofuran to give 2-methoxy-5-(α -cyclopropylcarbonyl-2-fluorobenzyl)-4,5,6,7,7*a*-hexahydrothieno[3,2-*c*]pyridine (**5**). The later compound is treated HCl in water to give 2-cyclopropyl-1-(2-fluorophenyl)-2-oxoethyl]-5,6,7,7*a*-tetrahydrothieno[3,2-*c*]pyridine-2(4*H*)-one (**6**). Acetylation of compound (**6**) with acetic anhydride is then carried out in the presence of sodium hydride in dimethylformamide to give prasugrel (Scheme 41).



Scheme 39 Preparation of prasugrel.

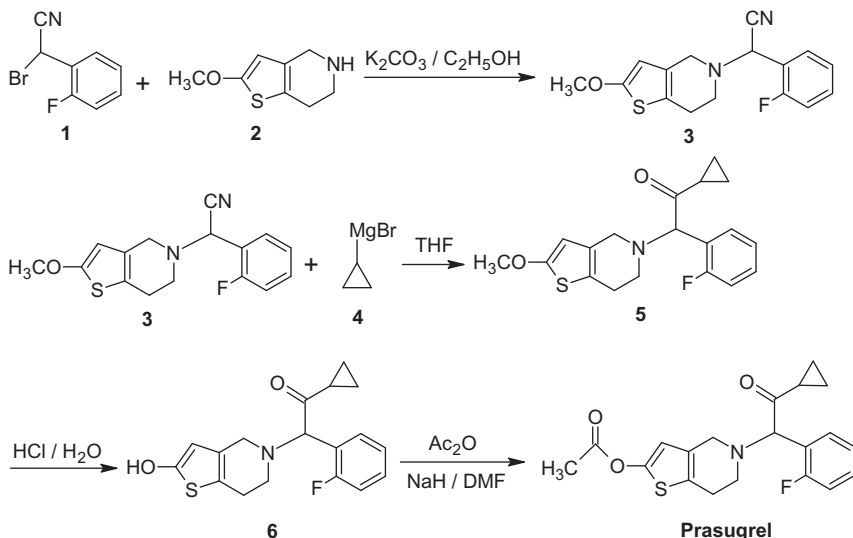


Scheme 40 Preparation of 2-(*tert*-butyldimethylsiloxy)-4,5,6,7-tetrahydrothieno[3,2-*c*]pyridine (**4**) (Scheme 39).

The 2-bromo-2-(2-fluorophenyl)acetonitrile (**1**) is prepared following the same procedure in Section 4.1.30 (Scheme 39) and the 2-methoxy-4,5,6,7-tetrahydrothieno[3,2-*c*]pyridine (**2**) is prepared following almost the same procedure in Section 4.1.4 (Scheme 6), but using tetrabutylammonium sulfate in the first step to assess the N-protection by benzyl group, whereas methylchloroformate and KOH to assess the de-protection of *N*-benzyl moiety.

2.1.32 Method 32 [41]

The method describes a process for preparing prasugrel using 1-cyclopropyl-2-(2-fluorophenyl)-2-*R*¹sulfonyl-ethanone and 2-*R*²-



Scheme 41 Preparation of prasugrel.

4,5,6,7-tetrahydrothieno[3,2-*c*]pyridine, where R^1 represents an alkyl group or an aryl group and R^2 represents an alkyl group.

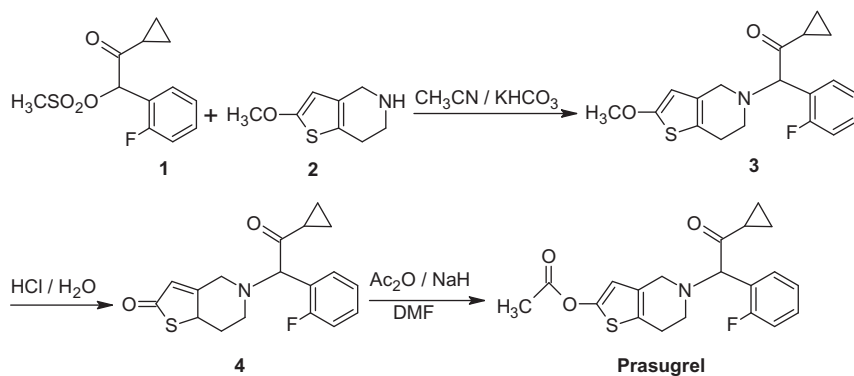
For example, 1-cyclopropyl-2-(2-fluorophenyl)-2-methanesulfonyl-ethanone (1) is reacted with 2-methoxy-4,5,6,7-tetrahydrothieno[3,2-*c*]pyridine (2) in the presence of potassium bicarbonate in acetonitrile to give 2-methoxy-5-(α -cyclopropylcarbonyl-2-fluorobenzyl)-4,5,6,7,7a-hexahydrothieno[3,2-*c*]pyridine (3), followed by reaction with HCl in water to give OXTP (4). Acetylation of compound (4) with acetic anhydride in the presence of sodium hydride in dimethylformamide gives prasugrel (Scheme 42).

1-Cyclopropyl-2-(2-fluorophenyl)-2-methanesulfonyl-ethanone (1) (Scheme 42) is prepared following the same procedure in Section 4.1.5 (Scheme 7).

2.1.33 Method 33 [42]

The method describes a process for preparing prasugrel intermediate 5-(α -cyclopropylcarbonyl-2-fluorobenzyl)-4,5,6,7,7a-hexahydrothieno[3,2-*c*]pyridine-2-boronic acid, which can be used to prepare prasugrel.

For example, 4,5,6,7-tetrahydrothieno[3,2-*c*]pyridine HCl (1) is reacted with trityl chloride in the presence of triethylamine in dichloromethane



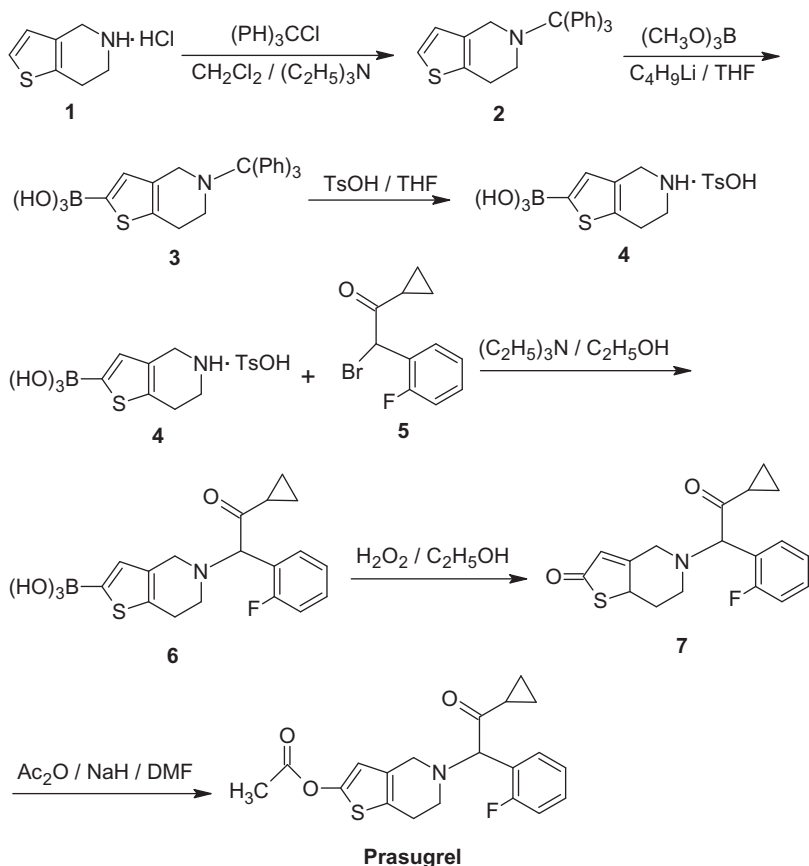
Scheme 42 Preparation of prasugrel.

to give 5-trityl-4,5,6,7-tetrahydrothieno[3,2-*c*]pyridine (**2**), followed by reaction with trimethyl borate in the presence of *n*-butyl lithium in tetrahydrofuran to give 5-trityl-4,5,6,7-tetrahydrothieno[3,2-*c*]pyridine-2-boronic acid (**3**). The later compound is N-deprotected by TsOH in tetrahydrofuran to give 5,6,7,7*a*-tetrahydrothieno[3,2-*c*]pyridin-2-boronic acid *p*-toluenesulfonate (**4**), followed by coupling with α -cyclopropylcarbonyl-2-fluorobenzyl bromide (**5**) in the presence of triethylamine in ethanol to give 5-(α -cyclopropylcarbonyl-2-fluorobenzyl)-4,5,6,7,7*a*-hexahydrothieno[3,2-*c*]pyridine-2-boronic acid (**6**). The later compound is reacted with hydrogen peroxide in ethanol to give OXTP (**7**). Prasugrel is prepared by reacting compound (**7**) with acetic anhydride in the presence of sodium hydride in dimethylformamide to give prasugrel (Scheme 43).

2.1.34 Method 34 [43]

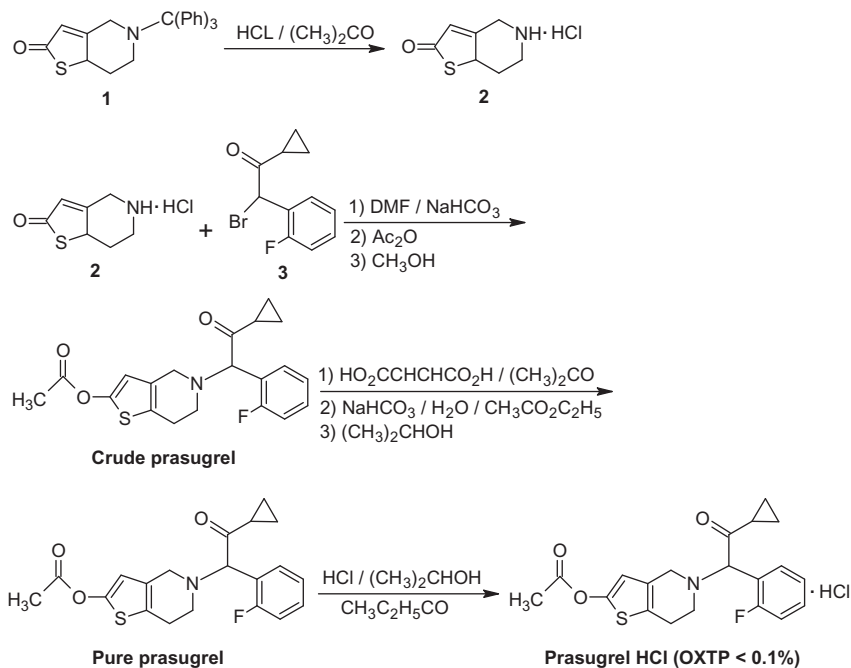
The method describes a process for preparing pure prasugrel HCl.

5-Trityl-5,6,7,7a-tetrahydrothieno[3,2-c]pyridin-2(4*H*)-one (**1**) is reacted with HCl in acetone to give 5,6,7,7a-tetrahydrothieno[3,2-c]pyridin-2(4*H*)-one HCl (**2**). Coupling of compound (**2**) with α -cyclopropylcarbonyl-2-fluorobenzyl bromide (**3**) in the presence of sodium bicarbonate in dimethylformamide, followed by reaction with acetic anhydride in dimethylformamide and then the obtained solid is treated with methanol to give crude prasugrel. Purification is done by converting prasugrel to its maleate salt in acetone, followed by precipitating prasugrel by sodium



Scheme 43 Preparation of prasugrel.

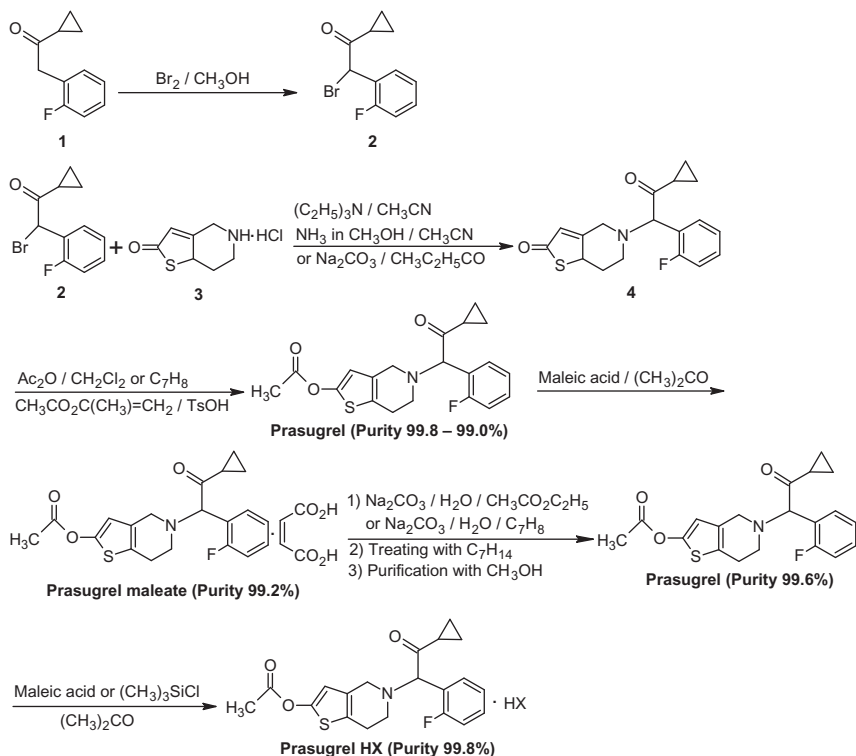
bicarbonate in water, extraction by ethyl acetate, and dried to give solid prasugrel, which is then treated with isopropanol to give pure prasugrel. Preparation of prasugrel HCl is carried out by dissolving pure prasugrel in methylethyl ketone, stirred at room temperature and filtered. HCl solution in isopropanol, prepared by purging with HCl gas in isopropanol, is added to the filtrate, heated up to 35–40 °C. The reaction mixture is maintained at 35–40 °C to obtain solid. The solid is filtered and washed with methylethyl ketone and dried in tray dryer at 50–55 °C under vacuum to obtain prasugrel HCl (Purity >99%) containing <0.1% OXTP impurity (Scheme 44).



Scheme 44 Preparation of prasugrel HCl containing <0.1% OXTIP impurity.

2.1.35 Method 35 [44]

α -Cyclopropyl-2-fluorobenzyl ketone (1) is reacted with bromine in methanol to give α -cyclopropylcarbonyl-2-fluorobenzyl bromide (2). Condensation of compound (2) with 5,6,7,8-tetrahydrothieno[3,2-c]pyridin-2 (4*H*)-one HCl (3) in the presence of base (ammonia in methanol, triethylamine or sodium carbonate) in organic solvent (acetonitrile or methyl ethyl ketone) gives OXTIP (4), which is finally reacted with acetic anhydride in the presence of triethylamine in organic solvent (dichloromethane or toluene) or with isopropenyl acetate in the presence of TsOH to yield prasugrel (Purity 99.8–99.0%). The maleate salt of prasugrel with high purity (99.2%) is prepared by reacting prasugrel-free base with maleic acid in acetone. Prasugrel with high purity (99.6%) is prepared by reacting prasugrel maleate with sodium carbonate in an extraction mixture (water and ethylacetate or water and toluene), collecting the organic layer and then drying is carried out. The residue is mixed with methyl cyclohexane, filtered, and washed with methanol. Also pure prasugrel is prepared by purification of crude prasugrel with methanol. Pure maleate (99.8%) and



Scheme 45 Preparation of prasugrel and its maleate and HCl salts. HX is maleic acid or HCl.

HCl (99.8%) salts of prasugrel are prepared by reacting pure prasugrel with maleic acid or trimethylsilyl chloride, respectively, in acetone (Scheme 45).

2.2 Drug Intermediates and Its Acid Salts

2.2.1 Method 1 [45,46]

The method describes preparation of 2-X-5-benzyl-4,5,6,7-tetrahydrothieno[3,2-c]pyridine derivatives, which are intermediates for preparing prasugrel, where X is halo or alkoxyl group.

For example, benzyl chloride (1) is reacted with 4,5,6,7-tetrahydrothieno[3,2-c]pyridine (2) in the presence of potassium carbonate with or without sodium iodide in acetonitrile or dimethylformamide to give 5-benzyl-4,5,6,7-tetrahydrothieno[3,2-c]pyridine (3), which is then brominated by hydrobromic acid in the presence of hydrogen peroxide in a mixture of acetic acid and methanol to give 2-bromo-5-benzyl-4,5,6,7-tetrahydrothieno[3,2-c]pyridine (4). The later compound is reacted

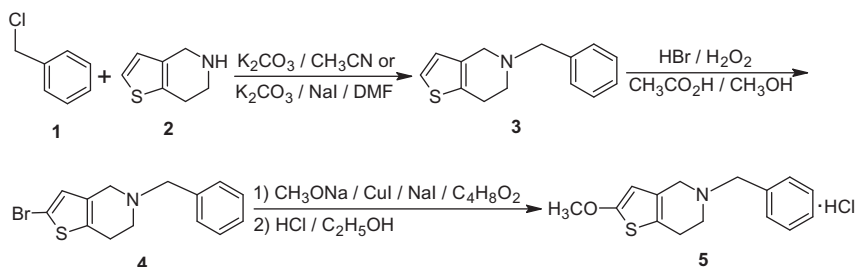
with sodium methoxide in the presence of cuprous bromide and sodium iodide in 1,4-dioxane and then with HCl in ethanol to give 2-methoxy-5-benzyl-4,5,6,7-tetrahydrothieno[3,2-c]pyridine HCl (**5**) (Scheme 46).

2.2.2 Method 2 [47]

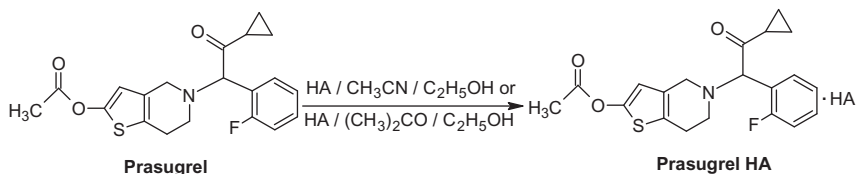
Different organic and inorganic salts of prasugrel are prepared by carrying out reaction between prasugrel base and acids at a molar ratio of 1:(1–2) in a mixture of acetonitrile and ethanol or acetone and ethanol at 0–100 °C for 1–24 h to obtain prasugrel HA salts (HA is selected from organic acids (namely, methanesulfonic, fumaric, acetic, oxalic, succinic, tartaric, salicylic, or acetylsalicylic acid) and inorganic acids (namely, HBr, HI, H₂SO₄, or H₃PO₄ acid) (Scheme 47).

2.2.3 Method 3 [48]

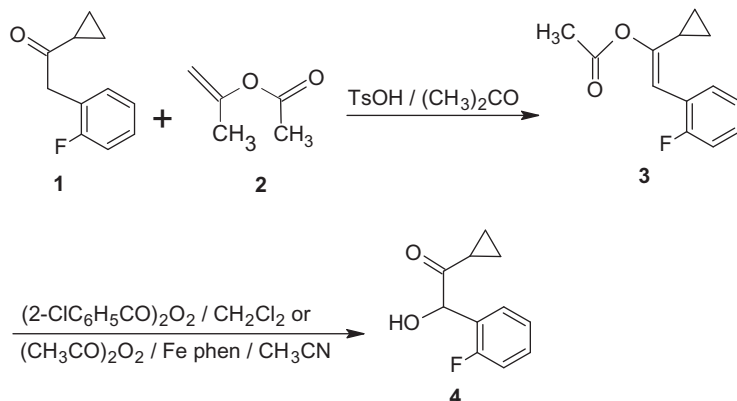
The method describes a process for preparing prasugrel intermediate 1-cyclopropyl-2-(2-fluorophenyl)-2-hydroxyethanone.



Scheme 46 Preparation of prasugrel intermediates 2-bromo-5-benzyl-4,5,6,7-tetrahydrothieno[3,2-c]pyridine (**4**) and 2-methoxy-5-benzyl-4,5,6,7-tetrahydrothieno[3,2-c]pyridine (**5**).



Scheme 47 Preparation of prasugrel salts. HA is methanesulfonic, fumaric, acetic, oxalic, succinic, tartaric, salicylic, acetylsalicylic, HBr, HI, H₂SO₄, or H₃PO₄ acid.



Scheme 48 Preparation of 1-cyclopropyl-2-(2-fluorophenyl)-2-hydroxyethanone (**4**).

For example, α -cyclopropyl-2-fluorophenyl ketone (**1**) is reacted with isopropenyl acetate (**2**) in the presence of TsOH in acetone to give 1-cyclopropyl-2-(2-(2-fluorophenyl)vinyl) acetate (**3**), followed by oxidation with 2-chlorobenzoyl peroxide in dichloromethane or with peracetic acid in the presence of $[(\text{phen})_2(\text{H}_2\text{O})\text{Fe}_2(\mu\text{-O})](\text{ClO}_4)_4$ (Fe phen) as a catalyst in acetonitrile to give 1-cyclopropyl-2-(2-fluorophenyl)-2-hydroxyethanone (**4**) (Scheme 48).

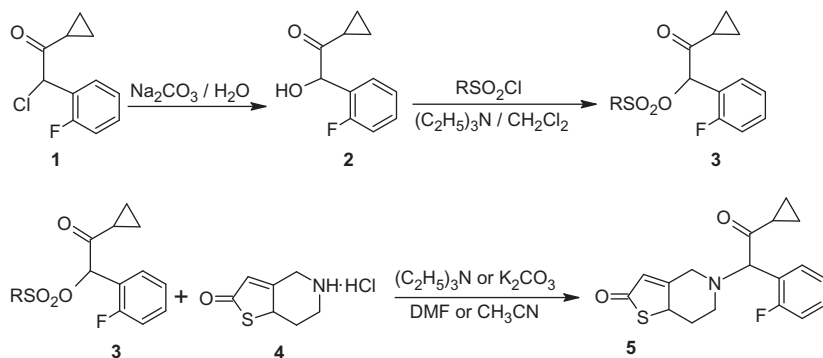
2.2.4 Method 4 [49]

The method describes a process for preparing 5-(2-cyclopropyl-1-(2-fluorophenyl)-2-oxoethyl)-5,6,7,7a-tetrahydrothieno[3,2-c]pyridin-2(4H)-one which can be used as intermediate for prasugrel.

For example, hydrolysis of α -cyclopropylcarbonyl-2-fluorobenzyl chloride (**1**) in the presence of sodium carbonate in water gives 1-cyclopropyl-2-(2-fluorophenyl)-2-hydroxyethanone (**2**), followed by reaction with R-sulfonyl chloride (R is methane or *p*-toluene) to give 1-cyclopropyl-2-(2-fluorophenyl)-2-R-sulfonylethanone (**3**) and then condensation with 5,6,7,7a-tetrahydrothieno[3,2-c]pyridin-2(4H)-one HCl (**4**) in the presence of triethylamine in dimethylformamide to give OXTP (**5**) (Scheme 49).

2.2.5 Method 5 [50]

This method describes a process for the preparation of acid addition salts of prasugrel especially sulfonic acids salts such as methanesulfonic,



Scheme 49 Preparation of 5-(2-cyclopropyl-1-(2-fluorophenyl)-2-oxoethyl)-5,6,7,7a-tetrahydrothieno[3,2-c]pyridin-2(4H)-one (**5**). R is methane or *p*-toluene.

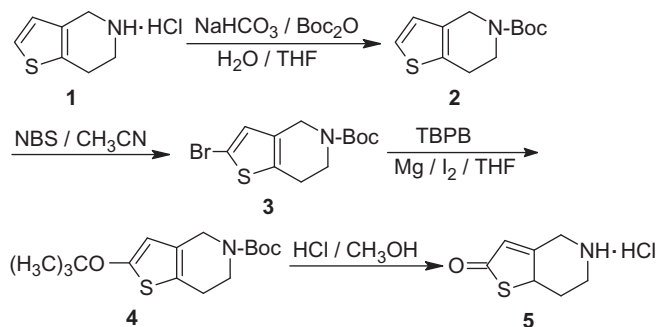
ethanesulfonic, ethane-1,2-disulfonic, 2-hydroxyethanesulfonic, benzene sulfonic, *p*-toluenesulfonic, 2-naphthalenesulfonic, or naphthalene-1,5-disulfonic acid.

Prasugrel base is dissolved in organic solvent such as acetone or ethanol and then added to a solution of 1 equiv. acid in the organic solvent. After completion of the addition, the reaction mixture is stirred and the formed crystals are isolated by filtration and dried under reduced pressure. The acid addition salts of prasugrel exhibit improved physical and pharmaceutical properties when formulated in solid dosage forms and have an improved toxicological profile.

2.2.6 Method 6 [51]

The method describes a process for the preparation of 5,6,7,7a-tetrahydrothieno[3,2-c]pyridin-2(4H)-one HCl as an intermediate for producing prasugrel.

For example, 4,5,6,7-tetrahydrothieno[3,2-c]pyridine HCl (**1**) is reacted with (Boc)₂O in a mixture of water and tetrahydrofuran in the presence of sodium bicarbonate to give 5-*tert*-butoxycarbonyl-4,5,6,7-tetrahydrothieno[3,2-c]pyridine (**2**), followed by bromination with NBS in acetonitrile to give 2-bromo-5-*tert*-butoxycarbonyl-4,5,6,7-tetrahydrothieno[3,2-c]pyridine (**3**). Alkoxylation with TBPB in tetrahydrofuran is then carried out in the presence of Mg/I₂ to give 2-*tert*-butoxy-5-*tert*-butoxycarbonyl-4,5,6,7-tetrahydrothieno[3,2-c]pyridine (**4**), followed by hydrolysis with HCl gas in methanol to give 5,6,7,7a-tetrahydrothieno[3,2-c]pyridin-2(4H)-one HCl (**5**) (Scheme 50).



Scheme 50 Preparation of 5,6,7,7a-tetrahydrothieno[3,2-c]pyridin-2(4H)-one HCl (**5**). Boc is *tert*-butyl carbonate.

2.2.7 Method 7 [52]

The same procedure in [Section 4.2.6 \(Scheme 50\)](#), but the alkoxylation is carried out using a mixture of potassium *tert*-butoxide, CuBr, and anhydrous ethanol instead of TBPB in the presence of Mg/I₂ in tetrahydrofuran to give 2-ethoxy-5-*tert*-butoxycarbonyl-4,5,6,7-tetrahydrothieno[3,2-c]pyridine.

2.2.8 Method 8 [53]

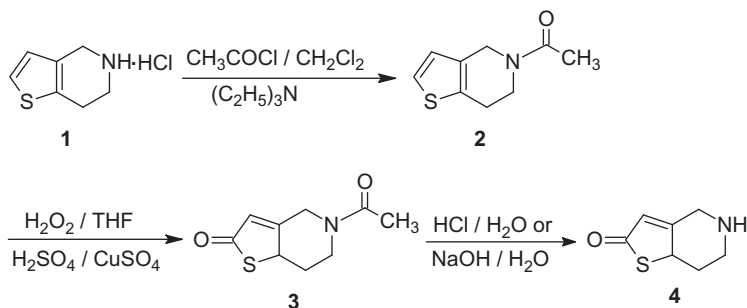
The method describes a process for preparing prasugrel intermediate 5-alkylcarbonyl-5,6,7,7a-tetrahydrothieno[3,2-c]pyridin-2(4H)-one (C₁ to C₂₀ alkyl), which is subsequently converted to 5,6,7,7a-tetrahydrothieno[3,2-c]pyridin-2(4H)-one.

For example, 4,5,6,7-tetrahydrothieno[3,2-c]pyridine HCl (**1**) is reacted with acetyl chloride in the presence of triethylamine in dichloromethane to give 5-acetyl-4,5,6,7-tetrahydrothieno[3,2-c]pyridine (**2**). The later compound is oxidized with hydrogen peroxide in the presence of sulfuric acid and copper sulfate in tetrahydrofuran to give 5-acetyl-5,6,7,7a-tetrahydrothieno[3,2-c]pyridin-2(4H)-one (**3**), followed by aqueous hydrolysis with HCl or NaOH to give 5,6,7,7a-tetrahydrothieno[3,2-c]pyridin-2(4H)-one (**4**) ([Scheme 51](#)).

2.2.9 Method 9 [24]

The method describes a process for preparing a highly pure prasugrel or its salts.

For example, 5,6,7,7a-tetrahydrothieno[3,2-c]pyridin-2(4H)-one HCl (**1**) is reacted with TsOH in a mixture of triethylamine, methanol, and acetone to give 5,6,7,7a-tetrahydrothieno[3,2-c]pyridin-2(4H)-one TsOH (**2**). The later compound is reacted with α -cyclopropylcarbonyl-2-fluorobenzyl



Scheme 51 5,6,7,7a-Tetrahydrothieno[3,2-c]pyridin-2(4H)-one (**4**).

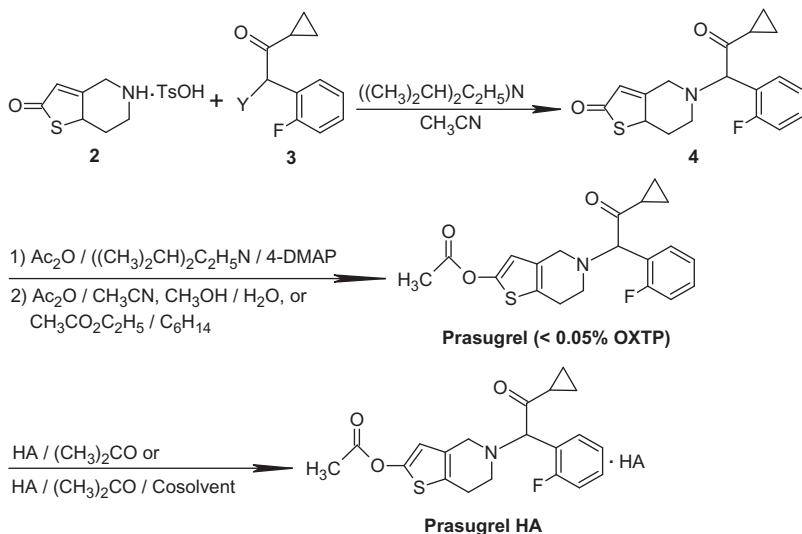
bromide, methanesulfonate, or *p*-toluene sulfonate (**3**) in the presence of diisopropylethylamine in acetonitrile to give OXTP (**4**), followed by reaction with acetic anhydride in the presence of diisopropylethylamine and dimethylaminopyridine as a catalyst to give prasugrel with a low content of the OXTP as undesired impurity (<0.1%). Crude prasugrel is further treated with acetic anhydride in acetonitrile to give pure prasugrel (OXTP <0.05%). In an alternative way, purification of crude prasugrel by recrystallization from a mixture of acetone and water, methanol and water, or ethyl acetate and hexane gives prasugrel with low content of OXTP (<0.05%). Furthermore, different salts of prasugrel are prepared by reaction with inorganic such as HBr and HI or organic acid such as benzenesulfonic or cyclamic acid in acetone in the absence and presence of cosolvent such as water, toluene, and diethyl ether (Scheme 52).

2.2.10 Method 10 [54]

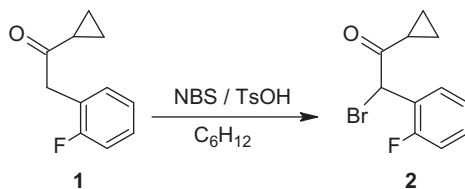
Prasugrel bisulfate is prepared by dissolving prasugrel base in an organic solvent such as acetone, methanol, or diethyl ether and then concentrated H_2SO_4 is added dropwise to the solution. The precipitate crystals are washed with the solvent and then dried under vacuum. Prasugrel bisulfate is claimed to have good stability, oral absorbability, metabolic activity and platelet aggregation inhibition effect, and low toxicity.

2.2.11 Method 11 [55]

The method describes a process for preparing the prasugrel intermediate α -cyclopropylcarbonyl-2-fluorobenzyl halides, whereby the halide is Br or Cl. The halogenation of 1-cyclopropyl-2-fluorobenzyl ketone with NBS, *N*-chlorosuccinimide, DBDMH, or 1,3-dichloro-5,5-dimethylhydantoin is carried out in the presence of a catalyst.



Scheme 52 Preparation of prasugrel acid salts. Y is Br, methanesulfonate or *p*-toluenesulfonate. HA is HBr, HI, benzenesulfonic or cyclamic acid.



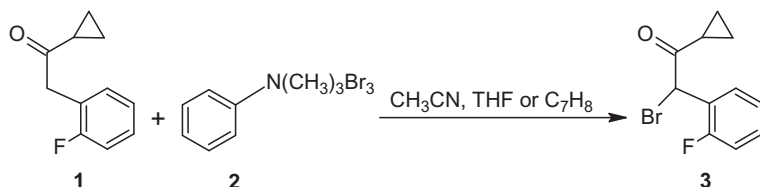
Scheme 53 Preparation of α -cyclopropylcarbonyl-2-fluorobenzyl bromide (**2**).

For example, 1-cyclopropyl-2-fluorobenzyl ketone (**1**) is reacted with NBS in cyclohexane in the presence of TsOH to give α -cyclopropylcarbonyl-2-fluorobenzyl bromide (**2**) with 96.5% purity (Yield 97.2%) (Scheme 53).

2.2.12 Method 12 [56]

The method describes a process for preparing α -cyclopropylcarbonyl-2-fluorobenzyl bromide, which is used as a prasugrel intermediate.

For example, bromination of α -cyclopropyl-2-fluorobenzyl ketone (**1**) with tri-methylphenylammonium tribromide (**2**) in organic solvent such as tetrahydrofuran, dichloromethane, or toluene gives α -cyclopropylcarbonyl-2-fluorobenzyl bromide (**3**) (Scheme 54).



Scheme 54 Preparation of α -cyclopropylcarbonyl-2-fluorobenzyl bromide (**3**).

2.2.13 Method 13 [57]

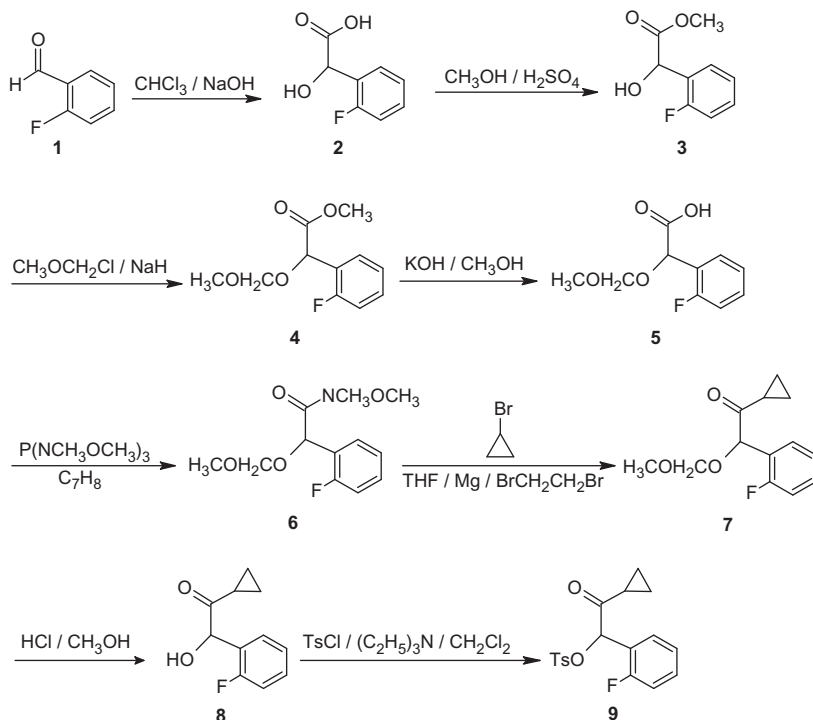
The method describes a process for preparing prasugrel intermediate 1-cyclopropyl-2-(2-fluorophenyl)-2-*p*-toluenesulfonyl ethanone.

For example, 2-fluorobenzaldehyde (**1**) is reacted with chloroform in the presence of NaOH, followed by acidification with HCl to give 2-fluoromandelic acid (**2**), which is esterified with methanol in the presence of concentrated H₂SO₄ to give 2-fluoromandelic acid methyl ester (**3**). The later compound is further reacted with methoxymethyl chloride and sodium hydride to give 2-(2-fluorophenyl)-2-(methoxymethoxy) acetic acid methyl ester (**4**), followed by hydrolysis with KOH in methanol to give 2-(2-fluorophenyl)-2-(methoxymethoxy) acetic acid (**5**). Amidation of compound (**5**) with P(NCH₃OCH₃)₃ in toluene gives 2-(2-fluorophenyl)-*N*-methoxy-2-(methoxymethoxy)-*N*-methyl-acetamide (**6**), followed by reaction with cyclopropyl bromide in the presence of magnesium turnings and BrCH₂CH₂Br to initiate the reaction in tetrahydrofuran to give 1-cyclopropyl-2-(2-fluorophenyl)-2-(methoxymethoxy)ethanone (**7**). Compound (**7**) is further reacted with HCl in methanol to give 1-cyclopropyl-2-(2-fluorophenyl)-2-hydroxyethanone (**8**), which is reacted with *p*-toluenesulfonyl chloride in dichloromethane to give 1-cyclopropyl-2-(2-fluorophenyl)-2-methanesulfonyl ethanone (**9**) (Scheme 55).

It is worth mentioning that the different proposed methods mentioned in this section to prepare prasugrel and its different intermediates offer different advantages. These advantages are starting materials easy to obtain, reaction conditions are mild and easily controlled, good selectivity, no employment of combustible, explosive and toxic reagents, high safety, high purity and yield, lower cost, and suitability for large-scale industrial production.

2.3 Drug Analogues

Preparation of prasugrel analogue compounds for anticoagulant treatment has been reported [58–62].



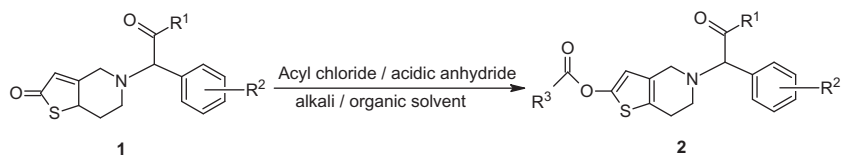
Scheme 55 Preparation of 1-cyclopropyl-2-(2-fluorophenyl)-2-methanesulfonyl-ethanone (**9**).

2.3.1 Method 1 [58]

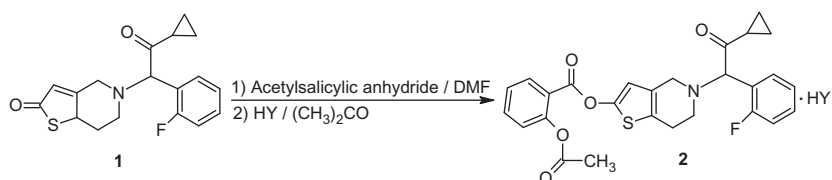
A method for preparing 4,5,6,7-tetrahydrothieno[3,2-*b*]pyridine aryl derivatives (**2**) is described. They are prepared from compound (**1**) and acyl chloride or acidic anhydride through esterification in the presence of an alkali such as sodium hydride or lithium diisopropylamide in organic solvent such as dimethylformamide, dimethylsulfoxide, or tetrahydrofuran (Scheme 56).

2.3.2 Method 2 [59]

A method for preparing 2-(2-acetoxy)benzoyl-5-(α -cyclopropylcarbonyl-2-fluorobenzyl)-4,5,6,7-tetrahydrothieno[3,2-*c*]pyridine (**2**) is described. For example, it is prepared through esterification of OXTP (**1**) with acetylsalicyl anhydride in dimethylformamide. Different salts of compound (**2**) are prepared by reaction with inorganic acids (HCl, HBr, H_3PO_4 , or H_2SO_4 acid) or organic acids (methanesulfonic, maleic, or fumaric acid) in acetone (Scheme 57).



Scheme 56 Preparation of 4,5,6,7-tetrahydrothieno[3,2-*b*]pyridine aryl derivatives (**2**). R^1 is halo (un)substituted C_1 – C_6 alkyl, C_1 – C_6 alkoxy, C_3 – C_8 cycloalkyl, or C_3 – C_8 cycloalkoxy. R^2 is halo, CN, NO_2 , NH_2 , OH, or halo (un)substituted C_1 – C_6 alkyl, C_3 – C_8 cycloalkyl, C_1 – C_6 alkoxy, C_3 – C_8 cycloalkoxy. R^3 is (un)substituted aryl or heteroaryl.



Scheme 57 Preparation of 2-(2-acetoxy)benzoyl-5-(α -cyclopropylcarbonyl)-2-fluorobenzyl)-4,5,6,7-tetrahydrothieno[3,2-*c*]pyridine (**2**). HY is HCl, HBr, H_3PO_4 , H_2SO_4 , methanesulfonic, maleic, or fumaric acid.

2.3.3 Method 3 [60]

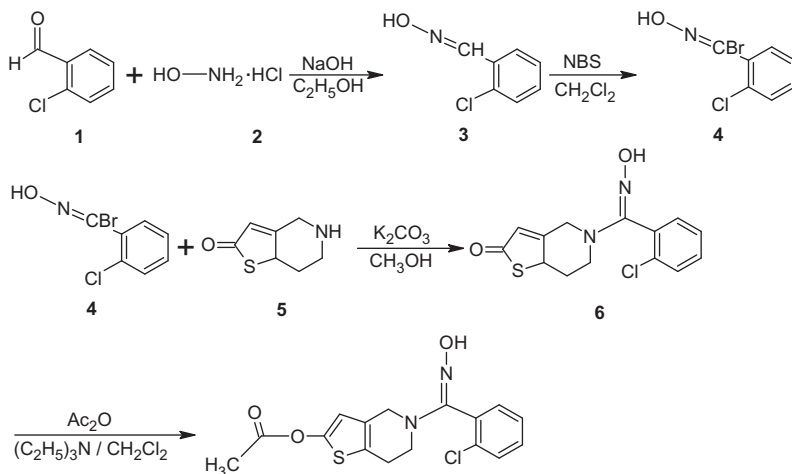
Prasugrel deuterated acid additive salts (acid is DCl, DBr, DI, D_2SO_4 , D_3PO_4 , DNO_3 , or maleic- d_2 acid) have been prepared.

For example, prasugrel is reacted with 20% DCl/ D_2O in acetone to give prasugrel DCl with less hygroscopicity and stability in comparison with prasugrel HCl. Formulations of prasugrel DCl as tablet and capsule have excellent bioavailability, metabolism, and less toxicity.

2.3.4 Method 4 [61]

Prasugrel analogue hydroxyimino derivatives have been prepared.

For example, condensation of 2-chlorobenzaldehyde (**1**) and hydroxylamine HCl (**2**) in the presence of NaOH in ethanol gives 2-chlorophenyl hydroxyimino methane (**3**), followed by bromination with NBS in dichloromethane to give bromo-2-chlorophenyl hydroxyimino methane (**4**), coupling with 5,6,7,7a-tetrahydrothieno[3,2-*c*]pyridin-2(4*H*)-one (**5**) in the presence of potassium carbonate in anhydrous methanol gives 5-((2-chlorophenyl)(hydroxyimino))methyl)-2-oxo-2,4,5,6,7,7a-hexahydrothieno[3,2-*c*]pyridine (**6**) and then acetylation with acidic anhydride in dichloromethane is carried out in the presence of triethylamine to give 5-((2-chlorophenyl)(hydroxyimino))methyl)-4,5,6,7-tetrahydrothieno[3,2-*c*]pyridin-2-yl-acetate (**7**) (Scheme 58).



Prasugrel analogue hydroxyimino derivatives (7)

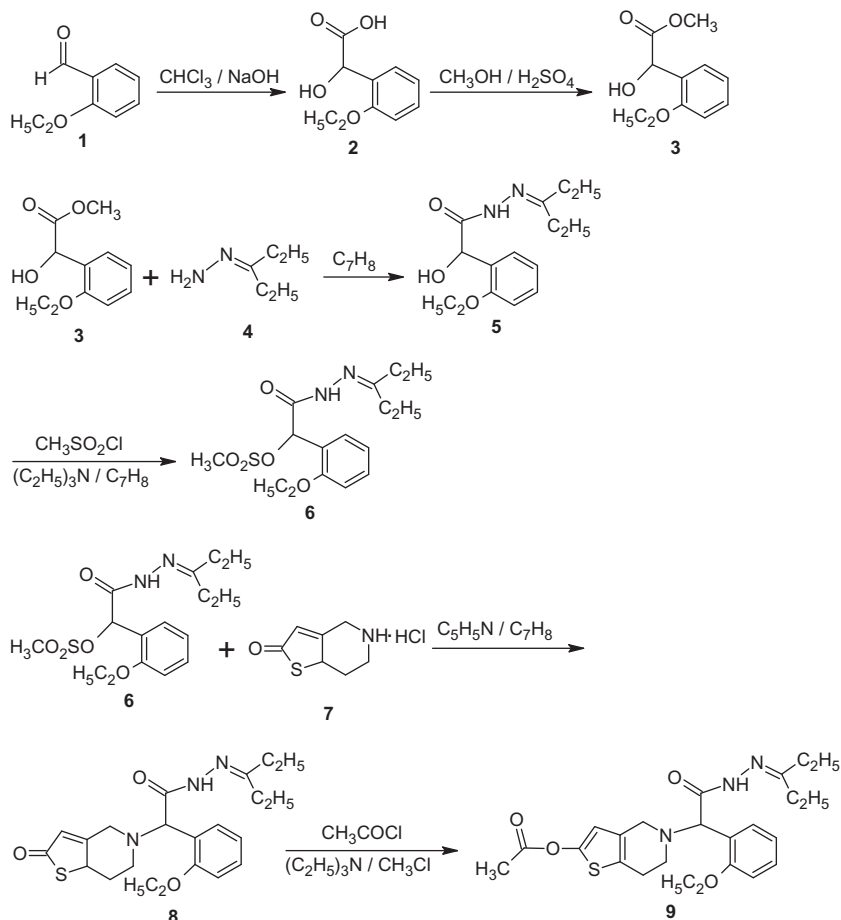
Scheme 58 Preparation of prasugrel analogue hydroxyimino derivative 5-((2-chlorophenyl)(hydroxyimino)methyl)-4,5,6,7-tetrahydrothieno[3,2-*c*]pyridin-2-yl-acetate (7).

2.3.5 Method 5 [62]

Prasugrel analogue Schiff base derivatives have been prepared.

For example, 2-ethoxybenzaldehyde (**1**) is reacted with bromoform in the presence of tetrabutylammonium bromide and sodium carbonate, followed by reaction with HCl to give 2-hydroxy-2-(2-ethoxyphenyl) acetic acid (**2**). Esterification of compound (**2**) with methanol in the presence of H_2SO_4 gives methyl 2-hydroxy-2-(2-ethoxyphenyl) acetate (**3**), followed by reaction with 3-pentanone hydrazone (**4**) in toluene to give 3-pentanone-(2-hydroxy-2-(2-ethoxyphenyl) acetyl) hydrazone (**5**). The later compound is reacted with methanesulfonyl chloride in the presence of triethylamine in toluene to give 3-pentanone-(2-methylsulfonate-2-(2-ethoxyphenyl) acetyl) hydrazone (**6**), followed by coupling with 5,6,7,8-tetrahydrothieno[3,2-*c*]pyridin-2(4*H*)-one HCl (**7**) in the presence of pyridine in toluene to give 3-pentanone-(2-(5,6,7,8-tetrahydrothieno[3,2-*c*]pyridine-2(4*H*)-one)-2-(2-ethoxyphenyl) acetyl) hydrazone (**8**). Acetylation with acetyl chloride in the presence of triethylamine in chloroform gives 3-pentanone-(2-(2-(acetyloxy)-6,7-dihydrothieno[3,2-*c*]pyrazol-5-yl)-2-(2-ethoxyphenyl) acetate (**9**) (Scheme 59).

Table 2 represents the published preparation patents as obtained from the “Intellectual Properties India” Indian Web site, in addition to some pharmaceutical compositions, polymorphs, and analytical patents [63].



Scheme 59 Preparation of prasugrel analogue Schiff base derivative 3-pentanone-(2-(2-(acetoxy)-6,7-dihydrothieno[3,2-*c*]pyrazol-5-yl)-2-(2-ethoxyphenyl) acetate (9).



3. PHYSICAL CHARACTERISTICS

3.1 Ionization Constants

Prasugrel is a basic compound, which contains a tertiary arylamine with ionization constant ($\text{pK}_{\text{a}1}$) value of 5.1 [1]. Two predicted pK_{a} values are also reported (5.48, strongest basic and 14.25, strongest acidic) [5]. A calculated pK_{a} value by Advanced Chemistry Development (ACD) software was found to be 3.65 ± 0.20 [64].

Table 2 The List of Patents Obtained from the Intellectual Properties India Web Site Including Preparations, Polymorphs, Compositions, and Chromatographic Analysis

No.	Application Number	Title of Invention	Priority Country
1	2683/CHE/2007	Improved process for the preparation of prasugrel and its pharmaceutically acceptable salts	—
2	2609/MUM/2008	A process for the preparation of prasugrel and its pharmaceutically acceptable salts thereof	—
3	3005/CHE/2008	Improved process for preparing prasugrel	—
4	1008/MUMNP/2009	An article of manufacture for prasugrel	USA
5	2428/CHE/2009	Improved process for the preparation of prasugrel and its pharmaceutically acceptable salts	—
6	3106/KOLNP/2009	Process for production of prasugrel hydrochloride having high purity	Japan
7	263/MUM/2010	An improved process for the preparation of prasugrel and its pharmaceutically acceptable salts there	—
8	1509/DEL/2010	An improved process for the preparation of prasugrel hydrochloride and its intermediates	—
9	1645/MUM/2010	A process for the preparation of prasugrel and its pharmaceutically accept salts thereof by using novel intermediate 5,6,7,7a-tetrahydrothieno[3,2-c] pyridine-2(4H)-one hydrobromide	—
10	2027/MUM/2010	Prasugrel and its pharmaceutically acceptable salts thereof	—
11	3431/CHENP/2010	Processes for the preparation of prasugrel, and its salts and polymorphs	India
12	3672/DELNP/2010	Process for the preparation of pharmaceutical intermediates	Hungary
13	3677/DELNP/2010	Process for the preparation of pharmaceutical intermediates	Hungary

Continued

Table 2 The List of Patents Obtained from the Intellectual Properties India Web Site Including Preparations, Polymorphs, Compositions, and Chromatographic Analysis—cont'd

No.	Application Number	Title of Invention	Priority Country
14	343/MUM/2011	An improved process for preparation of prasugrel hydrochloride	—
15	1307/CHENP/2011	Prasugrel bisulfate, pharmaceutical composition thereof, and use thereof	China
16	1430/MUM/2011	Process for preparation of prasugrel and its intermediates	—
17	2231/CHE/2011	An improved process for the preparation of prasugrel	—
18	2773/CHE/2011	Process for the preparation of prasugrel hydrobromide	—
19	34/CHE/2012	Process for the preparation of 5,6,7,7 <i>a</i> -tetrahydro-4- <i>H</i> -thieno[3,2- <i>c</i>]pyridine-2-one	—
20	1140/CHE/2008	Prasugrel pharmaceutical compositions	—
21	2208/MUM/2009	Pharmaceutical composition comprising prasugrel	—
22	244/CHE/2010	Pharmaceutical composition of prasugrel and its pharmaceutically acceptable salts	—
23	146/MUM/2011	Pharmaceutical composition comprising prasugrel and aspirin	—
24	2599/CHE/2008	Process for preparing amorphous prasugrel hydrochloride	—
25	1596/MUM/2009	Crystalline form of prasugrel hydrobromide and process for the preparation thereof	—
26	2344/MUM/2010	Prasugrel salts, polymorphs and process for preparation thereof	—
27	2377/CHE/2010	Prasugrel hydrochloride crystalline particles	—
28	2831/CHE/2010	Novel pseudopolymorphs of prasugrel hydrochloride	—
29	2287/MUM/2011	An improved method for the quantitative determination of prasugrel HCl	—
30	2852/DEL/2012	Validated HPLC and stability indicating HPLC method for prasugrel hydrochloride	—

3.2 Solubility Characteristics

Prasugrel HCl is soluble at pH 2, slightly soluble at pH 3–4, practically insoluble at pH 6–7.5. In addition, it dissolves freely in methanol and is slightly soluble in *n*-propanol, isopropanol, and acetone. It is practically insoluble in diethylether and ethyl acetate [65].

The solubility of prasugrel HCl is pH-dependent (Figure 2), it increases with decreasing pH. The dramatic decrease in solubility at pH 6.8 is due to the formation of free-base prasugrel ($pK_{a1}=5.1$) [66].

According to the WHO [67], EMA [68], and USFDA [69] guidelines, prasugrel HCl can be considered as a low-soluble drug based on the Biopharmaceutics Classification System (BCS). The drug exhibits a dose/solubility (D/S) of >250 ml at the pH value of 6.86 (Table 3).

3.3 Partition Coefficients

The apparent partition coefficient of prasugrel ($\log P$) is 3.536 [5]. A calculated $\log P$ value by ACD Software was found to be 2.718 ± 0.904 [64]. Based upon solubility determination results and permeability and metabolism information, prasugrel HCl can be classified as a BCS class 2 compound [1].

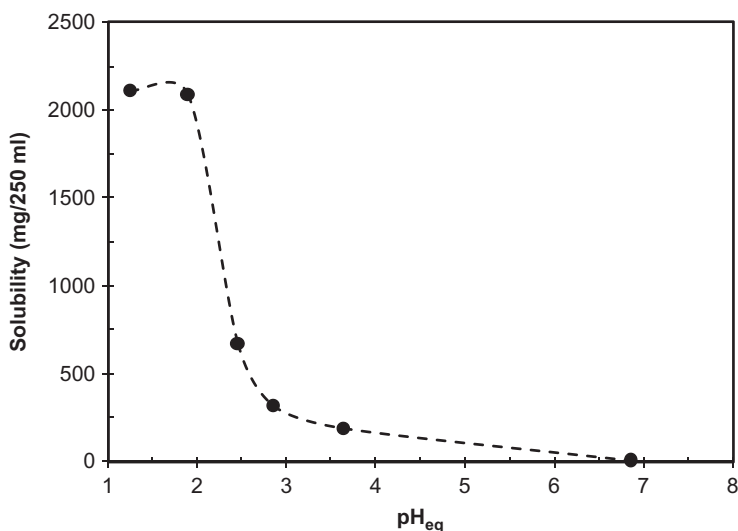


Figure 2 The pH solubility of prasugrel HCl in 0.05 M phosphate buffer at 30 °C (pH 1.2 corresponds to 0.1 N HCl solution).

Table 3 The pH Solubility (*S*) Data of Prasugrel HCl and the Calculated Dose/Solubility (*D/S*)

pH _{eq}	<i>S</i> (mg/ml)	<i>D/S</i> (ml)
1.25	8.43	1.2
1.89	8.34	1.2
2.45	2.67	3.7
2.85	1.26	7.9
3.64	0.75	13.3
6.86	0.026	372.6

The highest single dose (*D*) is 10 mg.

3.4 Optical Activity

Prasugrel HCl exists as a racemic mixture; therefore, it shows no optical rotation [1].

It has one chiral center, located at the benzylic carbon, leading to possible formation of *R*- and *S*-enantiomers (Figure 3). Both enantiomers of prasugrel show similar activity; therefore, it was approved for use in its racemic form [70].

3.5 Polymorphism

Prasugrel HCl exists in different crystalline forms as shown in Table 4. The amorphous form can be prepared by dissolving prasugrel HCl in an organic solvent and then spray dried.

Different forms of prasugrel HCl can be obtained from different aqueous and organic solvents under controlled experimental conditions (Table 4). They are characterized by distinctive X-ray powder diffraction (XRPD) patterns, differential scanning calorimetry (DSC), and Fourier transform infrared (FT-IR).

Also prasugrel as free base and its different salts, other than hydrochloride, may exist in different polymorphic forms as shown in Table 5.

3.6 Particle Morphology

Crystal particles of prasugrel or prasugrel HCl, as reported by Anumula *et al.*, can be in needle shape, rod shape, or flake shape [34]. It is also reported by Khan *et al.* that prasugrel and its HCl salt can be in flake shape and condensation floc shape, respectively [18]. Forms A and B of prasugrel HCl

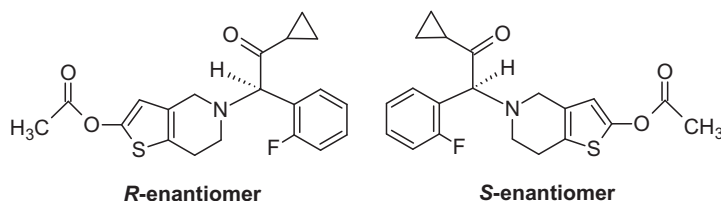


Figure 3 The chemical structures of *R*- and *S*-enantiomers of prasugrel.

(designated as Form II and I by Du *et al.* [74], respectively) were prepared and examined by using Olympus BX51 polarizing microscope [74]. They show platelike (Figure 4A) and needlelike (Figure 4B) shapes, respectively. However, Form B of prasugrel HCl, obtained from a particular drug supplier, was examined by FEI Quanta-600 scanning electron microscope (SEM) [66]. As shown in SEM image (Figure 4C), the sample has irregular shape crystals with flocs and flakes.

3.7 Hygroscopicity

Prasugrel HCl is slightly hygroscopic material [1].

3.8 Molecular Modeling

Conformational analysis of prasugrel has been investigated by Bano *et al.* [82]. All conformational analysis studies were performed on a window-based computer using Argus Lab and ACD Lab chem sketch softwares. From the studies, the best conformation of the molecule is present at a minimum potential energy of $-99,561$ kcal/mol. At this point, the molecule will be more active as P2Y₁₂ receptor antagonist and reduce platelets aggregation more effectively (Figure 5).

3.9 Crystallographic Properties

3.9.1 Single Crystal Structure

The single crystal structure of prasugrel has been investigated using Bruker Smart CCD diffractometer [70]. The molecular structure of prasugrel is shown in Figure 6. The tetrahydropyridine ring of the bicyclic thienopyridine system shows a half-chair conformation with the N1 and C8 atoms displaced by -0.408 and 0.411 Å from the plane of C5, C6, C7, and C9 atoms, which are coplanar within 0.003 Å. The dihedral angle formed by the planes of the benzene and thiophene rings (C₁₁–C₁₆ and C3, C4, C5, C6, S1, respectively) is equal to 83.17° .

Table 4 The List of Different Forms of Prasugrel HCl with Their Preparations and Methods of Characterization

Form	Preparation	Characterization	Reference
Crystal A	Prasugrel (10 g) is dissolved in acetone (150 ml) and 36% HCl (2.71 g) is added dropwise with stirring at 25 °C. Seeding with crystal A, prepared by other procedure, is done and then the mixture is stirred for 90 min at 25 °C. The crystals are filtered, washed with acetone, and then dried at 50 °C under reduced pressure for 4 h.	Melting point: 133–136 °C, IR: 1762 and 1720 cm ⁻¹	[7]
Crystal B1	Prasugrel (10 g) is dissolved in acetone (100 ml) and 36% HCl is added dropwise over 1 min with stirring at 40 °C. The mixture is stirred at 40 °C for 60 min. The crystals are filtered, washed with acetone, and then dried at 60 °C under reduced pressure for 2 h.	Melting point: 166–174 °C, IR: 1758 and 1690 cm ⁻¹	
Crystal B2	Prasugrel (50 g) is dissolved in acetone (750 ml) and 36% HCl (6.78 g) is added over 5 min at 40 °C. Seeding with crystal B and then stirred at 40 °C for 60 min. 36% HCl (6.10 g) is added over 60 min and then stirred at 40 °C for 120 min. The crystals are filtered, washed with acetone, and then dried at 70 °C under reduced pressure for 3 h.	Melting point: 165–178 °C, IR: 1758 and 1690 cm ⁻¹	
Crystal B2	Prasugrel (50 g) is dissolved in acetone (750 ml) and 36% HCl (6.78 g) is added dropwise over 5 min with stirring at 55 °C. Crystals of B1 (0.1 g) are added to the mixture as seed crystals and then stirred at 55 °C for 60 min. Further 36% HCl (6.08 g) is added to the mixture over 60 min and then stirred at 40 °C for 120 min. The crystals are filtered, washed with acetone, and then dried at 70 °C under reduced pressure for 3 h.	Melting point: 164–178 °C, IR: 1758 and 1690 cm ⁻¹	
Form G1	Prasugrel HCl (5 g) is dissolved in dichloromethane (200 ml) and cyclohexane (830 ml) is added dropwise over 10 min with stirring at 25–30 °C. Then mixture is stirred for 20–24 h at 25 °C. The crystals are filtered, washed with cyclohexane, and then dried at 50 °C under reduced pressure for 12 h.	XRPD, DSC	[18]

Form G2	Prasugrel HCl (5 g) is dissolved in 2-propanol (375 ml) and hexane (375 ml) is added dropwise over 10 min with stirring at reflux temperature. Then allowed the mixture to reach ~25 °C and stirred for ~20–24 h. The crystals are filtered, washed with hexane, and then dried at 50 °C under reduced pressure for 12 h.		
Amorphous	Prasugrel HCl (5 g) is dissolved in dichloromethane (250 ml) and then spray dried at 65 °C and obtained solid is dried at 50 °C for 20 h under reduced pressure.		
Form C	An aqueous HCl (0.27 g) is added to a mixture of prasugrel (1 g) and 2-butanol (20 ml) at 40 °C, stirred for 60 min, filtered and dried at 60 °C for 2 h.	XRPD, FT-IR, DSC	[21]
Form C	A mixture of 2-butanol (2 ml) and aqueous HCl (0.135 g) is added to a mixture of prasugrel (0.5 g) and 2-butanol (10 ml) at 28 °C, stirred for 15 min, seeded with 2 mg of Form C, stirred for 60 min, filtered, washed with 2-butanol (5 ml), and dried at 60 °C for 4 h.		
Form D	A solution of 2-propanol HCl (0.15 g) is added to a mixture of prasugrel (0.5 g) and 2-propanol (10 ml), previously heated at 40 °C for 15 min, to pH 2. The contents are stirred for 60 min, filtered, and dried at 60 °C for 2 h.		
Form E	The same as in Form D preparation, but using ethyl acetate instead of 2-propanol.		
Form B1 (Crystal B1)	HCl gas purged in acetone (1.95 g) is added to a mixture of prasugrel (0.5 g) and acetone (10 ml) at 40 °C, stirred for 2 h, filtered, and dried at 60 °C for 3 h.		
Form B2 (Crystal B2)	A mixture of acetone (5 ml) and aqueous HCl (0.25 ml) is added to a mixture of prasugrel maleate (1 g) and acetone (10 m) at 25 °C, stirred for 90 min, seeded with 2 mg of Form B2, stirred for 60 min, filtered, washed with acetone (5 ml), and dried at 55 °C for 4 h.		

Continued

Table 4 The List of Different Forms of Prasugrel HCl with Their Preparations and Methods of Characterization—cont'd

Form	Preparation	Characterization	Reference
Amorphous	A mixture of methanol (2 ml) and aqueous HCl (0.135 g) is added to a mixture of prasugrel (0.5 g) and dichloromethane (10 ml) at 25 °C, heated to 40 °C and then the solvent is distilled off. 2-Propanol (10 ml) is added to the residue and then the solvent is distilled off completely. The obtained solid is dried for 4 h at 40 °C.		
Amorphous	Prasugrel HCl (0.5 g) is dissolved in a mixture of 2-propanol (10 ml) and water (0.1 ml). The solvent is evaporated at 30 °C under vacuum. The solid is dried at the same temperature for 3 h.		
Form A (Crystal A)	Amorphous prasugrel HCl (11 g) is dissolved in acetone (100 ml) at 25 °C. The resulting solution is stirred for 1.5 h at 25 °C and then Form A is collected by filtration at 25 °C, washed with acetone, and then dried under vacuum at 65 °C for 3.5 h.	XRPD	[34]
Form C	Amorphous prasugrel HCl (11 g) is dissolved in 2-propanol (100 ml) at 25 °C. The resulting solution is stirred for 1.75 h at 25 °C and then Form C is collected by filtration, washed with 2-propanol, and then dried under vacuum at 65 °C for 3.5 h.		
Amorphous	Prasugrel (30 g) is dissolved in dichloromethane (300 ml) at 25 °C, 9.8% HCl in 2-propanol (30 ml) is added dropwise in 15 min, and the reaction mass is stirred for 30 min at 25 °C. The solvent is evaporated under vacuum at 40 °C to result in a solid material, which is further dried under vacuum for 3.5 h at 40 °C.		
Form B (Crystals B1 and B2)	Prasugrel (5 g) is dissolved in acetone (75 ml) at room temperature, followed by addition of acetic acid (0.92 ml) and trimethylchlorosilane (2.05 ml) under stirring. Immediately after addition a white precipitate is obtained, filtered, and dried at room temperature under vacuum for 6 h.	XRPD, IR: 1758 and 1690 cm ⁻¹	[71]

Amorphous	Prasugrel HCl is dissolved in methanol at 20–40 °C and stirred to give a clear solution. The methanol is distilled off and the solid dried at 25–30 °C.		[72]
Form B2 (Crystal B2)	Prasugrel (100 g) is dissolved in acetone (800 ml) and then heated to 35–40 °C. Carbon (5 g) is added, stirred for 15 min, and then filtered. The filtrate is cooled to 0–5 °C and then ethyl acetate HCl (500 ml) is added. The reaction mixture is stirred for 45 min at 0–5 °C, filtered, and washed with acetone. Acetone (800 ml) is added to the wet material, stirred for 45 min at 25–30 °C, filtered, washed with acetone, and then dried.		[73]
Form B2 (Crystal B2)	Prasugrel (100 g) is dissolved in acetone (800 ml) and then heated to 35–40 °C. Carbon (5 g) is added, stirred for 15 min, and then filtered. The filtrate is cooled to 0–5 °C and ethyl acetate (500 ml) is added. Then HCl gas is bubbled through it. The precipitated solid is filtered and washed with acetone. Acetone (800 ml) is added to the wet material, stirred for 45 min at 25–30 °C, filtered, washed with acetone, and then dried.		
Form I (Form B)	Prasugrel (2 g) and 1 mol equiv. of HCl are added to 150 ml of 2-propanol at 20 °C to produce prasugrel HCl Form I.	XRPD, Raman, microscope	[74]
Form II (Form A)	Prasugrel (15 g) and 1 mol equiv. of HCl are added to 150 ml of 2-propanol at 20 °C to produce prasugrel HCl Form II.		
Form A (Crystal A)	Prasugrel (2.55 g) is dissolved in ethyl methyl ketone (25 ml) by heating up to 35 °C, cooled with stirring to 0 °C, and a solution of HCl (0.24 g) in ethanol (1.45 ml) is added dropwise with stirring at the temperature 0 °C. The mixture is stirred at the same temperature for 1 h. The separated crystals are aspirated and dried freely in air.	XRPD, DSC	[75]

Continued

Table 4 The List of Different Forms of Prasugrel HCl with Their Preparations and Methods of Characterization—cont'd

Form	Preparation	Characterization	Reference
Form B	Prasugrel (1.324 g) is dissolved in isopropyl acetate (13 ml) by heating up to 45 °C, cooled to the room temperature, and a solution of HCl (0.123 g) in ethanol (0.753 g) is added dropwise with stirring. The mixture is stirred at the room temperature for 1 h. The separated crystals are aspirated and dried in air.		
Form B	Prasugrel (1.430 g) is dissolved in ethyl acetate at 40 °C, cooled to the room temperature, and a 16.3% solution of HCl in ethanol is added dropwise. The solution is inoculated, left to crystallize under stirring at the temperature of 20–25 °C for 2 h, and the separated crystals are aspirated.		
Form B	To a suspension of prasugrel (1.627 g) in ethanol (5 ml), 1 equiv. of HCl in an ethanol solution is added dropwise. To the resulting solution, 28 ml of ethyl acetate is added, the mixture is inoculated with Form B crystals, and stirred at the room temperature. The separated white crystals are aspirated.		

Table 5 The List of Different Forms of Prasugrel-Free Base, Its Different Salts, and Solvates

Form	Drug Form Used/Recrystallization System	Reference
Form I	Free base/diisopropyl ether	[4,76]
Form A (HBr salt)	Free base/aqueous HBr and acetone	[24]
Form A (HBr salt)	Free base/gaseous HBr, acetone, and toluene	
Form A (free base)	Free base/ethanol or 2-propanol	[37]
Acetonitrile solvate (HCl salt)	Free base/acetonitrile, acetic acid, and trimethylchlorosilane	[71]
Form II	Free base/1,4-dioxane	[76]
Amorphous	Free base/organic solvents	
Amorphous (free base)	Free base/hydrophobic polymer	[77]
Form I (hydrogen sulfate salt)	Free base/H ₂ SO ₄ and 2-propanol or 2-butanol	[78]
Form I (hydrogen sulfate salt)	Free base/H ₂ SO ₄ and 2-propanol and ethyl acetate	
Form II (hydrogen sulfate salt)	Sulfate salt (Form I)/methyl ethyl ketone or acetone	
Form II (hydrogen sulfate salt)	Sulfate salt (Form I)/ethyl acetate and acetone	
Form II (hydrogen sulfate salt)	Free base/H ₂ SO ₄ , methyl ethyl ketone, and Form II (seeding)	
Crystalline form (HBr salt)	Free base/aqueous HBr and acetone	[79]
Form C (HBr salt)	Free base/gaseous HBr, ethyl acetate, and toluene	[80]
Form B (HBr salt)	HBr salt/ethanol and ethyl acetate	

Continued

Table 5 The List of Different Forms of Prasugrel-Free Base, Its Different Salts, and Solvates—cont'd

Form	Drug Form Used/Recrystallization System	Reference
Nitromethane solvate (HCl salt)	HCl salt/nitromethane	[81]
Form F (HCl salt, acetic acid solvate)	HCl salt/glacial acetic acid or acetic anhydride	
Form F (HCl salt, acetic acid solvate)	HCl salt/acetic anhydride and Form F (seeding)	
Form F (HCl salt, acetic acid solvate)	Free base/glacial acetic acid (alkyl acetate, methyl- <i>tert</i> -butyl ether, <i>p</i> -cymol, mesitylene, or tetrachloromethane) and trimethylchlorosilane	
Form I (HBr salt)	HBr salt (Form II)/ethyl acetate or methyl ethyl ketone	
Form I (HBr salt)	Free base/aqueous HBr, isopropyl acetate, and methanol	
Form I (HBr salt)	Free base/aqueous HBr, methyl isobutyl ketone, methanol, and Form I (seeding)	
Form IA (HBr salt)	Free base/aqueous HBr, 1-pentanol, or isopentanol	
Form IA (HBr salt)	Free base/aqueous HBr, methyl acetate, and methanol	
Form II (HBr salt)	Free base/aqueous or gaseous HBr and acetone	
Form III (HBr salt)	Free base/HBr and 2-propanol	
Form IV (HBr salt)	HBr (Form II)/96% ethanol	
Form V (HBr salt)	HBr (Form II)/acetic acid	
Form VI (HBr salt)	HBr (Form II)/tetrahydrofuran	
Form VII (HBr salt)	Free base/aqueous HBr and methyl ethyl ketone	
Form VIII (HBr salt)	Free base/aqueous HBr and 1-butanol	

Form IX (HBr salt)	Free base/gaseous HBr, methyl acetate, methanol, and Form I (seeding)
Form XI (HBr salt)	Free base/gaseous HBr, isobutyl acetate, and methanol
Form X (HBr salt)	Free base/gaseous HBr, toluene, methanol, and Form I (seeding)
Form XII (HBr salt)	Free base/gaseous HBr, methyl acetate, and methanol
Form XIII (HBr salt)	Free base/aqueous HBr and <i>n</i> -butyl acetate
Form P1 (phosphate salt)	Free base/H ₃ PO ₄ , methyl acetate, and ethanol
Form P2 (phosphate salt)	Free base/H ₃ PO ₄ and dichloromethane
Form S1 (Hydrogen sulfate salt)	Free base/H ₂ SO ₄ , methyl acetate, and methanol
Form S1 (hydrogen sulfate salt)	Free base/H ₂ SO ₄ , methyl acetate, ethanol, and Form S1 (seeding)
Form S1 (hydrogen sulfate salt)	Free base/H ₂ SO ₄ and acetone
Form S2 (hydrogen sulfate salt)	Free base/H ₂ SO ₄ , ethyl formate, ethanol, and Form S1 (seeding)
Form S3 (hydrogen sulfate salt)	Free base/H ₂ SO ₄ and ethyl acetate

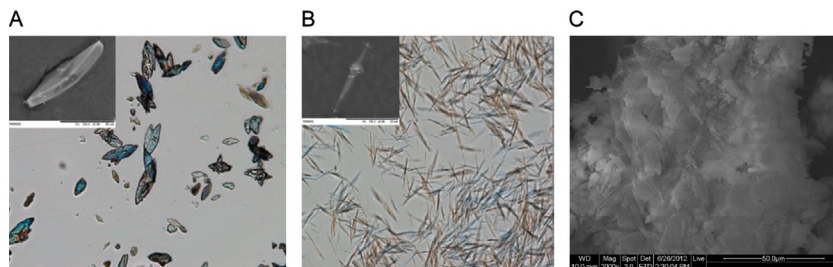


Figure 4 The polarizing microscope images of (A) Form A (magnified by 500), (B) Form B (magnified by 100), and (C) scanning electron microscope image of Form B (magnified by 2000).

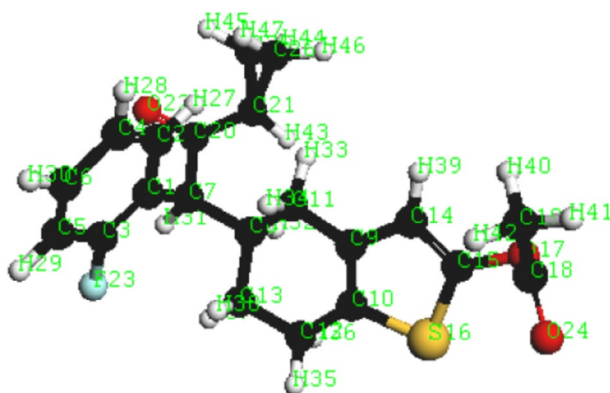


Figure 5 The prospective view of active conformation of prasugrel.

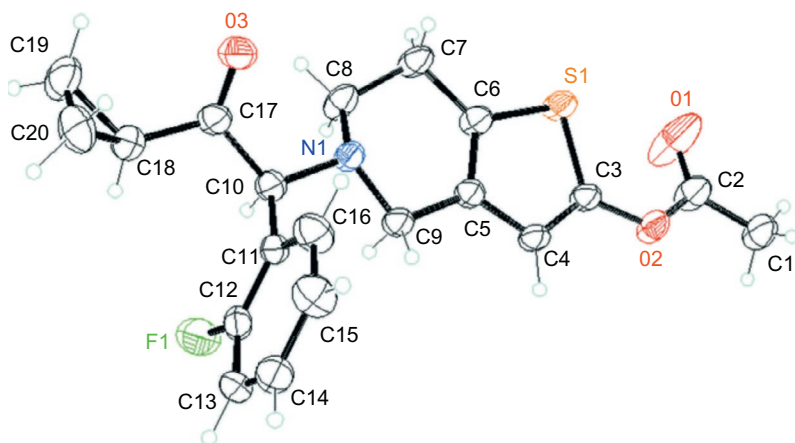


Figure 6 The molecular structure of prasugrel with thermal ellipsoids drawn at the 30% probability level.

Table 6 The Crystal Data, Data Collection, and Refinement of Prasugrel^a

Crystal Data	Data Collection	Refinement
C ₂₀ H ₂₀ FN ₃ O ₃ S	Bruker SMART CCD	$R[F^2 > 2\sigma(F^2)] = 0.106$
Mr = 373.43	diffractometer	$wR(F^2) = 0.198$
Triclinic, $P\bar{1}$	Absorption correction: multi-	$S = 1.08$
$a = 7.910$ (2) Å	scan (SADABS; Sheldrick, 2000)	3201 reflections
$b = 9.943$ (3) Å	$T_{\min} = 0.936$, $T_{\max} = 0.947$	235 parameters
$c = 12.450$ (4) Å	5345 measured reflections	H atom parameters
$\alpha = 112.938$ (5)°	3201 independent reflections	constrained
$\beta = 90.644$ (5)°	2379 reflections with $I > 2\sigma(I)$	$\Delta\rho_{\max} = 0.73 \text{ e \AA}^{-3}$
$\gamma = 92.591$ (6)°	$R_{\text{int}} = 0.027$	$\Delta\rho_{\min} = -0.26 \text{ e \AA}^{-3}$
$V = 900.3$ (5) Å ³		
$Z = 2$		
Mo $K\alpha$ radiation		
$\mu = 0.21 \text{ mm}^{-1}$		
$T = 291 \text{ K}$		
$0.32 \times 0.28 \times 0.26 \text{ mm}$		

^aPrasugrel is dissolved in methanol and then slowly evaporated.

The material crystallizes in the triclinic space group $P\bar{1}$ with $a = 7.910$ Å, $b = 9.943$ Å, $c = 12.450$ Å, $\alpha = 112.938^\circ$, $\beta = 90.644^\circ$, and $\gamma = 92.591^\circ$ (Table 6).

3.9.2 X-ray Powder Diffraction Pattern

In the patent of Sankyo Co., three different polymorphic forms of prasugrel HCl are described, namely, crystal A, B1, and B2 [7]. The XRPD pattern of crystal A, as reported by Inoue *et al.* [11], differs from those of crystal B1 and B2. On the other hand, the XRPD patterns of both crystal B1 and B2 are almost identical [11].

Furthermore, the patent of Zentiva used XRPD to describe Form A (similar to crystal A) and Form B (similar to crystal B1 and B2) [75]. The XRPD patterns were recorded with an X'Pert Pro MPD PANalytical powder diffractometer using CuK α ($\lambda = 1.542$ Å) radiator (Figure 7A and B). The crystallographic data of both forms are listed in Table 7.

The XRPD pattern of the amorphous form of prasugrel HCl prepared by dissolving in a mixture of 2-propanol and water or 2-propanol followed by evaporation is shown in Figure 7C [21]. The plain halo shape of the pattern proves the amorphous nature of the obtained powder.

In addition to these three forms and as mentioned previously in Section 3.5, there are other crystalline forms of prasugrel HCl that can be clearly characterized using this technique.

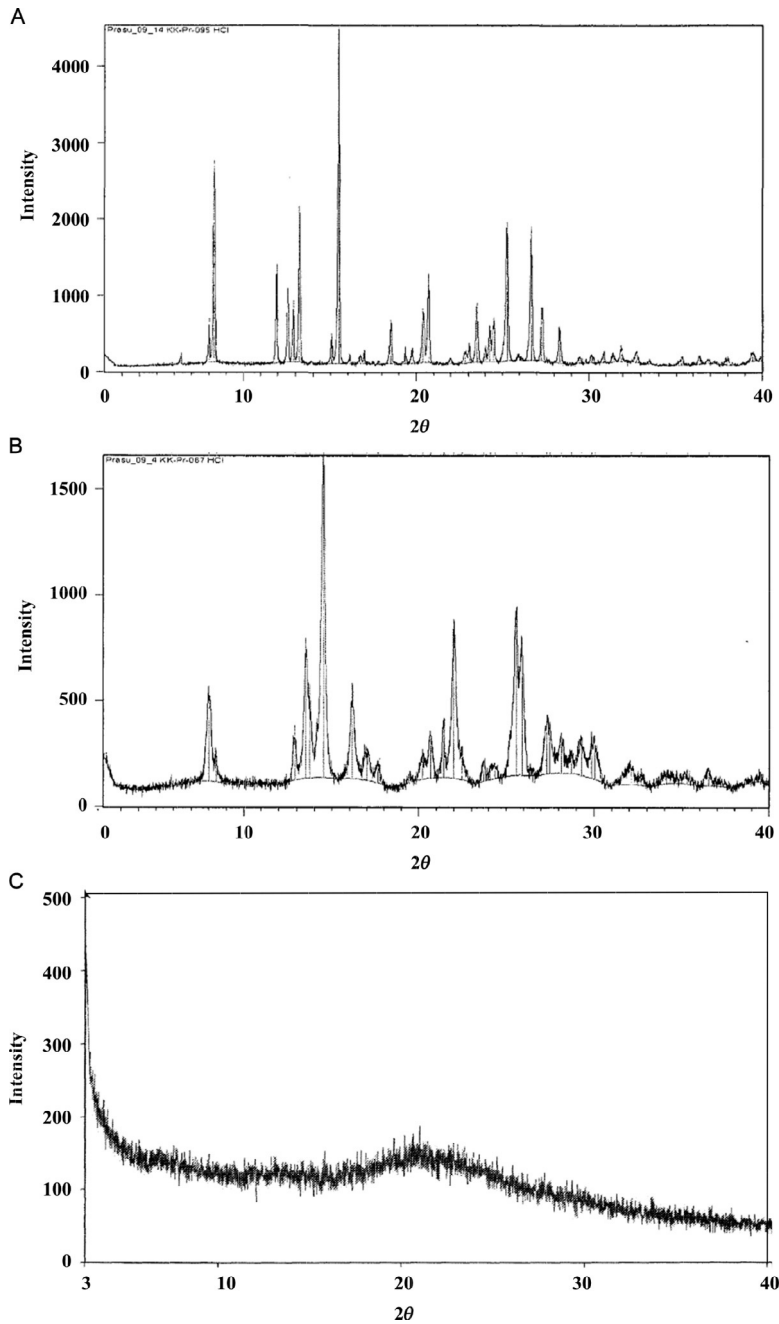


Figure 7 The XRPD patterns of prasugrel HCl (A) Form A, (B) Form B, and (C) amorphous form.

Table 7 The Crystallographic Data from the X-ray Powder Diffraction Patterns of Prasugrel HCl (Form A and Form B)

Form A			Form B		
Scattering Angle (2 θ)	d-Spacing (Å)	Relative Intensity (%)	Scattering Angle (2 θ)	d-Spacing (Å)	Relative Intensity (%)
8.33	10.600	59.9	8.01	11.028	27.1
11.94	7.407	41.5	12.88	6.870	15.2
12.55	7.045	23.4	13.52	6.545	41.4
12.88	6.869	18.4	14.52	6.095	100.0
13.24	6.681	45.8	16.17	5.476	27.0
15.52	5.705	100.0	22.01	4.035	47.7
18.52	4.786	12.7	25.57	3.481	47.0
20.41	4.348	16.0	27.28	3.267	16.2
20.72	4.283	27.7	28.17	3.165	10.7
25.29	3.518	40.4	29.27	3.049	11.8
26.68	3.339	39.0			
27.31	3.263	15.6			
28.35	3.146	10.1			

3.10 Thermal Analysis

3.10.1 Melting Behavior

The melting points of prasugrel and prasugrel HCl are listed in [Table 8](#). The data indicate that prasugrel melts within the temperature range of 120–125 °C excluding the lower value (114–118 °C) reported by Thijs *et al.* [23].

As shown in [Table 8](#), prasugrel HCl exists in different polymorphic forms each with different melting points. For example, crystals A and B (B1 and B2) melt within the temperature range of 133–136 °C and 165–178 °C, respectively [7]. Stepankova *et al.* [75] described different procedures to prepare prasugrel HCl Forms A and B with melting range of 122–124 °C and 165–168 °C, respectively. It is worth mentioning that Forms A and B have the same XRPD patterns of crystal A and crystal B (B1 and B2), respectively, which indicates that they are almost the same forms [7,75]. The significant difference between the melting points of Form A and crystal A may be justified on the basis of differences in

Table 8 The Melting Point and DSC Endothermic Peak of Different Forms of Prasugrel and Prasugrel HCl

Compound	Form	Melting Point (°C)	Endothermic Peak (°C)
Prasugrel	–	120–122 [4,7]	121 ($T_{\text{onset}} = 118.0$) [21]
	–	120–121 [9,24,25,36]	120.7 ($T_{\text{onset}} = 118.7$) [24]
	–	122–124 [10]	117.1 ($T_{\text{onset}} = 116.0$) [77]
	–	120–123 [15,38]	–
	–	120–125 [19,38]	–
	–	114–118 [23]	–
	Form A	121–125 [37]	–
	Form I	120–121.5 [4,76]	–
Prasugrel HCl	Crystal A	133–136 [7]	–
	Form A	122–124 [75]	188.4 ($T_{\text{onset}} = 179.8$) [75]
	Crystal B1	166–174 [7]	–
	Crystal B2	165–178 [7]	–
	Form B	165–168 [75]	184.6 ($T_{\text{onset}} = 179.3$) [75]
	Form B	$\sim 175^+$ $\sim 181^s$ [66]	192 ($T_{\text{onset}} = 185$) [66]
	Seed by crystal B2	192–196 [10]	192.5 ($T_{\text{onset}} = 188.2$) [43]
	Seed by crystal B2	194–197 [10]	–
	Form C	–	128 ^a , 165 ($T_{\text{onset}} = \sim 140$) [21]
	Form D	–	~ 175 ($T_{\text{onset}} = \sim 140$) [21]
	Form E	–	~ 175 ($T_{\text{onset}} = \sim 140$) [21]
	Form G1	–	135, 145.7 ($T_{\text{onset}} = \sim 140$) [18]
	Form G2	–	135, 166.0 ($T_{\text{onset}} = \sim 150$) [18]

^aIt is characterized by a weight loss of 11% by TGA analysis.^{+,s} Heating rates 1 and 2°/min, respectively.

experimental conditions and purity of the tested samples. Miyata *et al.* prepared, by seeding with crystal B2, prasugrel HCl crystals with higher melting point range of 192–197 °C [10].

3.10.2 Differential Scanning Calorimetry

The DSC thermograms of prasugrel HCl (Form A and Form B) were recorded using Perkin Elmer Pyris 1 DSC instrument with a heating rate of 10 °C/min under N₂ atmosphere [75]. Figure 8 shows the DSC thermograms of both forms after holding the sample in the pan for 1 min at 50 °C, followed by heating from 50 to 250 °C at 10 °C/min. From the DSC results, prasugrel HCl Forms A and B have endothermic peaks at 188.4 and 184.6 °C, respectively (Table 8).

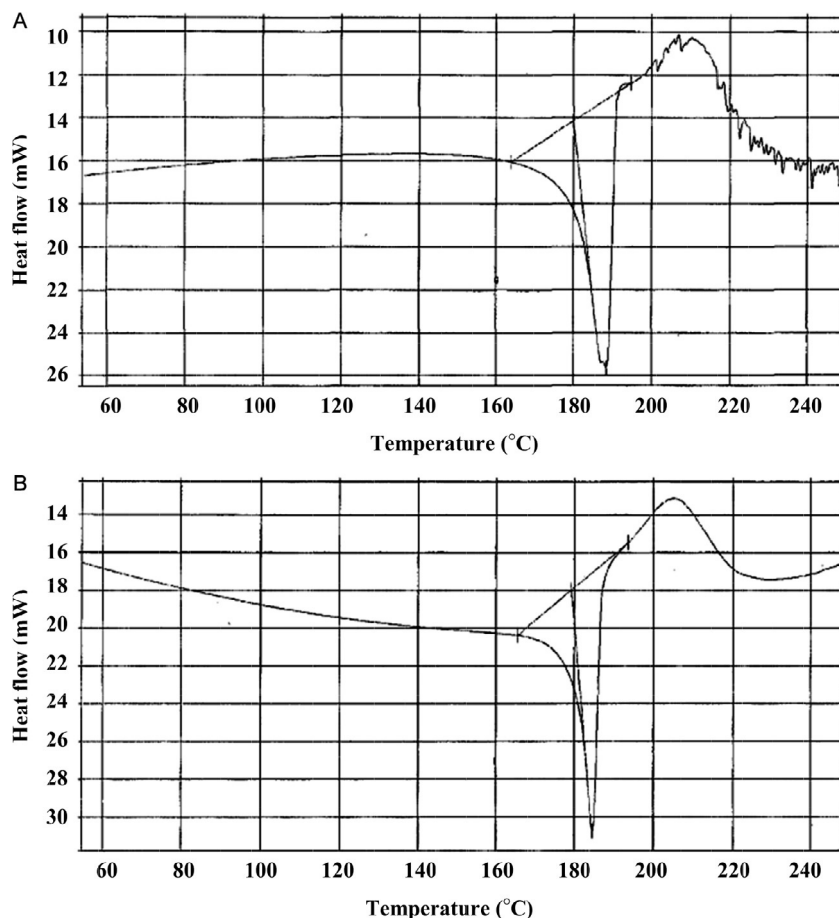


Figure 8 The DSC thermograms of prasugrel HCl (A) Form A and (B) Form B.

The DSC results in Table 8 show that the endothermic peak of prasugrel is within the temperature range of 117–121 °C, which is in agreement with the melting point value. On the other hand, the different forms of prasugrel HCl have different endothermic peaks ranging from 145 to 192 °C (Table 8). It is worth mentioning that the melting point of the same form is generally lower than the endothermic peak obtained by DSC (Table 8). This may indicate that the melting of prasugrel HCl (with decomposition) is sensitive to method parameters such as the heating rate, starting point, and atmosphere (e.g., under ambient or nitrogen atmosphere).

3.10.3 Thermogravimetric Analysis

The thermogravimetric analysis thermogram of prasugrel HCl (Form B) was recorded using a Mettler Toledo DSC 823e [66]. Sample (5 mg) was weighed in silica crucible and heated from 25 to 250 °C with a heating rate of 10 °C/min under nitrogen purge (80 ml/min). Prasugrel HCl exhibits no loss in weight until heated beyond the temperature of its thermal decomposition at ~185 °C (Figure 9).

3.11 Spectroscopy

3.11.1 UV/VIS Spectroscopy

The ultraviolet/visible (UV/VIS) absorption spectra of prasugrel HCl in different solvents were recorded using the Beckman Coulter DU-650 spectrophotometer [66]. Figure 10 shows the UV/VIS absorption spectrum of prasugrel HCl (0.02 mg/ml) in methanol. The maximum recorded at

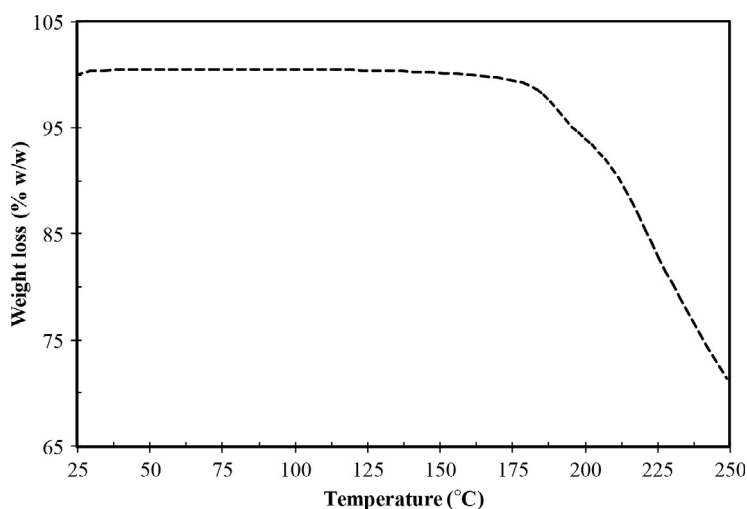


Figure 9 The TGA thermogram of prasugrel HCl (Form B).

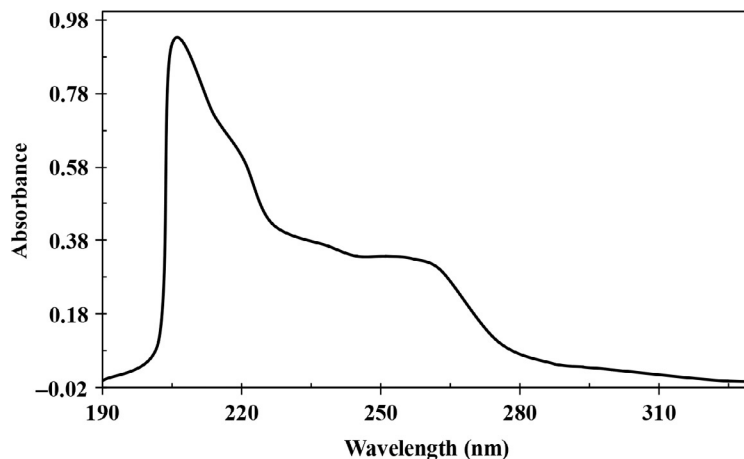


Figure 10 The UV/VIS absorption spectrum of prasugrel HCl (0.02 mg/ml) in methanol.

Table 9 The UV/VIS Absorption Data of Prasugrel HCl in Different Solvents

Solvent	λ_{\max} (nm)	A (1%, 1 cm) (g/100 ml) ⁻¹ cm ⁻¹
Methanol	205	440
	~250	164
Water	195	747
	~250	141
0.1 N HCl	205	474
	~250	146
0.1 N NaOH ^a	220	377
	265	140

^aAs prasugrel degrades in basic media, the absorbance was measured immediately.

205 nm is apparently due to the $\pi \rightarrow \pi^*$ electronic transitions in the aromatic ring. The longest wavelength maximum recorded at ~250 nm (Broad shoulder) is due to an $n \rightarrow \pi^*$ electronic transition.

The UV/VIS absorption summary data including solvent type, λ_{\max} , and the intensity of absorption (A (1%, 1 cm)) are listed in [Table 9](#).

3.11.2 Vibrational Spectroscopy

3.11.2.1 Fourier Transform Infrared Spectroscopy

The FT-IR absorption spectrum of prasugrel HCl (Form B) was recorded using the Perkin Elmer Paragon 1000 FT-IR Spectrometer (KBr disc) in the range of 4400–400 cm⁻¹ [66]. The FT-IR spectrum is shown in [Figure 11](#) and its corresponding assignments are given in [Table 10](#). As mentioned in [Section 3.5](#), FT-IR technique can be used to distinguish between different

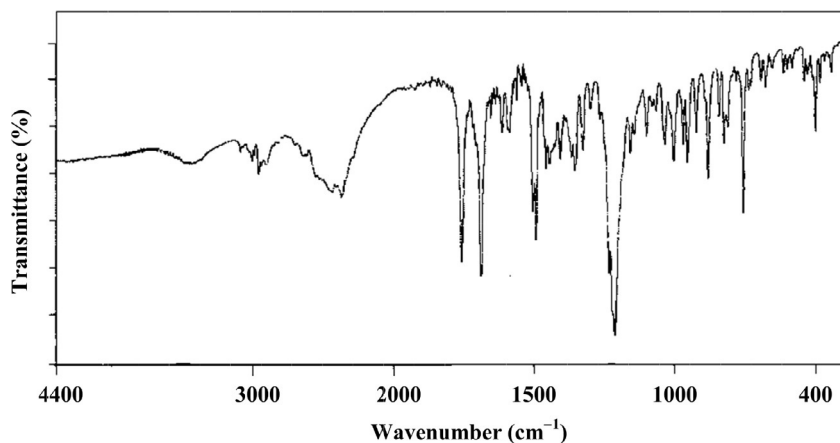


Figure 11 The FT-IR absorption spectrum of prasugrel HCl (Form B) using KBr disc.

Table 10 The Assignments of the FT-IR Absorption Bands of Prasugrel HCl (Form B)

Wavenumber (cm ⁻¹)	Assignment
3425	$\nu(\text{H}_2\text{O})$; broad
3100–3005	$\nu(\text{C—H})$; aromatic
2985–2890	$\nu(\text{C—H})$; aliphatic
2440	$\nu(\text{—NH}^+)$; broad
1758	$\nu(\text{C=O})$; carboxylate
1690	$\nu(\text{C=O})$; cyclopropylcarbonyl
1615 – 1590	$\nu(\text{C=C})$; aromatic
1505–1490	$\delta_b(\text{C—H})$
1405	$\nu(\text{C—F})$
1355, 1325	$\nu(\text{C—N})$
1215, 1235	$\nu(\text{C—O})$
1155, 1140	$\nu(\text{C—C})$
1100–1135	$\delta_b(\text{=C—H})$, in plane
955–880	$\delta_b(\text{=C—H})$, out of plane
825, 755	$\nu(\text{C—S})$
690–485	Ring deformation

ν , stretching; δ_b , bending.

forms of prasugrel HCl. For example, Form A of prasugrel HCl has characteristic IR bands at 1762 and 1720 cm^{-1} , while Form B has characteristic IR bands at 1758 and 1690 cm^{-1} [7].

3.11.2.2 Raman Spectroscopy

The Raman absorption spectra of prasugrel and Forms A and B of prasugrel HCl were recorded using the Kaiser RXN2 Raman spectrometer [74]. The Raman spectra of prasugrel and both forms of prasugrel HCl are shown in Figure 12 and the assignments of part of distinctive Raman bands are given in Table 11. As shown in Figure 12, the minimal differences in the spectra of the two forms are observed in the range of 1800–1300 cm^{-1} , but the spectrum of Form A has sharp characteristic peaks in the range of 900–600 cm^{-1} in comparison with that of Form B.

3.11.3 Nuclear Magnetic Resonance Spectrometry

3.11.3.1 ^1H NMR Spectrum

The ^1H NMR spectrum of prasugrel HCl was obtained using the Bruker Avance-300 spectrometer [66]. The sample was dissolved in DMSO- d_6 and all resonance bands were referenced to the tetramethylsilane (TMS) internal standard. The ^1H NMR and COSY ^1H NMR spectra of prasugrel HCl are shown in Figures 13 and 14, respectively. In Figure 13, the presence of broad signal at 11.75 ppm is due to the hydrochloride proton. The assignments of the resonance bands are given in Table 12.

3.11.3.2 ^{13}C NMR Spectrum

The ^{13}C NMR spectrum of prasugrel HCl was obtained using the Bruker Avance-300 spectrometer [66]. The sample was dissolved in DMSO- d_6 and all resonance bands were referenced to the TMS internal standard. The ^{13}C NMR, DEPT, HMQC, and HMBC spectrum of prasugrel HCl are shown in Figures 15, 16, 17, and 18, respectively. The ^{13}C NMR assignments are given in Table 13 with their relative intensities (DMSO peak is observed at ~ 40 ppm).

3.11.3.3 Solid ^{13}C NMR Spectrum

The solid ^{13}C NMR spectra of different forms of prasugrel HBr were recorded using Bruker Avance II⁺ spectrometer [81]. Figure 19 shows the spectra of prasugrel HBr Forms I, III, and VII (methyl ethyl ketone solvate) and the assignments of Form I are given in Table 14. The solid ^{13}C NMR spectra show some differences between the different forms of

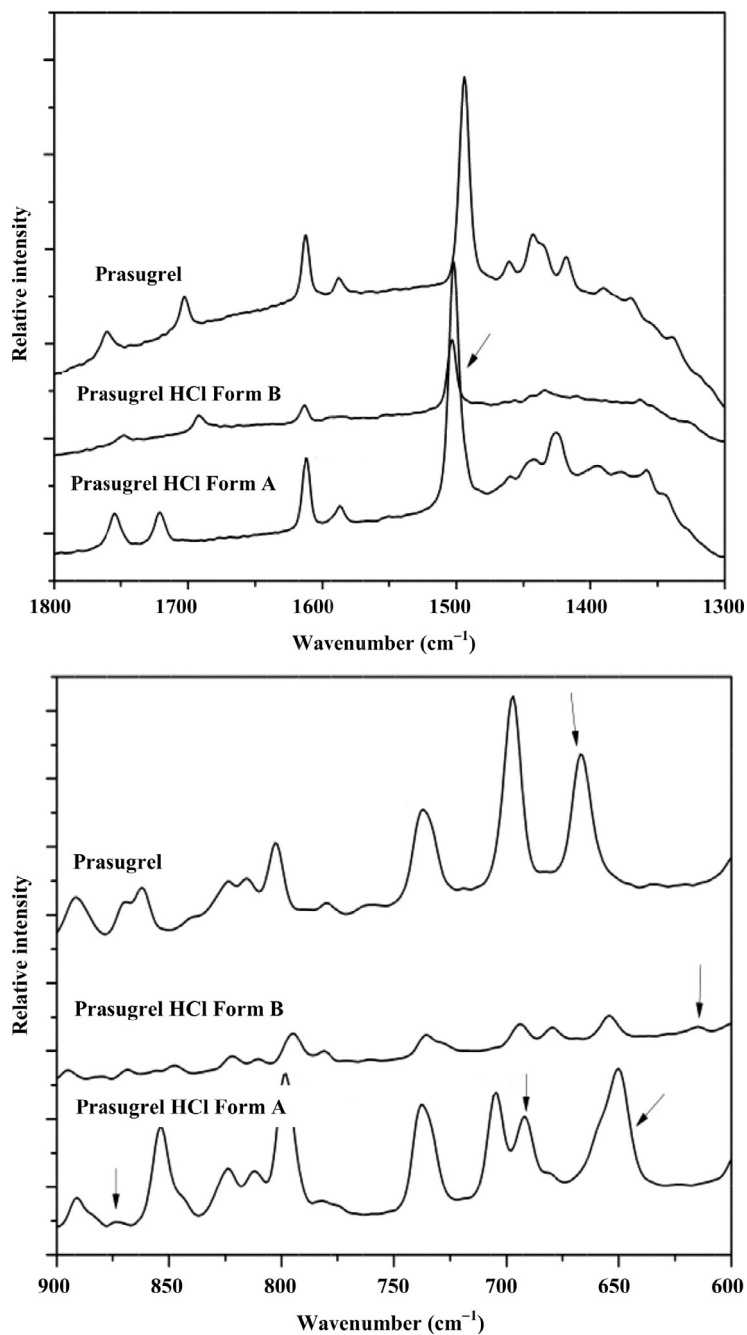


Figure 12 The Raman absorption spectrum of prasugrel and Forms A and B of prasugrel HCl in the wavenumber ranges of 1800–1300 and 900–600 cm^{-1} .

Table 11 The Assignments of Some of the Raman Absorption Bands of Prasugrel HCl

Wavenumber (cm ⁻¹)	Assignment
1750	$\nu(\text{C=O})$; carboxylate
1695	$\nu(\text{C=O})$; cyclopropylcarbonyl
1615, 1585	$\nu(\text{C=C})$; aromatic
1510	$\delta_{\text{b}}(\text{CH}_3)$
1420	$\delta_{\text{b}}(\text{CH}_2)$
740	$\nu(\text{C-S})$
650	$\nu(\text{C-F})$

ν , stretching; δ_{b} , bending.

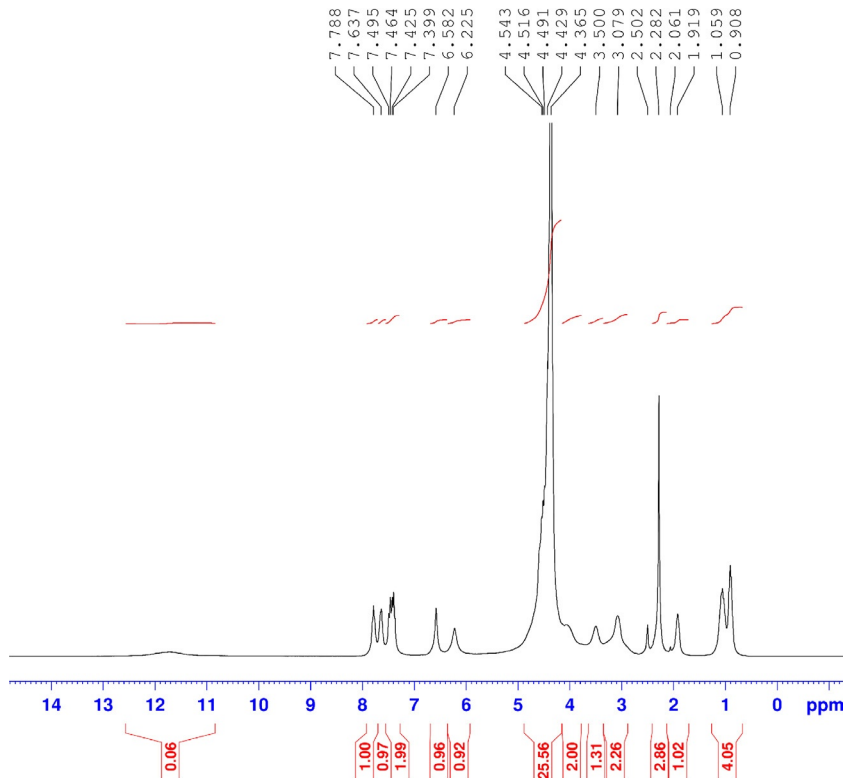


Figure 13 The ¹H NMR spectrum of prasugrel HCl in DMSO-*d*₆.

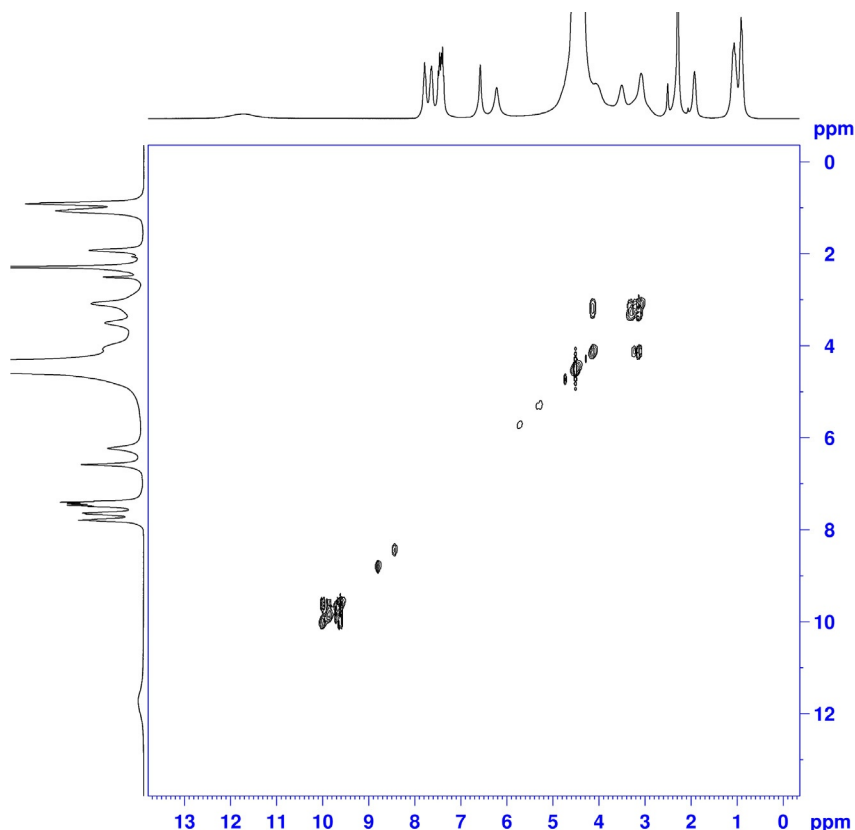


Figure 14 The COSY ^1H NMR spectrum of prasugrel HCl in $\text{DMSO-}d_6$.

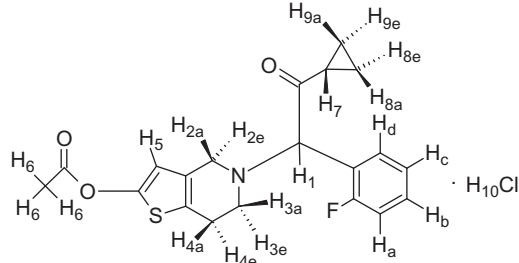
prasugrel HBr in chemical shift and peak intensity as shown in [Figure 19](#). It is worth mentioning that solid ^{13}C NMR spectra is almost similar to that obtained for prasugrel HCl in DMSO solution ([Figure 15](#)) with some differences in the chemical shifts and broadness of the peaks.

3.12 Mass Spectrometry

The mass spectrum of prasugrel was performed using mass spectrometry equipped with an electro-spray ionization source [83]. [Figure 20](#) shows the full mass fragmentation pattern and [Table 15](#) shows its corresponding mass fragments.

The mass spectrum of prasugrel HCl was obtained by direct insertion (DI) into Shimadzu QP5050A gas chromatography mass spectrometer using electron impact ionization and analyzed using GC-MS solution

Table 12 The ¹H NMR Spectral Assignments for Prasugrel HCl



Chemical Shift (ppm)	Number of Proton	Multiplicity	Assignment
11.75	—	br	H ₁₀
7.71	2	m	H _b , H _d
7.46	2	m	H _a , H _c
6.58	1	s	H ₅
6.23	1	s	H ₁
4.50	1 (overlap with HOD)	m	H _{2e}
4.10	2	m	H _{2a} , H _{3e}
3.50	1	m	H _{3a}
3.08	2	m	H _{4a} , H _{4e}
2.28	3	s	H ₆
1.92	1	m	H ₇
1.06	2	m	H _{8e} , H _{9e}
0.91	2	m	H _{8a} , H _{9a}

s, singlet; m, multiplet; br, broad.

software [66]. The spectrum shows a peak at *m/z* of 374 corresponding to the molecular ion of prasugrel ([C₂₀H₂₀FNO₃S+H]⁺) (Figure 21).

4. METHODS OF ANALYSIS

4.1 Compendial Methods

Prasugrel HCl, as drug substance or drug product, is not official in any pharmacopeia. In United States Pharmacopeia Web site, prasugrel HCl and prasugrel tablet are listed in “Priority New Monograph” list [84]. They have been approved by the FDA and are published in the “Approved Drug Products with Therapeutic Equivalence Evaluations” in Orange Book [85].

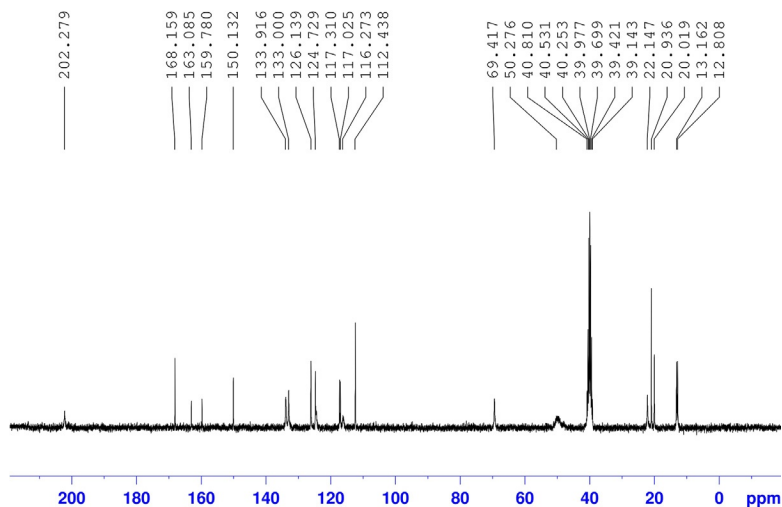


Figure 15 The ^{13}C NMR spectrum of prasugrel HCl in $\text{DMSO}-d_6$.

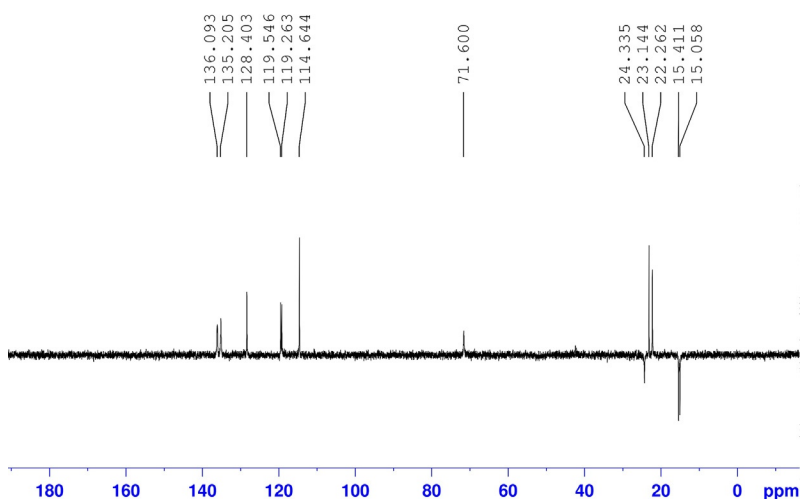


Figure 16 The DEPT spectrum of prasugrel HCl in $\text{DMSO}-d_6$.

4.2 Titrimetric Methods

4.2.1 Aqueous Titration

About 410 mg of prasugrel HCl, accurately weighed, are dissolved in 50 ml of water. The sample is potentiometrically titrated with 0.1 N NaOH VS. Each ml of 0.1 N NaOH is equivalent to 40.99 mg of $\text{C}_{20}\text{H}_{21}\text{ClFNO}_3\text{S}$ [66].

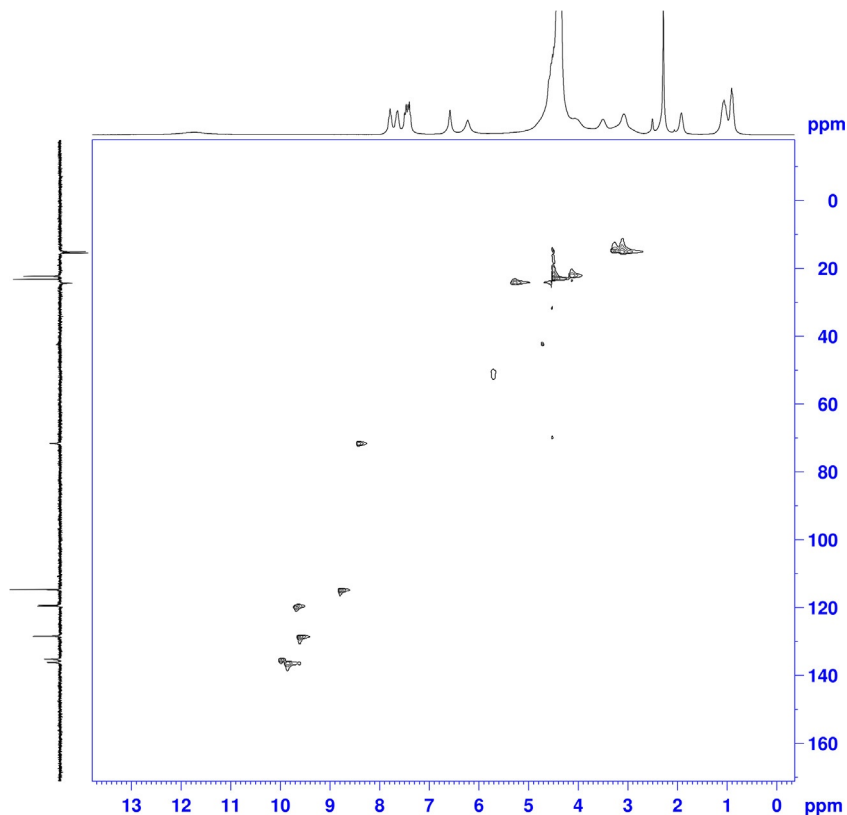


Figure 17 The HMQC spectrum of prasugrel HCl in DMSO- d_6 .

4.2.2 Nonaqueous Titration

About 410 mg of prasugrel HCl, accurately weighed, is dissolved in 50 ml of anhydrous glacial acetic acid. 10 ml of 6% mercuric acetate solution (in acetic acid) is added. The sample is potentiometrically titrated with 0.1 N HClO_4 VS. Each ml of 0.1 N HClO_4 is equivalent to 40.99 mg of $\text{C}_{20}\text{H}_{21}\text{ClFNO}_3\text{S}$ [66].

4.2.3 Argentometric Titration

About 410 mg of prasugrel HCl, accurately weighed, is dissolved in 50 ml of water. The sample is potentiometrically titrated with 0.1 N AgNO_3 VS. Each ml of 0.1 N AgNO_3 is equivalent to 40.99 mg of $\text{C}_{20}\text{H}_{21}\text{ClFNO}_3\text{S}$ [66].

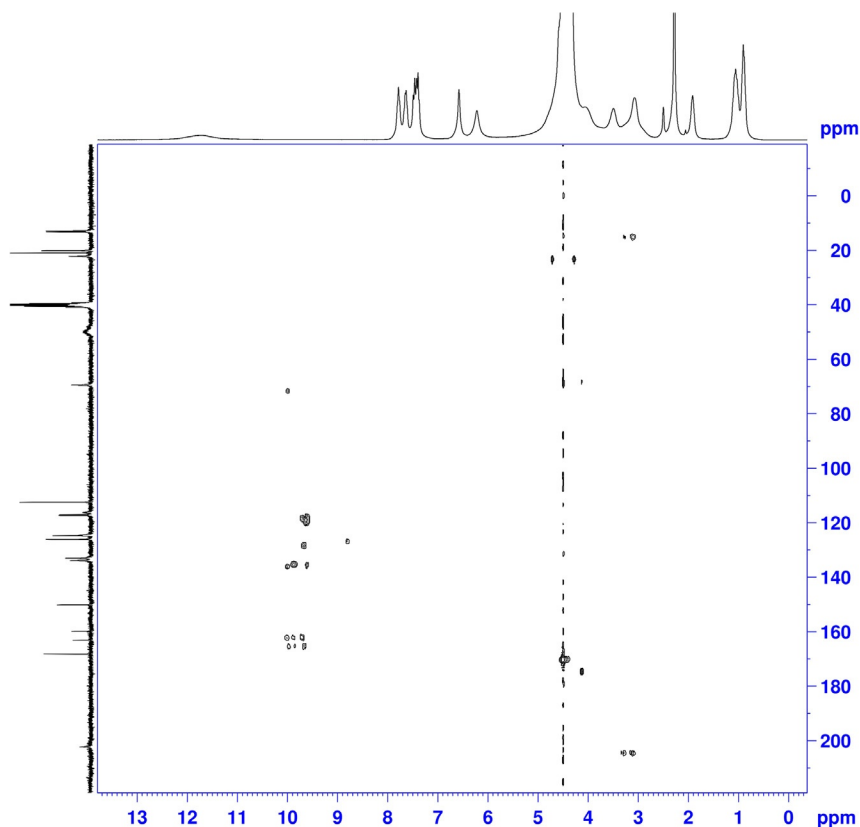


Figure 18 The HMBC spectrum of prasugrel HCl in DMSO- d_6 .

4.3 Spectroscopic Methods

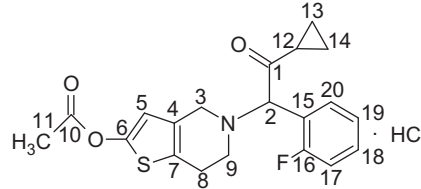
4.3.1 Spectrophotometry

Direct measurements of prasugrel as a bulk material alone or in combination with aspirin in its tablets by UV/VIS spectrophotometric methods were reported (Table 16). The determination is based on the use of different absorption modes including zero, 1st, and 2nd derivatives, and area under curve (AUC) methods. The solvents are 0.1 N HCl, 0.1 N NaOH, and methanol. The calibration range and quantitation limit for these methods are in the range of 1–60 $\mu\text{g/ml}$ and 0.4–1.9 $\mu\text{g/ml}$, respectively.

4.3.2 Colorimetry

The determination of prasugrel as a bulk material and in tablets by colorimetric method was reported [93]. It is based upon the formation of

Table 13 The ¹³C NMR Spectral Assignments for Prasugrel HCl



Chemical Shift (ppm)	Assignment	Relative Intensity (%)
202.28	1	9.09
168.16	10	48.48
161.44	16	24.42
150.13	6	36.36
133.92	4	24.24
133.00	20	27.27
126.14	18	45.45
124.73	19	42.42
117.31	15	33.33
117.03	7	33.33
112.44	5, 17	75.75
69.42	2	21.21
50.28	3	9.09
39.98	DMSO	—
22.15	9	25.00
20.94	8, 12	100.00
20.02	11	54.17
13.00	13, 14	48.48

extractable prasugrel-bromocresol green complex from phosphate buffer of pH 3.6 (chloroform extraction system). The colored complex is measured by spectrophotometry at 418 nm with a linearity range of 10–100 µg/ml. The proposed method was applied for the determination of prasugrel in tablet and gave acceptable % recovery (97.6–98.1%).

Another colorimetric method was developed for the determination of prasugrel as a bulk material, in tablets and in biological fluids [94]. It is based upon the formation of extractable ion pair complex of prasugrel and

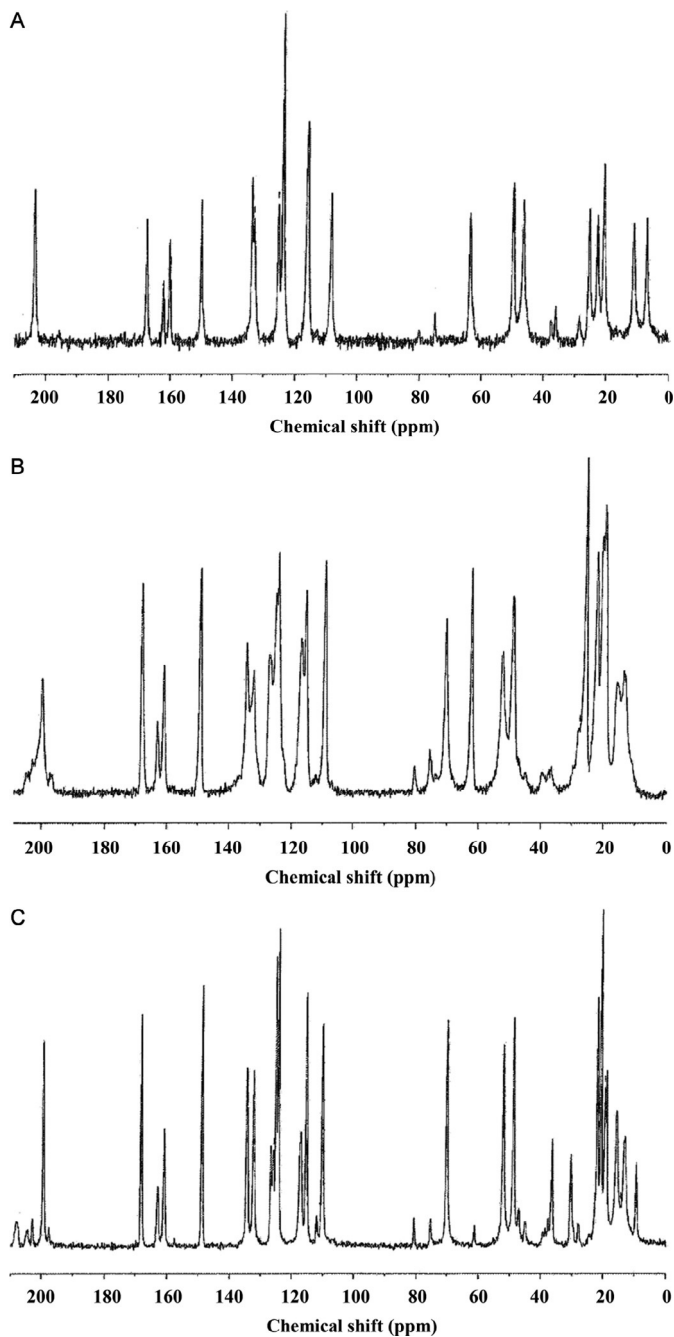
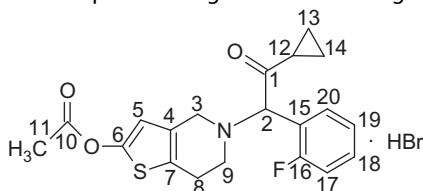


Figure 19 The solid ^{13}C NMR spectrum of prasugrel HBr (A) Form I, (B) Form III, and (C) Form VII (methyl ethyl ketone solvate).

Table 14 The Solid ^{13}C NMR Spectral Assignments for Prasugrel HBr (Form I)

Chemical Shift (ppm)	Assignment	Relative Intensity (%)
203.37	1	47.44
167.59	10	38.46
161.22	16	30.05
150.02	6	44.87
133.69	4	50.00
133.02	20	38.46
125.13	18	42.31
123.74	19	100.00
115.83	7, 15	66.67
108.26	5, 17	44.87
63.63	2	39.74
48.06	3,	50.00
25.40	9	42.31
22.79	8, 12	39.74
20.78	11	53.85
11.23	13, 14	38.46

bromophenol blue from acetate buffer of pH 3.8 (chloroform extraction system). The measurements were performed at 416 nm. The linearity was obtained over a concentration range of 5–10 $\mu\text{g/ml}$ and % recovery was obtained within a range of 99–100%.

The accurate, precise, and simple colorimetric method was developed for the determination of prasugrel in bulk and in tablets [95]. The proposed methods depend upon the reduction of Fe^{3+} to Fe^{2+} by prasugrel, followed by reaction of Fe^{2+} with 1,10-phenanthroline to give a soluble yellowish-orange complex. The colored complex was determined colorimetrically

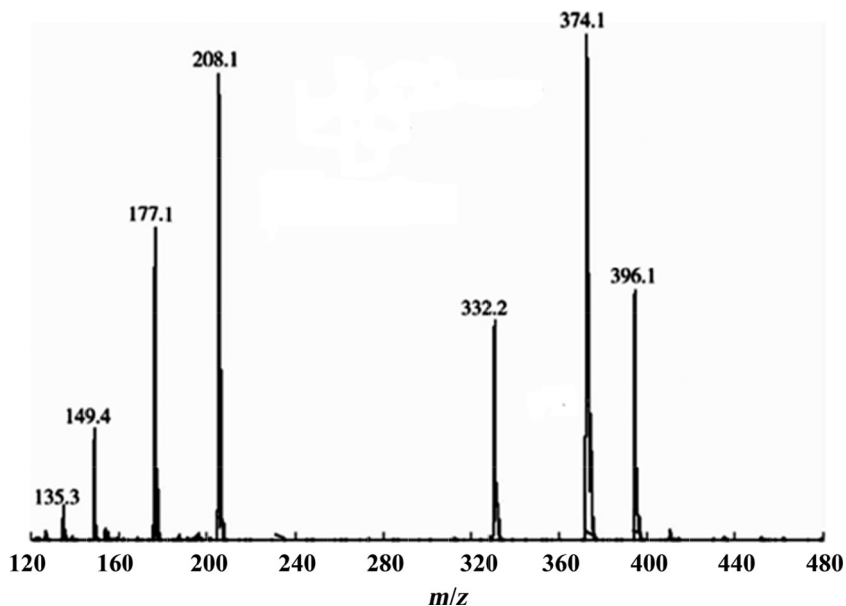


Figure 20 The mass spectrum of prasugrel obtained by mass spectrometer equipped with electro-spray ionization (ESI) source.

at 510 nm. The linearity was obtained over a concentration range of 5–30 $\mu\text{g/ml}$ and % recovery was within a range of 99.3–99.7%.

Furthermore, a simple, sensitive and selective colorimetric method was developed for the determination of prasugrel as bulk material and in tablets [96]. It involves the addition of excess NBS of known concentration in the presence of 1 N HCl, reactants are allowed to react and the unreacted NBS is estimated by the measurement in the decrease in the absorbance of the Rhodamine-B dye at 557 nm. The linearity was obtained over a concentration range of 0.6–4.2 $\mu\text{g/ml}$ and % recovery was within a range of 99.3–100.0%. Kabir *et al.* also reported a new colorimetric method for the determination of prasugrel in bulk and in tablets [97]. Bromophenol blue was used to form ion pair complex with the drug in 0.1 M H_2SO_4 . The maximum absorbance of the complex formed by bromophenol blue and the drug was found to be at 421 nm.

4.4 Chromatographic Methods

4.4.1 High-Performance Thin Layer Chromatography

High-performance thin layer chromatographic (HPTLC) method of the determination of prasugrel in the presence of its acid, base, oxidation, dry

Table 15 The Mass Spectral Fragmentation for Prasugrel

<i>m/z</i>	Relative Abundance (%)	Fragment	
		Formula	Structure
396.1	48.7	$[\text{C}_{20}\text{H}_{20}\text{FNO}_3\text{S} + \text{Na}]^+$	
374.1	100.0	$[\text{C}_{20}\text{H}_{21}\text{FNO}_3\text{S}]^+$	
332.2	43.6	$[\text{C}_{20}\text{H}_{21}\text{FNO}_3\text{S} + \text{H}]^+ - [\text{COCH}_3]$	
208.1	92.3	$[\text{C}_{12}\text{H}_{14}\text{FNO} + \text{H}]^+$	
177.1	61.5	$[\text{C}_{11}\text{H}_{10}\text{FO}]^+$	
149.4	23.1	$[\text{C}_7\text{H}_4\text{NOS}]^+$	
135.3	10.3	$[\text{C}_7\text{H}_5\text{NS}]^+$	

heat, and light degradation products was developed [98]. The TLC aluminum plates precoated with silica gel 60 F254 was used as the stationary phase. The solvent system consisted of dichloromethane/methanol (9.9:0.1 v/v) and densitometric analysis was carried out in the absorbance mode

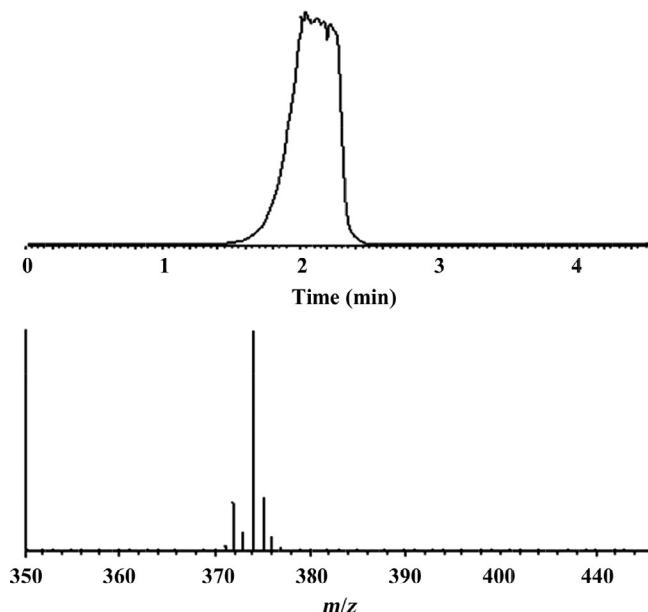


Figure 21 The mass spectrum of prasugrel HCl obtained by gas chromatography mass spectrometer using electron impact (EI) ionization source.

at 254 nm. The linearity was obtained in a range of 300–1500 ng/band and % recovery was within a range of 98–102%. The limits of detection and quantitation were found to be 287 ng/band and 869 ng/band, respectively.

4.4.2 High-Performance Liquid Chromatography

Various HPLC methods were reported for the determination of prasugrel, its impurities, and metabolites in bulk material, in pharmaceutical formulations and in biological fluids. HPLC systems with ultraviolet or mass spectrometric detection were applied in these studies. These HPLC methods with their full parameters and applications are listed in [Table 17](#).

4.4.3 Ultra Performance Liquid Chromatography

Different UPLC methods were reported to determine the prasugrel and its impurities in bulk material and tablets ([Table 18](#)).

4.4.4 Capillary Electrophoresis

A capillary electrophoresis method was developed to determine simultaneously prasugrel counter ion and other possible impurities during the synthesis process [123].

Table 16 The UV/Visible Spectrophotometric Methods for the Determination of Prasugrel HCl

Material	Mode/ λ (nm)/Solvent	Range ($\mu\text{g/ml}$)	LD/LQ ($\mu\text{g/ml}$)	Reference
Bulk material and tablets	Zero-order/249/0.1 N HCl	1–50	1.9/6.9	[86]
Bulk material and tablets	Zero-order/254/0.1 N HCl 1st derivative/272/0.1 N HCl AUC/244–264/0.1 N HCl	1–50	–	[87]
Bulk material and tablets	$\Delta A_{254-239}$ /0.1 N HCl, 0.1 N NaOH	5–30	0.7/2.0	[88]
Tablets with aspirin	Zero-order/254, 276/methanol Q-absorbance ratio method/ 274.7, 254/methanol	5–60	0.4/1.2 0.4/1.1	[89]
Bulk material, with aspirin and tablet excipients	2nd derivative/267.62, 252.40/ methanol Ratio 1st derivative/268, 290/ methanol	5–45 6–22	0.7/2.2 0.4/1.4	[90]
Bulk material and tablets	Zero-order/248/methanol 1st derivative/248/methanol	5–25 5–25	0.6/2.0 0.2/0.6	[91]
Bulk material and tablets	Zero-order/252/methanol	10–60	1.0/3.1	[92]

LD, detection limit; LQ, quantitation limit; AUC, area under curve.



5. STABILITY

5.1 Solid-State Stability

It was reported that the HCl salt of prasugrel has better hydrolytic stability and provides a better solubility at relevant physiological pHs than other salts and the free base [1,7].

Furthermore, stability studies of prasugrel HCl on long term (25 °C/60% RH) and accelerated conditions (40 °C/75% RH) showed no significant changes at 25 °C/60% RH nor at 40 °C/75% RH except for an impurity which increased, but still within the limit [1]. The photostability study of solid prasugrel HCl showed that it is stable against light. The stress degradation studies indicated that prasugrel HCl is susceptible to hydrolysis and therefore contact with water should be avoided [1]. Furthermore, the effect of exposure solid prasugrel HCl to light or moderate temperatures (<70 °C)

Table 17 The HPLC Parameters of the Method Used for the Determination of Prasugrel, Its Impurities, and Metabolites

Material	Stationary Phase	Mobile Phase (v/v)	Detection	Flow Rate (ml/min)	Reference
Bulk material, its impurities, and degradates	Gemini C ₁₈ (5 μ m, 250 \times 4.6 mm)	ACN:50 mM KH ₂ PO ₄ :H ₂ O (63:30:7)	UV: 220	1.2	[6]
Dog plasma, S-methyl metabolite	YMC Pack A302 C ₁₈ (5 μ m, 150 \times 4.6 mm)	ACN:2-PrOH:TFA:H ₂ O (10:12:0.01:78)	UV: 220	1.0	[7]
Bulk material, intermediate	TSK C ₁₈ 80TM (5 μ m, 150 \times 4.6 mm)	ACN:5 mM KH ₂ PO ₄ (4:1)	UV: 254	1.0	[9]
Bulk material and impurities	Hypersil BDS C ₁₈ (5 μ m, 250 \times 4.6 mm)	ACN:Buffer (60:40)	UV: 240	0.8	[15]
Bulk material and impurities	Cadenza CD C ₁₈ (3 μ m, 150 \times 4.6 mm)	Gradient system: (A) ACN:PO ₄ buffer (20:80) and (B) ACN:PO ₄ buffer (80:20), PO ₄ buffer: 0.272% KH ₂ PO ₄ and 0.15 TEA, pH 6.0 by dilute H ₃ PO ₄	UV: 210	1.2	[21]
Bulk material and impurities	C ₁₈ , (5 μ m, 250 \times 4.6 mm)	Gradient system: (A) 10 mM KH ₂ PO ₄ , pH 2.2 and (B) ACN	UV: 228	1.0	[24,30,75]
Bulk material and tablets	Shimadzu C ₁₈ column (5 μ m, 150 \times 4.6 mm)	ACN:TFA (45:55)	UV: 252	1.0	[92]
Human plasma, stereoisomers of active metabolite	BetaBasic C ₄ Javelin Guard (10 \times 2 mm) connected to two ProntoSIL Chiral AXQN (150 \times 2 mm and 250 \times 2 mm)	MeOH:AcOH: 0.1 M NH ₄ OAc: H ₂ O (200:1.2:0.0025:0.6)	MS/MS	0.17	[99]

Human plasma, active and inactive metabolites	Monochrome C ₁₈ (5 µm, 50 × 2 mm)	MeOH:1% HCO ₂ H (50:50) and (54:46) for the inactive and active metabolite assays, respectively	MS/MS	0.25	[100]
Tablets	L-CERI C ₁₈ (5 µm, 150 × 4.6 mm)	ACN:0.01 M PO ₄ buffer, pH 2.8 (35:65)	UV: 260	–	[101]
Tablets	XTerra C ₁₈ (5 µm, 250 × 4.6 mm)	ACN:30 mM K ₂ HPO ₄ , pH 3.2 (75:25)	UV: 210	1.0	[102]
Bulk material and tablets	Inertsil ODS-3V (5 µm, 250 × 4.6 mm)	ACN:20 mM KH ₂ PO ₄ and 20 mM K ₂ HPO ₄ (70:30)	UV: 210	1.0	[103]
Tablets	Inertsil C ₁₈ (5 µm, 150 × 4.6 mm)	ACN:20 mM KH ₂ PO ₄ , pH 3.1 by H ₃ PO ₄ : (85:15)	UV: 230	1.0	[104]
Bulk material and tablets	–	ACN:10 mM PO ₄ buffer, pH 6.5: H ₂ O (54:40:6)	UV: 235	1.2	[105]
Bulk material	Phenomenex C ₈ (5 µm, 250 × 4.6 mm)	ACN:10 mM NH ₄ OAc (85:15)	UV: 245	0.9	[106]
Bulk material	Kromasil C ₁₈ (5 µm, 250 × 4.6 mm)	MeOH:10 mM KH ₂ PO ₄ , pH 2.2 (70:30)	UV: 257	1.0	[107]
Tablets	Grace Smart C ₁₈ (5 µm, 150 × 4.6 mm)	ACN:MeOH:20 mM NaH ₂ PO ₄ , pH 3 by H ₃ PO ₄ (35:20:45)	UV: 220	1.0	[108]
Bulk material and tablets	Kromasil C ₁₈ (5 µm, 100 × 4.6 mm)	MeOH: 0.136% KH ₂ PO ₄ , pH 2.1 by H ₃ PO ₄ (70:30)	UV: 220	0.8	[109]

Continued

Table 17 The HPLC Parameters of the Method Used for the Determination of Prasugrel, Its Impurities, and Metabolites—cont'd

Material	Stationary Phase	Mobile Phase (v/v)	Detection	Flow Rate (ml/min)	Reference
Tablets	Zorbax XDB C ₈ (3.5 µm, 150 × 4.6 mm)	ACN:50 mM NH ₄ OAc, pH 4.5 by AcOH (60:40)	UV: 254	1.0	[110]
Bulk material	C ₁₈ , (5 µm, 250 × 4.6 mm)	ACN:MeOH (10:90)	UV: 240	1.0	[111]
Tablets with aspirin	Luna C ₁₈ (5 µm, 150 × 4.60 mm)	ACN:50 mM NH ₄ OAc, pH 4.5 (75:25)	UV: 245	0.6	[112]
Human plasma, active metabolite	Hypurity C ₁₈ (5 µm, 50 × 4.6 mm)	ACN:10 mM NH ₄ HCO ₂ , pH 3.0 (50:50)	MS/MS	–	[113]
Metabolism by human liver microsomes and human sera	Phenomenex Gemini C ₁₈ (3 µm, 100 × 2 mm)	Gradient system: (A) 10 mM NH ₄ OAc, pH 4.6 and (B) ACN/ MeOH/H ₂ O (7:2:1)	MS	0.2	[113]
Tablets with acetaminophen	Luna C ₁₈ (5 µm, 150 × 4.60 mm)	ACN:50 mM NH ₄ OAc, pH 4.5 (75:25)	UV: 245	0.6	[114]
Metabolism by human liver microsomes	Shimadzu Shimpack C ₁₈ (2.3 µm, 75 × 2.1 mm)	Gradient system: (A) 2 mM NH ₄ OAc and 0.2% HCO ₂ H, pH 4.6 and (B) ACN/H ₂ O/HCO ₂ H (980:18:2)	MS	0.25	[115]
Bulk material and impurities	Waters symmetry C ₈ (5 µm, 250 × 4.6 mm)	Gradient system: (A) 0.1% TEA, pH 2.5 by H ₃ PO ₄ and (B) ACN	UV: 220	1.0	[116]

Bulk material, impurities identification	Merck Symmetry shield RP8 (5 μ m, 250 \times 4.6 mm)	Gradient system: (A) 0.01 mM NH ₄ OAc, pH 2.3 and (B) ACN: H ₂ O (70:30)	MS/MS	1.0	[117]
Bulk material and tablets	XTerra C ₁₈ (5 μ m, 150 \times 4.6 mm)	ACN:0.272% KH ₂ PO ₄ , pH 3.0 by H ₃ PO ₄ (60:40)	UV: 210	1.0	[118]
Bulk material and tablets with aspirin	Kromasil 100 C ₁₈ (5 μ m, 150 \times 4.6 mm)	ACN:MeOH:H ₂ O (30:10:60), pH 3.0 by H ₃ PO ₄	UV/PDA	1.0	[119]
Bulk material and tablets with aspirin	Phenomenex C ₈ (5 μ m, 250 \times 4.6 mm)	MeOH:H ₂ O (80:20)	236	1.0	[120]

ACN, acetonitrile; TFA, trifluoroacetic acid; AcOH, acetic acid; OAc, acetate; 2-PrOH, 2-propanol; TEA, triethylamine; HCO₂H, fumaric acid.

Table 18 The UPLC Parameters of the Method Used for the Determination of Prasugrel HCl

Material	Stationary Phase	Mobile Phase (v/v)	Detection	Flow Rate (ml/min)	Reference
Bulk material, impurities determination	Acquity BEH C ₁₈ (1.7 μ m, 50 \times 2.1 mm)	Gradient system: (A) 2.5 mM NaH ₂ PO ₄ , pH 5.5 and (B) ACN	UV:220	0.45	[76]
Bulk material	Waters Acquity BEH C ₁₈ (1.7 μ m, 150 \times 2.1 mm)	ACN:H ₂ O (80:20)	UV:245	0.2	[106]
Bulk material, impurities identification	Acquity BEH phenyl (1.7 μ m, 100 \times 2.1 mm)	Gradient system: (A) 0.01 mM KH ₂ PO ₄ , 1.0 ml DEA, pH 3.0 and (B) ACN:H ₂ O (70:30)	UV: 215	0.25	[117]
Tablets	Acquity BEH C ₁₈ (1.7 μ m, 100 \times 2.1 mm)	ACN: MeOH:0.2% TEA, pH 2.5 by H ₃ PO ₄ (25:25:50)	UV: 210	0.4	[121]
Human urine with aliskiren and rivaroxaban	Zorbax RRHD SB-C ₁₈ (1.8 μ m, 50 \times 2.1 mm)	ACN:0.1% HCO ₂ H (30:70)	MS/MS	0.8	[122]

ACN, acetonitrile; MeOH, methanol; TEA, triethylamine; DEA, diethylamine.

on its stability was investigated and the results proved its stability [6,106]. It was found that storage of prasugrel and prasugrel HCl in the presence of desiccant provides a greater stability with respect to impurities such as desacetyl impurity [34].

On the other hand, 50% degradation of prasugrel HCl can be obtained by dry heating at 100 °C for 6 h as measured by HPTLC. Also it was

degraded by 22.6% and 23.5% upon exposure to UV light and fluorescent light (after UV light exposure), respectively [98]. Another study reveals that stress degradation of solid prasugrel HCl at high temperature of 90 °C for 3 h leads to a decrease in assay by ~6% [110], while exposure to short (254 nm) and long (366 nm) lamp for 2 h does not affect its stability.

Comparison between the stability of prasugrel HCl of Form B, which is contained in the original product Effient, with prasugrel HBr of Form C was reported [124]. The results revealed that prasugrel HBr (Form C) exhibits higher chemical stability at 25 °C for 4 months in comparison to prasugrel HCl (Form B) when both packed in double PE foil with dark top layer and desiccant. The increase in % impurities is up to 0.04% in the case of the prasugrel HBr as compared to 0.6% in prasugrel HCl. A dry granulation formulation of prasugrel HBr was proposed using a mixture of mannitol, crosscarmellose sodium, microcrystalline cellulose, and magnesium stearate in a core tablet and Opadry II® 85G (polyvinyl alcohol, polyethylene glycol 3350, talc, titanium dioxide, and lecithin) as a coating material. However, comparison between the stability of prasugrel HBr and prasugrel HCl in such formulation was not considered [124].

In solid dosage form, it was reported that prolonged exposure of prasugrel HCl to air and moisture leads to hydrolysis and oxidation. It was suggested to avoid the use of certain excipients such as povidone and crospovidone (containing trace peroxides) and wet granulation in prasugrel formulation. In addition, using air and moisture impervious gas-inserted blister packs was recommended to improve the stability of prasugrel in solid formulation [125]. Also a sort of interaction between prasugrel HCl and an excipient was observed leading to a partial and irreversible formation of prasugrel-free base in the tablets [1]. Further investigation indicated that salt-to-base formation of at least up to 70% had no clinical impact. It is worth mentioning that Effient label information published by FDA describes the composition as “Original Formulation: During manufacture and storage, partial conversion from prasugrel HCl to prasugrel-free base may occur. Other ingredients include mannitol, hypromellose, crosscarmellose sodium, microcrystalline cellulose, and vegetable magnesium stearate. The color coatings contain lactose, hypromellose, titanium dioxide, triacetin, iron oxide yellow, and iron oxide red (only in Effient 10 mg tablet). Revised Formulation: Other ingredients include mannitol, hypromellose, low-substituted hydroxypropyl cellulose, microcrystalline cellulose, sucrose stearate, and glyceryl behenate. The color coatings contain lactose, hypromellose, titanium dioxide,

triacetin, iron oxide yellow, and iron oxide red (only in Effient 10 mg tablet).” This change in formulation includes addition of low-substituted hydroxypropyl cellulose, sucrose stearate, and glyceryl behenate and deletion of crosscarmellose sodium and vegetable magnesium stearate. Also the statement “During manufacture and storage, partial conversion from prasugrel HCl to prasugrel free base may occur” was removed [2].

Different works to improve the stability of prasugrel HCl in tablet formulation were reported. For example, the stability of prasugrel HCl in tablets was enhanced by using pregelatinized starch as a binder, ethyl cellulose as a hydrophobic polymer in the coating material to protect the drug against absorption of moisture, Al–Al cold packing having no air gap in the pocket of Al blister to prevent any moisture around the tablet, and avoiding the use of inert gases/liquid pressure in packing which is difficult to handle [73]. Use of dry or hot melt granulation in the presence of xylitol and microcrystalline cellulose and with the absence of lactose and mannitol offered higher stability in both Al blisters–normal and –nitrogen atmospheres with comparison with Effient tablets, which packed in Al blisters–nitrogen atmosphere [76]. Furthermore, use one or more of polyvinyl alcohol, sodium carboxymethyl cellulose, and pullulan [101] and water-soluble polymers such as hydroxypropyl methylcellulose, hydroxypropyl cellulose, or polyvinylpyrrolidone [126] improved the stability of prasugrel tablets.

The stability of prasugrel HCl formulation was improved in the presence of sodium bisulfate as antioxidant, a citrate or phosphate buffer, excipients with low moisture content, and package with at least one of a desiccant and an oxygen scavenger [127]. The use of an air and/or moisture impervious container under a positive liquid nitrogen pressure, optionally adding a desiccant an oxygen scavenger, was found to improve the stability of prasugrel HCl in tablet formulation [128].

Furthermore, using polyvinyl alcohol as film coating agent showed excellent storage stability of prasugrel tablets [129]. To improve the content uniformity of prasugrel in tablet, mannitol, or lactose has a particle distribution in which the 90% cumulative diameter is 80–300 μm was used in direct compression formulation [130]. A pharmaceutical composition containing micronized prasugrel base ($<10 \mu\text{m}$) with improved stability and quick dissolution profile was reported [131]. It was prepared by granulating prasugrel base with an aqueous solution, drying the granules thus obtained, and mixing the dry granules with a starch or starch derivatives and sodium stearyl fumarate or stearic acid, followed by pressing into tablets.

5.2 Solution-Phase Stability

The stability of prasugrel HCl in solution was studied by different authors using chromatographic methods (HPTLC, HPLC, and UPLC). The summary of these studies was listed in Table 19. The drug is highly degraded in NaOH, while in H₂O₂ and HCl, it is relatively more stable. It can be considered stable in neutral media at temperature below 60 °C. The desacetyl impurity (OXTP) as a major degrade is formed in solution.

Based upon the different methods of preparation and stability in solution and in solid state, prasugrel may be contaminated by different types of impurities including synthetic impurities, by-products, intermediates, and degradation products. Table 20 represents these potential impurities with their chemical names and structures.

Various impurities of prasugrel HCl were identified by LC/MS and prepared by Sastry *et al.* [134]. These impurities were observed during laboratory optimization and later its bulk synthesis. Most of the impurities were synthesized and their assigned constitutions confirmed by co-injection in HPLC.

5.3 Stability in Biological Fluids

Prasugrel HCl, a racemic prodrug, is rapidly converted to inactive and active metabolites. It is metabolized by esterases to a thiolactone (R-95913, inactive), which is then oxidatively metabolized by several cytochrome P450 enzymes to thiol metabolite (R-138727, active). The active metabolite is further metabolized to its *S*-methyl metabolite (R-106583, inactive) and cysteine conjugate (R-119251, inactive) [1,100,135]. Accordingly, stability of prasugrel metabolites is monitored in the biological fluids rather than the parent compound.

For example, after oral administration of prasugrel and its HCl salt to male beagle dogs, the metabolite (2*Z*)-[1-[α -cyclopropylcarbonyl-2-fluorobenzyl]-4-methylthio-3-piperidinylidene]acetic acid (*S*-methyl metabolite, R-106583) was measured by HPLC/UV method [7]. It was stated that the blood samples were centrifuged to obtain the plasma and then the plasma samples were kept at -30 °C until analysis.

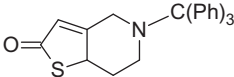
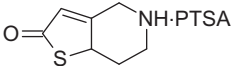
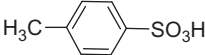
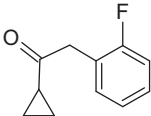
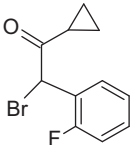
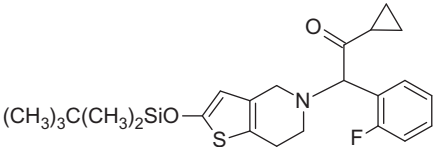
The stability of four stereoisomers of thiol metabolite (R-138727) with concentrations of 4, 16, 64, and 256 ng/ml was investigated by HPLC/MS method after derivatization with 2-bromo-3'-methoxyacetophenone to stabilize the molecule [99]. The ratio of the four stereoisomers of R-138727 remained constant when they were exposed to room temperature for

Table 19 The Stability Results of Prasugrel HCl in Solution

Media	Concentration (mg/ml)	Degradation Condition	Method	Result (%Drop in assay)	Reference
0.1 N NaOH	5.0	60 °C/15 min	HPLC	73	[6]
1 N HCl		60 °C/2 h		3	
50% ACN	0.5	60 °C/2 h		3	
50% H ₂ O ₂	12.5	60 °C/30 min		29	
0.001 N NaOH (in 90% MeOH)	0.1	RT/5 min	HPTLC	46	[98]
0.01 N HCl (in 90% MeOH)		RT/4 h		62	
H ₂ O		Reflux/1 h		Stable	
H ₂ O ₂		Reflux/1 h		72	
ACN	0.5	RT/3 h	HPLC	Stable	[103]
ACN		Refrigerator/8 h		Stable	
0.013 N NaOH	2.0	80 °C/4 h	HPLC/UPLC	80	[106]
0.1 N HCl		80 °C/4 h		50	
H ₂ O		80 °C/6 h		–	
ACN		Sunlight/2 days		Stable	
6.0% H ₂ O ₂	3.0	RT/5 days		–	
0.004 N NaOH ^a	6.7	RT/30 min	HPLC	14	[110]
1 N HCl		RT/1 h		12	
12% H ₂ O ₂		RT/3 h		19	
0.013 N NaOH	0.1	RT/1.5 h	UPLC	95	
0.2 N HCl		RT/5 h		97	[117]
H ₂ O		70 °C/2 h		97	
6.0% H ₂ O ₂		RT in dark/16 h		99	

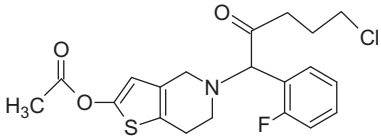
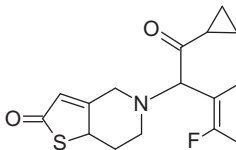
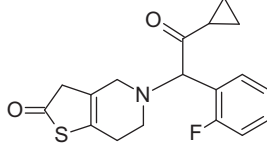
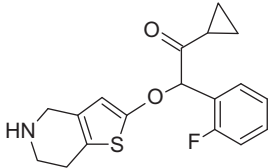
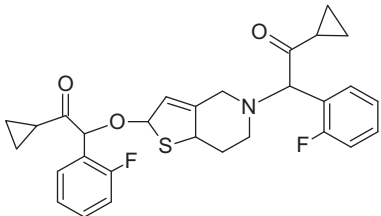
^aIn a mixture of ACN and H₂O (1:4); ACN, acetonitrile; MeOH, methanol.

Table 20 The List of Potential Impurities of Prasugrel

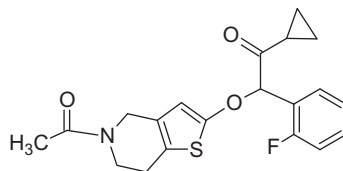
Chemical Name/Common Name	Chemical Structure	Type	Reference
5-Trityl-5,6,7,7a-tetrahydro-4 <i>H</i> -thieno[3,2- <i>c</i>]pyridin-2-one/SC-II		Synthetic	[6,116]
5,6,7,7a-Tetrahydro-4 <i>H</i> -thieno[3,2- <i>c</i>]pyridine-2(4 <i>H</i>)-one- <i>p</i> -toluenesulfonate/SC-II, Impurity C		Synthetic	
<i>p</i> -Toluenesulfonic acid/PTSA		Synthetic	
α -Cyclopropyl-2-fluorophenyl ketone/MC-I, Impurity A		Synthetic	
α -Cyclopropylcarbonyl-2-fluorobenzyl bromide/MC-II, Impurity B		Synthetic	
2-(<i>Tert</i> -butyldimethylsilyloxy)-5-(2-cyclopropyl-1-(2-fluorophenyl)-2-oxoethyl)-5,6,7,7a-tetrahydrothieno[3,2- <i>c</i>]pyridine/MC-III		Intermediate	

Continued

Table 20 The List of Potential Impurities of Prasugrel—cont'd

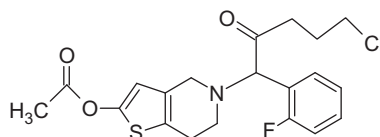
Chemical Name/Common Name	Chemical Structure	Type	Reference
5-(5-Chloro-1-(2-fluorophenyl)-2-oxopentyl)-4,5,6,7-tetrahydrothieno[3,2- <i>c</i>]pyridin-2-yl-acetate/CATP		By-product	[10]
5-(2-Cyclopropyl-1-(2-fluorophenyl)-2-oxoethyl)-5,6,7,7 <i>a</i> -tetrahydrothieno[3,2- <i>c</i>]pyridine-2(4 <i>H</i>)-one/OXTP	<div style="display: flex; align-items: center; justify-content: center;">  <div style="margin: 0 10px; text-align: center;"> \rightleftharpoons Tautomer </div>  </div> <div style="display: flex; justify-content: space-around; margin-top: 5px;"> OXTP1 and OXTP2 diastereomers OXTP </div>	Intermediate, hydrolytic, and hydrolysis	[11,24,30, 34,73,75, 116,125,128]
2-(α -Cyclopropylcarbonyl-2-fluorobenzoyloxy)-5- <i>H</i> -4,5,6,7-tetrahydrothieno[3,2- <i>c</i>]pyridine/IMP-1		By-product	[15]
2-(α -Cyclopropylcarbonyl-2-fluorobenzoyloxy)-5-(α -cyclopropylcarbonyl-2-fluorobenzyl)-4,5,6,7-tetrahydrothieno[3,2- <i>c</i>]pyridine/IMP-2		By-product	

2-(α -Cyclopropylcarbonyl-2-fluorobenzyloxy)-5-acetoxy-4,5,6,7-tetrahydrothieno[3,2-*c*]pyridine/IMP-3



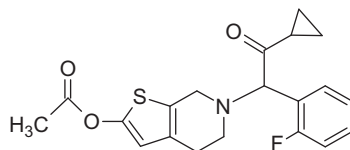
By-product

5-(5-Chloro-1-(2-fluorophenyl)-2-oxopentyl)-4,5,6,7-tetrahydrothieno[3,2-*c*]pyridin-2-yl-acetate/IMP-4



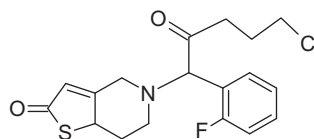
By-product

6-(2-Cyclopropyl-1-(2-fluorophenyl)-2-oxoethyl)-4,5,6,7-tetrahydrothieno[2,3-*c*]pyridin-2-yl-acetate/IMP-5



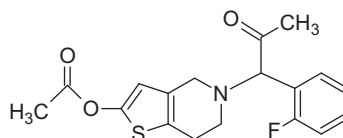
By-product

5-(5-Chloro-1-(2-fluorophenyl)-2-oxopentyl)-5,6,7,7*a*-tetrahydrothieno[3,2-*c*]pyridin-2(4*H*)-one/IMP-6



By-product

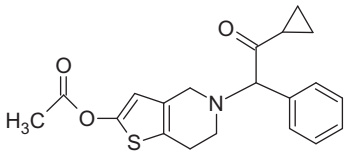
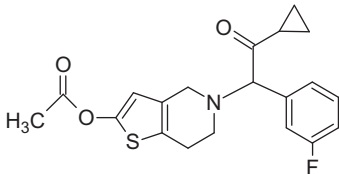
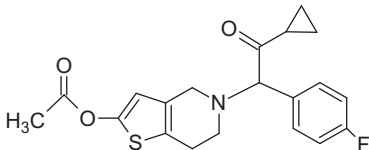
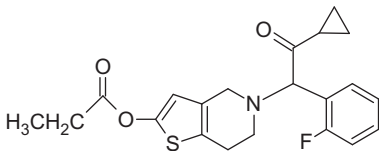
5-[(1*RS*)-2-methyl-1-(2-fluorophenyl)-2-oxoethyl]-4,5,6,7-tetrahydrothieno[3,2-*c*]pyridin-2-yl acetate/methyl impurity



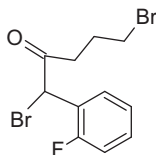
By-product [\[34,117,132\]](#)

Continued

Table 20 The List of Potential Impurities of Prasugrel—cont'd

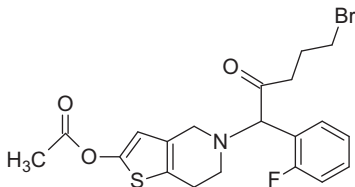
Chemical Name/Common Name	Chemical Structure	Type	Reference
5-[(1 <i>R</i> S)-2-cyclopropyl-2-oxo-1-phenylethyl]-4,5,6,7-tetrahydrothieno[3,2- <i>c</i>]pyridin-2-yl acetate/desfluoro impurity		By-product	
5-[(1 <i>R</i> S)-2-cyclopropyl-1-(3-fluorophenyl)-2-oxoethyl]-4,5,6,7-tetrahydrothieno[3,2- <i>c</i>]pyridin-2-yl acetate/3-fluoro impurity		By-product	
5-[(1 <i>R</i> S)-2-cyclopropyl-1-(4-fluorophenyl)-2-oxoethyl]-4,5,6,7-tetrahydrothieno[3,2- <i>c</i>]pyridin-2-yl acetate/4-fluoro impurity		By-product	
5-[(1 <i>R</i> S)-2-cyclopropyl-1-(2-fluorophenyl)-2-oxoethyl]-4,5,6,7-tetrahydrothieno[3,2- <i>c</i>]pyridin-2-yl propionate/propionyl impurity		By-product	

1,5-Dibromo-1-(2-fluorophenyl)-2-pentanone/dibromo impurity



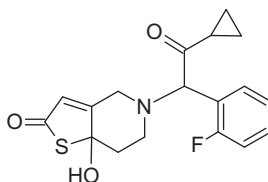
By-product [\[36,133\]](#)

5-(5-Bromo-1-(2-fluorophenyl)-2-oxopentyl)-4,5,6,7-tetrahydrothieno[3,2-*c*]pyridin-2-yl-acetate/bromopentyl impurity



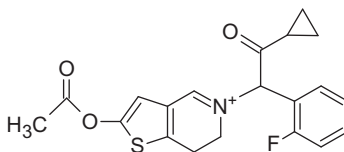
By-product

5-(2-Cyclopropyl-1-(2-fluorophenyl)-2-oxoethyl)-7*a*-hydroxy-5,6,7,7*a*-tetrahydrothieno[3,2-*c*]pyridin-2(4*H*)-one/HYTP



Oxidation [\[125,128\]](#)

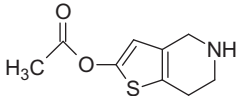
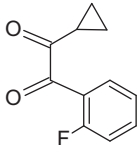
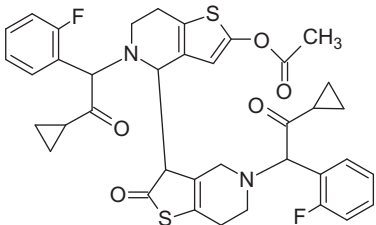
2-Acetoxy-5-(2-cyclopropyl-1-(2-fluorophenyl)-2-oxoethyl)-6,7-dihydrothieno[3,2-*c*]pyridin-5-ium/iminium



Oxidation

Continued

Table 20 The List of Potential Impurities of Prasugrel—cont'd

Chemical Name/Common Name	Chemical Structure	Type	Reference
4,5,6,7-Tetrahydrothieno[3,2- <i>c</i>]pyridin-2-yl acetate/acetylated TTPO		Hydrolysis	
1-Cyclopropyl-2-(2-fluorophenyl)ethane-1,2-dione/diketone		Hydrolysis	
5,5'-Bis(2-cyclopropyl-1-(2-fluorophenyl)-2-oxoethyl)-2-oxo-2,3,4,4',5,5',6,6',7,7'-decahydro-[3,4'-bithieno[3,2- <i>c</i>]pyridin]-2'-yl acetate/dimeric isomers		Dimerization, which is further degraded	

24 h, subjected to four freeze/thaw cycles, or held during long-term frozen storage for 31 days at -20°C .

The stability of the three inactive metabolites (R-95913, R-106583, and R-119251) in human plasma with concentrations of 2.5, 400, and 2000 ng/ml were evaluated by HPLC/MS method [100]. It was found that they are stable in human plasma at room temperature for 3.5 h, when frozen and thawed for three cycles at both -20°C and -70°C , and in plasma extracts with concentration range of 2.5 and 400 ng/ml stored at room temperature for 24 h. In addition, they are stable at -20°C and -70°C storage conditions at all concentration levels up to 6 and 267 days, respectively.

The stability of derivatized R-138727 with *N*-ethylmaleimide to protect thiol group was evaluated by HPLC/MS [136]. The derivatized R-138727 was found to be stable in human plasma for 3 months at -20°C .



6. PHARMACOLOGY

6.1 Uses, Applications, and Pertinent History

Prasugrel belongs to the thienopyridine class that was discovered by Daiichi Sankyo Co. with Ube industries Ltd. and developed in collaboration with Eli Lilly and Company [137]. Its use was approved in Europe and USA in 2009 [1,2], in Canada in 2010 and in Japan in 2014 [137,138]. It is marketed under the trademarks of Effient in USA and Canada and Efient in Europe and Japan.

Prasugrel, as a platelet aggregation inhibitor, is indicated for the prevention of atherothrombotic events in adult patients with acute coronary syndrome (ACS). Such syndrome can comprise patients with unstable angina, non-stent thrombosis segment elevation myocardial infarction or stent thrombosis segment elevation myocardial infarction undergoing primary or delayed percutaneous coronary intervention (PCI). It is prescribed initially with a single 60 mg oral loading dose followed by 10 mg once daily with or without food. Patients with ACS are consistently prescribed a dual antiplatelet therapy of a P2Y₁₂ receptor inhibitor and aspirin (75–325 mg daily) [2,139]. In Japan, prasugrel has been indicated also for the treatment of patients with ischemic heart disease undergoing PCI. It should be initiated orally with a single 20 mg loading dose and then continued at a 3.75 mg once daily dose for adults [137].

6.2 Absorption

Prasugrel is rapidly absorbed and extensively metabolized after oral administration. In rats and dogs, the time to achieve maximum plasma

concentration (T_{\max}) was <1 h after an oral [^{14}C]prasugrel dose [138,140]. The absolute oral bioavailability of prasugrel is considered high in animals. For example, the oral bioavailability was estimated to be approximately 77% in rats administered a single oral dose of [^{14}C]prasugrel [138].

In human, the absorption and metabolism of prasugrel seems faster. It is estimated that more than 79% of the dose was absorbed after oral administration in human [141]. The peak plasma concentrations (C_{\max}) of radioactivity and the active thiol metabolite (R-138727) occurring approximately in 0.5 h after dosing, representing 26% of the $\text{AUC}_{0-12\text{h}}$ of the radioactivity. The sum of all prasugrel four key metabolites (R-95913, R-138727, R-119251, and R-106583) comprised approximately 70% of the plasma radioactivity at 15 and 30 min after dosing, suggesting rapid metabolism of prasugrel via the pathway leading to the active metabolite. Moreover, the sum of $\text{AUC}_{0-0.25}$ of R-138727, R-106583, and R-119251 represented about 55% of the comparable area for plasma radioactivity [142,143].

In a study of healthy subjects given a single 15 mg dose, the AUC of the active metabolite was unaffected by a high fat, high calorie meal, but the C_{\max} was decreased by 49% and the T_{\max} was increased from 0.5 to 1.5 h. Still, prasugrel can be administered without regard to food [1,2,138].

In another study, a single dose of either 2.5, 10, 30, and 75 mg prasugrel was administered to healthy humans and three inactive metabolites (R-95913, R-100932, and R-106583) were determined and their pharmacokinetic parameters were calculated [144]. The C_{\max} and the $\text{AUC}_{(0-24\text{h})}$ of the metabolites increased proportionally to the dose administered. The three metabolites appeared in the plasma soon after administration and reached C_{\max} in approximately 1 h. The most abundant metabolite was the S-methyl metabolite (R-106583).

Furthermore, a multiple-dose of 2.5–20 mg study in healthy humans, the three prasugrel inactive metabolites (R-95913, R-100932, and R-106583) showed almost a proportional increase in C_{\max} and the $\text{AUC}_{(0-24\text{h})}$ on both day 1 and day 10 as a function of dose. No significant accumulation was apparent for any metabolites during multiple doses for 10 days [145,146].

6.3 Distribution

The C_{\max} of [^{14}C]prasugrel is reported at about 1-h post dose in most tissues involved in the absorption and elimination of the drug and its metabolites, including the stomach, intestines, liver, kidneys, and the urinary bladder. Placental transfer of prasugrel metabolites to the fetus of pregnant rats

was low. However, the transfer of [^{14}C]prasugrel into the milk of lactating rats was verified [138].

In general, protein binding of prasugrel's inactive metabolites is high (>80%) in rats, dogs, and human plasma [138,141]. The fraction bound to plasma proteins at various concentrations, determined by ultracentrifugation, was reported as 94.6% for R-95913 (50, 100, and 500 ng/ml), 95.1% for R-106583 (100 and 500 ng/ml), and 76.4% for R-119251 (100, 500, and 1000 ng/ml) [1,141]. The binding of thiol metabolite (R-138727) to plasma proteins could not be determined, however, it was measured as 98% in a 4% human serum albumin solution in phosphate buffer, pH 7.4 [141,143].

In subjects with stable atherosclerosis, estimates of the apparent volume of distribution of prasugrel active metabolite ranged from 30 to 84 l, and estimates of apparent clearance ranged from 73 to 266 l/h [141].

6.4 Metabolism

Prasugrel is a prodrug. It is metabolized by intestinal and plasma esterases to form its active and inactive metabolites. The metabolites that were identified by radiochromatographic profiling and mass spectral analysis in the human plasma, urine, and feces were also identified in mice, rats, and dogs [140,142].

As shown in Figure 22, an inactive thiolactone metabolite (M2, R-95913) was initially formed by de-esterification, which was subsequently metabolized to thiol active (M3, R-138727) and inactive (M4, R-104434) metabolites [140,142–144,147,148]. The later metabolite M4 was not detected in plasma after the 15 mg p.o. dose of [^{14}C]prasugrel; however, its downstream metabolites M6 (R-100932) and M8 (R-118443) were observed (Figure 22). On the other hand, S-methyl metabolite M5 was the major prasugrel metabolite found in human plasma, which represents >10% of the plasma radioactivity, followed by metabolites M3 and M2 [142]. The relatively small contribution of other thiol metabolites, formed by opening the thiolactone ring of metabolite M2 (M6 (R-100932) and M8 (R-118443)), indicated that the pathway leading to the formation of the active metabolite M4 is predominant in humans. Furthermore, the concentrations of glucuronide conjugates (M13, M14, M15, M16, M17, and M19) were very low for further isolation and/or analysis for absolute structural confirmation.

The hydroxyl metabolite M1, a minor one in plasma, was the major metabolite detected in urine. Its formation was suggested by conversion

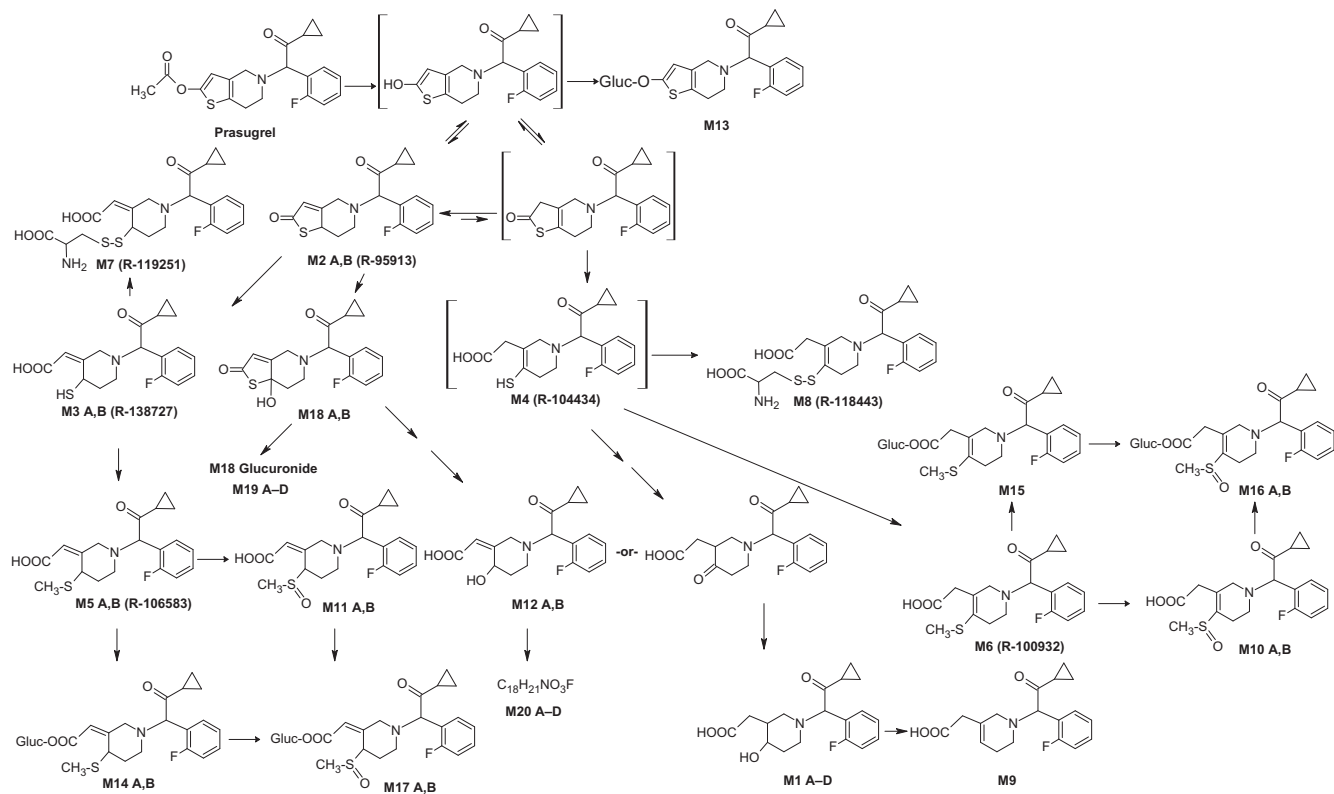


Figure 22 The proposed metabolic pattern of prasugrel in humans.

of a thione derived from metabolite M4 to metabolite M12 (ketone form), which was then reduced to form metabolite M1. Also it was proposed that metabolite M12 (alcohol form) was produced as a result of hydrolysis of metabolite M18 and then reduction of the formed ketone to form metabolite M1 [142].

Due to the presence of 2 chiral carbons in the active metabolite M3, it exists in four stereoisomers (*RS*, *SR*, *SS*, and *RR* isomers) and the most active isomer is *RS* one [149]. The formation of metabolite M3 involves two steps of enzymatic reaction including: (1) hydrolysis of prasugrel to thiolactone metabolite M2, which mainly catalyzed by the hCE₂ enzyme in human [150] and (2) oxidative cleavage of the thioester bond of metabolite M2, which is catalyzed by cytochromes P450 3A4, 2B6, 2C9, or 2C19 in humans [143]. The detail mechanism of metabolite M3 formation is presented in Figure 23, which involves a P450-catalyzed oxidative opening of metabolites M2 leading to the formation of sulfenic acid intermediate and then a reduction of this sulfenic acid into the thiol metabolite M3 by glutathione (GSH) [151,152].

However, the second competing pathway to form the metabolite M4 (*Endo*) was investigated by using human liver microsomes and human sera [113]. The analysis was carried out by HPLC-MS under conditions allowing a complete separation of the thiol metabolite isomers, after derivatization with 3'-methoxy phenacyl bromide. The results revealed that there are two competing pathways as shown in Figure 23. The major pathway results from a P450- and NADPH-dependent redox bioactivation of metabolite M2 leading to metabolite M4 with an exocyclic double bond. It occurs with NADPH-supplemented human liver microsomes but not with human sera. The second one results from a hydrolysis of metabolite M2 leading to metabolite M4 isomer (*Endo*), in which the double bond has migrated from an exocyclic to an endocyclic position in the piperidine ring. It occurs both with human liver microsomes and human sera, and does not require NADPH. However, it requires Ca²⁺ and is inhibited by paraoxon, which suggests that it is catalyzed by a thioesterase such as PON-1. The study also showed that the chemical reaction of prasugrel with CH₃ONa in CH₃OH led to the hydrolysis of its acetate function and the opening of the metabolite M2 ring with the formation of only the methyl ester of metabolite M4 (*Endo*) isomer, with an 80% yield [113].

To support the major proposition, the sulfoxide intermediate was trapped by a series of nucleophiles such as amines, thiols, or cyclopentane-1,3-dione, an equivalent of dimedone [115]. The result of

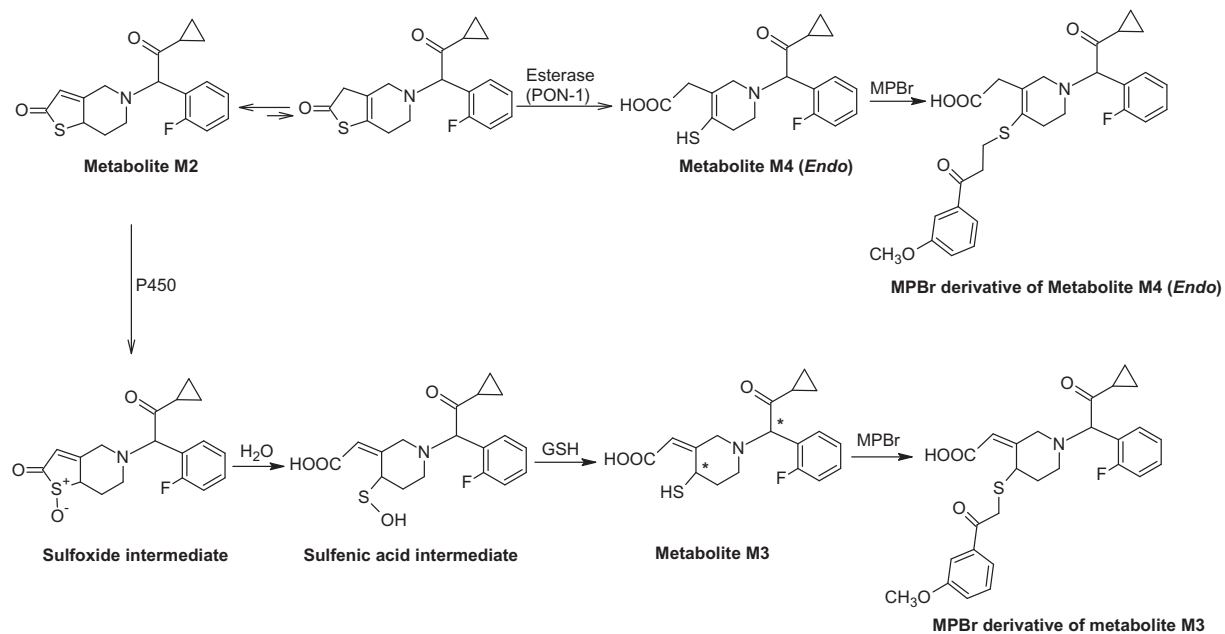


Figure 23 The competing two pathways involved in metabolic opening of the thiophene ring of prasugrel.

HPLC-MS analysis showed that various bis-adducts having incorporated two nucleophile molecules were formed in these reactions (Figure 24). Also all metabolites derived from an attack of H₂O or an amine at the CO carbon of the intermediate thiolactone sulfoxide existed as a mixture of two diastereomers having a *cis* configuration, whereas those formed in the presence of thiols appeared as a mixture of four diastereomers with a *cis* or *trans* configuration.

6.5 Elimination

In rats and dogs, biliary excretion was the major route of elimination for prasugrel's metabolites. The elimination $t_{1/2}$ of radioactivity for the mouse was approximately 1 day, in dogs, however it was 3 days. Approximately, 73–79% of the oral dose was excreted in the feces. In mice, approximately 52% of the dose was eliminated in the urine, and 37% was eliminated in the feces [138,140].

Approximately, 21% of a 15 mg [¹⁴C]prasugrel dose was eliminated in the feces within the first 48 h after an oral administration to human, indicating that at least 79% of the prasugrel dose was absorbed. Overall, about 68% of the [¹⁴C]prasugrel dose was excreted in the urine and 27% in the feces in the form of inactive metabolites over a period of 10 days, indicating that urinary excretion is the major pathway for the elimination of prasugrel metabolites [142,143].

6.6 Pharmacological Effects

Prasugrel is classified as a thienopyridine P2Y₁₂ platelet ADP-receptor antagonist. The irreversible binding of its active metabolite to the P2Y₁₂ class of ADP receptors on platelets makes prasugrel a potent inhibitor of platelet activation and aggregation. Prasugrel is mainly used to reduce the risk of thrombotic cardiovascular events such as stent thrombosis or myocardial infarctions in patients with ACS [2,153]. When vascular injury occurs, inactive platelets become activated through binding to exposed vascular collagen. Platelet activation results in degranulation and secretion ADP, thromboxane A₂, and platelet-activating factor. In addition, P2Y₁ and P2Y₁₂ are G protein-coupled receptors that are responsible for platelet aggregation. The P2Y₁ receptor is claimed to initiate weak platelet activation while binding of a P2Y₁₂ receptor results in a slower but progressive platelet aggregation [153–155].

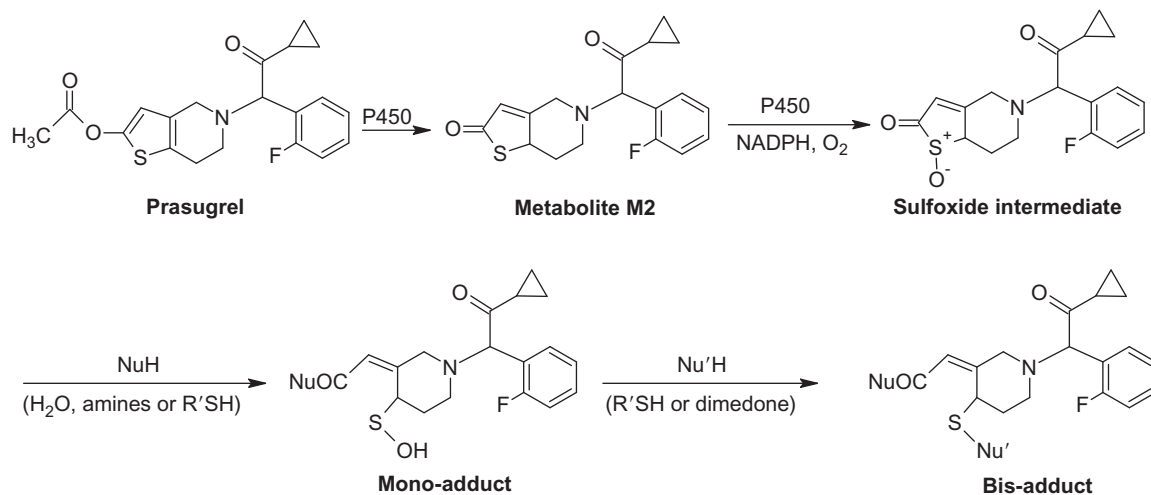


Figure 24 The pathway of formation of mono- and bis-adducts by trapping of thiolactone sulfoxide by nucleophiles such as amines, thiols (R'SH), or cyclopentane-1,3-dione (CPDH), an equivalent of dimedone.

The ADP receptor blockers (P2Y₁₂ inhibitors) prevent binding of the ADP to a specific platelet receptor, therefore, inhibiting the activation of the GP IIb/IIIa complex and thus platelet aggregation [153]. Prasugrel's active metabolite irreversibly inactivates P2Y₁₂ receptors through the covalent linkage of a sulfhydryl group. Early preclinical studies demonstrate that following oral administration of prasugrel there is a rapid and potent inhibition of ADP-induced platelet activation and aggregation [144,147,148,156]. Clopidogrel and prasugrel are equipotent at inhibiting P2Y₁₂ receptors, however, preclinical studies demonstrated that the dose required achieving a given degree of platelet inhibition or inhibition of thrombus formation was approximately one-tenth and one-hundredth that of the dose of clopidogrel and ticlopidine, respectively [144]. Later, prasugrel was clinically seen more efficacious than clopidogrel and produces less variable antiplatelet response, with a faster onset of action [157,158].

Using light transmission aggregometry, prasugrel was found capable of inhibiting ADP-induced platelet aggregation. It takes about one hour in most of patients receiving prasugrel to reach 50% platelet aggregation. It is claimed that the maximum platelet inhibition was about 80% in patients treated with Effient. However, mean steady-state inhibition of platelet aggregation is reported to be about 70% following 3–5 days of dosing at 10 mg daily after a 60 mg loading dose of Effient [2]. After discontinuation of prasugrel, platelet aggregation gradually returns to baseline values over 5–9 days. This might be attributed to new platelet production rather than pharmacokinetics of prasugrel [2].

REFERENCES

- [1] CHMP/EMA assessment report for Efiect, http://www.ema.europa.eu/docs/en_GB/document_library/EPAR_-_Public_assessment_report/human/000984/WC500021975.pdf, 2014 (accessed June 2014).
- [2] FDA product label information for Effient, http://www.accessdata.fda.gov/drugsatfda_docs/label/2013/022307s010lbl.pdf, 2014 (accessed June 2014).
- [3] Medsafe datasheet for Effient, <http://www.medsafe.govt.nz/profs/datasheet/e/Effientab.pdf>, 2014 (accessed June 2014).
- [4] H. Koike, F. Asai, Fumitoshi, A. Sugidachi, T. Kimura, T. Inoue, S. Nishino, Y. Tsuzaki, Tetrahydrothienopyridine derivatives, furo and pyrrolo analogs thereof and their preparation and uses for inhibiting blood platelet aggregation, European patent EP054241181, 1993.
- [5] Prasugrel monograph, Drug Bank Website, <http://www.drugbank.ca/drugs/DB06209>, 2014 (accessed June 2014).
- [6] V. Sriram, K. Sriram, J. Angirekula, U.M. Tripathi, D. Nayakanti, Development and validation of reverse phase HPLC method for the determination of impurities in prasugrel hydrochloride, Int. J. PharmTech Res. 4 (2012) 1407–1416. [http://sphinxσαι.com/2012/oct-dec/Pharmpdf/PT=08\(1407-1416\)OD12.pdf](http://sphinxσαι.com/2012/oct-dec/Pharmpdf/PT=08(1407-1416)OD12.pdf) (accessed June 2014).

- [7] F. Asai, T. Ogawa, H. Naganuma, N. Yamamura, T. Inoue, K. Nakamura, Hydropyridine derivative acid addition salts, European patent EP1298132, 2003.
- [8] M.A. Goldsmith, E. Vadas, Oral dosage forms including an antiplatelet agent and an acid inhibitor, United States patent US20070243243, 2007.
- [9] K. Ataka, H. Miyata, M. Kono, N. Yokota, Y. Yamamoto, 2-Silyloxytetrahydrothienopyridine, salt thereof, and process for producing the same, European patent EP0785205, 1997.
- [10] H. Miyata, Y. Wada, N. Yokota, Process for production of prasugrel hydrochloride having high purity, European patent EP2123656, 2009.
- [11] T. Inoue, K. Nakamura, M. Hagihara, H. Miyata, Y. Wada, N. Yokota, Process for producing high-purity prasugrel and acid addition salt thereof, European patent EP2003136, 2008.
- [12] W. Xuesong, C. Junda, G. Heng, Method for preparing 5-(α -cyclopropylcarbonyl-2-fluorobenzyl)-2-oxo-2,4,5,6,7,7a-hexahydrothiophene[3,2-c]pyridine, Chinese patent CN101250192, 2008.
- [13] W. Xuesong, C. Junda, G. Heng, Method for preparation of 2-methoxy-5-(α -cyclopropylcarbonyl-2-fluorobenzyl)-4,5,6,7-tetrahydrothieno[3,2-c]pyridine by one-step reaction, Chinese patent CN101250193, 2008.
- [14] W. Guoping, H. Jian, S. Zhiguo, Z. Qiang, Y. Zhenpeng, Process for preparation of 2-cyclopropyl-1-(2-fluorophenyl)-2-oxoethanol derivatives as intermediate compounds for preparing prasugrel, Chinese patent CN101402593, 2009.
- [15] M. Satyanarayana Reddy, S. Eswaraiiah, G. Venkat Reddy, Improved process for the preparation of prasugrel and its pharmaceutically acceptable salts, World Organization patent WO2009066326, 2009.
- [16] Z. Gaojun, H. Yanzhen, X. Tao, Z. Fangjiang, Method for synthesis of prasugrel intermediate and prasugrel, Chinese patent CN101531667, 2009.
- [17] A.V.V.S. Rao, J. Jaware, S. Goud, G.P. Bijukumar, S.S. Nadkarni, Process for the preparation of 2-acetoxy-5-(α -cyclopropylcarbonyl-2-fluorobenzyl)-4,5,6,7-tetrahydrothieno[3,2-c]pyridine, World Organization patent WO2009122440, 2009.
- [18] A.M. Khan, S.R. Sanikommu, B.R. Antyakula Pydi, S. Sangnabhatla, A process for the preparation of prasugrel and its pharmaceutically acceptable salts thereof, World Organization patent WO2010070677, 2010.
- [19] H. Stepankova, J. Hajicek, A method of manufacturing 5-[2-cyclopropyl-1-(2-fluorophenyl)-2-oxoethyl]-4,5,6,7-tetrahydrothieno[3,2-c]pyridin-2-yl acetate (prasugrel), European patent EP2176269, 2010.
- [20] L. Jindou, S. Ke, C. Sen, A process for preparing prasugrel and its intermediates, Chinese patent CN101812069, 2010.
- [21] P.R. Padi, S.R.S. Peri, M.R. Ganta, S. Polavarapu, P. Cherukupally, B. Irent, S. Padamata, K. Jonnada, K. Vinigari, K. Nerella, Processes for the preparation of prasugrel, and its salts and polymorphs, United States patent US20100261908, 2010.
- [22] T. Mezei, G. Lukács, E. Molnár, J. Barkóczy, B. Volk, M. Porcs-Makkay, J. Szulágyi, M. Vajjon, Maria, Process for the preparation of pharmaceutical intermediates, European patent EP2242736, 2010.
- [23] L. Thijs, J. Zhu, A. Overeem, A process for making prasugrel and its intermediates, World Organization patent WO2011029456, 2010.
- [24] H. Stepankova, K. Kaminska, J. Hajicek, Method of producing highly pure prasugrel and pharmaceutically acceptable salts thereof, World Organization patent WO2011057592, 2011.
- [25] M. Porcs-Makkay, T. Gregor, B. Volk, G. Németh, J. Barkóczy, B. Nyulasi, T. Mezei, G. Ruzsics, A. Pandur, E. Szilágyi, K. Nagy, P. Slégel, E. Molnár, J. Debreczeni, Improved process for preparing a pharmaceutical compound, World Organization patent WO2011077173, 2011.

- [26] L. Thijs, J. Zhu, A. Overeem, R. Keltjens, A process for making prasugrel, World Organization patent WO2011110219, 2011.
- [27] C. Xingdong, Y. Zhedong, Y. Yulei, Z. Xueyan, Y. Xiong, Process for preparation of prasugrel, Chinese patent CN102212070, 2011.
- [28] S. Liang, W. Zhe, Z. Aiqing, B. Zhijian, S. Jian, Z. Qing, New method for preparing prasugrel, Chinese patent CN102219792, 2011.
- [29] X. Baizhong, Z. Liang, W. Hongying, X. Yan, L. Hongda, L. Na, Q. Yan, J. Linzhou, Method for preparing prasugrel intermediate and application of method in synthesizing prasugrel, Chinese patent CN102241689, 2011.
- [30] H. Stepankova, J. Hajicek, M. Dousa, Method for the manufacture of highly pure prasugrel, United States patent US20110282064, 2011.
- [31] S. Shi, Q. Huanghua, S. Fan, D. Wei, Method for preparing prasugrel by using organosilicon protective agent, Chinese patent CN102276623, 2011.
- [32] C.S.N. Krishnamurthy, J. Singh, M.Y. Khan, An improved process for the preparation of prasugrel hydrochloride and its intermediates, World Organization patent WO2012001486, 2011.
- [33] L. Aiguo, A process for preparing prasugrel, Chinese patent CN101812070, 2012.
- [34] R.R. Anumula, G. Gilla, S. Aalla, D.S. Metil, S. Kurella, K. Charagondla, Preparation of prasugrel hydrochloride, World Organization patent WO2012018791, 2012.
- [35] F. Jianpeng, S. Tianjiang, Z. Yubin, Y. Bixi, Z. Feng, G. Zhongqiang, New method for preparing prasugrel, Chinese patent CN101775025, 2012.
- [36] B. Nyulasi, M. Porcsmakay, G. Németh, T. Gregor, J. Barkóczy, B. Volk, K. Nagy, G. Ruzsics, Z. Papp-Fúzfai, E. Molnár, A. Pandur, A. Keszthelyi, T. Mezei, D. Frigyes, Method for preparing pharmaceutically active ingredient and intermediates thereof, World Organization patent WO2012052788, 2012.
- [37] C. Liu, Q. Lu, C. Chen, Method for preparing prasugrel, European patent EP2471795, 2012.
- [38] M.S. Reddy, S.T. Rajan, S. Eswaraiyah, K.R.S. Reddy, B.K. Reddy, G.V. Reddy, Processes for preparing prasugrel and pharmaceutically acceptable salts thereof, United States patent US20120202066, 2012.
- [39] L. Jiang, P. Xianhua, H. Kunlun, Z. Dunfeng, Prasugrel intermediate and preparation method thereof, Chinese patent CN102030761, 2012.
- [40] X. Pan, R. Huang, J. Zhang, L. Ding, W. Li, Q. Zhang, F. Liu, Efficient synthesis of prasugrel, a novel P2Y₁₂ receptor inhibitor, *Tetrahedron Lett.* 53 (2012) 5364–5366.
- [41] W. Guoping, H. Jian, S. Zhiguo, Z. Qiang, Y. Zhenpeng, A process for preparing prasugrel, Chinese patent CN101402642, 2013.
- [42] H. Kunlun, P. Xianhua, P. Xijiang, L. Xin, C. Qing, B. Yi, C. Shuhua, Z. Yu, Y. Zhenyan, Prasugrel intermediate and preparation method thereof, Chinese patent CN101948479, 2013.
- [43] J.V. Raman, S. Patel, A. Kadam, V. Patel, J. Patel, Process for the preparation of prasugrel HCl salt, United States patent US20130053569, 2013.
- [44] R.V. Newadkar, A. Purushottam Joshi, S. Raghunath Bendre, D. Hemant Jere, P. Dalmas Barjoan, I. Navarro Munoz, J. Huguet Clotet, Process for preparing prasugrel, World Organization patent WO2013014295, 2013.
- [45] W. Xuesong, C. Junda, G. Heng, A process for preparing 2-substituted-5-(phenylmethyl)-4,5,6,7-tetrahydro-thieno[3,2-c]pyridine derivatives as intermediates for synthesizing prasugrel, Chinese patent CN101245072, 2008.
- [46] W. Xuesong, C. Junda, G. Heng, D. Ren, A process for preparing 2-substituted-5-(phenylmethyl)-4,5,6,7-tetrahydro-thieno[3,2-c]pyridine derivatives as intermediates for synthesizing prasugrel, Chinese patent CN101245073, 2008.
- [47] L. Zhaopeng, D. Yuehui, Method for preparing salts of prasugrel, Chinese patent CN101255169, 2008.

- [48] W. Guoping, H. Jian, S. Zhiguo, Z. Qiang, Y. Zhenpeng, Process for preparation of 1-cyclopropyl-2-(2-fluorophenyl)-2-hydroxyethanone as prasugrel intermediate, Chinese patent CN101402556, 2009.
- [49] L. Junzhi, X. Wenbin, W. Xinguang, N. Jing, Z. Xianggen, J. Huirong, Z. Xiaolong, L. Xiaoyu, A process for preparing 5-[2-cyclopropyl-1-(2-fluorophenyl)-2-oxoethyl]-5,6,7,7a-tetrahydro-thieno[3,2-c]pyridin-2(4H)-one useful as intermediate for manufacturing prasugrel, Chinese patent CN101735240, 2010.
- [50] K. Doser, Prasugrel salts with improved properties, United States patent US20110003847, 2011.
- [51] A. Xinmiao, Z. Jiang, Y. Yan, A process for preparing 5,6,7,7a-tetrahydro-thieno[3,2-c]pyridin-2(4H)-one hydrochloride as intermediate for manufacturing prasugrel, Chinese patent CN101985451, 2011.
- [52] A. Xinmiao, Z. Jiang, Y. Yan, Method for preparing 2-oxo-2,4,5,6,7,7a-hexahydrothieno[3,2-c]pyridine hydrochloride as prasugrel intermediate, Chinese patent CN102002056, 2011.
- [53] L. Xin, Z. Fuqiang, M. Jun, Prasugrel intermediate and its preparation method, Chinese patent CN102020656, 2011.
- [54] Z. Zhao, The hydrosulfate of prasugrel, its pharmaceutical combination and use thereof, United States patent US 20110124675, 2011.
- [55] L. Jindu, L. Huailin, W. Junjun, C. Sen, Process for preparation of α -cyclopropylcarbonyl-2-fluorobenzyl halides, Chinese patent CN102101827, 2011.
- [56] W. Lixin, Z. Yong, X. Xiaoying, T. He, H. Qingchun, J. Junhui, Preparation method of α -(cyclopropylcarbonyl)-2-fluorobenzyl bromide as prasugrel intermediate, Chinese patent CN102190569, 2011.
- [57] H. Danfeng, L. Xiguo, H. Yulai, X. Changming, N. Teng, Process for preparation of 1-cyclopropyl-2-tosyloxy-2-(2-fluorophenyl)ethanone as prasugrel intermediate, Chinese patent CN102241612, 2011.
- [58] W. Zhen, Z. Lei, Synthesis of 4,5,6,7-tetrahydrothieno[3,2-b]pyridine derivative with anticoagulant activity, and medical application, Chinese patent CN101684124, 2010.
- [59] W. Fujian, G. Baiying, L. Hanxing, Tetrahydrothieno[3,2-c]pyridine derivative and their preparation, pharmaceutical compositions and use in the treatment of thrombopoiesis and embolism, Chinese patent CN102229616, 2011.
- [60] W. Fujian, G. Baiying, L. Hanxing, Preparation of deuterated acid addition salt of prasugrel, Chinese patent CN102399232, 2012.
- [61] L. Dengke, L. Ying, L. Bingni, L. Mo, H. Changjiang, Z. Shuang, L. Li, W. Jingyang, Preparation of prasugrel derivatives as platelet aggregation inhibitors, Chinese patent CN101974015, 2012.
- [62] L. Dengke, L. Ying, Z. Shuang, M. Shuai, L. Peng, F. Xiaoli, W. Jiang, Z. Meixiang, Preparation of prasugrel derivatives as platelet inhibitors, Chinese patent CN102093385, 2013.
- [63] Intellectual Properties India Website, Published Applications, <http://ipindiaservices.gov.in/patentsearch/search/index.aspx>, 2014 (accessed June 2014).
- [64] Chemical Abstracts Services (CAS) Registry File for Prasugrel (accessed June 2014).
- [65] Effient Product Monograph, Eli Lilly Website, <http://www.lilly.ca/en?t=/documentManager/sfdoc.file.supply&i=1306943185696&fileID=1317404027858>, 2014 (accessed June 2014).
- [66] A.A. Badwan, M.M.H. Al Omari, The Jordanian Pharmaceutical Manufacturing Co. (personal communication).
- [67] WHO Technical Report Series, No 937, 40th Report, Annex 8, 2006. http://whqlibdoc.who.int/trs/who_trs_937_eng.pdf (accessed June 2014).
- [68] EMA guideline on the investigation of bioequivalence, http://www.emea.europa.eu/docs/en_GB/document_library/Scientific_guideline/2010/01/WC500070039.pdf, 2010 (accessed June 2014).

- [69] USFDA guidance for waiver of in vivo bioavailability and bioequivalence studies for immediate-release solid oral dosage forms based on a Biopharmaceutics Classification System, <http://www.fda.gov/downloads/Drugs/GuidanceComplianceRegulatoryInformation/Guidances/UCM070246.pdf>, 2000 (accessed June 2014).
- [70] Z.-M. Wang, J. Zhao, G. Xu, Prasugrel, a new medicine for preventing blockages in the arteries, *Acta Crystallogr. E: Struct. Rep. Online* E66 (2010) o1354. <http://www.ncbi.nlm.nih.gov/pmc/articles/PMC2979458/pdf/e-66-o1354.pdf> (accessed June 2014).
- [71] J. Wieser, H. Lengauer, E. Klingler, A. Pichler, H. Sturm, Method for salt preparation, United States patent US 20100204470, 2010.
- [72] G.K Vijay, P. Rajendra, K.N. Praveen, P.N. Sharadchandra, Process for preparing an amorphous form of prasugrel hydrochloride, Indian patent IN2008CH02599, 2011.
- [73] M. Satyanarayana Reddy, S. Thirumalai Rajan, M. Elevathingal Nicholas, K. Rama Subba Reddy, Pharmaceutical composition of prasugrel and its pharmaceutically acceptable salts, World Organization patent WO2011092720, 2011.
- [74] W. Du, Q. Yin, Y. Bao, C. Xie, B. Hou, H. Hao, W. Chen, J. Wang, J. Gong, Concomitant polymorphism of prasugrel hydrochloride in reactive crystallization, *Ind. Eng. Chem. Res.* 52 (2013) 16182–16189.
- [75] H. Stepankova, K. Kaminska, J. Hajicek, A method for the preparation of prasugrel hydrochloride in polymorphous form B, World Organization patent WO2011069473, 2011.
- [76] S. Kuček, M. Štukelj, F. Vrečer, F. Trošt, S. Trošt, Sabina, K. Mežnar, A. Kljajic, Pharmaceutical compositions comprising prasugrel base or its pharmaceutically acceptable acid addition salts and processes for their preparation, World Organization patent WO2010094471, 2010.
- [77] S. Brueck, J. Paetz, Prasugrel in non-crystalline form and pharmaceutical composition thereof, United States patent US20120149727, 2012.
- [78] C.H. Park, J.O. Baek, K.H. Suh, T.H. Ha, M.S. Ko, G.S. Lee, E.Y. Byun, Novel polymorphic form of prasugrel-hydrogen sulfate, World Organization patent WO2011027988, 2011.
- [79] S.S. Reddy, S. Sanganabhatla, A.P.B. Rao, M.A. Khan, Crystalline form of prasugrel hydrobromide, preparation and application thereof, World Organization patent WO2011004392, 2011.
- [80] K. Kaminska, H. Stepankova, J. Hajicek, Preparation of polymorphic form C of prasugrel hydrobromide, World Organization patent WO 2012089180, 2012.
- [81] M. Tuksar, T. Biljan, M. Zegarac, Crystalline forms of prasugrel salts, United States patent US20130085154, 2013.
- [82] K. Bano, A.K. Sherwani, U. Asif, S. Naeem, M.H. Shoaib, N. Akhtar, Conformational analysis and geometry optimization of Prasugrel as P2Y₁₂ receptor antagonist, *Pak. J. Biochem. Mol. Biol.* 45 (2012) 11–14.
- [83] H.-H. Zhu, W.-Z. Li, Y.B. Wei, One-pot synthesis of prasugrel, *J. Nanjing Univ. Technol.* 32 (2010) 77–81. http://en.cnki.com.cn/Article_en/CJFDTOTAL-NHXB201005016.htm (accessed June 2014).
- [84] Priority new monograph list, United States Pharmacopeia (USP) Website, <http://www.usp.org/usp-nf/development-process/priority-new-monographs/priority-new-monograph-list>, 2014 (accessed June 2014).
- [85] Approved drug products with therapeutic equivalence evaluations in Orange Book, USFDA Website, <http://www.accessdata.fda.gov/scripts/Cder/ob/docs/tempai.cfm>, 2014 (accessed June 2014).
- [86] A.A. Kumar, A.A. Kumar, D.G. Sankar, Development, estimation and validation of prasugrel in bulk and in its pharmaceutical formulation by UV–vis spectroscopic method, *Pharmanest: Int. J. Adv. Pharm. Sci.* 2 (2011) 37–39. <http://pharmanest.net/development-estimation-and-validation-of-prasugrel-in-bulk-and-in->

- its-pharmaceutical-formulation-by-UV-vis-spectroscopic-method-54.html (accessed June 2014).
- [87] F.M. Jena, B.V.V.R. Kumar, R.K. Viriyala, M.M. Annapurna, S.P.S. Bisht, Validated new spectrophotometric methods for the estimation of prasugrel in bulk and pharmaceutical dosage forms, *Pharm. Globale: Int. J. Comp. Pharm.* 2 (2011) 3 pages. http://www.pharmacie-globale.info/index.php?option=com_docman&task=search_result&Itemid=41 (accessed June 2014).
 - [88] D.D. Satishkumar, B.B. Subhash, W.S. Gomaji, Difference spectrophotometric estimation of prasugrel hydrochloride in bulk and tablet dosage form, *Int. Res. J. Pharm.* 3 (2011) 449–451. http://www.irjponline.com/admin/php/uploads/1145_pdf.pdf (accessed June 2014).
 - [89] S.M. Patel, C.N. Patel, V.B. Patel, Development and validation of spectrophotometric methods for simultaneous estimation of prasugrel and aspirin in tablet dosage form, *Am. J. PharmTech. Res.* 2 (2012) 818–827. <http://www.ajptr.com/search-result.php?search=prasugrel&btnG=Go> (accessed June 2014).
 - [90] S.N. Alvi, M.N. Patel, P.B. Kathiriyi, B.A. Patel, S.J. Parmar, Simultaneous determination of prasugrel and aspirin by second order and ratio first order derivative ultraviolet spectrophotometry, *J. Quant. Spectrosc. Radiat. Transf.* 2013 (2013) 7 pages. <http://dx.doi.org/10.1155/2013/705363> (Article ID 705363, accessed June 2014).
 - [91] S.M. Patel, C.N. Patel, V.B. Patel, Validation and derivative spectroscopy of prasugrel HCl in bulk and formulation, *Am. J. PharmTech. Res.* 3 (2013) 424–430. <http://www.ajptr.com/search-result.php?search=prasugrel&btnG=Go> (accessed June 2014).
 - [92] R.K. Rajendhirana, V.K. Sekar, B.D. Namadevan, J.K. Annamalai, S. Devarajan, UV-spectrophotometric and RP-HPLC methods for the estimation of prasugrel hydrochloride in bulk and tablet formulation, *Int. J. Pharm. Pharm. Sci.* 6 (2014) 220–225. <http://www.ijppsjournal.com/Vol6Issue1/8007.pdf> (accessed July 2014).
 - [93] B. Harshini, S.V.R. Alekhya, G. Manasa, K.V. Prakash, Extractive spectrophotometric estimation of prasugrel in pharmaceutical formulation, *Res. J. Pharm. Biol. Chem. Sci.* 2 (2011) 426–430. [http://www.rjpbcs.com/pdf/2011_2\(3\)/50.pdf](http://www.rjpbcs.com/pdf/2011_2(3)/50.pdf) (accessed July 2014).
 - [94] A.L. Lavanya, J.V.S. Kumar, P.G. Swarupa, K.R.S. Prasad, Spectrophotometric determination of prasugrel in bulk, dosage and biological fluids, *Int. J. Pharm. Pharm. Sci.* 4 (2012) 280–281. <http://www.ijppsjournal.com/Vol4Suppl5/4912.pdf> (accessed July 2014).
 - [95] S. Mastanamma, K. Gujjarlupudi, K.S. Deepthi, K. Harith, P. Saidulu, Development and validation of colorimetric method for the determination of prasugrel HCl in bulk and dosage form, *Int. J. Pharm. Ind. Res.* 3 (2013) 323–328. http://www.ijpir.com/view_content.php?quat=3&date=2013&issue=4 (accessed July 2014).
 - [96] B. Sailaja, T.V. Kumar, G. Venkateshwarlu, Spectrophotometric determination of a few commercial drugs using NBS and Rhodamine-B couple, *IOSR J. Appl. Chem.* 6 (2013) 25–30. <http://iosrjournals.org/iosr-jac/papers/vol6-issue1/C0612530.pdf?id=7283> (accessed July 2014).
 - [97] S.S. Kabir, A. Naveed, S.Z. Ul Quasim, V.K. Nandipati, Spectrophotometric method development and its validation for estimation of prasugrel HCl in bulk and pharmaceutical formulations, *Res. J. Pharm. Technol.* 6 (2013) 641–644. http://www.rjptonline.org/RJPT/RJPT_6_6_2013_Abstract.pdf (accessed July 2014).
 - [98] T.C. Borole, R. Mehendre, M.C. Damle, K.G. Bothara, Development and validation of stability indicating HPTLC method for determination of prasugrel, *J. Chem. Pharm. Res.* 2 (2010) 907–913. <http://jocpr.com/vol2-iss4-2010/JCPR-2-4-907-913.pdf> (accessed July 2014).
 - [99] E.R. Wickremsinhe, Y. Tian, K.J. Ruterbories, E.M. Verburg, G.J. Weerakkody, A. Kurihara, N.A. Farid, Stereoselective metabolism of prasugrel in humans using a

- novel chiral liquid chromatography–tandem mass spectrometry method, *Drug Metab. Dispos.* 35 (2007) 917–921.
- [100] N.A. Farid, M. McIntosh, F. Garofolo, E. Wong, A. Shwajch, M. Kennedy, M. Young, P. Sarkar, K. Kawabata, M. Takahashi, H. Pang, Determination of the active and inactive metabolites of prasugrel in human plasma by liquid chromatography/tandem mass spectrometry, *Rapid Commun. Mass Spectrom.* 21 (2007) 169–179.
- [101] T. Watanabe, K. Maeda, Film-coated preparation having improved stability, United States patent US20090291138, 2009.
- [102] R.P. Pulla, B.S. Sastry, Y.R. Prasad, N.A. Raju, Estimation of prasugrel in tablet dosage form by RP-HPLC, *Int. J. Chem. Res.* 2 (2011) 34–36. <http://www.ijcr.info/Vol2Issue3/182.pdf> (accessed July 2014).
- [103] B.M. Ishaq, K.V. Prakash, G.K. Mohan, Development and validation of HPLC method for determination of prasugrel in bulk and its pharmaceutical formulation, *J. Chem. Pharm. Res.* 3 (2011) 404–409. <http://jocpr.com/vol3-iss4-2011/JCPR-2011-3-4-404-409.pdf> (accessed July 2014).
- [104] A.E. Prabahar, N.R. Rao, K.R.S.S. Rao, P.V. Kumar, Method development and validation for the HPLC potency assay of prasugrel tablets, *J. Pharm. Res.* 4 (2011) 980–982. <http://jpronline.info/index.php/jpr/article/view/6834/3482> (accessed July 2014).
- [105] R.K.R. Seerapu, V.A. Rao, P. Lavanya, P.A.D. Kumar, R.K. Krishna, P.V.S. Reddy, Development of validated RP-HPLC method for the estimation of prasugrel HCl in pure and pharmaceutical formulations, *J. Pharm. Res.* 4 (2011) 3105–3107. <http://jpronline.info/index.php/jpr/article/view/9301/4744> (accessed 2014).
- [106] K. Sahu, C. Karthikeyan, N.S.H.N. Moorthy, P. Trivedi, Comparative study of forced degradation behavior of prasugrel by UPLC and HPLC and the development of validated stability indicating assay method, *J. Liq. Chromatogr. Relat. Technol.* 34 (2011) 1870–1884.
- [107] S.J. Parmar, B.A. Patel, A.P. Jain, Development and validation of RP-HPLC method for prasugrel, *J. Chem. Pharm. Res.* 4 (2012) 3373–3376. <http://jocpr.com/vol4-iss7-2012/JCPR-2012-4-7-3373-3376.pdf> (accessed July 2014).
- [108] I. Srikanth, P. Sharmila, K.V. Bharathi, M. Raju, M.L. Naik, K. Nagarjuna, A validated reverse phase HPLC method for the estimation of prasugrel hydrochloride in pharmaceutical dosage forms, *J. Innov. Trends Pharm. Sci.* 2 (2011) 140–148. www.itpsonline.net (accessed July 2014).
- [109] V.J. Modi, P.L. Pingale, Development and validation of analytical method for estimation of prasugrel hydrochloride in bulk and in pharmaceutical formulations, *Int. J. Pharma Bio. Sci.* 3 (2012) 292–298. <http://www.ijpbs.net/vol-3/issue-4/Pharma/34.pdf> (accessed July 2014).
- [110] V.K. Ahirrao, C.S. Patil, S.B. Bembalkar, S.B. Ubale, R.P. Marathe, R.B. Nawale, M.G. Landge, R.P. Pawar, Stability-indicating LC method for the determination of prasugrel hydrochloride in pharmaceutical dosage form, *Sci. Pharm.* 80 (2012) 379–391. <http://www.ncbi.nlm.nih.gov/pmc/articles/PMC3383204/pdf/scipharm-2012-80-379.pdf> (accessed July 2014).
- [111] D.S. Desai, B.S. Barnecha, S.G. Walode, Stability indicating method for quantitation of prasugrel hydrochloride in presence of its degradation products, *Int. J. Pharm. Technol.* 4 (2012) 4711–4720. <http://www.ijptonline.com/wp-content/uploads/2009/10/4711-4721.pdf> (accessed July 2014).
- [112] D.K. Jain, N. Jain, J. Verma, RP-HPLC method for simultaneous estimation of aspirin and prasugrel in binary combination, *Int. J. Pharm. Sci. Drug Res.* 4 (2012) 218–221. <http://www.ijpsdr.com/pdf/vol4-issue3/10.pdf> (accessed July 2014).
- [113] P.M. Dansette, J. Rosi, J. Debernardi, G. Bertho, D. Mansuy, Metabolic activation of prasugrel: nature of the two competitive pathways resulting in the opening of its thiophene ring, *Chem. Res. Toxicol.* 25 (2012) 1058–1065.

- [114] V. Nigam, P.M. Paarekh, Simultaneous estimation of acetaminophen and prasugrel in binary combination by RP-HPLC method, *Am. J. PharmTech Res.* 2 (2012) 920–929. <http://www.ajptr.com/archive/volume-2/december-2012-issue-6/article-519.html> (accessed July 2014).
- [115] P.M. Dansette, D. Levent, A. Hessani, G. Bertho, D. Mansuy, Thiolactone sulfoxides as new reactive metabolites acting as bis-electrophiles: implication in clopidogrel and prasugrel bioactivation, *Chem. Res. Toxicol.* 26 (2013) 794–802.
- [116] V. Jayaraman, S.K. Balaji, S. Dixit, J. Kadia, Improved method for quantitative determination of prasugrel hydrochloride, World Organization patent WO2013024399, 2013.
- [117] V. Malati, A. Raghupatireddy, K. Mukkanti, M.V. Suryanarayana, Identification of prasugrel (An antiplatelet drug) impurities by LC-MS/MS, rapid determination of prasugrel hydrochloride-related substances, and degradation products in active pharmaceutical ingredient and pharmaceutical dosage forms by stability indicating ultra-performance liquid chromatographic method, *J. Liq. Chromatogr. Relat. Technol.* 36 (2013) 61–79.
- [118] S.A. Kumar, J.V.L.N.S. Rao, K.J. Rani, S.S.S.J. Madhuri, T.S.R.K.V. Prasad, Development and validation of RP-HPLC method for the estimation of prasugrel in bulk as well in pharmaceutical dosages form, *Int. Res. J. Pharm.* 4 (2013) 254–260. http://www.irjponline.com/admin/php/uploads/1711_pdf.pdf (accessed July 2014).
- [119] S.M. Patel, C.N. Patel, V.B. Patel, Stability-indicating HPLC method for simultaneous determination of aspirin and prasugrel, *Indian J. Pharm. Sci.* 75 (2013) 413–419. <http://www.ncbi.nlm.nih.gov/pmc/articles/PMC3831722/> (accessed July 2014).
- [120] S.N. Konari, J.T. Jacob, Development and validation of RP-HPLC method for the simultaneous estimation of prasugrel and aspirin in bulk and pharmaceutical dosage form, *Inventi Impact: Pharm. Anal. Qual. Assur.* 1 (2013) 71–74. <http://www.inventi.in/Article/ppaqa/559/12.aspx> (accessed July 2014).
- [121] V. Bhavani, B. Jameelunnisa, M. Prakash, R.T. Siva, Stability indicating RP-UPLC method for the estimation of prasugrel HCl in pharmaceutical formulations, *Int. J. Biol. Pharm. Allied Sci.* 1 (2012) 946–956. <http://ijbpas.com/pdf/1343514644MS%20IJBPA%202012%201099.pdf> (accessed July 2014).
- [122] S. Magiera, Fast, simultaneous quantification of three novel cardiac drugs in human urine by MEPS-UHPLC-MS/MS for therapeutic drug monitoring, *J. Chromatogr. B Anal. Technol. Biomed. Life Sci.* 938 (2013) 86–95.
- [123] W. Maruszak, M. Cybulski, Simultaneous CE determination of counterion and possible impurity from synthetic route in pharmaceutical substance prasugrel hydrochloride, <http://science24.com/event/mknol2014/journal/?item=2> (accessed July 2014).
- [124] M. Benes, Pharmaceutical formulation of prasugrel hydrobromide, World Organization patent WO2013091595, 2013.
- [125] D.B. Dziennik, T.B. Edelman, P.L. Oren, R.L. Ternik, Formulation of a thienopyridine platelet aggregation inhibitor, European patent EP1896019, 2009.
- [126] T. Watanabe, K. Maeda, Pharmaceutical composition having improved storage stability, United States patent US20100280064, 2010.
- [127] S. Mhetre, A.S. Patil, N.B. Vishwanathan, Prasugrel pharmaceutical formulations, United States patent US20090281136, 2009.
- [128] M.J. Moon, P.L. Oren, Article of manufacture for prasugrel, United States patent US20100179184, 2010.
- [129] A.K. Nair, B. Srinivas, V. Jayaramreddy, C.S. Kandi, P.S. Reddy, Stabilized compositions of prasugrel hydrochloride tablets, *Int. J. Sci. Innov. Discov.* 2 (2012) 351–358. http://www.ijsidonline.info/admin/pdf_files/0203_2012_002.pdf (accessed July 2014).

- [130] T. Watanabe, K. Maeda, Solid medicinal preparation containing mannitol or lactose, United States patent US20100004279, 2010.
- [131] A. Féher, Z. Zsigmong, P. Tonka-Nagy, G.T. Ujfalussy, Prasugrel containing quickly released stable oral pharmaceutical compositions, United States patent US8603537, 2013.
- [132] A. Sampath, V.P. Reddy, G. Goverdhan, G. Nagaraju, P.P. Reddy, Identification, synthesis and characterization of related substances of prasugrel, *J. Pharm. Res. Opin.* 2 (2012) 102–106. <http://innovativejournal.in/index.php/jpro/article/view/713/616> (accessed July 2014).
- [133] M. Cybulski, W. Maruszak, Evaluation of potential genotoxic impurities in prasugrel intermediate by HPLC chromatography, <http://science24.com/event/mknol2014/journal/?item=2> (accessed July 2014).
- [134] T.U. Sastry, K.N. Rao, T.A. Reddy, P. Gandhi, Identification and synthesis of impurities formed during prasugrel hydrochloride preparation, *Asian J. Chem.* 25 (2013) 7783–7789.
- [135] J.L.F. Rehm, J.A. Eckstein, N.A. Farid, J.B. Heim, S.C. Kasper, A. Kurihara, S.A. Wrighton, B.J. Ring, Interactions of two major metabolites of prasugrel, a thienopyridine antiplatelet agent, with the cytochromes P450, *Drug Metab. Dispos.* 34 (2006) 600–607.
- [136] O. Lukram, M. Zarparkar, Jha C. Kumar, S. Parmar, K.S. Tomar, A. Hande, Electrospray ionization LC-MS/MS validated method for the determination of the active metabolite (R-138727) of prasugrel in human plasma and its application to a bioequivalence study, *Drug Test. Anal.* 4 (2012) 158–166.
- [137] Press releases, Daiichi Sankyo launches the antiplatelet agent Effient 3.75 mg/5mg tablets, Daiichi Sankyo Website, http://www.daiichisankyo.com/media_investors/media_relations/press_releases/detail/006133.html, 2014 (accessed July 2014).
- [138] Summary of Product Characteristics (SPC) for Effient, Electronic Medicines Compendium (eMC) Website, [http://www.medicines.org.uk/emc/medicine/21504/SPC/Effient+5mg+%26+10mg+film-coated+tablets+\(Eli+Lilly+and+Company+Ltd+Daiichi+Sankyo+UK+Limited\)/](http://www.medicines.org.uk/emc/medicine/21504/SPC/Effient+5mg+%26+10mg+film-coated+tablets+(Eli+Lilly+and+Company+Ltd+Daiichi+Sankyo+UK+Limited)/), 2014 (accessed July 2014).
- [139] Summary Basis of Decision (SBD) for Effient, Health Canada Website, http://www.hc-sc.gc.ca/dhp-mps/prodpharma/sbd-smd/drug-med/sbd_smd_2010_effient_121143-eng.php, 2014 (accessed July 2014).
- [140] R.L. Smith, T.A. Gillespie, T.J. Rash, A. Kurihara, N.A. Farid, Disposition and metabolic fate of prasugrel in mice, rats, and dogs, *Xenobiotica* 37 (2007) 884–901.
- [141] Prasugrel secondary review, FDA: Center for Drug Evaluation and Research (CDER) Website, <http://www.fda.gov/ohrms/dockets/ac/09/briefing/2009-4412b1-01-FDA.pdf>, 2014 (accessed July 2014).
- [142] N.A. Farid, R.L. Smith, T.A. Gillespie, T.J. Rash, P.E. Blair, A. Kurihara, M.J. Goldberg, The disposition of prasugrel, a novel thienopyridine, in humans, *Drug Metab. Dispos.* 35 (2007) 1096–1104.
- [143] N.A. Farid, A. Kurihara, S.A. Wrighton, Metabolism and disposition of the thienopyridine antiplatelet drugs ticlopidine, clopidogrel, and prasugrel in humans, *J. Clin. Pharmacol.* 50 (2010) 126–142.
- [144] F. Asai, J.A. Jakubowski, H. Naganuma, J.T. Brandt, N. Matsushima, T. Hirota, S. Freestone, K.J. Winters, Platelet inhibitory activity and pharmacokinetics of prasugrel (CS-747) a novel thienopyridine P2Y₁₂ inhibitor: a single ascending dose study in healthy humans, *Platelets* 17 (2006) 209–217.
- [145] N. Matsushima, J.A. Jakubowski, F. Asai, H. Naganuma, J.T. Brandt, T. Hirota, S. Freestone, K.J. Winters, Platelet inhibitory activity and pharmacokinetics of prasugrel (CS-747) a novel thienopyridine P2Y₁₂ inhibitor: a multiple-dose study in healthy humans, *Platelets* 17 (2006) 218–226.

- [146] J.A. Jakubowski, N. Matsushima, F. Asai, H. Naganuma, J.T. Brandt, T. Hirota, S. Freestone, K.J. Winters, A multiple dose study of prasugrel (CS-747), a novel thienopyridine P2Y₁₂ inhibitor, compared with clopidogrel in healthy humans, *Br. J. Clin. Pharmacol.* 63 (2006) 421–430.
- [147] A. Sugidachi, F. Asai, T. Ogawa, T. Inoue, H. Koike, The *in vivo* pharmacological profile of CS-747, a novel antiplatelet agent with platelet ADP receptor antagonist properties, *Br. J. Pharmacol.* 129 (2000) 1439–1446.
- [148] A. Sugidachi, F. Asai, K. Yoneda, R. Iwamura, T. Ogawa, K.-I. Otsuguro, H. Koike, Antiplatelet action of R-99224, an active metabolite of a novel thienopyridine-type G_i-linked P2T antagonist, CS-747, *Br. J. Pharmacol.* 132 (2001) 47–54.
- [149] M. Hasegawa, A. Sugidachi, T. Ogawa, T. Isobe, J.A. Jakubowski, F. Asai, Stereoselective inhibition of human platelet aggregation by R-138727, the active metabolite of CS-747 (prasugrel, LY640315), a novel P2Y₁₂ receptor inhibitor, *Thromb. Haemost.* 94 (2005) 593–598.
- [150] E.T. Williams, K.O. Jones, G.D. Ponsler, S.M. Lowery, E.J. Perkins, S.A. Wrighton, K.J. Ruterbories, M. Kazui, N.A. Farid, The biotransformation of prasugrel, a new thienopyridine prodrug, by the human carboxylesterases 1 and 2, *Drug Metab. Dispos.* 36 (2008) 1227–1232.
- [151] P.M. Dansette, S. Thebault, G. Bertho, D. Mansuy, Formation and fate of a sulfenic acid intermediate in the metabolic activation of the antithrombotic prodrug prasugrel, *Chem. Res. Toxicol.* 23 (2010) 1268–1274.
- [152] K. Hagihara, M. Kazui, A. Kurihara, H. Iwabuchi, M. Ishikawa, H. Kobayashi, N. Tanaka, O. Okazaki, N.A. Farid, T. Ikeda, Biotransformation of prasugrel, a novel thienopyridine antiplatelet agent, to the pharmacologically active metabolite, *Drug Metab. Dispos.* 38 (2010) 898–904.
- [153] A.D. Oprea, W.M. Popescu, P2Y₁₂ Receptor inhibitors in acute coronary syndromes: what is new on the horizon? *Cardiol. Res. Pract.* 2013 (2013) 15 pages. <http://www.hindawi.com/journals/crp/2013/195456/> (Article ID 195456, accessed July 2014).
- [154] G.H. Stone, H.D. Aronow, Long-term care after percutaneous coronary intervention: focus on the role of antiplatelet therapy, *Mayo Clin. Proc.* 81 (2006) 641–652.
- [155] P. Gladding, M. Webster, J. Ormiston, S. Olsen, H. White, Antiplatelet drug non-responsiveness, *Am. Heart J.* 155 (2008) 591–599.
- [156] Y. Niitsu, J.A. Jakubowski, A. Sugidachi, F. Asai, Pharmacology of CS-747 (prasugrel, LY640315), a novel, potent antiplatelet agent with *in vivo* P2Y₁₂ receptor antagonist activity, *Semin. Thromb. Hemost.* 31 (2005) 184–194.
- [157] S.A. Mousa, W.P. Jeske, J. Fareed, Antiplatelet therapy prasugrel: a novel platelet ADP P2Y₁₂ receptor antagonist, *Clin. Appl. Thromb. Hemost.* 16 (2010) 170–176.
- [158] G. Cayla, J. Silvain, S.A. O'Connor, J.-P. Collet, G. Montalescot, Current antiplatelet options for NSTEMI-ACS patients, *QJM: Int. J. Med.* 105 (2012) 935–948.



Salmeterol Xinafoate

Manal M. Anwar*, Radwan S. El-Haggar^{†,‡}, Wafaa A. Zaghary^{†,§,1}

*Therapeutical Chemistry Department, National Research Centre, Dokki, Cairo, Egypt

[†]Department of Pharmaceutical Chemistry, Faculty of Pharmacy, Helwan University, Cairo, Egypt

[‡]Department of Medicinal Chemistry, Pharmacy Program, Batterjee Medical College, Jeddah, Saudi Arabia

[§]Department of Pharmaceutical Chemistry, College of Pharmacy, King Saud University, Riyadh, Saudi Arabia

¹Corresponding author: e-mail address: wafaa.zaghary@pharm.helwan.edu.eg; wzaghary@yahoo.com

Contents

1. Description	321
1.1 Nomenclature	321
1.2 Formula	322
1.3 Elemental Analysis	323
1.4 Appearance	323
1.5 Uses and Applications	323
2. Methods of Preparation	324
3. Physical Characteristics	329
3.1 Solubility Characteristics	329
3.2 X-ray Powder Diffraction Pattern	329
3.3 Thermal Methods of Analysis	329
3.4 Spectroscopy	330
3.5 Mass Spectroscopy	334
4. Methods of Analysis	335
4.1 Compendial Methods	335
4.2 Reported Methods	349
5. Stability	364
6. Pharmacokinetics, Metabolism, and Excretion	365
6.1 Pharmacokinetics	365
Acknowledgment	366
References	366



1. DESCRIPTION

1.1 Nomenclature

1.1.1 Systemic Chemical Names

(*RS*)-2-(Hydroxymethyl)-4-(1-hydroxy-2-[6-(4-phenylbutoxy)hexylamino]ethyl)phenol.

(±)-1,3-Benzenedimethanol-4-hydroxy- α -[[[6-(4-phenylbutoxy)hexyl]-amino)methyl].

4-Hydroxy- α^1 -[[[6-(4-phenylbutoxy)hexyl]amino)methyl]-1,3-benzenedimethanol [1].

(±)-4-Hydroxy- α^1 -[[[6-(4-phenylbutoxy)hexyl]amino)methyl]-*m*-xylene- α, α^1 -diol [1].

(1*RS*)-1-[4-hydroxy-3-(hydroxymethyl)phenyl]-2-[[6-(4-phenylbutoxy)hexyl]amino]ethanol [2].

1.1.2 Nonproprietary Names

Base: Salmeterol

Salt: Salmeterol xinafoate

1.1.3 Proprietary Names

Arial; Advair Diskus; Salmeterdur; Serevent Diskus

1.2 Formula

1.2.1 Empirical Formula, Molecular Weight, and CAS Number

1.2.1.1 Salmeterol

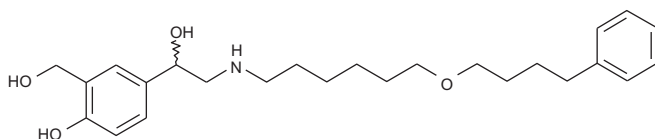
$C_{25}H_{37}NO_4$	415.56	[89365-50-4]
--------------------	--------	--------------

1.2.1.2 Salmeterol Xinafoate

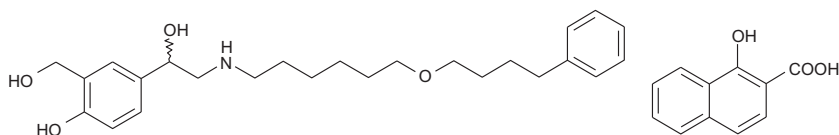
$C_{25}H_{37}NO_4 \cdot C_{11}H_8O_3$	603.47	[94749-08-3]
---------------------------------------	--------	--------------

1.2.2 Structural Formula

Salmeterol



Salmeterol xinafoate



1.3 Elemental Analysis

Salmeterol

C 72.26%, H 8.97%, N 3.37%, O 15.40%.

Salmeterol xinafoate

C 71.62%, H 7.51%, N 2.32%, O 18.55%.

1.4 Appearance

Salmeterol base is white or almost white powder. Salmeterol xinafoate is white or almost white powder [1,2].

1.5 Uses and Applications

Salmeterol xinafoate has been developed as a potent β_2 -adrenoceptor agonist having the desired pharmacological profile of a long-acting bronchodilator [3,4]. Salmeterol xinafoate as a long-acting β -agonist (LABA) is prescribed for the treatment of asthma and chronic obstructive pulmonary disease [5–7]. The principal action of salmeterol, like other β_2 -agonists, is to relax airway smooth muscle by stimulating β_2 -adrenergic receptors. This increases the intracellular messenger cyclic AMP that is responsible for the control of smooth muscle tone [8]. Thus, activation of the β_2 -adrenergic receptor results directly in bronchodilation. Muscarinic antagonists also facilitate bronchodilation but work by competing with acetylcholine for muscarinic receptors [9]. Salmeterol xinafoate as LABA with a 12-h duration of action showed positive experience in asthma [10], providing improvements in bronchodilator efficacy and patient outcomes compared with short-acting β -agonist (SABA), which have duration of action of only 4–6 h [11]. Salmeterol is usually prescribed only for severe persistent asthma following previous treatment with SABA, such as salbutamol and is prescribed concurrently with an inhaled corticosteroid (ICS), such as fluticasone [12,13]. The combination of the LABA and the ICS has been shown to have superior efficacy to either

component given separately [14], a higher dose of ICS alone [15–18], or a combination of ICS and a leukotriene antagonist [19,20] or theophylline [21].



2. METHODS OF PREPARATION

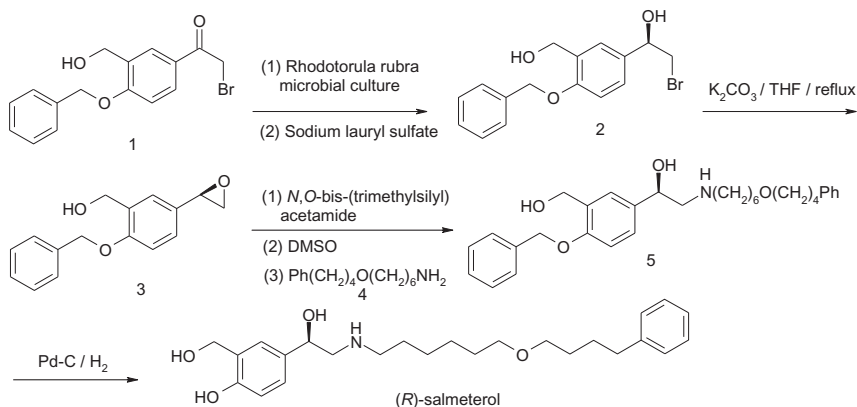
1. (*R*)-(–)-Salmeterol was prepared by Goswami and coworkers [22], their method to synthesize salmeterol in a highly enantioselective way was started with mixing a sample of 4-benzyloxy-3-hydroxymethyl- ω -bromoacetophenone **1** with sodium lauryl sulfate (in a 1:3, w/w ratio) and the mixture was added to the microbial culture of *Rhodotorula rubra*.

The pH of the reaction mixture was maintained at 7. The mixture was kept under an argon atmosphere and shaken at 200 rpm at 30 °C for 48 h. The reaction afforded (*R*)-(–)-2-bromo-1-(4-benzyloxy-3-hydroxymethylphenyl)ethanol **2** in 78–80% yield with 95% ee (as determined by the method described above).

Enantiomerically pure alcohol **2** was then transformed into the corresponding epoxide **3** without any loss of integrity of the stereogenic center by heating with potassium carbonate in refluxing THF.

Finally, this epoxide was reacted with 6-(4-phenylbutoxyhexyl)-1-amine **4** by heating in DMSO in the presence of *N,O*-bis(trimethylsilyl)acetamide at 85 °C, to afford (*R*)-(–)-2-(4-phenylbutoxyhexyl)amino-1-(4-benzyloxy-3-hydroxymethylphenyl)ethanol **5**. Catalytic hydrogenation of **5** then cleaved the benzyl-protecting group to furnish (*R*)-(–)-salmeterol with 96% ee in 61% yield (Scheme 1).

2. (*R*)-(–)-Salmeterol was also prepared by Ley and coworkers [23]. It was reported the synthesis of (*R*)-salmeterol using a sequence of supported reagents and scavenging agents. Treatment of **1** with Eschenmoser's salt and carbonate exchange resin cleanly afforded the desired tertiary amine **2**. Displacement of dimethylamine from **2** with acetic anhydride and catalytic sulfonic acid resin followed by a highly selective monobromination with polyvinylpyridinium bromide perbromide resin furnished diacetate-protected α -bromoketone **3** in good yield. The acetate groups of **3** were removed under HBr catalysis to preserve the α -bromoketone functionality. Reprotection of the diol as the acetonide was efficiently achieved by using 2-methoxypropene catalyzed by sulfonic acid resin, conditions under which all by-products are volatile. N-alkylation then proceeded without any observed dialkylation



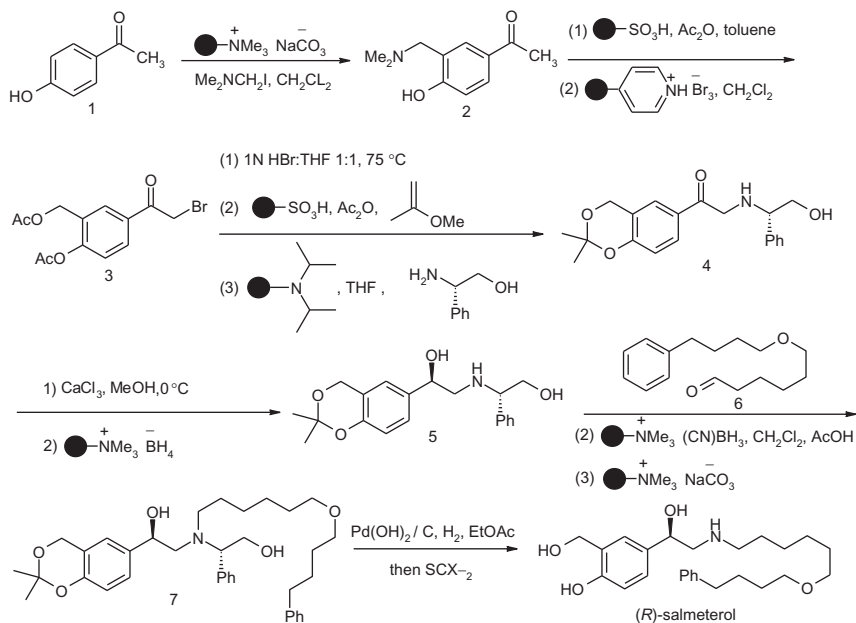
Scheme 1 Synthesis of (*R*)-(-)-Salmeterol starting with a mixing sample of 4-benzyloxy-3-hydroxymethyl- ω -bromoacetophenone **1** with sodium lauryl sulfate.

furnished α -aminoketone **4**. Treatment of **4** with calcium chloride at 0 ° C followed by the addition of BER pleasingly delivered the desired amino alcohol **5** as a 10:1 mixture of diastereomers favoring the desired (*R*)-alcohol. Recrystallization from acetonitrile afforded enantiomerically pure **5** in 76% yield.

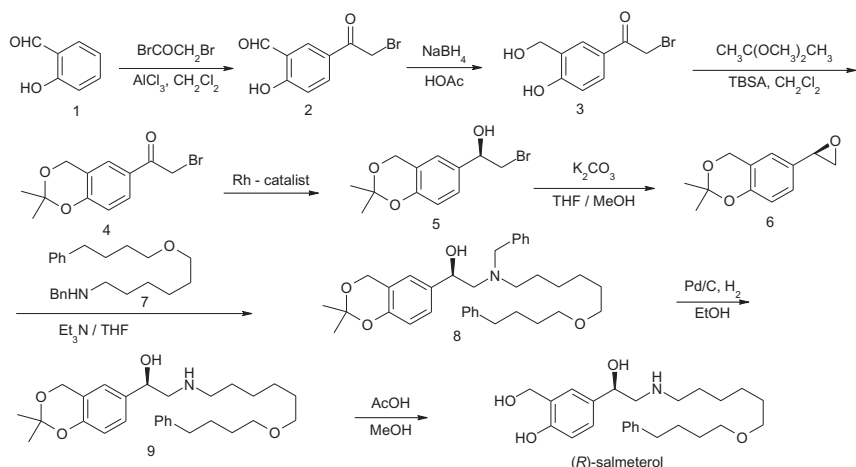
The desired reductive amination with aldehyde **6** was accomplished by using polymer-supported cyanoborohydride [24], activated by acetic acid. Filtration and evaporation afforded a mixture of the desired tertiary amine product **7** and its acetate salt, which was conveniently converted to the free base after being stirred briefly with carbonate resin. Application of the crude product **7** to an acidic SCX-2 cartridge [25], eluting with methanol, allowed the removal of the phenethyl alcohol by-product. Elution with 2 N ammonia in methanol then released the product with simultaneous removal of the acetamide group afforded (*R*)-salmeterol in 87% yield in two steps. Enantioselectivity (es) was determined by chiral HPLC to be 97.4% (Scheme 2).

- In addition, Xingshu Li reported a convenient synthesis of (*R*)-salmeterol via Rh-catalyzed asymmetric transfer hydrogenation (Scheme 3) [26].

In the presence of aluminum chloride, bromoacetyl bromide reacted with salicaldehyde **1** to give acetophenone derivative **2** [27]. Then, the aldehyde group of compound **2** was reduced regioselectively by sodium borohydride in acetic acid to give the intermediate **3** [28]. Ketal formation by the reaction of intermediate **3** with 2,2-dimethoxypropane



Scheme 2 Synthesis of (*R*)-salmeterol using a sequence of supported reagents and scavenging agents.

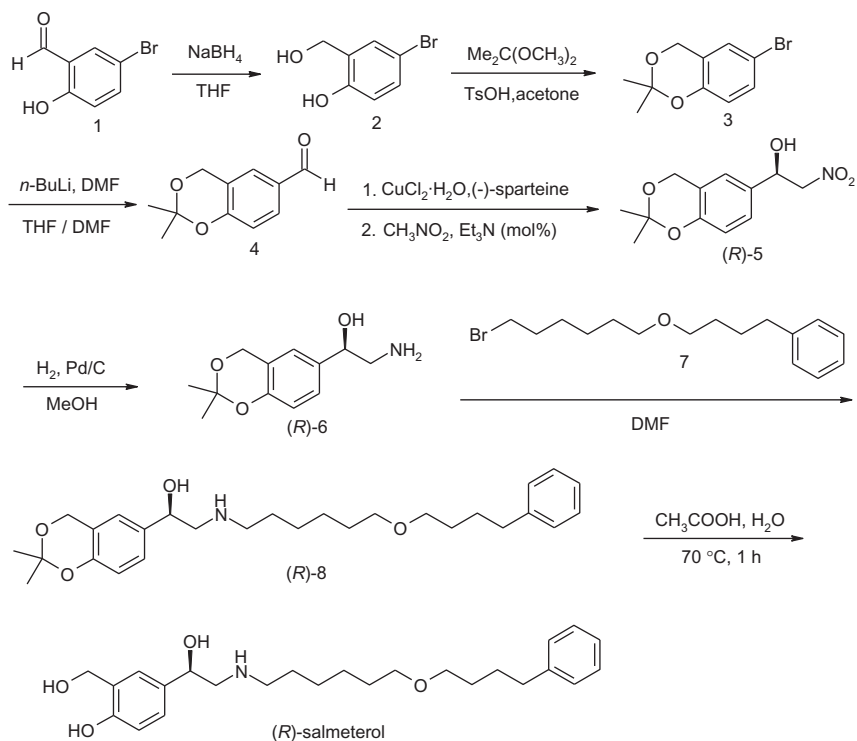


Scheme 3 Synthesis of (*R*)-salmeterol via Rh-catalyzed asymmetric transfer hydrogenation.

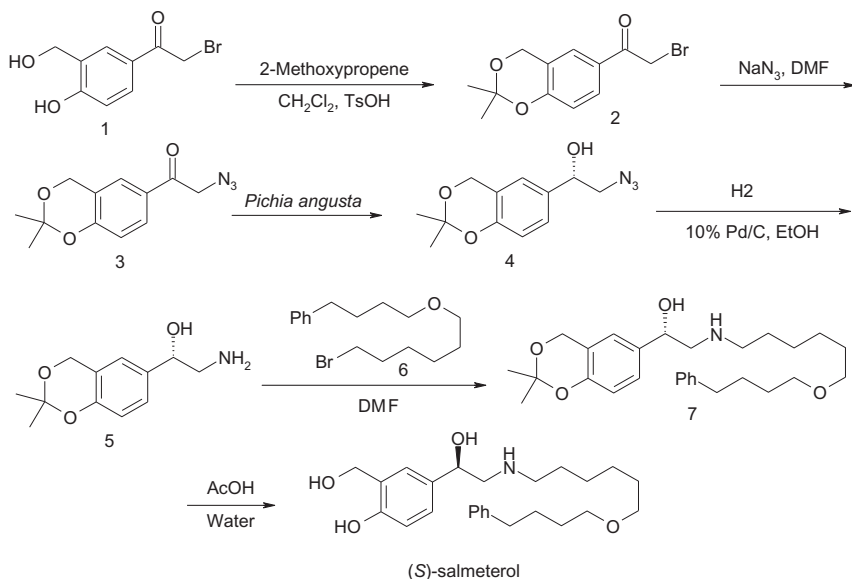
catalyzed by *p*-toluenesulfonic acid gave the desired prochiral α -bromoketone **4**. Rh-catalyzed asymmetric transfer hydrogenation of α -bromoketone **4** in water gave the desired product α -bromoalcohol **5** with good yield and enantioselectivity (98% ee).

The α -bromoalcohol **5** could be quantitatively transformed into epoxide **6** in the presence of potassium carbonate in a mixture of THF and MeOH at room temperature. Heating the mixture of epoxide **6** and amine **7** at 120 °C in the presence of triethylamine under neat conditions gave the ring-opening product **8**. Removal of the benzyl group by Pd/C-catalyzed hydrogenolysis, followed by acidolysis of the ketal protective group with acetic acid afforded (R)-salmeterol (Scheme 3).

4. Also, Lu and coworker reported the enantioselective synthesis of (R)-salmeterol employing an asymmetric Henry reaction as the key step [29]. The reduction of 3-bromosalicylaldehyde **1** with sodium borohydride proceeded quantitatively to afford **2**. Compound **2** underwent acetalization to give compound **3** in good yield. Carbonylation of **3** with *n*-butyllithium in dry DMF afforded the aldehyde **4**. After optimization of the Henry reaction conditions, the key intermediate (R)-**5** was obtained in excellent ee, compound (R)-**5** was reduced to (R)-**6** by Pd/C catalyst in quantitative yield. Another key intermediate **7** was prepared by the direct alkylation of 4-phenylbutan-1-ol with 1,6-dibromohexane [30]. The controlled alkylation of **7** with (R)-**6** was smoothly carried out using less bromide **7** to avoid the possible bis-ether by-product. Compound (R)-**8** can be purified by flash chromatography with petroleum ether/ethyl acetate as eluent. Next, refluxing (R)-**8** in 85% acetic acid solution for 45 min afforded (R)-salmeterol (Scheme 4).
5. On the other hand, interest in the (S)-enantiomer of salmeterol had recently been stimulated since it is claimed that the (S)-enantiomer of salmeterol had a higher selectivity for β_2 receptors and that it did not precipitate certain adverse effects associated with the administration of (\pm)- or (R)-salmeterol [29], which motivated Procopiou and coworker to report the enantioselective synthesis of (S)-salmeterol via asymmetric reduction of azidoketone by *Pichia angusta* (Scheme 4) [31]. The salmeterol intermediate **1** was first protected as the acetonide **2** and then converted to the azidoketone **3**. The biotransformation of the azidoketone **3** to the (S)-enantiomer of **4** is achieved using *P. angusta* yeast that produced **4** with excellent enantioselectivity (ee >98%) and 94% yield. The azido alcohol **4** was then hydrogenated over palladium on charcoal in ethanol to provide the amino alcohol **5** in 86% yield. Reaction of **5** with the bromide **6** (prepared from 4-phenyl-1-butanol and 1,6-dibromohexane under phase-transfer conditions) [32] gave the secondary amine **7**. Deprotection of **7** with aqueous acetic acid gave (S)-salmeterol acetate salt in quantitative yield and 98.6% ee (Scheme 5).



Scheme 4 Synthesis of (R)-salmeterol employing an asymmetric Henry reaction as the key step.



Scheme 5 Synthesis of (S)-salmeterol via asymmetric reduction of azidoketone by *Pichia angusta*.



3. PHYSICAL CHARACTERISTICS

3.1 Solubility Characteristics

Freely soluble in methanol; slightly soluble in ethanol, chloroform, and isopropanol; sparingly soluble in water.

3.2 X-ray Powder Diffraction Pattern

The X-ray powder diffraction pattern of salmeterol xinafoate was performed using (Bruker-Nonius KappaCCD). Figure 1 shows the X-ray powder diffraction pattern of salmeterol xinafoate, which was obtained in a pure sample of the drug substance. Table 1 shows the values of the interplanar d -spacing (Å) and the relative intensities (%) observed for the major diffraction peaks of salmeterol xinafoate.

3.3 Thermal Methods of Analysis

Salmeterol base melts at 75.5–76.5 °C. Salmeterol xinafoate melts at 137–138 °C.

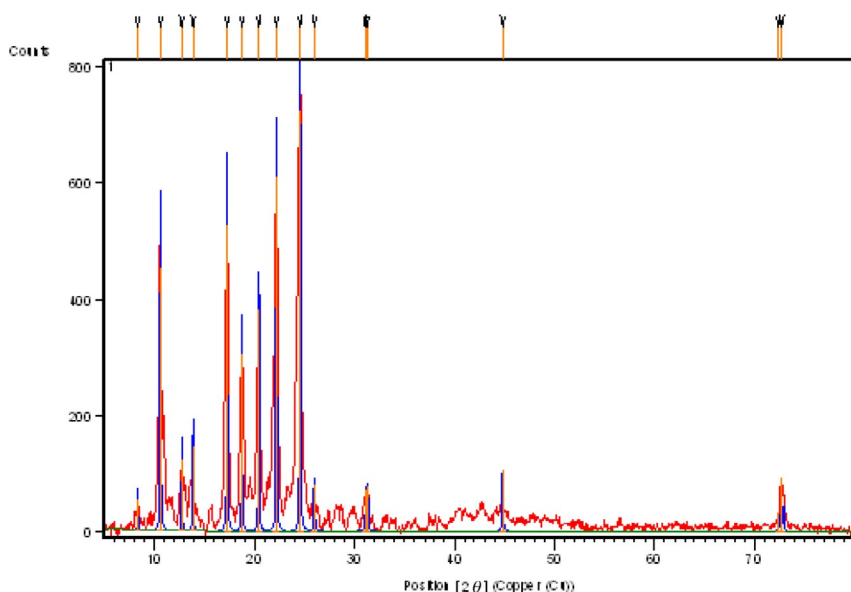


Figure 1 The X-ray powder diffraction pattern of salmeterol xinafoate.

Table 1 Crystallographic Data from the X-ray Powder Diffraction Pattern of Salmeterol Xinafoate

Pos. ($^{\circ}$, 2θ)	Height (cts)	FWHM Left ($^{\circ}$, 2θ)	d-Spacing (\AA)	Rel. Int. (%)
8.3485	55.23	0.090	10.58246	7.62
10.6065	452.79	0.090	8.33413	62.45
12.7418	122.32	0.090	6.94185	16.87
13.8629	144.60	0.090	6.38289	19.95
17.2552	528.00	0.090	5.13494	72.83
18.7490	307.00	0.090	4.72905	42.34
20.4365	381.00	0.090	4.34220	52.55
22.1875	611.00	0.090	4.00332	84.28
24.5649	725.00	0.090	3.62100	100.00
25.9662	81.00	0.090	3.42867	11.17
31.0966	73.00	0.090	2.87370	10.07
31.3014	77.00	0.090	2.85537	10.62
44.7814	105.43	0.090	2.02220	14.54
72.3719	33.73	0.090	1.30469	4.65
72.6772	93.77	0.090	1.29996	12.93

3.4 Spectroscopy

3.4.1 Ultraviolet Spectroscopy

The ultraviolet absorption spectrum of salmeterol xinafoate in methanol shown in [Figure 2](#) was recorded using Labomed, INC. Spectro UV–vis double beam PC 8 scanning auto cell spectrophotometer model UVD-3000. The compound exhibited a maximum peak at 217 nm (λ 1%, 1 cm = 340.8).

3.4.2 Vibrational Spectroscopy

The infrared (IR) absorption spectrum of salmeterol xinafoate was obtained in a KBr pellet using Jasco F/IR-4100 IR spectrophotometer. The IR spectrum is shown in [Figure 3](#), where the principle peaks were observed at 3322, 3025, 2940, 2859, 2359–3300, 1581, 1470, 1275, and 1098 cm^{-1} . Assignment for the major IR absorption bands are provided in [Table 2](#).

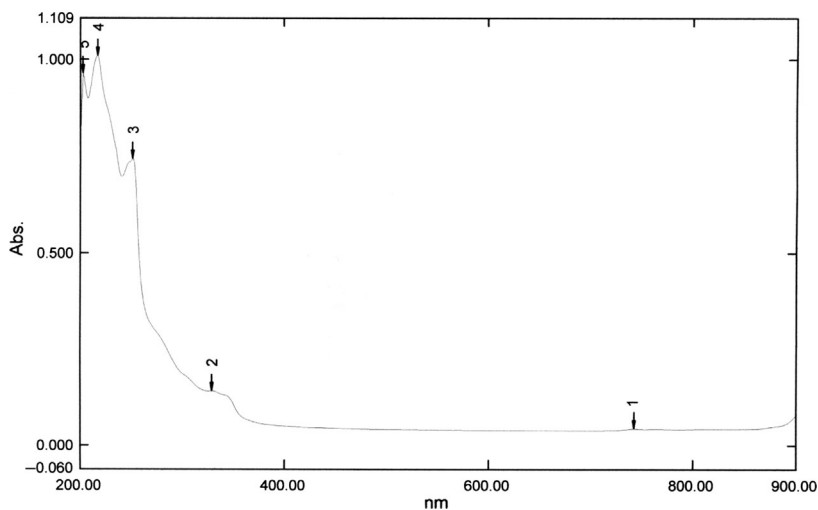


Figure 2 The ultraviolet absorption spectrum of salmeterol xinafoate.

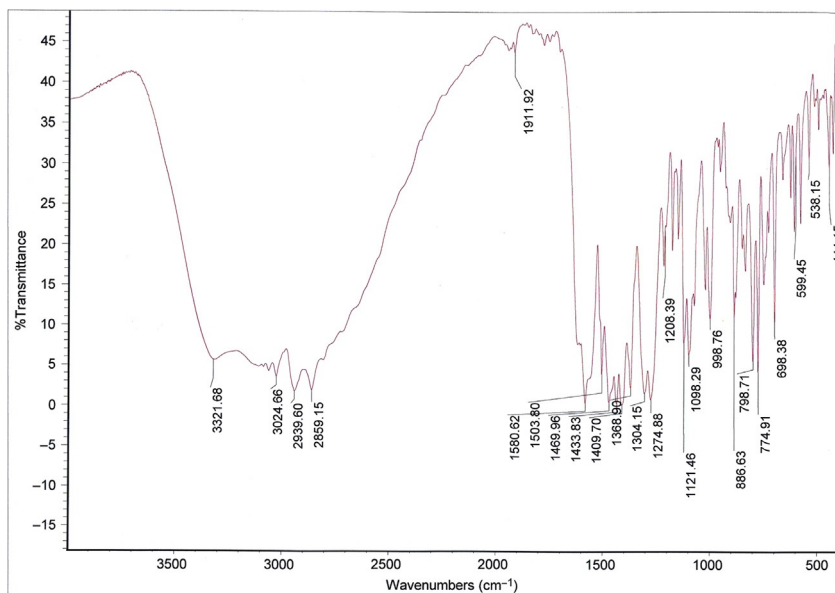


Figure 3 The infrared absorption spectrum of salmeterol xinafoate (KBr disc).

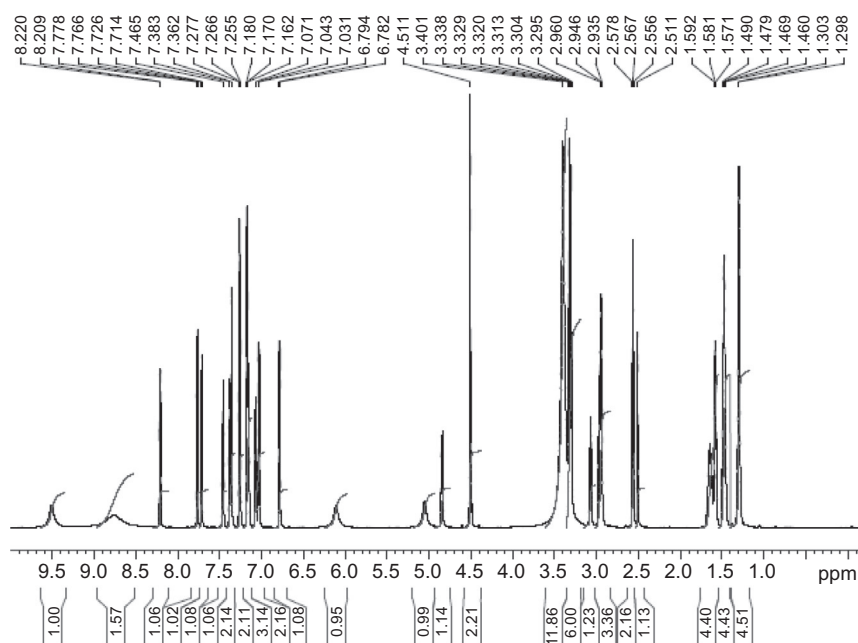
3.4.3 Nuclear Magnetic Resonance Spectroscopy

3.4.3.1 ¹H NMR Spectrum

The proton nuclear magnetic resonance (NMR) spectrum of salmeterol xinafoate was obtained using a Bruker instrument operating at 700 MHz.

Table 2 Vibrational Assignments for Salmeterol Xinafoate Infrared Absorption Bands

Frequency (cm^{-1})	Assignments
3322	OH stretch, NH stretch
3025	Aromatic CH stretch
2940, 2859	CH stretch (aliphatic)
2359–3300	Carboxylic acids
1581	C=C aromatic
1470	—CH ₂ — (bend)
1275	C—N stretch
1098	C—O stretching

**Figure 4** The ^1H NMR spectrum of salmeterol xinafoate in $\text{DMSO}-d_6$.

Standard Bruker software was used to execute the recording of ^1H NMR and COSY spectra. The sample was dissolved in $\text{DMSO}-d_6$ and all resonance bands were referenced to the tetramethylsilane (TMS) internal standard. The ^1H NMR spectra of salmeterol are shown in [Figures 4–7](#), and the COSY spectra are shown in [Figures 8–11](#). The ^1H NMR assignments for salmeterol are provided in [Table 3](#).

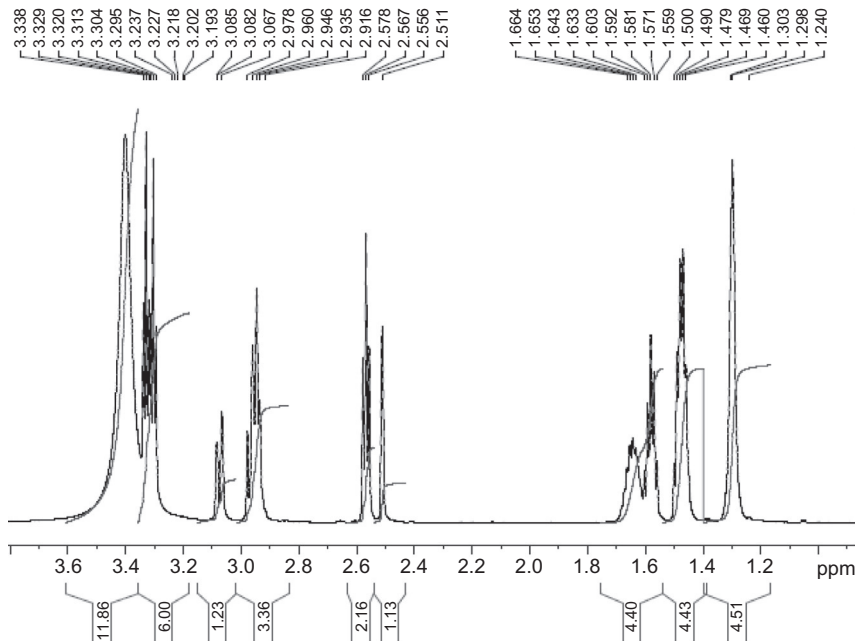


Figure 5 Expanded ^1H NMR spectrum of salmeterol xinafoate in $\text{DMSO}-d_6$.

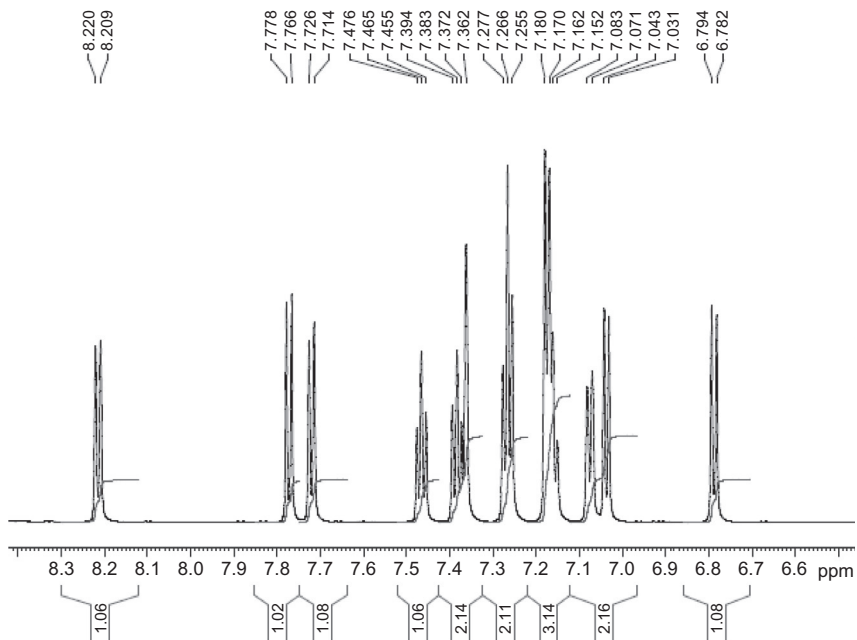


Figure 6 Expanded ^1H NMR spectrum of salmeterol xinafoate in $\text{DMSO}-d_6$.

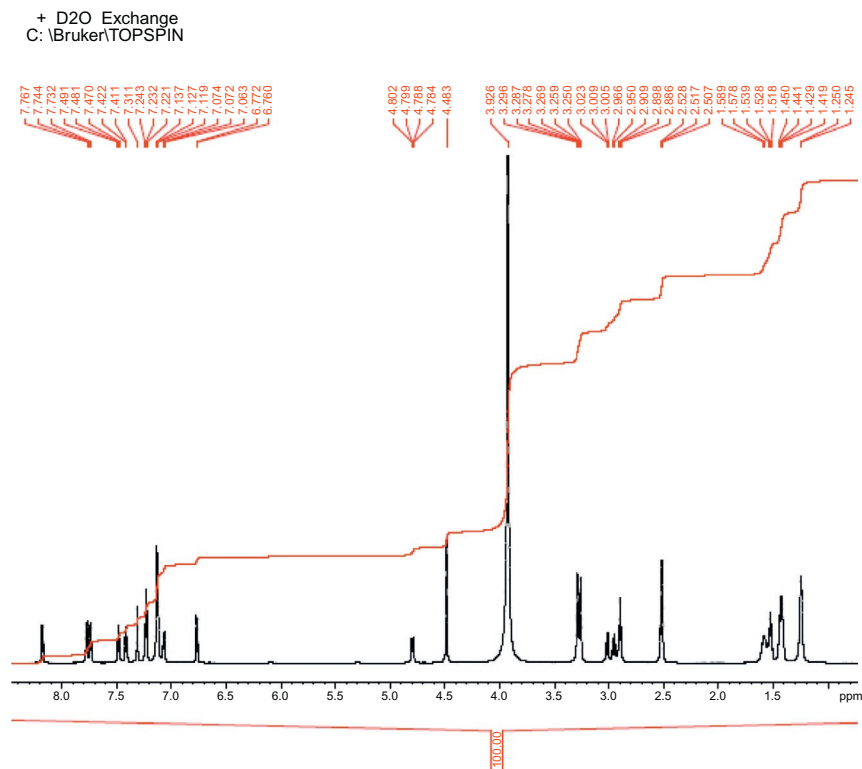


Figure 7 Expanded ^1H NMR spectrum of salmeterol xinafoate in $\text{DMSO}-d_6 + \text{D}_2\text{O}$ exchange.

3.4.3.2 ^{13}C NMR Spectrum

The ^{13}C NMR spectrum of salmeterol xinafoate was obtained using a Bruker instrument operating at 175 MHz. The sample was dissolved in $\text{DMSO}-d_6$ and TMS was added to act as internal standard. The ^{13}C NMR spectra of salmeterol xinafoate are shown in [Figures 12–14](#), and the HSQC and HMBC NMR spectra are shown in [Figures 15–21](#). The DEPT 90 and DEPT 135 are shown in [Figures 22–27](#). The ^{13}C NMR assignments for the observed resonance bands associated with the various carbons are listed in [Table 4](#). Summary of assignments for the NMR bands of salmeterol xinafoate is shown in [Table 5](#).

3.5 Mass Spectroscopy

The mass spectrum of salmeterol xinafoate was obtained using Shimadzu QP-2012 plus mass spectrometer. The parent ion collided with helium as the carrier gas. [Figure 28](#) shows the detailed mass fragmentation pattern and [Table 6](#) shows the mass fragmentation pattern of the drug substance.

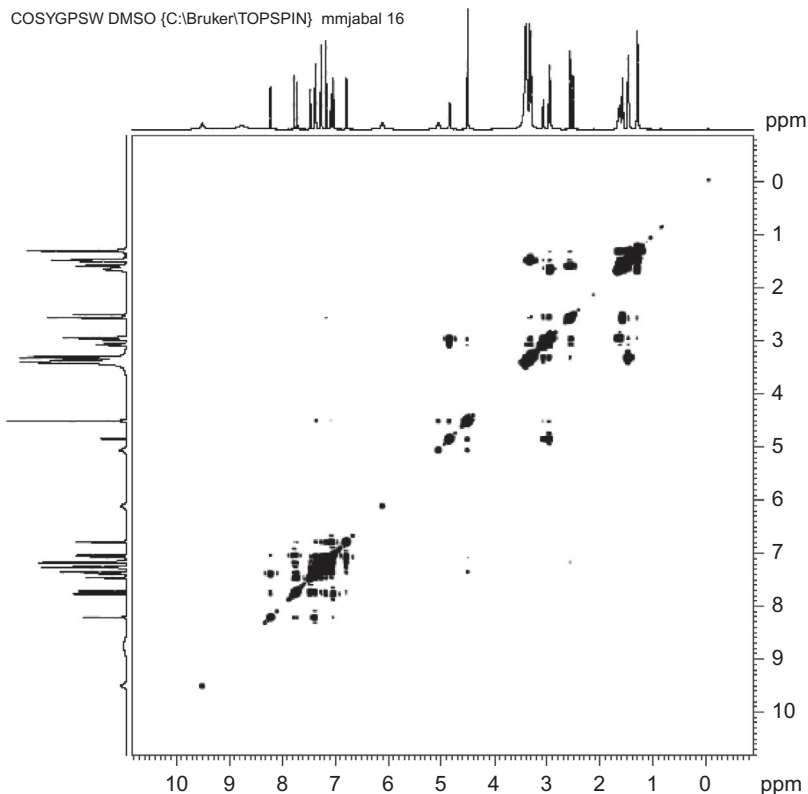


Figure 8 COSY ^1H NMR spectrum of salmeterol xinafoate in $\text{DMSO}-d_6$.



4. METHODS OF ANALYSIS

4.1 Compendial Methods

4.1.1 British Pharmacopoeia Methods [2]

Content

97.0–102.0% (anhydrous substance).

Identification

IR absorption spectrophotometry (2.2.24).

Comparison: salmeterol xinafoate CRS.

Tests

Related substances

Liquid chromatography (2.2.29). Protect the solutions from light.

Solvent mixture: acetonitrile R, water R (50:50, v/v).

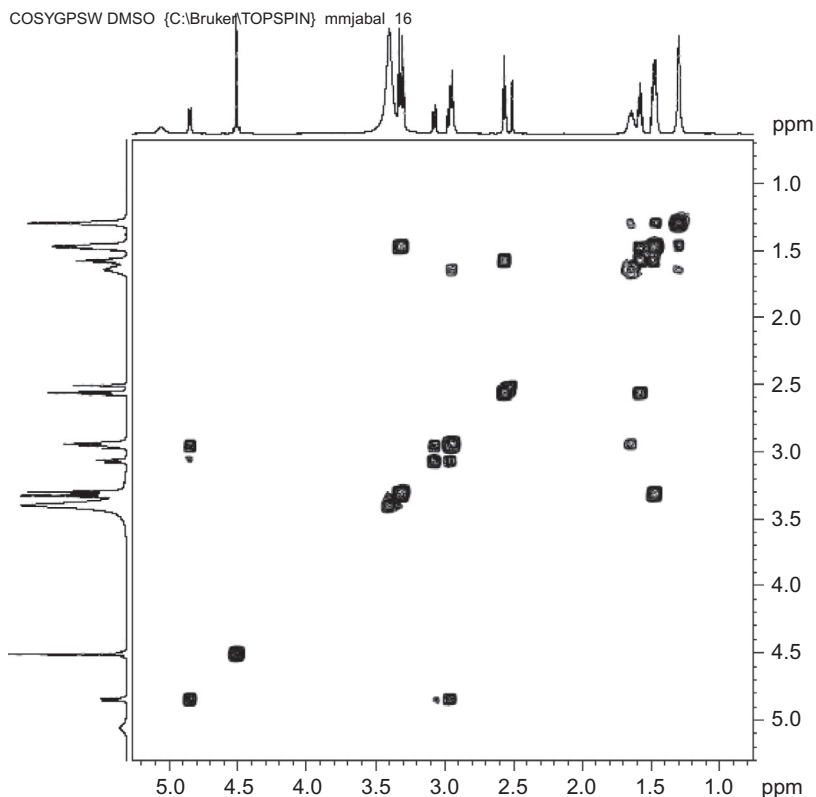


Figure 9 Expanded COSY ^1H NMR spectrum of salmeterol xinafoate in $\text{DMSO}-d_6$.

Test solution: Dissolve 50.0 mg of the substance to be examined in the solvent mixture and dilute to 10.0 mL with the solvent mixture.

Reference solution (a): Dissolve 11 mg of salmeterol xinafoate for system suitability CRS (salmeterol containing impurities E and G) in the solvent mixture and dilute to 2 mL with the solvent mixture.

Reference solution (b): Dilute 1.0 mL of the test solution to 100.0 mL with the solvent mixture. Dilute 1.0 mL of this solution to 10.0 mL with the solvent mixture.

Column:

Size: $l=0.15$ m, $\varnothing=4.6$ mm;

Stationary phase: octadecylsilyl silica gel for chromatography R (5 μm).

Mobile phase:

Mobile phase A: mix 24 volumes of a 7.71 g/L solution of ammonium acetate R with 24 volumes of a 28.84 g/L solution of sodium

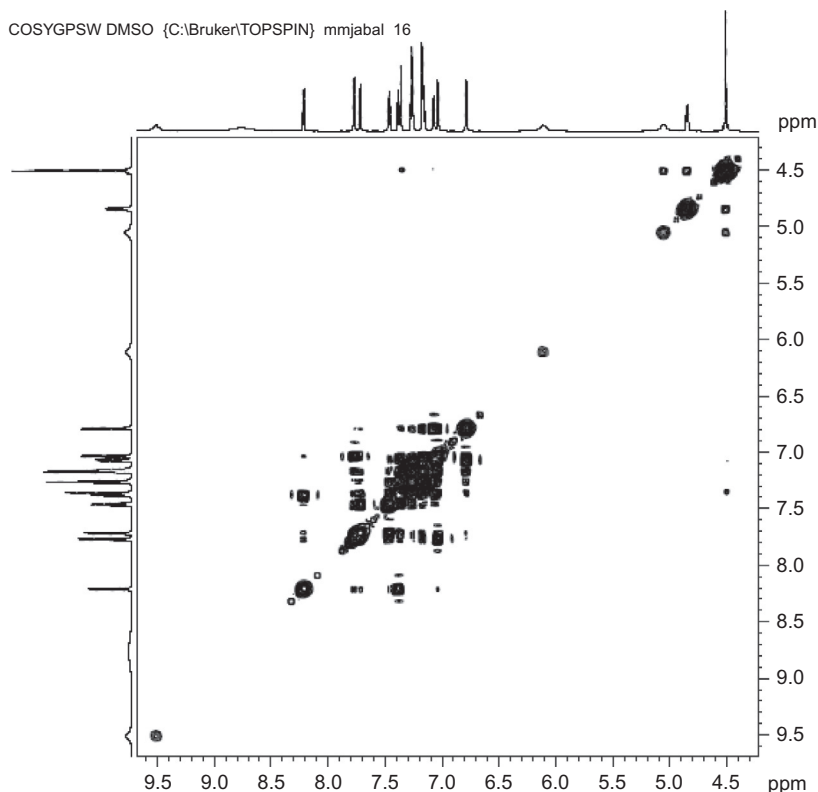


Figure 10 Expanded COSY ^1H NMR spectrum of salmeterol xinafoate in $\text{DMSO}-d_6$.

dodecyl sulfate R and adjust to pH 2.7 with glacial acetic acid R; mix with 52 volumes of acetonitrile R;

Mobile phase B: acetonitrile R;

Flow rate: 2 mL/min.

Detection: Spectrophotometer at 278 nm.

Injection: 20 μL ; inject the solvent mixture as a blank solution.

Relative retention with reference to salmeterol (retention time = about 13 min): xinafoic acid = about 0.2; impurity A = about 0.3; impurity B = about 0.5; impurity C = about 0.7; impurity D = about 0.8; impurity E = about 0.9; impurity F = about 1.6; impurity G = about 2.7.

System suitability: Reference solution (a):

Peak-to-valley ratio: minimum 10, where H_p = height above the baseline of the peak due to impurity E and H_v = height above the baseline of the lowest point of the curve separating this peak from the peak due to salmeterol;

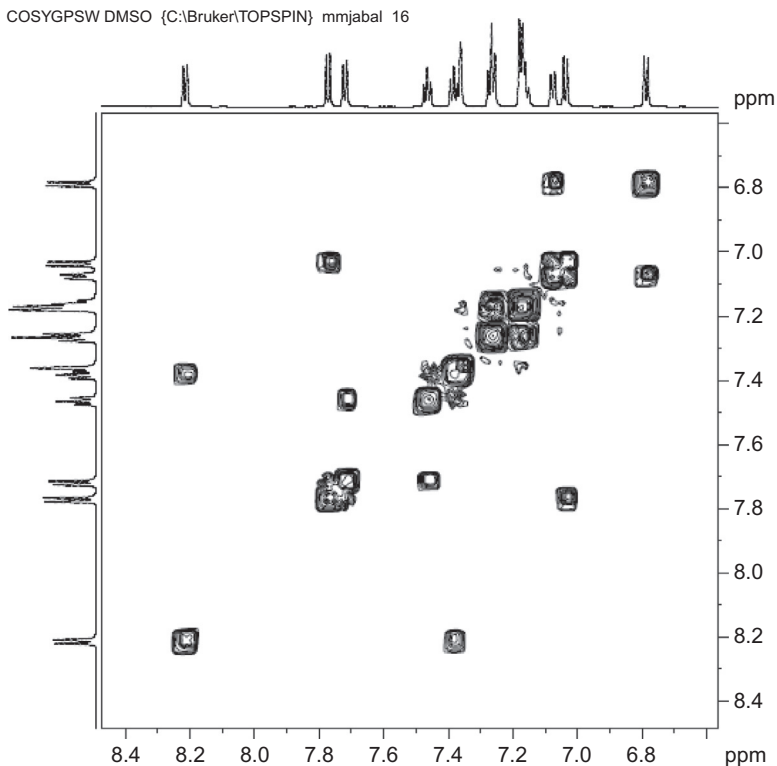


Figure 11 Expanded COSY ^1H NMR spectrum of salmeterol xinafoate in $\text{DMSO}-d_6$.

The chromatogram obtained is similar to the chromatogram supplied with salmeterol xinafoate for system suitability CRS.

Limits

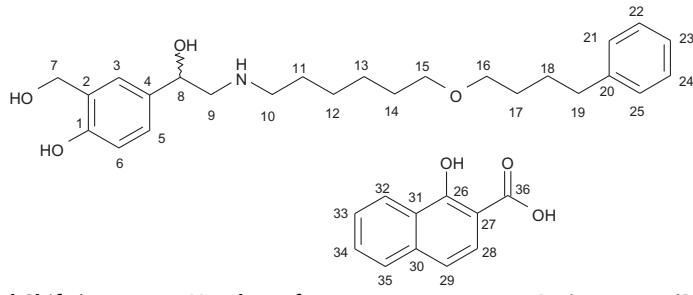
Impurity D: not more than three times the area of the principal peak in the chromatogram obtained with reference solution (b) (0.3%);

Impurities A, F, and G: for each impurity, not more than twice the area of the principal peak in the chromatogram obtained with the reference solution (b) (0.2%);

Impurities B, C, and E: for each impurity, not more than the area of the principal peak in the chromatogram obtained with the reference solution (b) (0.1%);

Any other impurity: for each impurity, not more than the area of the principal peak in the chromatogram obtained with reference solution (b) (0.1%);

Table 3 ¹H NMR (δ, ppm) Assignments of the Resonance Bands in Salmeterol Xinafoate



Chemical Shift (ppm, Relative to TMS)	Number of Protons	Multiplicity ^a	Assignments (Proton at Carbon Number)
1.29–1.30	4	m	H-12 and H-13
1.46–1.50	4	m	H-14 and H-17
1.56–1.66	4	m	H-11 and H-18
2.57	2	t, $J=7.7$	H-19
2.95	2	m	H-10
2.97	1	dd, $J=7.7$, 12.6	H-9a
3.08	1	dd, $J=2.1$, 12.6	H-9b
3.30–3.43	4	m	H-15 and H-16
4.51	2	s	H-7
4.79	1	dd, $J=10.5$, 2.1	H-8
6.79	1	d, $J=8.4$	H-6
7.04	1	d, $J=8.4$	H-29
7.08	1	d, $J=8.4$	H-5
7.15–7.18	3	m	H-22, H-23, and H-24
7.27	2	t, $J=7.7$	H-21 and H-25
7.36	1	s	H-3
7.38	1	t, $J=7.7$	H-33
7.47	1	t, $J=7.7$	H-34
7.72	1	d, $J=8.4$	H-35
7.77	1	d, $J=8.4$	H-28
8.21	1	d, $J=7.7$	H-32

^as, singlet; d, doublet; triplet; m, multiplet.

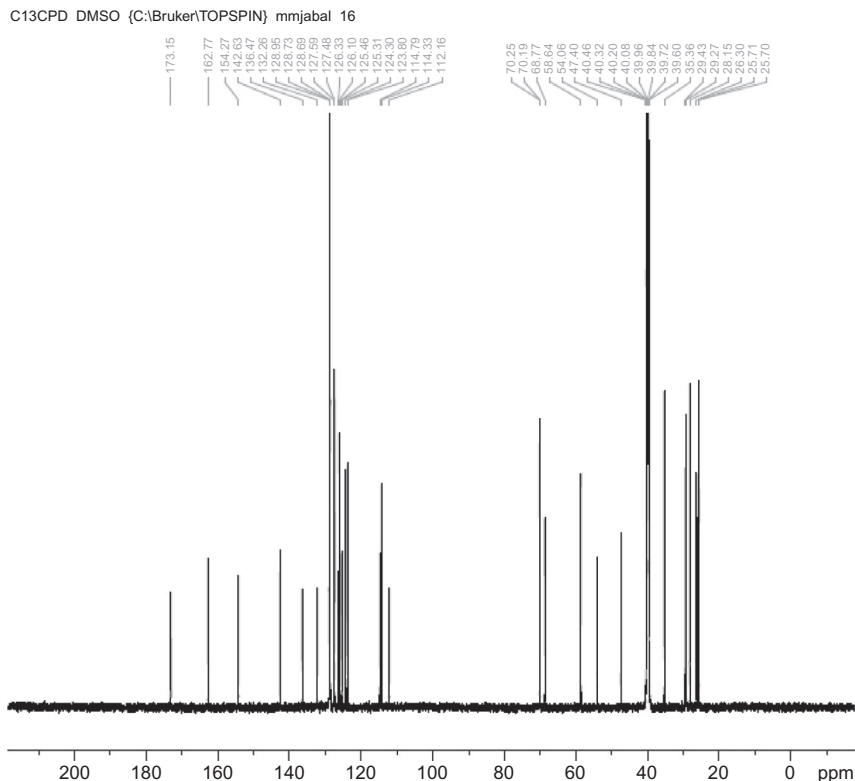


Figure 12 ^{13}C NMR spectrum of salmeterol xinafoate in $\text{DMSO-}d_6$.

Total: not more than nine times the area of the principal peak in the chromatogram obtained with the reference solution (b) (0.9%);

Disregard limit: 0.5 times the area of the principal peak in the chromatogram obtained with the reference solution (b) (0.05%); disregard the peak due to xinafoic acid and any peaks due to the blank.

Water (2.5.12)

Maximum 0.5%, determined on 1.000 g.

Dissolve the sample with 30 mL of anhydrous methanol R.

Sulfated ash (2.4.14)

Maximum 0.1%, determined on 1.0 g.

Assay

Liquid chromatography (2.2.29).

Test solution: Dissolve 12.50 mg of the substance to be examined in the mobile phase and dilute to 50.0 mL with the mobile phase.

C13CPD DMSO {C:\Bruker\TOPSPIN} mmjabal 16

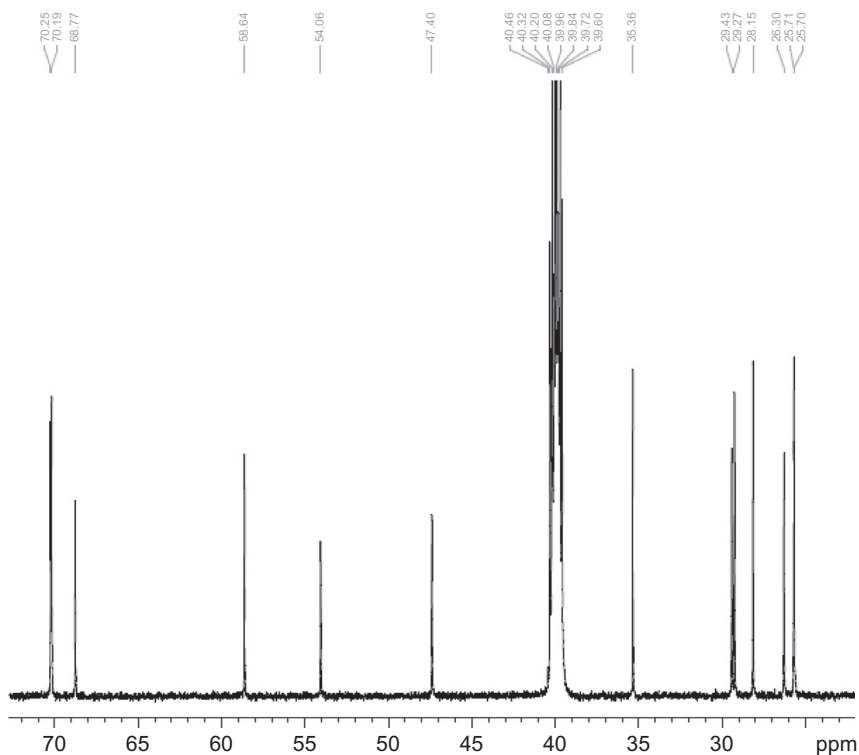


Figure 13 Expanded ^{13}C NMR spectrum of salmeterol xinafoate in DMSO- d_6 .

Reference solution (a): Dissolve 12.50 mg of salmeterol xinafoate CRS in the mobile phase and dilute to 50.0 mL with the mobile phase.

Reference solution (b): Dilute 1 mL of reference solution (a) described in the test for related substances to 20 mL with the mobile phase.

Column:

Size: $l=0.15$ m, $\varnothing=4.6$ mm;

Stationary phase: octadecylsilyl silica gel for chromatography R (5 μm).

Mobile phase: Mix 24 volumes of a 7.71 g/L solution of ammonium acetate R with 24 volumes of a 28.84 g/L solution of sodium dodecyl sulfate R and adjust to pH 2.7 with glacial acetic acid R. Mix with 52 volumes of acetonitrile R.

Flow rate: 2 mL/min.

Detection Spectrophotometer: at 278 nm.

Injection: 20 μL .

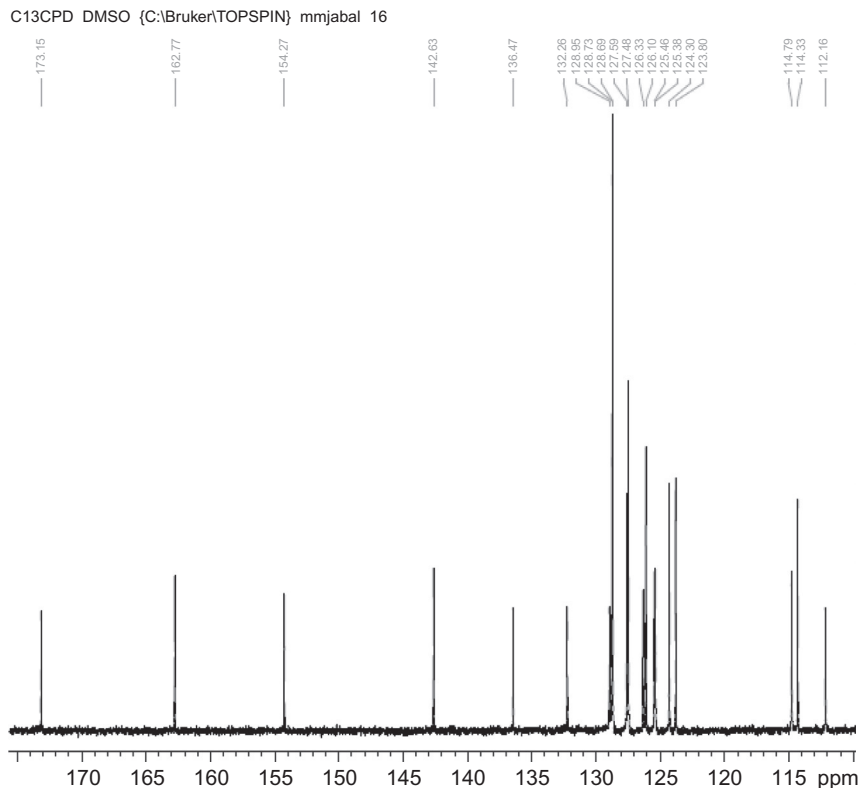


Figure 14 Expanded ^{13}C NMR spectrum of salmeterol xinafoate in $\text{DMSO}-d_6$.

Run time: Until complete elution of the peak due to salmeterol (about 16 min).

System suitability: Reference solution (b):

Peak-to-valley ratio: minimum 10, where H_p = height above the baseline of the peak due to impurity E and H_v = height above the baseline of the lowest point of the curve separating this peak from the peak due to salmeterol.

The stationary phase may be regenerated using the gradient described under the test for related substances.

Calculate the content percentage of $\text{C}_{36}\text{H}_{45}\text{NO}_7$ using the chromatogram obtained with reference solution (a) and the declared content of $\text{C}_{36}\text{H}_{45}\text{NO}_7$ in salmeterol xinafoate CRS.

Storage

Protected from light.

Impurities

HMBCGP DMSO {C:\Bruker\TOPSPIN} mmjabal 16

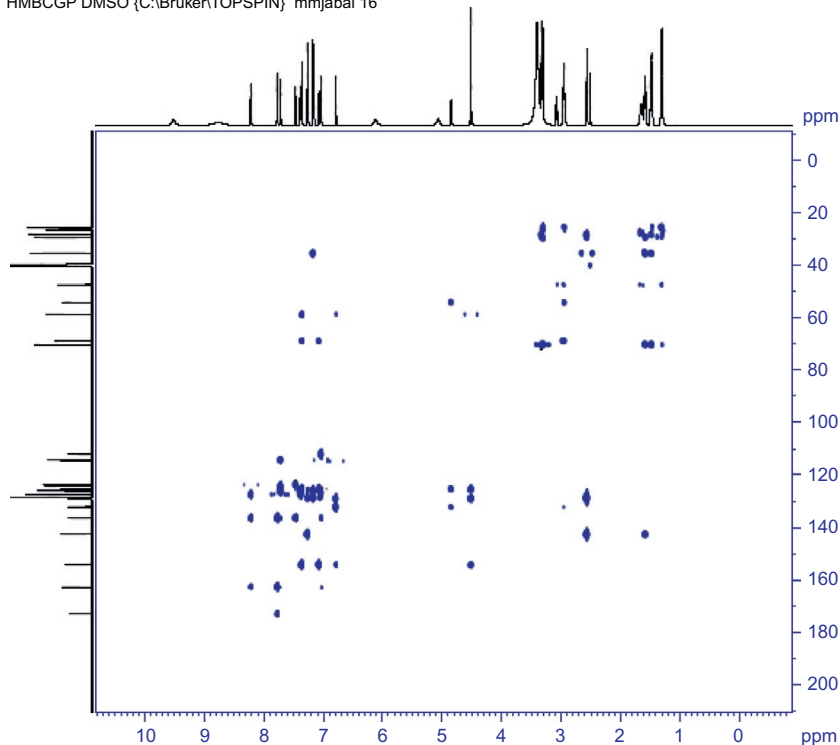
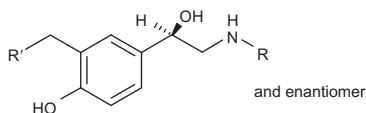


Figure 15 The HMBC spectrum of salmeterol xinafoate in DMSO- d_6 .

Specified impurities: A, B, C, D, E, F, G.



- A.** $R = [CH_2]_4-C_6H_5$, $R' = OH$: (1*RS*)-1-[4-hydroxy-3-(hydroxymethyl)phenyl]-2-[(4-phenylbutyl)amino]ethanol,
- B.** $R = [CH_2]_6-O-[CH_2]_2-C_6H_5$, $R' = OH$: (1*RS*)-1-[4-hydroxy-3-(hydroxymethyl)phenyl]-2-[[6-(2-phenylethoxy)hexyl]amino]ethanol,
- C.** $R = [CH_2]_6-O-[CH_2]_3-C_6H_5$, $R' = OH$: (1*RS*)-1-[4-hydroxy-3-(hydroxymethyl)phenyl]-2-[[6-(3-phenylpropoxy)hexyl]amino]ethanol,

HMBCGP DMSO {C:\Bruker\TOPSPIN} mmjabal 16

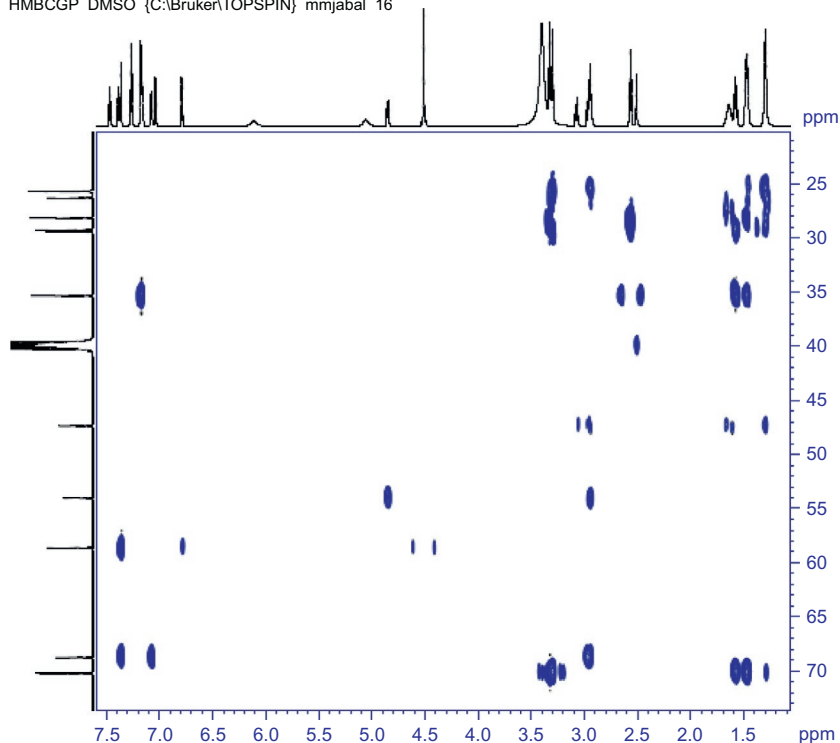
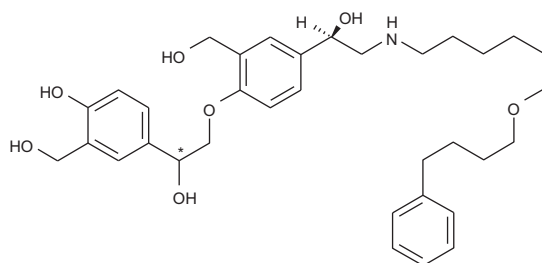


Figure 16 Expanded HMBC spectrum of salmeterol xinafoate in DMSO- d_6 .

F. $R = [CH_2]_6-O-[CH_2]_4-C_6H_5$, $R' = H$: (1*RS*)-1-(4-hydroxy-3-methylphenyl)-2-[[6-(4-phenylbutoxy)hexyl]amino]ethanol,



D. 1-[4-[2-Hydroxy-2-[4-hydroxy-3-(hydroxymethyl)phenyl]-ethoxy]-3-(hydroxymethyl)phenyl]-2-[[6-(3-phenylbutoxy)hexyl]amino]ethanol,

HMBCGP DMSO {C:\Bruker\TOPSPIN} mmjabal 16

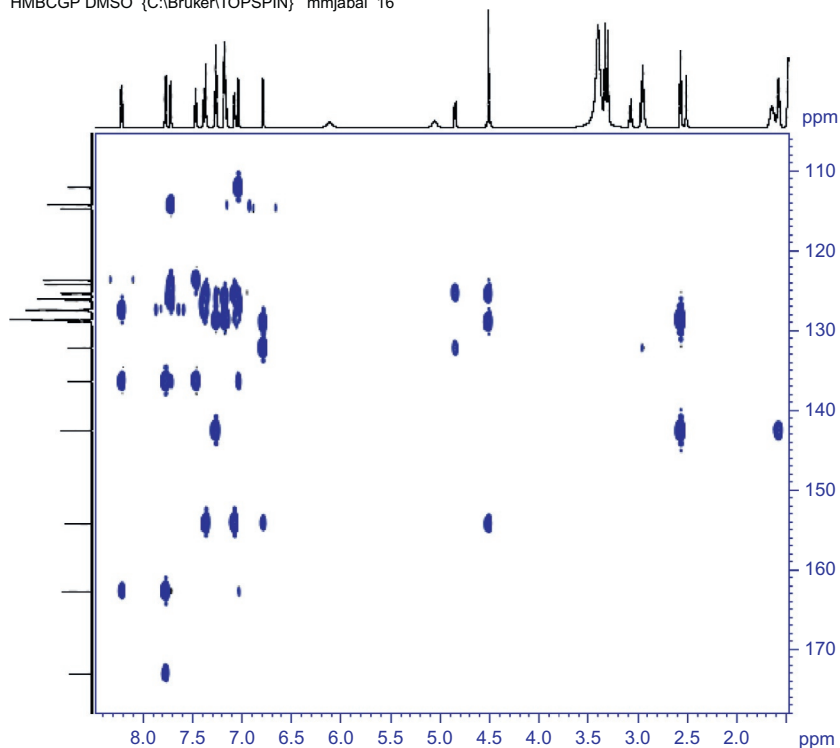
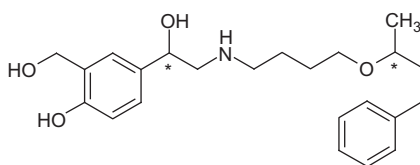
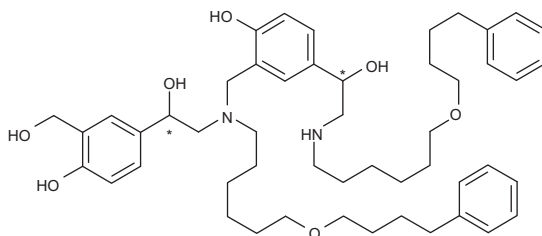


Figure 17 Expanded HMBC spectrum of salmeterol xinafoate in DMSO- d_6 .



E. 1-[4-Hydroxy-3-(hydroxymethyl)phenyl]-2-[[6-(1-methyl-3-phenylpropoxy)hexyl]amino]ethanol.



HMBCGP DMSO {C:\Bruker\TOPSPIN} mmjabal 16

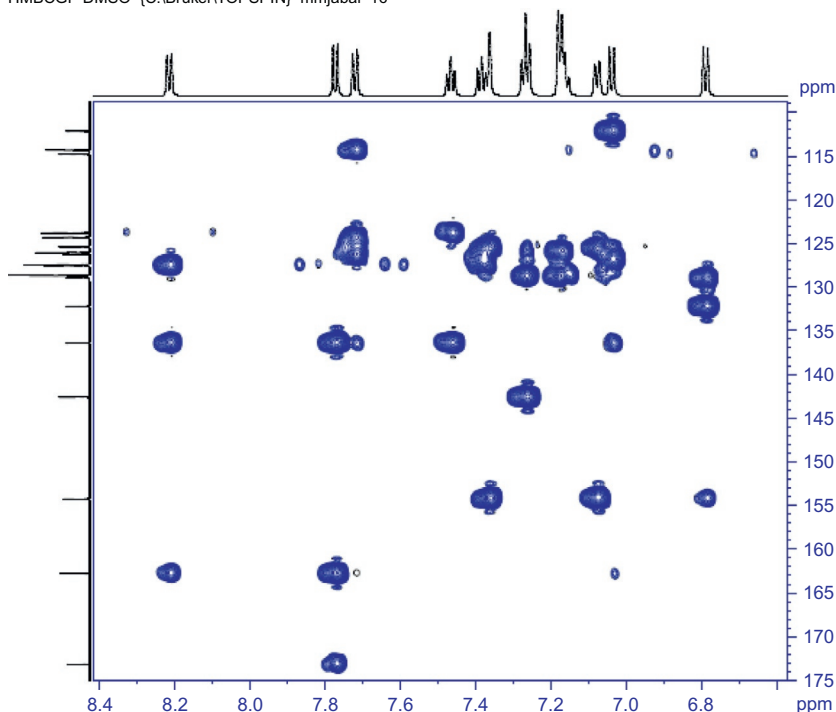


Figure 18 Expanded HMBC spectrum of salmeterol xinafoate in DMSO- d_6 .

- G.** 1-[4-Hydroxy-3-[[[2-hydroxy-2-[4-hydroxy-3-(hydroxymethyl)-phenyl]ethyl][6-(4-phenylbutoxy)hexyl]amino]methyl]phenyl]-2-[[6-(4-phenylbutoxy)hexyl]amino]ethanol.

4.1.2 United States Pharmacopoeia Methods [33]

Definition

Salmeterol xinafoate contains not less than 98.0% and not more than 102.0% of $C_{25}H_{37}NO_4 \cdot C_{11}H_8O_3$, calculated on the water and solvent-free basis.

Identification

- A.** IR absorption.
B. The retention time of the major peak from the sample solution corresponds to that from the standard solution, as obtained in assay.

Assay

Procedures

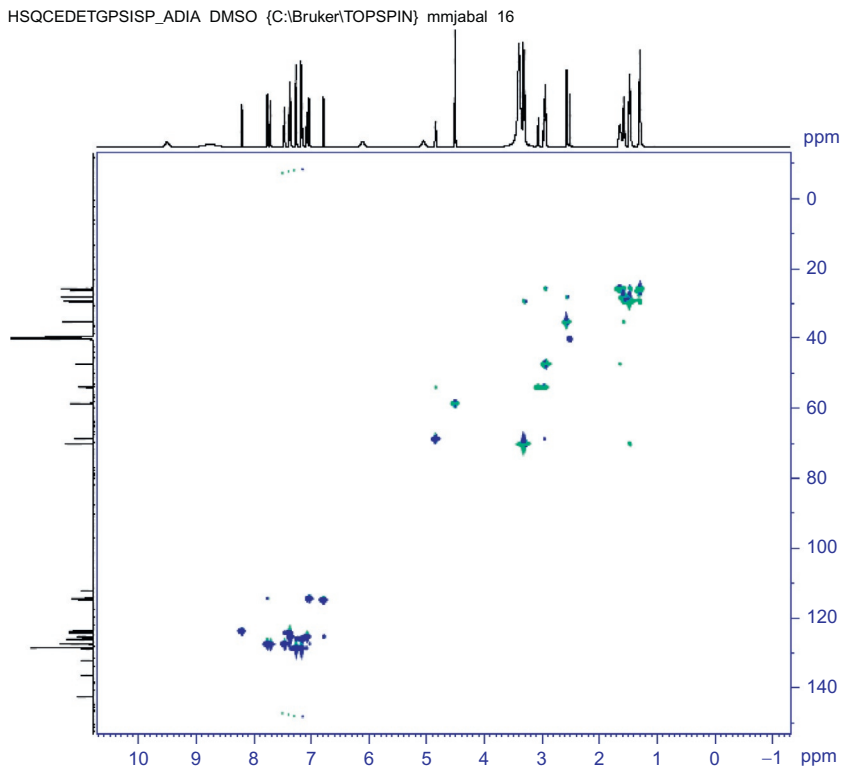


Figure 19 The HSQC spectrum of salmeterol xinafoate in DMSO- d_6 .

Solution A: 0.1 M sodium dodecyl sulfate

Solution B: 0.1 M ammonium acetate

Mobile phase: acetonitrile, Solution A, and Solution B (13:6:6).
Adjust with glacial acetic acid to a pH of 3.8.

System suitability solution: 0.25 mg/mL of USP salmeterol xinafoate RS and 0.017 mg/mL of USP salmeterol-related compound B RS in mobile phase, prepared by diluting system suitability solution 1 in the test for organic impurities.

Standard solution: 0.25 mg/mL of USP salmeterol xinafoate RS in mobile phase.

Sample solution: 0.25 mg/mL of salmeterol xinafoate in mobile phase.

Chromatographic system

Mode: LC

Detector: UV 278 nm

Column: 4.6 mm \times 15 cm; packing L1

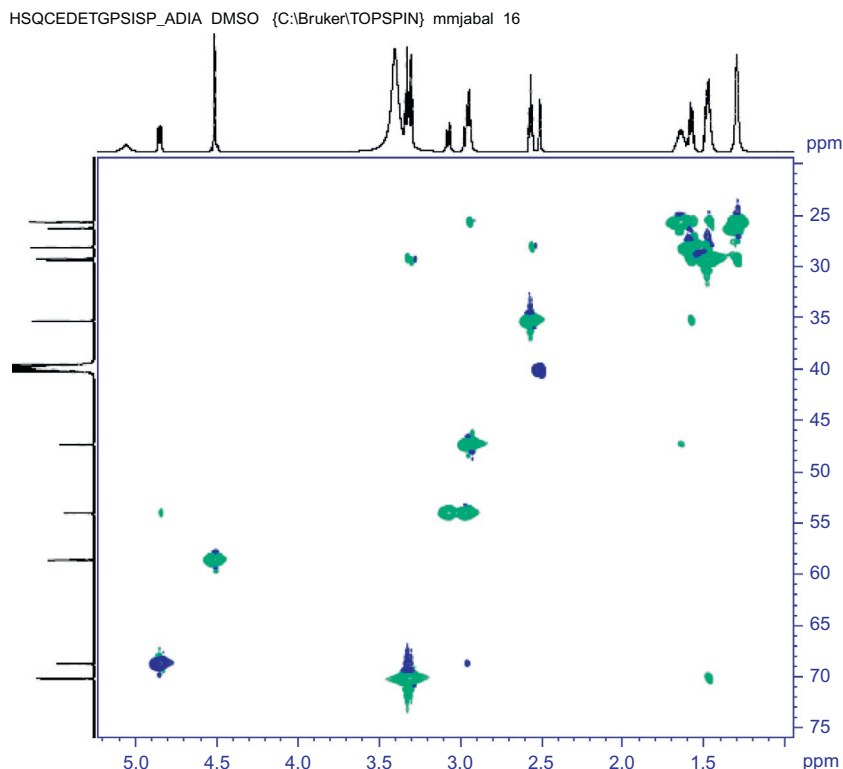


Figure 20 Expanded HSQC spectrum of salmeterol xinafoate in DMSO- d_6 .

Flow rate: 2 mL/min

Injection size: 20 μ L

System suitability

Sample: System suitability solution

Suitability requirements

Resolution: not less than 1.0 between salmeterol- and salmeterol-related compound B.

Relative standard deviation: not less than 2.0% for salmeterol.

Analysis

Sample: standard solution and sample solution.

Calculate the percentage of $C_{25}H_{37}NO_4 \cdot C_{11}H_8O_3$ in the portion of salmeterol xinafoate taken

Results = $(rU/rS) \times (CS/CU) \times 100$

rU = peak response from the sample solution

rS = peak response from the standard solution

HSQCEDETGPSISP_ADIA DMSO {C:\Bruker\TOPSPIN} mmjabal 16

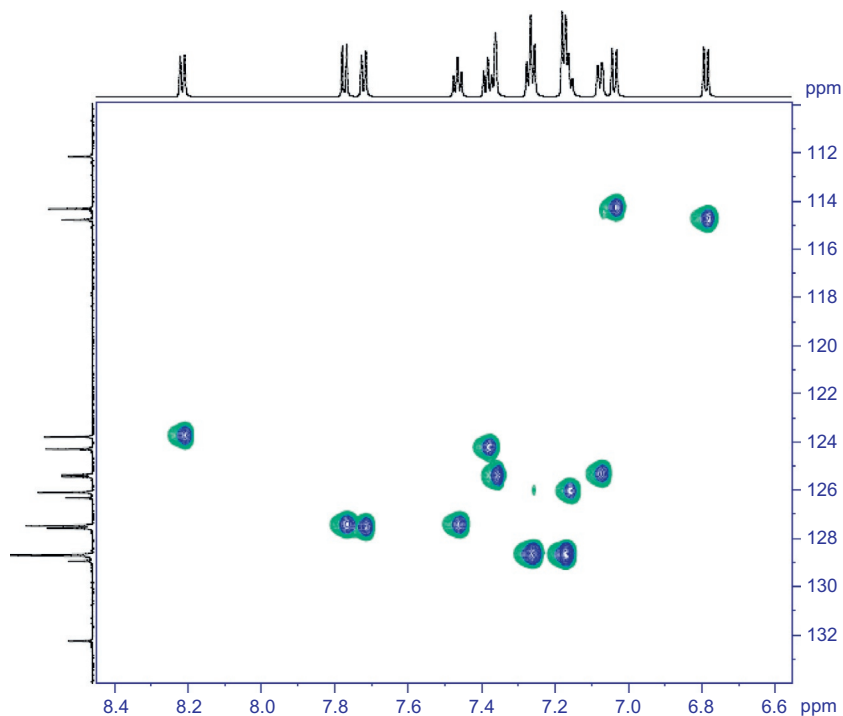


Figure 21 Expanded HSQC spectrum of salmeterol xinafoate in DMSO- d_6 .

CS = concentration of USP salmeterol xinafoate *RS* in the standard solution (mg/mL)

CU = concentration of salmeterol xinafoate in the sample solution (mg/mL)

Acceptance criteria: 98.0–102.0% on the water and solvent-free basis.

4.2 Reported Methods

4.2.1 Spectrophotometric Methods

4.2.1.1 Ultraviolet Spectrometry

Shah *et al.* [34] reported the ultraviolet spectrophotometric method for simultaneous estimation of salmeterol xinafoate and fluticasone propionate in bulk and dosage using UV–visible double beam spectrophotometer, Make: JASCO spectrophotometer, model V-550 with a pair of 10 mm matched quartz cells. The absorption spectra of reference and test solution were carried out in a 1-cm quartz cell over the range of 200–400 nm. 20 capsules of marketed formulation of salmeterol xinafoate and fluticasone propionate

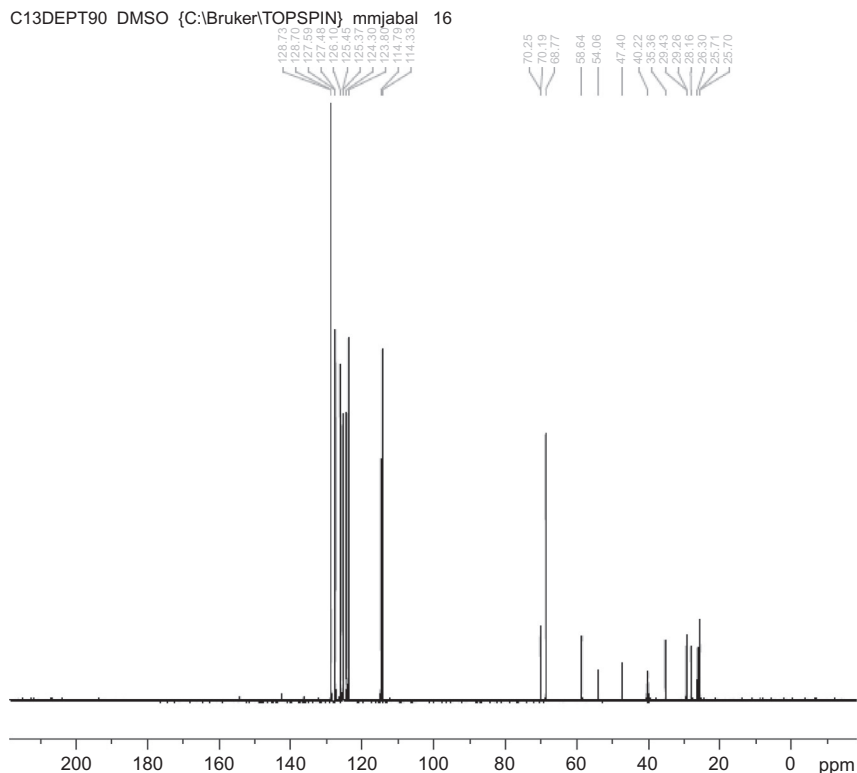


Figure 22 The DEPT 90 ^{13}C NMR spectrum of salmeterol xinafoate in $\text{DMSO}-d_6$.

corresponding to 50 and 100 μg , respectively, were weighed; their average weights determined. The correct amount of drug powder equivalent to label claim was weighed and transferred to 10 mL volumetric flask, dissolved in phosphate buffer pH 7.4: ethanol (90:10) and sonicated for 15 min. The volume was then made up to the mark using same solvent. The resultant solution was filtered through 0.45 μm membrane filter. The filtrate was having concentration 5 $\mu\text{g}/\text{mL}$ for salmeterol xinafoate and 10 $\mu\text{g}/\text{mL}$ for fluticasone propionate. Absorbance of these sample solutions was recorded at 214 nm (λ_{max} of salmeterol xinafoate) and 246 nm (λ_{max} of fluticasone propionate) and concentrations of two drugs in the sample were determined by using simultaneous equations [35].

Abdelkawy *et al.* [36] reported a new developed spectrophotometric method for simultaneous determination of salmeterol xinafoate and fluticasone propionate in bulk powder and inhalation dosage forms using UV-visible spectrophotometer, Shimadzu UV-1800, connected to an

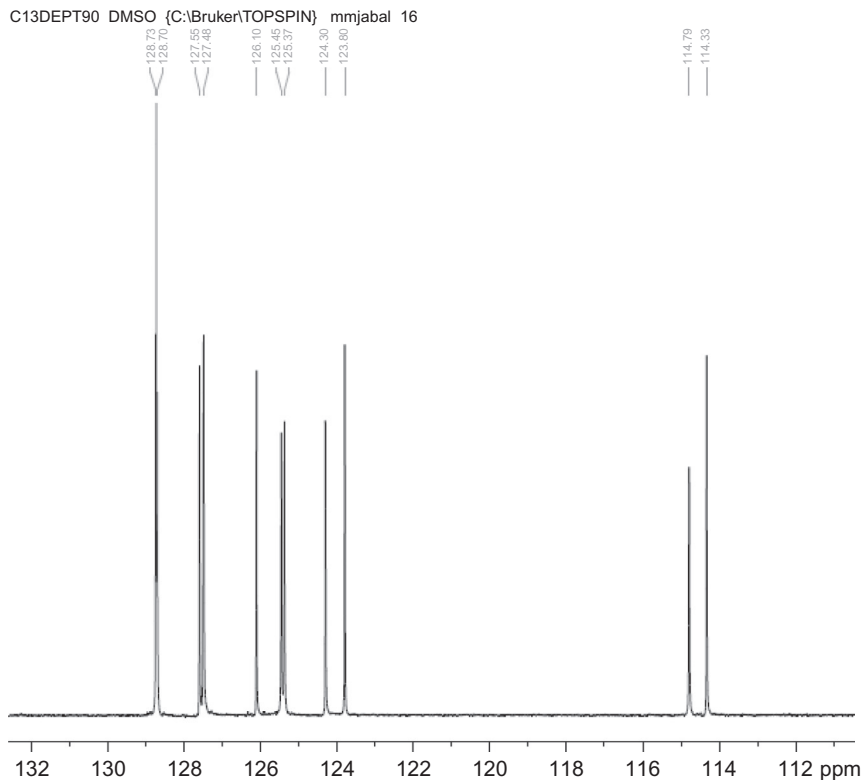


Figure 23 Expanded DEPT 90 ^{13}C NMR spectrum of salmeterol xinafoate in $\text{DMSO}-d_6$.

IBM compatible computer. The software was UVPC personal spectroscopy software version 3.7 (Shimadzu). The absorption spectra of the reference and test solutions were carried out in 1 cm quartz cells. Stock standard solutions of salmeterol xinafoate and fluticasone propionate were prepared separately by dissolving 40 mg of each drug in methanol and completing the volume to 100 mL using the same solvent. Working stock solutions were prepared by diluting 20 mL of each stock solution to 100 mL in a volumetric flask using the same solvent to get working solutions containing 80 $\mu\text{g}/\text{mL}$ of salmeterol xinafoate or fluticasone propionate. Series of concentration of each drug is prepared by diluting these working solutions in a series of 10 mL volumetric flasks to obtain a concentration range of 4–60 $\mu\text{g}/\text{mL}$ for salmeterol xinafoate and 4–28 $\mu\text{g}/\text{mL}$ for fluticasone propionate. From the first derivative spectra of the laboratory prepared mixtures, the concentration of salmeterol xinafoate obtained

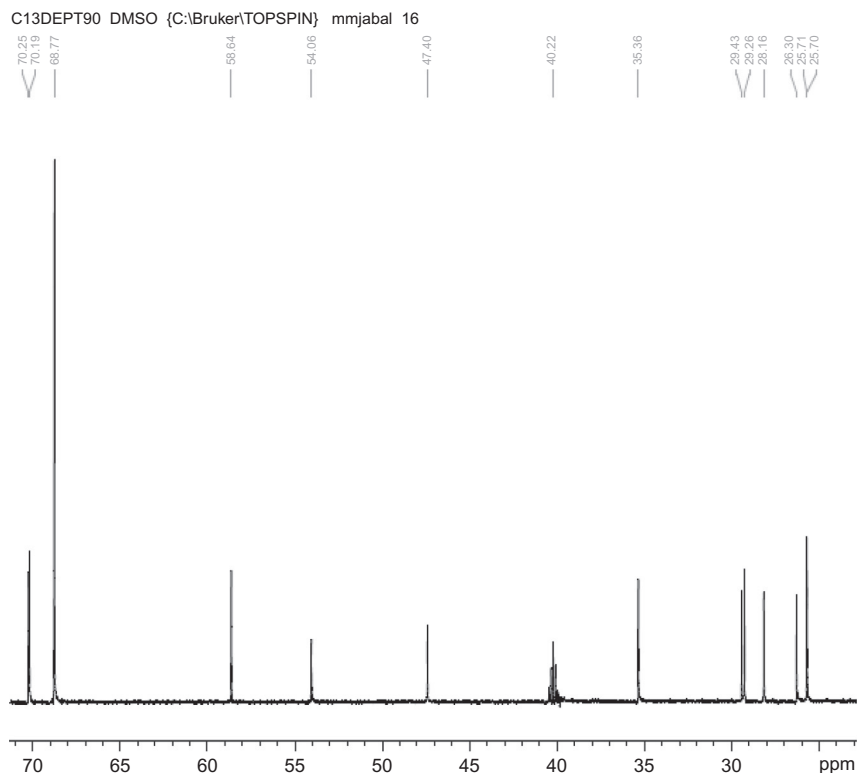


Figure 24 Expanded DEPT 90 ^{13}C NMR spectrum of salmeterol xinafoate in $\text{DMSO}-d_6$.

at 352 nm by substituting in regression equation, the corresponding concentration of fluticasone propionate is obtained by subtracting the concentration of salmeterol xinafoate from the results obtained by substitution in regression equations at absorptivity factor points (225 and 256.5 nm) then multiplying by two.

4.2.2 Chromatographic Methods

4.2.2.1 Thin Liquid Chromatography

Mohamed *et al.* [37] reported a high-performance thin layer chromatography (HPTLC)-densitometric method for simultaneous determination of salmeterol xinafoate and fluticasone propionate in dry-powder inhalers using precoated silica gel 60 F-254 glass plates (10 × 10 cm with 200 mL, thickness HPTLC; Merck, Germany). The sample solution and 10 different concentration levels of working standard solutions were freshly prepared by diluting suitable volumes of the stock sample solution and the stock standard

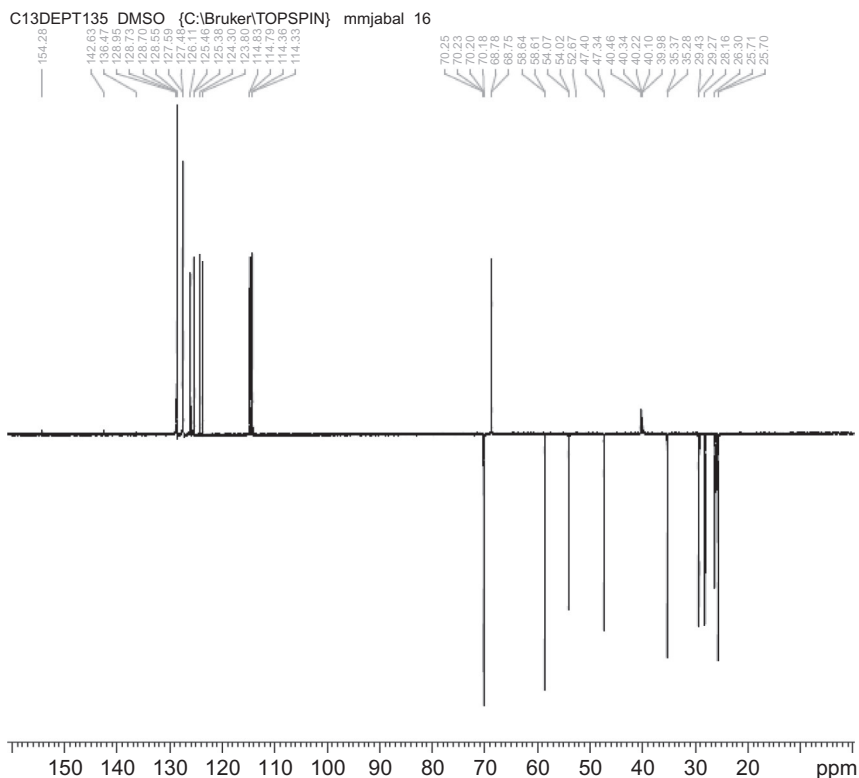


Figure 25 The DEPT 135 ^{13}C NMR spectrum of salmeterol xinafoate in $\text{DMSO}-d_6$.

solution to 25 mL with methanol in appropriate volumetric flasks. The sample was applied to the plate 10 mm from the bottom and 10 mm from the side edges in the form of band or streak with band length of 6 mm. The mobile phase consisted of *n*-hexane:ethyl acetate:acetic acid (5:10:0.2, v/v/v) and 15 mL of the mobile phase was used in each chromatographic run. Ascending development technique was carried out in a twin trough chamber. The optimized chamber saturation time for the mobile phase was 25 min at room temperature ($20 \pm 2^\circ\text{C}$) that was assisted by saturation pad. The distance covered by the solvent front was 8 cm, which took about 15 min. The spots were scanned using the TLC scanner 3 in the reflectance/absorbance mode at 250 nm and all measurements were operated by winCATS software. Concentrations of the separated compounds were determined from the intensity of reflected light and peak areas were used for comparison.

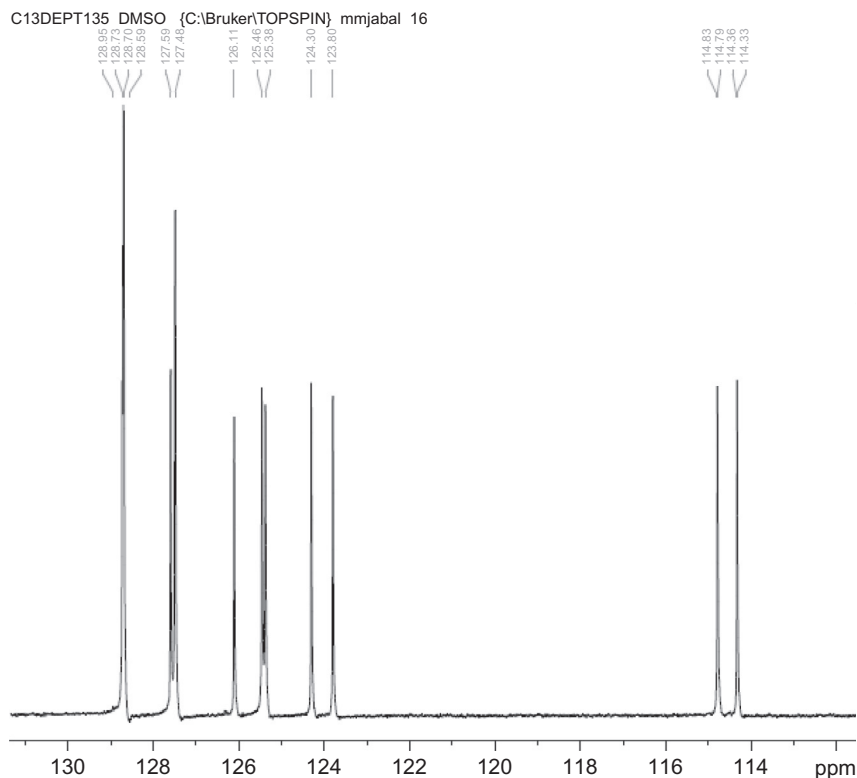


Figure 26 Expanded DEPT 135 ^{13}C NMR spectrum of salmeterol xinafoate in $\text{DMSO}-d_6$.

4.2.2.2 High-Performance Liquid Chromatography

Farhadi *et al.* [38] described a novel analytical method for the determination of salmeterol in dried blood spot using an ionic liquid-based dispersive liquid–liquid microextraction coupled with HPLC. Chromatographic quantification of salmeterol was carried out using a Knauer (Berlin, Germany) liquid chromatography, equipped with a smart line 1000 solvent pump unit, a Rheodyne 7725 injector of 20 μL loop volume (USA), and an Shimadzu RF 10AXL fluorescence detector (Kyoto, Japan) operating at excitation wave length of 230 nm and emission wave length of 340 nm. Separation was performed on a reversed-phase analytical column (C18, 5 μm , 250 \times 4.6 mm i.d.) and precolumn (Knauer, Germany). The temperature was maintained at 25 $^{\circ}\text{C}$ by a column-thermostat Jet-stream Knauer oven and Chromgate software was used for data acquisition and integration. The mobile phase was 50:50 (v/v) acetonitrile–ammonium acetate buffer (0.2%, pH 6). The flow rate was kept at 1 mL/min. A Hettich centrifuge (Model Universal 320 R) was used to accomplish DLLME procedure.

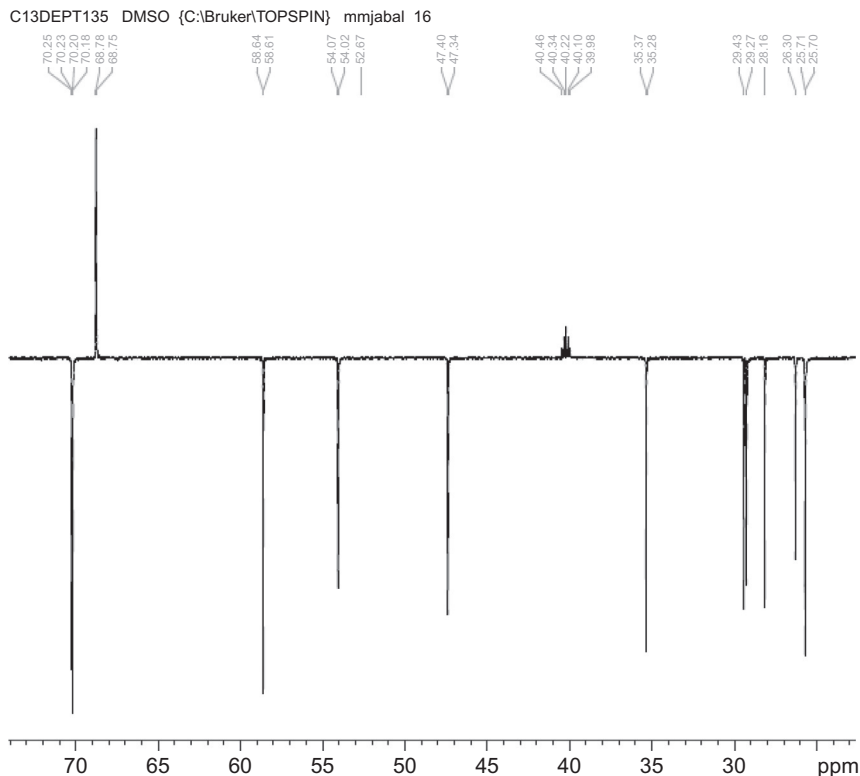
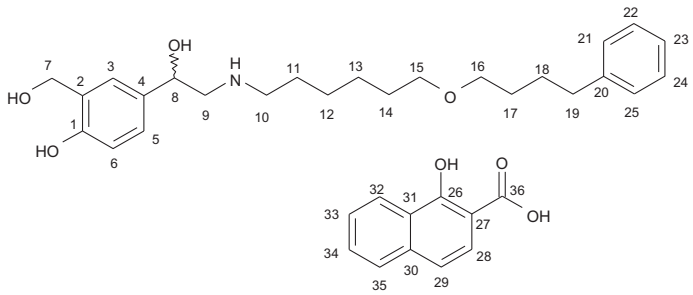


Figure 27 Expanded DEPT 135 ^{13}C NMR spectrum of salmeterol xinafoate in $\text{DMSO}-d_6$.

A standard stock solution of salmeterol (1 mg/mL) was prepared by dissolving 10 mg of salmeterol in 10 mL methanol. Salmeterol working solutions for spiked blood spots were prepared freshly as follows: the stock solution was diluted with distilled water to produce different working solutions of 10,000, 1000, and 100 ng/mL. Spiked blood standards were prepared by spiking different samples of fresh blood (200 μL) with appropriate amount of one of the above-mentioned working solutions to yield final blood salmeterol for calibration concentrations (500, 200, 100, 50, 20, 10, 5, 2, and 1 ng/mL). A blank blood sample was prepared by spiking with 10 μL of distilled water.

A stock solution of the internal standard, salmeterol (1 mg/mL), was prepared in methanol and working solution of internal standard was prepared by diluting stock solution in distilled water to produce a 1 $\mu\text{g/mL}$ concentration.

The venous blood samples (1 mL) were drawn between 8.00 and 10.00 a. m. from healthy volunteers and asthma patients treated with salmeterol and

Table 4 Assignment for the Resonance Bands in the ^{13}C NMR Spectrum of Salmeterol Xinafoate


Chemical Shift (ppm Relative to TMS)	Assignment (Carbon Number)	Chemical Shift (ppm Relative to TMS)	Assignment (Carbon Number)
25.7	12/13	124.3	33
26.3	14	125.4	5
28.2	17	125.5	3
29.3	18	126.1	23
29.4	11	126.3	31
35.4	19	127.5	34/35
47.4	10	127.6	28
54.1	9	128.7	22/24 and 21/25
58.6	7	129	2
68.8	8	132.3	4
70.2	15	136.5	30
70.3	16	142.6	20
112.2	27	154.3	1
114.3	29	162.8	26
114.8	6	173.2	36
123.8	32		

put into test tubes containing citrate as anticoagulant. Before spotting, spiked bloods were kept at room temperature for 20 min to allow for the equilibration of salmeterol in the sample. Ten microliters of spiked or real whole blood were spotted on a filter paper using a volumetric micropipette. The samples were allowed to dry at room temperature in the dark for at least 4 h and

¹³ C			DEPT ^b		
No.	(δ _C)	¹ H(δ _H) ^a	135	COSY	HMBC
1	154.3	—	0	—	H-3(³ <i>J</i>), H-5(³ <i>J</i>), H-6(² <i>J</i>), H-7(³ <i>J</i>)
2	129	—	0	—	H-3(² <i>J</i>), H-6(³ <i>J</i>), H-7(² <i>J</i>)
3	125.5	7.36 (1 <i>H</i> , s)	1	—	H-5(³ <i>J</i>), H-7(³ <i>J</i>), H-8(³ <i>J</i>)
4	132.3	—	0	—	H-6(³ <i>J</i>), H-8(² <i>J</i>)
5	125.4	7.08 (1 <i>H</i> , d, <i>J</i> =8.4)	1	H-6	H-3(³ <i>J</i>)
6	114.8	6.79 (2 <i>H</i> , d, <i>J</i> =8.4)	1	H-5	—
7	58.6	4.51 (2 <i>H</i> , s)	2	—	H-3(³ <i>J</i>)
8	68.8	4.79 (1 <i>H</i> , dd, <i>J</i> =10.5; <i>J</i> =2.1)	1	H-9	H-3(³ <i>J</i>), H-5(³ <i>J</i>), H-9(² <i>J</i>)
9a	54.1	2.97 (1 <i>H</i> , dd, <i>J</i> =7.7; <i>J</i> =12.6)	2	H-10, H-8	H-8(² <i>J</i>), H-10(³ <i>J</i>)
9b		3.08 (1 <i>H</i> , dd, <i>J</i> =2.1; <i>J</i> =12.6)			
10	47.4	2.95 (2 <i>H</i> , m)	2	H-11, H-9	H-9(³ <i>J</i>), H-11(² <i>J</i>), H-12(³ <i>J</i>)
11	29.4	1.56–1.66 (2 <i>H</i> , m)	2	H-10, H-12	H-12(² <i>J</i>)
12	25.7	1.29–1.30 (2 <i>H</i> , m)	2	H-11	H-10(³ <i>J</i>), H-13(² <i>J</i>)
13	25.7	1.29–1.30 (2 <i>H</i> , m)	2	H-14	H-12(² <i>J</i>), H-15(³ <i>J</i>)
14	26.3	1.46–1.50 (2 <i>H</i> , m)	2	H-13, H-15	H-13(² <i>J</i>), H-15(² <i>J</i>)
15	70.2	3.30–3.34 (2 <i>H</i> , m)	2	H-14	H-13(³ <i>J</i>), H-14(² <i>J</i>), H-16(³ <i>J</i>)

Continued

Table 5 NMR Correlation of Salmeterol Xinafoate—cont'd

No.	¹³ C		DEPT	COSY	HMBC
	(δ_C)	¹ H(δ_H)	135		
16	70.3	3.30–3.34 (2H, m)	2	H-17	H-15(³ J), H-17(² J), H-18(³ J)
17	28.2	1.46–1.50 (2H, m)	2	H-18, H-16	H-16(² J), H-18(² J)
18	29.3	1.56–1.66 (2H, m)	2	H-17, H-19	H-16(³ J), H-17(² J), H-19(² J)
19	35.4	2.57 (2H, t, $J=7.7$)	2	H-18	H-17(³ J), H-18(² J)
20	142.6	–	0	–	H-18(³ J), H-19(² J), H-22(³ J), H-24(³ J)
21	128.7	7.27 (1H, t, $J=7.7$)	1	–	H-19(³ J), H-22(² J)
22	128.7	7.15–7.18 (1H, m)	1	–	H-21(² J)
23	126.1	7.15–7.18 (1H, m)	1	–	H-21(³ J), H-22(² J), H-24(² J), H-25(³ J)
24	128.7	7.15–7.18 (1H, m)	1	–	H-25(² J)
25	128.7	7.27 (1H, t, $J=7.7$)	1	–	H-19(³ J), H-24(² J)
26	162.8	–	0	–	H-28(³ J), H-32(³ J)
27	112.2	–	0	–	H-29(³ J)
28	127.6	7.77 (1H, d, $J=8.4$)	1	H-29	H-29(² J)
29	114.3	7.04 (1H, d, $J=8.4$)	1	H-28	H-28(³ J), H-35(³ J)
30	136.5	–	0	–	H-28(³ J), H-29(² J), H-32(³ J), H-34(³ J), H-35(² J)
31	126.3	–	0	–	H-29(³ J), H-32(² J), H-33(³ J), H-35(³ J)
32	123.8	8.21 (1H, d, $J=7.7$)	1	H-33	H-34(³ J)
33	124.3	7.38 (1H, t, $J=7.7$)	1	H-32	H-34(² J), H-35(³ J)
34	127.5	7.47 (1H, t, $J=7.7$)	1	H-35	H-32(³ J), H-33(² J), H-35(² J)
35	127.5	7.72 (1H, d, $J=8.4$)	1	H-34	H-33(³ J)
36	173.2	–	0	–	H-28(³ J)

^a δ ppm in DMSO-*d*₆, J in Hz, 175 MHz for ¹³C, 700 MHz for ¹H.^bDEPT is the number of attached protons.

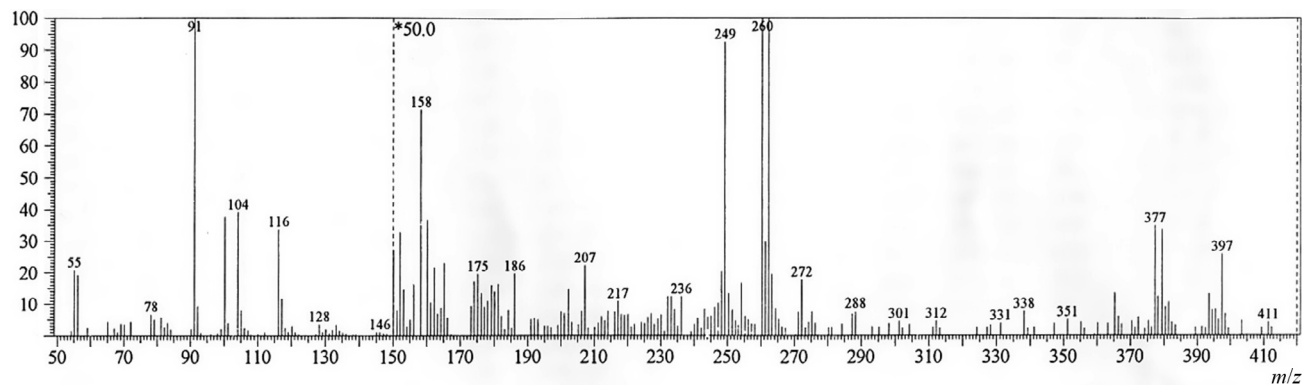
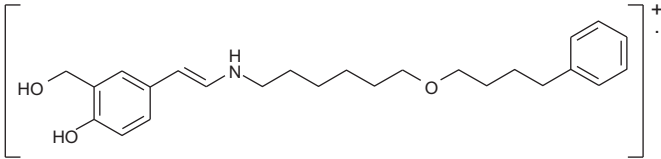
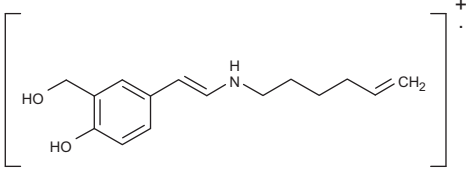
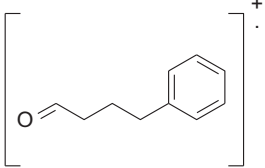
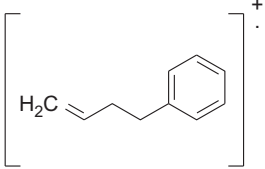


Figure 28 Mass spectrum of salmeterol xinafoate.

Table 6 Mass Fragmentation of Salmeterol Xinafoate

<i>m/z</i>	Relative Intensity (%)	Fragment	
		Formula	Structure
397	0.5	C ₂₅ H ₃₅ NO ₃	
249	2	C ₁₅ H ₂₁ NO ₂	
148	0.5	C ₁₀ H ₁₂ O	
132	2	C ₁₀ H ₁₂	

121	1	$\text{C}_8\text{H}_{11}\text{N}$	$\left[\text{C}_6\text{H}_5\text{CH}_2\text{CH}_2\text{NH}_2 \right]^+$
104	39	C_8H_8	$\left[\text{H}_2\text{C}=\text{CH}-\text{C}_6\text{H}_5 \right]^+$
91	100	C_7H_7	$\left[\text{H}_2\text{C}-\text{C}_6\text{H}_5 \right]^+$
78	7	C_6H_6	$\left[\text{C}_6\text{H}_6 \right]^+$

packed in a zip lock pouches, which were stored in laboratory cupboard until analysis. Salmeterol had been inhaled by the patient as two puffs daily, each puff separated by 1 min via metered-dose inhaler (MDI).

Extraction procedure of DBS samples is as follows: a 5-mm disk was punched out from the center of the DBS sample and transferred to a microcentrifuge tube. A 500- μ L volume of extraction solvent consisting of methanol (disperser) and 54 μ L ionic liquid plus internal standard (20 ng/mL) was added to microtube. Sample tubes were then sonicated for 10 min and were centrifuged for 5 min at 3000 rpm. The microtube content was withdrawn into a 2-mL syringe and rapidly injected in 1 mL salinated (10% NaCl) and alkalized (pH 12) water. A cloudy solution that consists of very fine droplets of ionic liquid dispersed into aqueous sample was formed, and the analyte was extracted into the fine droplets. After centrifugation for 5 min at 3000 rpm, the dispersed fine ionic liquid droplets were settled to the bottom of the test tube. Twenty microliters of sedimented phase was removed using a 50- μ L HPLC microsyringe and injected into the HPLC system for analysis.

4.2.2.3 Reversed-Phase High-Performance Liquid Chromatography

Nayak *et al.* [39] reported the determination of salmeterol in metered-dose and dry-powder inhalers by reversed-phase high-performance liquid chromatography. A liquid chromatograph (TOSOH Corporation, Japan) consisting of a CCPE dual-piston reciprocating pump, a UV-8011 UV-visible detector and a Rheodyne injector fitted with a 20- μ L loop were used. The column used was a 150 mm \times 4.6 mm i.d. column packed with 5 μ m C18 TSK GEL from TOSOH. Detection was at 225 nm. Data acquisition were accomplished by using an integrator, Chromatocorder from TOSOH.

Analytical reagent grade triethylamine, orthophosphoric acid (85%, w/w), HPLC grade acetonitrile, methanol (E. Merck India Ltd., Bombay, India), and distilled water prepared in the laboratory were used to prepare the mobile phase consisting of methanol-acetonitrile-water-diethylamine-orthophosphoric acid (85%) 55:10:35:0.1:0.1 (v/v/v/v/v). A flow rate of 1.0 mL/min was used.

Determination of salmeterol MDI; 40 sprays of salmeterol were actuated into a 250-mL beaker containing 80 mL of methanol by immersing a canister together with its adaptor body in the solution. Two appropriate washings (5 mL each) with methanol were applied to the adaptor body collected in the same solution. The contents were then warmed at 50 °C for 10 min to

expel propellents from the solution. The resulting solution was cooled to ambient temperature and diluted to 100 mL with methanol. The canister was shaken after actuation of every five sprays to achieve uniform delivery of the drug into the solution. Each actuation of canister delivered 25 µg of salmeterol equivalent to salmeterol hydroxynaphthoate.

Determination of salmeterol dry-powder inhaler; 20 capsules of salmeterol were actuated into a 250-mL beaker containing 50 mL of methanol with the aid of a Rotahaler device by immersing in the solution. Two appropriate washings (5 mL each) with methanol were applied the device collected in the same solution. The contents were then sonicated for 10 min. The resulting solution was filtered through a Whatman No. 42 filter and diluted to 100 mL with methanol. Each actuation delivered 25 µg of salmeterol equivalent to salmeterol hydroxynaphthoate.

Martin *et al.* [40] described the validation of a reversed-phase high-performance liquid chromatographic method for concurrent assay of salmeterol xinafoate as a weak base and fluticasone propionate using a HP 1050 modular liquid chromatography system for the analysis. The variable wavelength detector of the system was interfaced to a HP Chemstation for data acquisition using a HP 35900C multichannel interface (Agilent Technologies UK Ltd., Wokingham, UK). Integration was carried out using the HP Chemstation LC data analysis module enhanced integrator (revision A.07.01). Separation was achieved using an Inertsil ODS2 column (5 µm, 200 mm × 4.6 mm) (Capital HPLC Ltd., Broxburn, UK), maintained at 40 °C using a column block heater (Jones Chromatography Ltd., Pontypridd, UK). The mobile phase was a mixture of methanol–0.6% (w/v) aqueous ammonium acetate solution (75:25%, v/v), filtered through a 0.45-µm nylon membrane (Whatman International Ltd., Maidstone, UK) and degassed. The mobile phase flow rate was 1.0 mL/min. The injection volume was 20 µL and detection was at 228 nm. Data and statistical analysis were performed using Microsoft Excel and Minitab, respectively. The choice of 228 nm as the detection wavelength was determined by using a Dionex PDA 100 photodiode array detector, with Chromeleon Client Version 6.60 for analysis (Dionex Corporation, Sunnyvale, CA, USA) following injection of a standard solution of SX and FP.

Srinivasaro *et al.* [41] reported a simple, sensitive, rapid, and reproducible reversed-phase HPLC method, which has been developed and validated for estimation of salmeterol xinafoate in metered-dose inhalation form using Shimadzu HPLC system LC-2010 CHT consisting of UV/VIS detector and LC solutions software. Separation was carried out on Kromosil C18

(150 × 4.6 mm i.d.) column using Buffer pH 3.0: acetonitrile in ratio of (65:35, v/v) as mobile phase at flow rate of 2.0 mL/min and column oven temperature 30 °C. Samples were injected using auto injector with 100 µL loop and detection was carried out at 235 nm. All weighings were done on Shimadzu balance (Model AY-120). After setting the chromatographic conditions and stabilizing the instrument to obtain a steady baseline, the metered-dose sample solution A and actuator retention B solution was injected, chromatogram was obtained and the peak areas were recorded. The injections were repeated six times and the amount of each drug present per inhalation was estimated from the respective calibration curves.

$$\begin{aligned} &\text{Content of Active Ingredient Delivered per Actuation} \\ &= \mu\text{g of Sample A} - \mu\text{g of Sample B} \end{aligned}$$

$$\begin{aligned} &\% \text{ Labeled Amount of Active Ingredient Delivered per Actuation} \\ &= \frac{[\mu\text{g of Sample A} - \mu\text{g of Sample B}] \times 100}{\text{Label Claim}} \end{aligned}$$



5. STABILITY

Storage

Oral Inhalation

Powder

Salmeterol Serevent Diskus alone or in fixed combination with fluticasone Advair Diskus: 20–25 °C in a dry place away from direct heat and sunlight [42–44].

Discard Serevent Diskus 6 weeks after removal from foil pouch or when every blister used (when the dose counter reads “0”), whichever comes first [42].

Discard Advair Diskus 1 month after removal from foil pouch or when every blister used, whichever comes first [45,46].

Aerosol

Fixed combination with fluticasone: 25 °C (may be exposed to 15–30 °C) with mouthpiece down [47,48].

Contents under pressure; do not puncture, use or store near heat or open flame, or place into fire or incinerator [47,48]. Exposure to temperatures >49 °C may cause canister to burst [47].

Discard when dose counter reads “000” [47].



6. PHARMACOKINETICS, METABOLISM, AND EXCRETION

6.1 Pharmacokinetics

Absorption

Bioavailability

Most of an orally inhaled drug actually is swallowed [42,49–52]. Bronchodilating action of orally inhaled sympathomimetic agents is believed to result from a local action of the portion of the dose that reaches the bronchial tree [42,49–52].

Low or undetectable systemic concentrations occur after inhalation of the recommended dosage and are not predictive of therapeutic effects [42,49–52].

Onset

Time to onset of effective bronchodilation 60 min with salmeterol oral inhalation powder [42]. Initial improvement in asthma control may occur within 30 min following oral inhalation of salmeterol in fixed combination with fluticasone propionate. Maximum benefit may not be achieved for 1 week or longer after initiating treatment with salmeterol in fixed combination with fluticasone propionate [43,47].

Maximum improvement in forced expiratory volume in 1 s generally occurs within 3 h after administration of salmeterol oral inhalation powder [42].

Duration

Clinically important improvements are maintained for up to 12 h in most patients receiving salmeterol oral inhalation powder [42]. In the prevention of exercise-induced bronchospasm in adolescents and adults, salmeterol oral inhalation powder provides protection for up to 9 h and up to 12 h in children 4–11 years of age [42].

Distribution

Extent

Crosses the blood–brain barrier in trace amounts [51,53].

Not known whether the drug and/or its metabolites cross the placenta [54].

Distributed into milk in rats; it is not known whether is distributed into human milk [44].

Plasma Protein Binding
94–98% [3,54].

Elimination

Metabolism

Extensively metabolized in the liver by hydroxylation [46,49–51].

Elimination Route

Eliminated in feces (60%) and urine (25%), [42,49–51] principally as metabolites [42,49–51].

Half-life

About 5.5 h (oral administration) [3,42,49].

Special Populations

Pharmacokinetics not studied in patients with hepatic impairment; however, increased plasma concentrations may occur since drug is predominantly cleared by hepatic metabolism [42].

ACKNOWLEDGMENT

This research project was supported by a grant from the “Research Center of Female Scientific and Medical Colleges,” Deanship of Scientific Research, King Saud University.

REFERENCES

- [1] The Merck Index, Electronic copy, Monograph number 8416.
- [2] The British Pharmacopoeia, electronic copy, 2009, p. 8416.
- [3] R.N. Brogden, D. Faulds, Salmeterol xinafoate. A review of its pharmacological properties and therapeutic potential in reversible obstructive airways disease, *Drugs* 42 (5) (1991) 895–912.
- [4] D.I. Ball, R.T. Brittain, R.A. Coleman, L.H. Denyer, D. Jack, M. Johnson, L.H. Lunts, A.T. Nials, K.E. Sheldrick, I.F. Skidmore, Salmeterol, a novel, long-acting beta 2-adrenoceptor agonist: characterization of pharmacological activity in vitro and in vivo, *Br. J. Pharmacol.* 104 (3) (1991) 665–671.
- [5] M. Johnson, P.R. Butchers, R.A. Coleman, A.T. Nials, P. Strong, M.J. Sumner, C.J. Vardey, C.J. Whelan, The pharmacology of salmeterol, *Life Sci.* 52 (1993) 2131–2143.
- [6] A.T. Nials, R.A. Coleman, M. Johnson, C. Vardey, The β -adrenoceptor pharmacology of the enantiomers of salmeterol, *Am. J. Respir. Crit. Care Med.* 149 (4) (1994) A481.
- [7] M. Johnson, Beta2-adrenoceptors: mechanisms of action of beta2-agonists, *Paediatr. Respir. Rev.* 2 (2001) 57–62.
- [8] M. Johnson, The beta-adrenoceptor, *Am. J. Respir. Crit. Care Med.* 158 (1998) 146–153.
- [9] E. Roux, M. Molimard, J.P. Savineau, R. Marthan, Muscarinic stimulation of airway smooth muscle cells, *Gen. Pharmacol.* 31 (1998) 349–356.
- [10] S. Shrewsbury, S. Pyke, M. Britton, Meta-analysis of increased dose of inhaled steroid or addition of salmeterol in symptomatic asthma (MIASMA), *Br. Med. J.* 320 (2000) 1368–1373.

- [11] G. Boyd, A.H. Morice, J.C. Pounsford, M. Siebert, N. Peslis, C. Crawford, An evaluation of salmeterol in the treatment of chronic obstructive pulmonary disease (COPD), *Eur. Respir. J.* 10 (1997) 815–821.
- [12] N.A. Hanania, P. Darken, D. Horstman, The efficacy and safety of fluticasone propionate (250 microg)/salmeterol (50 microg) combined in the Diskus inhaler for the treatment of COPD, *Chest* 124 (2003) 834–843.
- [13] N. Svedmyr, C.G. Löfdahl, The use of beta 2-adrenoceptor agonists in the treatment of bronchial asthma, *Pharmacol. Toxicol.* 78 (1996) 3–11.
- [14] G. Shapiro, W. Lumry, J. Wolfe, Combined salmeterol 50 microg and fluticasone propionate 250 microg in the diskus device for the treatment of asthma, *Am. J. Respir. Crit. Care Med.* 161 (2000) 527–534.
- [15] A.P. Greening, P.W. Ind, M. Northfield, G. Shaw, Added salmeterol versus higher-dose corticosteroid in asthma patients with symptoms on existing inhaled corticosteroid. Allen & Hanburys Limited UK Study Group, *Lancet* 344 (1994) 219–224.
- [16] A. Woolcock, B. Lundback, N. Ringdal, L.A. Jacques, Comparison of addition of salmeterol to inhaled steroids with doubling of the dose of inhaled steroids, *Am. J. Respir. Crit. Care Med.* 153 (1996) 1481–1488.
- [17] J.J. Condemni, S. Goldstein, C. Kalberg, S. Yancey, A. Emmett, K. Rickard, The addition of salmeterol to fluticasone propionate versus increasing the dose of fluticasone propionate in patients with persistent asthma. Salmeterol Study Group, *Ann. Allergy Asthma Immunol.* 82 (1999) 383–389.
- [18] W. Busse, S.M. Koenig, J. Oppenheimer, Steroid-sparing effects of fluticasone propionate 100 microg and salmeterol 50 microg administered twice daily in a single product in patients previously controlled with fluticasone propionate 250 microg administered twice daily, *J. Allergy Clin. Immunol.* 111 (1) (2003) 57–85.
- [19] H.S. Nelson, W.W. Busse, E. Kerwin, Fluticasone propionate/salmeterol combination provides more effective asthma control than low-dose inhaled corticosteroid plus montelukast, *J. Allergy Clin. Immunol.* 106 (2000) 1088–1095.
- [20] N. Ringdal, A. Eliraz, R. Pruzinec, The salmeterol/fluticasone combination is more effective than fluticasone plus oral montelukast in asthma, *Respir. Med.* 97 (2003) 234–241.
- [21] B. Davies, G. Brooks, M. Devoy, The efficacy and safety of salmeterol compared to theophylline: meta-analysis of nine controlled studies, *Respir. Med.* 92 (1998) 256–263.
- [22] J. Goswami, R.L. Bezbaruah, A. Goswami, N. Borthakur, A convenient stereoselective synthesis of (R)-(–)-denopamine and (R)-(–)-salmeterol, *Tetrahedron Asymmetry* 2 (2001) 3343–3348.
- [23] R.N. Bream, S.V. Ley, P.A. Procopiou, Synthesis of the β_2 agonist (R)-salmeterol using a sequence of supported reagents and scavenging agents, *Org. Lett.* 4 (2002) 3793–3796.
- [24] (Polystyrylmethyl) trimethylammonium cyanoborohydride. Available from: Novabiochem, catalogue no. 01-64-0337.
- [25] SCX-2 (alkylsulfonic acid) cartridge. Available from: Jones Chromatography, catalogue no. 532-0100-C.
- [26] L. Juntao, Z. Di, J. Xian, H. Ling, L. Xingshu, S.C.C. Albert, A convenient synthesis of (R)-salmeterol via Rh-catalyzed asymmetric transfer hydrogenation, *Tetrahedron Asymmetry* 19 (2008) 1824–1828.
- [27] S. Hbaieb, Z. Latiri, H. Amri, Stereoselective synthesis of 2-ethylidene-3-aminonitriles, *Synth. Commun.* 29 (6) (1999) 981–988.
- [28] G.W. Gribble, Sodium borohydride in carboxylic acid media: a phenomenal reduction system, *Chem. Soc. Rev.* 27 (1998) 395–404.
- [29] Z. Guo, Y. Deng, S. Zhong, G. Lu, Enantioselective synthesis of (R)-salmeterol employing an asymmetric Henry reaction as the key step, *Tetrahedron Asymmetry* 22 (2011) 1395–1399.

- [30] J. Liu, D. Zhou, X. Jia, L. Huang, X. Li, A.S.C. Chan, Asymmetric transfer hydrogenation of ketones with a polyethylene glycol bound Ru catalyst in water, *Tetrahedron Asymmetry* 19 (2008) 832–837.
- [31] P.A. Procopiou, G.E. Morton, M. Todd, G. Webb, Enantioselective synthesis of (S)-salmeterol via asymmetric reduction of azidoketone by *Pichia angusta*, *Tetrahedron Asymmetry* 12 (2001) 2005–2008.
- [32] C.E. Clark, A.D. Ferguson, J.A. Siddorn, Respiratory arrests in young asthmatics on salmeterol, *Respir. Med.* 87 (3) (1993) 227–228.
- [33] The United States Pharmacopoeia, 35.
- [34] M.S. Kondawar, R.R. Shah, J.J. Waghmare, M.K. Malusare¹, N.D. Shah, UV spectrophotometric method for simultaneous estimation of Salmeterol xinafoate and Fluticasone propionate in bulk and dosage form, *Int. J. Pharm. Tech. Res.* 3 (2011) 1801–1806.
- [35] ICH topic Q-2B validation of analytical procedure: methodology (CPMP/ICH/281/95) the European agency for the evaluation of medicinal product, human medicines evaluation unit, 1996, pp. 1–9.
- [36] A. Samir, H. Salem, M. Abdelkawy, New developed spectrophotometric method for simultaneous determination of salmeterol xinafoate and fluticasone propionate in bulk powder and Seritide[®] diskus inhalation, *Bull. Fac. Pharm.* 50 (2012) 121–126, Cairo University.
- [37] L. Kasaye, A. Hymete, A.I. Mohamed, HPTLC–densitometric method for simultaneous determination of salmeterol xinafoate and fluticasone propionate in dry powder inhalers, *Saudi Pharm. J.* 18 (2010) 153–159.
- [38] M. Hatami, E. Karimnia, K. Farhadi, Determination of salmeterol in dried blood spot using an ionic liquid based dispersive liquid-liquid microextraction coupled with HPLC, *J. Pharm. Biomed. Anal.* 85 (2013) 283–287.
- [39] V.G. Nayak, S.G. Belapure, C.D. Gaitonde, A.A. Sule, Determination of salmeterol in metered-dose and dry-powder inhalers by reversed-phase high performance liquid chromatography, *J. Pharm. Biomed. Anal.* 14 (1996) 511–513.
- [40] D. Murnane, G.P. Martin, C. Marriott, Validation of a reverse-phase high performance liquid chromatographic method for concurrent assay of a weak base (salmeterol xinafoate) and a pharmacologically active steroid (fluticasone propionate), *J. Pharm. Biomed. Anal.* 40 (2006) 1149–1154.
- [41] K. Srinivasaro, V. Gorule, V.K. Akula, Development and validation for simultaneous estimation of Budesonide and Salmeterol Xinafoate in metered dose inhalation form by RP-HPLC, *Int. J. Pharm. Phytopharmacol. Res.* 1 (2012) 271–275.
- [42] GlaxoSmithKline. Serevent Diskus (salmeterol xinafoate) inhalation powder prescribing information. Research Triangle Park, NC, 2010 December.
- [43] GlaxoSmithKline. Advair Diskus (fluticasone propionate/salmeterol xinafoate) inhalation powder prescribing information. Research Triangle Park, NC, 2010 June.
- [44] GlaxoSmithKline. Serevent (salmeterol xinafoate inhalation powder) Diskus medication guide. Research Triangle Park; NC, 2010 December.
- [45] GlaxoSmithKline. Advair Diskus (fluticasone propionate and salmeterol) medication guide. Research Triangle Park, NC, 2011 January.
- [46] GlaxoSmithKline. Advair Diskus (fluticasone propionate/salmeterol xinafoate) inhalation powder patient instructions for use. Research Triangle Park, NC, undated.
- [47] GlaxoSmithKline. Advair HFA (fluticasone propionate and salmeterol) prescribing information. Research Triangle Park, NC, 2010 June.
- [48] GlaxoSmithKline. Advair HFA (fluticasone propionate and salmeterol) medication guide. Research Triangle Park, NC, 2011 January.
- [49] Glaxo Wellcome. Serevent (salmeterol xinafoate) inhalation aerosol prescribing information. Research Triangle Park, NC, 1999 November.

- [50] J.M. Meyer, C.L. Wenzel, W.A. Kradjan, Salmeterol: a novel, long-acting beta 2-agonist, *Ann. Pharmacother.* 27 (1993) 1478–1487.
- [51] G.R. Manchee, A. Barrow, S. Kulkarni, Disposition of salmeterol xinafoate in laboratory animals and humans, *Drug Metab. Dispos.* 21 (1993) 1022–1028.
- [52] D.S. Davies, Pharmacokinetics of inhaled substances, *Scand. J. Respir. Dis.* 103 (1979) 44–49.
- [53] M.F. Fitzpatrick, T. Mackay, H. Driver, N.J. Douglas, Salmeterol in nocturnal asthma: a double blind, placebo controlled trial of a long acting inhaled beta 2 agonist, *Br. Med. J.* 301 (1990) 1365–1368.
- [54] Allen & Hanburys, Research Triangle Park, NC, Personal communication.



Telmisartan

**Ahmed H.H. Bakheit^{*,1}, Ahmed A. Abd-Elgalil[†], Bakheit Mustafa[‡],
Anzarul Haque[§], Tanveer A. Wani^{*}**

^{*}Department of Pharmaceutical Chemistry, College of Pharmacy, King Saud University, P.O. Box 2457, Riyadh, Kingdom of Saudi Arabia

[†]Research Center, College of Pharmacy, King Saud University, P.O. Box 2457, Riyadh, Kingdom of Saudi Arabia

[‡]Chemistry Department, Faculty of Science and Technology, Al-Neelain University, Khartoum, Sudan

[§]Department of Phytochemistry and Pharmacognosy, College of Pharmacy, Salman bin Abdul Aziz University, Alkharj, Kingdom of Saudi Arabia

¹Corresponding author: e-mail addresses: abujazz76@gmail.com; abakheit@ksu.edu.sa

Contents

1. Description	372
1.1 Nomenclature	372
1.2 Formula	373
1.3 Elemental Analysis	373
1.4 Appearance	373
2. Uses and Applications	373
3. Methods of Preparation	373
4. Physical Characteristics	384
4.1 Ionization Constant	384
4.2 Solubility Characteristics	384
4.3 Optical Activity	385
4.4 Partition Coefficient	385
4.5 Particle Morphology	385
4.6 X-ray Powder Diffraction Pattern	385
4.7 Hygroscopicity	385
4.8 Thermal Methods of Analysis	385
4.9 Spectroscopy	387
4.10 Mass Spectrometry	389
5. Methods of Analysis	393
5.1 Compendial Methods of Analysis	393
5.2 Titrimetric Methods of Analysis	406
5.3 Electrochemical Methods of Analysis	406
5.4 Spectroscopic Methods of Analysis	410
5.5 Chromatographic Methods of Analysis	413
5.6 Determination in Body Fluids and Tissues	420
6. Stability	421
7. Pharmacology	422

7.1	Pharmacological Actions	422
7.2	Pharmacokinetics Parameters	422
7.3	Therapeutic Uses and Dosing	422
7.4	Adverse Effects and Precautions	423
7.5	Interactions	423
	Acknowledgments	424
	References	424



1. DESCRIPTION

1.1 Nomenclature

1.1.1 Systematic Chemical Names

4'-{[4-Methyl-6-(1-methyl-2-benzimidazolyl)-2-propyl-1-benzimidazolyl]methyl}-2-biphenylcarboxylic acid.

2-(4-{[4-Methyl-6-(1-methyl-1*H*-1,3-benzodiazol-2-yl)-2-propyl-1*H*-1,3-benzodiazol-1-yl]methyl}phenyl)benzoic acid.

4'-[[2-*n*-Propyl-4-methyl-6-(1-methylbenzimidazol-2-yl)benzimidazol-1-yl]methyl]biphenyl-2-carboxylic acid.

4'-[(1,7'-Dimethyl-2'-propyl[2,5'-bis-1*H*-benzimidazol]-3'-yl)methyl][1,1'-biphenyl]-2-carboxylic acid.

2-[4-Methyl-6-(1-methylbenzimidazol-2-yl)-2-propyl-benzimidazol-1-yl]methyl]phenyl] benzoic acid.

2-(4-{[4-Methyl-6-(1-methyl-1*H*-1,3-benzodiazol-2-yl)-2-propyl-1*H*-1,3-benzodiazol-1-yl]methyl}phenyl)benzoic acid.

4'-[[4-Methyl-6-(1-methyl-1*H*-benzimidazol-2-yl)-2-propyl-1*H*-benzimidazol-1-yl]methyl]biphenyl-2-carboxylic acid [1-7].

1.1.2 Nonproprietary Names

Generic: Telmisartan (BAN, USAN, rINN).

Synonyms: BIBR-277; BIBR-277-SE; Telmisartaani; Telmisartán; Telmisartanum [1,5].

1.1.3 Proprietary Names

Gliosartan[®]; Micardis[®]; Pritor[®]; Kinzalmono[®]; Samertan[®]; Telma[®]; Telpres[®]; Indon[®]; Combinations: Gliosartan Plus[®]; Micardis Plus[®] [1].

1.2 Formula

1.2.1 Empirical Formula, Molecular Weight, CAS Number

Empirical Formula	Molecular Weight	CAS Number [8]
$C_{33}H_{30}N_4O_2$	514.62	144701-48-4

1.2.2 Structural Formula

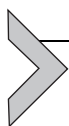
See [Figure 1](#).

1.3 Elemental Analysis

C: 77.02%, H: 5.88%, N: 10.89%, O: 6.22%.

1.4 Appearance

A white or slightly yellowish, odorless crystalline powder [7,10].



2. USES AND APPLICATIONS

Telmisartan is an angiotensin receptor blocker (ARB), it is used in the treatment of hypertension also effective in cardiovascular risk reduction.



3. METHODS OF PREPARATION

The first total synthesis of telmisartan was introduced by, Ries *et al.* [11] as shown in [Scheme 1](#), which starts with the acylation of the 4-amino-3-methylbenzoic acid methyl ester **2** with butyryl chloride, followed by nitration, to the nitro product reduction of the nitro group, and subsequent cyclization of the resulting amine **3** to the benzimidazole

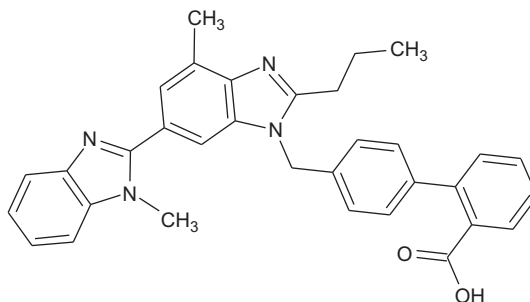
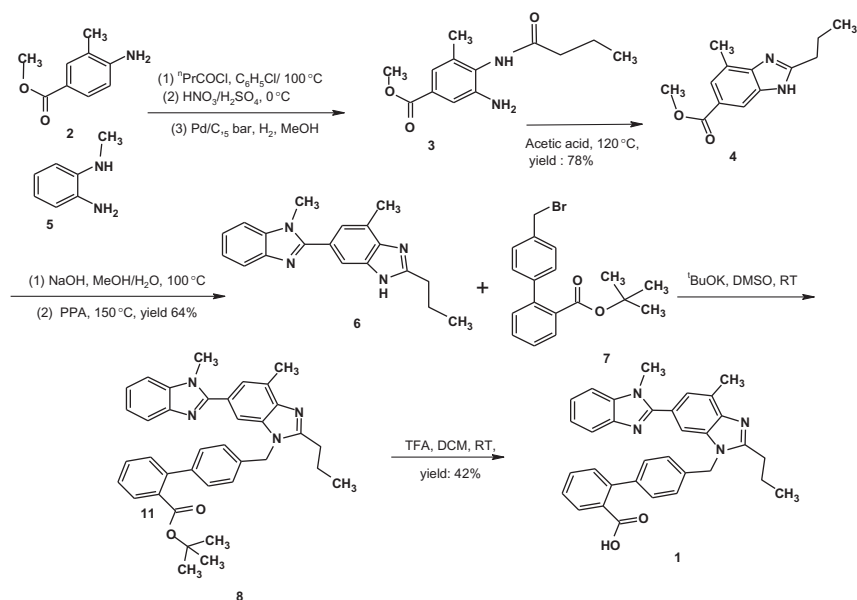


Figure 1 Structural formula of telmisartan **1** [9].

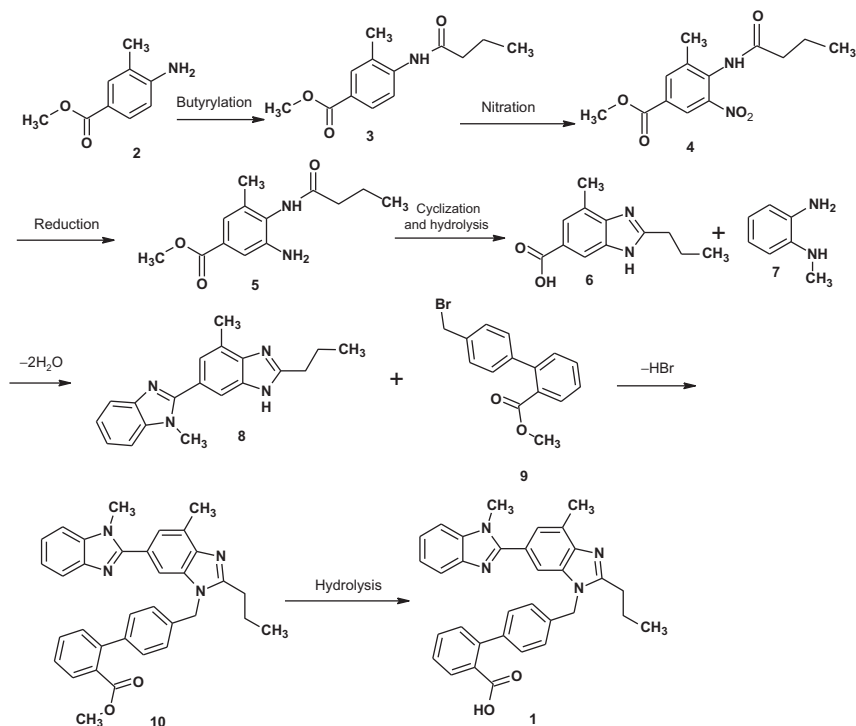


Scheme 1 Synthesis of telmisartan **1** [11].

derivative **4**. After its saponification, the free carboxyl group is condensed with *N*-methyl-1,2-phenylenediamine **5** to afford the bis-benzimidazole **6**, which is finally alkylated with the 4'-(bromomethyl)-2-biphenylcarboxylic acid *tert*-butyl ester **7** to give **8** from which telmisartan **1** was obtained after hydrolysis of the ester group of **8** in 21% overall.

Xia *et al.* [12] synthesized Telmisartan from methyl-4-amino-3-methyl benzoate **2** via butyrylation to give 4-butylamino-3-methyl-benzoic acid methyl ester **3**, follow by nitration of compound **3** to form 4-butylamino-3-methyl-5-nitro-benzoic acid methyl ester **4**, then it was reduced to give 3-amino-4-butylamino-3-methyl-benzoic acid methyl ester **5**, and subsequent cyclization and hydrolysis of the compound **5** to give 2-*n*-propyl-4-methyl-6-methoxycarbonyl benzimidazole **6**, which condensed with *N*-methyl-*O*-phenylenediamine **7** gives compound **8** (prepared in Scheme 1) which was condensed with 3-methyl 4' bromomethyl biphenyl-2-carboxylic acid methyl ester **9** to give compound **10**. From which Telmisartan **1** was obtained from hydrolysis of the ester **10** in (Scheme 2).

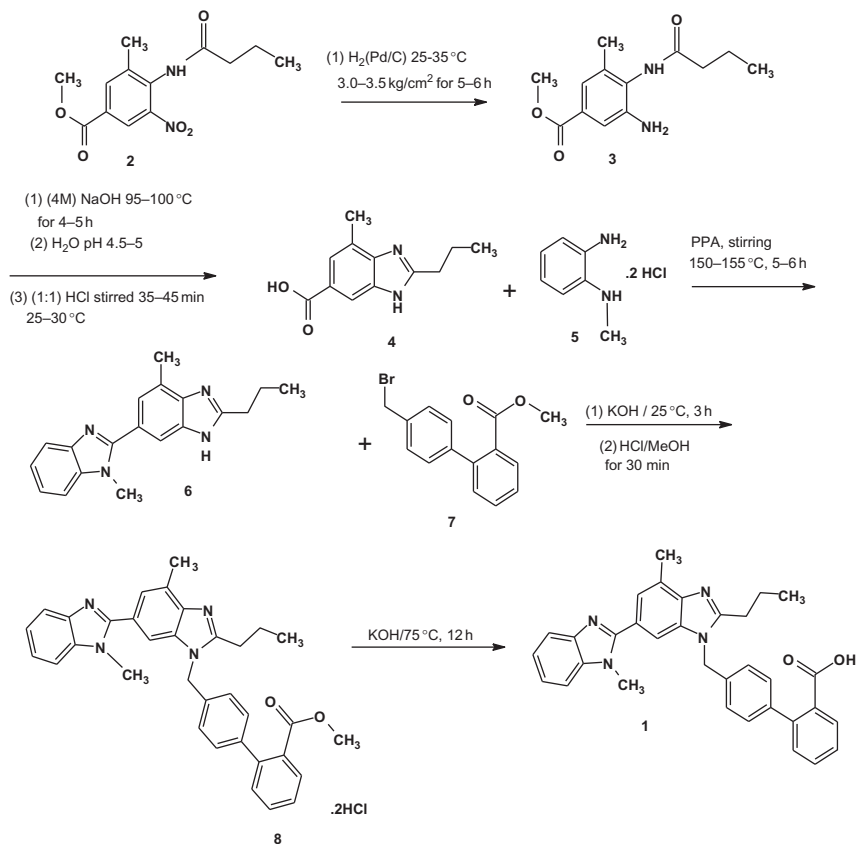
Venkataraman *et al.* [13] prepared Telmisartan **1** by reduction of methyl 4-butylamido-3-methyl-5-nitrobenzoate **2**, by hydrogenation, using palladium on charcoal in methanol, to form methyl 3-amino-4-butylamido-5-methylbenzoate **3**, subsequent hydrolysis of **3** followed



Scheme 2 Synthesis of telmisartan **1** [12].

by ring closure forms 2-*n*-propyl-4-methylbenzimidazole-6-carboxylic acid **4**. Condensation of **4** with *N*-methyl-*O*-phenylenediamine hydrochloride **5** to form 2-*n*-propyl-4-methyl-6-(1-methylbenzimidazole-2-yl) benzimidazole **6**; condensation of **6**, with methyl 4'-(bromomethyl) biphenyl-2-carboxylate **7** in the presence of a base to form methyl-4'-[(2-*n*-propyl-4-methyl-6-(1-methylbenzimidazol-2-yl)-benzimidazol-1-yl)-methyl]-biphenyl-2-carboxylate **8**. Hydrolysis of compound **8**, on treatment with a base form telmisartan **1** (Scheme 3).

Chava and Satyanarayana [14] prepared telmisartan **1** according to the following steps, 4-methyl-2-*n*-propyl-1*H*-benzimidazole-6-carboxylic acid **2** with *N*-methyl-*O*-phenylenediamine dihydrochloride **3** in the presence of polyphosphoric acid (PPA) followed by purification gives 4-methyl-6-(1-methylbenzimidazol-2-yl)-2-*n*-propyl 1*H*-benzimidazole **4** prepared in Scheme 1 which on condensation with 4'-(bromo methyl)-2-biphenyl carboxylate methyl ester **5** in the presence of base followed by acidification gives 4'-[4-methyl-6-(1-methyl-1*H*-benzimidazol-2-yl)-2-*n*-propyl-1*H*-benzimidazol-1-yl-methyl] biphenyl-2-carboxylate ester **6**,

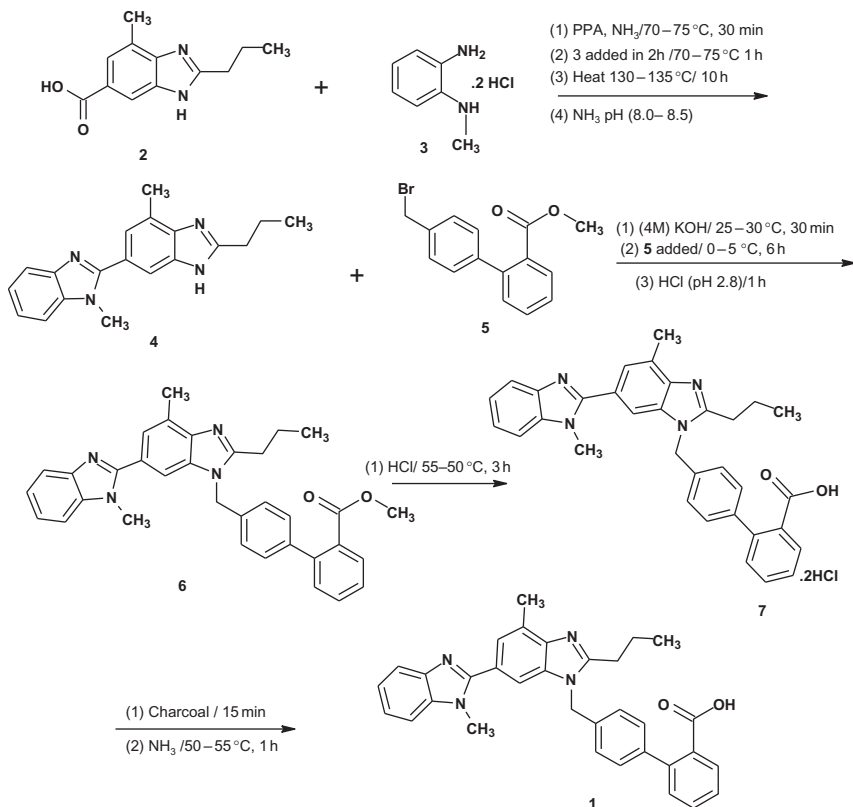


Scheme 3 Synthesis of telmisartan **1** [13].

which hydrolysis with hydrochloric acid gives the 4'-[4-methyl-6-(1-methyl-1*H*-benzimidazol-2-yl)-2-*n*-propyl-1*H*-benzimidazol-1-yl-methyl]biphenyl-2-carboxylic acid dihydrochloride salt (Telmisartan dihydrochloride) **7**. Telmisartan dihydrochloride on treatment with a base in the presence of suitable solvent gives the Telmisartan **1** (Scheme 4).

Goossen and Knauber [15] prepared telmisartan according to the following steps, potassium isopropylphthalate **3** prepared in one simple step from phthalic anhydride **2** by anhydride esterification with a potassium *tert*. butoxide.

Compound **5** was prepared by reaction of compound **3** with the dioxalane arylchloride **4** using a combination of Cu_2O and $\text{Pd}(\text{dba})_2$. Reduction of the nitro group of compound **6** followed by acylation with butyrylchloride and nitration afforded compound **7** in an excellent overall

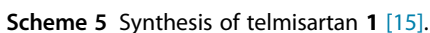


Scheme 4 Synthesis of telmisartan **1** [14].

yield of 87%. The carboxyl group of this compound was condensed with *N*-methyl-2-phenyldiamine **8** to give the benzimidazole derivative and its nitro group was smoothly reduced to afford the key intermediate **9**. Compounds **5** and **9** were coupled via a reductive amination reaction followed by cyclisation to construct the second benzimidazol ring.

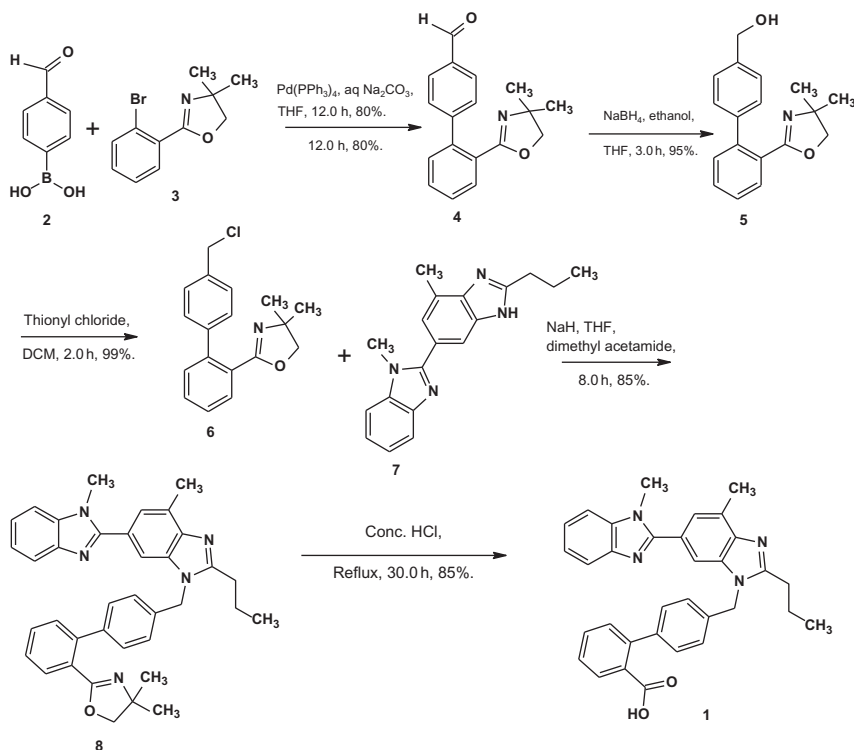
The resulting telmisartan isopropyl ester **10** was saponified and subsequent acidification led to precipitation of pure telmisartan **1** in 92% yields over the two final steps (Scheme 5).

Kumar *et al.* [16] developed an improved three-stage process employing Suzuki coupling [17,18] for the preparation of 2-[4'-(chloromethyl) biphenyl-2-yl]-4,4-dimethyl-4,5-dihydro-1,3-oxazolin **6**. Subsequent alkylation with dibenzimidazole derivative **7** [19,20] and acid hydrolysis of intermediate **8** provided Telmisartan **1** in good yield.



4-Formyl phenylboronic acid **2** and 2-(2-bromophenyl)-4,4-dimethyl-2-oxazoline **3** [21] identified as key starting materials for the preparation of key intermediate 2-[4'-(chloromethyl)biphenyl-2-yl]-4,4-dimethyl-4,5-dihydro-1,3-oxazoline **6**. Suzuki coupling was accomplished for the preparation of intermediate, 2'-(4,4-dimethyl-4,5-dihydro-1,3-oxazolin-1,3-yl)biphenyl-4-carbaldehyde **4** by reacting 2-(2-bromophenyl)-4,4-dimethyl-4,5-dihydro-1,3-oxazoline **3** with 4-formyl phenylboronic acid **2** in the presence of aqueous sodium carbonate and tetrakis(triphenyl)phosphine palladium (0) produced in 80% yield. Reduction of this intermediate with sodium borohydride furnished [2'-(4,4-dimethyl-4,5-dihydro-1,3-oxazolin-2-yl)biphenyl-4-yl]methanol **5** in 95% yield. Chlorination of intermediate **5** with thionyl chloride at low temperature afforded the key intermediate 2-[4'-(chloromethyl)biphenyl-2-yl]-4,4-dimethyl-4,5-dihydro-1,3-oxazoline **6** in 99% yield (Scheme 6).

Treatment of compounds **6** was coupled with **7** prepared in [Scheme 1](#) with sodium hydride in tetrahydrofuran and dimethyl acetamide gives compound **8** which was hydrolysed to telmisartan **1**.

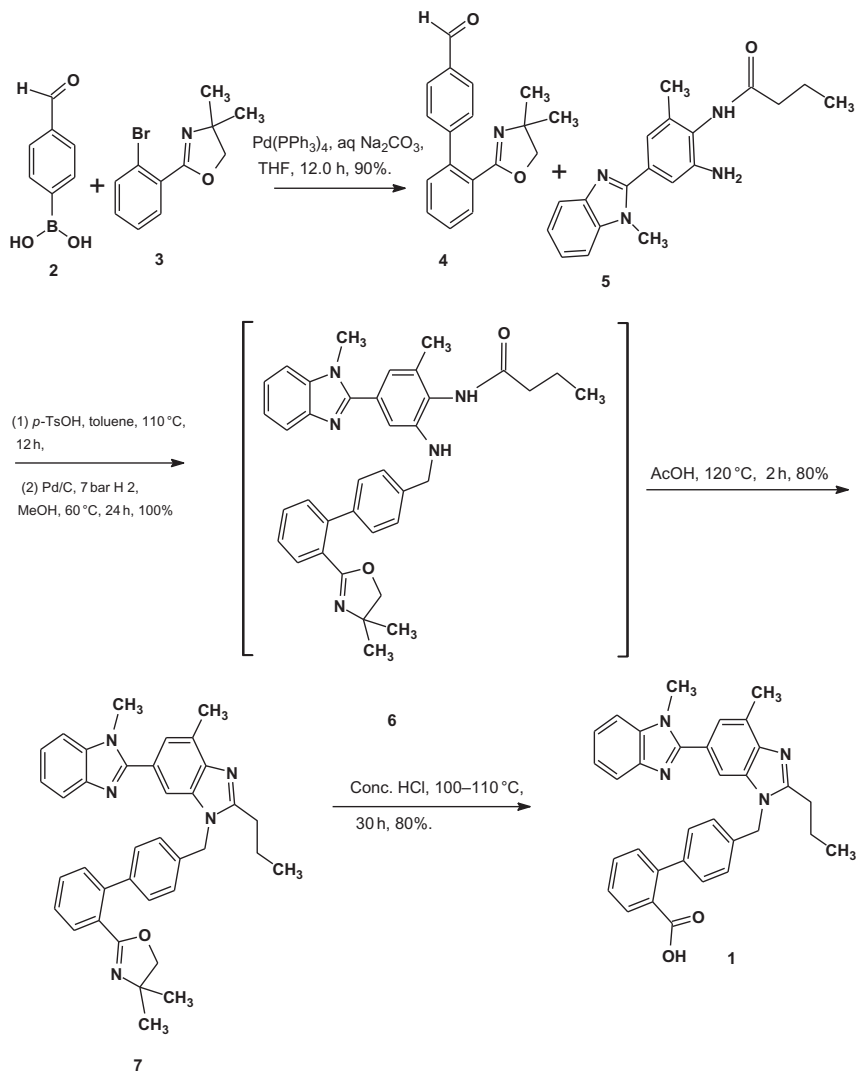


Scheme 6 Synthesis of telmisartan **1** [16].

Kumar *et al.* [22] identified 4-formylphenylboronic acid **2** and 2-(2-bromophenyl)-4,4-dimethyl-dihydro-2-oxazoline **3** [23] as the ideal starting materials for the preparation of the key biaryl intermediate **4**. Thus, Suzuki coupling of 2-(2-bromophenyl)-4,4-dimethyl-dihydro-2-oxazoline **3** with 4-formylphenylboronic acid **2** in the presence of aqueous sodium carbonate and tetrakis(triphenylphosphine)-palladium(0) in THF solvent gave 2'-(4,4-dimethyl-4,5-dihydro-1,3-oxazol-2-yl)-biphenyl-4-carbaldehyde **4** in over 90% yield (Scheme 7).

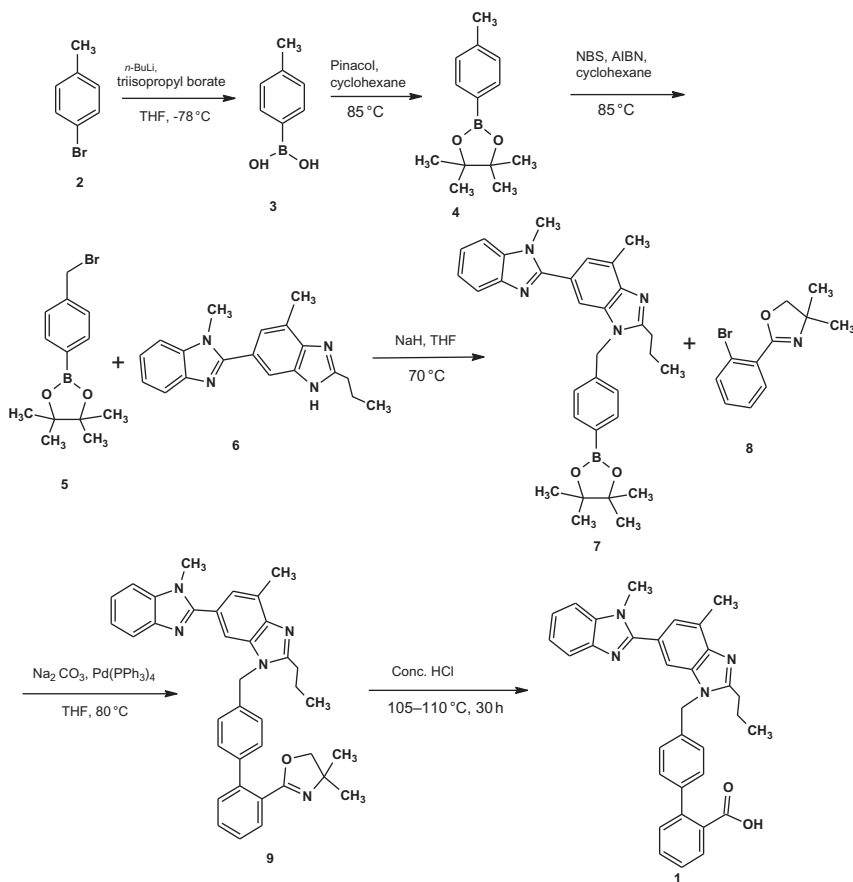
The reductive amination of the biaryl aldehyde **4** with amine **5** (in Scheme 5) was carried out in the presence of *p*-toluenesulfonic acid in toluene and followed by hydrogenation in methyl alcohol. The resulting amine **6** was not isolated but cyclized *in situ* to the *n*-propyl benzimidazole **7** in 80% yield in refluxing glacial acetic acid. Finally, cleavage of the oxazoline moiety in **7** by acid afforded Telmisartan **1** (Scheme 7).

Kumar *et al.* [24] synthesized Telmisartan in three segments, the first segment of this synthesis was construction of 2-(4-(bromomethyl)



Scheme 7 Synthesis of telmisartan **1** [22].

phenyl)-4,4,5,5-tetramethyl-1,3,2-dioxaborolane **5** (Scheme 8). First, *p*-tolyl boronic acid **3** was prepared from 4-bromo toluene **2** by reacting with *n*-BuLi and triisopropyl borate at -70°C and stirred for 2 h at the same temperature to afford the *p*-tolyl boronic acid **3** (85%). Second, the mixture of *p*-tolyl boronic acid **3** and pinacol in cyclohexane was refluxed for 10 h to remove water and then the 4,4,5,5-tetramethyl-2-*p*-tolyl-1,3,2-dioxaborolane **4** was obtained in 80% yield. Third, compound **4**, with



Scheme 8 Synthesis of telmisartan **1** [24].

N-bromosuccinimide (NBS) and 2,2'-azoisobutyronitrile (AIBN) in cyclohexane were refluxed for 5 h to provide the bromomethyl intermediate **5** (82%).

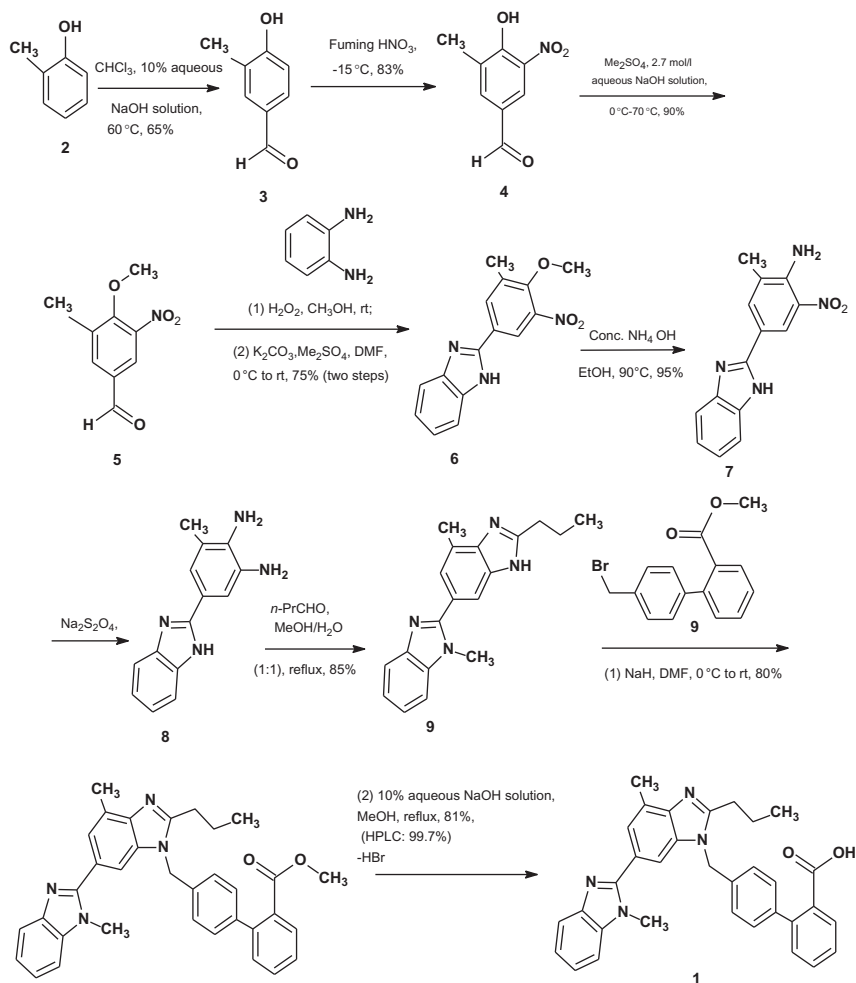
The second segment is the preparation of the key intermediate **7** for Suzuki coupling (Scheme 8). First, 1,4'-dimethyl-2'-propyl-1*H*,3'*H*-2,6'-bibenzo[*d*]imidazole **6**, sodium hydride, and 2-(4-(bromomethyl)phenyl)-4,4,5,5-tetramethyl-1,3,2-dioxaborolane **5** in THF were allowed to heated at 70 °C for 3 h to give 1,4'-dimethyl-2'-propyl-3'-(4-(4,4,5,5-tetramethyl-1,3,2-dioxaborolan-2-yl)benzyl)-1*H*,3'*H*-2,4'-bibenzo[*d*]imidazole **7** (60%).

Finally biaryl coupling, which was conducted with the borate ester **7** and 2-(2-bromophenyl)-4,4-dimethyl-4,5-dihydro-2-(1,3) oxazoline [9] **8** in

the presence of sodium carbonate and $\text{Pd}(\text{PPh}_3)_4$ at 80 °C for 48 h to afford the coupling product **9** in 70% (Scheme 8).

The third segment of our synthesis was deprotection oxazoline to carboxylic acid. Hydrolysis of oxazoline **8** is carried out by refluxing in concentrated hydrochloric acid for 30 h at 105–110 °C to afford the telmisartan **1** in 85% (Scheme 8).

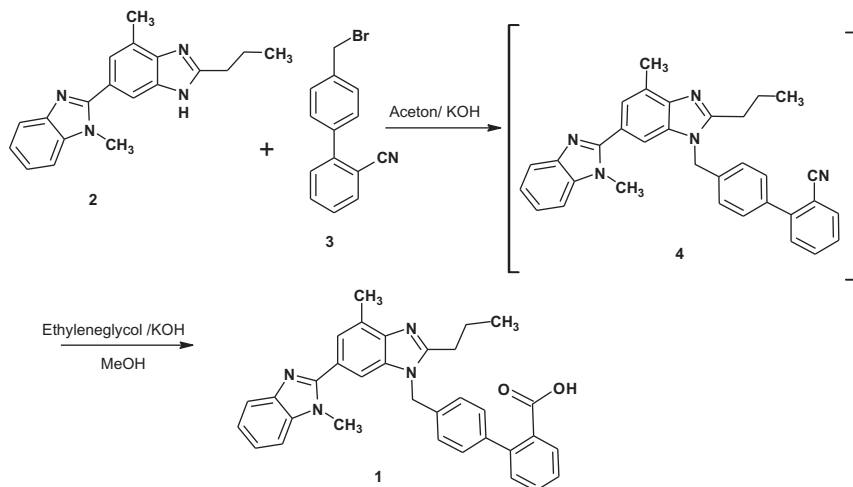
Wang *et al.* [25] detailed the total synthesis of telmisartan in Scheme 9. First, starting material *o*-cresol **2** was treated with chloroform in 10% sodium hydroxide solution to give aldehyde **3**, which was purified by crystallization



Scheme 9 Total synthesis of telmisartan **1** [25].

from ethyl acetate and petroleum ether. Then, the nitration of aldehyde **3** was accomplished via reacting with fuming nitric acid at $-15\text{ }^{\circ}\text{C}$. The result demonstrated that the nitration step was highly sensitive to the reaction conditions, and only fuming nitric acid as the nitration agent at below $-15\text{ }^{\circ}\text{C}$ could achieve the best outcome. Under most other conditions tested, in which a variety of the ratios of concentrated $\text{HNO}_3/\text{H}_2\text{SO}_4$ or fuming $\text{HNO}_3/\text{H}_2\text{SO}_4$ were performed, either the aldehyde group was partially nitrated off or the yield was rather low. Furthermore, temperature is critical to this reaction, and there was little desired product if the temperature was over $5\text{ }^{\circ}\text{C}$. The phenolic hydroxyl group of compound **4** was protected with dimethyl sulfate in 2.7 mol/l sodium hydroxide solution, and after that, the resulting reaction mass was filtered to obtain the anisole **5** with the yield of 90%. Anisole **5** was subsequently reacted with *o*-phenylenediamine rather than *N*-methyl-1,2-phenylenediamine under oxidative condition at room temperature because the latter costs more. Diluted solution of hydrogen peroxide adopted as oxidizing agent, because it is a universal, ecologically clean, and easy-to-handle reagent for different oxidations in the liquid phase. At the same time, the reaction was carried out at normal temperature and pressure, and the workup was that pouring the resulting reaction mass into ice-water then collected by filtration, avoiding the explosion hazard in use of hydrogen peroxide solution. Followed by *N*-methylation with dimethyl sulfate could afford compound **6**, which was recrystallized from ethyl acetate in 75% yield over two steps. Remarkably, conversion of methoxy group of compound **6** into the amino group was conducted via treatment with concentrated ammonia solution in autoclave at $90\text{ }^{\circ}\text{C}$ with the yield of 95%. The bis-benzimidazole **9** was prepared from the reduction an *o*-nitroaniline **7**, using butyl aldehyde in the presence of sodium dithionite in the mixture of methanol and water at reflux in 85% yield gives the phenylene diamine **8** which was then *N*-alkylate to give the bis-benzimidazole **9**. Compound **9** was reacted with the bromides **9** in DMF in the presence of sodium hydride, the resulting Telmisartan methyl ester **10** was saponified with 10% aqueous sodium hydroxide solution in methanol, and subsequent acidification with acetic acid led to the precipitation of crude telmisartan **1**, which was recrystallized from ethanol via adjustment of pH with ammonia solution and acetic acid to obtain qualified product (high-performance liquid chromatography (HPLC): 99.7%) in 81% yield.

Patil *et al.* [8] have developed a cost-effective and an improved one-pot synthesis for telmisartan which is described in Scheme 10.



Scheme 10 Synthesis of telmisartan **1** [8].

For the preparation of 4'-((1,4'-dimethyl-2'-propyl(2,6'-bi-1H-benzimidazole)-1'-yl)methyl)-1,1'-biphenyl-2-carbonitrile **4**, 4'-(bromomethyl) biphenyl-2-carbonitrile **3** was condensed with 2-*n*-propyl-4-methyl-6-(1'-methylbenzimidazol-2'-yl) benzimidazole **2** in acetone using potassium hydroxide as a base to give 4'-((1,4'-dimethyl-2'-propyl(2,6'-bi-1H benzimidazole)-1'-yl) methyl)-1,1'-biphenyl-2-carbonitrile **4** *in situ* which was hydrolysed by using potassium hydroxide in ethylene glycol to give potassium salt of telmisartan **1**. It is isolated by acetic acid to give pure telmisartan **1** in good yield and high purity.



4. PHYSICAL CHARACTERISTICS

The molar volume of telmisartan was 414.9 cm^3 ; the surface tension is 48.7 dyne/cm ; and the density: 1.24 g/cm^3 .

4.1 Ionization Constant

Cagigal *et al.* [26] determined the pKa of telmisartan by spectrofluorimetry, it is 4.45 ± 0.09 .

4.2 Solubility Characteristics

Telmisartan is practically insoluble in water, slightly soluble in methanol, sparingly soluble in methylene chloride strong acid; soluble in strong base. It dissolves in 1 M sodium hydroxide [7,10].

4.3 Optical Activity

The index of refraction of telmisartan is 1.667; and the molar refractivity: 154.51 cm^3 .

4.4 Partition Coefficient

Telmisartan is the most lipophilic compound with a partition coefficient $\log P=3.2$ (*n*-octanol buffer at pH 7.4). Due to its physicochemical properties, telmisartan shows excellent oral absorption and tissue penetration [27].

4.5 Particle Morphology

Doney [28] described methods for preparing solid materials. One aspect of the method include the steps of providing a mixture comprising an organic material, distributing the mixture into either droplets or granules, and evaporating the solvent and nonsolvent mixture to form particles having an average size of from about 0.5 to about 5000 μm .

4.6 X-ray Powder Diffraction Pattern

The X-ray powder diffraction pattern of telmisartan has been measured using a XRD-COMPACT 3 K using Powder X-ray diffractometer, equipped with a single channel analyzer and using a copper K_α radiation, a voltage of 40 kV and a current of 20 mA. The samples were scanned at the scanning rate of $0.02^\circ/\text{min}$ over the $5\text{--}60^\circ 2\theta$ range. The diffraction pattern of pure telmisartan was highly crystalline in nature as indicated by numerous peaks. Three peaks at 7.0° , 14.0° , 20.0° , 23.0° , and 25.0° were noticeable and the main peak at 7.0° was particularly distinctive [29].

4.7 Hygroscopicity

Telmisartan is commercially available in particular in its free acid form, which is poorly soluble in neutral or acidic media. Thus, telmisartan is typically formulated together with a basic agent or in the form of a basic salt for improved solubility [30].

4.8 Thermal Methods of Analysis

4.8.1 Melting Behavior

The melting range of telmisartan is between 261 and 263°C , determined after drying at $100\text{--}105^\circ\text{C}$ for 4 h [31,32].

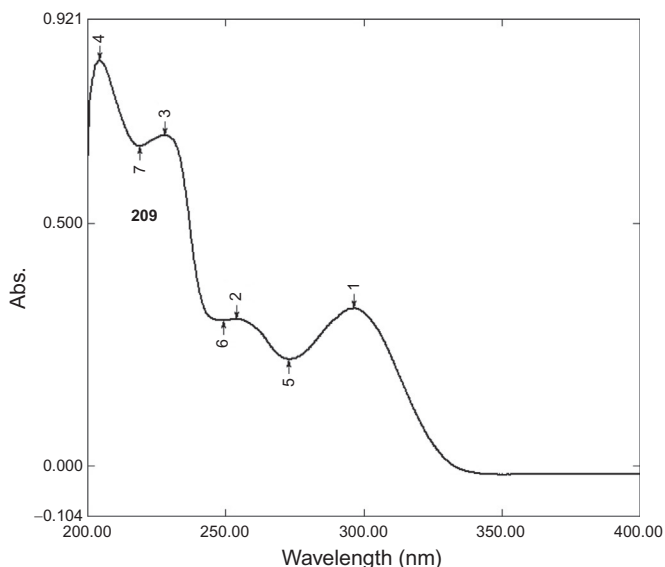


Figure 2 Ultraviolet absorption spectrum of telmisartan dissolved in methanol.

4.8.2 Differential Scanning Calorimetry

The differential scanning calorimetry (DSC) thermogram of telmisartan was obtained using a TA Instruments differential scanning calorimeter DSC-60 (Shimadzu). The data were collected from 30 to 300 °C using a heating rate of 10 °C/min. using nitrogen as a purge gas at heat flow of 40 ml/min. It was found that the compound melted at 269.06 °C with an enthalpy of fusion equal to 59.06 J/g [33,34].

4.8.3 Thermogravimetric Analysis

The thermogravimetric measurement of the crystalline form of telmisartan was carried out with a Perkin Elmer TGA 1 thermal analyzer in a platinum measuring cell, with the use of Pyris program for data handling. Measurements were performed in a nitrogen atmosphere as a purge gas at heat flow of 40 ml/min. The samples were heated up to 873 K, starting from room temperature. The data were collected from 300 to 800 K using a heating rate of 10 K/min. It was found that the compound melted around 542 K, and it was thermally stable up to 587 K. At that temperature, a thermal decomposition of the sample began and was nearly complete at about 773 K (mass loss 77%), gave a final residue of less than 20%. The sample was decomposed in a single weight loss. This was supported by the derivative curve which exhibits only a single peak [35,36].

4.8.4 Boiling Point, Enthalpy of Vapor, Flash Point, and Vapor Pressure

The calculated value of the boiling point of telmisartan under a pressure of 760 Torr was $771.9\text{ }^{\circ}\text{C} \pm 45.0\text{ }^{\circ}\text{C}$. The enthalpy of vaporization: 117.87 kJ/mol. The flash point was found $420.6\text{ }^{\circ}\text{C}$, and the vapor pressure was found $4.58\text{E}-25\text{ mmHg}$ at $25\text{ }^{\circ}\text{C}$ [37].

4.9 Spectroscopy

4.9.1 UV-vis Spectroscopy

The UV absorption spectra of telmisartan in methanol shown in Figure 2. The figures were recorded using a JASCO spectrophotometer, model no. V-530 with 1 cm matched quartz cells was used for experiments. The absorption spectra of reference and test solution were carried out in a 1 cm quartz cell over the range of 200–400 nm.

The values of the molar absorptivity of telmisartan at 298 nm are $4.04 \times 10^4\text{ l/mol cm}$ [38].

4.9.2 Fourier Transform Infrared Spectroscopy

The infrared absorption spectrum of telmisartan is shown in Figure 3. It was obtained in a KBr disc using a spectrophotometer FTIR-88101A (Shimadzu). The peaks were collected from 300 to 4000 cm^{-1} (Table 1).

4.9.3 Nuclear Magnetic Resonance Spectrometry

The ^1H NMR (nuclear magnetic resonance) and the ^{13}C NMR spectra of telmisartan were obtained using a Varian INOVA. Instruments system

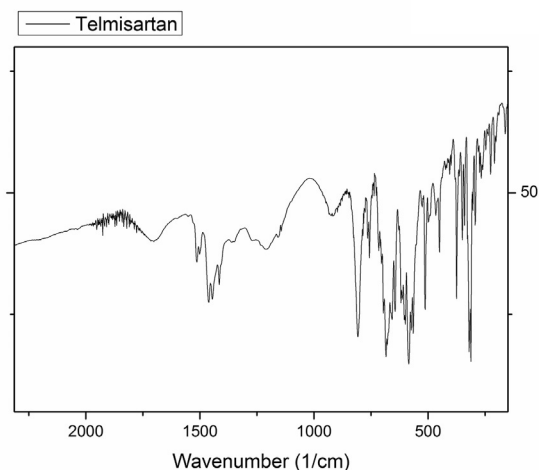


Figure 3 Infrared absorption spectrum of pure telmisartan.

Table 1 IR Interpretation of Telmisartan

Sr. No.	Peak at Wave Number (cm^{-1})	Peak Height
1	418.9334	66.6355
2	451.3314	62.0772
3	542.0964	56.0247
4	574.6112	53.8226
5	643.6542	54.7111
6	705.4500	43.1696
7	741.1014	14.9437
8	757.6413	17.1611
9	795.7474	42.9614
10	814.3524	40.1706
11	862.6864	27.9690
12	875.0962	52.7077
13	1007.4545	37.4949
14	1039.3459	45.2814
15	1128.9226	25.7250
16	1230.0128	20.9717
17	1267.1643	14.8085
18	1304.2769	23.8387
19	1382.9243	25.5885
20	1459.7599	16.2751
21	1599.1706	36.5372
22	1696.0723	20.3135
23	2868.4779	31.1139
24	2926.9424	28.0960
25	2956.8467	27.4844
26	3034.3057	37.3909
27	3057.1382	35.7713

operating sweep width was 9820 at 600 MHz (proton NMR), or at 20,000 and 30,000 Hz (carbon NMR). MestReNova software was used to obtain ^1H – ^{13}C -HSQC, DQF-COSY, and ^1H – ^{13}C HMBC spectra. All measurements were obtained with the compound being dissolved in deuterated dimethyl sulfoxide (DMSO-d_6).

4.9.3.1 ^1H NMR Spectrum

The full ^1H NMR spectrum of telmisartan is shown in Figure 4A–C with various regions being expanded for easier viewing. Confirmation of the spectral assignments was derived from a 2D DQF-COSY, and NESY experiment, see Figures 5A–D to 8A–C, respectively, and these assignment are summarized in Table 2.

4.9.3.2 ^{13}C NMR Spectrum

The ^{13}C NMR spectrum of telmisartan is interpretation in Table 3. The assignments for the observed bands are provided in Table 3, which are consistent with the 13 carbon contents of telmisartan.

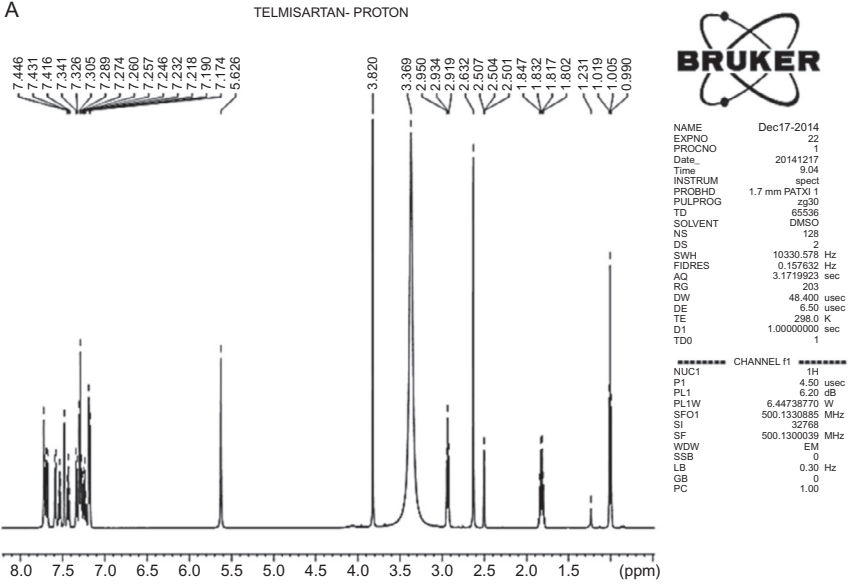
The ^{13}C NMR spectrum of telmisartan was recorded by broadband proton spin decoupling at ambient probe temperature using an internal deuterium lock. All chemical shift values are reported in ppm to the nearest 0.01 ppm. An internal reference of δ_{C} 77.0 was used for DMSO-d_6 . Verification of the carbon chemical shifts was obtained through ^{13}C NMR, 2D heteronuclear HSQC and HMBC spectra, see Figures 7A–C and 6A–C, respectively (Figure 9).

4.10 Mass Spectrometry

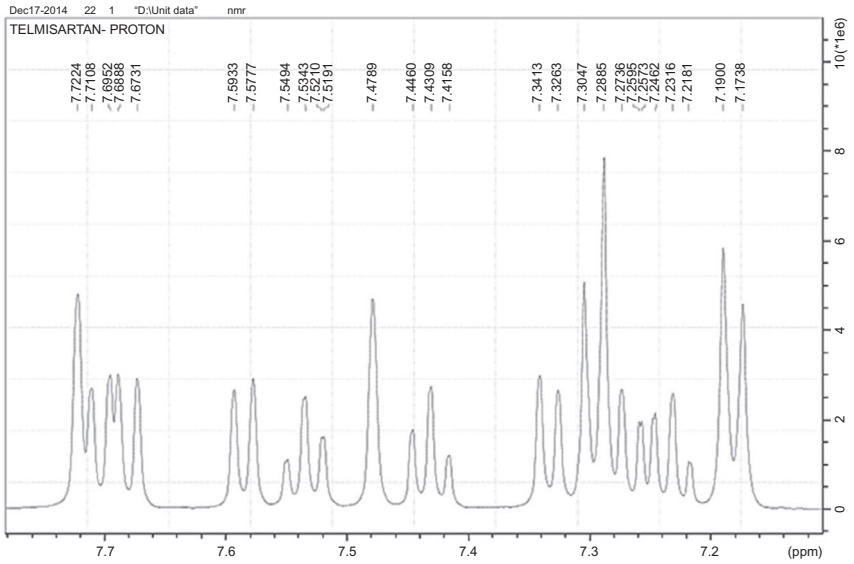
The mass spectrum of telmisartan was obtained using Waters TQD triple quadrupole mass spectrometer with Waters Acquity liquid chromatography (Waters Corp., Milford, Massachusetts, USA). The UPLC-MS/MS system was controlled by Mass Lynx software (SCN 805; Version 4.1).

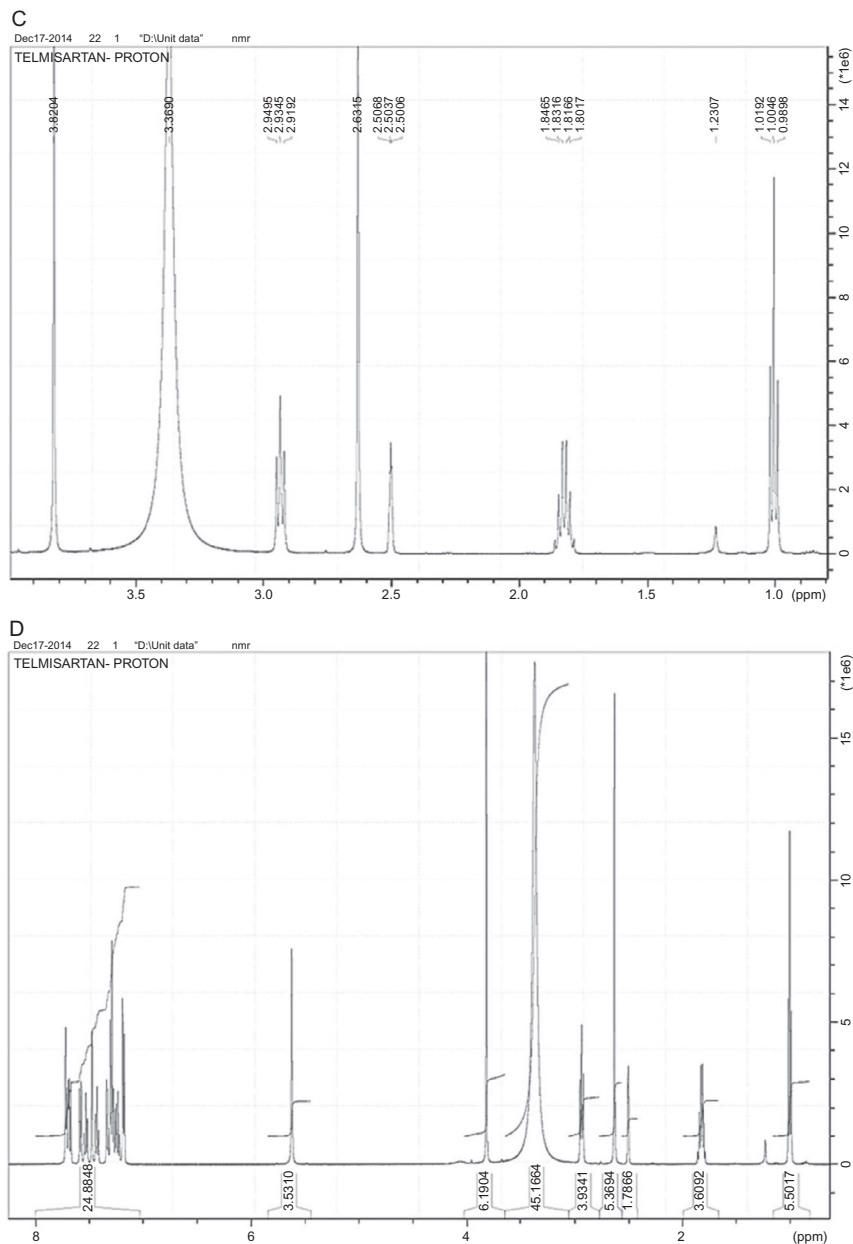
Figure 10A–D shows the detected mass fragmentation pattern of telmisartan. Tuning of the mass spectrometer for telmisartan was performed using negative and positive ionization modes with ESI as the ionization source. Parameters that included cone voltage and collision energy, desolvation temperature, ESI source temperature, and flow rate of desolvation gas and cone gas were optimized in order to achieve the maximum intensity of protonated or deprotonated molecules. The mass fragmentation pattern of the telmisartan is detailed in Table 4. The most abundant ion

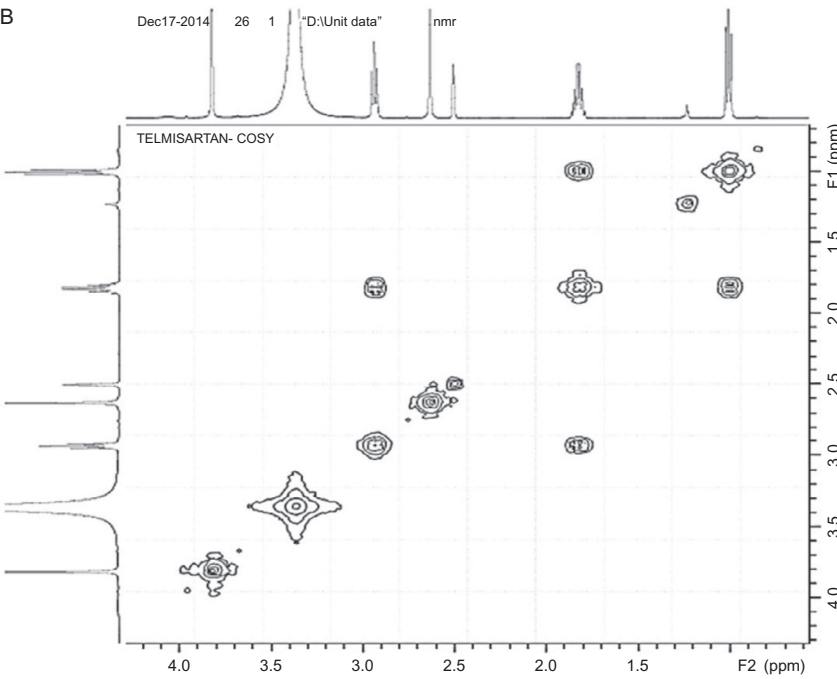
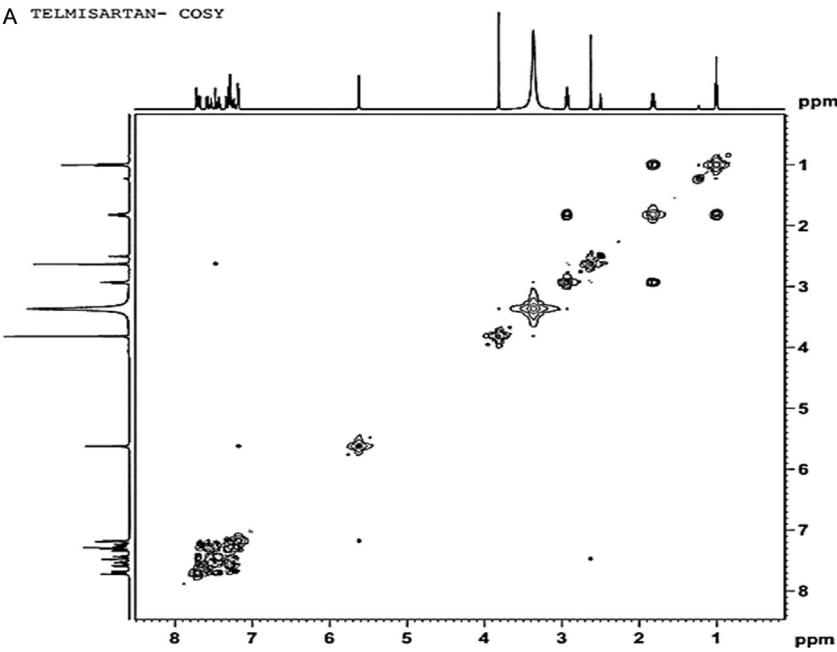
A



B







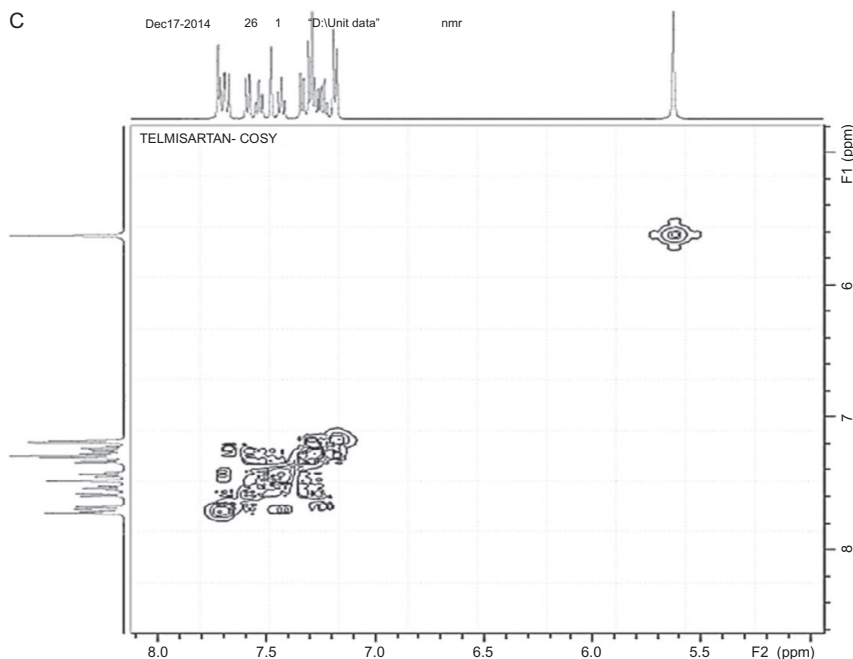


Figure 5 (A) COSY ^1H NMR spectrum of telmisartan in DMSO-d_6 . (B) Expanded-1 COSY ^1H NMR spectrum of telmisartan in DMSO-d_6 . (C) Expanded-2 COSY ^1H NMR spectrum of telmisartan in DMSO-d_6 .

(the base-peak) was found at m/z 276.1 in positive ionization mode and the most abundant ion (the base-peak) at m/z 469.16 in the negative ionization mode.

5. METHODS OF ANALYSIS

5.1 Compendial Methods of Analysis

5.1.1 British Pharmacopoeia Methods [7]

Definition

4'-[[4-Methyl-6-(1-methyl-1*H*-benzimidazol-2-yl)-2-propyl-1*H*-benzimidazol-1-yl]methyl]biphenyl-2-carboxylic acid.

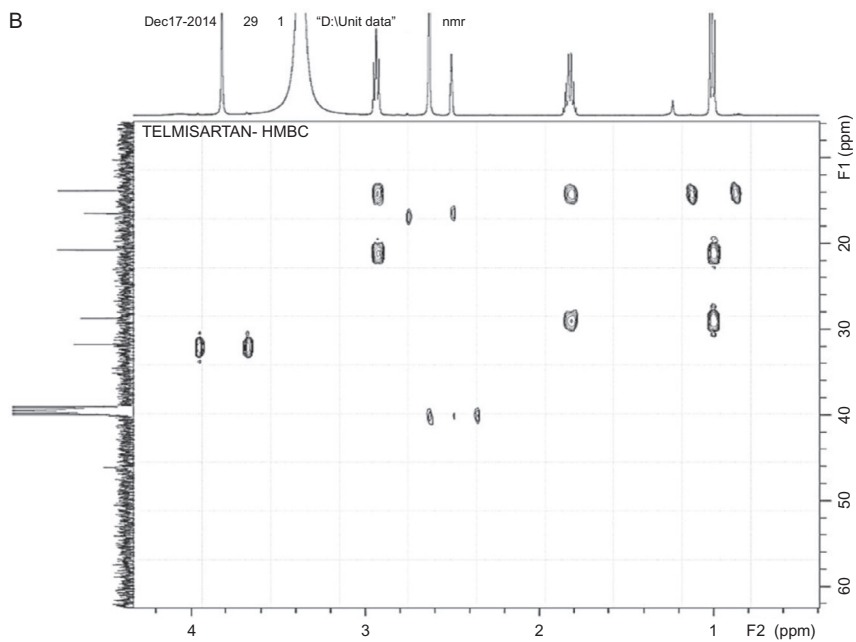
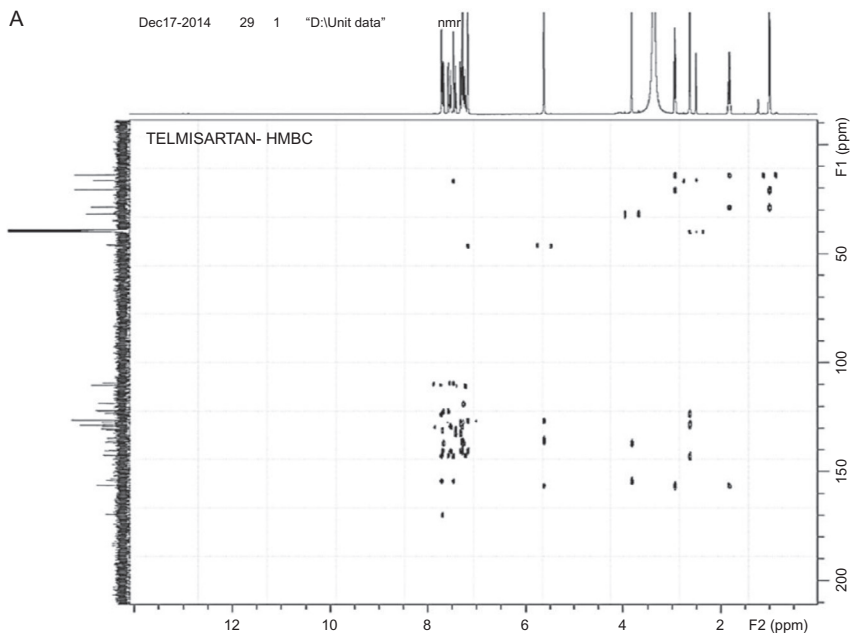
Content

99.0–101.0% (dried substance).

Characters

Appearance

White or slightly yellowish, crystalline powder.



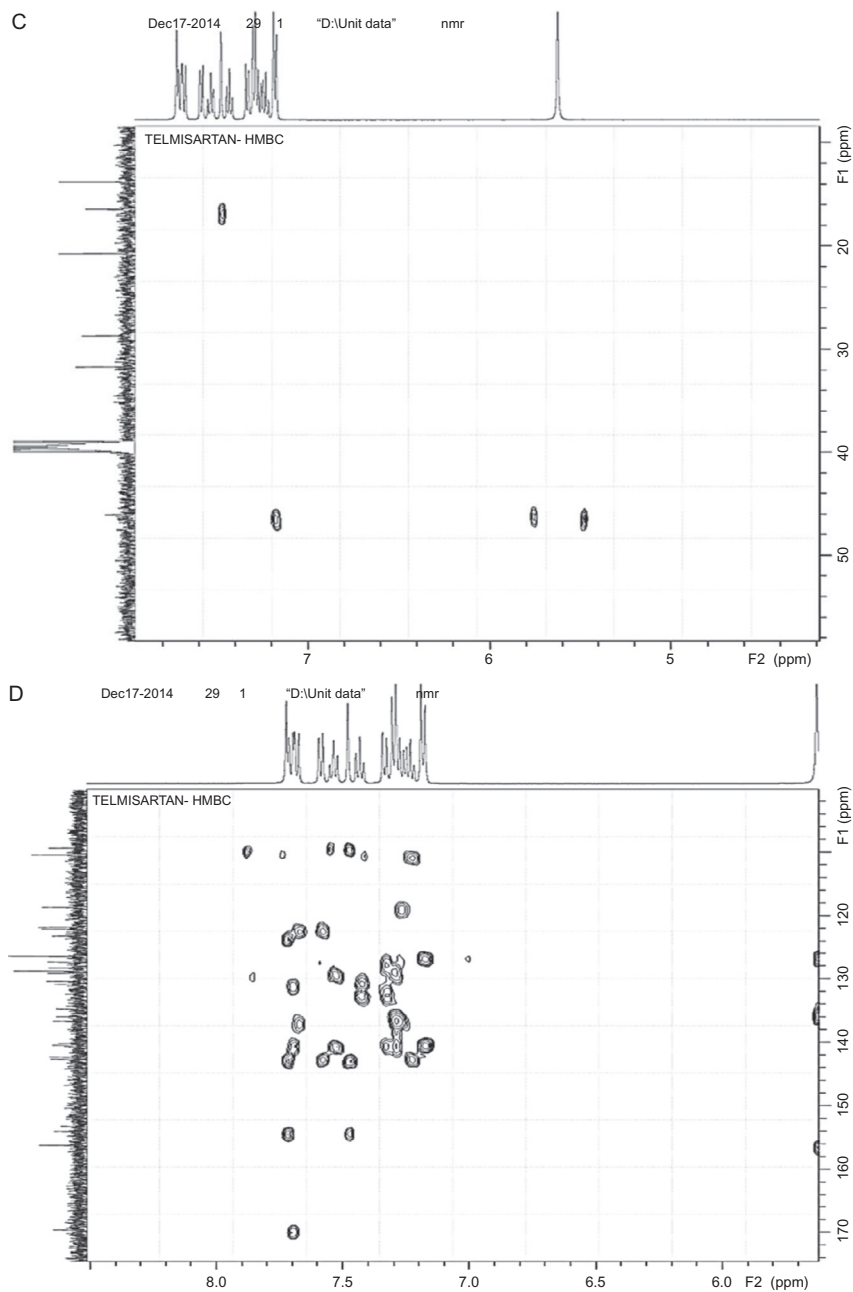
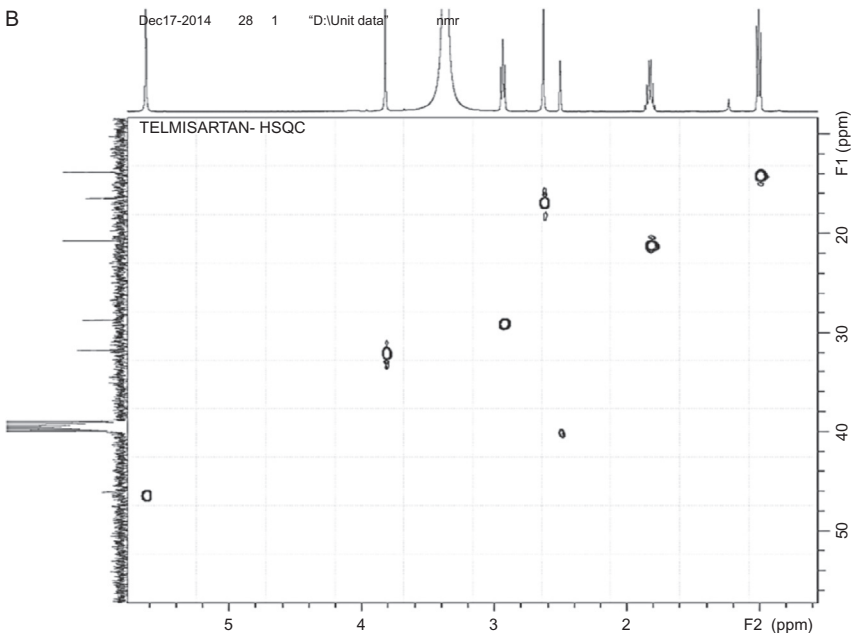
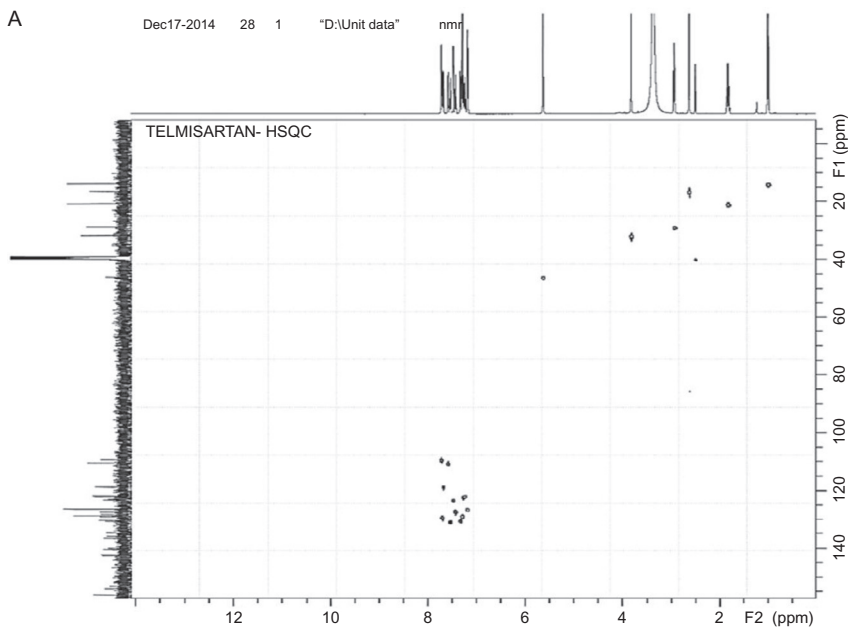


Figure 6 (A) HMBC ^1H NMR spectrum of telmisartan in DMSO- d_6 . (B) Expanded-1 HMBC ^1H NMR spectrum of telmisartan in DMSO- d_6 . (C) Expanded-2 HMBC ^1H NMR spectrum of telmisartan in DMSO- d_6 . (D) Expanded-3 HMBC ^1H NMR spectrum of telmisartan in DMSO- d_6 .



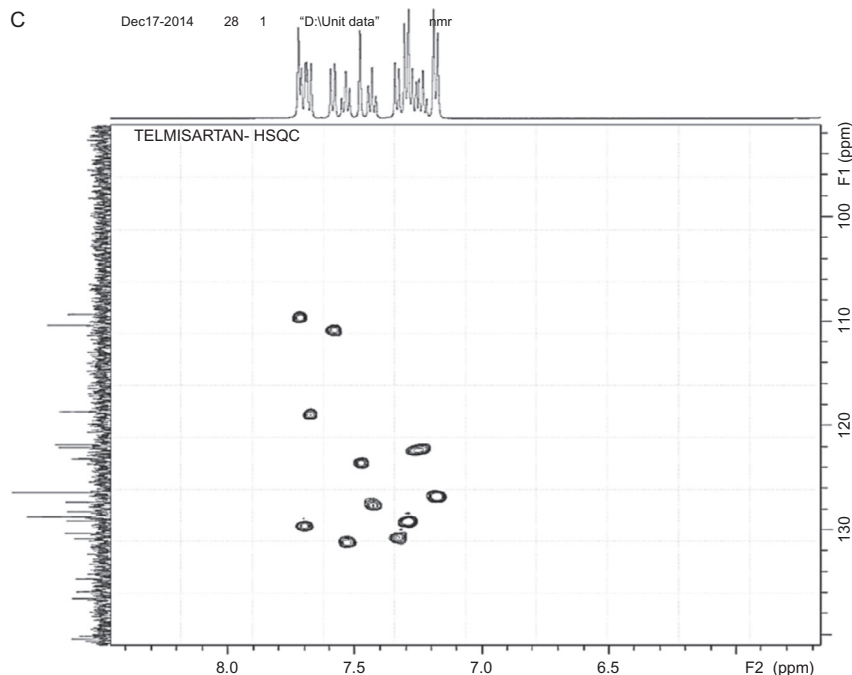


Figure 7 (A) HSQC ^1H NMR spectrum of telmisartan in DMSO-d_6 . (B) Expanded-1 HSQC ^1H NMR spectrum of telmisartan in DMSO-d_6 . (C) Expanded-2 HSQC ^1H NMR spectrum of telmisartan in DMSO-d_6 .

Solubility

Practically insoluble in water, slightly soluble in methanol, sparingly soluble in methylene chloride. It dissolves in 1 M sodium hydroxide. It shows polymorphism (5.9).

Identification

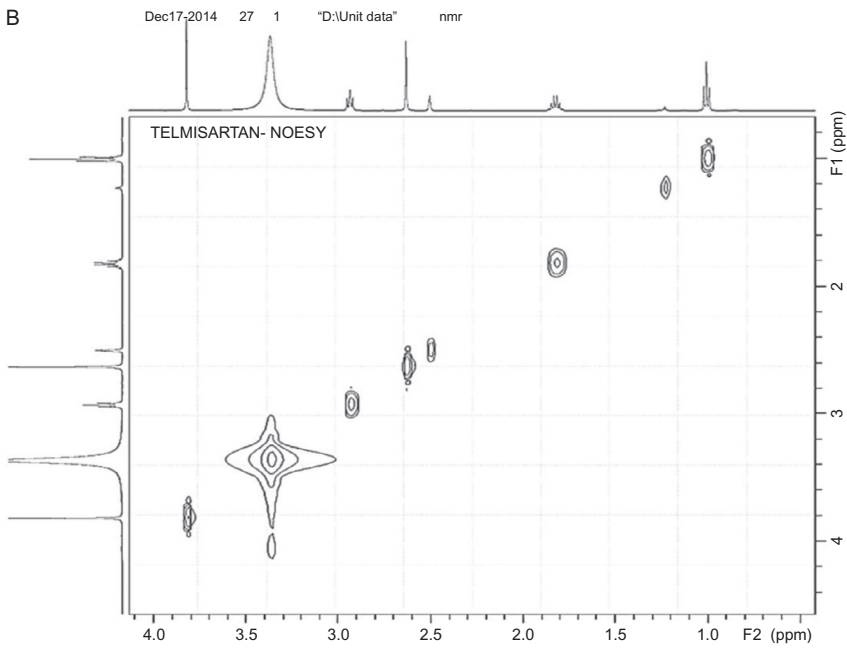
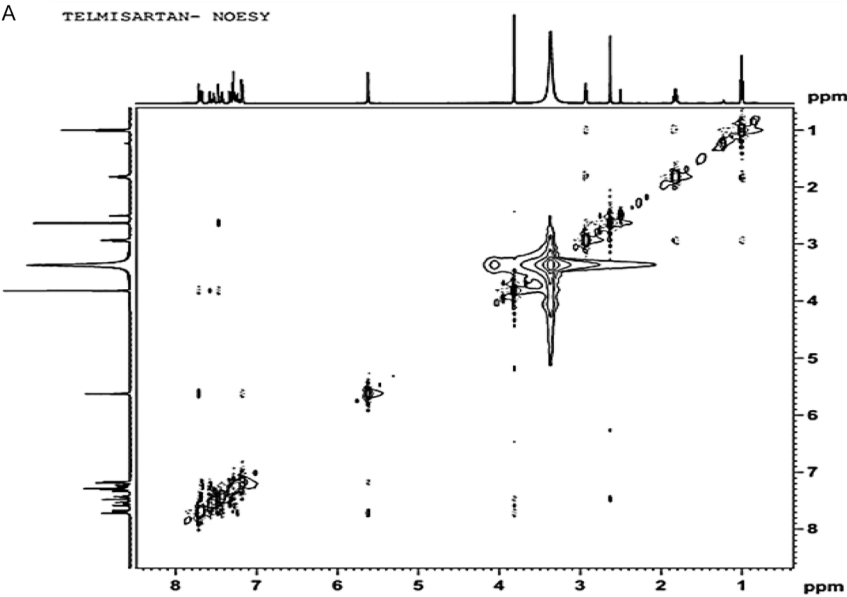
Infrared absorption spectrophotometry (2.2.24). *Comparison telmisartan CRS.*

If the spectra obtained in the solid state show differences, dissolve the substance to be examined and the reference substance separately in hot *anhydrous ethanol R*, evaporate to dryness and record new spectra using the residues.

Tests

Appearance of solution

The solution is not more intensely coloured than reference solution Y_4 (2.2.2, *Method II*).



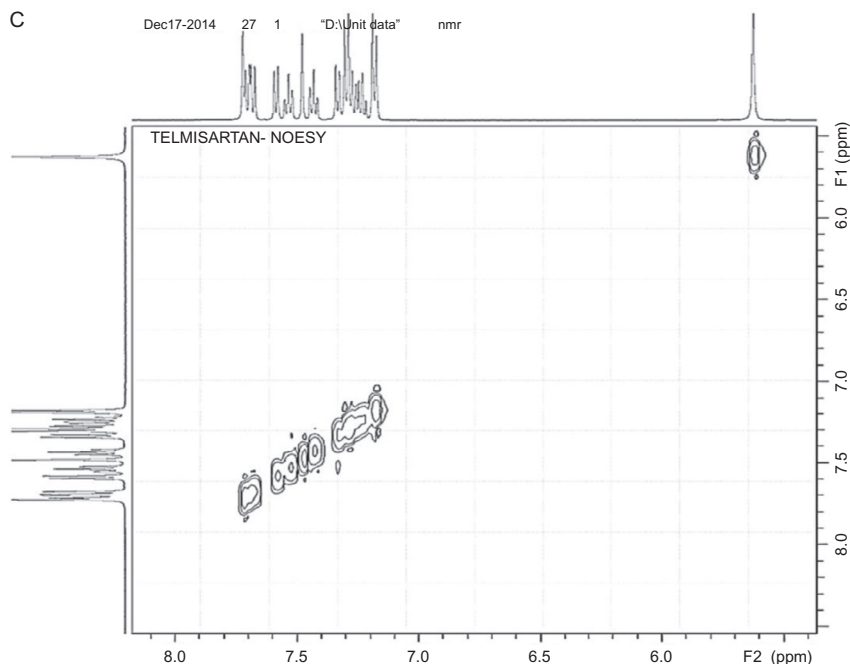


Figure 8 (A) NESY ^1H NMR spectrum of telmisartan in DMSO-d_6 . (B) Expanded-1 NESY ^1H NMR spectrum of telmisartan in DMSO-d_6 . (C) Expanded-2 NESY ^1H NMR spectrum of telmisartan in DMSO-d_6 . (D) Expanded-2 NESY ^1H NMR spectrum of telmisartan in DMSO-d_6 .

Dissolve 0.5 g in 1 M sodium hydroxide and dilute to 10 ml with the same solvent.

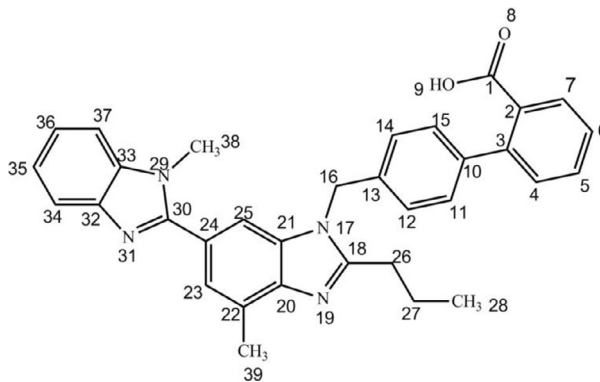
Related substances

Liquid Chromatography (2.2.29)

Test solution: To 25 mg of the substance to be examined, add about 5 ml of *methanol R* and 100 μl of a 40 g/l solution of *sodium hydroxide R*. Dissolve with the aid of ultrasound and dilute to 50 ml with *methanol R*.

Reference solution (a): Dilute 1.0 ml of the test solution to 10.0 ml with *methanol R*. Dilute 1.0 ml of this solution to 100.0 ml with *methanol R*.

Reference solution (b): Dissolve the contents of a vial of *telmisartan for system suitability CRS* (containing impurities A, B, C, E, and F) in 2 ml of *methanol R*.

Table 2 Assignments for the Resonance Bands Observed in the ^1H NMR Spectrum of Telmisartan

Chemical Shift (ppm)	Number of Protons	Multiplicity and Coupling Constant (J)	Assignment
0.99	3H	Triplet, $J=7.6$ Hz	(C28) <u>CH</u> ₃
1.83	2H	Multiplet, $J=7.6$ Hz	(C27) <u>CH</u> ₂
2.63	3H	Singlet	(C39) <u>CH</u> ₃
2.97	2H	Triplet, $J=7.6$ Hz	(C26) <u>CH</u> ₂
3.81	3H	Singlet	(C38) <u>CH</u> ₃
5.62	2H	Singlet	(C16) <u>CH</u> ₂
7.18	2H	Singlet	(C12, C14) Ar <u>H</u>
7.28	2H	Doublet, $J=8.0$ Hz	(C11, C15) Ar <u>H</u>
7.58–7.26	7H	Multiplet	(C4, C5, C6, C23, C37, C36, C35) Ar <u>H</u>
7.67–7.71	3H	Doublet, $J=8.02$ Hz	(C34, C7, C25) Ar <u>H</u>
–	1H	Singlet	(C9) COO <u>H</u>

Reference solution (c): To 5 mg of telmisartan for peak identification CRS (containing impurity D) add about 5 ml of methanol R and 100 μl of a 40 g/l solution of sodium hydroxide R. Dissolve with the aid of ultrasound and dilute to 10 ml with methanol R.

Column:

- size: $l=0.125$ m, $\varnothing=4.0$ mm;
- stationary phase: octadecylsilyl silica gel for chromatography R (5 μm) with a pore size of 10 nm;
- temperature: 40 $^{\circ}\text{C}$.

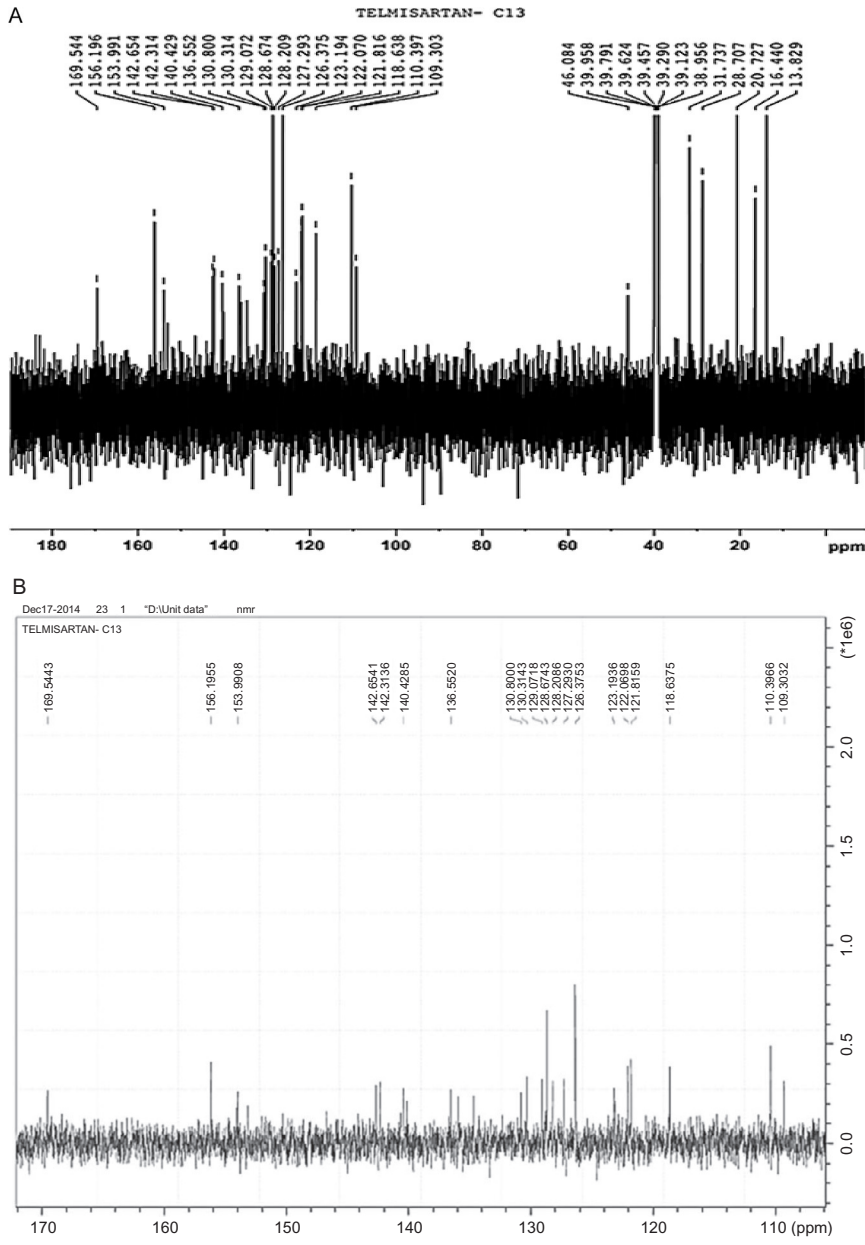


Figure 9 (A) ^{13}C NMR spectrum of telmisartan in DMSO-d_6 . (B) Expanded-1 ^{13}C NMR spectrum of telmisartan in DMSO-d_6 .

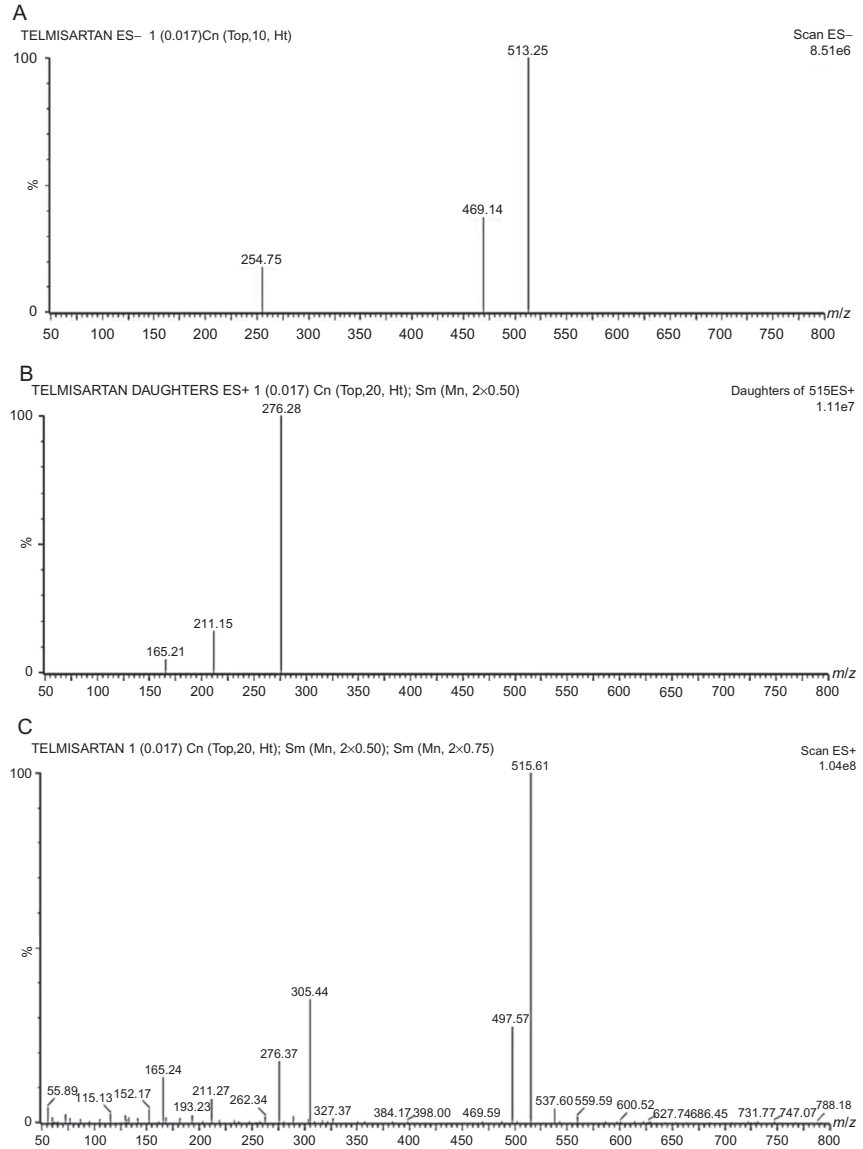


Figure 10 (A) (ES-) Mass spectrum of telmisartan in methanol. (B) (ES-) Mass spectrum of telmisartan in methanol (daughters). (C) (ES+) Mass spectrum of telmisartan in methanol (parent). (D) (ES+) Mass spectrum of telmisartan in methanol (daughters).
(Continued)

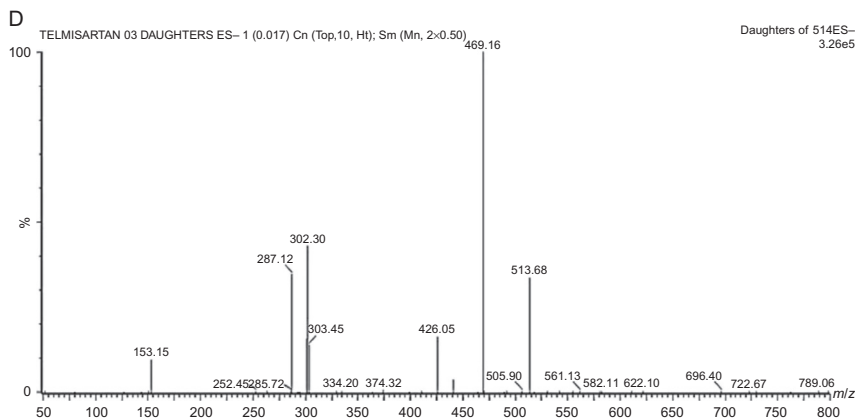


Figure 10—Cont'd

Table 4 MSⁿ Fragmentation of the Telmisartan

	Precursor Ion	Product Ions
Positive ion mode	515	276, 211, 165
Negative ion mode	513	469, 426, 302, 303, 287, 154
	317	302 ^a , 288 ^a , 274 ^a
	303	288 ^a , 275 ^a , 262 ^a , 261 ^a
	289	274 ^a , 261 ^a
	276	262 ^a , 261 ^a

^aFragments had low intensity, so could not be captured for further MSⁿ.

Time (min)	Mobile phase A (percent v/v)	Mobile phase B (percent v/v)
0–3	70	30
3–28	70–20	30–80

Flow rate: 1 ml/min.

Detection: Spectrophotometer at 230 nm.

Injection: 10 µl.

Identification of impurities: Use the chromatogram supplied with *telmisartan* for system suitability CRS and the chromatogram obtained with reference solution (b) to identify the peaks due to impurities A, B, C, E, and F; use the chromatogram supplied with *telmisartan* for peak identification CRS

and the chromatogram obtained with reference solution (c) to identify the peak due to impurity D.

Relative retention: With reference to telmisartan (retention time = about 15 min), impurity A = about 0.2; impurity E = about 0.6; impurity F = about 0.7; impurity B = about 0.9; impurity C = about 1.5; impurity D = about 1.6.

System suitability: Reference solution (b):

- the chromatogram obtained with reference solution (b) is similar to the chromatogram supplied with *telmisartan for system suitability CRS*;
- *resolution:* minimum 3.0 between the peaks due to impurity B and telmisartan.

Limits:

- *impurities C and D:* for each impurity, not more than twice the area of the principal peak in the chromatogram obtained with reference solution (a) (0.2%);
- *impurities A and B:* for each impurity, not more than 1.5 times the area of the principal peak in the chromatogram obtained with reference solution (a) (0.15%);
- *unspecified impurities:* for each impurity, not more than the area of the principal peak in the chromatogram obtained with reference solution (a) (0.10%);
- *total:* not more than 10 times the area of the principal peak in the chromatogram obtained with reference solution (a) (1.0%);
- *disregard limit:* 0.5 times the area of the principal peak in the chromatogram obtained with reference solution (a) (0.05%).

Loss on drying (2.2.32)

Maximum 0.5%, determined on 1.000 g by drying in an oven at 105 °C.

Sulfated ash (2.4.14)

Maximum 0.1%, determined on 1.0 g.

Assay

Dissolve 0.190 g in 5 ml of *anhydrous formic acid R*. Add 75 ml of *acetic anhydride R*. Titrate with 0.1 M *perchloric acid*, determining the end-point potentiometrically (2.2.20).

1 ml of 0.1 M *perchloric acid* is equivalent to 25.73 mg of $C_{33}H_{30}N_4O_2$.

The IR spectra of the drug were obtained in the solid state. If the spectra obtained in the solid state show differences, dissolve the substance to be

examined and the reference substance separately in hot anhydrous ethanol R, evaporate to dryness, and record new spectra using the residues.

Test 1: Dissolve 50 mg of Telmisartan of 1 M sodium hydroxide dilute to 10 ml with the same solvent. The solution is not more intensely coloured than reference solution.

Impurity analysis

The specified impurities (A–H) of telmisartan were determined using liquid chromatography (Table 5).

5.2 Titrimetric Methods of Analysis

5.2.1 Aqueous and Potentiometric Titration Methods

Patil and Janjale [39] developed and validated a novel and simple method of titrations for determination of telmisartan. The direct acid–base titration of eprosartan mesylate, irbesartan, telmisartan, and valsartan, was carried out in the mixture of ethanol:water (1:1) as solvent using standardized sodium hydroxide aqueous solution as titrant, either visually using phenolphthalein as an indicator or potentiometrically using combined pH electrode. The method was found to be accurate and precise, having relative standard deviation of less than 2% for telmisartan and all angiotensin-II-receptor antagonists (ARA-IIs) studied.

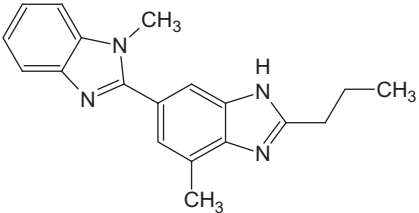
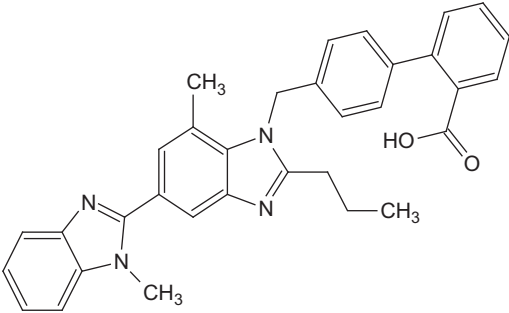
5.3 Electrochemical Methods of Analysis

Electrochemical methods have proved to be very sensitive for the determination of organic molecules, including drugs and related molecules in pharmaceutical dosage forms and biological fluids. The advance in experimental electrochemical techniques in the field of analysis of drugs is due to their simplicity, low cost, and relatively short analysis time as compared with the other techniques. However, since most drugs are less active electrochemically, little attention has been paid so far to the use of electrochemical detection methods [40–43].

5.3.1 Voltammetry

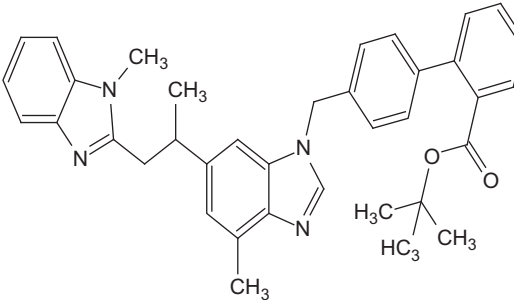
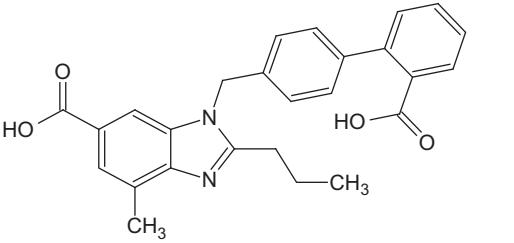
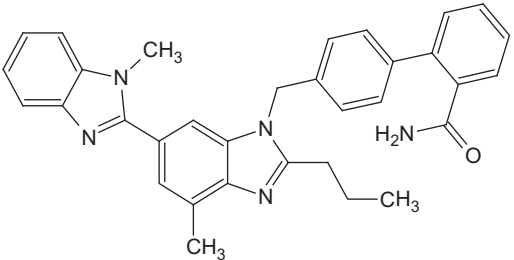
Tasemir *et al.* [40] investigated the electrochemical behavior of Telmisartan and optimum conditions for its assay by using cyclic voltammetry and square-wave voltammetry. They based all studies on the quasi-reversible and adsorption-controlled electrochemical reduction signal of TS at about -1.50 V versus Ag/AgCl at pH 10.0 in Britton–Robinson buffer. They found that the peak current was change linearly with concentration from 1.69 nM (0.87 mg/l) to 27.5 nM (14.15 mg/l) and found the limit of

Table 5 The Specified Impurities of Telmisartan

Specified Impurities	Name	Structure
A	4-Methyl-6-(1-methyl-1 <i>H</i> -benzimidazol-2-yl)-2-propyl-1 <i>H</i> -benzimidazole	
B	4'-[[7-methyl-5-(1-methyl-1 <i>H</i> -benzimidazol-2-yl)-2-propyl-1 <i>H</i> -benzimidazol-1-yl]methyl]biphenyl-2-carboxylic acid	

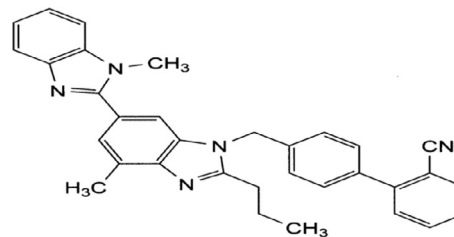
Continued

Table 5 The Specified Impurities of Telmisartan—cont'd

Specified Impurities	Name	Structure
C	1,1-Dimethylethyl 4'-[[4-methyl-6-(1-methyl-1 <i>H</i> -benzimidazol-2-yl)-2-propyl-1 <i>H</i> -benzimidazol-1-yl]methyl]biphenyl-2-carboxylate	
D	Unidentified impurity	
E	1-[(2'-Carboxybiphenyl-4-yl)methyl]-4-methyl-2-propyl-1 <i>H</i> -benzimidazol-6-carboxylic acid	
F	4'-[[4-Methyl-6-(1-methyl-1 <i>H</i> -benzimidazol-2-yl)-2-propyl-1 <i>H</i> -benzimidazol-1-yl]methyl]biphenyl-2-carboxamide	

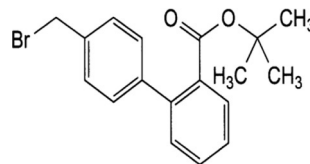
G

4'-[[4-Methyl-6-(1-methyl-1*H*-benzimidazol-2-yl)-2-propyl-1*H*-benzimidazol-1-yl]methyl]biphenyl-2-carbonitrile



H

1,1-Dimethylethyl 4'-(bromomethyl)biphenyl-2-carboxylate



detection and the limit of quantification were 1.05 nM (0.54 mg/l) and 3.49 nM (1.79 mg/l), respectively.

Alarfaj [41] investigated the adsorptive stripping voltammetry of telmisartan with a hanging mercury drop electrode. This compound produced a catalytic hydrogen wave at -1.5 V in Britton–Robinson buffer of pH 10.38, and the peak current increased with adsorptive accumulation at the electrode. Adsorptive stripping voltammetry with the catalytic hydrogen wave could provide a sensitive novel method for the determination of telmisartan. Various chemical and instrumental parameters affecting the monitored electroanalytical response were investigated and optimized for telmisartan determination. Under these optimized conditions, the square-wave adsorptive stripping voltammetric peak current showed a linear dependence on drug concentration over the range of 0.05 – 3.00 $\mu\text{g/ml}$ (1×10^{-7} – 6×10^{-6} M) ($r=0.999$) with accumulation for 120 s at -1.0 V versus Ag/AgCl.

5.3.2 Polarography

Xu *et al.* [42] investigated the polarographic characteristics of telmisartan in 0.8 mol/l $\text{NH}_3 \cdot \text{H}_2\text{O}$ – NH_4Cl (pH 8.9)– 0.01 mol/l H_2O_2 as supporting electrolyte. The calibration curve is linear in the range of 2.0×10^{-8} – 2.0×10^{-6} mol/l and the detection limit is 1.0×10^{-8} mol/l. The precision is excellent with relative standard deviations of 2.6% at a concentration of 1.0×10^{-7} mol/l telmisartan.

Xu *et al.* [43] investigated the polarographic behaviors of telmisartan in 0.8 mol/l $\text{NH}_3 \cdot \text{H}_2\text{O}$ – NH_4Cl (pH 8.9) supporting electrolyte. The results demonstrated that the reduction peak is obtained at ca. -1.30 V, which corresponds to a catalytic hydrogen wave. Based on the catalytic hydrogen wave, a novel method has been developed for the determination of telmisartan by linear sweep polarography. Calibration curve is linear in the range of 2.0×10^{-7} – 3.0×10^{-6} mol/l and the detection limit is 1.0×10^{-7} mol/l.

5.3.3 Coulometry

Adrianowicz *et al.* [35] determined the water content by the Karl Fischer method. For cryomilled Telmisartan sample, they have found 4% of water.

5.4 Spectroscopic Methods of Analysis

5.4.1 Spectrophotometry

Bhat *et al.* [44] developed a difference spectrophotometric method for the estimation of telmisartan in bulk drug and in pharmaceutical formulations.

Telmisartan exists in two different forms in acidic and basic mediums that differ in their UV spectra. Difference spectrum, obtained by keeping telmisartan in 0.01 N NaOH in reference cell and telmisartan in 0.01 N HNO₃ in sample cell, showed two characteristic peaks at 295 and 327 nm with positive and negative absorbance, respectively. Difference of absorbance between these two maxima was calculated to find out the amplitude, which was plotted against concentration. The method was found to be linear in the range of 2–12 µg/ml.

Telmisartan assayed by the UV spectrophotometric (Amax) method directly by Tatane [45] has been developed the development of a UV estimation method for telmisartan in tablet formulation. The wavelength (λ_{max}) selected for the telmisartan was 230 nm. The linearity for this drug at the selected wavelength is lies between 1 and 8 µg/m. Beer's law was obeyed in this concentration range with correlation coefficient of 0.999.

Pandey *et al.* [46] developed and validated a simple, precise, and accurate UV spectrophotometric method for the estimation of telmisartan in bulk and tablet dosage form. The zero-order spectra of telmisartan in 0.1 N NaOH shows λ_{max} at 234.0 nm and estimation was carried out by A (1% 1 cm) and by comparison with standard. Calibration graph was found to be linear ($r^2=0.999$) over the concentration range of 4–24 µg/ml.

Rathod *et al.* [47] developed and validated a simple, precise, and accurate UV spectrophotometric method for the estimation of telmisartan in bulk and tablet dosage form. The spectra of telmisartan in 0.1 N NaOH and distilled water (20:80) show λ_{max} at 234 nm and estimation was carried out by A (1% 1 cm) and by comparison with standard. Calibration graph was found to be linear ($r^2=0.999$) over the concentration range of 2–10 µg/ml.

Jat *et al.* [48] developed a sensitive and rapid extractive spectrophotometer method for the assay of Telmisartan in bulk drug and tablets. Telmisartan shows maximum absorbance at 216 nm. Beer's law was obeyed in the concentration range of in the range of 5–25 µg/ml. Beer's law was obeyed in this concentration range with correlation coefficient of 0.999.

Singh *et al.* [49] developed UV first derivative spectrophotometric methods for the determination of telmisartan in pharmaceutical formulation. They prepared the solutions of standard and sample in 0.1 M sodium hydroxide. They carried in the UV spectrophotometric method, the quantitative determination of the drug at 295 nm, and they found the linearity range to be 4–20 µg/ml. They were determined the drug at 311 nm for the first-order derivative spectrophotometric method, with the linearity ranges of 4–20 µg/ml.

Kreny and Mehta [50] developed a simple, precise, and accurate method for the estimation of telmisartan and Chlorthalidone in bulk and pharmaceutical dosage form using first-order derivative spectrophotometry. Wavelength selected for quantitation 264.85 nm for telmisartan (zero-crossing point of Chlorthalidone) and 222.38 nm for Chlorthalidone (zero-crossing point of telmisartan). The method was validated with respect to linearity, accuracy, precision, limit of detection, and limit of quantitation in accordance with the International Conference on Harmonisation guidelines. Linearity was observed in concentration range of 8–48 $\mu\text{g/ml}$ for telmisartan and 2.5–15 $\mu\text{g/ml}$ for Chlorthalidone. The limit of detection and limit of quantitation were found to be 0.234 and 0.712 $\mu\text{g/ml}$ for telmisartan and 0.102 $\mu\text{g/ml}$ and 0.309 $\mu\text{g/ml}$ for Chlorthalidone, respectively.

Bebawy *et al.* [51] described four sensitive methods for the direct determination of telmisartan and hydrochlorothiazide in combined dosage forms without prior separation. The first method is a first derivative spectrophotometry using a zero-crossing technique of measurement at 241.6 and 227.6 nm for telmisartan and hydrochlorothiazide, respectively. The second method is the first derivative of ratio spectrophotometry where the amplitudes were measured at 242.7 nm for telmisartan and 274.9 nm for hydrochlorothiazide.

Lakshmi and Lakshmi [52] utilize Chemometric-Assisted Spectrophotometric for the simultaneous determination of telmisartan and hydrochlorothiazide. The chemometric methods applied were principal component regression and partial least square (PLS-1). These approaches were applied to quantify the two drugs in the mixture using the information included in the UV absorption spectra of appropriate solutions in the range of 200–350 nm with the intervals $\Delta\lambda = 1$ nm. The PCR and PLS-1 methods require neither any separation step nor any prior graphical treatment of the overlapping spectra of the two drugs in a mixture.

5.4.2 Colorimetry

Srihari *et al.* [53] developed two simple, sensitive, and economical spectrophotometric methods for the estimation of telmisartan in pharmaceutical dosage forms. A method was based on the formation of chloroform extractable complex of telmisartan with a wool fast blue. The absorbance of the extractable ion pair complex is measured at the wavelength of maximum absorbance 585 nm against the reagent blank. Method B was based on the charge transfer reaction of telmisartan as n -electron donor with acceptor,

2,5-dichloro-3,6-dihydroxy-1,4-benzoquinone. The absorbance of the highly intensive colored solution was measured at 460 nm against reagent blank treated similarly.

Kumbhar *et al.* [54] proposed a new, simple, sensitive, reproducible, economical, accurate, and precise method, and it can be successfully applied in estimation of telmisartan from urine. This method can find applications in clinical studies and therapeutic drug monitoring. This method of colorimetric estimation of telmisartan from urine is based on the formation of yellow-colored chromogen when it is reacted with alizarin in the presence of thionyl chloride. The concentration of telmisartan over a range of 10–60 µg/ml was found to obey Beer's law in the stated range. The yellow-colored complex has absorption maxima at 427 nm with molar absorptivity and Sandell's sensitivity 2.2387×10^4 lit mol/cm and $0.0154 \mu\text{g}/\text{cm}^2/0.001$ absorbance units, respectively.

Qin *et al.* [55] developed new method for the estimation of telmisartan. This method of colorimetric estimation of telmisartan is based on the formation of red colored chromogen when it is reacted with congo red in the presence of buffer solution in pH 2.50 HCl–NaAc, which has the maximum absorbance at 593 nm in the spectrophotometric experiment. Under this wavelength, the Beer's law was obeyed within the concentration range of 1.08×10^{-6} – 2.24×10^{-5} M. The linear regression equation was $A = -0.1913 \times 10^5 c + 0.0286$ (C:M). The regression coefficient r was 0.9986. The apparent molar coefficient ϵ_{593} was 1.63×10^4 l/mol/cm and the detection limit was 5.66×10^{-7} M.

Rani Tulja *et al.* [56] developed simple, accurate, rapid, and sensitive method for the estimation of telmisartan and irbesartan in bulk and pharmaceutical formulations. The method is based on the formation of ion association complex of the drug with eriochrome black-T in acidic buffer of pH 3.5 followed by extraction into chloroform. The linearity range of telmisartan and irbesartan with eriochrome black-T was found to be 50–250 µg/ml.

5.5 Chromatographic Methods of Analysis

5.5.1 Electrophoresis

As a powerful complementary new technique to HPLC and GC, capillary electrophoresis (CE) has rapidly spread into a wide array of analytical areas due to its excellent separation efficiency, short analysis time, minimal need of samples and solvents, and high versatility in terms of separation modes.

However, one of the main drawbacks of CE is its low sensitivity in terms of solute concentration compared to other separation techniques, which is due to both the small optical path length of the capillary used as a detection cell and the small volumes (usually a few nanoliters) that can be injected [57,58].

González *et al.* [59] optimized a capillary zone electrophoretic (CZE) method for the separation of telmisartan and four other ARA-IIs (losartan, irbesartan, valsartan, and eprosartan) and two of their metabolites (EXP 3174 and Candesartan M1) by means of experimental design methodologies. Successful results were obtained with a 50 mM potassium dihydrogen phosphate:boric acid (25:75, v/v) buffer at pH 5.5 in the presence of 5% methanol and application of a 25 kV voltage. Analysis time was 8 min in a conventional fused-silica capillary (50 cm effective length) in a normal cationic mode (anode at the inlet and cathode at the outlet) after hydrostatical sample injection for 30 s.

Hillaert and Van Den Bossche [60] optimized a CZE method for separation of telmisartan and five other ARA-IIs: candesartan, eprosartan, irbesartan, losartan potassium, and valsartan. A three-level, full-factorial design was applied to study the effect of the pH and molarity of the running buffer on separation. Combination of the studied parameters permitted the separation of the six ARA-IIs, which was best carried out using 60 mM sodium phosphate buffer (pH 2.5). The same system can also be applied for the quantitative determination of these compounds, but only for the more soluble ones. Some parameters (linearity, precision, and accuracy) were validated.

5.5.2 Thin Layer Chromatography

Few methods use this technique for determination of telmisartan. Also some stability study was performed by researchers. Establishment of a stability-indicating assay is mandatory for study of degradation pathways of drug. Prabhu *et al.* [61] developed a stability-indicating HPTLC for telmisartan. This method is suitable for quantification for telmisartan in the presence of degradation product.

Vekariya *et al.* [62] developed and validated a rapid, selective, and stability-indicating high-performance thin layer chromatographic method for simultaneous estimation of telmisartan and amlodipine besylate in pharmaceutical dosage forms. TLC aluminium plates precoated with silica gel 60 F 254 was employed as the stationary phase in the method. The solvent system consisted of tetrahydrofuran:dichloroethane:methanol:ammonia solution (3.0:1.0:0.5:0.2, v/v). That system was found to give compact spots

for both telmisartan (R_f value of 0.22 ± 0.02) and amlodipine besylate (R_f value of 0.45 ± 0.02). Spectrodensitometric scanning-integration was performed at a wavelength of 326 nm. The polynomial regression data for the calibration plots showed good linear relationship with $r^2 = 0.9993$ in the concentration range of 1200–7200 ng for telmisartan.

Chabukswar *et al.* [63] described an HPTLC method for the simultaneous determination of telmisartan and amlodipine besylate from tablet dosage form. This employs a precoated silica gel 60 F 254 (0.2 mm thickness) on aluminium sheets and a mobile phase ethyl acetate:1,4 dioxane:methanol:25% ammonia in the ratio of 15:1.5:3:1.5 (v/v), having chamber saturation for 30 min at room temperature. The developing chamber was run up to 8 cm. The R_f values were found to be 0.16 and 0.33 for telmisartan and amlodipine, respectively. The plates were scanned and quantified at 323 nm. The linear detector response was observed between 100–500 $\mu\text{g/ml}$ and 200–1000 $\mu\text{g/ml}$ for telmisartan and amlodipine, respectively. The method so developed was validated for its accuracy and precision. The LOD and LOQ were found to be 0.025, 0.0747 $\mu\text{g/ml}$ and 0.0236, 0.0714 $\mu\text{g/ml}$, respectively, for telmisartan and amlodipine.

5.5.3 High-Performance Liquid Chromatography

Sujana *et al.* [64] developed and validated a simple, selective, precise, and stability-indicating reverse phase high-performance liquid chromatographic (RP-HPLC) method of an analysis of telmisartan in pure and pharmaceutical dosage form. The chromatographic conditions comprised of a reversed phase C8 column (4.6×150 mm, 3.5 μm , Make: XTerra), with a mobile phase composed of buffer and methanol (40:60, v/v, adjusted the pH to 3.0 with ortho phosphoric acid).

Flow rate was 0.5 ml/min, detection was carried out at 230 nm. The retention time of telmisartan was 2.6 min. The linear regression analysis data for the calibration plots showed good linear relationship in the concentration range of 20–100. The values of correlation coefficient, slope, and intercept were 0.9998, 2.326, and -6.708 , respectively.

Vijayamirtharaj *et al.* [65] developed a RP-HPLC method for the determination of telmisartan and atorvastatin calcium in bulk and in formulation using UV detector. Selected mobile phase was a combination of acetonitrile: buffer (0.01 M potassium dihydrogen phosphate) 65:35, pH 4.00 (adjusted with orthophosphoric acid), and the wavelength selected was 250 nm. The flow rate was kept at 2.0 ml/min, and the injection volume was 10 μl . The separation was performed at ambient temperature. Retention time of

telmisartan and atorvastatin calcium was found to be 3.72 and 6.14 min, respectively. Linearity of the method was found to be 319–480 µg/ml for telmisartan and 86–130 µg/ml for atorvastatin calcium. The correlation coefficient of telmisartan was found to be 0.9998 and the correlation coefficient of atorvastatin calcium was found to be 0.9999. Accuracy of the method was determined through recovery studies by adding known quantities of standard drug to the preanalyzed test solution and was found to be 98.92–100.02 for telmisartan and 99.93–100.96 for atorvastatin calcium, respectively. The system suitability parameters such as theoretical plates and tailing factor were found to be 6347, 1.652, and 9720, 1.394, respectively, for telmisartan and atorvastatin calcium. This method was validated according to ICH guidelines.

Kurade *et al.* [66] described a rapid high-performance liquid chromatographic method for the estimation of ramipril and telmisartan simultaneously in combined dosage form. A Genesis C18 column having dimensions of 4.6×250 mm and particle size of 5 µm in isocratic mode, with mobile phase containing a mixture of 0.01 M potassium dihydrogen phosphate buffer (adjusted to pH 3.4 using orthophosphoric acid):methanol:acetonitrile (15:15:70, v/v/v) was used.

The mobile phase was pumped at a flow rate of 1.0 ml/min and the eluents were monitored at 210 nm. The selected chromatographic conditions were found to effectively separate ramipril (RT: 3.68 min) and telmisartan (RT: 4.98 min) having a resolution of 3.84. The method was validated in terms of linearity, accuracy, precision, and specificity, limit of detection, and limit of quantitation. Linearity for ramipril and telmisartan were found in the range of 3.5–6.5 and 28.0–52.0 µg/ml, respectively. The percentage recoveries for ramipril and telmisartan ranged from 99.09–101.64% to 99.45–100.99%, respectively. The limit of detection and the limit of quantitation for ramipril were found to be 0.5 and 1.5 µg/ml, respectively, and for telmisartan were found to be 1.5 and 3.0 µg/ml, respectively. The method was found to be robust and can be successfully used to determine the drug content of marketed formulations.

Wankhede *et al.* [67] described a validated RP-HPLC method for simultaneous estimation of telmisartan and hydrochlorothiazide in tablet formulation. Chromatography was performed on a ODS Hypersil C18 (25 cm \times 4.6 mm I.D.) column from Thermo in isocratic mode with mobile phase containing acetonitrile:0.05 M KH_2PO_4 , pH 3.0 (60:40). The flow rate was 1.0 ml/min and the eluent was monitored at 271 nm. The selected chromatographic conditions were found to effectively separate telmisartan

(RT: 5.19 min) and hydrochlorothiazide (RT: 2.97 min). Linearity for telmisartan and hydrochlorothiazide were found in the range of 4.1–20.48 and 1.28–6.4 µg/ml, respectively. The proposed method was found to be accurate, precise, reproducible, and specific and can be used for simultaneous analysis of these drugs in tablet formulation.

Charde *et al.* [68] developed and validated a simple, rapid, precise, sensitive, and reproducible RP-HPLC method for determination of telmisartan in tablet dosage form.

Chromatographic separation was achieved on a 250 × 4.6 mm, 5 µm, Waters symmetry column in gradient mode, with mobile phase consisting of a mixture of solution (10 mM potassium dihydrogen phosphate, pH 3.5 ± 0.01):acetonitrile (64:40) was used.

The quantitation performed at flow rate of 1.0 ml/min at 230 nm and run time was 12 min. The analytical method was validated as per ICH guideline for linearity, accuracy, precision, specificity, limit of detection, limit of quantification, robustness, and stability, and method can be extended to the analysis of telmisartan in tablet formulations. The relative standard deviation values for precision was less than 2%, and % recovery was greater than 98% for telmisartan. The drug undergoes oxidative degradation, thermal degradation, and in alkali medium.

Li *et al.* [69] developed a rapid, selective, and sensitive method for the determination of telmisartan, in human plasma, telmisartan and the internal standard, diphenhydramine, were extracted from plasma using diethyl ether–dichloromethane (60:40, v/v), and separated on a Zorbax extend C18 column using methanol–10 mM ammonium acetate (85:15, v/v) adjusted to pH 4.5 after mixing with formic acid as mobile phase. Detection was carried out by multiple reactions monitoring on a Q-trap™ LC–MS/MS system with an ESI interface. The assay was linear over the range 0.5–600.0 ng/ml with a limit of quantitation of 0.5 ng/ml and a limit of detection of 0.05 ng/ml. Intra- and interday precision were <6.7% and <8.1%, respectively, and the accuracy was in the range of 88.9–111.0%. The assay was applied to a pharmacokinetic study of telmisartan given as a single oral dose (80 mg) to healthy volunteers.

Zhang *et al.* [70] developed a rapid HPLC method using a monolithic column with fluorescence detection has been for determination of telmisartan in human plasma. Sample preparation was done by protein precipitation with acetonitrile and naproxen was used as internal standard. The compounds were detected by fluorescence detection, using an excitation wavelength of 300 nm and emission wavelength of 385 nm. Calibration

curves of telmisartan were linear in the range of 1–200 ng/ml. The assay was high throughput, sensitive, and precise, and it was applied to a bioequivalence study of two formulations of telmisartan.

Londhe *et al.* [71] developed a sensitive and reproducible HPLC method for quantitative analysis of telmisartan. The drug was separated from its degradation products on a C18 column at ambient temperature with methanol–water 80:20 (v/v), pH 4.0 (adjusted by addition of orthophosphoric acid), as mobile phase at a flow rate of 1.0 ml/min. Under these conditions, the retention time of telmisartan was 4.85 ± 0.05 min. Quantification on the basis of peak area was achieved by UV detection at 225 nm; calibration plots were linear in the concentration range 10–60 µg/ml. When the method was applied to a pharmaceutical formulation, there was no chromatographic interference from tablet excipients. The method was validated for precision, robustness, recovery, and limits of detection and quantification. The drug was subjected to acidic and alkaline hydrolysis, and oxidising, dry heat, wet heat, and photodegrading conditions. Because the method could effectively separate the drug from its degradation products, it can be regarded as stability indicating.

Bhat *et al.* [72] developed a simple, selective, and precise RP-HPLC method for the simultaneous determination of telmisartan and hydrochlorothiazide from pharmaceutical formulation. The mobile phase consisted of methanol and acetonitrile (70:30, v/v) at a flow rate of 1 ml/min and the wavelength of detection was 270 nm. Rabeprazole was used as an internal standard. The retention times of telmisartan, hydrochlorothiazide and rabeprazole were 1.79 ± 0.01 , 2.80 ± 0.01 , and 3.19 ± 0.01 min, respectively.

The developed method was validated according to ICH guidelines. The method can be used for determination of these drugs in combined dosage forms (Table 6).

5.5.4 Liquid Chromatography–Mass Spectrometry

Li *et al.* [69] describe Q-trap TM LC–MS/MS method for the determination of the telmisartan, in human plasma using internal standard, diphenhydramine that requires only 50 µl of plasma and allows high sample throughput due to a simple sample preparation procedure and short run time. Samples were extracted from plasma using diethyl ether–dichloromethane (60:40, v/v), and separated on a Zorbax extend C18 column using methanol–10 mM ammonium acetate (85:15, v/v) adjusted to pH 4.5 after mixing with formic acid as mobile phase. The assay was linear over the range of

Table 6 List the Condition of the Other HPLC Method That Has Been Reported for the Determination Of Drug [72–78]

Material	Column	Mobile Phase and [Flow Rate]	Detection	References
Human urine	A Waters Atlantis dC18, 10063.9 mm id, 3 lm, 100 Å. A Waters lBondapak C18 guard column 10 lm was placed in front of the analytical column	(Acetonitrile 0.1% TFA:water 0.1% TFA, 30:70, v/v) [1 ml/min]	Photodiode array detection	[73]
Tablet	Lichrospher RP-18 column (250 × 4.6 mm, 5 µm)	(20 mM Ammonium acetate containing 0.1% (v/v) triethylamine (pH: 3.0): acetonitrile) at 25 °C [1 ml/min]	UV detection at 254 nm	[74]
Rat tissue	COSMOSIL-packed column 5C18-MS-II (250 mm × 64.6 mm ID; 5lm) (NACALAI TESQUE)	ACN: 5 mM NaAc buffer solution at pH 6 (45:55, v/v) [0.6 ml/min]	Fluorescence detection λ_{ex} (300 nm), λ_{em} (370 nm)	[75]
Urine sample	Novapak C18 column 3.9 × 150 mm, 4 µm	Acetonitrile/phosphate buffer (pH 6.0, 5 mM) (45:55, v/v) [0.5 ml/min]	Fluorimetric detection λ_{ex} (305 nm), λ_{em} (365 nm)	[76]
Human plasma	Chromolith (RP-18e 100 mm × 4.6 mm, Merck, Germany) at 25 °C	(Acetonitrile: methanol:water: acetic acid) (30:20:50:0.05, v/v) [3 ml/min]	Fluorimetric detection λ_{ex} (300 nm), λ_{em} (385 nm)	[77]
Urine sample	Chromolith RP-18e monolithic column	5 mM Phosphate buffer (pH 3.8): acetonitrile: methanol (65:20:15, v/v/v) [3.0 ml/min]	Fluorescence detection λ_{ex} (259 nm), λ_{em} (399 nm)	[78]
Human plasma and urine	Betasil C18 column (250 mm × 4.6 mm i.d.; 5 µm)	Acetonitrile: 5 mM NaAc buffer solution at pH 3.5 (40:60; v/v) [1.0 ml/min]	UV detection: 250 nm λ_{em} : 380 nm, λ_{ex} : 250 nm	[79]

0.5–600.0 ng/ml with a limit of quantitation of 0.5 ng/ml and a limit of detection of 0.05 ng/ml. Intra- and interday precision were <6.7% and <8.1%, respectively, and the accuracy was in the range of 88.9–111.0%. Acceptable precision and accuracy is obtained within the standard curve range of 0.5–600.0 ng/ml. The LOD of the method is 0.05 ng/ml.

Shah and Singh [80] described specific SIAM HPLC-MS method under ICH prescribed conditions of hydrolysis (acidic, neutral, and basic), photolysis, oxidation, and thermal stress. Telmisartan showed labiality under only photo-acidic condition by forming a single degradation product. HPLC separation of the drug and the degradation product was achieved on C-8 column using gradient method. Subsequently, the degradation product peak was subjected to LC-MS/TOF and on-line H/D exchange mass studies. Based on these studies, a tentative structure was assigned to the product as 3-((1,7-dimethyl-2-propyl-1*H*,3*H*-2,5-bibenzo(*d*)imidazol-3-yl)methyl)-6*H*-benzo(*c*)chromen-6-one, which was verified through ¹H LC-NMR experiments.

Yan *et al.* [81] developed a rapid and sensitive method using liquid chromatography–tandem mass spectrometry (LC-MS/MS) for the simultaneous determination of telmisartan and hydrochlorothiazide in human plasma. Sample preparation involved liquid–liquid extraction with diethyl ether–dichloromethane (60:40, v/v). The analytes and internal standard, probenecid, were separated on a Venusil XBP-C8 column using gradient elution with acetonitrile–10 mM ammonium acetate–formic acid at a flow rate of 1.2 ml/min. Detection was by electrospray negative ionization mass spectrometry using multiple reaction monitoring of the transitions at m/z 513.0 → 469.4 for telmisartan, m/z 295.9 → 268.9 for hydrochlorothiazide, and m/z 283.9 → 239.9 for probenecid. For both analytes, the method was linear in the range of 1.00–600 ng/ml with intra- and interday precision (as relative standard deviation) ≤ 10.6% and accuracy (as relative error) ≤ 4.2%.

5.6 Determination in Body Fluids and Tissues

Li *et al.* [69] developed a rapid, selective, and sensitive method for the determination telmisartan in human plasma.

Torrealday *et al.* [76] developed a high-performance liquid chromatographic method with fluorimetric detection for the quantitation of telmisartan in urine.



6. STABILITY

Ebner *et al.* [82] characterized telmisartan 1-*O*-acylglucuronide as the principal metabolite of telmisartan in humans, in terms of chemical stability and the structure of its isomerization products was elucidated. In addition, pharmacokinetics of telmisartan 1-*O*-acylglucuronide was assessed in rats after i.v. dosing. Similar to other acylglucuronides, telmisartan 1-*O*-acylglucuronide and diclofenac 1-*O*-acylglucuronide, which was used for comparison, showed the formation of different isomeric acylglucuronides on incubation in aqueous buffer. The isomeric acylglucuronides of telmisartan consisted of the 2-*O*-, 3-*O*-, and 4-*O*-acylglucuronides (a,b-anomers). First-order degradation half-lives of 26 and 0.5 h were observed on incubation in buffer of pH 7.4 for the 1-*O*-acylglucuronides of telmisartan and diclofenac, respectively. This indicated that the 1-*O*-acylglucuronide of telmisartan was among the most stable acylglucuronides reported to date. The high stability of telmisartan 1-*O*-acylglucuronide was confirmed by in vitro experiments that indicated only very low covalent binding of telmisartan acylglucuronide to human serum albumin but a considerable amount of covalently bound radioactivity with the acylglucuronide of diclofenac.

Bhavani *et al.* [83] studied the stability of telmisartan drug substance and drug products in bulk samples and pharmaceutical dosage forms in the presence of its degradation products and impurities by gradient reverse phase ultra-performance liquid chromatographic method. Telmisartan was found to degrade significantly in acid stress condition when it was subjected for various stress conditions.

Sujana *et al.* [64] was developed a simple, selective, precise, and stability-indicating RP-HPLC method of analysis of telmisartan in pure and pharmaceutical dosage form and validated. The method was successfully validated in accordance to ICH guidelines acceptance criteria for specificity, linearity, precision, recovery, ruggedness, and robustness. The drug undergoes degradation under acidic, basic, peroxide, and thermal degradation conditions.

Patil and Shinde [84] developed a simple, rapid, precise, and stability-indicating method for the quantitative simultaneous estimation of telmisartan and hydrochlorothiazide in combined pharmaceutical dosage form. Telmisartan, hydrochlorothiazide, and their combination drug products stressed samples were analyzed by this method.



7. PHARMACOLOGY

7.1 Pharmacological Actions

Telmisartan, belongs to ARB group, which are potently and selectively inhibit most of the biological effects of Ang-II, including Ang-II-induced (1) contraction of vascular smooth muscle, (2) rapid pressor responses, (3) slow pressor responses, (4) thirst, (5) vasopressin release, (6) aldosterone secretion, (7) release of adrenal catecholamines, (8) enhancement of noradrenergic neurotransmission, (9) increases in sympathetic tone, (10) changes in renal function, and (11) cellular hypertrophy and hyperplasia. ARBs reduce arterial blood pressure in animals with renovascular and genetic hypertension, as well as in transgenic animals overexpressing the renin gene. ARBs, however, have little effect on arterial blood pressure in animals with low-renin hypertension (e.g., rats with hypertension induced by NaCl and deoxycorticosterone) [85,86]. Telmisartan recently was found to prevent adipogenesis and weight gain through activation of PPAR- δ -dependent lipolytic pathways and energy uncoupling in several tissues [87].

7.2 Pharmacokinetics Parameters

Telmisartan is rapidly absorbed from the gastrointestinal tract; the absolute oral bioavailability is dose dependent and is about 42% after a 40 mg dose and 58% after a 160 mg dose. Peak plasma levels are obtained 0.5–1 h after oral administration, and the plasma $t_{1/2}$ is \sim 24 h. Telmisartan is over 99% bound to plasma proteins. It is excreted from the circulation almost entirely in the feces via bile; mainly as unchanged drug. The plasma clearance of telmisartan affected by hepatic but not renal insufficiency [1,85].

7.3 Therapeutic Uses and Dosing

Telmisartan is used in the management of hypertension and cardiovascular risk reduction. The drug is given orally. After a dose, the hypotensive effect peaks within 3 h and persists for at least 24 h. The maximum hypotensive effect occurs within about 4 to 8 weeks after starting therapy. In hypertension, telmisartan is given in an initial dose of 40 mg once daily. This may be increased, if necessary, to a maximum dose of 80 mg once daily. Lower doses should be considered in patients with hepatic or renal impairment [1,88].

7.4 Adverse Effects and Precautions

Telmisartan and other ARBs are generally well tolerated. The incidence of angioedema and cough with ARBs is less than that with ACE inhibitors. As with angiotensin converting enzyme inhibitors, ARBs have teratogenic potential and should be discontinued in pregnancy. In patients whose arterial blood pressure or renal function is highly dependent on the RAS (e.g., renal artery stenosis), ARBs can cause hypotension, oliguria, progressive azotemia, or acute renal failure. ARBs may cause hyperkalemia in patients with renal disease or in patients taking K^+ supplements or K^+ -sparing diuretics. ARBs enhance the blood pressure-lowering effect of other antihypertensive drugs, a desirable effect but one that may necessitate dosage adjustment. There are rare postmarketing reports of anaphylaxis, abnormal hepatic function, hepatitis, neutropenia, leukopenia, agranulocytosis, pruritus, urticaria, hyponatremia, alopecia, and vasculitis.

Telmisartan should be used with caution in patients with hepatic impairment or biliary obstruction [1,85].

7.5 Interactions

Digoxin. When telmisartan was coadministered with digoxin, median increases in digoxin peak plasma concentration (49%), and in trough concentration (20%) were observed. Therefore, monitor digoxin levels when initiating, adjusting, and discontinuing telmisartan for the purpose of keeping the digoxin level within the therapeutic range, but the interaction is probably not clinically significant.

Lithium. Reversible increases in serum lithium concentrations and toxicity have been reported during concomitant administration of lithium with ARA-IIs including telmisartan. Therefore, monitor serum lithium levels during concomitant use. The antihypertensive effects of telmisartan may be potentiated by drugs or other agents that lower blood pressure [1,87,89]. Also an additive hyperkalemic effect is possible with potassium supplements, potassium-sparing diuretics, or other drugs that can cause hyperkalemia; Telmisartan and potassium-sparing diuretics should not generally be given together. *Nonsteroidal antiinflammatory drugs (NSAIDs)* should be used with caution in patients taking telmisartan as the risk of renal impairment may be increased, particularly in those who are inadequately hydrated; use of NSAIDs may also attenuate the hypotensive effect of telmisartan.

Other drugs. Coadministration of telmisartan did not result in a clinically significant interaction with acetaminophen, amlodipine, glyburide,

simvastatin, hydrochlorothiazide, warfarin, or ibuprofen. Telmisartan is not metabolized by the cytochrome P450 system and had no effects in vitro on cytochrome P450 enzymes, except for some inhibition of CYP2C19. Telmisartan is not expected to interact with drugs that inhibit cytochrome P450 enzymes; it is also not expected to interact with drugs metabolized by cytochrome P450 enzymes, except for possible inhibition of the metabolism of drugs metabolized by CYP2C19.

ACKNOWLEDGMENTS

The authors wish to express their gratitude and thanks to Dr. Abdullah A. Al-Badr, Department of Pharmaceutical Chemistry, College of Pharmacy, King Saud University, for his invaluable advice, assistance, encouragement and constant guidance, during the course of this work.

REFERENCES

- [1] S.C. Sweetman, *Martindale: The Complete Drug Reference*, thirty-sixth ed., Pharmaceutical Press, London, 2009, 1409.
- [2] <http://www.chemicalize.org/structure/#!/mol=Pritor>.
- [3] I. Halasz, R.E. Dinnebier, Structural and thermal characterization of zolpidem hemitartrate hemihydrate (form E) and its decomposition products by laboratory X-ray powder diffraction, *J. Pharm. Sci.* 99 (2) (2010) 871–878.
- [4] P. Allegrini, M. Rasparini, G. Razzetti, A. Bologna, G. Barreca, A process for the preparation of telmisartan, 2006, EP Patent 1,719,766.
- [5] T. Kalyankar, M. Khan, N. Rangari, R. Kakde, A rapid colorimetric method for the estimation of ammonia in telmisartan in bulk and solid dosage form, *Inter. J. Pharm. World Res.* 1 (2) (2010) 1–9.
- [6] <http://en.wikipedia.org/wiki/Telmisartan>.
- [7] *Pharmacopeia, British*, vol. 2, Published by British Pharmacopoeia Commission, The Stationery Office, London, 2009, pp. 5872–5877.
- [8] P.B. Patil, A. Pandey, D.B.S.A.B.R. Chaudhari, An improved, scalable and cost effective one-pot synthesis of telmisartan, *Int. J. Res. Pharm. Biomed. Sci.* 4 (2013) 293–295.
- [9] <http://www.drugbank.ca/drugs/DB00966>. Drug Bank.
- [10] A.C. Moffat, M.D. Osselton, B. Widdop, *Clarke's Analysis of Drugs and Poisons*, Pharmaceutical Press, London, 2005.
- [11] U.J. Ries, G. Mihm, B. Narr, K.M. Hasselbach, H. Wittneben, M. Entzeroth, J.C.A. van Meel, W. Wienen, N.H. Huel, 6-Substituted benzimidazoles as new non-peptide angiotensin II receptor antagonists: synthesis, biological activity, and structure-activity relationships, *J. Med. Chem.* 36 (25) (1993) 4040–4051.
- [12] C. Xia, F.G. Ling, R.Y. Ming, Improved synthesis of telmisartan, *Chin. J. Pharm.* 6 (2003) 001.
- [13] S. Venkataraman, V. Thippannachar, S.R. Kikkuru, S. Neti; R.R. Chinta, M. Arunagiri, L.K. Routhu, Process for preparing Telmisartan, 2007, US 2007/0287840 A1.
- [14] S. Chava, S. Gorantla, S. Gijupalli, B. Prasanna, A process for the preparation of Telmisartan, 2007, WO Patent 2,007,010,558.
- [15] L.J. Goossen, T. Knauber, Concise synthesis of telmisartan via decarboxylative cross-coupling, *J. Org. Chem.* 73 (21) (2008) 8631–8634.
- [16] A.S. Kumar, S. Ghosh, R. Soundararajan, G. Mehta, An improved synthesis of telmisartan: an antihypertensive drug, *ARKIVOC* 10 (2009) 247–254.

- [17] (a) N. Miyaara, A. Suzuki, Palladium-catalyzed cross-coupling reactions of organoboron compounds, *Chem. Rev.* 95 (7) (1995) 2457–2483. (b) A. Suzuki, Recent advances in the cross-coupling reactions of organoboron derivatives with organic electrophiles, 1995–1998, *J. Organomet. Chem.* 576 (1) (1999) 147–168. (c) The Stille reaction has also been widely applied in biaryl synthesis: S.P. Stanfort, *Tetrahedron*, 54 (1998) 263. (d) J.P. Genet, M. Savignac, Recent developments of palladium(0) catalyzed reactions in aqueous medium, *J. Organomet. Chem.* 576 (1) (1999) 305–317. (e) M.G. Johnson, R. Foglesong, The preparation of hindered biphenyls via the Suzuki reaction, *Tetrahedron letters*, 38 (40) (1997) 7001–7002. (f) S. Caron, J.M. Hawkins, Directed ortho metalation of neopentyl benzoates with LDA: preparation of arylboronic acids, *J. Org. Chem.* 63 (7) (1998) 2054–2055. (g) V. Snieckus, Directed ortho metalation. Tertiary amide and O-carbamate directors in synthetic strategies for poly-substituted aromatics, *Chem. Rev.* 90 (1990) 879.
- [18] For recent examples, see: (a) C. Dupuis, K. Adiey, L. Charruault, V. Michelet, M. Savignac, J.-P. Genet, Suzuki cross-coupling of arylboronic acids mediated by a hydrosoluble Pd (0)/TPPTS catalyst, *Tetrahedron Lett.* 42 (37) (2001) 6523–6526. (b) M. Feuerstein, H. Doucet, M. Santelli, Tetraphosphine/palladium-catalysed Suzuki cross-coupling with sterically hindered aryl bromides and arylboronic acids, *Tetrahedron Lett.* 42 (38) (2001) 6667–6670. (c) K.H. Shaughnessy, R.S. Booth, Sterically demanding, water-soluble alkylphosphines as ligands for high activity Suzuki coupling of aryl bromides in aqueous solvents, *Org. Lett.* 3 (17) (2001) 2757–2759. (d) G.Y. Li, The first phosphine oxide ligand precursors for transition metal catalyzed cross-coupling reactions: C–C, C–N, and C–S bond formation on unactivated aryl chlorides, *Angew. Chem. Int. Ed.* 40 (8) (2001) 1513–1516. (e) R.B. Bedford, C.S. Cazin, Highly active catalysts for the Suzuki coupling of aryl chlorides, *Chem. Commun.* 17 (2001) 1540–1541. (f) B. Vaz, R. Rosana, M. Nieto, A.I. Paniello, A.R. deLera, Suzuki cross-coupling of meso-dibromoporphyrins for the synthesis of functionalized A 2 B 2 porphyrins, *Tetrahedron Lett.* 42 (42) (2001) 7409–7412. (g) Wang, W., C. Xiong, J. Yang, V.J. Hruby, Practical, asymmetric synthesis of aromatic-substituted bulky and hydrophobic tryptophan derivatives, *Tetrahedron Lett.* 42 (44) (2001) 7717–7719. (h) M.A. Zhuravel, S.T. Nguyen, Preparation of 3-aryl-substituted salicylaldehydes via Suzuki coupling, *Tetrahedron Lett.* 42 (45) (2001) 7925–7928. (i) J.M. Schomaker, T.J. Delia, Arylation of halogenated pyrimidines via a Suzuki coupling reaction, *J. Org. Chem.* 66 (21) (2001) 7125–7128. (j) M.R. Netherton, G.C. Fu, Air-stable trialkylphosphonium salts: simple, practical, and versatile replacements for air-sensitive trialkylphosphines. Applications in stoichiometric and catalytic processes, *Org. Lett.* 3 (26) (2001) 4295–4298. (k) J. Yin, M.P. Rainka, X. Zhang, S.L. Buchwald, *J. Am. Chem. Soc.* 124 (2002) 1162. (l) G.A. Molander, M.R. Rivero, Suzuki cross-coupling reactions of potassium alkenyltrifluoroborates, *Org. Lett.* 4 (1) (2002) 107–109.
- [19] S. Venkataraman, V.T. Mathad, S.R. Kikkuru, S. Neti, R.R. Chinta, M. Arunagiri, L.K. Routhu, *KPCT WO 06/044754A2*, 2006.
- [20] S. Venkataraman, V.T. Mathad, S.R. Kikkuru, S. Neti, R.R. Chinta, B. Apuraba, Y. Anjaneyulu, K. Naveenkumar, An efficient and impurity-free process for telmisartan: an antihypertensive drug, *Org. Process Res. Dev.* 11 (1) (2007) 81–85.
- [21] A. Marxer, H.R. Rodriguez, J.M. McKenna, H.M. Tsai, Spiro piperidines. I. Synthesis of Spiro [isobenzofuran-1 (3H), 4'-piperidines] and Spiro [isobenzofuran-1 (3H), 3'-piperidines], *J. Org. Chem.* 40 (10) (1975) 1427–1433.
- [22] A.S. Kumar, S. Ghosh, G. Mehta, Efficient and improved synthesis of telmisartan, *Beilstein J. Org. Chem.* 6 (1) (2010) 25.
- [23] M. Reuman, A.I. Meyers, The synthetic utility of oxazolines in aromatic substitution, *Tetrahedron* 41 (5) (1985) 837–860.
- [24] A.S. Kumar, S. Ghosh, G. Mehta, Alternative synthesis of telmisartan via Suzuki coupling, *Arch. Appl. Sci. Res.* 2 (5) (2010) 135–141.

- [25] P. Wang, G.J. Zheng, Y.P. Wang, X.J. Wang, H.G. Wei, W.S. Xiang, Highly practical and cost-efficient synthesis of telmisartan: an antihypertensive drug, *Tetrahedron* 68 (11) (2012) 2509–2512.
- [26] E. Cagigal, L. Gonzalez, R. Alonso, R. Jimenez, pKa determination of angiotensin II receptor antagonists (ARA II) by spectrofluorimetry, *J. Pharm. Biomed. Anal.* 26 (3) (2001) 477–486.
- [27] W. Wienen, M. Entzeroth, J.C. Meel, J. Stangier, U. Busch, T. Ebner, J. Schmid, H. Lehmann, K. Matzek, J. Kempthorne-Rawson, A review on telmisartan: a novel, long-acting angiotensin II-receptor antagonist, *Cardiovasc. Drug Rev.* 18 (2) (2000) 127–154.
- [28] J. Doney, Method to improve characteristics of spray dried powders and granulated materials, and the products thereby produced, 2007, WO Patent 2,007,016,435.
- [29] A. Patil, V. Keny Ramchandra, S. Saindane Dhananjay, S. Khade Trushali, B. Gavitre Bhaskar, S. Kulkarni Vivek, R. Bobe Kisan, T. Gaikwad Dinanath, Formulation and evaluation of solid dispersion of telmisartan with KOH as alkaliser by hot melt method, *J. Pharm. Biomed. Sci.* 1 (2010) 1–7.
- [30] G. Sedmak, S. Zupancic, Multilayer pharmaceutical composition comprising telmisartan and amlodipine, 2012, WO Patent 2,012,055,941.
- [31] http://www.chemicalbook.com/ChemicalProductProperty_US_CB4266172.aspx.
- [32] <http://www.drugbank.ca/drugs/DB00966>.
- [33] M. Patil, R. Keny, S. Mandlik, D. Saindane, D. Gaikwad, T. Khade, B. Gavitre, V. Kulkarni, K. Bobe, U. Gaikwad, Characterization and formulation of solid dispersion of telmisartan using NaHCO₃ by hot melt method, *IJPI's J. Pharm. Cosmetol.* 1 (3) (2011) 20–33.
- [34] J. Gaja, B.F. Sayyad, Enhancement of solubility and dissolution rate of telmisartan by using water soluble polymers, *Inventi Rapid: Pharm Tech* (2) (2013) 676.
- [35] K. Adrjanowicz, K. Grzybowska, K. Kaminski, L. Hawelek, M. Paluch, D. Zakowiecki, Comprehensive studies on physical and chemical stability in liquid and glassy states of telmisartan (TEL): solubility advantages given by cryomilled and quenched material, *Philos. Mag.* 91 (13–15) (2011) 1926–1948.
- [36] H. Schneider, M. Schneider, Polymorphs of telmisartan, 2002, Google Patents.
- [37] <http://www.lookchem.com/Telmisartan/.lookchem>.
- [38] M. Kondawar, K. Kamble, K. Raut, K. Maharshi, UV spectrophotometric estimation of amlodipine besylate and telmisartan in bulk drug and dosage form by multiwavelength analysis, *Int. J. ChemTech Res.* 3 (2011) 1274–1278.
- [39] S.H. Patil, M.V. Janjale, Novel and validated titrimetric method for determination of selected angiotensin-II-receptor antagonists in pharmaceutical preparations and its comparison with UV spectrophotometric determination, *J. Pharm. Anal.* 2 (6) (2012) 470–477.
- [40] İ.H. Taşdemir, M.A. Akay, N. Erk, E. Kılıç, Voltammetric behavior of telmisartan and cathodic adsorptive stripping voltammetric method for its assay in pharmaceutical dosage forms and biological fluids, *Electroanalysis* 22 (17–18) (2010) 2101–2109.
- [41] N.A. Alarfaj, Square-wave adsorptive stripping voltammetric determination of antihypertensive agent telmisartan in tablets and its application to human plasma, *J. Anal. Chem.* 68 (4) (2013) 335–340.
- [42] M.T. Xu, J.F. Song, N. Li, Rapid determination of telmisartan in pharmaceuticals and serum by the parallel catalytic hydrogen wave method, *Anal. Bioanal. Chem.* 377 (7–8) (2003) 1184–1189.
- [43] M. Xu, J. Song, Y. Liang, Rapid determination of telmisartan in pharmaceutical preparations and serum by linear sweep polarography, *J. Pharm. Biomed. Anal.* 34 (3) (2004) 681–687.
- [44] A. Bhat, M. Palled, M. Chatter, P.M.N. Rajesh, Difference spectrophotometric determination of telmisartan in tablet dosage forms, *Indian J. Pharm. Sci.* 68 (5) (2006) 685–686.

- [45] S. Tatane, Development of UV spectrophotometric method of telmisartan in tablet formulation, *J. Adv. Pharm. Healthcare Res.* 1 (2011) 23–26.
- [46] A. Pandey, H. Sawarkar, M. Singh, P. Kashyap, P. Ghosh, UV-spectrophotometric method for estimation of telmisartan in bulk and tablet dosage form, *Int. J. ChemTech Res.* 3 (2) (2011) 657–660.
- [47] S.D. Rathod, P. Patil, S.S. Waghmare, P. Chaudhari, UV-spectrophotometric method for estimation of telmisartan in bulk and tablet dosage form, *Int. J. Pharmaceut. Sci. Res.* 3 (10) (2012) 3936–3939.
- [48] R.K. Sharma, R.C. Chippa, R. Singh, I. Alam, Quantitative estimation of telmisartan in bulk drug and tablets by uv spectroscopy, *Int. J. Drug Res. Tech.* 2 (3) (2012) 268–272.
- [49] S. Singh, A.K. Yadav, H. Gautam, First order derivative spectrophotometric determination of telmisartan in pharmaceutical formulation, *Bull. Pharm. Res.* 2 (2) (2012) 83–86.
- [50] E.P. Kreny, R.S. Mehta, First order derivative spectrophotometric method for simultaneous estimation of Telmisartan and chlorthalidone in bulk and pharmaceutical dosage form, *Int. Res. J. Pharm.* 4 (2013) 224–228.
- [51] L.I. Bebawy, S.S. Abbas, L.A. Fattah, H.H. Refaat, Application of first-derivative, ratio derivative spectrophotometry, TLC-densitometry and spectrofluorimetry for the simultaneous determination of telmisartan and hydrochlorothiazide in pharmaceutical dosage forms and plasma, *Farmaco* 60 (10) (2005) 859–867.
- [52] K. Lakshmi, S. Lakshmi, Design and optimization of a chemometric-assisted spectrophotometric determination of telmisartan and hydrochlorothiazide in pharmaceutical dosage form, *J. Young Pharm.* 2 (1) (2010) 85–89.
- [53] G. Srihari, N. Rami Reddy, I.E. Chakravarthi, Spectrophotometric determination of telmisartan sulfate in pharmaceutical dosage forms, *Asian J. Pharm. Health Sci.* 1 (3) (2011) 142–144.
- [54] S. Kumbhar, G. Chougule, G. Gajeli, V. Tegeli, Y. Thorat, U. Shivsharan, Visible spectrophotometric determination of telmisartan from urine, *Int. J. Pharm. Sci. Res.* 2 (2011) 1254–1258.
- [55] Z. Qin, W. Niu, R. Tan, Spectrophotometric method for the determination of telmisartan with Congo red, *J. Anal. Chem.* 64 (5) (2009) 449–454.
- [56] R.G. Tulja, D.G. Sankar, L. Madhavi, B. Satyanarayana, Extractive visible spectrophotometric method for determination of telmisartan and irbesartan in bulk and pharmaceutical formulations, *Asian J. Pharm. Clin. Res.* 5 (1) (2012) 41–44.
- [57] D.M. Osbourn, D.J. Weiss, C.E. Lunte, On-line preconcentration methods for capillary electrophoresis, *Electrophoresis* 21 (14) (2000) 2768.
- [58] M.C. Breadmore, Recent advances in enhancing the sensitivity of electrophoresis and electrochromatography in capillaries and microchips, *Electrophoresis* 28 (1–2) (2007) 254–281.
- [59] L. González, U. Akesolo, R.M. Jiménez, R.M. Alonso, Application of capillary zone electrophoresis to the screening of some angiotensin II receptor antagonists, *Electrophoresis* 23 (2) (2002) 223–229.
- [60] S. Hillaert, W. Van den Bossche, Optimization and validation of a capillary zone electrophoretic method for the analysis of several angiotensin-II-receptor antagonists, *J. Chromatogr. A* 979 (1–2) (2002) 323–333.
- [61] C. Prabhu, G.S. Subramanian, A. Karthik, S. Kini, M.S. Rajan, N. Udupa, Determination of telmisartan by HPTLC—a stability indicating assay, *JPC J. Plan. Chromatogr. Modern TLC* 20 (6) (2007) 477–481.
- [62] N. Vekariya, G. Patel, H. Bhatt, M. Patel, R. Dholakiya, G. Ramani, Application of TLC-densitometry method for simultaneous estimation of telmisartan and amlodipine besylate in pharmaceutical dosage form, *Int. J. Pharm. Tech. Res* 1 (4) (2009) 1644–1649.

- [63] A.R. Chabukswar, S.C. Jagdale, S. Kumbhar, V.J. Kadam, V.D. Patil, B.S. Kuchekar, P. Lokhande, Simultaneous HPTLC estimation of telmisartan and amlodipine besylate in tablet dosage form, *Arch. Appl. Sci. Res.* 2 (2010) 94–100.
- [64] K. Sujana, D. Gowri Sankar, O. Bala Souri, G. Swathi Rani, Stability indicating RP-HPLC method for the determination of telmisartan in pure and pharmaceutical formulation, *Int. J. Pharm. Pharm. Sci.* 3 (2) (2011) 164–167.
- [65] R. Vijayamirtharaj, J. Ramesh, B. Jayalakshmi, H.B. Hashim, Development and validation of RP-HPLC method for the simultaneous estimation of telmisartan and atorvastatin calcium in tablet dosage forms, *Int. J. Comprehens. Pharm.* 1 (4) (2010) 1–4.
- [66] V. Kurade, M. Pai, R. Gude, RP-HPLC estimation of ramipril and telmisartan in tablets, *Indian J. Pharm. Sci.* 71 (2) (2009) 148.
- [67] S.B. Wankhede, M. Tajne, K. Gupta, S.G. Wadodkar, RP-HPLC method for simultaneous estimation of telmisartan and hydrochlorothiazide in tablet dosage form, *Indian J. Pharm. Sci.* 69 (2) (2007) 298.
- [68] M.S. Charde, A. Gupta, R. Chakole, Determination of telmisartan and forced degradation behavior by RP-HPLC in tablet dosage form, *Int. J. Adv. Pharm. Anal.* 1 (2) (2012) 38–44.
- [69] L. Pengfei, Y. Wang, Y. Wang, Y. Tang, J.P. Fawcett, Y. Cui, J. Gu, Determination of telmisartan in human plasma by liquid chromatography–tandem mass spectrometry, *J. Chromatogr. B* 828 (1) (2005) 126–129.
- [70] H. Zhang, Y. Jiang, J. Wen, T. Zhou, G. Fan, Y. Wu, Rapid determination of telmisartan in human plasma by HPLC using a monolithic column with fluorescence detection and its application to a bioequivalence study, *J. Chromatogr. B* 877 (29) (2009) 3729–3733.
- [71] S. Londhe, N. Kaul, H. Agrawal, K. Mahadik, Stability-indicating RP-HPLC method for analysis of telmisartan in the bulk drug and in formulations, *Acta Chromatogr.* 22 (4) (2010) 539–548.
- [72] L.R. Bhat, R.K. Godge, A.T. Vora, M.C. Damle, Validated RP-HPLC method for simultaneous determination of telmisartan and hydrochlorothiazide in pharmaceutical formulation, *J. Liq. Chromatogr. Relat. Technol.* 30 (20) (2007) 3059–3067.
- [73] N. Ferreiros, G. Iriarte, R.M. Alonso, R.M. Jimenez, E. Ortiz, Separation and quantitation of several angiotensin II receptor antagonist drugs in human urine by a SPE-HPLC–DAD method, *J. Sep. Sci.* 31 (4) (2008) 667–676.
- [74] R. Nageswara Rao, K. Guru Prasad, C. Gangu Naidu, P.K. Maurya, Development of a validated liquid chromatographic method for determination of related substances of telmisartan in bulk drugs and formulations, *J. Pharm. Biomed. Anal.* 56 (3) (2011) 471–478.
- [75] J. Nie, Q. Zhao, J. Huang, B. Xiang, Y.Q. Feng, Determination of telmisartan in rat tissues by in-tube solid-phase microextraction coupled to high performance liquid chromatography, *J. Sep. Sci.* 29 (5) (2006) 650–655.
- [76] N. Torrealday, L. Gonzalez, R. Alonso, R. Jimenez, E. Ortiz Lastra, Experimental design approach for the optimisation of a HPLC–fluorimetric method for the quantitation of the angiotensin II receptor antagonist telmisartan in urine, *J. Pharm. Biomed. Anal.* 32 (4) (2003) 847–857.
- [77] Y.L. Shen, F. Feng, J. Wu, Evaluation of HPLC–fluorescence and LC–ESI/MS for determination of telmisartan in human plasma, *Yaowu Fenxi Zazhi* 26 (1) (2006) 71–75.
- [78] M. del Rosario Brunetto, Y. Contreras, S. Clavijo, D. Torres, Y. Delgado, F. Ovalles, C. Ayala, M. Gallignani, J.M. Estela, V.C. Martin, Determination of losartan, telmisartan, and valsartan by direct injection of human urine into a column-switching liquid chromatographic system with fluorescence detection, *J. Pharm. Biomed. Anal.* 50 (2) (2009) 194–199.

- [79] J. Nie, M. Zhang, Y. Fan, Y. Wen, B. Xiang, Y.-Q. Feng, Biocompatible in-tube solid-phase microextraction coupled to HPLC for the determination of angiotensin II receptor antagonists in human plasma and urine, *J. Chromatogr. B* 828 (1) (2005) 62–69.
- [80] R.P. Shah, S. Singh, Identification and characterization of a photolytic degradation product of telmisartan using LC–MS/TOF, LC–MSⁿ, LC–NMR and on-line H/D exchange mass studies, *J. Pharm. Biomed. Anal.* 53 (3) (2010) 755–761.
- [81] T. Yan, H. Li, L. Deng, Y. Guo, W. Yu, J.P. Fawcett, D. Zhang, Y. Cui, J. Gu, Liquid chromatographic–tandem mass spectrometric method for the simultaneous quantitation of telmisartan and hydrochlorothiazide in human plasma, *J. Pharm. Biomed. Anal.* 48 (4) (2008) 1225–1229.
- [82] T. Ebner, G. Heinzel, A. Prox, K. Beschke, H. Wachsmuth, Disposition and chemical stability of telmisartan 1-O-acylglucuronide, *Drug Metab. Dispos.* 27 (10) (1999) 1143–1149.
- [83] V. Bhavani, T.S. Rao, S. Raju, B. Madhusudan, J. Begum, Stability indicating UPLC method for the estimation of telmisartan related substances in tablets formulation, *Int. J. Sci. Res. Pub.* 3 (2) (2013) 2250–3153.
- [84] K.R. Patil, D.B. Shinde, Stability-indicating LC method for the simultaneous determination of telmisartan and hydrochlorothiazide in dosage form, *J. Chil. Chem. Soc.* 57 (1) (2012) 1017–1021.
- [85] L.L. Bruntoni, Goodman and Gilman's the pharmacological basis of therapeutics, *JAMA* 12 (2011) 1732–1734.
- [86] C. Csajka, T. Buclin, H.R. Brunner, J. Biollaz, Pharmacokinetic-pharmacodynamic profile of angiotensin II receptor antagonists, *Clin. Pharmacokinet.* 32 (1) (1997) 1–29.
- [87] H. He, D. Yang, L. Ma, Z. Luo, S. Ma, X. Feng, T. Cao, Z. Yan, D. Liu, M. Tepel, Z. Zhu, Telmisartan prevents weight gain and obesity through activation of peroxisome proliferator-activated receptor-delta-dependent pathways, *Hypertension* 55 (4) (2010) 869–879.
- [88] P. Verdecchia, F. Angeli, G. Gentile, G. Mazzotta, G. Reboldi, Telmisartan for the reduction of cardiovascular morbidity and mortality, *Expert. Rev. Clin. Pharmacol.* 4 (2) (2011) 151–161.
- [89] <http://dailymed.nlm.nih.gov/dailymed/lookup.cfm?setid=3bb7bc69-7752-4c16-9c60-e61eb5355a4d>.



Valsartan

Febry Ardiana*, **Suciati[†]**, **Gunawan Indrayanto^{†,1}**

*Research & Development, Bernofarm Pharmaceutical Company, Buduran-Sidoarjo, Indonesia

[†]Faculty of Pharmacy, Airlangga University, Dharmawangsa Dalam, Surabaya, Indonesia

¹Corresponding author: e-mail address: gunawanindrayanto@yahoo.com

Contents

1. General Information	432
1.1 Solubility	432
1.2 Chemical Name	432
1.3 Synonym	432
1.4 CAS Number	433
1.5 pK_a and Partition Coefficient	433
1.6 Proprietary Preparations	433
1.7 Structural Formula	433
1.8 Molecular Formula, Molecular Weight, and Elementary Analysis	433
2. Thermal Analysis	433
3. Polymorph	435
4. Related Compounds and Impurities	436
5. Spectroscopy	440
5.1 Ultraviolet Spectroscopy	440
5.2 Infrared Spectroscopy	446
5.3 Mass Spectroscopy	446
5.4 Nuclear Magnetic Spectroscopy	449
6. Compendial Method	450
6.1 Identification Test	450
6.2 Related Compounds	453
6.3 Assay	454
6.4 Dissolution Test	454
7. Method of Analysis	455
7.1 Spectrophotometer	455
7.2 Capillary Electrophoresis	456
7.3 High-Performance Liquid Chromatography	457
7.4 Thin-Layer Chromatography	457
8. Analysis of Valsartan in Biological Fluids and Herbal Preparation	469
Acknowledgments	486
References	486



1. GENERAL INFORMATION

Valsartan is an antihypertensive drug which selectively inhibits angiotensin receptor type II [1,2]. This tetrazole derivative was first developed by Novartis and marketed under brand name Diovan[®] [3]. This compound is orally active and is rapidly absorbed after oral doses, having a bioavailability of approximately 23% [4].

Valsartan appears as a white or almost white hygroscopic powder [5]. This compound must be kept in an air-tight container and should be protected from light and heat [6].

It is available in film-coated tablets containing valsartan 40, 80, 160, or 320 mg, and capsules with dosage of 80 or 160 mg. Tablet combinations of valsartan with hydrochlorothiazide or amlodipine are also available [3,7].

1.1 Solubility

Valsartan is practically insoluble in water, sparingly soluble in methylene chloride, and freely soluble in anhydrous ethanol and methanol [3,5]. Solubility of valsartan in water is affected by pH; solubility in pH 4.07, 7.02, 9.18, and 10.06 are 56.6, 62.8, 71.6, and 100.0 mg/100 mL, respectively [8].

1.2 Chemical Name

N-(1-Oxophentyl)-*N*-[[2'-(1*H*-tetrazole-5-yl)[1,1'-biphenyl]-4-yl]methyl]-L-valine
L-Valine, *N*-(1-oxopentyl)-*N*-[[2'-(1*H*-tetrazol-5-yl)[1,1'-biphenyl]-4-yl]methyl]
N-[*p*-(*o*-1*H*-Tetrazol-5-yl)phenyl]benzyl]-*N*-valeryl-L-valine
 (2*S*)-3-Methyl-2-[pentanoyl[[2'-(1*H*-tetrazol-5-yl)biphenyl-4-yl]methyl]amino]butanoic acid
 3-Methyl-2-[pentanoyl-[[4-[2-(2*H*-tetrazol-5-yl)phenyl]phenyl]methyl]amino]butanoic acid
N-Pentanoyl-*N*-[[2'-(1*H*-tetrazol-5-yl)biphenyl-4-yl]methyl]-L-valine
 (*S*)-*N*-(1-Carboxy-2-methylprop-1-yl)-*N*-pentanoyl-*N*-[2'-(1*H*-tetrazol-5-yl)-biphenyl-4-ylmethyl]amine [2,4-6,9].

1.3 Synonym

CGP-48993, Diovan[®], and Tareg[®] [1,4,9]

1.4 CAS Number

137862-53-4 [4–6]

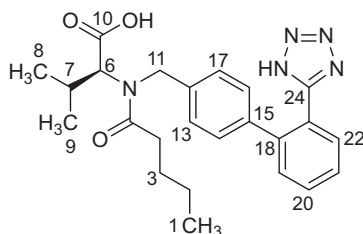
1.5 pK_a and Partition Coefficient

The pK_a of valsartan is 4.9 [10]; partition coefficient in octanol–water system is 22.2; *n*-octanol–phosphate buffer is 0.033 [8,9]

1.6 Proprietary Preparations

Diovan[®], Co-Diovan[®] (combination with hydrochlorothiazide), and Exforge (combination with amlodipine) [3,4]

1.7 Structural Formula



1.8 Molecular Formula, Molecular Weight, and Elementary Analysis

Molecular formula: $C_{24}H_{29}N_5O_3$ [4–6]

Molecular weight: 435.52 [6]

Elementary analysis: HRMS (calculated): 436.23432 $[M + H]^+$ [11].

C: 66.19%, H: 6.71%, N: 16.08%, and O: 11.02% [9].



2. THERMAL ANALYSIS

The melting point of valsartan crystallized from diisopropyl ether is 116–117 °C [9]. Unfortunately, the melting point measurement of the USP valsartan RS (lot L0L195) and valsartan raw material from TEVA, India (Control No. 761120512; using a Mettler Toledo MP 70 system) did not show sharp light intensity curves (see Figure 1), so their melting points cannot be determined accurately.

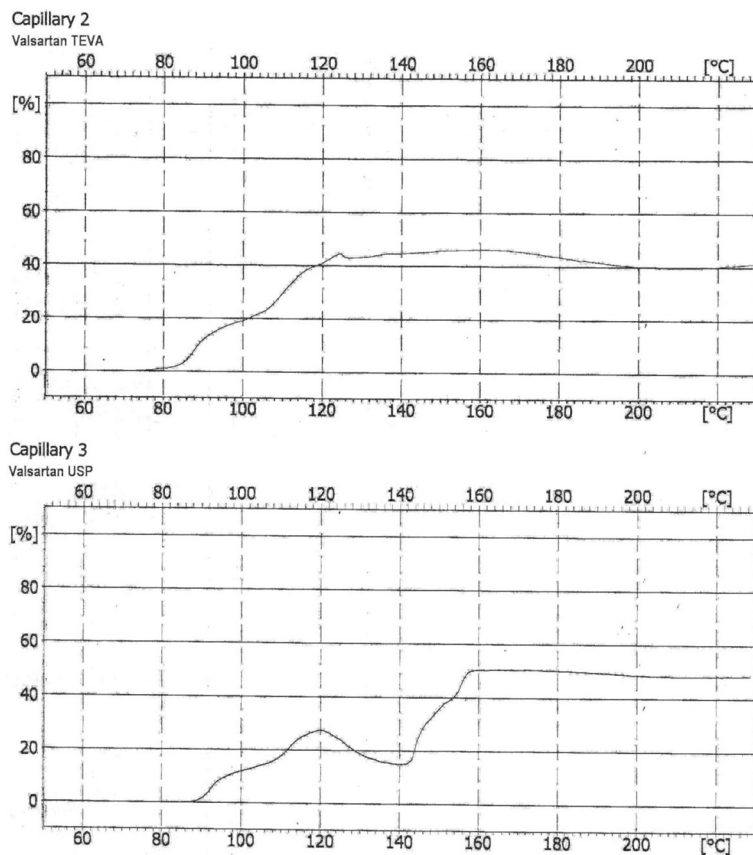


Figure 1 Light intensity curves of USP valsartan RS and valsartan bulk drug (TEVA, India) recorded on a Mettler Toledo MP 70. Y-axis: light intensity (%); X-axis: temperature (°C).

Nalluri *et al.* [12] reported that recrystallization of valsartan from methanol, ethanol, isopropanol, and acetonitrile could yield different endothermic (broad) peaks according to their DSC thermograms (75.2, 65.9, 64.6, and 80.6 °C, respectively). These results indicated that crystallization of valsartan from different solvents could yield different crystal forms. The broad endothermic peak of valsartan was reported at 102.8 °C [13] and 100.8 °C [14], while a sharp endothermic peak was reported at around 118 °C [15], 115 °C [16], and 115.77 °C [17]. Skotnicki *et al.* [18] reported that valsartan gave two endothermic peaks at approximately 80 °C (a small

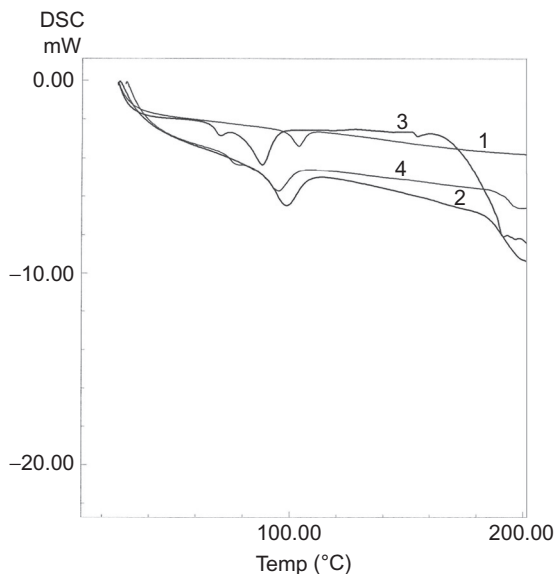


Figure 2 DSC curves of USP valsartan RS and valsartan bulk drug (TEVA, India) recorded on a DSC-60A Shimadzu Thermal Analyzer. (1) USP valsartan RS rate 20 °C/min, (2) USP valsartan RS rate 40 °C/min, (3) valsartan TEVA rate 20 °C/min, and (4) valsartan TEVA rate 40 °C/min.

broad peak) and at 100.6 °C (a sharp peak). These peaks are related to water evaporation and enthalpy relaxation. The glass transition of valsartan appeared at around 76 °C. [Figure 2](#) shows the DSC thermograms of USP valsartan RS and valsartan TEVA measured by using a DSC-60A Shimadzu Thermal Analyzer. The DSC of valsartan TEVA exhibits two endothermic peaks (2 and 3), which are similar to that of DSC reported by Skotnicki *et al.* [\[18\]](#). Based on our data and several published results, it can be suggested that crystal forms of valsartan available in the market are not identical.

3. POLYMORPH

Valsartan may occur in 12 different polymorphs and an amorphous form. X-Ray data of various crystal forms are presented in [Table 1](#).

Burgbacher *et al.* [\[21\]](#) reported the invention of a highly crystalline form of valsartan. The crystal was characterized by its XRPD pattern that

Table 1 X-Ray Powder Diffraction of Valsartan Polymorphs

Polymorph	Scattering Angle (Degree 2θ)	Reference
Form I	$(5.4; 13.0; 16.3; 19.5; 20.7; 23.4) \pm 0.2^\circ$	[19]
Form II	$(5.8; 12.7; 14.0; 17.6; 20.8; 22.5) \pm 0.2^\circ$	[19]
Form III	$(5.1; 10.1; 15.3; 18.6) \pm 0.2^\circ$	[19]
Form IV	$(6.2; 10.7; 14.5; 15.7; 19.0; 23.5; 24.8) \pm 0.2^\circ$	[19]
Form VI	$(5.5; 13.3; 14.3; 17.7; 21.1; 22.3) \pm 0.2^\circ$	[19]
Form VII	$(5.2; 15.2; 15.9; 18.6; 22.8; 23.6) \pm 0.2^\circ$	[19]
Form VIII	$(5.7; 13.6; 18.0)$	[19]
Form IX	$(6.3; 14.0; 17.9) \pm 0.2^\circ$	[19]
Form X	$(5.6) \pm 0.2^\circ$ broad peaks: $(15.0; 20.6) \pm 0.2^\circ$	[19]
Form XI	$(5.2; 10.5; 12.9; 13.9; 18.8) \pm 0.2^\circ$	[19]
Form XIII	$(5.1; 11.6; 15.8; 18.6; 26.2) \pm 0.2^\circ$	[19]
Amorphous	Very broad peak	[20]
Valsartan highly crystalline form	$(9.308; 10.74; 11.643; 13.854; 15.136; 16.056; 16.686; 17.643; 18.561; 19.186; 20.024; 20.567; 21.335; 21.595; 21.858; 22.879; 24.597; 25.051; 26.292; 31.032) \pm 0.2^\circ$	[21]

had a scattering angle peak ($2^\circ\theta$) about $(31.0 \pm 10.2)^\circ$; its melting point was $(140.8 \pm 3)^\circ\text{C}$. The invention stated that this highly crystalline form of valsartan can be easily dried compared to other forms of valsartan. This crystal has less residual solvent, higher stability, and better purity compared to the other forms of valsartan. The highly crystalline form of valsartan can also be characterized with SEM that showed very low water content. The quasi flower-like conglomerates and the formation of spheroid conglomerates were assumed for high flowability of the highly crystalline valsartan.



4. RELATED COMPOUNDS AND IMPURITIES

Valsartan has one chiral center in the valine moiety, and usually the pure (S)-enantiomer is used for pharmaceutical purposes. This S enantiomer

is derived from the L-valine that is used in the synthesis [22]. Method for testing enantiomer impurity is described in BP 2013 [5].

There are three related compounds or impurities described in the USP 36 [6] and BP 2013 [5]. These compounds are impurities A, B, and C in BP 2013 [5] which are identical to USP valsartan-related compound A RS, USP valsartan-related compound B RS, and USP valsartan-related compound C RS.

Nie *et al.* [23] isolated three impurities from crude valsartan, and one of the impurities was identified as impurity A. This compound may be formed by hydrolysis of a methyl ester intermediate in the last step of valsartan synthesis; the methyl group can react with the nitrogen of the tetrazole acid isostere to form impurity A. Approximately 80% of valsartan could be recovered by dissolving impurity A in methanol (pH 11) over 24 h. Impurity A described by Nie *et al.* [23] is different from impurity A in BP 2013 [5].

Sampath *et al.* [24] detected five impurities, i.e., impurities I, II, III, IV, and V from crude drug valsartan. The characterization and structure elucidation of the impurities were achieved by spectroscopic methods (IR, NMR, and MS) as well as by synthesis. The mechanism of impurities formation has been described in detail.

Mehta *et al.* [25] reported three impurities (DP-1, DP-2, and DP-3) from the results of degradation studies using acidic (in 1 N HCl), alkaline (in 2 N NaOH), neutral (in water), oxidative (in 30% H₂O₂), and photolytic studies (exposure to UV radiation). The structure of DP-1 reported by Mehta and coworkers [25] was identical to that of impurity I described by Sampath *et al.* [24].

Bianchini *et al.* [26] reported two degradation products of valsartan (DP-1 and DP-2) from exposure of valsartan to UV–VIS radiation (320 nm). DP-1 was formed by light-induced decarboxylation of valsartan, while DP-2 could be formed by further decomposition of tetrazole moiety from the loss of nitrogen and cyclization. The chemical structures of DP-1 and DP-2 are not identical to those of DP-1 and DP-2 reported by Mehta *et al.* [25].

Table 2 summarizes known impurities and related substances of valsartan, and their chemical structures are presented in Figure 3. The compendial method of separation and analysis of the impurities are summarized in Table 3. Raw pharmaceutical substances are required to have related substances or impurities less than 0.05% [24].

Table 2 Impurities and Related Compounds of Valsartan

Compound Number	Chemical Name	Other Name	Chemical Formula	Degradation Process or Formation	Ref.
1	(<i>R</i>)- <i>N</i> -Valeryl- <i>N</i> -{[2'-(1 <i>H</i> -tetrazole-5-yl)biphenyl-4-yl]-methyl} valine	Compound A RS, impurity A	C ₂₄ H ₂₉ N ₅ O ₃		[5,6]
2	(<i>S</i>)- <i>N</i> -Butyryl- <i>N</i> -{[2'-(1 <i>H</i> -tetrazole-5-yl)biphenyl-4-yl]-methyl} valine	Compound B RS, impurity C, CGP 55390	C ₂₃ H ₂₇ N ₅ O ₃		[5,6,27]
3	(<i>S</i>)- <i>N</i> -Valeryl- <i>N</i> -{[2'-(1 <i>H</i> -tetrazole-5-yl)biphenyl-4-yl]-methyl} valine benzyl ester	Compound C RS, impurity B	C ₃₁ H ₃₅ N ₅ O ₃		[5,6]
4	(<i>S</i>)- <i>N</i> -Valeryl- <i>N</i> -{[2'-(1-methyl-tetrazole-5-yl)biphenyl-4-yl]-methyl} valine	Impurity A ^a	C ₂₅ H ₃₁ N ₅ O ₃	Hydrolysis of the methyl ester in the last step of crude synthesis	[23]
5	(<i>S</i>)- <i>N</i> -(1-Carboxy-2-methylprop-1-yl)- <i>N</i> -[2'-(1 <i>H</i> -tetrazol-5-yl)-biphenyl-4ylmethyl]amine	Impurity I, DP-1 ^b	C ₁₉ H ₂₁ N ₅ O ₂	Intermediate product of valsartan Simple amide hydrolysis under acidic and neutral conditions	[24,25]
6	(<i>S</i>)- <i>N</i> -(1-Carboxy-2-methylprop-1-yl)- <i>N</i> -(5-phenylthio)pentanoyl- <i>N</i> -[2'-(1 <i>H</i> -tetrazol-5-yl)-biphenyl-4ylmethyl]amine	Impurity II	C ₃₀ H ₃₃ N ₅ O ₃ S	Intermediate product of valsartan	[24]

7	(S)-N-(1-Carboxy-2-methylprop-1-yl)-N-(5-phenyl)pentanoyl-N-[2'-(1H-tetrazol-5-yl)-biphenyl-4ylmethyl]amine	Impurity III	C ₃₀ H ₃₃ N ₅ O ₃	Condensation of impurity I with 5-phenylvaleroyl chloride in the presence of pyridin	[24]
8	(S)-N-(1-Carboxy-2-methylprop-1-yl)-N-4-pentenoyl-N-[2'-(1H-tetrazol-5-yl)-biphenyl-4ylmethyl]amine	Impurity IV	C ₂₄ H ₂₇ N ₅ O ₃	Condensation of impurity I with 4-pentanoic acid	[24]
9	(S)-N-(1-Carboxy-2-methylprop-1-yl)-N-(5-hydroxy)pentanoyl-N-[2'-(1H-tetrazol-5-yl)-biphenyl-4ylmethyl]amine	Impurity V	C ₂₄ H ₂₉ N ₅ O ₄	Condensation of impurity I with 5-chlorovaleric acid	[24]
10	n/a	DP-2 ^b	C ₁₉ H ₂₁ N ₅ O ₃	N-Dealkylation in photoneutral condition	[25]
11	n/a	DP-3 ^b	C ₂₄ H ₂₈ N ₅ O	Cyclization of tetrazole ring in photo acidic condition	[25]
12	N-[2'-(1H-Tetrazol-5-yl)-biphenyl-4ylmethyl]-N-isobutylpentanamide	DP-1	C ₂₃ H ₃₀ N ₅ O [M + H] ⁺	Photodegradation of valsartan	[26]
13	N-(Diazirinol[1,3-f]phenanthridin-4ylmethyl)-N-isobutylpentanamide	DP-2	C ₂₃ H ₂₇ N ₃ O	Photodegradation of valsartan	[26]

^aDegradation product from Nie *et al.* [23].

^bDegradation products from Mehta *et al.* [25].

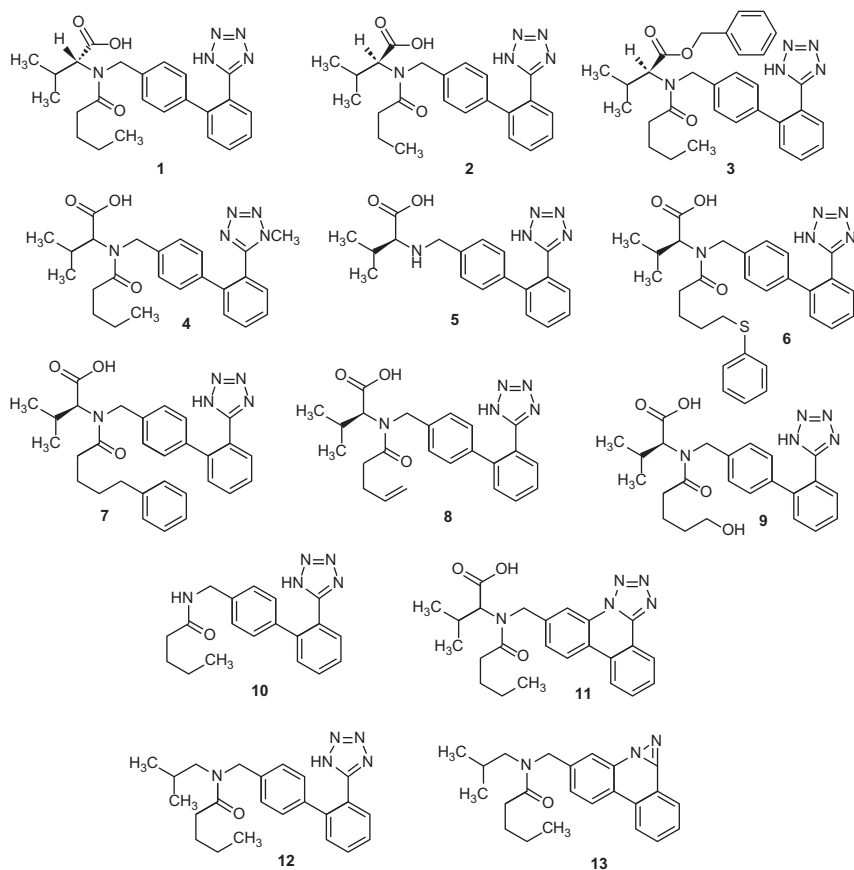


Figure 3 Chemical structures of impurities and related compound of valsartan. Compound numbers were described in [Table 2](#).



5. SPECTROSCOPY

5.1 Ultraviolet Spectroscopy

The UV spectra of valsartan in methanol (10 ppm, scanned 200–400 nm) are presented in [Figure 4](#). These spectra were recorded using a Spectrophotometer Shimadzu UV-1800 series; valsartan showed emission wavelength at 399 nm (excitation 259 nm), and the intrinsic fluorescence was decreased in basic pH [\[32\]](#).

Table 3 Compendial LC Methods and Their Validation Report

Analyte(s)	Sample	Test	Solvent	Column and Condition	Mobile Phase, Flow Rate, Injection Volume	Ref.
Valsartan	Raw material	Compendial USP assay method	Water:ACN:glacial acetic acid (500:500:1, v/v/v)	Column: L1 (125 mm × 3 mm; 5 µm) Temperature: n/a Detector: 273 nm	Water:ACN:glacial acetic acid (500:500:1, v/v/v) Flow rate: 0.4 mL/min Injection volume: 5 µL	[6]
Valsartan	Raw material	Assay method in USP/MC validation report	Water:ACN:glacial acetic acid (500:500:1, v/v/v)	Column: L10 Zorbax SB-CN (250 mm × 4.6 mm; 5 µm) Temperature: 25 °C Detector: 273 nm	Water:ACN:glacial acetic acid (500:500:1, v/v/v) Flow rate: 0.7 mL/min Injection volume: 10 µL	[28]
Valsartan-related compound A	Raw material	Compendial USP method for related compound A	<i>n</i> -Hexane:2-propanol:trifluoroacetic acid (85:15:0.1, v/v/v)	Column: L40 (250 mm × 4.6 mm; 5 µm) Temperature: n/a Detector: 230 nm	<i>n</i> -Hexane:2-propanol:trifluoroacetic acid (85:15:0.1, v/v/v) Flow rate: 0.8 mL/min Injection volume: 10 µL	[6]
Valsartan-related compounds B, C, and other related compounds	Raw material	Compendial USP method for related compounds B, C, and other related compounds	Water:ACN:glacial acetic acid (500:500:1, v/v/v)	Column: L1 (125 mm × 3 mm; 5 µm) Temperature: n/a Detector: 225 nm	Water:ACN:glacial acetic acid (500:500:1, v/v/v) Flow rate: 0.4 mL/min Injection volume: 5 µL	[6]

Continued

Table 3 Compendial LC Methods and Their Validation Report—cont'd

Analyte(s)	Sample	Test	Solvent	Column and Condition	Mobile Phase, Flow Rate, Injection Volume	Ref.
Valsartan	Raw material	Organic impurities test in USP/MC validation report	Water:ACN:acetic glacial acid (500:500:1, v/v/v)	Column: L10 Zorbax SB-CN (250 mm × 4.6 mm; 5 μm) Column oven temp: 25 °C Auto sampler temp: 4 °C Detector: 225 nm MS condition: Detector: MS Source: ES Scan (+ and –) Capillary (kv): 3.00 Cone (v): 20.0 Extractor (v): 2.0 RF lens (v): 0.1 Source temperature: 80 °C Desolvation temperature: 400 °C	Water:ACN:acetic glacial acid (500:500:1, v/v/v) Flow rate: 0.7 mL/min Injection volume: 10 μL	[28]
Valsartan	Tablet, organic impurities	Compendial USP assay method	ACN:water (1:1, v/v)	Column: L1 (250 mm × 4.6 mm; 10 μm) Column temperature: 30 °C Detector: 230 nm	Water:ACN:glacial acetic acid (50:50:1, v/v/v) Flow rate: 1.0 mL/min Injection volume: 20 μL	[6]
Valsartan	Tablet	Assay method in USP/MC validation report	Water:ACN:glacial acetic acid (500:500:1, v/v/v)	Column: L10 Zorbax SB-CN (250 mm × 4.6 mm; 5 μm) Column oven temp: 25 °C Auto sampler temp: 4 °C Detector: 225 nm	Water:ACN:glacial acetic acid (500:500:1, v/v/v) Flow rate: 0.7 mL/min Injection volume: 10 μL	[29]

Valsartan	Tablet	Organic impurities test in USP/MC validation report	Water:ACN: glacial acetic acid (500:500:1, v/v/v)	Column: L10 Zorbax SB-CN (250 mm × 4.6 mm; 5 μm) Column oven temp: 25 °C Auto sampler temp: 4 °C Detector: 225 nm MS condition: Detector: MS Source: ES Scan (+ and –) MS condition: Capillary (kv): 3.00 Cone (v): 20.0 Extractor (v): 2.0 RF lens (v): 0.1 Source temperature: 80 °C Desolvation temperature: 400 °C	Water:ACN:glacial acetic acid (500:500:1, v/v/v) Flow rate: 0.7 mL/min Injection volume: 10 μL	[29]
Valsartan, hydrochlorothiazide	Tablet, organic impurities	Compendial USP assay method	ACN:water (1:1, v/v)	Column: L1 (125 mm × 3.0 mm; 5 μm) Column temperature: n/a Detector: 265 nm	Solution A: ACN:water: trifluoroacetic acid (10:90:0.1, v/v/v) Solution B: ACN:water: trifluoroacetic acid (90:10:0.1, v/v/v) (gradient) Flow rate: 0.4 mL/min Injection volume: 10 μL	[6]

Continued

Table 3 Compendial LC Methods and Their Validation Report—cont'd

Analyte(s)	Sample	Test	Solvent	Column and Condition	Mobile Phase, Flow Rate, Injection Volume	Ref.
Valsartan, hydrochlorothiazide	Tablet	Assay method in USP/MC validation report	Solution A: 0.2% acetic acid in water Solution B: ACN Solvent: solution A: solution B (1:1, v/v)	Column: L10 Zorbax SB-CN (250 mm × 4.6 mm; 5 µm) Column oven temp: 25 °C Auto sampler temp: 10 °C Detector: 272 nm	Solution A: 0.2% acetic acid in water Solution B: ACN (gradient) Flow rate: 1 mL/min Injection volume: 10 µL	[30]
Valsartan, hydrochlorothiazide	Tablet	Organic impurities test in USP/MC validation report	Solution A: 0.2% acetic acid in water Solution B: ACN Solvent: solution A: solution B (1:1, v/v)	Column: L10 Zorbax SB-CN (250 mm × 4.6 mm; 5 µm) Column oven temp: 25 °C Auto sampler temp: 10 °C Detector: 272 nm MS condition: Detector: MS Source: ES Scan (+ and –) MS condition: Capillary (kv): 3.00 Cone (v): 25.0 Extractor (v): 2.0 RF lens (v): 0.1 Source temperature: 90 °C Desolvation temperature: 500 °C	Solution A: 0.2% acetic acid in water Solution B: ACN (gradient) Flow rate: 1 mL/min Injection volume: 10 µL	[30]

Valsartan, amlodipine	Tablet	Assay method in USP/MC validation report	Water:MeOH (3:7, v/v)	Column: L1 Purosphere Star RP18 (150 mm × 4.6 mm; 5 µm) Column oven temp: 40 °C Auto sampler temp: 10 °C Detector: 237 nm	Solution A: 25 mM ammonium acetate pH 7.5 Solution B: ACN (gradient) Flow rate: 1 mL/min Injection volume: 20 µL	[31]
Valsartan	Raw material	Organic impurities test in USP/MC validation report	Water:MeOH (3:7, v/v)	Column: L1 Purosphere Star RP18 (150 mm × 4.6 mm; 5 µm) Column oven temp: 40 °C Auto sampler temp: 10 °C Detector: 237 nm MS condition: Detector: MS Source: ES Scan (+ and –) MS condition: Capillary (kv): 3.00 Cone (v): 25.0 Source temperature: 90 °C Desolvation temperature: 500 °C	Solution A: 25 mM ammonium acetate pH 7.5 Solution B: ACN (gradient) Flow rate: 1 mL/min Injection volume: 20 µL	[31]
Valsartan	Raw material	Compendial BP method of enantiomer purity	Trifluoroacetic acid:2- propanol: hexane (0.1:15:85, v/v/v)	Column: silica gel OD for chiral separations (250 mm × 4.6 mm) Temperature: n/a Detector: 230 nm	Trifluoroacetic acid:2- propanol:hexane (0.1:15:85, v/v/v) Flow rate: 0.8 mL/min Injection volume: 5 µL	[5]
Valsartan	Raw material	Compendial BP method for related substances	Glacial acetic acid:ACN: water (1:500:500, v/v/v)	Column: end-capped octadecylsilyl silica gel (125 mm × 3.0 mm; 5 µm) Temperature: n/a Detector: 230 nm	Glacial acetic acid:ACN:water (1:500:500, v/v/v) Flow rate: 0.4 mL/min Injection volume: 10 µL	[5]

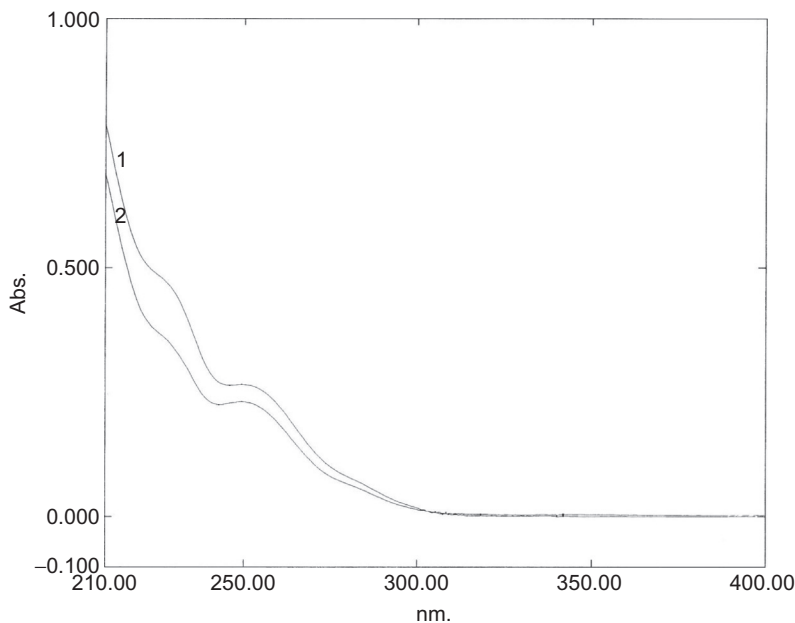


Figure 4 UV spectra of valsartan in methanol (10 ppm) recorded on a Shimadzu UV-1800 series spectrophotometer. (1) USP valsartan RS and (2) valsartan (TEVA, India).

5.2 Infrared Spectroscopy

The IR spectra of USP valsartan RS in KBr (2 mg/200 mg) pellets are shown in [Figure 5](#). IR spectra were obtained by using a Shimadzu IR Prestige-21 Spectrophotometer. The principle peaks and their assignments are listed in [Table 4](#).

Several authors used IR spectrum to characterize nanoparticles of valsartan with Eudragit[®] L 100 [33], solid dispersion of valsartan and cyclodextrin [34,35], and hydrogel formulations [13]. Data from these references suggested that the IR spectrum of valsartan bulk drug is not fully identical, which confirmed the results of DSC (see [Section 2](#)).

5.3 Mass Spectroscopy

The ESI-MS of valsartan (TEVA) is shown in [Figure 6A](#). The ESI-M-S (positive ion mode) is measured by using a UPLC Waters H Class and MS: XEVO TQD (direct injection to MS; cone voltage 30 V), while MS/MS (collision; 20 V) is presented in [Figure 6B](#). The important

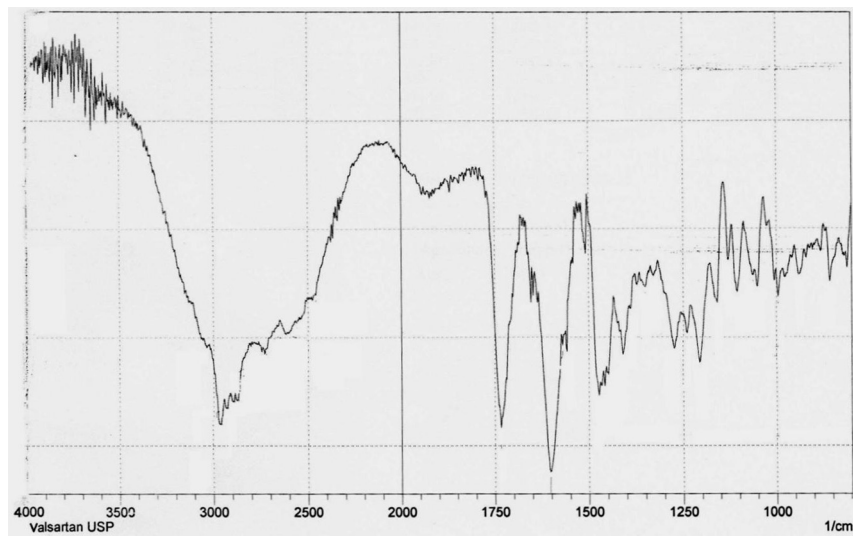


Figure 5 IR spectrum of USP valsartan RS recorded on a Shimadzu IR Prestige-21 spectrophotometer using KBr pellet sampling (2 mg/200 mg).

Frequency (cm ⁻¹)	Assignment
3035.96	O—H stretch
2873.94	C—H stretch
2927.94	C—H stretch
1734.01	C=O stretch, acid
1602.85	C=O stretch, amide
1570.06	N—N bending
1473.62	C—OH plane bend
1448.54	C—OH plane band
1390.68	C—O stretch
995.27	C—N stretch

³Assignments were compared to previous published data [13,24].

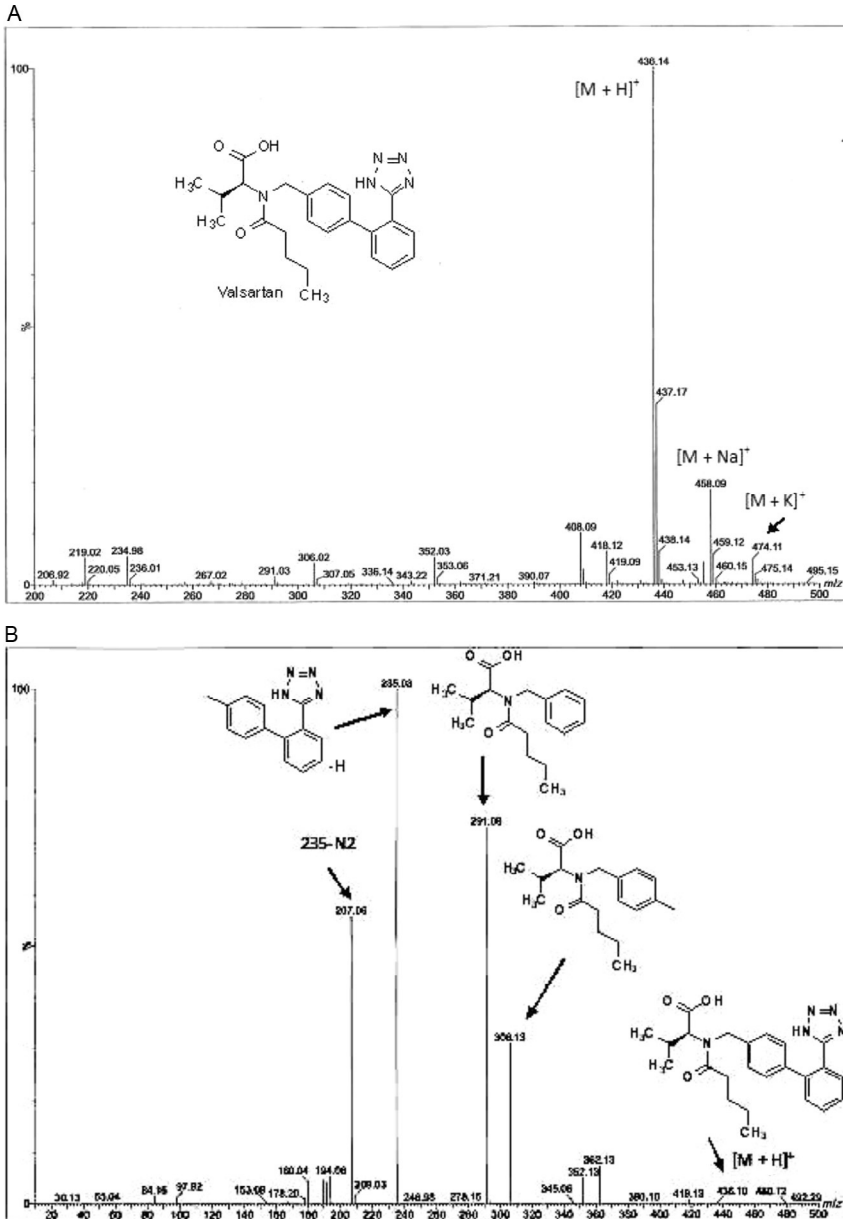


Figure 6 (A) ESI-MS spectrum of valsartan (TEVA) recorded on a UPLC Waters H Class and MS: XEVO TQD (direct injection to MS; cone voltage 30 V). (B) MS/MS spectrum of valsartan (precursor ion m/z 436, collision energy 20 V).

fragments are also described. The MS data are similar to that of described in the literature [36–39]. The ESI negative ion mode is also reported; the important fragments (m/z) are 434.25 ($M-H^-$), 390.1, 350.1, and 179.2 [40,41]. Both positive and negative ion modes are used for determination of valsartan by LC–MS/MS (see Section 8).

The EI–MS of valsartan dimethyl ester was reported by Maurer *et al.* [42]. The important fragments (m/z) were 463 ($[M]^+$, valsartan dimethyl ester), 378 $[M-57]$, 320 $[M-115]$, 268 $[M-115-57]$, and 250 $[M-115-78]$.

5.4 Nuclear Magnetic Spectroscopy

Li *et al.* [43] reported two conformations for valsartan based on the result of 2D NOESY experiment and quantum chemistry calculations. The two conformers, namely conformers A (major) and B (minor), are presented in Figure 7 (ChemBio3D Ultra 13, energy minimization with MM2 software to an RMS gradient of 0.100). These *cis/trans* isomer existed as the result of the conformational interchange via rotation around the peptide C(O)—N bond. Potamitis and coworkers [44] as well as Li *et al.* [43] suggested that the two conformers can be distinguished by NOESY experiment. A NOESY experiment was conducted on valsartan sample. In the major conformer A, NOESY cross peaks were observed from H-2, H-3, and H-4 to the methylene protons at C-11 (Figures 7 and 8). Other NOESY correlation observed was between H-4 and the aromatic proton H-13/H-17.

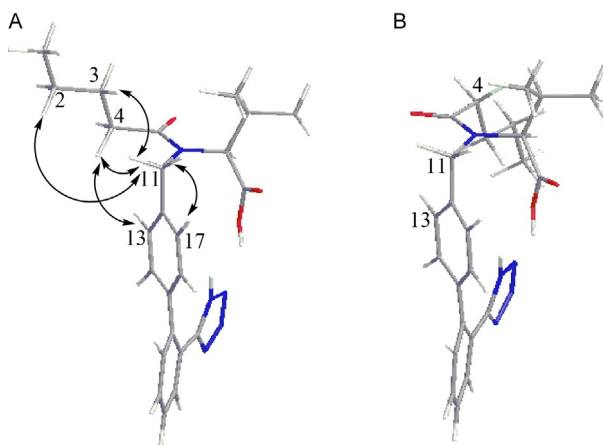


Figure 7 Conformers of valsartan and their NOESY correlation. Structures were drawn by ChemBio3D Ultra 13, energy minimization with MM2 software to an RMS gradient of 0.100: (A) major and (B) minor.

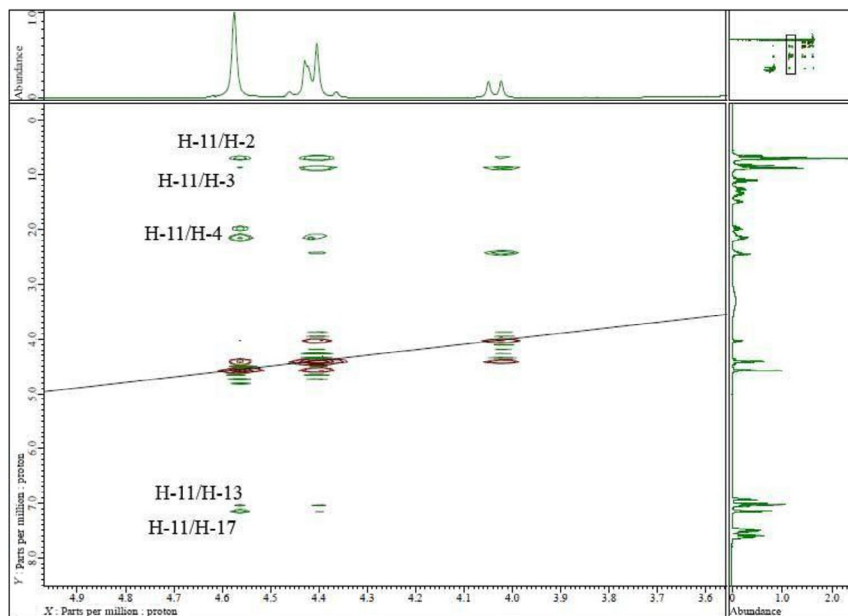


Figure 8 Selected 2D NOESY spectrum for valsartan (TEVA, India) recorded on a JEOL ECS-400, NMR spectrometer in DMSO- d_6 at 294 K with mixing time 500 ms.

These data indicated the closeness of the aliphatic *n*-butyl side chain to the aromatic ring. In the minor conformer, these NOESY correlations were absent. The composition of the two conformers was calculated at different temperature ranging from 293 to 313 K by using ^1H NMR spectroscopy. The data suggested that population of the minor conformer B increased as the temperature increased. Potamitis *et al.* [44] suggested that between 50 and 65 °C the ratio of isomer A:B is $\sim 60:40$. The ^1H and ^{13}C NMR spectra also indicated two sets of data which are presented in Table 5.



6. COMPENDIAL METHOD

6.1 Identification Test

USP 36 [6] described two methods for identification of valsartan bulk drug, i.e., IR absorption and LC system (by comparison of the retention time). This LC method has also been applied for identification of valsartan in tablets (valsartan tablets, valsartan, and hydrochlorothiazide tablets;

Table 5 NMR Data of Two Conformers of Valsartan

#	Major Conformer						Minor Conformer			
	δ_C			δ_H			δ_C		δ_H	
	CD ₃ OD ^{a,b}	DMSO- <i>d</i> ₆ ^b	DMSO- <i>d</i> ₆ ^c	CD ₃ OD ^{a,b}	DMSO- <i>d</i> ₆ ^b	DMSO- <i>d</i> ₆ ^c	CD ₃ OD ^{a,b}	DMSO- <i>d</i> ₆ ^b	CD ₃ OD ^{a,b}	DMSO- <i>d</i> ₆ ^b
1	14.5	13.6	14.1	0.84 (<i>t</i> , 7.4)	0.75	0.74 (<i>t</i> , 7.2)	14.5	13.6	0.95 (<i>t</i> , 7.4)	0.88
2	23.7	21.6	22.1	1.24	1.15	1.10–1.18	23.8	21.7	1.38	1.31
3	28.8	26.7	28.0	1.51	1.37; 1.39	1.52 (<i>sextet</i> , 6.9)	28.9	26.9	1.66	1.54
4	34.8	32.4	32.9	2.19; 2.33	2.04; 2.20	2.41–2.51 (<i>m</i>)	34.7	32.4	2.50; 2.64	2.46
5	177.5	173.4	172.4	–	–	–	177.3	173.4	–	–
6	65.2	62.9	63.4	4.58 (<i>d</i> , 10.1)	4.45	4.03 (<i>d</i> , 6.5)	68.2	65.7	4.14 (<i>d</i> , 10.7)	4.08
7	29.6	27.5	27.2	2.31	2.21	2.17 (<i>septet</i> , 6.5)	29.5	27.5	2.24	2.13
8	19.7	18.7	19.2	0.84 (<i>d</i> , 6.5)	0.75	0.73 (<i>d</i> , 6.5)	19.6	18.4	0.79 (<i>d</i> , 6.7)	0.70
9	20.9	20.0	20.5	1.00 (<i>d</i> , 6.5)	0.93	0.91 (<i>d</i> , 6.5)	20.3	19.3	1.01 (<i>d</i> , 6.5)	0.93
10	173.9	171.8	174.2	–	–	–	173.3	171.5	–	–
11	50.9	48.7	49.1	4.62; 4.80	4.62	4.41(<i>d</i> , 13.6) 4.49 (<i>d</i> , 13.6)	47.6	45.5	4.60	4.47
12	139.1	137.7	138.1	–	–	–	139.8	137.1	–	–
13	128.1	126.2	126.7	7.24	7.20	7.05 (<i>br d</i> , 8.0)	129.0	126.9	7.18	7.09
14	130.6	128.7	128.2	7.10	7.06	7.18 (<i>d</i> , 8.0)	130.1	128.2	7.02	6.97

Continued

Table 5 NMR Data of Two Conformers of Valsartan—cont'd

#	Major Conformer						Minor Conformer			
	δ_C			δ_H			δ_C		δ_H	
	CD ₃ OD ^{a,b}	DMSO- <i>d</i> ₆	DMSO- <i>d</i> ₆	CD ₃ OD ^{a,b}	DMSO- <i>d</i> ₆	DMSO- <i>d</i> ₆	CD ₃ OD ^{a,b}	DMSO- <i>d</i> ₆	CD ₃ OD ^{a,b}	DMSO- <i>d</i> ₆
15	140.0	137.7	138.2	—	—	—	139.1	138.2	—	—
16	130.6	128.7	128.7	7.10 (<i>d</i> , 8.3)	7.06	6.95 (<i>d</i> , 8.0)	130.1	128.2	7.02 (<i>d</i> , 8.3)	6.97
17	128.1	126.2	128.7	7.24 (<i>d</i> , 8.3)	7.20	7.08 (<i>d</i> , 8.0)	129.0	126.9	7.18 (<i>d</i> , 8.3)	7.09
18	143.4	141.1	141.6	—	—	—	143.6	141.3	—	—
19	132.1	130.5	129.2	7.55	7.53	7.48–7.59 (<i>m</i>)	132.1	130.5	7.53	7.53
20	131.9	130.5	131.0	7.67	7.63	7.59–7.71 (<i>m</i>)	132.8	130.5	7.66	7.63
21	129.3	127.6	127.4	7.56	7.57	7.48–7.59 (<i>m</i>)	129.2	127.6	7.54	7.57
22	132.8	130.9	131.6	7.65	7.68	7.59–7.71 (<i>m</i>)	132.0	130.9	7.64	7.68
23	124.7	123.5	123.8	—	—	—	124.5	123.5	—	—
24	156.9	155.0	155.0	—	—	—	157.0	155.0	—	—
NH	—	—	—	—	—	1.97 (<i>s</i>)				

^aData from Li *et al.* [43].

^bData from Potamitis *et al.* [44].

^cData from Bianchini *et al.* [26].

see Table 3). In addition, a TLC method has also been used for identification of valsartan and hydrochlorothiazide tablets [201]. The sample ground tablets (the weight is equivalent to a single tablet) was dissolved in a 2 mL of acetone by sonication for 5 min, followed by centrifugation. The mobile phase was a mixture of EtOAc:dehydrated alcohol:3.6 M ammonium hydroxide. The R_f of the samples should be identical to that of the standard solutions.

British Pharmacopeia 2013 [5] described three methods (A, B, and C) for identification of valsartan, i.e., (A) IR absorption, (B) enantiomeric purity, and (C) specific optical rotation. The identification must be conducted by using either methods A and B or A and C. Method B should be performed by using LC system (see Table 3). The sample used in this method contains impurity A, and the area of the impurity should not be more than the area of the principle peak in the standard solution. For method C, 0.2000 g sample was dissolved in 20 mL methanol, and the value should be between -64.0 and -69.0 .

6.2 Related Compounds

USP 36 [6] described two limit tests for valsartan-related compounds using LC methods. Test 1 is the limit test for related compound A (RS A), while test 2 is for related compound B (RS B), related compound C (RS C), and other related compounds. The percentage of the related compounds can be calculated by using the formula:

$$100(C_s/C_u)(r_u/r_s)$$

in which C_s is the concentration (mg/mL) of the valsartan-related compound A RS in the standard solutions, while C_u is the concentration of valsartan (mg/mL) in the test solutions; r_u and r_s are the peak responses of RS A from the test and standard solutions, respectively. The acceptability limit is 1%. Details of LC methods are described in Table 3.

British Pharmacopeia 2013 [5] described an LC method for determination of the impurity in bulk drugs (see Table 3). The area of impurity C should not be more than twice the area of the principle peak in the chromatogram of reference solution A (0.2%). The area of each unspecified impurity should be less than that of reference solution A (0.1%), and the area of total impurities must not be more than the reference solution A (0.3%).

6.3 Assay

USP 36 [6] described LC methods for the determination of valsartan bulk drugs, valsartan tablets, and valsartan and hydrochlorothiazide tablets. All three LC methods used the same material for column (L1) but with different dimensions and particle sizes, while mobile phases are identical. A gradient elution was applied for analysis of valsartan and hydrochlorothiazide. Details of LC conditions are presented in Table 3.

British Pharmacopeia 2013 [5] used potentiometry for assay of valsartan in bulk drugs. The sample (0.170 g) in 70 mL of 2-propanol R was then titrated with 0.1 M tetrabutylammonium hydroxide in 2-propanol. Analyses were performed under nitrogen, and the end point was determined potentiometrically. In this method, 1 mL of 0.1 M tetrabutylammonium hydroxide in 2-propanol is equivalent to 21.78 mg $C_{24}H_{29}N_5O_3$.

6.4 Dissolution Test

6.4.1 Valsartan Tablets

USP 36 [6] described the determination of valsartan in dissolution medium (phosphate buffer pH 6.8) by using spectrophotometer at UV 250 nm against blank (medium). The percentage of dissolved valsartan can be calculated by using the equation:

$$\text{Result} = (A_u/A_s) \times (C_s/L) \times V \times 100$$

A_u = absorbance of sample solution; A_s = absorbance of standard solution; C_s = concentration of USP valsartan RS in standard solution (mg/mL); L = label claim (mg/tablet); V = volume medium (1000 mL); tolerance is not less than 80% (Q value).

6.4.2 USP Valsartan and Hydrochlorothiazide Tablets

6.4.2.1 Spectrophotometer

The determination of valsartan and hydrochlorothiazide in dissolution medium (phosphate buffer pH 6.8) was performed by using spectrophotometer at UV 250 nm (valsartan) and at 272 nm (hydrochlorothiazide) against blank (medium). The percentage of the dissolved valsartan and hydrochlorothiazide can be calculated using equations:

$$\text{Valsartan : Result} = [(AT_2 \times D) - (AT_1 \times E)/(C \times D) - (B \times E)] \times 12,500$$

$$\text{Hydrochlorothiazide : Result} : [(AT_1 \times C) - (AT_2 \times B)/(D \times C) - (E \times B)] \times 80,000$$

AT_1 = absorbance of sample solution at 272 nm; AT_2 = absorbance of sample solution at 250 nm; $B = A1\% V_{272}$ absorptivity (1%, 0.2 cm, 272 nm) valsartan in medium; $C = A1\% V_{272}$ absorptivity (1%, 0.2 cm, 250 nm) valsartan in medium; $D = A1\% V_{272}$ absorptivity (1%, 0.2 cm, 272 nm) hydrochlorothiazide in medium; $E = A1\% V_{272}$ absorptivity (1%, 0.2 cm, 250 nm) hydrochlorothiazide in medium.

6.4.2.2 Liquid Chromatography

Valsartan and hydrochlorothiazide can be analyzed in dissolution medium using an LC method. The sample diluents are ACN:water (1:1). Details of the LC condition are described in Table 3. The percentage of dissolved valsartan and hydrochlorothiazide can be calculated by equation:

$$\text{Result} = (r_u/r_s) \times (C_s/L) \times D \times V \times 100$$

r_u = peak response valsartan or hydrochlorothiazide in the sample solution; r_s = peak response valsartan or hydrochlorothiazide in the standard solution; C_s = concentration of valsartan or hydrochlorothiazide in standard solution; L = label claim of valsartan or hydrochlorothiazide in tablet (mg/tablet); D = dilution factor (if applicable); V = volume of medium (1000 mL). Tolerance is 80% (Q value).



7. METHOD OF ANALYSIS

7.1 Spectrophotometer

Gupta *et al.* [45] described analysis of valsartan in bulk drugs and tablets. The standard and samples were dissolved in methanol, and the determination of analytes in samples was performed by comparing with standards and value of A (1%, 1 cm). Comparison with standards was performed by using two methods, i.e., zero-order absorption (at 250 nm) and second-order spectra (at 241 nm). Calibration ranges were linear in the range of 10–50 $\mu\text{g/mL}$ ($r=0.999$). Recovery studies were in the range of 99.08–100.31%. A statistical evaluation showed no significant difference among three methods of estimation. A similar spectrophotometric method was proposed by Kumar *et al.* [46]; in this case, the analysis was performed at λ 249 nm (in methanol), and recovery showed good values (97.77–101.4%).

Dinç *et al.* [47] reported two simultaneous spectrophotometric determination of valsartan and hydrochlorothiazide in tablets. The first method applied ratio derivative method; in this case, first amplitude derivatives were at λ 231.5 and 260.5 nm (valsartan) and 270.6 nm (hydrochlorothiazide);

mean recover for valsartan was 100.4% (RSD = 1.76%). Second method applied inverse least square absorbance matrix of zero-order spectra in the range of 225–280 nm ($\Delta\lambda = 5$ nm, at 12 wavelengths). Spectra were measured in various binary mixtures; in this case, recovery of valsartan was 101.2% (RSD = 1.58%).

Chaudhary *et al.* [48] determined valsartan and hydrochlorothiazide simultaneously in tablets by using absorption ratio method. Molar absorptivity was calculated at both wavelengths 270.5 nm (λ_{max} of hydrochlorothiazide) and 231.5 nm (isoabsorptive point). The recovery showed satisfactory results (valsartan: 99.05–102.23%; hydrochlorothiazide: 97.42–100.22%). RSD of intra- and interday precision was below 2%.

Gupta *et al.* [49] reported analysis of valsartan and amlodipine in tablets by using simultaneous equation method and absorption correction method. A simultaneous equation method was developed by using λ_{max} of valsartan (250 nm, MeOH) and amlodipine (238 nm, MeOH), while absorption correction method applied at iso-bestic wavelength of the drugs (236 nm). Recoveries were in the range of 99.48–100.13% for both spectrophotometric methods.

Ramachandran *et al.* [50] developed method for simultaneous determination of valsartan and ezetimibe in tablets by using complex formation with bromophenol blue (BPB) and bromocresol green (BCG). Valsartan–dye complex shows λ_{max} at 425 and 428 nm, respectively, while ezetimibe cannot react with both BPB and BCG. The analysis was then performed by using two wavelengths for each method of complexation (λ 425 or 428 for valsartan) and at λ_{max} for ezetimibe (250 nm). Good recovery was achieved using this method (99.3–100.3%).

Birajdar *et al.* [51] reported simultaneous determination of valsartan and nebivolol in tablets using Q method of analysis and simultaneous equations (at λ 280.2 and 246.6 nm). Isoabsorptive point of valsartan and nebivolol (at λ 275 nm) and λ 246.6 nm were selected for Q method. Recoveries for both analytes were in the range of 98.80–101.2% by using both spectrophotometric methods.

7.2 Capillary Electrophoresis

Hillaert and van den Bossche [52] described the separation of six ARA-IIs, i.e., valsartan, candesartan, eprosartan mesylate, irbesartan, losartan potassium, and telmisartan, by using capillary zone electrophoretic method

(CZE). Best separation was achieved by using 60 mM phosphate buffer pH 2.5. In 2003, these authors reported the separation of the same six ARA-IIIs by using micellar electrokinetic capillary chromatography (MEKC) in a 55 mM sodium phosphate buffer solution (pH 6.5) containing 15 mM SDS. Both CZE and MEKC methods were performed in a fused silica capillary column and detected by using UV 214 nm.

Hillaert and van den Bossche [53] also reported simultaneous analysis of combination of the six ARA-IIIs and hydrochlorothiazide by using CZE and MEKC methods. The experiments were conducted on a fused silica capillary (total length was 85 cm, 33 cm to the detector; 50 μm i.d.) and by UV 214 nm detection. The running buffers were similar to that of in the previous publications [52,54]. Sulfanilamide (CZE) and eprosartan mesylate (MEKC) were used as internal standard for a quantitative evaluation. The recovery of valsartan, losartan potassium, and irbesartan at three-level concentrations for both methods was in the range of 96.1–102.3%.

7.3 High-Performance Liquid Chromatography

Table 6 summarizes HPLC analysis of valsartan and other drugs in pharmaceutical preparations and raw materials. Most of the methods used C18 as the stationary phase.

7.4 Thin-Layer Chromatography

Silica gel has been reported as the stationary phase in most of the analysis of valsartan by (HP)TLC. The mobile phase usually contains a small amount of acid or base (ammonia), and UV was used for detection. Summary of these works is presented in Table 7.

Inglot and coworkers [102,103] reported the retention behavior of several antihypertension drugs on diol, silica, RP-8, RP-18, and CN plates in various mobile phases. The best separation on diol plate was achieved by using hexane:dioxane:formic acid (3:7:0.1, v/v/v), while a mixture of hexane:isopropanol:formic acid (4:6:0.1, v/v/v) was the best mobile phase for CN plate. An effective separation on RP-8 and RP-18 plates can be achieved by using simple mobile phase containing DMSO:phosphate buffer pH 5 (8:2, v/v). The detection limit of valsartan as determined by using densitometry at 254 nm and video densitometry were 0.1 and 0.2 $\mu\text{g}/\text{spot}$, respectively.

Table 6 Summary of HPLC Analysis of Valsartan

Analyte (s)	Sample	Solvent	Column and Condition	Mobile Phase, Flow Rate, Injection Volume	LOD, LOQ, Recovery (Rec) Valsartan	Ref.
Valsartan, hydrochlorothiazide	Tablet	ACN:acetate buffer (pH 4.0, 0.1 M; 40:60, v/v)	Column: RP Hypersil ODS (200 mm × 4.6 mm, 5 µm) Temperature: (20–25) °C Detector: 220 nm	ACN:acetate buffer (pH 4.0, 0.1 M; 40:60, v/v) Flow rate: 1.0 mL/min Injection volume: n/a	LOD: 1.0 µg/mL LOQ: n/a Rec: 99.75%	[55]
Valsartan, hydrochlorothiazide	Tablet, synthetic mixtures	MeOH	Column: Supelcosil C18 (150 mm × 4.6 mm; 5 µm) Temperature: n/a Detector: 225 nm	0.02 M Phosphate buffer pH 3.2:ACN (55:45, v/v) Flow rate: 0.9 mL/min Injection volume: 20 µL	LOD: 0.017 µg/mL LOQ: 0.058 µg/mL Rec: Tablet: 102.2% Synthetic mixtures: 100.8%	[56]
Valsartan,	Capsule	Std: ACN, diluted with mobile phase Sample: ACN	Column: Shim-pack C18 (250 mm × 4.6 mm; 10 µm) Temperature: room Detector: 265 nm	ACN:PO ₄ buffer pH 2.7 (45:55, v/v) Flow rate: 1.3 mL/min Injection volume: 20 µL	LOD: 0.2 µg/mL LOQ: 1 µg/mL Rec: 99.91%	[57]
Valsartan	Crude valsartan	MeOH	Column: ODS Hypersil C18 (200 mm × 4.6 mm; 5 µm); Temperature: ambient Detector: 254 nm MS: ESI (–) ion mode Scan range: 80–600 <i>m/z</i> 434.2 <i>m/z</i> valsartan	Acetic acid 0.2%:water (55:45, v/v) Flow rate: 1.0 mL/min Injection volume: 20 µL	LOD: n/a LOQ: n/a Rec: n/a	[23]
Valsartan, hydrochlorothiazide	Tablet, impurities	ACN:water (4:6; v/v)	Column: Hypersil 120–5 ODS (250 mm × 4.6 mm; 5 µm) Column temperature: 25 °C Detector: 256 nm	Mobile phase A: ACN: water = 10:90 (v/v, pH 2.5) Mobile phase B: ACN: water = 90:10 (pH 2.5) Gradient time program Flow rate: 1.0 mL/min Injection volume: 50 µL	LOD: 0.02 µg/mL LOQ: 0.004 µg/mL Rec: (103.7–105.3)%	[27]

Valsartan, amlodipine	Capsule	ACN:phosphate buffer (0.02 M, pH 3.0; 56:44, v/v)	Column: Kromasil RP18 (250 mm × 4.6 mm) Column temperature: 25 °C Detector: 234 nm	ACN:phosphate buffer (0.02 M, pH 3.0; 56:44, v/v) Flow rate: 1.0 mL/min Injection volume: 20 µL	LOD: 0.018 µg/mL LOQ: 0.054 µg/mL Rec: (99.09–101.79)%	[58]
Valsartan, nebivolol hydrochloride	Capsule	MeOH:1-hexanesulfonic acid monohydrate sodium salt (80:20, v/v)	Column: HIQ sil C18 ODS (250 mm × 4.6 mm, 5 µm) Temperature: ambient Detector: 289 nm	MeOH:1-hexanesulfonic acid monohydrate sodium salt (80:20, v/v) Flow rate: 1.0 mL/min Injection volume: 20 µL	LOD: 17.58 µg/mL LOQ: 53.29 µg/mL Rec: (99.08 ± 1.05)%	[59]
Valsartan, hydrochlorothiazide	Tablet	MeOH:ACN:water: isopropyl alcohol (22:18:68:2, pH 8.0, v/v/v/v)	Column: Diamonsil C18 (250 mm × 4.6 mm; 5 µm) Temperature: n/a Detector: 270 nm	MeOH:ACN:water: isopropylalcohol (22:18:68:2, pH 8.0, v/v/v/v) Flow rate: 1.0 mL/min Injection volume: 20 µL	LOD: n/a LOQ: n/a Rec: n/a	[60]
Valsartan	Raw material	n/a	Column: Kromasil C18 (250 mm × 4.6 mm, 5 µm) Temperature: n/a Detector: 265 nm	ACN:water:0.5% orthophosphoric acid (40:60, v/v) Flow rate: 1.0 mL/min Injection volume: 20 µL	LOD: 0.25 µg/mL LOQ: 1.0 µg/mL Rec: (98.76–101.30)%	[61]
Valsartan, amlodipine	Tablet	Water:ACN (50:50, v/v)	Column: Xterra RP18 (150 mm × 4.6 mm, 5 µm) Temperature: 25 °C Detector: Valsartan: UV 265 nm	A: 1000 mL water + 0.2 mL trifluoroacetic acid B: Water:ACN:trifluoroacetic acid (400:600:1, v/v/v) Flow rate: 1.5 mL/min Injection volume: 10 µL	LOD: 0.95 µg/mL LOQ: 1.6 µg/mL Rec: (99.76–99.91)%	[62]

Continued

Table 6 Summary of HPLC Analysis of Valsartan—cont'd

Analyte (s)	Sample	Solvent	Column and Condition	Mobile Phase, Flow Rate, Injection Volume	LOD, LOQ, Recovery (Rec) Valsartan	Ref.
Valsartan	Tablet	NH ₄ H ₂ PO ₄ 0.01 M, pH 3.5:MeOH (50:50, v/v)	Column: Phenomenex Gemini C18 (250 mm × 4.6 mm; 5 µm) Temperature: 25 °C Detector: 210 nm	NH ₄ H ₂ PO ₄ 0.01 M, pH 3.5: MeOH = 50:50 Flow rate: 1.0 mL/min Injection volume: 20 µL	LOD: 0.0388 µg/mL LOQ: 0.1176 µg/mL Rec: (99.63–100.587)%	[63]
Valsartan	Degradation product	MeOH	Column: HIQ sil C18 (250 mm × 4.6 mm; 5 µm) Temperature: ambient Detector: 250 nm	MeOH:water (pH 7.2; 70:30, v/v) Flow rate: 1.2 mL/min Injection volume: 20 µL	LOD: n/a LOQ: n/a Acid hydrolysis (valsartan) (98.50–100.20)% Oxidation (valsartan): (98.70–101.50)%	[64]
Valsartan, ramipril	Synthetic mixture, degradation studies	ACN:water (55:45, v/v) pH 3.6	Colum: Hypersil C18 (250 mm × 4.6 mm, 5 µm) Temperature: (25 ± 2) °C Detector: 215 nm	ACN:water = 55:45 pH 3.6 Flow rate: 1 mL/min Injection volume: 20 µL	LOD: 0.0280 µg/mL LOQ: 0.0849 µg/mL Rec: (98.42–99.34)%	[65]
Valsartan, amlodipine besylate	Tablet	ACN:phosphate buffer (50:50, v/v)	Column: Zorbax ODS (250 mm × 4.6 mm, 5 µm) Temperature: room Detector: 210 nm	ACN:phosphate buffer (50:50, v/v) Flow rate: 1.0 mL/min Injection volume: n/a	LOD: 0.36 µg/mL LOQ: 1.28 µg/mL Rec: 100.48%	[66]
Valsartan	Capsule	0.1 M phosphate buffer:ACN (20:80, v/v)	Column: Venusil XBP C18 (250 mm × 4.6 mm, 5 µm) Temperature: ambient Detector: 273 nm	0.1 M Phosphate buffer:ACN (20:80, v/v) Flow rate: 1.0 mL/min Injection volume: 20 µL	LOD: 0.5 µg/mL LOQ: 1.5 µg/mL Rec: 100.57–100.80%	[67]
Valsartan	Tablet	Water:ACN (50:50, v/v)	Column: Thermo-Hypersil ODS (150 mm × 4.6 mm; 5 µm) Temperature: 25 °C Detector: 273 nm	Water:ACN:glacial acetic acid (500:500:01, v/v/v) Flow rate: 1.0 mL/min Injection volume: 20 µL	LOD: 2.72 µg/mL LOQ: 8.25 µg/mL Rec: (99.0–100.4)%	[68]

Valsartan, nebivolol HCl	Capsule	ACN:water (1:1, v/v)	Column: Phenomenex RP C18 (250 mm × 4.6 mm, 5 µm) Temperature: n/a Detector: 275 nm	Ammonium acetate 50 mM, pH 3.5:ACN (30:70, v/v) Flow rate: 0.8 mL/min Injection volume: 50 µL	LOD: 0.032 µg/mL LOQ: 0.095 µg/mL Rec: 99.58%	[51]
Valsartan, hydrochlorothiazide	Tablet	MeOH	Column: Phenomenex Luna C18 (150 mm × 4.6 mm; 5 µm) Temperature: (20 ± 1) °C Detector: 250 nm	ACN:MeOH:PO ₄ buffer 50 mM, pH (3 ± 0.1) (20:50:30, v/v/v) Flow rate: 1.0 mL/min Injection volume: 20 µL	LOD: 0.2077 µg/mL LOQ: 0.6294 µg/mL Rec: (100.73–102.22)%	[69]
Valsartan, atorvastatin	Tablet	Diluent 1: ACN: MeOH (50:50, v/v) Diluent 2: Water: MeOH (50:50, v/v)	Column: Hypersil BDS C18 (250 mm × 4.6 mm, 5 µm) Temperature: 40 °C Detector: 225 nm	0.1% Acetic acid:ACN (50:50, v/v) Flow rate: 2.0 mL/min Injection volume: 10 µL	LOD: n/a LOQ: n/a Rec: 99.2%	[70]
Valsartan	Pure, tablet	Phosphate buffer pH 3:ACN (50:50, v/v)	Column: Xterra C18 (100 mm × 4.6 mm, 5 µm) Temperature: ambient Detector: 210 nm	Phosphate buffer pH 3:ACN (50:50, v/v) Flow rate: 1.0 mL/min Injection volume: 20 µL	LOD: 0.012 µg/mL LOQ: 0.040 µg/mL Rec: 100.2%	[71]
Valsartan	Tablet	MeOH	Column: C18 (250 mm × 4.6 mm; 5 µm) Temperature: n/a Detector: 265 nm	Ammonium dihydrogen phosphate:MeOH (33.5:66.5, v/v) Flow rate: 1.0 mL/min Injection volume: 20 µL	LOD: 6 ng/mL LOQ: 18 ng/mL Rec: (99.4–100.6)%	[72]
Valsartan, amlodipine	Tablet	MeOH	Column: Microbondapak C18 (250 mm × 4.6 mm, 5 µm) Temperature: n/a Detector: 210 nm	MeOH:potassium dihydrogen phosphate 0.1 M, pH 3.0 (65:35, v/v) Flow rate: 1.0 mL/min Injection volume: 20 µL	LOD: 0.02 µg/mL LOQ: 0.06 µg/mL Rec: (98.95–99.76)%	[73]

Continued

Table 6 Summary of HPLC Analysis of Valsartan—cont'd

Analyte (s)	Sample	Solvent	Column and Condition	Mobile Phase, Flow Rate, Injection Volume	LOD, LOQ, Recovery (Rec) Valsartan	Ref.
Valsartan	Capsule	Ammonium dihydrogen orthophosphate pH 3.5:MeOH (50:50, v/v)	Column: Inertsil C18 (250 mm × 4.6 mm, 5 µm) Temperature: room temp Detector: 210 nm	Ammonium dihydrogen orthophosphate pH 3.5: MeOH (50:50, v/v) Flow rate: 1.0 mL/min Injection volume: 20 µL	LOD: 0.056 µg/mL LOQ: 0.156 µg/mL Rec: (100.01–100.04)%	[74]
Valsartan, hydrochlorothiazide	Tablet	MeOH and mobile phase	Column: C18 Inertsil (250 mm × 4.6 mm; 10 µm) Temperature: room Detector: 259 nm	0.02 M potassium dihydrogen orthophosphate:MeOH: triethylamine (25:75:0.2, v/v/v, pH 6.0) Flow rate: 1.0 mL/min Injection volume: 20 µL	LOD: 16 µg/mL LOQ: 48 µg/mL Rec: (99.39–100.05)%	[75]
Valsartan	Tablet	Phosphate buffer: ACN=55:45	Column: Kromasil C18 (250 mm × 4.6 mm, 5 µm) Temperature: ambient Detector: 233 nm	Phosphate buffer:ACN (55:45, v/v) Flow rate: 1.0 mL/min Injection volume: 20 µL	LOD: 0.034 µg/mL LOQ: 0.104 µg/mL Rec: 99.97%	[76]
Valsartan, aliskiren hemifumarate	Tablet	ACN:0.05 M potassium dihydrogen PO ₄ buffer pH 3.5 (45:55, v/v)	Column: Hyperchrom ODS BP (200 mm × 4.6 mm, 5 µm) Temperature: n/a Detector: 224 nm	ACN:0.05 M Potassium dihydrogen PO ₄ buffer pH 3.5 (45:55, v/v) Flow rate: 1.0 mL/min Injection volume: 20 µL	LOD: 0.93 µg/mL LOQ: 2.84 µg/mL Rec: (99.32–99.92)%	[77]
Valsartan, ramipril	Capsule	MeOH	Column: RP 18 (250 mm × 4.6 mm, 5 µm) Temperature: n/a Detector: 225 nm	Phosphate buffer 1%:ACN (40:60, v/v, pH 3.2) Flow rate: 1.0 mL/min Injection volume: 20 µL	LOD: 1 µg/mL LOQ: 3 µg/mL Rec: (97.67–100.23)%	[78]

Valsartan, irbesartan, losartan potassium, telmisartan	Tablet	MeOH	Column: ACE RP-C18 (250 mm × 4.6 mm, 5 µm) Temperature: 40 °C Detector: 220 nm	Potassium dihydrogen phosphate 0.025 M, pH 6.0 (65:35, v/v) Flow rate: 1.5 mL/min Injection volume: 50 µL	LOD: 0.13 µg/mL LOQ: 0.4 µg/mL Rec: (99.87–101.35)%	[79]
Valsartan, amlodipine, hydrochlorothiazide	Tablet	ACN:phosphate buffer (0.05 M) pH 2.8 (40:60, v/v)	Column: Phenomenex Kinetex (150 mm × 4.6 mm, 5 µm) Temperature: (22–25) °C Detector: 227 nm	ACN:phosphate buffer (0.05 M) pH 2.8 (40:60, v/v) Flow rate: 0.8 mL/min Injection volume: 20 µL	LOD: 1.42 µg/mL LOQ: 4.31 µg/mL Rec: (98.9–101.0)%	[80]
Valsartan	Tablet	MeOH	Column: Phenomenex Luna C18 (250 mm × 4.6 mm; 5 µm) Temperature: n/a Detector: 210 nm	MeOH:PO ₄ buffer pH 3.0 (65:35, v/v) Flow rate: 1.0 mL/min Injection volume: 20 µL	LOD: 0.02 µg/mL LOQ: 0.06 µg/mL Rec: (98.79–99.81)%	[81]
Valsartan	Tablet	MeOH	Column: Kromasil C18 (250 mm × 4.6 mm, 5 µm) Temperature: n/a Detector: 250 nm	Gradient condition of ACN and PO ₄ buffer pH 3.5 Flow rate: 1.0 mL/min Injection volume: 20 µL	LOD: n/a LOQ: n/a Rec: (99.27–99.92)%	[82]
Valsartan, hydrochlorothiazide	Tablet	ACN:water (1:1, v/v)	Column: Xterra (250 mm × 4.6 mm, 5 µm) Temperature: room Detector: 265 nm	Ammonium acetate 0.20 M, pH 5.6:ACN (gradient elution) Flow rate: 1.5 mL/min Injection volume: 20 µL	LOD: 0.0375 µg/mL LOQ: 0.064 µg/mL Rec: (100.1–102.3)%	[83]
Valsartan	Tablet	Water:ACN (1:1, v/v)	Column: Phenomenex C18 (250 mm × 4.6 mm; 5 µm) Temperature: ambient Detector: 240 nm	ACN:5 mM ammonium acetate pH 4.5 (75:25, v/v) Flow rate: 1.0 mL/min Injection volume: 50 µL	LOD: 10 ng/mL LOQ: 28 ng/mL Rec: (99.85 ± 1.03)%	[84]

Continued

Table 6 Summary of HPLC Analysis of Valsartan—cont'd

Analyte (s)	Sample	Solvent	Column and Condition	Mobile Phase, Flow Rate, Injection Volume	LOD, LOQ, Recovery (Rec) Valsartan	Ref.
Valsartan, amlodipine besylate	Capsule	MeOH	Column: Waters Symmetry C18 (150 mm × 4.6 mm; 5 µm) Temperature: 25 °C Detector: 238 nm	MeOH:KH ₂ PO ₄ buffer 0.01 M, pH 2.5 (60:40, v/v) Flow rate: 1.0 mL/min	LOD: 44 ng/mL LOQ: 300 ng/mL Rec: (98.97–99.97)%	[85]
Valsartan, hydrochlorothiazide	Tablet	0.02 M Phosphate buffer:ACN: MeOH = 50:40:10	Column: Supelcosil C18 (150 mm × 4.6 mm; 5 µm) Temperature: ~25 °C Detector: 225 nm	0.02 M Phosphate buffer pH 2.9:ACN:MeOH (50:40:10, v/v/v) Flow rate: 1.4 mL/min Injection volume: 50 µL	LOD: n/a LOQ: n/a Rec: 99.94%	[86]
Valsartan	Tablet	KH ₂ PO ₄ buffer: ACN (pH 3.0 ± 0.1, 55:45, v/v)	Column: Xterra C18 (150 mm × 4.6 mm; 5 µm) Temperature: 23 ± 1 °C Detector: 286 nm	KH ₂ PO ₄ buffer:ACN (pH 3.0 ± 0.1, 55:45, v/v) Flow rate: 0.7 mL/min Injection volume: 20 µL	LOD: 0.0180 µg/mL LOQ: 0.01016 µg/mL Rec: (99.40–99.68)%	[87]
Valsartan, ramipril	Capsule	n/a	Column: Hypersil C18 (150 mm × 4.6 mm, 5 µm) Temperature: n/a Detector: 220 nm	20 mM Phosphate buffer: ACN (35:65, v/v) Flow rate: 0.8 mL/min Injection volume: 20 µL	LOD: n/a LOQ: n/a Rec: (98.4–99.6)%	[88]
Valsartan, amlodipine besilate, olmesartan medoxomil, hydrochlorothiazide	Tablet	MeOH diluted with ACN MeOH water (7:13:80, v/v/v)	Column: CN (200 mm × 4.6 mm, 5 µm) Temperature: 30 °C Detector: 235 nm	ACN:MeOH:10 mM phosphoric acid (pH 2.5, 7:13:80, v/v/v) Flow rate: 1.0 mL/min Injection volume: 20 µL	LOD: 0.1 µg/mL LOQ: 0.3 µg/mL Rec: 95.8%	[89]

Valsartan, amlodipine hydrochlorothiazide	Tablet	MeOH	Column: Zorbax SB-C8 (250 mm × 4.6 mm; 5 µm) Temperature: 25 °C Detector: 225 nm	0.025 M phosphoric acid: ACN (gradient) Flow rate: 1.0 mL/min Injection volume: 20 µL	LOD: 0.24 µg/mL LOQ: 0.80 µg/mL Rec: 100.65 ± 1.23%	[90]
Valsartan, amlodipine besylate, hydrochlorothiazide	Tablet	MeOH	Column: Kromasil KR-5 C18 (250 mm × 4.6 mm; 5 µm) Temperature: n/a Detector: 232 nm	50 mM KH ₂ PO ₄ pH 3.7: ACN (56:44, v/v) Flow rate: 1.0 mL/min Injection volume: 20 µL	LOD: 1.1 µg/mL LOQ: 3.3 µg/mL Rec: 99.69 ± 0.63% to 100.20 ± 0.07%	[91]
Valsartan, propranolol hydrochloride	Raw material, gel formulation	ACN: MeOH:0.01 M Na ₂ PO ₄ pH 3.5 = 50:35:15	Column: Hypersil ODS C18 (250 mm × 4.6 mm, 5 µm) Temperature: 25 ± 0.2 °C Detector: 250 nm	ACN:MeOH:0.01 M Na ₂ HPO ₄ pH 3.5 = 50:35:15 Flow rate: 1.0 mL/min Injection volume: 20 µL	LOD: 0.45 µg/mL LOQ: 1.39 µg/mL Rec: (99.79–102.93)%	[92]

Table 7 Summary of TLC Analysis of Valsartan

Analyte(s)	Sample	Stationary Phase	Mobile Phase, Solvent	Detection	LOD, LOQ, Recovery, Precision (Valsartan)	Ref.
Valsartan, amlodipine	Bulk drug, tablet	Silica gel F254	Mobile phase: toluene: MeOH:acetic acid (7:3:0.1, v/v/v) Solvent: MeOH	UV 244 nm	LOD: 50 ng/spot LOQ: 100 ng/spot Recovery: (98.72 ± 0.5)% RSD precision: Intraday: (0.14–0.39)% Interday: (0.19–0.52)%	[93]
Valsartan, ramipril	Capsules	Silica gel F254	Mobile phase: ethyl acetate: chloroform:glacial acetic acid (8:2:0.2, v/v/v) Solvent: MeOH	UV 220 nm	LOD: 42.4 ng/spot LOQ: 1400.8 ng/spot Recovery: (98.92–101.22)% RSD precision: Intraday: 0.037% Interday: 0.046%	[94]
Valsartan, telmisartan	Tablets	Silica gel F254	Mobile phase:1,4-dioxane: hexane:formic acid 99% (5:5:0.1, v/v/v) Solvent: MeOH	Video scanning	LOD: n/a LOQ: n/a Recovery: (99.62–101.59)% Intermediate precision (RSD): 5.14%	[95]
Valsartan, ramipril	Capsule	Silica gel 60F ₂₅₄	Mobile phase: chloroform: ethyl acetate:methanol: glacial acetic acid (5:5:1:0.2, v/v/v/v) Solvent: n/a	UV 210 nm	LOD: 100 ng/spot LOQ: 330 ng/spot Recovery: 99.099.7% RSD precision: Intraday: 0.136–0.277% Interday: 0.172–0.259%	[96]

Valsartan, hydrochlorothiazide	Tablet	Silica gel 60F ₂₅₄	Mobile phase: CHCl ₃ : MeOH:NH ₄ OH (8:2:1, v/v/v) Solvent: MeOH	UV 225 nm	Recovery: 99.94% RSD precision: Intraday: 1.22% Interday: 1.59%	[86]
Valsartan, telmisartan, potassium losartan	Tablet	Silica gel 60F ₂₅₄	Mobile phase: CHCl ₃ : MeOH:acetone:toluene: acetic acid (7.5:1.5:5:5:0.01:0.003, v/v/v/v/v) Solvent: mobile phase	UV 254 nm	Recovery: 98.74–101.1% Precision (RSD): 0.85%	[97]
Valsartan	Bulk drug, formulation	Silica gel 60F ₂₅₄	Mobile phase: toluene: ethyl acetate:MeOH: formic acid (60:20:20:1, v/v/v/v) Solvent: MeOH	UV 250 nm	LOD: 25 ng/band LOQ: 150 ng/band Recovery: 99.30–101.09% RSD precision: Intraday: 0.76–1.52% Interday: 0.40–1.35%	[98]
Valsartan, hydrochlorothiazide	Tablets	Silica gel 60F ₂₅₄	CHCl ₃ :MeOH:acetone: toluene:acetic acid (6:2:1:0.1, v/v/v/v) Solvent: MeOH	UV 260 nm	LOD: 100 ng/spot LOQ: 300 ng/spot Precision: 0.27–1.19%	[99]

Continued

Table 7 Summary of TLC Analysis of Valsartan—cont'd

Analyte(s)	Sample	Stationary Phase	Mobile Phase, Solvent	Detection	LOD, LOQ, Recovery, Precision (Valsartan)	Ref.
Valsartan, losartan, irbesartan, candesartan, eprosartan mesylate, telmisartan	Tablets	HPTLC F ₂₅₄	CH ₂ Cl ₂ :EtOA:EtOH: Glacial acetic acid:H ₂ O (45:40:5:1:0.5, v/v/v/v/v) Solvent: n/a	UV 260 nm	LOD: 0.02 µg/spot LOQ: 0.5 µg/spot Recovery: 98–102% Precision: n/a	[101]
		RP-Diphenyl-F	ACN:MeOH:0.1 M ammonium acetate:25% ammonia (30:20:50:0.5, v/v/v/v/v) Solvent: n/a			
Valsartan, nebivolol HCl	Dosage form	Silica gel	EtOA:MeOH:25% ammonia (12:2:1, v/v/v) Solvent: n/a	UV 280 nm	LOD: n/a LOQ: n/a Recovery: n/a Precision: n/a	[101]
Valsartan, hydrochlorothiazide, amlodipine besylate	Tablets	Silica gel	EtOA:MeOH:10% ammonia (17:4:2, v/v/v) Solvent: n/a	UV 320 nm	LOD: 3200 ng/zone LOQ: 6400 ng/zone Recovery: (98–101)% Precision (RSD): Intraday and interday: <0.8%	[101]



8. ANALYSIS OF VALSARTAN IN BIOLOGICAL FLUIDS AND HERBAL PREPARATION

HPLC is the most common method used in the analysis of valsartan and related compounds, biological fluids, and samples. In this technique, an RP-18 column is normally fitted, and detection was performed by various methods including UV, fluorescent, and MS (SIM and MRM (multiple reaction monitoring)).

Maurer and coworkers [42] reported the analysis of the methylation product of valsartan and other drugs in human urine by using GC-EIMS. The GC conditions used were splitless injection, column 12 mm \times 0.2 mm i.d. HP column, injection temperature of 280 °C, column temperature of 100–310 °C at 30 °C/min, carrier gas He 1 mL/min, EI mode (70 eV, source 220 °C, interface 260 °C).

Valsartan is metabolized by CYP-450 isoenzyme into valeryl-4-hydroxy-valsartan in human. This metabolite has 200-fold lower affinities to the AT1 receptor than valsartan. The renal clearance of valsartan has reported only 30% of the total plasma clearance. The recovery of valsartan are 83% in feces and 13% in urine from oral solution administration of valsartan [2,3,104].

In the quantitative analysis of valsartan in a complex matrix, it is recommended to use an LC–MS technique with MRM due to its low LOQ and specificity. In this method, two daughter ions should be selected: one ion for qualification and the other for quantification purposes. The intensity ratio of qualifier and quantification ions must be compared between standard and samples. The qualifier and quantification ions as described by Ref. [105] in MS–MS Agilent (precursor ion m/z 436.2; ESI positive mode; fragmentation voltage: 98 V; collision energy: 14 eV; dwell time: 20 ms) for valsartan are m/z 235 and 291.1, respectively.

The HPLC methods that applied for analysis of valsartan and related compounds in biological fluids and samples are summarized in Table 8.

Kesting and coworkers [11] investigated the presence of adulterant in the Chinese herbal medicines which were used for the treatment of hypertension. The identification of adulterant was conducted by using LC–HRMS and LC–MS–SPE–NMR. The results showed the presence of valsartan, amlodipine, indapamide, and other drugs used for antihypertension as the commercial soft capsules of herbal drug preparations [11].

Table 8 Summary of Analysis of Valsartan, Other Compounds, and Their Metabolite in the Biological Fluids and Samples

Analyte(s)	Chromatography Conditions	Sample	Internal Standard (IS)	Preparation of Standards, Sample Extraction, and Cleanup	Accuracy, Precision (RSD), LOD, and LOQ Valsartan	Ref.
Valsartan, hydrochlorothiazide	Column: Zorbax SB-Aq C-18 (150 mm × 4.6 mm; 5 µm) Mobile phase: ACN:10 mM ammonium acetate (60:40, v/v; pH 4.5) Flow rate: 1.2 mL/min Column temperature: 35 °C Detection: MRM (negative ion mode): valsartan (<i>m/z</i> , quantification: 434.2 → 350.2; identification: 434.2 → 179.1) HCT (<i>m/z</i> quantification: 295.9 → 268.9; identification: 295.9 → 204.9) Probenecid: (<i>m/z</i> 283.9 → 239.9)	Human plasma	Probenecid	Standard solutions: Stock solutions of valsartan (4 mg/mL), HCT (1 mg/mL), and probenecid (5 mg/mL) were prepared by dissolving in ACN:water (80:20, v/v); working solution IS (150 ng/mL) Samples: 100 µL IS + 100 µL plasma sample + 300 µL ACN vortex-mixed 1 min, then centrifuged 10 min (10,000 × <i>g</i>), upper layer collected; 15 µL aliquot was injected into LC-MS/MS	Accuracy: ±7.85% Precision: Intraday: (1.92–4.81)%; Interday: (2.21–7.12)% LOD: n/a LOQ: 4 ng/mL	[106]
Valsartan	SPE column (20 mm × 2.1 mm) packed with OASIS MAX 30 µm; SPE was connected 10-port switching valve Samples (40 µL) was flushed from sample loop at 2 mL/min using water:acetic acid (85:15), after loading in SPE, and then SPE was washed with water and THF for 0.5 min. Elution was performed using THF:water:formic acid (95:5:5, v/v/v)	Human plasma and urine	Candesartan	Standard solutions: Stock solutions, valsartan (4 mg/mL) and candesartan (1 mg/mL), were dissolved in MeOH with 0.5% NH ₄ OH. Calibration and QC samples were prepared by spiking matrices with standard solutions Samples: Samples were centrifuged 5 min (2400 × <i>g</i>); 50 µL sample then deposited in 96-well polypropylene plate; after	Accuracy: Plasma: (101–108)% Urine: (41.7–46.4)% Precision: Intraday: Plasma: (2.0–8.5)% Urine: (0.6–9.3)% Interday: Plasma: (2.1–16.9)% Urine: (2.7–5.0)% LOD: n/a LOQ: n/a	[107]

	Detection: MRM (positive ion mode): valsartan: (m/z 436.2 \rightarrow 291.2.1) Candesartan: (m/z : 441.2 \rightarrow 263.2)			addition of 50 μ L acetic acid (15%, v/v) and 10 μ L IS solutions, the plates were sealed and vortexed at 1000 rpm (10 s), and kept 4 $^{\circ}$ C until injection		
Valsartan	Column: Phenomenex C18 (10 mm \times 4.6 mm; 5 μ m) equipped with guard column NovaPak C8 Column temperature: ambient Mobile phase: phosphate buffer pH 2.8:ACN (70:30, v/v) Flow rate: 1.3 mL/min Detection: fluorescent Excitation: 265 nm Emission: 378 nm	Human plasma	Losartan	Standard solutions: Stock solutions of valsartan (50 μ g/mL) were prepared by dissolving in 0.1 M KOH and pH was adjusted to 8 with 1 M HCl. IS was prepared with same method (2 μ g/mL) Samples: <ul style="list-style-type: none"> – 1 mL Human plasma + 100 μL IS, acidified with 125 μL phosphoric acid to pH 2.5, add 10 mL methyl-<i>tert</i>-butyl ether (MTBE) then vortex-mixed and centrifuged (1800 $\times g$ for 5 min) – Organic layer was transferred to tube containing 200 μL 0.05 M NaOH and then the mixture was vortexed and centrifuged (1800 $\times g$ for 5 min) – Organic layer was discarded, aqueous layer neutralized with 75 μL 0.2 M phosphoric acid, 125 μL was injected into HPLC 	Accuracy and precision: Intraday: (91.8–100.6)% RSD: (0.7–10.8%) Interday: (88.3–100.6)% RSD: (0.8–8.9%) LOD: n/a LOQ: 10 ng/mL	[108]

Table 8 Summary of Analysis of Valsartan, Other Compounds, and Their Metabolite in the Biological Fluids and Samples—cont'd

Analyte(s)	Chromatography Conditions	Sample	Internal Standard (IS)	Preparation of Standards, Sample Extraction, and Cleanup	Accuracy, Precision (RSD), LOD, and LOQ Valsartan	Ref.
Valsartan, losartan, irbesartan, candesartan cilexetil, and candesartan M1	Column: μ Bondapak C18 (300 mm \times 3.9 mm; 10 μ m) + guard column Novapak C18 (20 mm \times 3.9 mm; 4 μ m) Mobile phase: gradient elution 5 mM acetate buffer pH 4 and ACN Column temperature: room Detection: Fluorescence detector Excitation: 250 nm Emission: 375 nm	Human plasma	Bumetanide	Standard solutions: Stock solutions were prepared in MeOH and ACN Samples: – 0.25 mL plasma was spiked with appropriate amount of stock solutions and IS, then acidified with 0.25 mL 1 M H ₃ PO ₄ and the mixture was then shaken and centrifuged 5 min (10,000 $\times g$ at 4 $^{\circ}$ C) – Clean up was performed using Bond Elut C8 that was conditioned with 2 mL MeOH followed by 1 mL 0.1 M phosphate buffer pH 2 – Samples was slowly passed into the cartridge (0.5 mL) – Column was washed with 0.5 mL MeOH–1 M phosphate buffer pH 2 (50:50, v/v) and dried. – Analyte then eluted with 0.5 mL MeOH – 0.1 mL ethylene glycol 10% (v/v) was added	Accuracy and precision: Intraday: Relative errors: –2.6% to +3.7% RSD: 3.4–5.4% Interday: Relative error: –4.6% to +6.7% RSD: 5.0–8.0% LOD: n/a LOQ: 51.5 ng/mL	[32]

				<ul style="list-style-type: none"> – The eluate was vortexed and dried under N₂ at 40 °C – The residue was dissolved in starting mobile phase (0.25 mL) – 20 µL solution was injected to the HPLC system 		
Valsartan, amlodipine	Column: HICHROM Nucleosil 100-5 C18 (250 mm × 4.6 mm) Temperature: room Mobile phase: phosphate buffer (0.01 M, pH 3.6):ACN: MeOH (50:40:10, v/v/v) Flow rate: 1.0 mL/min Detection: UV 240 nm	Rat liver perfusate	n/a	Standard solutions: Standard solutions were prepared in MeOH (100 µg/mL) Samples: Spiked samples were prepared by adding 50 µL standard solutions into blank liver perfusate (100 µL) and then making up into 1000 µL by mobile phase, after filtering (0.45 µm) then injected into HPLC	Accuracy and precision Intraday: Bias: –1.03% to +12.67%; RSD: 2.20–4.19% Interday: Bias: +0.89% to +12.33%; RSD: 2.93–4.74% LOD: 0.02 µg/mL LOQ: 0.05 µg/mL	[109]
Valsartan	Column: Nucleosil C18 (50 mm × 4 mm) + guard column Phenomenex (4 mm × 3 mm) Mobile phase: ACN:15 mM KH ₂ (PO ₄) ₃ pH 2.0 (45:55, v/v) Flow rate: 1 mL/min Column temperature: 40 °C Detection: fluorescence Excitation: 234 nm Emission: 374 nm	Human plasma	n/a	Standard solutions: Stock solutions were prepared by dissolving standard (20 mg) in 25 mL MeOH; calibration, and QC samples were prepared by spiking standard solutions into drug-free plasma Samples: 0.2 mL plasma + 1 mL MeOH then vortex-mixed 30 s (2000 rpm) and then centrifuged 3 min (2500 × g); 5 µL supernatant injected into HPLC system	Intraday: Bias: +1.8% to +7.2%; RSD: 1.1–3.0% Interday: Bias: –0.8% to +1.4%; RSD: 1.3–4.9% LOD: 25 pg/mL LOQ: 97.9 ng/mL	[110]

Continued

Table 8 Summary of Analysis of Valsartan, Other Compounds, and Their Metabolite in the Biological Fluids and Samples—cont'd

Analyte(s)	Chromatography Conditions	Sample	Internal Standard (IS)	Preparation of Standards, Sample Extraction, and Cleanup	Accuracy, Precision (RSD), LOD, and LOQ Valsartan	Ref.
Valsartan	Column: Chromolith RP-18e (100 mm × 4.6 mm) Mobile phase: 0.01 M Na ₂ HPO ₄ buffer:ACN (60:40, v/v, adjusted to pH 3.5) Flow rate: 2 mL/min Column temperature: n/a Detection: fluorescence Excitation: 230 nm Emission: 295 nm	Human plasma	Atorvastatin	Standard solutions: Stock solutions (2 mg/mL) were prepared in MeOH Samples: 450 µL plasma + 50 µL IS (12 µg/mL) + 500 µL ACN then mixed and centrifuged for 10 min (8000 rpm); 20 µL was injected into HPLC	Recovery (average): 96.3 ± 1.3% Precision (%CV) Intraday: 2.6–4.3% Interday: 3.0–5.2% LOD: n/a LOQ: 20 ng/mL	[111]
Valsartan, losartan, telmisartan	Column: Chromolith RP-18e monolithic (25 mm × 4.6 mm) Mobile phase: 5 mM phosphate buffer pH 3.8:ACN:MeOH (65:20:15, v/v/v) Flow rate: 3.0 mL/min Temperature: room Detection: fluorescent Excitation: 259 nm Emission: 399 nm	Human urine	n/a	Standard solutions: Individual stock solution (1000 µg/mL) were prepared in MeOH Samples: – 1 mL sample were transferred into 16 mm × 125-mm disposable glass tubes and 3 mL of extraction solvent 1 (2% MeOH in 5 mM phosphate buffer pH 3.8) and then vortexed and centrifuged 10 min (2500 × g) – 2 mL of supernatant was transferred into glass screw-cap vials, then processed by using SPE (LiChrocart 25-4 LiChrospher RP-18 ADS (25 mm × 4 mm; 25 µm)), and extracted using solvent 1	Recovery: (92.9–102.5)% Precision (CV) Intraday: <3.5% Interday: <3.5% LOD: 0.001 µg/mL LLOQ: 0.003 µg/mL	[112]

Valsartan, hydrochlorothiazide	Column: Betabasic C8 (50 mm × 4.6 mm; 5 µm) Mobile phase: ACN: MeOH:0.001% aqueous ammonia (75:15:10, v/v/v) Flow rate: 0.5 mL/min Column temperature: 50 °C MRM: Valsartan: (negative ion mode: <i>m/z</i> 434.25 → 179.22) HCT: <i>m/z</i> 295.85 → 204.86 Clonazepam: <i>m/z</i> : 314.0 → 278.27	Human plasma	Clonazepam	Standard solutions: Stock solutions (5 mg/mL) and IS (1 mg/mL) were prepared in MeOH:water (50:50, v/v). This stock solution can be used for spiking in plasma Samples: <ul style="list-style-type: none"> – 500 µL plasma + 25 µL IS + 500 µL orthophosphoric acid 2% in 1.7-mL microtube then vortexed – The mixture then applied to HLB cartridge (30 mg, 1 cm³) previously conditioned with 1 mL MeOH and 2 mL water – The loaded cartridge was washed with 2 mL water, then 1 mL 5% MeOH in water, then eluted with 1.0 mL MeOH:ACN (90:10, v/v), and loaded into autosampler vial 	Mean recovery: 90.28% CV: 0.12% Precision: Intraday: <10.0% Interday: <10.0% LOD: n/a LLOQ: 50.0 ng/mL	[41]
Valsartan	Column: Zorbax SB-C18 (50 mm × 4.6 mm; 3.5 µm) Mobile phase: ammonium formate 8 mM, pH 3:MeOH (30:70, v/v) Flow rate: 1 mL/min Temperature: room Detection: MS/MS (no detailed data reported)	Human blood	Valsartan- <i>d</i> ₉	Standards: not reported Samples: <ul style="list-style-type: none"> – Plasma samples were vortexed (3000 rpm) and centrifuged (1900 × <i>g</i>, 5 min, 4 °C); – 100 µL aliquot + 600 µL solution of IS in MeOH were vortexed (3000 rpm) 	Accuracy: 98.66% Precision: 3.51% LLOQ: 20.18 ng/mL	[113]

Continued

Table 8 Summary of Analysis of Valsartan, Other Compounds, and Their Metabolite in the Biological Fluids and Samples—cont'd

Analyte(s)	Chromatography Conditions	Sample	Internal Standard (IS)	Preparation of Standards, Sample Extraction, and Cleanup	Accuracy, Precision (RSD), LOD, and LOQ Valsartan	Ref.
				and then centrifuged (1900 × g, 10 min, 4 °C). – 400 µL supernatant was evaporated into dryness with N ₂ – Residue was reconstituted in 200 µL in mobile phase and measured with LC–MS/MS		
Valsartan, nebivolol	Column: Gemini-C18 (50 mm × 2.0 mm; 3 µm) Guard column C18 (4 mm × 3 mm) Mobile phase: ACN:0.05 mM formic acid buffer (50:50, v/v, pH 3.5) Flow rate: 0.25 mL/min Column temperature: 20 °C	Human plasma	Tamsulosin	Standard solutions: Analytes and IS were prepared individually in ACN (100.0 µg/mL). The stocks were diluted with water to give serial of standard solutions; QC samples were prepared by spiking standards into plasma	Accuracy: 101.1–103.7% Precision: Intrarun (RSD): 1.6–2.5% Interrun (RSD): 2.9–4.8% LOD: n/a LLOQ: 1.0 ng/mL	[114]
	Detection: Valsartan (negative ion mode) <i>m/z</i> : 434.2 → 179.0 nebivolol (positive ion mode) <i>m/z</i> : 406.1 → 150.9 IS (positive ion mode) <i>m/z</i> 409.4 → 228.1			Samples: 200 µL plasma + 400 µL ACN contained IS (240 ng/mL), then vortexed (1 min) and centrifuged (14,000 rpm; 10 min); aliquots were filtered through 0.2 µm and injected into LC–MS–MS system		

Valsartan, valeryl-4-hydroxy-valsartan	<p>Column: Waters Atlantis dC18 (100 mm × 3.9 mm; 3.9 μm)</p> <p>Guard column: μBondapak C18 (10 μm)</p> <p>Mobile phase: gradient elution using 0.025% TFA in ACN and 0.025% TFA in buffer phosphate buffer (5 mM, pH 2.5)</p> <p>Flow rate: 1.3 mL/min</p> <p>Temperature: 40 ± 0.2 °C</p> <p>Detection: fluorescence</p> <p>Excitation: 234 nm</p> <p>Excitation: 378 nm</p>	Human plasma	Candesartan M1	<p>Standard solutions: Stock solutions valsartan, metabolite, and IS were prepared in MeOH with concentrations 107, 186, and 99.26 μg/mL, respectively. Working solutions prepared by diluting the stock solution</p> <p>Samples:</p> <ul style="list-style-type: none"> – 1 mL blank samples were spiked with valsartan, metabolite, and IS to achieve concentrations 1.1 μg/mL (analytes) and 1.2 μg/mL (IS) and then 1 mL of H₃PO₄ (0.5 M) was added, vortexed, and centrifuged (5 min, 10,000 rpm) – The mixtures were applied to a C8 SPE (conditioned with 2 mL MeOH and 1 mL phosphate buffer pH 2, 60 mM) – SPE was washed by 1 mL MeOH:phosphate buffer (40:60, v/v) – After drying for 8 min, SPE was eluted using solution of 	<p>Recovery:</p> <p>Valsartan: (96.6–101.2)% (RSD: 1.2–3.1%)</p> <p>Metabolite: 94.6–108.8% (RSD: 0.7–1.6%)</p> <p>LOD: n/a</p> <p>LLOQ: 5 ng/mL (valsartan and metabolites)</p>	[104]
--	---	--------------	----------------	--	--	-------

Continued

Table 8 Summary of Analysis of Valsartan, Other Compounds, and Their Metabolite in the Biological Fluids and Samples—cont'd

Analyte(s)	Chromatography Conditions	Sample	Internal Standard (IS)	Preparation of Standards, Sample Extraction, and Cleanup	Accuracy, Precision (RSD), LOD, and LOQ Valsartan	Ref.
				10% ethylene glycol in MeOH (0.1 mL) – The compounds were eluted using 0.5 mL diethylether. – Evaporated with N ₂ stream at 60 °C – Residue + 100 µL mobile phase was reconstituted, vortexed, mixed, and filtered with polypropylene membrane Ø = 13 mm, 0.45 µm – 20 µL was injected into HPLC system		
Valsartan, valeryl-4-hydroxy-valsartan	Same with Iriarte 2006	Human plasma	Candesartan M1	Same with Iriarte 2006 (except the nominal concentrations were different). This work reported the application of Iriarte 2006 for bioavailability studies	LOQ for both of analytes was 5 ng/mL Accuracy and precision of analytes: <15%	[115]
Valsartan, amlodipine, hydrochlorothiazide	Column: Gemini C18 (250 mm × 4.6 mm; 5 µm), protected with guard column C18 (4 mm × 2 mm) Column temperature: 35 °C Mobile phase: ACN:10 mM ammonium formate pH 3.5, v/v (gradient from 20:80 to 70:30)	Human plasma	Telmisartan	Standard solutions: Stock solutions (100 µg/mL) of the analytes were prepared in MeOH Samples: Plasma samples + 1 mL mixture of MeOH:ACN (50:50, v/v) + 15 µL IS solution, vortexed (3 min) and centrifuged 10,000 rpm (10 min),	Recovery: 76.5 ± 2.1%; Precision: Intraday: 101.1–101.8%; Interday: 101.7–107.0% LOD: 7 ng/mL LOQ: 20 ng/mL	[116]

	Flow rate: 1 mL/min Detector: PDA (254 nm)			supernatant filtered, and evaporated with N ₂ Dried residue + 0.5 mL mobile phase reconstituted, filtered, and then injected into HPLC		
Valsartan	Column: Hypersyl BDS C18 (250 mm × 4.6 mm; 5 µm) Mobile phase: buffer triethylamine pH 3.0:ACN (45:55, v/v) Flow rate: 0.7 mL/min Column temperature: 25 °C Detection: UV 215 nm	Human plasma	Losartan potassium	Standard solutions: not reported Samples: 0.2 mL plasma was transferred into 2-mL centrifuge tube + 25 µL IS (1 mg/mL), vortexed 30 s (2000 rpm) + 1 mL MeOH, vortexed for 10 min (2000 rpm), then centrifuged 10 min (2500 rpm), and 20 µL supernatant injected into HPLC	Accuracy: n/a Precision: n/a LOD: n/a LOQ: n/a	[117]
Valsartan, gliclazide, benazepril	Column: Shimadzu VP-ODS C18 (250 mm × 2.0 mm, 5 µm) Temperature: 40 °C Mobile phase: gradient elution of MeOH and 0.05% formic acid Flow rate: 0.2 mL/min Column temperature: n/a Detection: SRM: Valsartan (<i>m/z</i> 436 → 207) Gliclazide (<i>m/z</i> 324 → 110) Benazepril (<i>m/z</i> 425 → 351) IS (<i>m/z</i> 531 → 489)	Human plasma	Ketoconazole	Standard solutions: Stock solutions were prepared in MeOH (valsartan 500 µg/ mL; gliclazide and benazepril 50 µg/mL); calibration and QC samples were prepared by spiking into human blank samples Samples: 100 µL + 10 µL IS (125 µg/ mL) + 500 µL MeOH, then vortexed and centrifuged for 10 min (40,000 × <i>g</i>), supernatant transferred into another clean test tube, centrifuged again for 10 min (40,000 rpm), 10 µL clear supernatant was injected into LC-MS	Recovery: (93.52–99.94)% Precision: Intraday: 6.2% Bias: 0.1% Interday: 10.4% Bias: 9.0% LOD: n/a LOQ: 20 ng/mL	[38]

Continued

Table 8 Summary of Analysis of Valsartan, Other Compounds, and Their Metabolite in the Biological Fluids and Samples—cont'd

Analyte(s)	Chromatography Conditions	Sample	Internal Standard (IS)	Preparation of Standards, Sample Extraction, and Cleanup	Accuracy, Precision (RSD), LOD, and LOQ Valsartan	Ref.
Valsartan, verapamil, losartan, telmisartan, irbesartan, flecainide, beta blocker drugs	Column: Atlantis dC18 (150 mm × 2.1 mm; 3 μm) Mobile phase: gradient elution. Solvent A: 10 mM ammonium formate pH 3.1; B: ACN linear gradient from 90% A and 10% B to 10% A and 90% B in 10 min, then held 3 min Column temperature: 25 ± 0.8 °C Flow rate: 0.3 mL/min Detection: SIM (<i>m/z</i>): Valsartan (207.3); telmisartan (276.3); losartan (207.3); irbesartan (207.3)	Post mortem whole blood	Diazepam-d5	Standard solutions: Two stock solutions were prepared in MeOH (2500 μM); aqueous calibration solutions and aqueous control solutions were prepared from stock solutions; IS was dissolved in ACN (155 μM) and water (18.5 μM). Spiked calibration and QC samples were prepared by adding aqueous solutions into drug-free sodium fluoride whole blood Samples: 0.5 mL whole blood + 50 μL (18.5 μM IS), then this mixture was precipitated with 1 mL ice cold mixture of ACN:MeOH (85:15, v/v), then frozen for 30 min (−20 °C), and centrifuged (2260 × <i>g</i> , 4 °C, 10 min). Supernatant was decanted and mixed with 0.2 mL 4.5 M HCl before diluting with water, and the samples were applied to SPE (Oasis MCX)	Accuracy: n/a Precision: intraday Bias: −7.3%, and −22%; RSD: 21% and 4% for theoretical concentration 5 and 1 μM, respectively Interday: Bias: −20%, and −21%; RSD: 13% and 28% for theoretical concentration 5 and 1 μM LOD: n/a LOQ: n/a	[118]

Valsartan	<p>Column: XTerra MS (50 mm × 2.1 mm; 3.5 μm), guard column: Opti guard- mini C18 (15 mm × 1 mm) Mobile phase: 0.1% trifluoroacetic acid:MeOH: ACN (45:30:25, v/v/v) Flow rate: 0.2 mL/min Column temperature: 50 °C Detection: SRM (positive ion mode): Valsartan: m/z 436.2 and 291.2 IS: m/z 429.2 and 401.2</p>	Human plasma	CGP48791	<p>Standard solutions: Stock solutions were prepared in MeOH; Calibration standards and QC samples were prepared by spiking into heparinized human plasma Samples: Mixture of 500 μL plasma + 50 μL IS solution (500 ng/mL in MeOH:H₂O (50:50, v/v) + 250 μL 2% trifluoroacetic acid) was placed in 96-well collection plates, then the entire volume was transferred into 96-well Empore SPE that pretreated with 100 μL MeOH and 500 μL 1% trifluoroacetic acid, rinsed with various solvent, then the analytes were eluted using 500 μL mixture of MeOH:H₂O (90:10, v/v) Eluate dried under N₂, residue reconstituted with 100 μL MeOH/0.1% trifluoroacetic acid (50:50, v/v), filtered then centrifuged for 1900 × <i>g</i> (10 min) at 4 °C. Filtrate applied to LC-MS/MS</p>	<p>Recovery: (63.0–73.0)% Precision: Intraday: Precision (RSD): 2.19–5.40% Accuracy: 94.8–107% Interday: Precision (RSD): 1.87–5.67% Accuracy: 93.5–105% LOQ: 2 ng/mL LOQ: n/a</p>	[37]
-----------	---	-----------------	----------	---	--	----------------------

Continued

Table 8 Summary of Analysis of Valsartan, Other Compounds, and Their Metabolite in the Biological Fluids and Samples—cont'd

Analyte(s)	Chromatography Conditions	Sample	Internal Standard (IS)	Preparation of Standards, Sample Extraction, and Cleanup	Accuracy, Precision (RSD), LOD, and LOQ Valsartan	Ref.
Valsartan, amlodipine, indapamide	Column: Zorbax Eclipse Plus C18 (50 mm × 3 mm; 3 µm) Mobile phase: Solvent A: ACN; B: H ₂ O with 0.1% formic acid (gradient elution): A:B (10:90) to (95:5) in 5 min, then held 1 min Detection: Qualitative: HRMS and NMR Quantitative: UV (valsartan: 250 nm; amlodipine: 360 nm; and indapamide: 240 nm)	Capsules of Chinese herbal medicine	n/a	Standard solutions: Analytes were dissolved in ACN:H ₂ O (1:1) Samples: Capsules were cut and emptied into 100 mL volumetric flask + 30 mL H ₂ O, stirred 30 min + 30 mL ACN stirred 30 min, and then diluted to volume with ACN:H ₂ O (1:1)	Recovery: 108.51 ± 3.40% Precision: n/a LOD: n/a LOQ: n/a	[11]
Valsartan, amlodipine, hydrochlorothiazide	Column: Aquasil C-18 (50 mm × 2.1 mm; 5 µm) Column temperature: 20 °C Flow rate: 0.2 mL/min Mobile phase: ACN:H ₂ O containing 0.1% formic acid (50:50, v/v, for separating valsartan and amlodipine) ACN:H ₂ O containing 0.1% glacial acetic acid (60:40, v/v, for separating hydrochlorothiazide) Detection: MRM (positive ion mode): valsartan (<i>m/z</i> 436 → 418); losartan (<i>m/z</i> 423 → 406); amlodipine (<i>m/z</i> 409 → 238) Negative ion mode: hydrochlorothiazide (<i>m/z</i> 296 → 268); furosemide (<i>m/z</i> 328 → 285)	Rat plasma	Losartan Furosemide (only for hydrochlorothiazide)	Standard solutions: Stock solutions were prepared by dissolved analytes in ACN (10 mg/10 mL). Calibration and QC samples were prepared by spiking diluted stock solutions into drug-free rat plasma Samples: Analytes were extracted from plasma by adding ACN as precipitating agent, by vortexing (1 min), and centrifugating 10,000 rpm (10 min) Separated supernatant layer filters with 0.45-µm syringe, 20 µL was injected into LC-MS/MS	Recovery: Intraday: 87.9–106.3% Interday: 85.7–110% Precision: Intra- and interday: <14.3% LOQ: 1 ng/mL (all analytes)	[119]

Valsartan, amlodipine, olmesartan medoxomil, hydrochlorothiazide	Column: CN column (200 mm × 4.6 mm; 5 µm) Mobile phase: ACN: MeOH:10 mM phosphoric acid pH 2.5 (7:13:80, v/v/v) Flow rate: 1.0 mL/min Detection: UV 235 nm	Human plasma	n/a	Standard solutions: Stock solutions (1 mg/mL) were prepared in MeOH; dilution was performed using a mixture of ACN:MeOH:H ₂ O (7:13:80, v/v/v) Samples: – 1 mL plasma was spiked with various concentrations of working solutions and then basified with 0.5 mL NaOH – Analytes were extracted by vortex mixer (2 min) using mixture of 5 mL <i>n</i> -hexane: EtOA:isoamyl alcohol (88:10:2, v/v/v) – Samples were then centrifuged for 1 min (1500 rpm), and the organic layer was taken, evaporated, and then dissolved with 0.5 mL mobile phase	Recovery: 75.8–100.3% Precision: <5.8% LOD: 0.1 ng/mL LOQ: 0.3 µg/mL	[89]
Valsartan	The system comprised of 3-µL level pumps (A, B, C), an in-line degasser, a sample cooler, a syringe pump, and a switch valve Separation was performed in a 5 cm micro RP-C18 nano-flow column (150 µm i.d. and 375 µm o.d.; 3 µm).	Human plasma (microliter sample)	Losartan	Standard solutions: Stock solutions of valsartan were prepared in MeOH (1 mg/mL); IS solutions were prepared (10 µg/mL) in solutions of 100 g/L HFBA Samples: Human plasma samples (10 µL) were added in 500-µL vials and	Bias (relative error): Intraday: –4.69% to +4.50% Interday: –2.75% to 3.00% Precision: Intraday: 4.47–6.70%; Interday: 4.71–6.43% LOD: n/a LOQ: 1 µg/mL	[39]

Continued

Table 8 Summary of Analysis of Valsartan, Other Compounds, and Their Metabolite in the Biological Fluids and Samples—cont'd

Analyte(s)	Chromatography Conditions	Sample	Internal Standard (IS)	Preparation of Standards, Sample Extraction, and Cleanup	Accuracy, Precision (RSD), LOD, and LOQ Valsartan	Ref.
	Mobile phase: samples loading (pump A): ACN:1% formic acid (20:80, v/v) Flow rate: 3 $\mu\text{L}/\text{min}$ For sample analysis (pump B: pump C) 1% formic acid:ACN (20:80, v/v) Flow rate: 1 $\mu\text{L}/\text{min}$ Detection: SIR: valsartan m/z 436 ($[\text{M} + \text{H}]^+$)			then 5 μL solutions were added. Samples were vortexed (30 s) and centrifuged 10,000 rpm (2 min) 1 μL of supernatant was injected into the nanoscale LC–MS/MS		
Valsartan, losartan, irbesartan, candesartan cilexetil, candesartan cilexetil M1	Column: $\mu\text{Bondapak C18}$ (300 mm \times 3.9 mm; 10 μm) Guard column: Novapak C18 Mobile phase: ACN and sodium acetate 5 mM, pH 4 (gradient elution) Temperature: room Detector: UV 254 nm		Nimodipine	Standard solutions: Stock solutions (1000 $\mu\text{g}/\text{mL}$) prepared in MeOH and ACN Working solution were made daily by dilution with the same solvent Samples: 1. Frozen human urine (-20°C) thawed 2. 1 mL vortexed and mixed urine + PO_4 buffer (0.5 mL, 0.1 M, pH 2) \rightarrow shaken and centrifuged (3500 rpm) for 5 min 3. BondElut C8 cartridges + MeOH and 1 mL PO_4 buffer (0.1 M, pH 2)	Recovery (RSD): 1.85–2.27% Precision (RSD): Intraday: 0.82–0.97% Interday: 2.63–4.30% LOD: n/a LOQ: 0.43 $\mu\text{g}/\text{mL}$	[120]

-
4. Cartridges do not dry before application of 1 mL acidified sample under low vacuum (<5 mmHg)
 5. Column conditioned with MeOH:PO₄ buffer pH 2 (40:60, v/v) → dried at vacuum (>200 mmHg) for 20 min
 6. Analytes eluted with 1 mL MeOH
 7. Eluate dry at 40 °C with N₂
 8. Remaining residue dissolved with 0.5 mL mobile phase
 9. 20 µL injected into HPLC system
-

ACKNOWLEDGMENTS

The authors would like to thank Mr. Widi Tri Raharjo, PT. Kromtekindo Utama, Jakarta, and Mr. Tegar Achsendo, Yuniarta Institute of Tropical Diseases, Airlangga University, Surabaya for measuring ESI-MS and NMR of valsartan, respectively.

REFERENCES

- [1] C.H. Czendlik, A. Sioufi, G. Preiswerk, H. Howald, Pharmacokinetic and pharmacodynamic interaction of single dose of valsartan and atenolol, *Eur. J. Clin. Pharmacol.* 52 (1997) 451–459.
- [2] N. Siddiqui, A. Husain, L. Chaudhry, M. Shamser Alam, M. Mitra, P.S. Bhasin, Pharmacological and pharmaceutical profile of valsartan: a review, *J. Appl. Pharm. Sci.* 01 (04) (2011) 12–19.
- [3] Valsartan in DailyMed, <http://dailymed.nlm.nih.gov/dailymed/search.cfm?startswith=VALSARTAN&x=20&y=13>, 2014 (accessed 06.05.14).
- [4] S.C. Sweetman, Martindale: The Complete Drug Reference, 36th ed., The Pharmaceutical Press, London, 2009, pp. 1420–1421.
- [5] British Pharmacopoeia 2013, The Stationary Office, London, Data ©Crown Index +©System Simulation Ltd Copyright 2012. <http://pharmatechbd.blogspot.com/2013/01/british-pharmacopoeia-2013.html> (accessed 07.05.14).
- [6] The United States Pharmacopeial Convention, United States Pharmacopoeia—36 National Formulary 31, The United States Pharmacopeial Convention, Rockville, MD, 2012, pp. 5537–5542.
- [7] Xpil, Patient Information Leaflets Online, Valsartan 40mg, 80mg, 160mg, 320mg Film-Coated Tablets. <http://xpil.medicines.org.uk/ViewPil.aspx?DocID=26854>, 2014 (accessed 03.02.14).
- [8] C.J. Mbah, Physicochemical properties of valsartan and the effect of ethyl alcohol, propylene glycol and pH on its solubility, *Pharmazie* 60 (2005) 849–850.
- [9] Merck & Co., Inc., The Merck Index, Merck & Co., Inc., Whitehouse Station, NJ, USA, 2008.
- [10] C. Potamitis, P. Chatzigeorgiou, E. Siapi, K. Viras, T. Mavromoustakos, A. Hodzic, G. Pabst, F. Cacho-Nerin, P. Laggner, M. Rappolt, Interactions of the AT1 antagonist with dipalmitoyl-phosphatidylcholine bilayers, *Biochim. Biophys. Acta* 1808 (2011) 1753–1763.
- [11] J.R. Kesting, J. Huang, D. Sorensen, Identification of adulterants in a Chinese herbal medicine by LC–HRMS and LC–MS–SPE/NMR and comparative in vivo study with standards in a hypertensive rat model, *J. Pharm. Biomed. Anal.* 51 (2010) 705–711.
- [12] B.N. Nalluri, R.M. Krishna, T.P. Rao, P.A. Crooks, Effect of recrystallization on the pharmaceutical properties of valsartan for improved therapeutic efficacy, *J. Appl. Pharm. Sci.* 2 (10) (2012) 126–132.
- [13] K.R. Rajeswari, K. Abbulu, M. Sudhakar, R. Karki, B. Rajkumar, Development and characterization of valsartan loaded hydrogel beads, *Pharm. Lett.* 4 (4) (2012) 1044–1053.
- [14] M.S. Sokar, A.S. Hanafy, A.H. El-Kamel, S.S. El-Gamal, Pulsatile core-in-cup valsartan tablet formulations: in vitro evaluation, *Asian J. Pharm. Sci.* 8 (2013) 234–243.
- [15] P. Raviteja, S. Muralidhar, R. Ramesh, T.V. Narayana, P.V. Kumar, G.V. Kumar, Formulation and evaluation of valsartan fast disintegrating tablets using solid dispersion technique, *Int. J. Innov. Pharm. Res.* 4 (1) (2013) 274–280.
- [16] A. Sharma, C.P. Jain, Preparation and characterization of solid dispersions of valsartan with poloxamer 188, *Pharm. Lett.* 2 (2) (2010) 54–63.

- [17] P.D. Maheskumar, G.S. Shantha Kumar, D. Goli, M.P. Talsania, H. Shah, Design, development and evaluation of nanoparticles of poorly soluble valsartan, *World J. Pharm. Pharm. Sci.* 2 (6) (2013) 5737–5749.
- [18] M. Skotnicki, A. Gawel, P. Cebe, M. Pyda, Thermal behaviour and phase identification of valsartan by standard and temperature-modulated differential scanning calorimetry, *Drug Dev. Ind. Pharm.* 39 (10) (2013) 1508–1514.
- [19] I. Rukhman, E. Flyaks, T. Koltai, J. Aronhime, Polymorphs of valsartan, United States Patent US 7,105,557, September 12, 2006.
- [20] I. Rukhman, E. Flyaks, T. Koltai, J. Aronhime, Amorphous form of valsartan, European Patent Specification EP 1950204 A1, July 30, 2008.
- [21] J. Burgbacher, B.T. Hahn, F.A. Rampf, R. Schneeberger, Highly crystalline valsartan, United States Patent US 2013/0137737 A1, May 30, 2013.
- [22] Scientific Discussion EMEA. http://www.ema.europa.eu/docs/en_GB/document_library/EPAR_-_Scientific_Discussion/human/000716/WC500033006.pdf, 2007 (accessed 23.01.14).
- [23] J. Nie, B. Xiang, Y. Feng, D. Wang, Mass spectrometry and nuclear magnetic resonance spectroscopy, isolation and identification of process impurities in crude valsartan by HPLC, mass spectrometry, and nuclear magnetic spectroscopy, *J. Liq. Chromatogr. Relat. Technol.* 29 (2006) 553–568.
- [24] A. Sampath, A. Raghupathi Reddy, B. Yakambaran, A. Thirupathi, M. Prabhakar, P. Pratap Reddy, V. Prabhakar Reddy, Identification and characterization of potential impurities of valsartan AT1 receptor antagonist, *J. Pharm. Biomed. Anal.* 50 (2009) 405–412.
- [25] S. Mehta, R.P. Shah, S. Singh, Strategy for identification and characterization of small quantities of drug degradation products using LC and LC-MS: application to valsartan, a model drug, *Drug Test. Anal.* 2 (2010) 82–90.
- [26] R.M. Bianchini, P.M. Castellano, T.S. Kaufman, Characterization of two new potential impurities of valsartan obtained under photodegradation stress condition, *J. Pharm. Biomed. Anal.* 56 (2011) 16–22.
- [27] D. Ivanović, A. Malenović, B. Jančić, M. Medenica, M. Mašković, Monitoring of impurity level of valsartan and hydrochlorothiazide employing an RP-HPLC gradient mode, *J. Liq. Chromatogr. Relat. Technol.* 30 (2007) 2879–2890.
- [28] Valsartan Summary Validation Report. <https://mc.usp.org/sites/default/files/documents/ValidationReport/2012-06-11%20Valsartan%20Summary%20Validation%20Report.pdf>, 2012 (accessed 01.02.14).
- [29] Valsartan tablet summary validation report. <https://mc.usp.org/sites/default/files/documents/ValidationReport/2012-06-12%20Valsartan%20Tablets%20Summary%20Validation%20Report.pdf>, 2012 (accessed 01.02.14).
- [30] Hydrochlorothiazide and valsartan tablets summary validation report. <https://mc.usp.org/sites/default/files/documents/Hydrochlorothiazide%20and%20Valsartan%20Tablets%20Summary%20Validation%20Report%20-%202013-01-020.pdf>, 2012.
- [31] Amlodipine and valsartan tablets summary validation report. <https://mc.usp.org/sites/default/files/documents/Amlodipine%20and%20Valsartan%20Tablets%20Summary%20Validation%20Report%20-%202013-04-20.pdf>, 2013 (accessed 01.02.14).
- [32] L. González, J.A. Lopez, R.M. Alonso, R.M. Jiménez, Fast screening method for the determination of angiotensin II receptor antagonist in human plasma by high-performance liquid chromatography with fluorometric detection, *J. Chromatogr. A* 949 (2002) 49–60.
- [33] M. Bharathi, S.C.M. Prasad, R.L. Eswari, S. Wajim Raja, R.T. Allena, S. Brito Raj, K. Bhaskar Reddy, Preparation and in vitro & in vivo characterization of valsartan loaded eudragit nanoparticles, *Pharm. Sin.* 3 (5) (2012) 516–525.

- [34] A.K. Mahapatra, P.N. Murthy, S. Biswal, A.P.K. Mahapatra, S.P. Pradhan, Dissolution enhancement and physicochemical characterization of valsartan in solid dispersions with β -CD, HP β -CD, and PVP K-30, *Dissolution Technol.* 18 (2011) 39–45.
- [35] C.E.M. Jensen, R.A.S. Santos, A.M.L. Denadai, C.F.F. Santos, A.N.G. Braga, R.D. Sinisterra, Pharmaceutical composition of valsartan: β -cyclodextrin: physico-chemical characterization and anti-hypertensive evaluation, *Molecules* 15 (2010) 4067–4084.
- [36] B. Chen, Y. Liang, Y. Wang, Development and validation of liquid chromatography-mass spectrometry method for the determination of telmisartan in human plasma, *Anal. Chim. Acta* 540 (2005) 367–373.
- [37] N. Koseki, H. Kawashita, H. Hara, M. Niina, M. Tanaka, R. Kawai, Y. Nagae, N. Masuda, Development and validation of a method for quantitative determination of valsartan in human plasma by liquid chromatography-tandem mass spectrometry, *J. Pharm. Biomed. Anal.* 43 (2007) 1769–1774.
- [38] X. Hu, Y. Zheng, J. Sun, L. Shang, G. Wang, H. Zhang, Simultaneous quantification of benazepril, glimepiride and valsartan in human plasma by LC-MS-MS and application for rapidly measuring protein binding interaction between rhein and these three drugs, *Chromatographia* 69 (2009) 843–852.
- [39] C.Y. Lu, Y. Chang, W. Tseng, C. Feng, C. Lu, Analysis of angiotensin II receptor antagonist and protein markers at microliter level plasma by LC-MS/MS, *J. Pharm. Biomed. Anal.* 49 (2009) 123–128.
- [40] D. Zhang, X. Du, M. Liu, H. Li, Y. Jiang, L. Zhao, J. Gu, Determination of escabet in human plasma by high performance liquid chromatography-tandem mass spectrometry, *J. Chromatogr. B* 863 (2008) 223–228.
- [41] H.J. Shah, N.B. Kataria, G. Subbaiah, C.N. Patel, Simultaneous LC-MS-MS analysis of valsartan and hydrochlorothiazide in human plasma, *Chromatographia* 69 (2009) 1055–1060.
- [42] H.H. Maurer, T. Kraemer, J.W. Arit, Screening for the detection of angiotensin-converting enzyme inhibitors, their metabolites, and AT II receptor antagonists, *Ther. Drug Monit.* 20 (6) (1998) 706–713.
- [43] F. Li, H. Zhang, L. Jiang, W. Zhang, J. Nie, Y. Feng, M. Yang, M. Liu, Dynamic NMR study and theoretical calculations on the conformational exchange of valsartan and related compounds, *Magn. Reson. Chem.* 45 (2007) 929–936.
- [44] C. Potamitis, M. Zervou, V. Katsiaras, P. Zoumpoulakis, S. Durdagi, M.G. Papadopoulos, J.M. Hayes, S.G. Grdadolnik, I. Kyrikou, D. Argyropoulos, G. Vatougia, T. Mavromoustakos, Antihypertensive drug valsartan in solution and the AT receptor: conformational analysis, dynamic NMR spectroscopy, in silico docking, and molecular dynamics simulations, *J. Chem. Inf. Model.* 49 (3) (2009) 726–739.
- [45] K.R. Gupta, A.R. Wadodkar, S.G. Wadodkar, UV-spectrophotometric methods for estimation of valsartan in bulk and tablet dosage form, *Int. J. ChemTech Res.* 2 (2) (2010) 985–989.
- [46] P.K. Kumar, M.U. Shankar, P. Subasini, P. Ghanshyam, P. Gourishyam, S. Kanhu, Stress degradation studies of valsartan and development of a validated method by UV spectrophotometric in bulk and pharmaceutical dosage form, *J. Pharm. Biomed. Sci.* 8 (2) (2011) 1–8.
- [47] E. Dinç, B. Uslu, S.A. Özkan, Spectral resolution of a binary mixture containing valsartan and hydrochlorothiazide in tablets by ratio spectra derivative and inverse least square techniques, *Anal. Lett.* 37 (4) (2004) 679–693.
- [48] A.B. Chaudhary, R.K. Patel, S.A. Chaudhary, K.V. Gadhvi, Estimation of valsartan and hydrochlorothiazide in pharmaceutical dosage forms by absorption ratio method, *Int. J. Appl. Biol. Pharm. Technol.* 1 (2) (2010) 455–464.

- [49] K.R. Gupta, A.D. Mahapatra, A.R. Wadodkar, S.G. Wadodkar, Simultaneous UV spectrophotometric determination of valsartan and amlodipine in tablet, *Int. J. ChemTech Res.* 2 (1) (2010) 551–556.
- [50] S. Ramachandran, B.K. Mandal, S.G. Navalgund, Simultaneous spectrophotometric determination of valsartan and ezetimibe in pharmaceuticals, *Trop. J. Pharm. Res.* 10 (6) (2011) 809–815.
- [51] A.S. Birajdar, S.N. Meyyanathan, B. Suresh, Simultaneous determination of nebivolol HCl and valsartan in solid dosage form by spectrophotometric and RP-HPLC method, *Int. J. Pharm. Sci. Res.* 2 (2) (2011) 424–431.
- [52] S. Hillaert, W. Van den Bossche, Optimization and validation of a capillary zone electrophoretic method for the analysis of several angiotensin-II-receptor antagonists, *J. Chromatogr. A* 979 (2002) 323–333.
- [53] S. Hillaert, W. Van den Bossche, Simultaneous determination of hydrochlorothiazide and several angiotensin-II-receptor antagonists by capillary electrophoresis, *J. Pharm. Biomed. Anal.* 31 (2003) 329–339.
- [54] S. Hillaert, T.R.M. De Beer, J.O. De Beer, W. Van den Bossche, Optimization and validation of a micellar electrokinetic chromatographic method for the analysis of several angiotensin-II-receptor antagonists, *J. Chromatogr. A* 984 (2003) 135–146.
- [55] G. Carlucci, V. Di Carlo, P. Mazzeo, Simultaneous determination of valsartan and hydrochlorothiazide in tablets by high performance liquid chromatography, *Anal. Lett.* 33 (12) (2000) 2491–2500.
- [56] E. Şatana, Ş. Altınay, N.G. Göğçer, S.A. Özkan, Z. Şentürk, Simultaneous determination of valsartan and hydrochlorothiazide in tablets by first-derivative ultraviolet spectrophotometry and LC, *J. Pharm. Biomed. Anal.* 25 (2001) 1009–1013.
- [57] S. Tatar, S. Sağlık, Comparison of UV and second derivative-spectrophotometric and LC methods for the determination of valsartan in pharmaceutical formulation, *J. Pharm. Biomed. Anal.* 30 (2002) 371–375.
- [58] S.S. Chitlange, K. Bagri, D.M. Sakarkar, Stability indicating RP-HPLC method for simultaneous estimation of valsartan and amlodipine in capsule formulation, *Asian J. Res. Chem.* 1 (1) (2008) 15–18.
- [59] S.U. Kokil, M.S. Bhatia, Simultaneous estimation of nebivolol hydrochloride and valsartan using RP HPLC, *Indian J. Pharm. Sci.* 71 (2) (2009) 111–114.
- [60] D.F. Tian, X.L. Tian, T. Tian, Z.Y. Wang, F.K. Mo, Simultaneous determination of valsartan and hydrochlorothiazide in tablets by RP HPLC, *Indian J. Pharm. Sci.* 70 (3) (2008) 372–374.
- [61] V. Agrahari, V. Kabra, S. Gupta, R.K. Nema, M. Nagar, C. Karthikeyan, P. Trivedi, Determination of inherent stability of valsartan by stress degradation and its validation by HPLC, *Int. J. Pharm. Clin. Res.* 1 (2) (2009) 77–81.
- [62] S.B. Patel, B.G. Chaudhari, M.K. Buch, A.B. Patel, Stability indicating RP-HPLC method for simultaneous determination of valsartan and amlodipine from their combination product, *Int. J. ChemTech Res.* 1 (4) (2009) 1257–1267.
- [63] S.K. Patro, S.K. Kanungo, V.J. Patro, N.S.K. Choudhury, Stability indicating RP-HPLC method for determination of valsartan in pure and pharmaceutical formulation, *E-J. Chem.* 7 (1) (2010) 246–252.
- [64] B.M. Sudesh, K.S. Uttamrao, Determination and validation of valsartan and its degradation products by isocratic HPLC, *J. Chem. Metrol.* 3 (1) (2009) 1–12.
- [65] K.S. Lakshmi, L. Vasubramanian, A stability indicating HPLC method for the simultaneous determination of valsartan and ramipril in binary combination, *J. Chil. Chem. Soc.* 55 (2) (2010) 223–226.
- [66] N.H. Al-Shaalan, M.A. Alnowaiser, Simultaneous determination of amlodipine besilate and valsartan in pharmaceutical formulation using high performance liquid chromatography, *J. Chem. Pharm. Res.* 2 (6) (2010) 129–134.

- [67] G. Thanusha, C.J.G. Babu, K.P.C. Basavaraj, V.R. Panditi, C. Sharadha, Quantitative estimation of valsartan in bulk and pharmaceutical dosage forms, *Int. J. ChemTech Res.* 2 (2) (2010) 1194–1198.
- [68] D.U. Vinzuda, G.U. Sailor, N.R. Sheth, RP-HPLC method for determination of valsartan in tablet dosage forms, *Int. J. ChemTech Res.* 2 (3) (2010) 1461–1467.
- [69] D. Jothieswari, D. Priya, S. Brito Raj, E. Mohanambal, S. Wasim Raja, Design and RP-HPLC method for the simultaneous determination of valsartan and hydrochlorothiazide in bulk and in pharmaceutical formulation, *Int. J. Novel Trend. Pharm. Sci.* 1 (1) (2011) 18–22.
- [70] C.V.N. Prasad, C.S. Kumari, J. Sriramulu, A stability indicating RP-HPLC method for simultaneous estimation of valsartan and atorvastatin from their combination drug product, *Int. J. Pharm. Res. Anal.* 1 (1) (2011) 26–31.
- [71] V.B. Raju, A.L. Rao, Reversed phase HPLC analysis of valsartan in pharmaceutical dosage forms, *Int. J. Chem. Environ. Pharm. Res.* 2 (1) (2011) 56–60.
- [72] D.G.T. Parambi, M. Matthew, V. Ganesan, A validated stability indicating HPLC method for the determination of valsartan in tablet dosage forms, *J. Appl. Pharm. Sci.* 1 (4) (2011) 97–99.
- [73] A. Patnaik, M. Shetty, S. Sahoo, D.K. Nayak, S.K. Veliyath, A new RP-HPLC method for the determination of valsartan in bulk and its pharmaceutical formulations with its stability indicative studies, *Pharm. Sci. Monit.* 2 (3) (2011) 43–53.
- [74] K.S. Nataraj, S.S. Kumar, M.B. Duza, K. Reddy, Quantitative estimation of valsartan in pure and capsule dosage forms by RP-HPLC, *Int. J. Res. Pharm. Chem.* 1 (3) (2011) 587–590.
- [75] S. Rahila, P. Manisha, B. Deepali, M. Prabha, Y. Pramod, RP-HPLC method for simultaneous estimation of valsartan and hydrochlorothiazide in solid dosage form, *Int. Res. J. Pharm.* 2 (3) (2011) 162–164.
- [76] P.V. Santosh Kumar, M. Sahu, K.D. Prasad, M.C. Shekhar, Development and validation of analytical method for the estimation of valsartan in pure and tablet dosage form by RP-HPLC method, *Int. J. Res. Pharm. Chem.* 1 (4) (2011) 945–949.
- [77] P.V. Chokshi, K.J. Trivedi, N.S. Patel, Development and validation of RP-HPLC method for analysis of aliskiren hemifumarate and valsartan in their combination tablet dosage form, *Int. J. ChemTech Res.* 4 (4) (2012) 1623–1627.
- [78] N. Dubey, N. Dubey, M. Mandhanya, U. Bhadoriya, P. Sharma, Simultaneous estimation of ramipril and valsartan by RP-HPLC method in combined dosage form, *Asian J. Pharm. Med. Sci.* 2 (1) (2012) 23–28.
- [79] A.A. Elshanawane, L.M. Abdelaziz, H.M. Hafez, Stability indicating HPLC method for simultaneous determination of several angiotensin-II-receptor antagonists in their dosage forms. *Pharm. Anal. Acta* 3 (8) (2012) 175. <http://dx.doi.org/10.4172/2153-2435.1000175>.
- [80] S.M. El-Gizawy, O.H. Abdelmageed, M.A. Omar, S.M. Deryea, A.M. Abdel-Megied, Development and validation of HPLC method for simultaneous determination of amlodipine, valsartan, hydrochlorothiazide in dosage form and spiked human plasma, *Am. J. Anal. Chem.* 3 (2012) 422–430.
- [81] M.A. Haque, S.H. Amrohi, P. Kumar, G. Nivedita, P. Kumar, D. Mohanty, P.V. Diwan, Stability indicating RP-HPLC method for the estimation of valsartan in pharmaceutical dosage form, *IOSR J. Pharm.* 2 (4) (2012) 12–18.
- [82] M.D. Kendre, S.K. Banerjee, Precise and accurate RP-HPLC method development for quantification of valsartan in tablet dosage form, *Int. J. Pharm. Sci. Drug Res.* 4 (2) (2012) 137–139.
- [83] M. Kharoaf, N. Malkieh, M. Abualhasan, R. Shubitah, N. Jaradat, A.N. Zaid, Tablet formulation and development of a validates stability indicating HPLC method for quantification of valsartan and hydrochlorothiazide combination, *Int. J. Pharm. Pharm. Sci.* 4 (3) (2012) 284–290.

- [84] S. Muralidharan, J.R. Kumar, S.A. Dhanaraj, Simple and validated RP-HPLC method for the estimation of valsartan in pharmaceutical tablet dosage form, *J. Chem. Pharm. Res.* 4 (9) (2012) 4235–4239.
- [85] R.R. Nahire, S.S. Joshi, V. Meghnani, N. Shastri, K.V.S. Nath, J. Satish, Stability indicating RP-HPLC method for simultaneous determination of amlodipine besylate and valsartan combination in bulk and commercial dosage forms, *Asian J. Pharm. Life Sci.* 2 (2) (2012) 281–290.
- [86] M.R. Rezk, N.M. El Remali, A.E.A. Aleem, Simultaneous determination of valsartan and hydrochlorothiazide in their pharmaceutical formulations, *Pharm. Chem.* 4 (1) (2012) 529–537.
- [87] K.N.K. Reddy, G.D. Rao, P.H. Pratyusha, Isocratic RP HPLC method validation of valsartan in pharmaceutical formulation with stress test stability evaluation of drug substance, *J. Chem. Pharm. Sci.* 5 (1) (2012) 8–12.
- [88] B. Brahmaiah, K. Sujana, A.P. Rani, Development and validation of RP-HPLC method for simultaneous determination of ramipril and valsartan in bulk and pharmaceutical dosage forms, *Asian J. Pharm. Clin. Res.* 6 (1) (2013) 23–25.
- [89] S.E. Kepekci Tekkeli, Development of an HPLC-UV method for the analysis of drugs used for combined hypertension therapy in pharmaceutical preparations and human plasma, *J. Anal. Method. Chem.* 2013 (2013) 1–9.
- [90] R.A. Shaalan, T.S. Belal, F.A. El Yazbi, S.M. Elonsy, Validated stability-indicating HPLC-DAD method of analysis for the antihypertensive triple mixture of amlodipine besylate, valsartan and hydrochlorothiazide. *Arab. J. Chem.* (2013). <http://dx.doi.org/10.1016/j.arabjc.2013.04.012>.
- [91] M. Sharma, K. Chamy, O. Sherikar, P. Mehta, Concurrent estimation of amlodipine besylate, hydrochlorothiazide and valsartan by RP-HPLC, HPTLC and UV-spectrophotometry, *J. Chromatogr. Sci.* 52 (2014) 27–35.
- [92] S.S. Inam, A. Ahad, M. Aqil, Y. Sultana, A. Ali, A validated RP-HPLC method for simultaneous determination of propranolol and valsartan in bulk drug and gel formulation, *J. Pharm. Bioallied Sci.* 5 (1) (2013) 61–65.
- [93] S.R. Dhaneswar, N.G. Patre, M.V. Mahadik, Validated TLC method for simultaneous quantitation of amlodipine besylate and valsartan in bulk drug and formulation, *Chromatographia* 69 (1/2) (2009) 157–161.
- [94] A.V. Gaikwad, V.G. Rajurkar, T. Shivakumar, G.Y. Dama, H.L. Tara, Simultaneous estimation of ramipril & valsartan in tablets by HPTLC, *Indo-Global J. Pharm. Sci.* 1 (1) (2011) 99–112.
- [95] T. Inglot, A. Gumieniczek, P. Maczka, Thin layer chromatography (TLC) and video-scanning in a new method for the analysis of angiotensin AT1 receptor antagonists, telmisartan and valsartan, in pharmaceuticals, *Ann. Univ. Mariae Curie-Skłodowska Lublin-Polonia XXIII* (4) (2010) 43–50.
- [96] S.P. Lokhande, S.P. Gupta, K. Sureshkumar, J. Dharumar, G. Garg, N. Upmanyu, Development and validation of a HPTLC method for the simultaneous estimation of ramipril and valsartan, *Int. J. Pharm. Teach. Pract.* 3 (1) (2012) 225–227.
- [97] D.D. Tsvetkova, D.P. Obreshkova, Application of validated TLC-densitometric method for simultaneous identification and determination of losartan potassium, telmisartan, and valsartan in tablets, *J. Planar Chromatogr.* 24 (4) (2012) 326–330.
- [98] A.R. Shrivastava, C.R. Barhate, C.J. Kapadia, Stress degradation studies on valsartan using validated stability-indicating high-performance thin-layer chromatography, *J. Planar Chromatogr.* 22 (6) (2009) 411–416.
- [99] N.J. Shah, B.N. Suhagia, R.R. Shah, N.M. Patel, HPTLC method for the simultaneous estimation of valsartan and hydrochlorothiazide in tablet dosage form, *Indian J. Pharm. Sci.* 71 (1) (2009) 72–74. <http://www.ijpsonline.com/article.asp?issn=0250-474X;year=2009;volume=71;issue=1;page=72;epage=74;aualst=Shah> (accessed 30.03.14).

- [100] K. Czerwińska, A.P. Mazurek, Identification and determination of angiotensin II receptor antagonists with densitometric method, *Acta Pol. Pharm.* 63 (5) (2006) 402–404.
- [101] CAMAG Camag Bibliography Service CBS 51-112, Camag Muttentz (2014).
- [102] T.W. Inglot, K. Dabrowska, G. Misztal, The normal-phase retention behaviour of some angiotensin-II receptor antagonists, *J. Planar Chromatogr.* 20 (4) (2007) 293–301.
- [103] T.W. Inglot, K. Dabrowska, A. Gumieniczek, The reversed-phase retention behaviour of some angiotensin-II receptor antagonists, *J. Planar Chromatogr.* 22 (2) (2009) 145–155.
- [104] G. Iriarte, N. Ferreiros, I. Ibarrondo, R.M. Alonso, M.I. Maguregi, R.M. Jiménez, L. Gonzalez, Optimization via experimental design of an SPE-HPLC-UV-fluorescence method for the determination of valsartan and its metabolite in human plasma samples, *J. Sep. Sci.* 29 (2006) 2265–2283.
- [105] S. Kailasam, Simultaneous Determination of Therapeutic Drug Analytes in Human Plasma Using LC/MS/MS. Application Note, Agilent Technologies India, Bangalore, India, 2011.
- [106] H. Li, Y. Wang, Y. Jiang, Y. Tang, J. Wang, L. Zhao, J. Gu, A liquid chromatography/tandem mass spectrophotometry method for the simultaneous quantification of valsartan and hydrochlorothiazide in human plasma, *J. Chromatogr. B* 852 (2007) 436–442.
- [107] M. Levi, G. Wuerzner, E. Ezan, A. Pruvost, Direct analysis of valsartan and candesartan in human plasma and urines by on-line solid phase extraction coupled to electrospray tandem mass spectrometry, *J. Chromatogr. B* 877 (2009) 919–926.
- [108] N. Daneshdalan, R.Z. Lewanczuk, F. Jamali, High-performance liquid chromatographic analysis of angiotensin II receptor antagonist valsartan using a liquid extraction method, *J. Chromatogr. B* 766 (2002) 345–349.
- [109] M. Celebier, M.S. Kaynak, S. Altinöz, S. Şahin, Validated HPLC method development: the simultaneous analysis of amlodipine and valsartan in samples for liver perfusion studies, *Hacettepe Univ. J. Fac. Pharm.* 28 (1) (2008) 15–30.
- [110] J. Macek, J. Klíma, P. Ptáček, Rapid determination of valsartan in human plasma by protein precipitation and high-performance liquid chromatography, *J. Chromatogr. B* 832 (2006) 169–172.
- [111] A. Zarghi, A. Shafaati, S.M. Foroutan, H. Movahed, Rapid quantification of valsartan in human plasma by liquid chromatography using a monolithic column and a fluorescence detection: application in pharmacokinetics studies, *Sci. Pharm.* 76 (2008) 439–450.
- [112] M.R. Brunetto, Y. Contreras, S. Clavijo, D. Torres, Y. Delgado, F. Ovalles, C. Ayala, M. Galignani, J.M. Estela, V.C. Martin, Determination of losartan, telmisartan, and valsartan by direct injection of human urine into a column-switching liquid chromatographic system with fluorescence detection, *J. Pharm. Biomed. Anal.* 50 (2009) 194–199.
- [113] A.C.F. Spínola, S. Almeida, A. Filipe, R. Neves, F. Trabelsi, A. Farré, Results of single-center, single-dose, randomized-sequence, open-label, two-way crossover bioequivalence study of two formulations of valsartan 160-mg tablets in healthy volunteers under fasting conditions, *Clin. Ther.* 31 (9) (2009) 1992–2001.
- [114] P.S. Selvan, K.V. Gowda, U. Mandal, W.D. Sam Solomon, T.K. Pal, Simultaneous determination of fixed dose combination of nebivolol and valsartan in human plasma by liquid chromatographic-tandem mass spectrometry and its application to pharmacokinetic study, *J. Chromatogr. B* 858 (2007) 143–150.
- [115] G. Iriarte, N. Ferreiros, I. Ibarrondo, R.M. Alonso, M.I. Maguregi, R.M. Jiménez, Biovalidation of an SPE-HPLC-UV-fluorescence method for the determination of valsartan and its metabolite valeryl-4-hydroxy-valsartan in human plasma, *J. Sep. Sci.* 30 (2007) 2231–2240.

- [116] R.N. Sharma, S.S. Pancholi, Simple RP-HPLC method for the determination of triple drug combination of valsartan, amlodipine and hydrochlorothiazide in human plasma, *Acta Pharm.* 62 (2012) 45–58.
- [117] A.R. Dixit, S.R. Rajput, S.G. Patel, Preparation and bioavailability assessment of SMEDDS containing valsartan, *AAPS PharmSciTech* 11 (1) (2010) 314–321.
- [118] L. Kristoffersen, E.L. Øistad, M.S. Opdal, M. Krogh, E. Lundanes, A.S. Christophersen, Simultaneous determination of 6 beta-blockers, 3 calcium-channel antagonists, 4 angiotensin-II antagonists and 1 antiarrhythmic drug in post-mortem whole blood by automated solid phase extraction and liquid chromatography mass spectrometry method development and robustness testing by experimental design, *J. Chromatogr. B* 850 (2007) 147–160.
- [119] G.S. Ganesh, P. Deme, K. Madhusudana, R. Sistla, Simultaneous determination of amlodipine, valsartan and hydrochlorothiazide by LC-ECI-MS/MS and its application to pharmacokinetics in rats, *J. Pharm. Anal.* 4 (2014) 399–406. <http://dx.doi.org/10.1016/j.jpha.2013.12.003>.
- [120] L. González, R.M. Alonso, R.M. Jimenez, A high-performance liquid chromatographic method for screening angiotensin II receptor antagonists in human urine, *Chromatographia* 52 (2000) 735–740.

CUMULATIVE INDEX

Bold numerals refer to volume numbers.

A

Acebutolol, **19**, 1
Acetaminophen, **3**, 1; **14**, 551
Acetazolamide, **22**, 1
Acetohexamide, **1**, 1; **2**, 573; **21**, 1
Acetylcholine chloride, **31**, 3, 21
Acyclovir, **30**, 1
Adenosine, **25**, 1
Alendronate sodium, **38**, 1
Allopurinol, **7**, 1
Amantadine, **12**, 1
Amikacin sulfate, **12**, 37
Amiloride hydrochloride, **15**, 1
Aminobenzoic acid, **22**, 33
Aminogluthethimide, **15**, 35
Aminophylline, **11**, 1
Aminosalicylic acid, **10**, 1
Amiodarone, **20**, 1
Amitriptyline hydrochloride, **3**, 127
Amlodipine besylate, **37**, 31
Amobarbital, **19**, 27
Amodiaquine hydrochloride, **21**, 43
Amoxicillin, **7**, 19; **23**, 1
Amphotericin B, **6**, 1; **7**, 502
Ampicillin, **2**, 1; **4**, 518
Apomorphine hydrochloride, **20**, 121
Arginine, **27**, 1
Aripiprazole, **38**, 35
Aripiprazole: polymorphs and solvatomorphs, **37**, 1
Ascorbic acid, **11**, 45
Aspartame, **29**, 7
Aspirin, **8**, 1
Astemizole, **20**, 173
Atenolol, **13**, 1
Atorvastatin calcium, **35**, 1
Atropine, **14**, 325
Azathioprine, **10**, 29
Azintamide, **18**, 1
Azithromycin, **39**, 1
Aztreonam, **17**, 1

B

Bacitracin, **9**, 1
Baclofen, **14**, 527
Benazepril hydrochloride, **31**, 117
Bendroflumethiazide, **5**, 1; **6**, 597
Benperidol, **14**, 245
Benzocaine, **12**, 73
Benzoic acid, **26**, 1
Benzyl benzoate, **10**, 55
Betamethasone dipropionate, **6**, 43
Bretylum tosylate, **9**, 71
Brinzolamide, **26**, 47
Bromazepam, **16**, 1
Bromcriptine methanesulfonate, **8**, 47
Buclizine, **36**, 1
Bumetanide, **22**, 107
Bupivacaine, **19**, 59
Busulphan, **16**, 53
Butyl methoxy dibenzoylmethane, **38**, 87

C

Caffeine, **15**, 71
Calcitriol, **8**, 83
Camphor, **13**, 27
Candesartan cilexetil, **37**, 79
Captopril, **11**, 79
Carbamazepine, **9**, 87
Carbenoxolone sodium, **24**, 1
Carvedilol, **38**, 113
Cefaclor, **9**, 107
Cefamandole nafate, **9**, 125; **10**, 729
Cefazolin, **4**, 1
Cefdinir, **39**, 41
Cefixime, **25**, 39
Cefotaxime, **11**, 139
Cefoxitin sodium, **11**, 169
Ceftazidime, **19**, 95
Ceftriaxone sodium, **30**, 21
Cefuroxime sodium, **20**, 209
Celiprolol hydrochloride, **20**, 237
Cephalexin, **4**, 21
Cephalothin sodium, **1**, 319

Cephadrine, **5**, 21
Chitin, **36**, 35
Chloral hydrate, **2**, 85
Chlorambucil, **16**, 85
Chloramphenicol, **4**, 47; **15**, 701
Chlordiazepoxide, **1**, 15
Chlordiazepoxide hydrochloride, **1**, 39;
4, 518
Chloropheniramine maleate, **7**, 43
Chloroquine, **13**, 95
Chloroquine phosphate, **5**, 61
Chlorothiazide, **18**, 33
Chlorpromazine, **26**, 97
Chlorprothixene, **2**, 63
Chlortetracycline hydrochloride, **8**, 101
Chlorthalidone, **14**, 1
Chlorzoxazone, **16**, 119
Cholecalciferol, **13**, 655
Cimetidine, **13**, 127; **17**, 797
Cinnarizine, **40**, 1
Ciprofloxacin, **31**, 163, 179, 209
Cisplatin, **14**, 77; **15**, 796
Citric Acid, **28**, 1
Clarithromycin, **24**, 45
Clidinium bromide, **2**, 145
Clindamycin hydrochloride, **10**, 75
Clioquinol, **18**, 57
Clofazimine, **18**, 91; **21**, 75
Clomiphene citrate, **25**, 85
Clonazepam, **6**, 61
Clonfibrate, **11**, 197
Clonidine hydrochloride, **21**, 109
Clopido­grel bisulfate, **35**, 71
Clorazepate dipotassium, **4**, 91
Clotrimazole, **11**, 225
Cloxacillin sodium, **4**, 113
Clozapine, **22**, 145
Cocaine hydrochloride, **15**, 151
Cocrystal Systems of Pharmaceutical
Interest: 2007–2008, **35**, 373
Cocrystal Systems of Pharmaceutical
Interest: 2009, **36**, 361
Codeine phosphate, **10**, 93
Colchicine, **10**, 139
Cortisone acetate, **26**, 167
Creatine monohydrate, **34**, 1
Crospovidone, **24**, 87
Curcumin, **39**, 113
Cyanocobalamin, **10**, 183

Cyclandelate, **21**, 149
Cyclizine, **6**, 83; **7**, 502
Cyclobenzaprine hydrochloride, **17**, 41
Cycloserine, **1**, 53; **18**, 567
Cyclosporine, **16**, 145
Cyclothiazide, **1**, 65
Cyproheptadine, **9**, 155
Cytarabine, **34**, 37

D

Dapsone, **5**, 87
Dasatinib, **39**, 205
Dexamethasone, **2**, 163; **4**, 519
Diatrizoic acid, **4**, 137; **5**, 556
Diazepam, **1**, 79; **4**, 518
Dibenzepin hydrochloride, **9**, 181
Dibucaine, **12**, 105
Dibucaine hydrochloride, **12**, 105
Diclofenac sodium, **19**, 123
Didanosine, **22**, 185
Diethylstilbestrol, **19**, 145
Diflunisal, **14**, 491
Digitoxin, **3**, 149; **9**, 207
Dihydroergotoxine methanesulfonate, **7**, 81
Diloxanide furoate, **26**, 247
Diltiazem hydrochloride, **23**, 53
Diocetyl sodium sulfosuccinate, **2**, 199;
12, 713
Diosgenin, **23**, 101
Diperodon, **6**, 99
Diphenhydramine hydrochloride, **3**, 173
Diphenoxylate hydrochloride, **7**, 149
Dipivefrin hydrochloride, **22**, 229
Dipyridamole, **31**, 215
Disopyramide phosphate, **13**, 183
Direct Crystallization of Enantiomers and
Dissociable Diastereomers, **36**, 331
Disulfiram, **4**, 168
Dobutamine hydrochloride, **8**, 139
Donepezil, **35**, 117
Dopamine hydrochloride, **11**, 257
Dorzolamide hydrochloride, **26**, 283; **27**, 377
Doxorubicine, **9**, 245
Droperidol, **7**, 171

E

Echothiophate iodide, **3**, 233
Econazole nitrate, **23**, 127
Edetic Acid (EDTA), **29**, 57

Emetine hydrochloride, **10**, 289
Enalapril maleate, **16**, 207
Ephedrine hydrochloride, **15**, 233
Epinephrine, **7**, 193
Ergonovine maleate, **11**, 273
Ergotamine tartrate, **6**, 113
Erthromycin, **8**, 159
Erthromycin estolate, **1**, 101; **2**, 573
Estradiol, **15**, 283
Estradiol valerate, **4**, 192
Estrone, **12**, 135
Ethambutol hydrochloride, **7**, 231
Ethynodiol diacetate, **3**, 253
Etodolac, **29**, 105
Etomidate, **12**, 191
Etoposide, **18**, 121
Eugenol, **29**, 149
Ezetimibe, **36**, 103

F

Famotidine, **34**, 115
Fenoprofen calcium, **6**, 161
Fenoterol hydrobromide, **27**, 33
Flavoxate hydrochloride, **28**, 77
Fexofenadine hydrochloride, **34**, 153
Flecainide, **21**, 169
Fluconazole, **27**, 67
Flucytosine, **5**, 115
Fludrocortisone acetate, **3**, 281
Flufenamic acid, **11**, 313
Fluorouracil, **2**, 221; **18**, 599
Fluoxetine, **19**, 193
Fluoxymesterone, **7**, 251
Fluphenazine decanoate, **9**, 275; **10**, 730
Fluphenazine enanthate, **2**, 245; **4**, 524
Fluphenazine hydrochloride, **2**, 263; **4**, 519
Flurazepam hydrochloride, **3**, 307
Flurbiprofen, **37**, 113
Flutamide, **27**, 115
Fluvoxamine maleate, **24**, 165
Folic acid, **19**, 221
Furosemide, **18**, 153

G

Gadoteridol, **24**, 209
Gatifloxacin, **37**, 183
Gefitinib, **39**, 239
Gemifloxacin, **36**, 151
Gentamicin sulfate, **9**, 295; **10**, 731

Glafenine, **21**, 197
Glibenclamide, **10**, 337
Glimepiride, **36**, 169
Glutathione, **40**, 43
Gluthethimide, **5**, 139
Gramicidin, **8**, 179
Griseofulvin, **8**, 219; **9**, 583
Guaifenesin, **25**, 121
Guanabenz acetate, **15**, 319
Guar gum, **24**, 243

H

Halcinonide, **8**, 251
Haloperidol, **9**, 341
Halothane, **1**, 119; **2**, 573; **14**, 597
Heparin sodium, **12**, 215
Heroin, **10**, 357
Hexestrol, **11**, 347
Hexetidine, **7**, 277
Histamine, **27**, 159
Homatropine hydrobromide,
 16, 245
Hydralazine hydrochloride, **8**, 283
Hydrochlorothiazide, **10**, 405
Hydrocortisone, **12**, 277
Hydroflumethazide, **7**, 297
Hydroxyprogesterone caproate, **4**, 209
Hydroxyzine dihydrochloride, **7**, 319
Hyoscyamine, **23**, 155

I

Ibuprofen, **27**, 265
Imatinib mesylate, **39**, 265
Imipramine hydrochloride, **14**, 37
Impenem, **17**, 73
Indapamide, **23**, 233
Indinavar sulfate, **26**, 319
Indomethacin, **13**, 211
Iodamide, **15**, 337
Iodipamide, **2**, 333
Iodoxamic acid, **20**, 303
Iopamidol, **17**, 115
Iopanoic acid, **14**, 181
Ipratropium bromide, **30**, 59
Iproniazid phosphate, **20**, 337
Isocarboxazid, **2**, 295
Isoniazide, **6**, 183
Isopropamide, **2**, 315; **12**, 721
Isoproterenol, **14**, 391

Isosorbide dinitrate, **4**, 225; **5**, 556
Isosuprine hydrochloride, **26**, 359
Itraconazole, **34**, 193
Ivermectin, **17**, 155

K

Kanamycin sulfate, **6**, 259
Ketamine, **6**, 297
Ketoprofen, **10**, 443
Ketotifen, **13**, 239
Khellin, **9**, 371

L

Lactic acid, **22**, 263
Lactose, anhydrous, **20**, 369
Lamotrigine, **37**, 245
Lansoprazole, **28**, 117
Leucovorin calcium, **8**, 315
Levallorphan tartrate, **2**, 339
Levarterenol bitartrate, **1**, 149; **2**, 573;
11, 555
Levodopa, **5**, 189
Levothyroxine sodium, **5**, 225
Lidocaine, **14**, 207; **15**, 761
Lidocaine hydrochloride, **14**, 207; **15**, 761
Lincomycin, **23**, 275
Lisinopril, **21**, 233
Lithium carbonate, **15**, 367
Lobeline hydrochloride, **19**, 261
Lomefloxacin, **23**, 327
Lomustine, **19**, 315
Loperamide hydrochloride, **19**, 341
Lorazepam, **9**, 397
Lornoxicam, **36**, 205
Losartan, **40**, 159
Lovastatin, **21**, 277

M

Mafenide acetate, **24**, 277
Malic Acid, **28**, 153
Magnesium Silicate, **36**, 241
Maltodextrin, **24**, 307
Mandelic Acid, **29**, 179
Maprotiline hydrochloride, **15**, 393
Mebendazole, **16**, 291
Mebeverine hydrochloride, **25**, 165
Mefenamic acid, **31**, 281

Mefloquine hydrochloride, **14**, 157
Melatonin: comprehensive profile, **38**, 159
Melfhalan, **13**, 265
Menadione, **38**, 227
Meperidine hydrochloride, **1**, 175
Meprobamate, **1**, 207; **4**, 520; **11**, 587
Mercaptopurine, **7**, 343
Mesalamine, **25**, 209; **27**, 379
Mestranol, **11**, 375
Metformin hydrochloride, **25**, 243
Methadone hydrochloride, **3**, 365; **4**, 520;
9, 601
Methaqualone, **4**, 245
Methimazole, **8**, 351
Methixen hydrochloride, **22**, 317
Methocarbamol, **23**, 377
Methotrexate, **5**, 283
Methoxamine hydrochloride, **20**, 399
Methoxsalen, **9**, 427
Methylclothiazide, **5**, 307
Methylphenidate hydrochloride, **10**, 473
Methyprylon, **2**, 363
Metipranolol, **19**, 367
Metoclopramide hydrochloride, **16**, 327
Metoprolol tartrate, **12**, 325
Metronidazole, **5**, 327
Mexiletine hydrochloride, **20**, 433
Miconazole nitrate, **32**, 3
Minocycline, **6**, 323
Minoxidil, **17**, 185
Mitomycin C, **16**, 361
Mitoxanthrone hydrochloride, **17**, 221
Morphine, **17**, 259
Moxalactam disodium, **13**, 305
Moxidectin, analytical profile, **38**, 315
Moxifloxacin hydrochloride, **39**, 299

N

Nabilone, **10**, 499
Nadolol, **9**, 455; **10**, 732
Nalidixic acid, **8**, 371
Nalmefene hydrochloride, **24**, 351
Nalorphine hydrobromide, **18**, 195
Naloxone hydrochloride, **14**, 453
Naphazoline hydrochloride, **21**, 307
Naproxen, **21**, 345
Natamycin, **10**, 513; **23**, 405
Neomycin, **8**, 399

Neostigmine, **16**, 403
Niclosamide, **32**, 67
Nicotinamide, **20**, 475
Nifedipine, **18**, 221
Nimesulide, **28**, 197
Nimodipine, **31**, 337, 355, 371
Nitrazepam, **9**, 487
Nitrofurantoin, **5**, 345
Nitroglycerin, **9**, 519
Nizatidine, **19**, 397
Norethindrone, **4**, 268
Norfloxacin, **20**, 557
Norgestrel, **4**, 294
Nortriptyline hydrochloride, **1**, 233; **2**, 573
Noscapine, **11**, 407
Nystatin, **6**, 341

O

Ofloxacin, **34**, 265
Omeprazole, **35**, 151
Ondansetron hydrochloride, **27**, 301
Ornidazole, **30**, 123
Oxamniquine, **20**, 601
Oxazepam, **3**, 441
Oxyphenbutazone, **13**, 333
Oxytetracycline, **32**, 97
Oxytocin, **10**, 563

P

Paclitaxel, **34**, 299
Pantoprazole, **29**, 213
Papaverine hydrochloride, **17**, 367
Parbendazole, **35**, 263
Particle Size Distribution, **31**, 379
Paroxetine hydrochloride, **38**, 367
Paroxetine hydrochloride: polymorphs
and solvatomorphs, **38**, 407
Penicillamine, **10**, 601; **32**, 119, 131, 149
Penicillin-G, benzothine, **11**, 463
Penicillin-G, potassium, **15**, 427
Penicillin-V, **1**, 249; **17**, 677
Pentazocine, **13**, 361
Pentoxifylline, **25**, 295
Pergolide Mesylate, **21**, 375
Phenazopyridine hydrochloride, **3**, 465
Phenelzine sulfate, **2**, 383
Phenformin hydrochloride, **4**, 319; **5**, 429
Phenobarbital, **7**, 359

Phenolphthalein, **20**, 627
Phenoxymethyl penicillin potassium, **1**, 249
Phenylbutazone, **11**, 483
Phenylephrine hydrochloride, **3**, 483
Phenylpropanolamine hydrochloride, **12**,
357; **13**, 767
Phenytoin, **13**, 417
Physostigmine salicylate, **18**, 289
Phytonadione, **17**, 449
Pilocarpine, **12**, 385
Pimozide, **37**, 287
Piperazine estrone sulfate, **5**, 375
Pirenzepine dihydrochloride, **16**, 445
Piroxicam, **15**, 509
Polymorphism 2004, **32**, 263
Polythiazide, **20**, 665
Polyvinyl alcohol, **24**, 397
Polyvinylpyrrolidone, **22**, 555
Povidone, **22**, 555
Povidone-Iodine, **25**, 341
Pralidoxine chloride, **17**, 533
Prasugrel hydrochloride, **40**, 195
Pravastatin sodium, **39**, 433
Praziquantel, **25**, 463
Prazosin hydrochloride, **18**, 351
Prednisolone, **21**, 415
Primaquine diphosphate, **32**, 153
Primidone, **2**, 409; **17**, 749
Probenecid, **10**, 639
Procainamide hydrochloride, **4**, 333; **28**, 251
Procaine hydrochloride, **26**, 395
Procarbazine hydrochloride, **5**, 403
Promethazine hydrochloride, **5**, 429
Proparacaine hydrochloride, **6**, 423
Propiomazine hydrochloride, **2**, 439
Propoxyphene hydrochloride, **1**, 301;
4, 520; **6**, 598
Propyl paraben, **30**, 235
Propylthiouracil, **6**, 457
Pseudoephedrine hydrochloride, **8**, 489
Pyrazinamide, **12**, 433
Pyridoxine hydrochloride, **13**, 447
Pyrimethamine, **12**, 463

Q

Quinidine sulfate, **12**, 483
Quinine hydrochloride, **12**, 547

R

Ranitidine, **15**, 533
Reserpine, **4**, 384; **5**, 557; **13**, 737
Riboflavin, **19**, 429
Rifampin, **5**, 467
Risperidone, **37**, 313
Rocuronium bromide, **35**, 285
Rutin, **12**, 623

S

Saccharin, **13**, 487
Salbutamol, **10**, 665
Salicylamide, **13**, 521
Salicylic acid, **23**, 427
Salmeterol xinafoate, **40**, 321
Scopolamine hydrobromide, **19**, 477
Secobarbital sodium, **1**, 343
Sertraline hydrochloride, **24**, 443
Sertraline lactate, **30**, 185
Sildenafil citrate, **27**, 339
Silver sulfadiazine, **13**, 553
Simvastatin, **22**, 359
Sodium nitroprusside, **6**, 487; **15**, 781
Sodium valproate, **32**, 209
Solasodine, **24**, 487
Sorbitol, **26**, 459
Sotalol, **21**, 501
Spironolactone, **4**, 431; **29**, 261
Starch, **24**, 523
Streptomycin, **16**, 507
Strychnine, **15**, 563
Succinylcholine chloride, **10**, 691
Sucralose, **38**, 423
Sulfacetamide, **23**, 477
Sulfadiazine, **11**, 523
Sulfadoxine, **17**, 571
Sulfamethazine, **7**, 401
Sulfamethoxazole, **2**, 467; **4**, 521
Sulfasalazine, **5**, 515
Sulfathiazole, **22**, 389
Sulfisoxazole, **2**, 487
Sulfoxone sodium, **19**, 553
Sulindac, **13**, 573
Sulphamerazine, **6**, 515
Sulpiride, **17**, 607
Sunitinib malate, **37**, 363

T

Tadalafil, **36**, 287
Talc, **23**, 517
Telmisartan, **40**, 371
Teniposide, **19**, 575
Tenoxicam, **22**, 431
Terazosin, **20**, 693
Terbutaline sulfate, **19**, 601
Terfenadine, **19**, 627
Terpin hydrate, **14**, 273
Testolactone, **5**, 533
Testosterone enanthate, **4**, 452
Tetracaine hydrochloride, **18**, 379
Tetracycline hydrochloride, **13**, 597
Theophylline, **4**, 466
Thiabendazole, **16**, 611
Thiamine hydrochloride, **18**, 413
Thiamphenicol, **22**, 461
Thiopental sodium, **21**, 535
Thioridazine, **18**, 459
Thioridazine hydrochloride, **18**, 459
Thiostrepton, **7**, 423
Thiothixene, **18**, 527
Ticlopidine hydrochloride, **21**, 573
Timolol maleate, **16**, 641
Titanium dioxide, **21**, 659
Tobramycin, **24**, 579
 α -Tocopheryl acetate, **3**, 111
Tolazamide, **22**, 489
Tolbutamide, **3**, 513; **5**, 557; **13**, 719
Tolnaftate, **23**, 549
Tramadol hydrochloride, **38**, 463
Tranlycypromine sulfate, **25**, 501
Trazodone hydrochloride, **16**, 693
Triamcinolone, **1**, 367; **2**, 571; **4**, 521;
11, 593
Triamcinolone acetonide, **1**, 397; **2**, 571;
4, 521; **7**, 501; **11**, 615
Triamcinolone diacetate, **1**, 423;
11, 651
Triamcinolone hexacetonide, **6**, 579
Triamterene, **23**, 579
Triclobisonium chloride, **2**, 507
Trifluoperazine hydrochloride, **9**, 543
Triflupromazine hydrochloride, **2**, 523;
4, 521; **5**, 557
Trimethaphan camsylate, **3**, 545

Trimethobenzamide hydrochloride, **2**, 551
Trimethoprim, **7**, 445
Trimipramine maleate, **12**, 683
Trioxsalen, **10**, 705
Tripeleennamine hydrochloride, **14**, 107
Triprolidine hydrochloride, **8**, 509
Tropicamide, **3**, 565
Tubocurarine chloride, **7**, 477
Tybamate, **4**, 494

V

Validation, Analytical Methods,
 37, 439
Validation, Chromatographic Methods,
 32, 243
Valproate sodium, **8**, 529
Valproic acid, **8**, 529; **32**, 209
Valsartan, **40**, 431
Vardenafil dihydrochloride, **39**, 515
Varenicline, **37**, 389
Verapamil, **17**, 643
Vidarabine, **15**, 647

Vigabatrin, **35**, 309
Vinblastine sulfate, **1**, 443; **21**, 611
Vincristine sulfate, **1**, 463; **22**, 517
Vitamin D3, **13**, 655

W

Warfarin, **14**, 423

X

X-Ray Diffraction, **30**, 271
Xylometazoline hydrochloride, **14**, 135

Y

Yohimbine, **16**, 731

Z

Zaleplon, **35**, 347
Zidovudine, **20**, 729
Zileuton, **25**, 535
Zolpidem tartrate, **37**, 413
Zomepirac sodium, **15**, 673